



Reliable and Affordable Control Systems Active Combustor Pattern Factor Control

Bob McCarty, Chris Tomondi, and Ray McGinley
Honeywell Engines and Systems, Phoenix, Arizona

The NASA STI Program Office . . . in Profile

Since its founding, NASA has been dedicated to the advancement of aeronautics and space science. The NASA Scientific and Technical Information (STI) Program Office plays a key part in helping NASA maintain this important role.

The NASA STI Program Office is operated by Langley Research Center, the Lead Center for NASA's scientific and technical information. The NASA STI Program Office provides access to the NASA STI Database, the largest collection of aeronautical and space science STI in the world. The Program Office is also NASA's institutional mechanism for disseminating the results of its research and development activities. These results are published by NASA in the NASA STI Report Series, which includes the following report types:

- **TECHNICAL PUBLICATION.** Reports of completed research or a major significant phase of research that present the results of NASA programs and include extensive data or theoretical analysis. Includes compilations of significant scientific and technical data and information deemed to be of continuing reference value. NASA's counterpart of peer-reviewed formal professional papers but has less stringent limitations on manuscript length and extent of graphic presentations.
- **TECHNICAL MEMORANDUM.** Scientific and technical findings that are preliminary or of specialized interest, e.g., quick release reports, working papers, and bibliographies that contain minimal annotation. Does not contain extensive analysis.
- **CONTRACTOR REPORT.** Scientific and technical findings by NASA-sponsored contractors and grantees.

- **CONFERENCE PUBLICATION.** Collected papers from scientific and technical conferences, symposia, seminars, or other meetings sponsored or cosponsored by NASA.
- **SPECIAL PUBLICATION.** Scientific, technical, or historical information from NASA programs, projects, and missions, often concerned with subjects having substantial public interest.
- **TECHNICAL TRANSLATION.** English-language translations of foreign scientific and technical material pertinent to NASA's mission.

Specialized services that complement the STI Program Office's diverse offerings include creating custom thesauri, building customized databases, organizing and publishing research results . . . even providing videos.

For more information about the NASA STI Program Office, see the following:

- Access the NASA STI Program Home Page at <http://www.sti.nasa.gov>
- E-mail your question via the Internet to help@sti.nasa.gov
- Fax your question to the NASA Access Help Desk at 301-621-0134
- Telephone the NASA Access Help Desk at 301-621-0390
- Write to:
NASA Access Help Desk
NASA Center for Aerospace Information
7121 Standard Drive
Hanover, MD 21076



Reliable and Affordable Control Systems Active Combustor Pattern Factor Control

Bob McCarty, Chris Tomondi, and Ray McGinley
Honeywell Engines and Systems, Phoenix, Arizona

Prepared under Contract NAS3-27752, AOI Task 1.2

National Aeronautics and
Space Administration

Glenn Research Center

Document History

This research was originally published internally as AST034 in June 2000.

Trade names or manufacturers' names are used in this report for identification only. This usage does not constitute an official endorsement, either expressed or implied, by the National Aeronautics and Space Administration.

Note that at the time of research, the NASA Lewis Research Center was undergoing a name change to the NASA John H. Glenn Research Center at Lewis Field. Both names may appear in this report.

Available from

NASA Center for Aerospace Information
7121 Standard Drive
Hanover, MD 21076

National Technical Information Service
5285 Port Royal Road
Springfield, VA 22100

Available electronically at <http://gltrs.grc.nasa.gov>

TABLE OF CONTENTS

| | <u>Page</u> |
|--|-------------|
| 1. INTRODUCTION | 1 |
| 2. THIN-FILM SENSORS | 3 |
| 3. FUEL-FLOW MODULATORS | 16 |
| 4. FUEL-FLOW MODULATOR DRIVER BOX | 27 |
| 5. CONTROL SYSTEM DEVELOPMENT | 28 |
| 6. PATTERN FACTOR CONTROLLER | 30 |
| 7. COMBUSTOR RIG ASSEMBLY | 38 |
| 8. RAPID PROTOTYPE CONTROLLER BENCH TEST | 41 |
| 9. SIMULATOR BENCH TEST | 43 |
| 10. COMBUSTOR RIG TESTS | 50 |
| 11. CONCLUSIONS | 57 |
| 12. FURTHER DEVELOPMENT | 58 |

APPENDIXES

| | | |
|-----|--|-----|
| I | THIN-FILM SENSOR TEARDOWN REPORT (17 pages) | 59 |
| II | DEMONSTRATION OF A FUEL FLOW MODULATOR USING AN ADVANCED LATCHING MAGNETIC ACTUATOR (39 pages) | 77 |
| III | RELIABLE AND AFFORDABLE CONTROL SYSTEMS ACTIVE COMBUSTOR PATTERN FACTOR CONTROL SYSTEM MODES AND LOGIC DESIGN DOCUMENT (149 pages) | 117 |
| IV | SOFTWARE REQUIREMENTS SPECIFICATION FOR THE PATTERN FACTOR CONTROLLER (32 pages) | 295 |

**RELIABLE AND AFFORDABLE CONTROL SYSTEMS
ACTIVE COMBUSTOR PATTERN FACTOR CONTROL
NASA CONTRACT NO. NAS3-27752 (TASK 1.2)
FINAL REPORT**

1. INTRODUCTION

Active, closed-loop control of combustor pattern factor is a cooperative effort between Honeywell (formerly AlliedSignal) Engines & Systems and the NASA Glenn Research Center to reduce emissions and turbine-stator vane temperature variations, thereby enhancing engine performance and life, and reducing direct operating costs. Total fuel flow supplied to the engine is established by the speed/power control, but the distribution to individual atomizers will be controlled by the Active Combustor Pattern Factor Control (ACPFC). This system consists of three major components: multiple, thin-film sensors located on the turbine-stator vanes; fuel-flow modulators for individual atomizers; and control logic and algorithms within the electronic control. A program summary is shown in Figure 1.

Goal

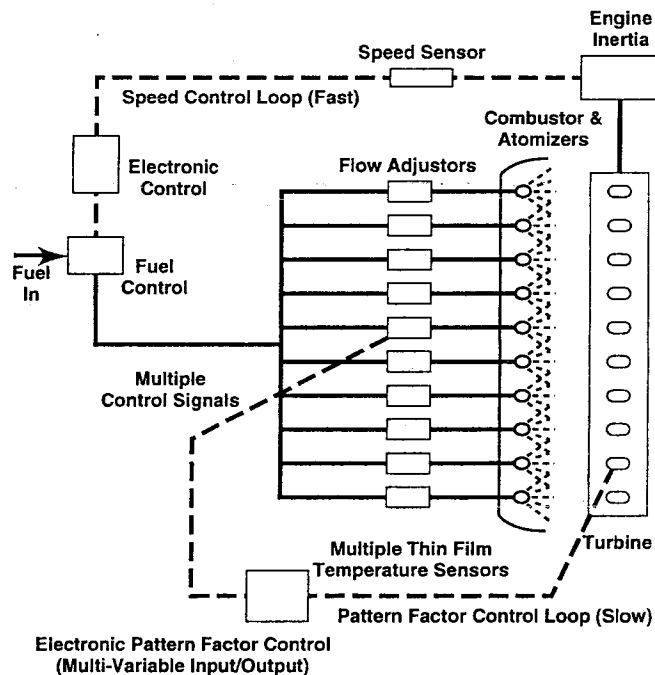
- Develop the methodology to control the burner pattern factor to reduce the temperature spread, or hot spots, and allow the average gaspath temperature to be increased to:
 - Increase engine specific thrust
 - Reduce direct operating costs by 2.4%

Approach

- Develop an active pattern factor control system to:
- Determine the turbine inlet stator temperature distribution using thin-film sensors
- Develop a method to modulate the fuel flow at individual atomizers
- Develop special logic in the engine electronic controller
- Evaluate the total system with existing rig test equipment

Payoff

- Uniform combustor exit temperatures allow increased turbine inlet temperatures of 200F
- Mission fuel burn improvement of 1.8%
- 2.4% DOC reduction
- Hot-section maintenance interval extended by 13%



**ACPFC Is Multi-Variable
Input/Output Control**

G6999-527

Figure 1. Program Goals, Approach, and Payoff.

This final report is organized to allow the reader to focus on the development of the individual elements of the control system (thin-film sensors, fuel-flow modulators, controller, rig assembly, etc.). The chronological report of events has been documented in the 22 bimonthly progress reports. This approach is expected to be more useful in assessing the technology readiness of the concept as a whole.

2. THIN-FILM SENSORS

Thin-film sensors are used to directly measure the turbine-stator temperature that is the thermal design point for the thermodynamic design. Indirect measurement of combustion airflow temperature requires the control system to provide sufficient allowance for hot spots and dynamic changes in radial airflow patterns, and the consequence is operation at average temperatures well below the thermal capability of the metal.

Initial testing was directed at evaluating three different base dielectrics. Thin-film, type-S (platinum and platinum 10% rhodium) thermocouples were fabricated on Hastelloy X bars (.75in x .25in x 11in) and then tested in the Metrology and Standards Laboratory to document accuracy and temperature capabilities. A total of seven thermocouples were tested to a maximum of 1200C (2192F) and accuracy was within two percent of standard. The limit of the wrought Hastelloy X bars was reached, as base material degraded above 1100C. The performance in the 1000 to 1100C range was excellent. Adherence of the metal films was best on the thermally grown, alpha-alumina dielectric. A standard thermocouple was installed in the furnace for reference comparisons.

Three types of aluminum-oxide dielectrics were used for the thermocouple basecoat. The first technique used a seed coat of sputtered alumina followed by a thermally grown gamma crystalline alumina layer. The second used an electron beam vapor deposition (EPVD) alpha-alumina dielectric and was supplied by NASA-GRC. The third method used a proprietary thermal cycle producing crystalline alpha aluminum oxide. Five of the thermocouples tested used the composite alumina dielectric, one used EPVD alumina, and one used the thermal alumina.

The bars were hung in a vertical furnace along with a standard type-S thermocouple. These were subjected to a ramp and soak cycle from ambient to the desired temperature where they were soaked for one to two hours and then ramped back to ambient for examination. Limitations of the attachment shim stock and potting were exceeded as well as encroaching on the Hastelloy X-substrate material limit. The thermocouples and output EMF were measured with respect to 0C. The total uncertainty of the temperature measurements is +/- 2C. Table 1 shows the results in accordance with ITS-90.

The thermally grown alpha-alumina dielectric showed the most stability.

Table 1. Results of Thin-Film, Type-S Thermocouple Testing.

| Bar ID | Dielectric Type Max | T @ failure | Number of cycles | Temp Dev | % Dev. |
|--------|---------------------|-------------|------------------|----------|--------|
| AE 1 | composite | 850C | 1 | -- | -- |
| AE4 | composite | 900C | 1 | -- | -- |
| AE5 | composite | 1037C | 3 | -44C | -4.2% |
| AE2 | composite | 817C | 1 | -24C | -3% |
| AE3 | composite | 1237C | 4 | -124C | - 10% |
| N1 | EPVD | 1237C | 4 | 449C | +36% |
| AE101 | Thermal | 1237C | 1 | 12C | +1% |

Development then focused on accelerated life testing of uncoated type S (platinum and platinum 10%rhodium) thin-film thermocouples sputtered on Hastelloy X bars. The thermocouples were sputtered on a thermally grown, alpha-alumina dielectric and tested by simulating engine operating hours in the Hot Corrosion Flow Facility. The thin-film transition consists of 3-mil wire that is spliced to 0.040-inch-diameter, type-S, magnesium oxide (MgO) insulated leadwire terminated in a standard thermocouple connector. The thermocouples were heat treated but are without any protective overcoat.

A 3-inch-diameter pipe rig fixture with 1-inch access mount ports was constructed for testing of the bars in the rig. The Mach 1 burner rig was initially set up with several small (3/8 inch wide) sample bars that had one type-S sputtered thermocouple on each. These were used to set the burner rig for the high-velocity flow and to allow automatic cyclical control.

A type-S, 0.040-inch-diameter thermocouple was tack welded in place adjacent to the thin-film sensors for reference (see Figure 2). A temperature profile of the gas flow across the pipe rig was also made. An analytical model was constructed to look at the correlation between the gas temperature and the recorded thin-film metal temperature.

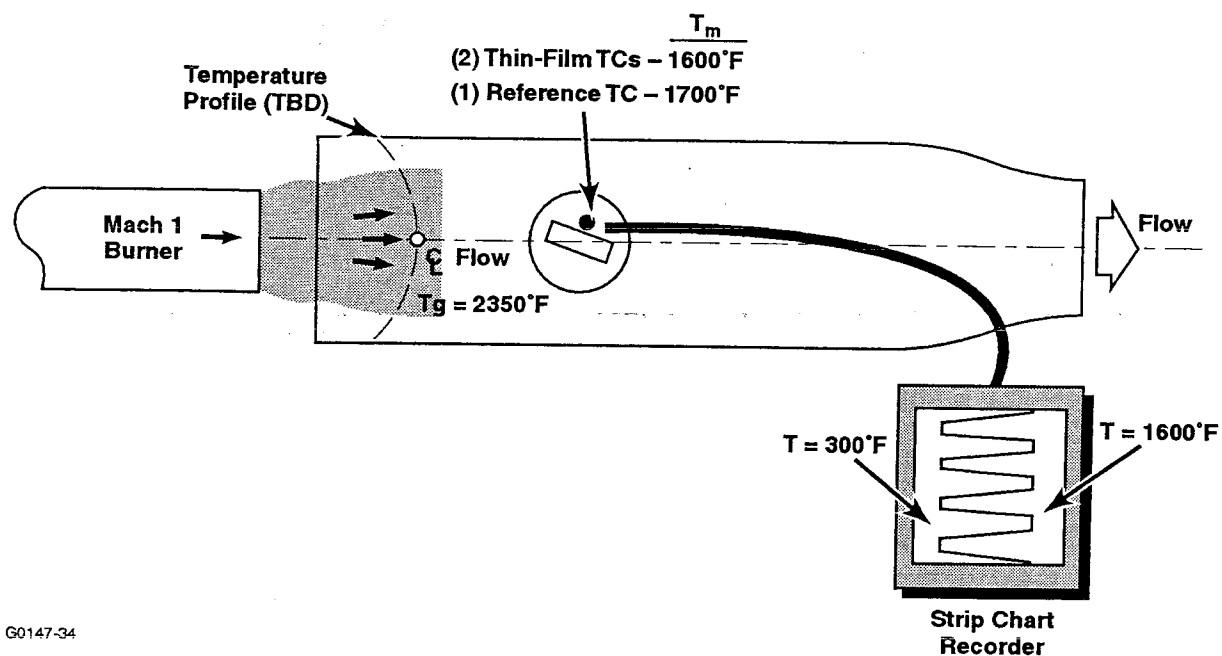


Figure 2. Burner Rig Test Configuration.

The first two bars were cycled to 1200F at Mach 1 and then the thin-film metal temperature was increased to 1600F, where the rig was controlled by one of the thin-film thermocouples. Each test cycle for the bars included seven minutes at temperature and three minutes of cooldown. For accelerated engine operation, sixty cycles on the rig to 1600F simulates 85 engine operating hours. The results are shown in Table 2. The early failure mode for the first two of the thermocouples occurred when the platinum leg delaminated. The longer term failure for the

balance of the sensors occurred when the sensor went open, as the platinum-10% rhodium leg eroded and delaminated. A maximum of 441 cycles to 1600F was reached on one of the thermocouples, which equates to 625 engine operational hours. The average of the five type-S thermocouples tested to 1600F was 249 cycles, or 353 engine hours.

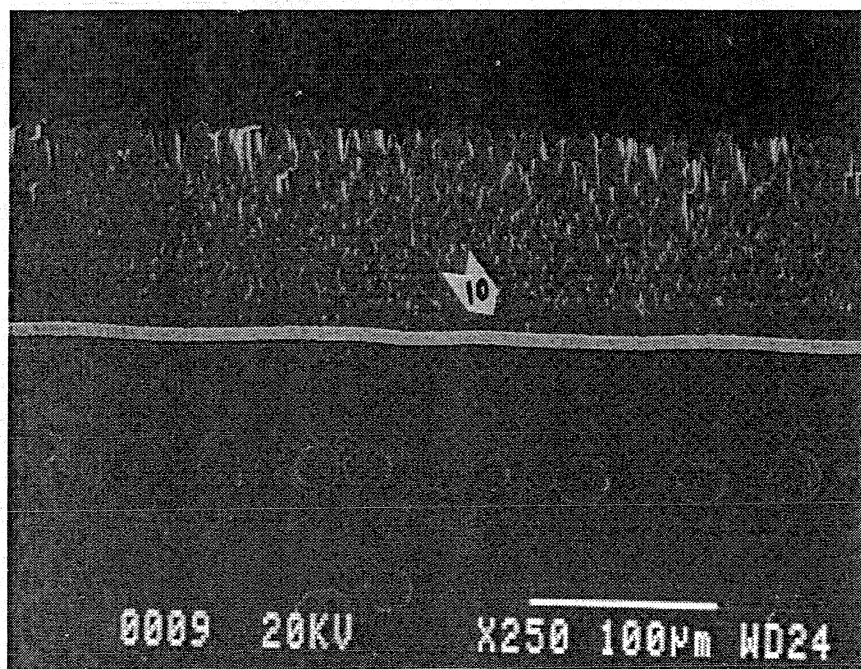
Table 2. Test Cycles and Results of Platinum and Platinum Alloy Bars.

| Test Specimen | Cycles to 1200F | Cycles to 1600F | Results to Date |
|---------------|-----------------|-----------------|-------------------------------------|
| Bar 1, TC 1 | 44 | n/a | Platinum leg delaminated |
| Bar 1, TC 2 | 74 | 441 | Platinum-10%Rhodium leg delaminated |
| Bar 2, TC 1 | 20 | 11 | Platinum leg delaminated |
| Bar 2, TC 2 | 20 | 135 | Platinum-10%Rhodium leg delaminated |
| Bar 3, TC 1 | 0 | 290 | Platinum-10%Rhodium leg delaminated |
| Bar 3, TC 2 | 0 | 369 | Platinum-10%Rhodium leg delaminated |

In addition, Honeywell Engines & Systems (Honeywell) reviewed the correlation between the gas temperature, the recorded thin-film temperature, and the standard 0.040-inch metal thermocouple reference for the thermocouples without overcoat. The measured difference was within expected errors due to the high-speed flow and large radial temperature gradient.

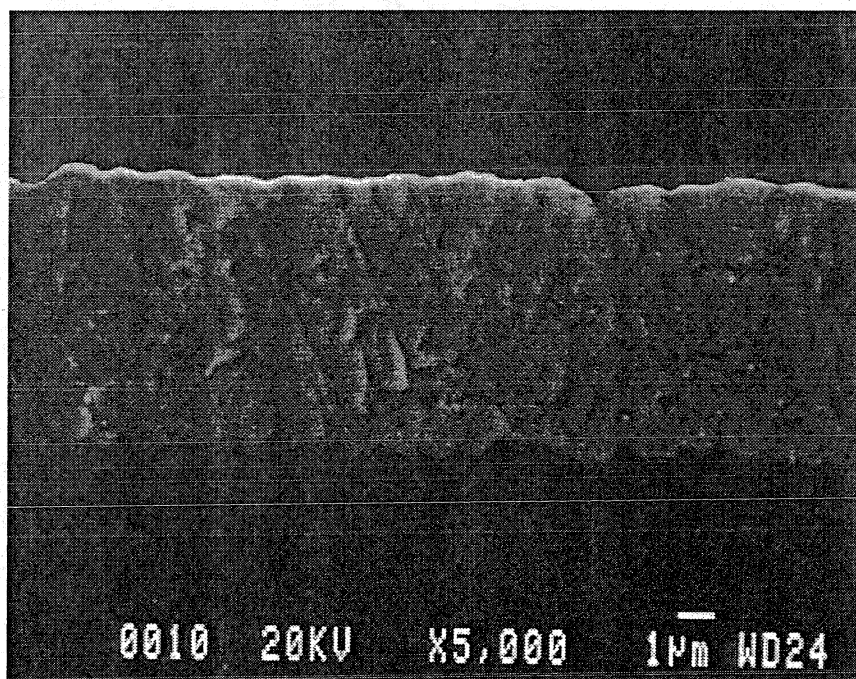
Testing was also conducted to validate the selection of overcoating. Scanning electron micrographs (SEM photos) were taken of bar specimens with sputtered chemical vapor deposition (CVD) overcoating. The photos were taken both before and after 500 thermal cycles to 1600F in the burner rig. The photos enable evaluation of the precious metal thin-film thermocouple integrity as well as the condition of the YSZ protective overcoating. In Figures 3 (before test) and 4 (after test), note the bar cross section and the YSZ overcoat. After testing it was noted that there was a fracture which initiated in the sputtered YSZ after 500 cycles. This testing indicates that the overcoating is not adversely affected by a fracture in the YSZ.

Bar specimens with thermal alumina only were compared to those with thermal alumina plus an additional two to three μM of chemical vapor deposited (CVD) alumina. This CVD process is done after the thermal oxidation forms the initial 15,000Å alpha aluminum oxide layer. The bars were cross-sectioned and SEM photos (Figures 5 and 6) taken which reveal random surface defects in the thermal alumina compared to a uniform surface when the CVD alumina is applied. Because of this it was decided to add the CVD alumina process to the baseline configuration.



G8404-3

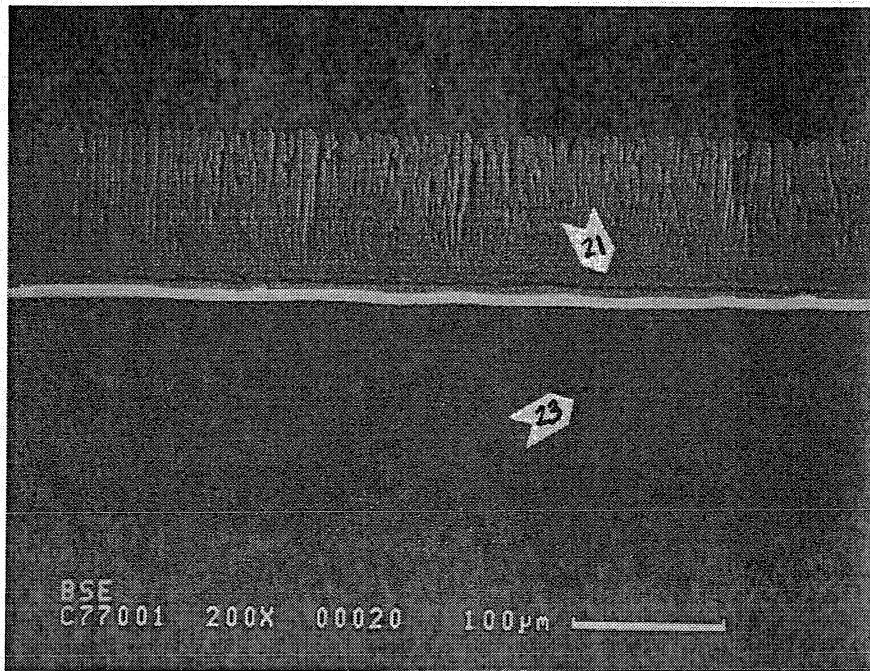
A. 250X Magnification



G8404-4

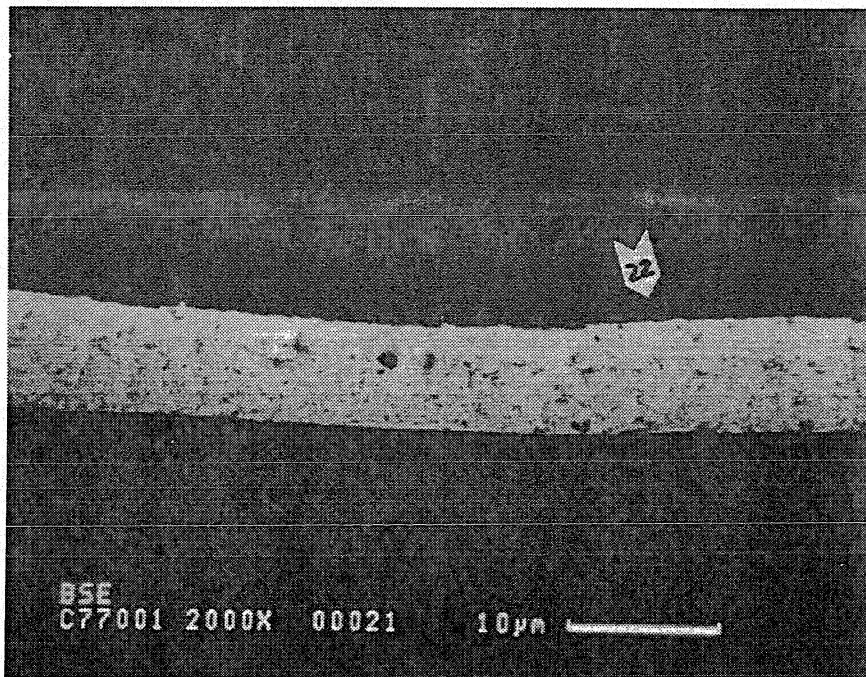
B. 5,000X Magnification

Figure 3. Type S Thermocouple (Pt leg) on Thermally-Grown Alpha-Alumina with YSZ Overcoating, Before Cyclical Testing.



G8404-1

A. 200X Magnification

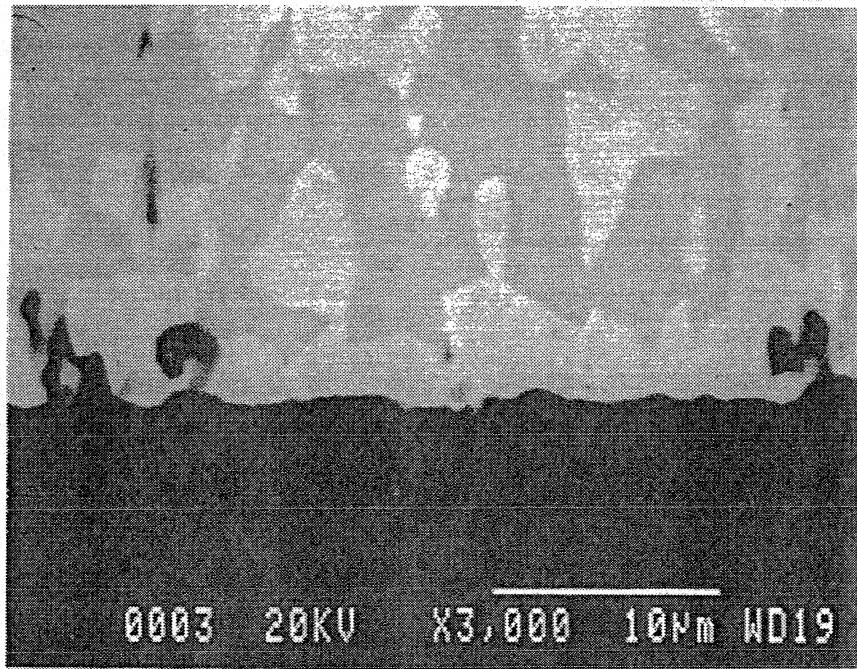


G8404-2

B. 2,000X Magnification

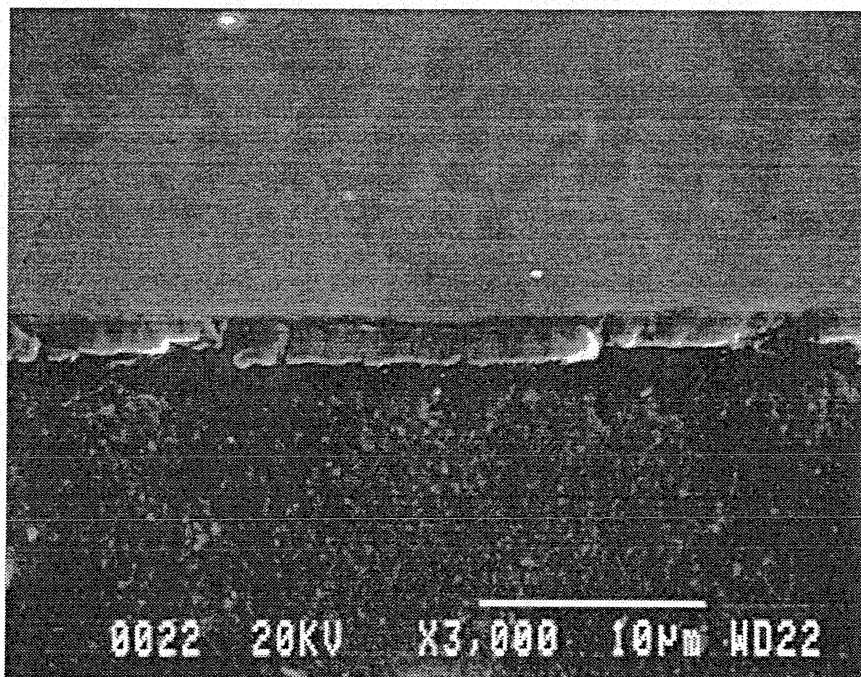
Figure 4. Type S Thermocouple on Thermally-Grown Alpha-Alumina with YSZ Overcoating After 500 Cycles to Mach 1 and 1600F.

Note the Fracture on the YSZ Overcoat After Testing.



G8404-5

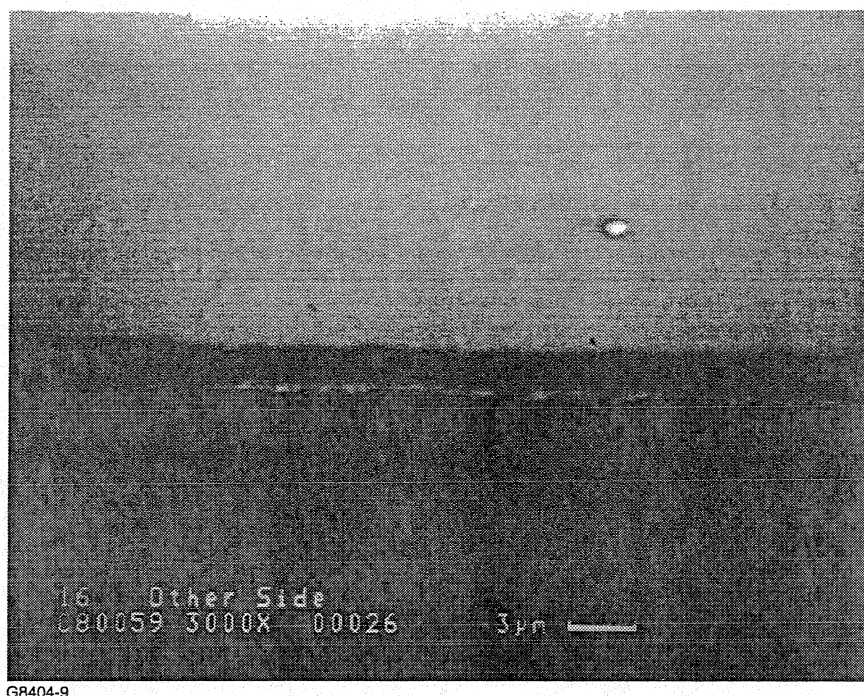
A. Approximately 12,500 Å Thick



G8404-6

B. Approximately 15,000 Å Thick

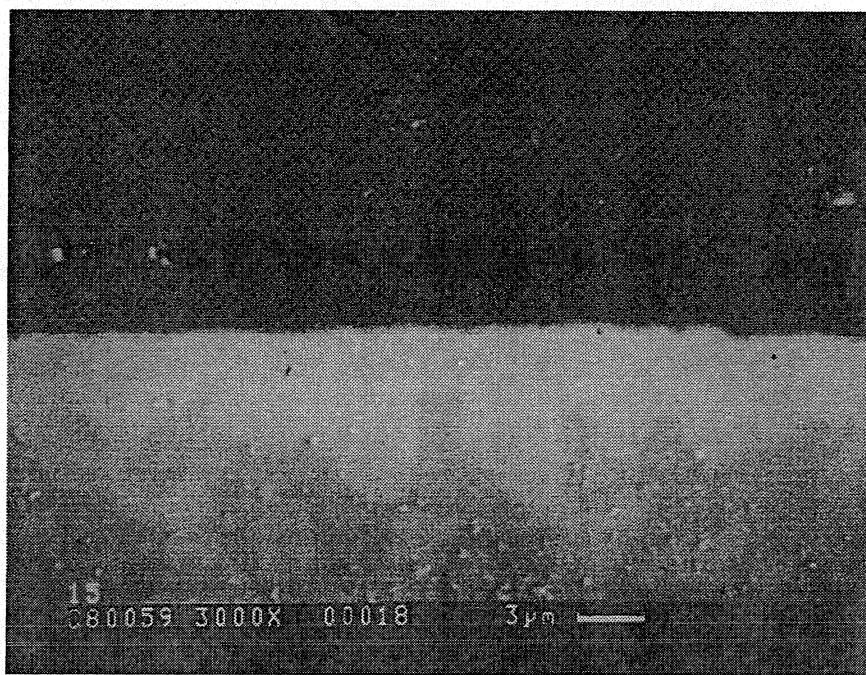
Figure 5. Thermally-Grown Alpha-Alumina Dielectric. Note Defects.



G8404-9

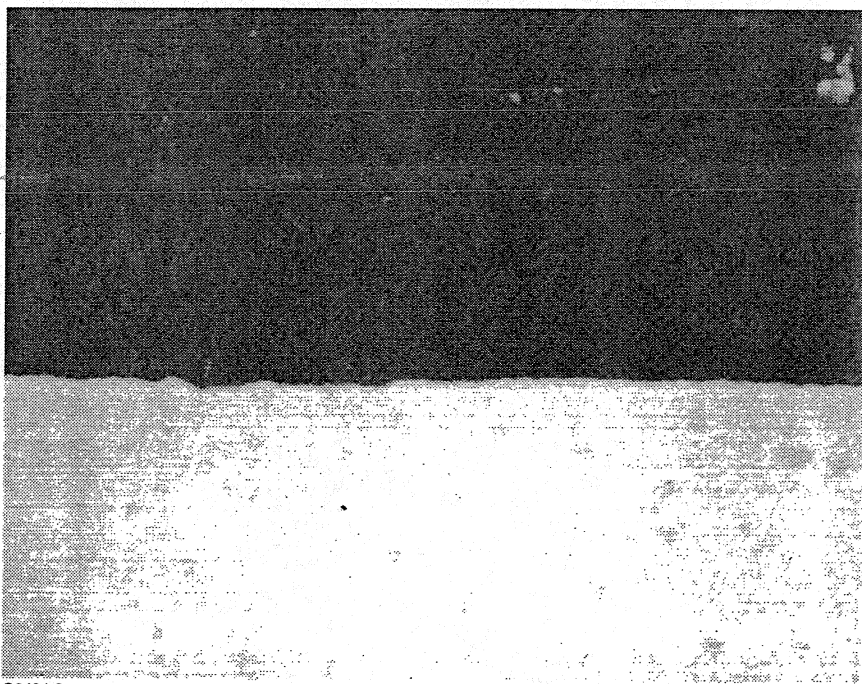
**Figure 6. Thermally-Grown Alpha-Alumina Dielectric, Approximately 17,500Å.
Note No Defects.**

The CVD process increases the dielectric strength by increasing the cross section of the alpha-alumina layer. Dr. Alan Constant at Iowa State University (ISU) has been developing the CVD deposition process for the alpha alumina in a 1-inch diameter reactor. Two samples received from ISU were sectioned and SEM photos (see Figure 6, photos of CVD alumina) taken to examine the thickness and density of the cross section. A total of 30,000Å of alumina was noted. This increased the dielectric strength from Kilohms to Megohms. A small layer of platinum was deposited on the ISU specimens to verify film adherence and the electrical isolation. The small bars were also thermally cycled to 1100C to verify film integrity.



G8404-7

A. 27,500Å Thick



G8404-8

B. 30,000Å Thick

Figure 7. Two Samples of CVD-Enhanced Alpha-Alumina Dielectrics, Processed at ISU.

The baseline configuration for the thin-film sensor processing is shown in Figure 8.

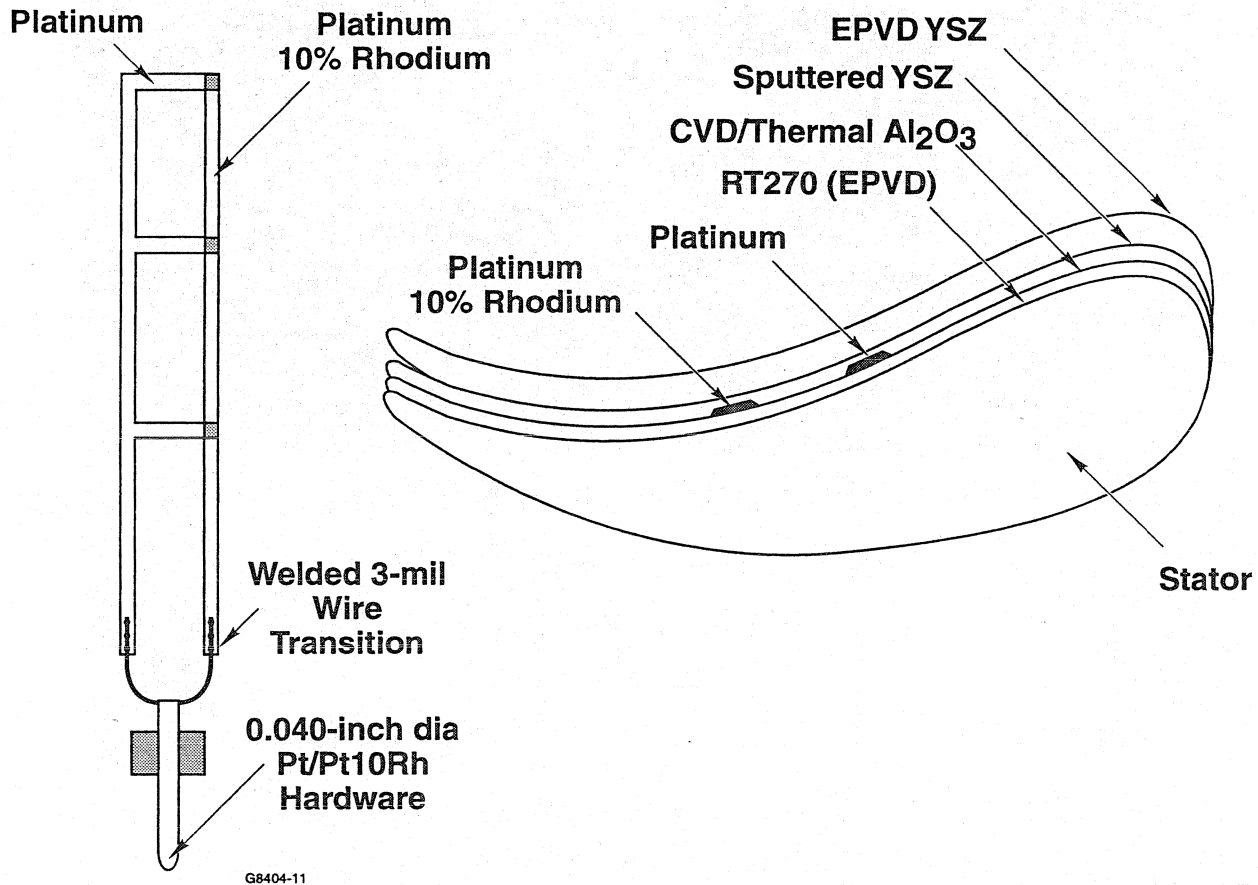
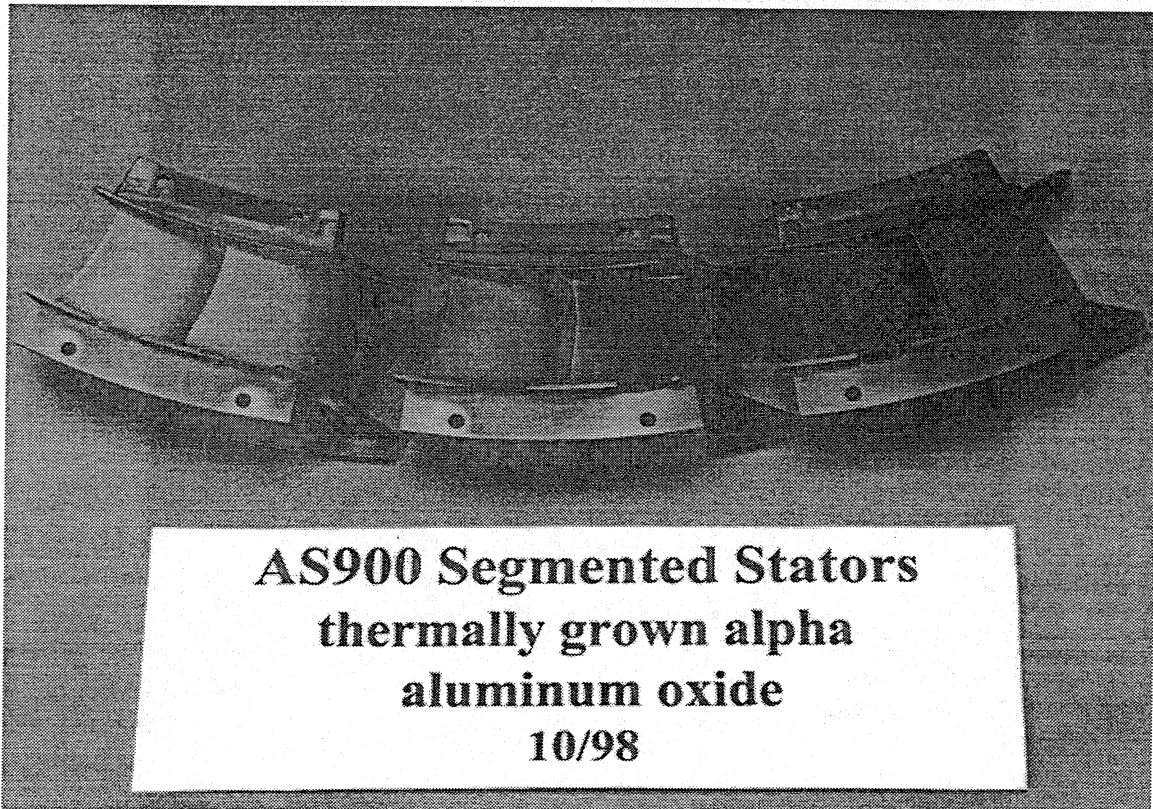


Figure 8. Baseline Thin-Film Sensor Configuration.

A turbine stator from the AS900 Technology Validation Team (TVT) development program was chosen to demonstrate this technology. (The AS900 is the new Honeywell business/regional propulsion-engine product line.) The AS 900 turbine stator was segmented into 19 pieces in order to facilitate processing of the thin-film sensors. The chemical vapor deposition (CVD) processing of the stator segments (see Figure 2) was performed at Iowa State University (ISU). The CVD reactor and holding fixture are shown in Figures 9, 10 and 11.

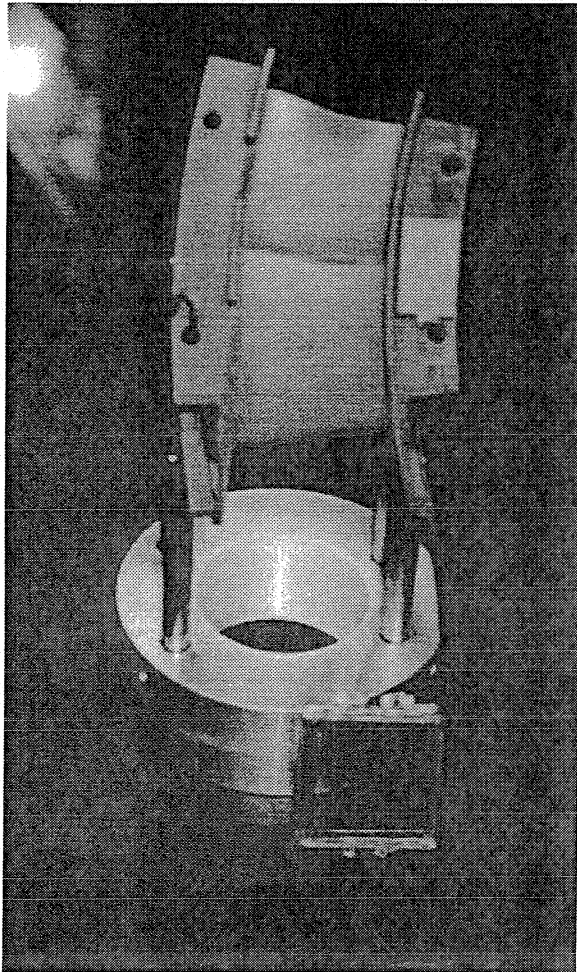


**AS900 Segmented Stators
thermally grown alpha
aluminum oxide
10/98**

G8880-1

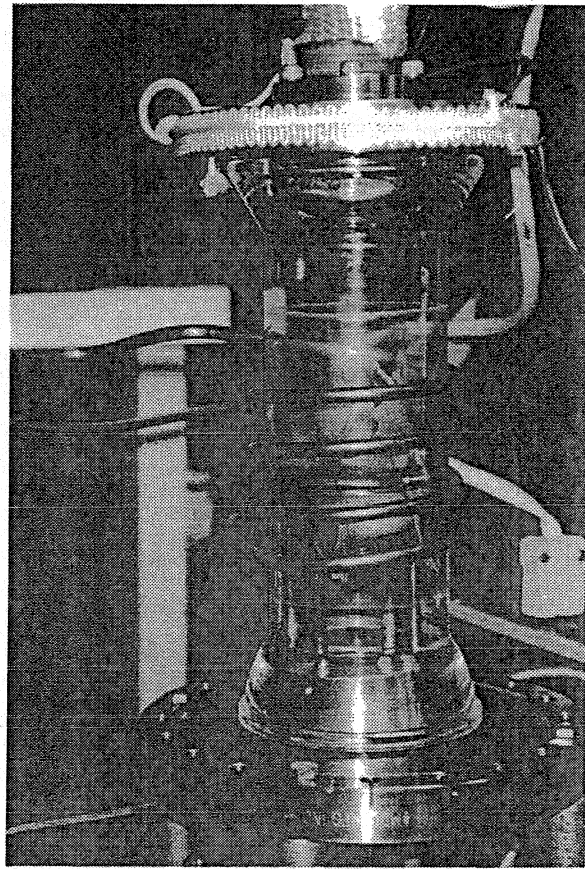
P141652-3

**Figure 9. AS900 Segment Stators with Thermally-Grown
Alpha-Aluminum Oxide Coating.**



G8880-2

Figure 10. Stator Segment in Reactor Holding Fixture.



G8880-3

Figure 11. Chemical Vapor Deposition Reactor at 1100C.

Spalling of the applied CVD aluminum oxide was observed where it delaminated from the thermally grown oxide on eight of the stator segments. This was attributed to an excessively high aluminum oxide growth rate in the CVD reactor at ISU. The high growth rate is caused by lack of control of the aluminum isopropoxide precursor and heated flow distribution in the cold wall CVD reactor. A softer columnar alumina is produced which created problems in the sensor photofabrication (with the resist) and delamination when the metal is sputtered. Changes in processing at ISU during the application improved this but did not eliminate the problem. Deposition of 30,000-40,000Å of CVD alumina was planned, but up to 150,000Å was deposited during processing. The growth rate increased as the aluminum isopropoxide precursor heated, creating an increase in the mass transfer rate to the gas phase. These changes were accommodated by reducing the growth cycle time in the reactor from 1.5 hours to 1.0 hours,

clearing out the bypass valve before deposition started, and installing a showerhead in the gas flow inlet to improve the distribution.

The first platinum sputtered on the CVD alumina at Honeywell delaminated where the CVD alumina debonded from the TGO alumina. This necessitated removal of as much of the “soft” CVD as possible in order to eliminate the metal delamination problem. As a result, the alumina quality on the 19 stator segments was reviewed and the process was modified. The CVD coated stators were tumbled in a walnut hull medium to remove the buildup and then baked at 700C. In addition the processing steps were changed to eliminate contamination from the photoresist under the metal film tracks. Tape is now used to define the sensor legs and the sensor metal film thickness was reduced to lower the residual stresses. An intermediate 700C “heat treat” of the films overnight between the sequential sputtering runs was introduced. The fabrication is now a four step metal deposition process. Sputtering of the platinum leg is followed by a second masking and sputtering of the weld pad. This is followed by the same two steps for the platinum-10% rhodium.

Six spare segments that were processed from the extra hardware set were used in the assembly of the ring to replace some of the stators with the “compromised” chemical vapor deposited (CVD) alumina, where the platinum and/or platinum-10% rhodium demonstrated adherence problems. The final set of stator segments for test consisted of ten segments with thermally grown oxide (TGO) only and nine with TGO and CVD alumina. Five of the stator segments with delaminated CVD oxide continued successfully through the processing sequence, but the long-term effects of the delamination were unknown. Table 1 provides the insulation resistance and processing history on an individual stator basis.

Based on the bench test and burner rig testing conducted earlier in the program, there was an expectation of success with the thin-film, type S thermocouples on the ACPFC stators in the Combustor Rig Test. However, results indicated sensor losses from the outset of the pattern factor testing. At the conclusion of the testing, it was noted that only eleven of the thin-film temperature sensors were providing in-range signals. On visual examination of the sensor installations at the conclusion of the test, the following items were noted. In several cases there was delamination of the metal platinum and platinum-rhodium thin-film legs, as well as cracking in the films. Splice locations also appeared to be compromised, with erosion and lifting of the WC16 ceramic cement, 3 mil to MGO conductors splices open, as well as damage to the 0.020-inch MGO.

The thin-film sensor failure analysis, from Report 21-9197(20), is provided in Appendix I.

Table 3. Stator Insulation Resistance and Processing History.

| Film Thermocouple Processing Status - 04/01/99 | | | | | | | | | | | | | | |
|--|---------------------------------|----------|-----------|----------|--------|---------------|-------------------|-----|--------------------------|-----------|-----|-------------|--------------|----|
| Stator ID | Polish, RT270, Peen, Repolish | TGO | CVD Oxide | Platinum | Pt10Rh | Rground | Buildup weld pads | YSZ | Chromalloy processing NA | 3mil wire | MGO | Rgnd: final | Rloop: final | MN |
| A1 | y - processed 1998 @ Chromalloy | Y-Refrac | delam | Y | Y | >.2Kohm short | Y | Y | | Y | Y | >20M | 53 | 1 |
| A2 | Y | Y | delam | Y | Y | >1Gohm | Y | Y | | Y | Y | >20M | 51 | 2 |
| B1 | Y | Y | N | Y | Y | >1Gohm | Y | Y | | Y | Y | >20M | 49 | 3 |
| B2 | Y | Y | N | Y | Y | >1Gohm | Y | Y | | Y | Y | >20M | 52 | 4 |
| C1 | Y | Y | delam | delam | Y | 100ohm short | Y | Y | | | | | | |
| C2 | Y | Y | delam | delam | Y | >14Kohm | Y | Y | | | | | | |
| D1 | Stator damaged by Chem Lab NG | | | NG | | | | | | | | | | |
| D2 | | | | NG | | | | | | | | | | |
| E1 | Y | Y | Y | Y | Y | >1Gohm | Y | Y | | Y | Y | >20M | 48 | 9 |
| E2 | Y | Y | Y | Y | Y | >1Gohm | Y | Y | | Y | Y | >20M | 59 | 10 |
| F1 | Y | Y | delam | NG | | | | | | | | | | |
| F2 | Y | Y | delam | NG | | | | | | | | | | |
| G1 | Y | Y | delam | Y | Y | 100ohms short | Y | Y | | Y | Y | .1K | 51 | 13 |
| G2 | Y | Y | delam | Y | Y | >1Gohm | Y | Y | | Y | Y | >20M | 50 | 14 |
| H1 | Y | Y | N | Y | Y | >12Mohm | Y | Y | | Y | Y | >20M | 50 | 15 |
| H2 | Y | Y | N | Y | Y | >30Mohm | Y | Y | | Y | Y | >20M | 52 | 16 |
| J1 | Y | Y | N | Y | Y | >20Mohm | Y | Y | | Y | Y | >20M | 51 | 17 |
| J2 | Y | Y | N | Y | Y | >20Mohm | Y | Y | | Y | Y | .1K | 56 | 18 |
| K1 | Y | Y | Y | Y | Y | >1Gohm | Y | Y | | Y | Y | >20M | 51 | 19 |
| K2 | Y | Y | Y | Y | Y | >1Gohm | Y | Y | | Y | Y | >20M | 50 | 20 |
| L1 | Y | Y | N | Y | Y | >300Kohm | Y | Y | | Y | Y | >20M | 32 | 21 |
| L2 | Y | Y | N | Y | Y | >20Mohm | Y | Y | | Y | Y | >20M | 27 | 22 |
| M1 | Y | Y | delam | Y | Y | >20Mohm | Y | Y | | Y | Y | >20M | 50 | 23 |
| M2 | Y | Y | delam | Y | Y | >20Mohm | Y | Y | | Y | Y | >20M | 49 | 24 |
| N1 | Y | Y | Y | Y | Y | >1Gohm | Y | Y | | Y | Y | >20M | 51 | 25 |
| N2 | Y | Y | Y | Y | Y | >800 Mohm | Y | Y | | Y | Y | >20M | 50 | 26 |
| O1 | Y | Y | delam | Y | Y | >200Kohm | Y | Y | | Y | Y | >20M | 65 | 27 |
| O2 | Y | Y | delam | Y | Y | >1Gohm | Y | Y | | Y | Y | >20M | 58 | 28 |
| P1 | Y | Y | delam | Y | Y | >1Gohm | Y | Y | | Y | Y | >20M | 50 | 29 |
| P2 | Y | Y | delam | Y | Y | >200Kohm | Y | Y | | Y | Y | >20M | 54 | 30 |
| Q1 | Y | Y | N | Y | delam | >25Mohm | Y | Y | | | | | | |
| Q2 | Y | Y | N | Y | delam | >1Gohm | Y | Y | | | | | | |
| R1 | Y | Y | Y | Y | Y | >1Gohm | Y | Y | | Y | Y | >20M | 47 | 33 |
| R2 | Y | Y | Y | Y | Y | >1Gohm | Y | Y | | Y | Y | >20M | 50 | 34 |
| S1 | Y | Y | delam | NG | | | | | | | | | | |
| S2 | Y | Y | delam | NG | | | | | | | | | | |
| T1 | Y | Y | delam | Y | NG | | | | | | | | | |
| T2 | Y | Y | delam | Y | NG | | | | | | | | | |
| U1 | Y - processed 1999 @ Chromalloy | YRefrac | N | Y | Y | >1Gohm | Y | Y | | Y | Y | >20M | 51 | 5 |
| U2 | Y | Y | N | Y | Y | >700Mohm | Y | Y | | Y | Y | >20M | 50 | 6 |
| V1 | Y | Y | N | Y | Y | >1Gohm | Y | Y | | Y | Y | >20M | 26 | 7 |
| V2 | Y | Y | N | Y | Y | >1Gohm | Y | Y | | Y | Y | >20M | 44 | 8 |
| W1 | Y | Y | N | Y | Y | >500Mohm | Y | Y | | Y | Y | .1K | 54 | 11 |
| W2 | Y | Y | N | Y | Y | >500Mohm | Y | Y | | Y | Y | >20M | 49 | 12 |
| X1 | Y | Y116 | N | Y | Y | >1Gohm | Y | Y | | Y | Y | >20M | 53 | 31 |
| X2 | Y | Y116 | N | Y | Y | >1Gohm | Y | Y | | Y | Y | >20M | 64 | 32 |
| Y1 | Y | Y | N | Y | Y | >1Gohm | Y | Y | | Y | Y | .1K | 49 | 35 |
| Y2 | Y | Y | N | Y | Y | >1Gohm | Y | Y | | Y | Y | .1K | 50 | 36 |
| Z1 | Y | Y | N | Y | Y | >1Gohm | Y | Y | | Y | Y | >20M | 50 | 37 |
| Z2 | Y | Y | N | Y | Y | >1Gohm | Y | Y | | Y | Y | >20M | 49 | 38 |
| NOTES | | | | | | | | | | | | | | |
| Summary | | | | | | | | | | | | | | |
| TGO - thermal grown oxide | | | | | | | | | | | | | | |
| CVD - chemical vapor deposition | | | | | | | | | | | | | | |
| Designation notes two separate airfoils on one stator eg: A1, A2 | | | | | | | | | | | | | | |
| 19 compl with wiring and ready for assembly | | | | | | | | | | | | | | |
| ASSEMBLY SEQUENCE: A,B,U,V,E,W,G,H,J,K,L,M,N,O,P,X,R,Y,Z | | | | | | | | | | | | | | |
| TGO Only [10] | | | | | | | | | | | | | | |
| TGO and good CVD [4] | | | | | | | | | | | | | | |
| Delam CVD [5] | | | | | | | | | | | | | | |

3. FUEL-FLOW MODULATORS

The fuel-flow modulator requirements were documented in procurement specification 21-9246. Nine fuel-flow modulator (FFM) proposals were submitted by eight suppliers in response to the Request for Proposal. These proposals were evaluated by a team consisting of three controls engineers and one combustion engineer. A summary of the principle of operation and the strengths and weaknesses of the concepts presented in the proposals follow, ranked from lowest (9) to highest (1 - best):

9. **Hydraulic Servo Controls** - This system consisted of 20 conventional torque motors on a common supply manifold. There was little program risk involved; however, little innovation or technology advancement was noted. System reliability, overall volume, and weight were all poor.
8. **Lucas Aerospace** - Lucas teamed with a small business, J.R. Buscher, to propose a system consisting of 20 torque motor valves that use a unique balanced poppet closure. Lack of production experience as well as very high production price and weight were noted.
7. **AlliedSignal Aerospace Equipment Systems** - This system consisted of 20 conventional torque motors on a common supply manifold. Lack of innovation, excessive envelope, and low reliability were noted. Low power consumption was a good point.
6. **Woodward Governor Company** - A centralized system using their H-MUX (hydraulic multiplexer) was proposed. A fast-acting, proportional solenoid communicates through a rotating sleeve valve to each of 20 hydraulic metering valves in the atomizer lines. The sleeve is rotated by an electric motor. System weight was high and it was noted that, although innovation was good, no knowledge of the metering valves' positions (and therefore individual nozzle flows) was available for nozzle or turbine vane plugging diagnostics. Both this and the other centralized system concept contain some failure modes where the total system can become inoperative.
5. **Moog** - Two concepts were proposed and judged individually. The first was a rotary impeller that drove a small generator in each atomizer line. The generator load, and therefore the flow resistance, was controlled electronically. Innovation was very good, as was reliability. However, insufficient pressure drop could be developed to meet the flow turndown ratio required. When the system was scaled to meet the turndown ratio, the system weight and power became excessive.
4. **Moog** - The second Moog concept involved the use of 20 proportional solenoids. Innovation was not particularly evident and the large hysteresis and high continuous current draw were noted as shortcomings. Low volume and moderate costs were deemed pluses. Weight was considered high.

3. **Chandler Evans** - A centralized distributor, using an electric-motor-driven, rotary, carbon-face-seal valve, was proposed in combination with 20 modulator valves (from Delawan). Two proportional solenoids either provide hydraulic signals to the modulators or vent them. This action moves the spring-loaded modulators to a new position and changes the flow to the nozzles. Cost, weight, and volume were all very favorable, as was the predicted reliability. A drawback to the system, as with the Woodward concept, is that no knowledge of the metering valve's position (and therefore individual nozzle flows) was available for nozzle or turbine vane plugging diagnostics.
2. **Defense Research Technology (DRT)** - A small business, with personnel experience at Harry Diamond Laboratories, teamed with AlliedSignal Aerospace Equipment Systems to propose a very innovative system. It consists of a fluidic vortex resistor, the vorticity of which was mechanically altered by insertion of a small tab into the fluid interaction region. In the research program, the tab would be moved by means of the NASA Langley "Thunder" piezo-electric actuator. In the production concept, the vortex valve and tab would be machined from silicon by the MEMS process. System cost, weight, volume, and reliability were all rated excellent. However, the vortex valve does not have sufficient turndown ratio when placed in series with another restriction (the atomizers). DRT proposed that the vortex valve be built into the atomizer as the primary restriction, and in-fact, the spray producing feature.

Honeywell felt that the program risk associated with developing an atomizer, actuator, and a modulator function was too high for the primary approach. However, the concept has such merit that Honeywell would encourage NASA to seek funding to develop this concept as a parallel path.

1. **Sturman Industries** - The design selected by the Honeywell evaluation team consists of 20 pulse-width-modulation valves. Sturman Industries is a Woodland, Colorado-based, woman-owned, small business that has developed a unique, magnetically latched, solenoid valve for use on small automotive, diesel engines. The valve consists of a high-speed, pressure-balanced spool and hermetically sealed magnetic circuit. Residual magnetism provides a small holding or latching force that requires a brief, high current to switch, but very low current to hold in position. The net result is overall low power consumption. Sturman will provide the driver circuits as well. In addition to scoring well in cost, size, weight and power, the digital valve concept permits almost infinite turn-down ratio. This will facilitate operation during the Phoenix scaled-flow combustion conditions, as well as the full-scale tests at NASA GRC. The high turndown in each flow line also provides a ready capability of staging the atomizers to enhance lightoff and resist blowout on rapid decels.

A preliminary design review of the fuel-flow modulator was conducted on December 17, 1996. Sturman representatives Pete Peterson and Jim Peña described the history of their company and the development of the residual-magnetism-latching feature of the proposed valve.

They emphasized that the low power consumption comes from the fact that only a very brief, high current is required to break the magnetic latching, thereby causing the valve to change states. Once having moved, no current is required to hold the valve in the new position. It was noted that this latching magnetic force would last for years under normal operating conditions.

Sturman presented a conceptual drawing of a proposed design for the NASA FFM as shown in Figure 12.

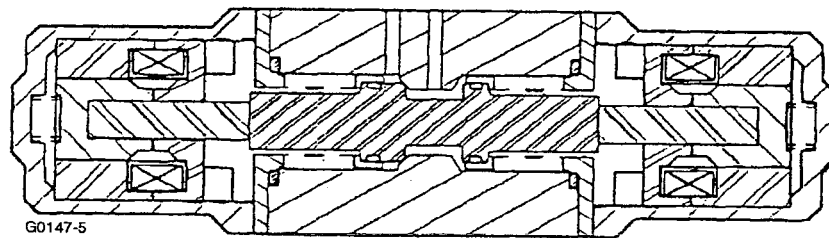


Figure 12. Dual-Coil FFM.

This is a dual, dry-coil device that uses an electroplating-formed bellows and an “O” ring to seal the working fluid from the magnetic parts. This configuration is often used when the fluid contains a significant number of iron particles that could agglomerate in the coil area. The valve shown is a Vespel poppet configuration that is often used when drip-free shutoff is required.

With the two coil configuration selected, three designs were considered. The first was a pressure balanced conical poppet valve that employed steel diaphragms. The valve would incorporate a semi-compliant seat to achieve positive sealing. The valve and diaphragm concepts are well understood by Sturman Industries and have been successfully applied to high reliability/high durability valves. Two diaphragms on the poppet valve would provide complete pressure balance and sealing; however, the diaphragms typically require a significant level of development to achieve infinite life and are costly to manufacture. Furthermore, the use of diaphragms introduced additional leakage paths, additional weight and complexity, all of which contributed to the decision to pass over this design.

The second design was based upon the use of a flat-lapped-disc-valving unit that is capable of high life and is simple to manufacture. For this valve, bellows were proposed to achieve the pressure balance. This valve had the benefits of the first option but would not require development effort for the bellows. Unfortunately, the problems of weight, complexity, and leakage paths and cost affect this design as they did the first.

The selected design was based upon some development work completed at Sturman Industries to determine the effects of subjecting the ends of a pressure-balanced spool to high pressure. If the pressure force can be limited, a simple spool valve has many advantages over the previously mentioned concepts with only one downside: leakage. Hydraulic pressure on the end of the spool causes a force imbalance when the spool is at the zero air gap position as the pressure affects the area of one end of the spool but not the other. To minimize the effects, the ends of the spool are profiled to limit contact area thereby limiting the hydraulic force component

to an acceptable level. These spools were tested to determine any detrimental effects of minimizing the contact area that absorbs the impact of the spool and were successfully operated to two billion cycles.

The leakage around the spool is diverted to the valve outlet, which will see a maximum pressure of 340 psi. The contact area on the ends of the spool is sized to limit the hydraulic force component to 1.5 pounds. The FFM employs a simple two-way-spool valve that is sized to provide an equivalent orifice diameter of 0.077 inch. Based upon this orifice, the estimated pressure drop at a flow rate of 100 pounds per hour will be 12 to 15 psi. The mass of the spool has been minimized to provide maximum performance for the response of the injector. Additional features have been added to minimize leakage through the valve.

Valve-to-valve flow tolerance is adjusted during assembly with a spacer shim that is used to account for tolerances in the manufacturing process. This method allows the unit to meet the ± 10 percent unit-to-unit allowable tolerance. Furthermore, this is the only adjustment required for proper operation of the valve; hence it is not "field adjustable."

A cross-section of the unit is shown in Figure 13.

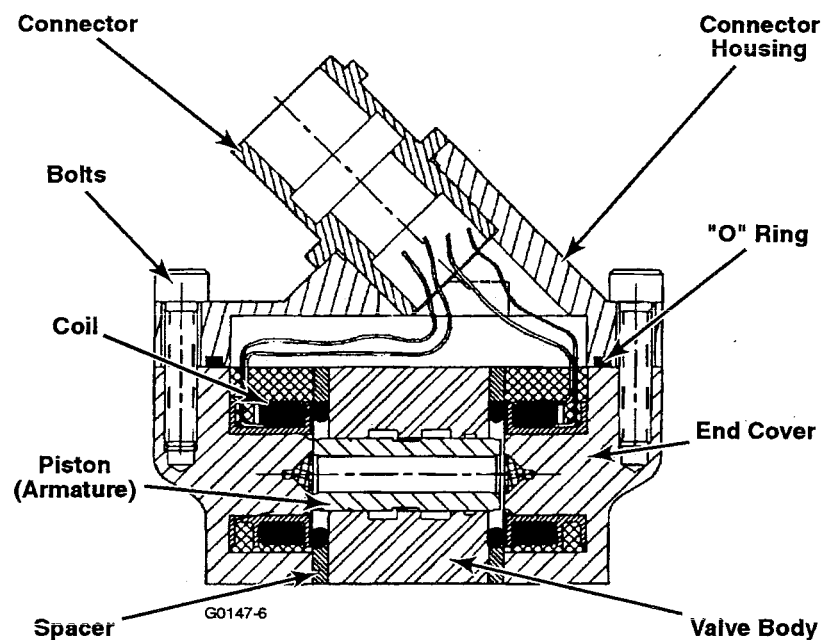


Figure 13. Cutaway of FFM.

Fuel leakage along the bobbin in the coils, which passed through the wires and connector, was experienced during testing of the original design of the FFM at Sturman. This was addressed by repotting the coils and applying a Loctite compound to the surface exposed to the fuel. Unfortunately, this was not successful in totally eliminating the leakage.

A redesign was then undertaken to place an O-ring groove on the coil bobbin and to rewind and pot the coils. This new design was then tested with both fuel and nitrogen, to pressures exceeding the ACPFC levels, and no leakage was observed. Figure 14 illustrates the addition of the O-ring groove. Figure 15 is a photo of the fuel-flow modulator.

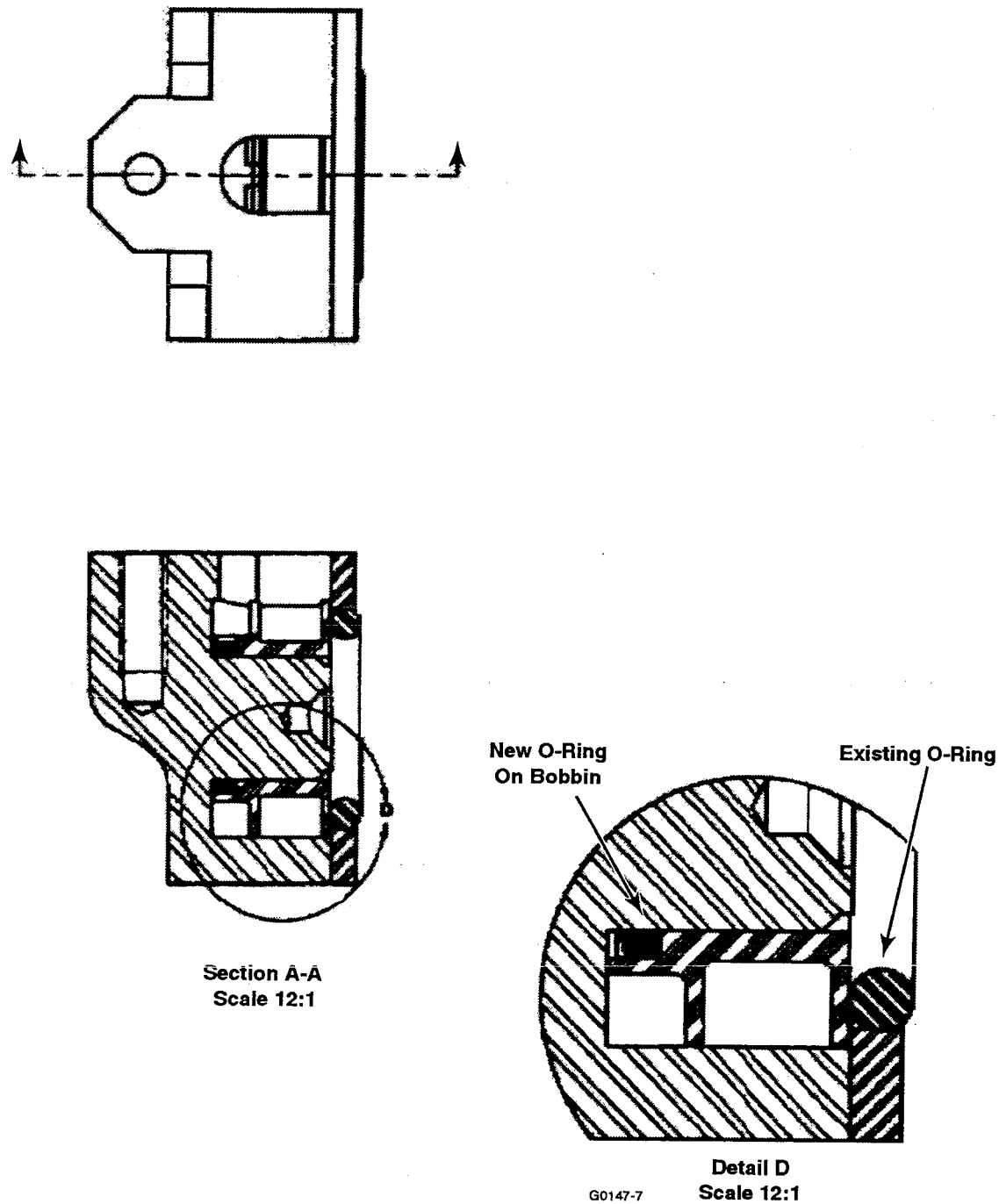
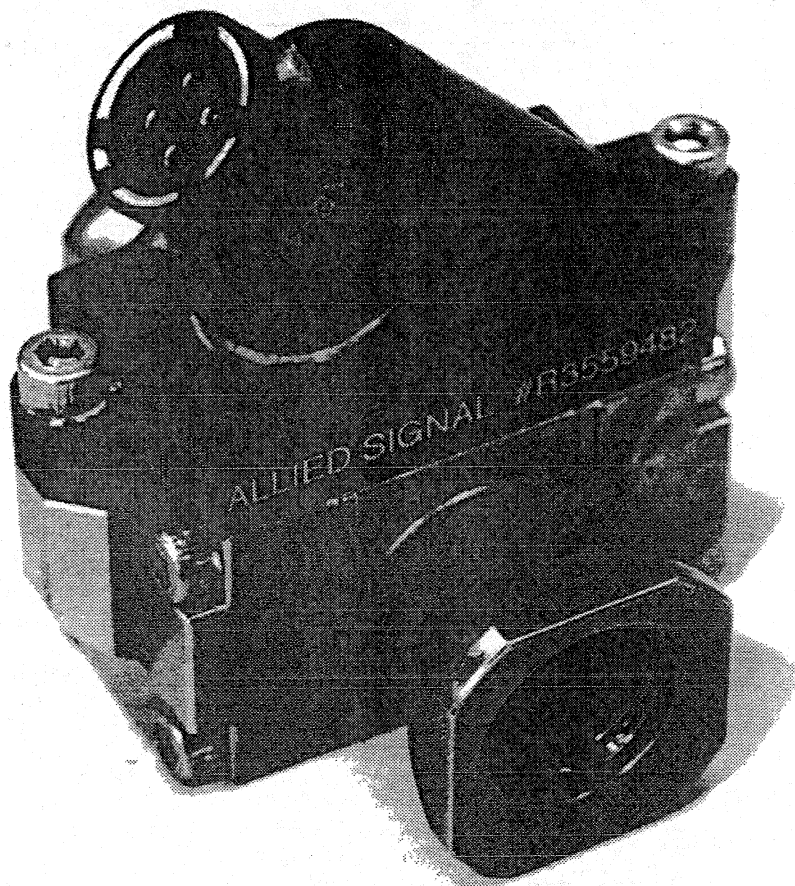


Figure 14. O-Ring Addition to Fuel-Flow Modulator.



G8538-1

141084-5

Figure 15. Photograph of Final Fuel-Flow Modulator.

The performance of the fuel-flow modulator can be seen in the oscilloscope traces shown in Figure 16. The logic or command signal is shown at the top. When the logic signal goes high, the valve is commanded to turn on. Below, the trace shows the current to coil one increases until a cusp is detected by the driver circuit, after which the coil is left energized for approximately 0.1 milliseconds to ensure a complete latch is achieved. When the logic goes low, coil two is turned on, again until the cusp is detected. The cursors are used to measure the maximum current. With the current probe set to 10 millivolts per amp, the measurement of 91.6 millivolts indicates 9.1 amps were required to open the valve.

Figure 17 shows the voltage signature on each coil for the same event. Here the back electromotive-force (EMF) voltage can be seen. This induced voltage signal is useful as a diagnostic tool.

The unit-to-unit variations in the modulator performance are minimal and can be seen in the plot in Figure 18, which overlays the performance of 20 valves.

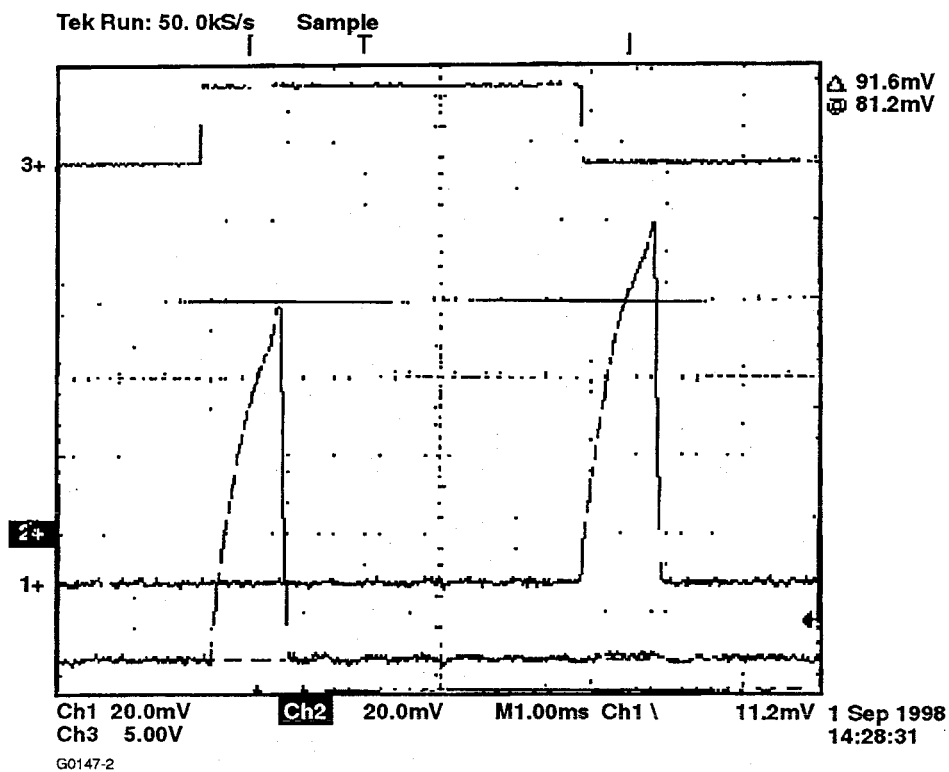


Figure 16. Oscilloscope Traces of FFM Performance.

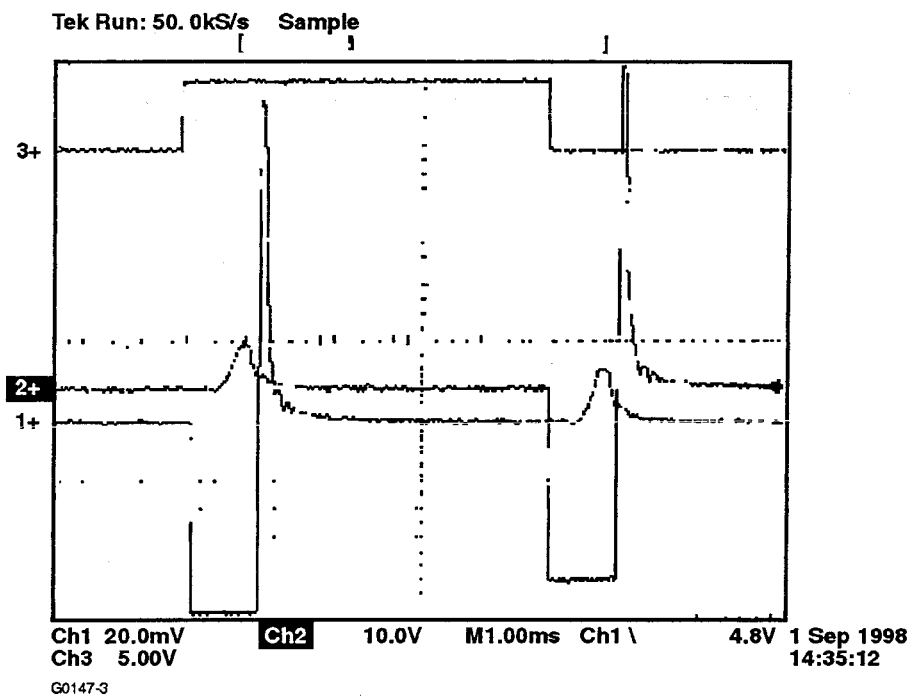


Figure 17. Back EMF Traces Used for Fault Detection.

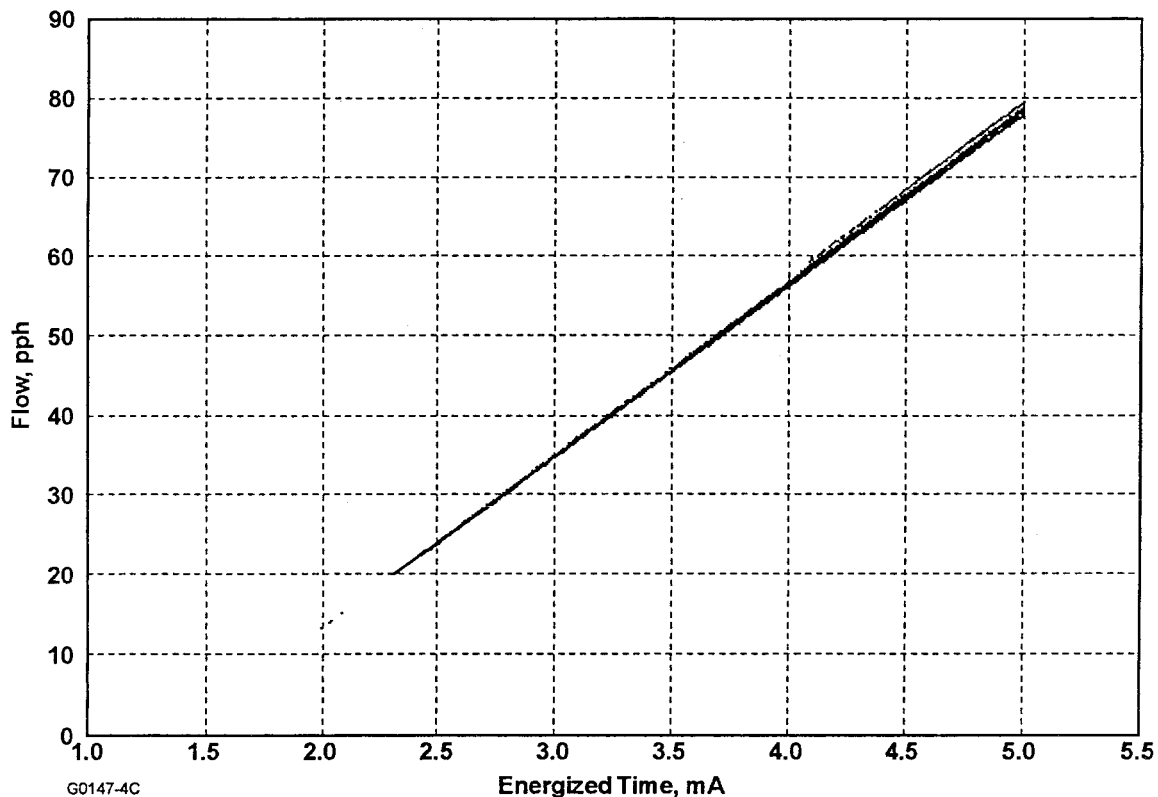


Figure 18. Linearity Plot of 20 Fuel-Flow Modulators.

The final report from Sturman Industries on the fuel-flow modulator design and performance is provided as Appendix II, and was previously an attachment to the sixteenth bimonthly progress report, Document No. 21-9197(16).

After the combustor rig test series, three fuel-flow modulators were returned (Serial Numbers 11, 23, 25) to Sturman. During testing the valves had stuck open or closed and one of the valves had been leaking fuel from the bottom of the coil housing, through what was originally the potting hole. Sturman determined that the coils had turn-to-turn short circuits. The effect of the short circuit was to reduce the number of turns within the coil and the resistance of the coil was reduced. The reduced resistance allowed the current to rise faster and to a higher current level. Total ampere-turns were enough that the valve actuated but inconsistently. The reason for the failure of the coils was not specifically determined, however it is suspected that the coils failed when the driver boards failed, as discussed in the fuel-flow modulator driver box section of this report.

The valves were cleaned in the ultrasonic system and microscope inspection of the spools showed some scratch marks of a very light nature on the ends of the cylindrical surface of the spools, but not of a level necessary to "stick" a spool. The spools received a very light polishing and afterwards the valves were reassembled with new coils. Testing of the valves showed the current traces and response all looked excellent per the original test specification and when

compared the master valve. The final test was to pressurize the valve with air to check for leaks. The test valve did not leak until about 250 psig after which some leakage was detected to 750 psig, when the seal completely let loose. Upon disassembly it was determined that the bobbin had actually deformed under pressure thereby allowing the o-ring additional area to extrude out of the groove. A fix was proposed to add a steel backup ring to the outside diameter of the bobbin (adjacent to the coil) to provide higher radial strength. The ring fit in the current assembly without any modification necessary and applied a light compressive loading on the bobbin. Follow-up testing showed that the ring allowed the fuel-flow modulators to operate to 750 psig with no leakage, thereby meeting the original RFP operational specification. At some point in the future, it is recommended that all valves be upgraded with the pressure ring, or an entirely new coil/bobbin design be fitted.

One concern about using a PWM fuel-delivery system was the unknown effect the pulsations would have on the combustion process. In order to alleviate this concern, a brief, proof-of-concept test was planned and conducted. Sturman provided a prototype injector and electronic driver, similar in concept to the ACPFC program except for the internal valve porting.

A test plan was developed and executed in which the unit was tested, first on the bench in a visualization spray chamber and then in a single-can combustor rig. Figure 19 shows the test setup for both.

The electronic circuit was driven by a square wave generator that could be adjusted to vary the percent-on versus percent-off time. Although the valve moves stop-to-stop in a very short time, the pressure rise time (and decay when closing) is proportional to the bulk modulus of the fluid and inversely proportional to the line volume downstream of the FFM. A large accumulator upstream of the FFM to provide a constant supply pressure was used during the test (not shown in Figure 20). This was done so that the performance could be compared with the model.

Two different downstream line volumes were used, and the data taken during the bench tests revealed that the performance was very close to the model predictions in both cases. This is shown in Figure 19 for the small (18 inches of 0.25-inch line) volume case.

As evident in Figure 20, the shape of the curves is very similar except for the high-frequency waves (667 Hz) riding on the experimental data. This phenomenon was assumed to be the fundamental frequency of a closed-at-one-end pipe. To test this theory, the fundamental was calculated by:

$$f = \frac{V}{\lambda} = \frac{V}{4L} = \frac{3800}{4(1.4)} = 678. \text{ Hz}$$

where:

λ = wave length, L = line length, and 3800 = speed of sound in diesel fuel, ft/sec.

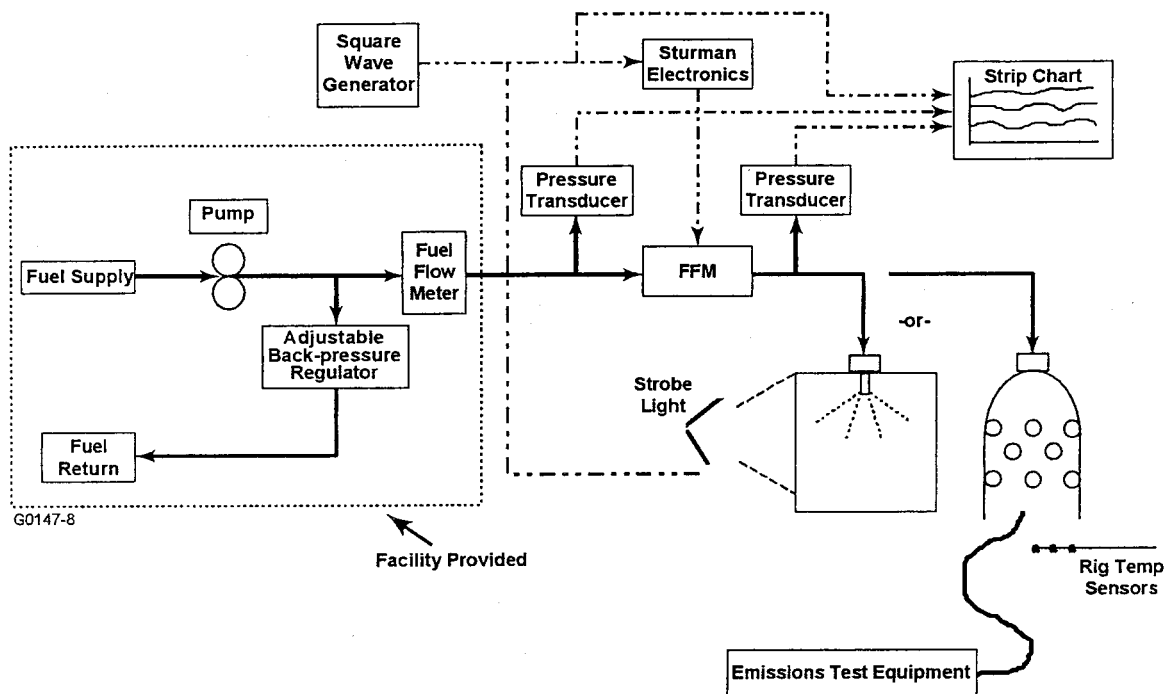


Figure 19. Bench and Combustor Test Setup for Prototype FFM.

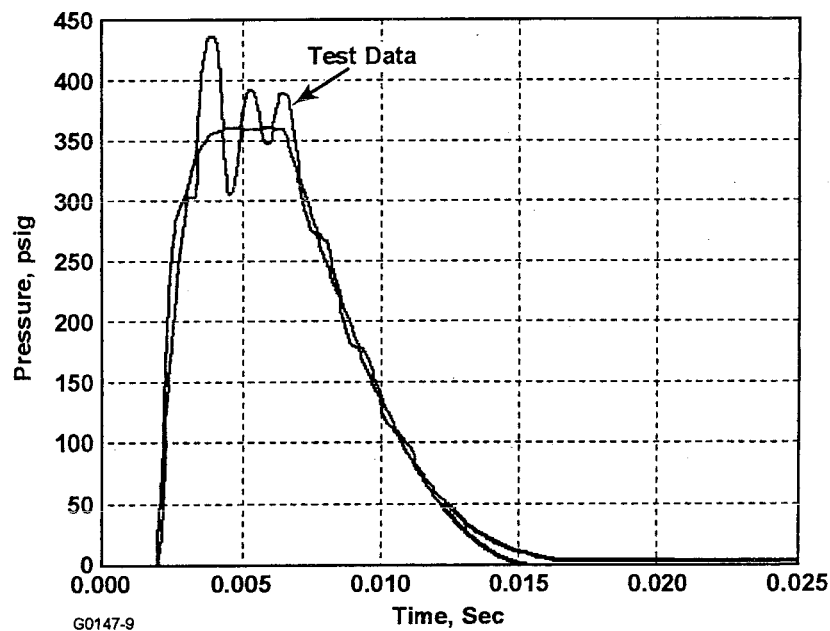


Figure 20. Comparison of Predicted with Actual Line Pressures.

The close correlation indicates that the acoustic assumption is correct. There is no adverse effect of these high-frequency waves. Spray pattern angles and visual quality seemed to be unaffected by the PWM fuel delivery.

The FFM and associated electronics were taken to the combustion facility and connected to a small, single-can burner being tested for use in an industrial application. The same fuel nozzle tested on the bench test was used in the combustor rig. Data was taken with no pulses (analog fuel delivery) and with PWM (digital fuel delivery). Exhaust emissions data was taken using gas chromatography for both fuel delivery systems. As shown in Figure 21, the effects of digital fuel delivery (PWM at 20 Hz) versus analog or continuous delivery on NO_x and HC are minimal and within the accuracy of the measurement equipment. As noted by the dashed lines, the values for NO_x and HC could be expected to change slightly over the temperature range tested.

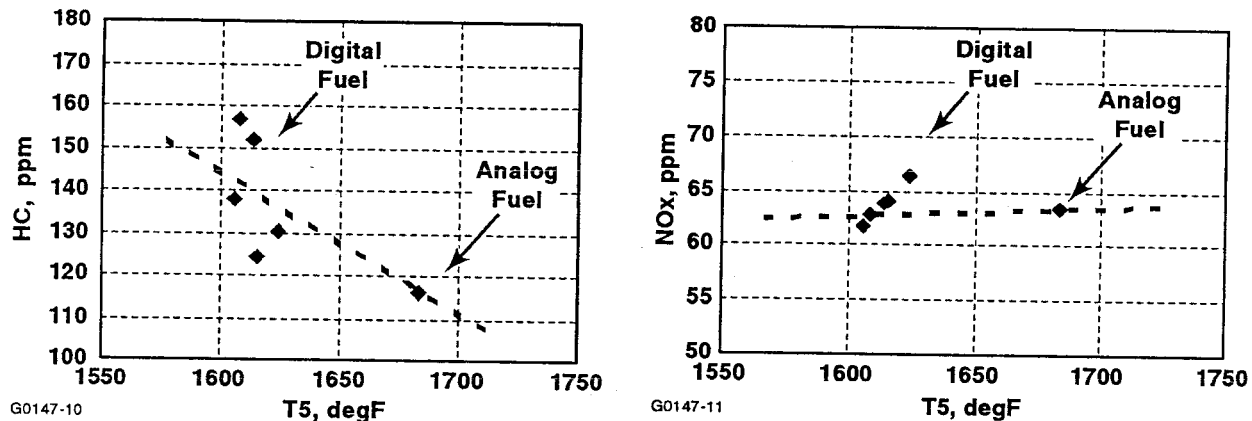


Figure 21. Effect of Digital Fuel Delivery on Emissions.

Surprisingly, the combustor continued to operate at very low flow rates and at low PWM frequencies. At 20 Hz and low delivery, the fuel flow was actually zero for up to 40 milliseconds, suggesting a kernel of flame persists in the primary zone that sustains combustion during the “off” periods. Very little effect on overall combustor blowout limits was observed with PWM, as shown in Figure 22.

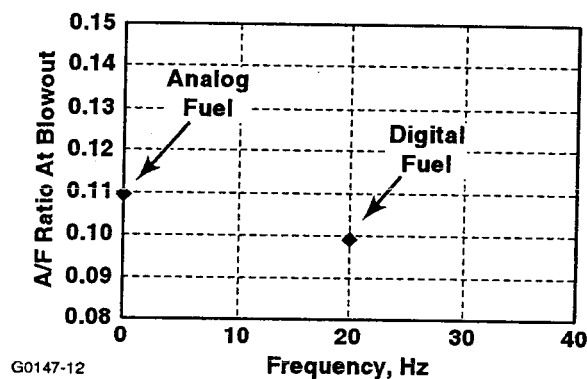


Figure 22. Air/Fuel Ratio at Blowout.

4. FUEL-FLOW MODULATOR DRIVER BOX

Sturman provided the driver box that consisted of a driver card for each of the fuel-flow modulators (19 plus one spare). An internal view of the box is shown in Figure 23. Each driver circuit uses a transistor connected in an H-bridge configuration to allow bidirectional current control. A built-in test circuit uses current sensing and back EMF voltage from the deenergized coil to infer the end of spool travel. Each driver circuit has a dedicated linear voltage regulator to regulate supply voltage.

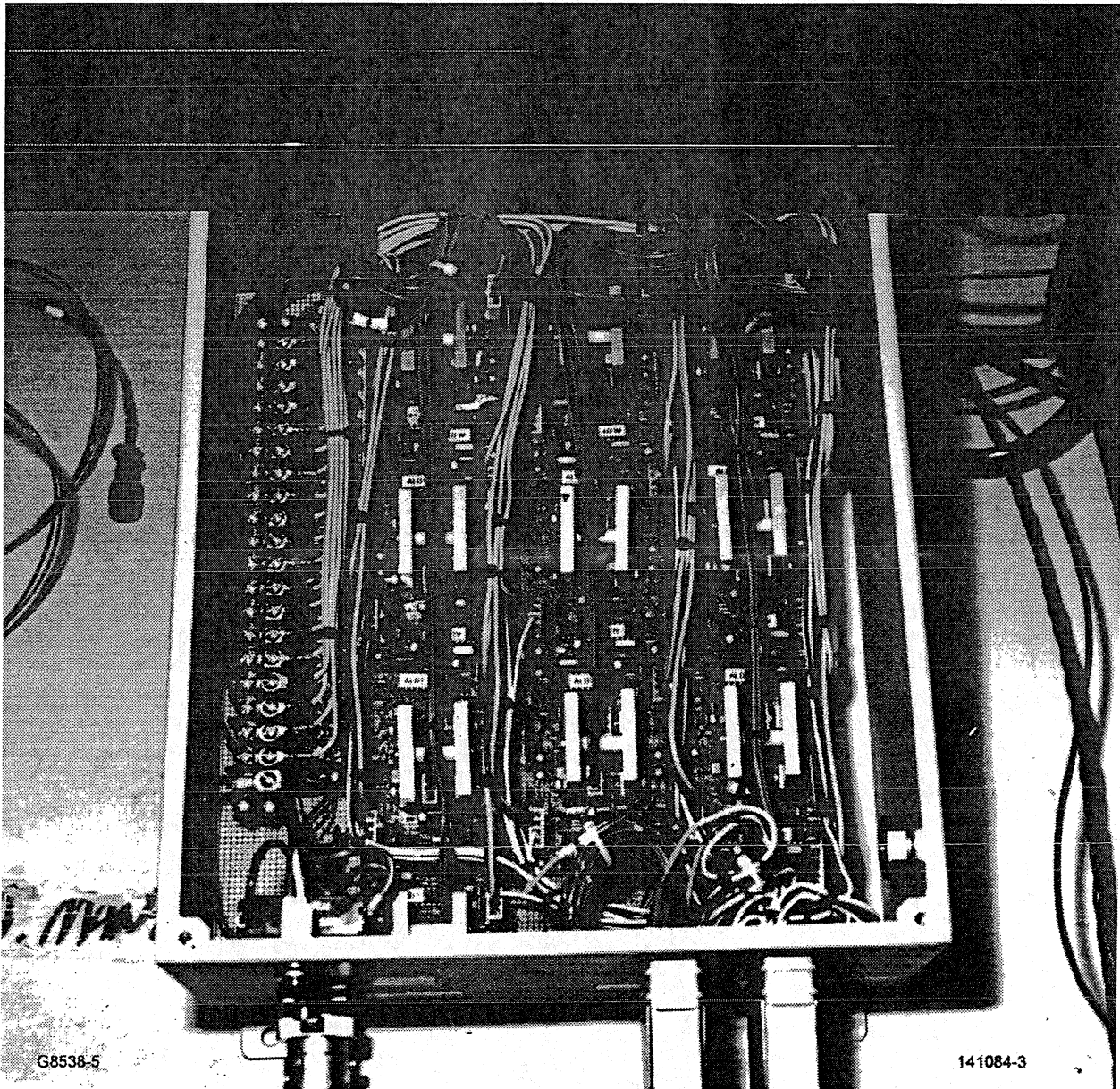


Figure 23. Fuel-Flow Modulator Driver Box.

5. CONTROL SYSTEM DEVELOPMENT

The control system was evaluated using both fuzzy logic and various closed-loop control methods. The evaluation is documented in Report 21-9690, System Modes and Logic Design Document, which was sent to NASA on June 12, 1997, and is provided as Appendix III.

Included in the report are details of the development and simulation results for the following control designs:

- (1) An optimization approach
- (2) A spatial averaging Proportional plus Integral (PI) multi-input-multi-output (MIMO) control
- (3) A harmonic control, using fast Fourier transforms (FFT) to identify controllable spatial modes
- (4) A Peak detection/switching control
- (5) An optimized parallel Single-Input-Single-Output (SISO) PI control
- (6) Control algorithms based on fuzzy logic.

The conclusion from these studies is that methods 4, 5, and 6 offer comparable benefits and that other tradeoff factors such as ease of implementation, execution time, size of code, etc., need to be considered to make the final selection. It was decided to program a closed loop method (peak detection) as well as a fuzzy logic method, so comparison testing can be done during the hardware rig test phase. The Simulink block diagram for the peak detection method is shown in Figure 24.

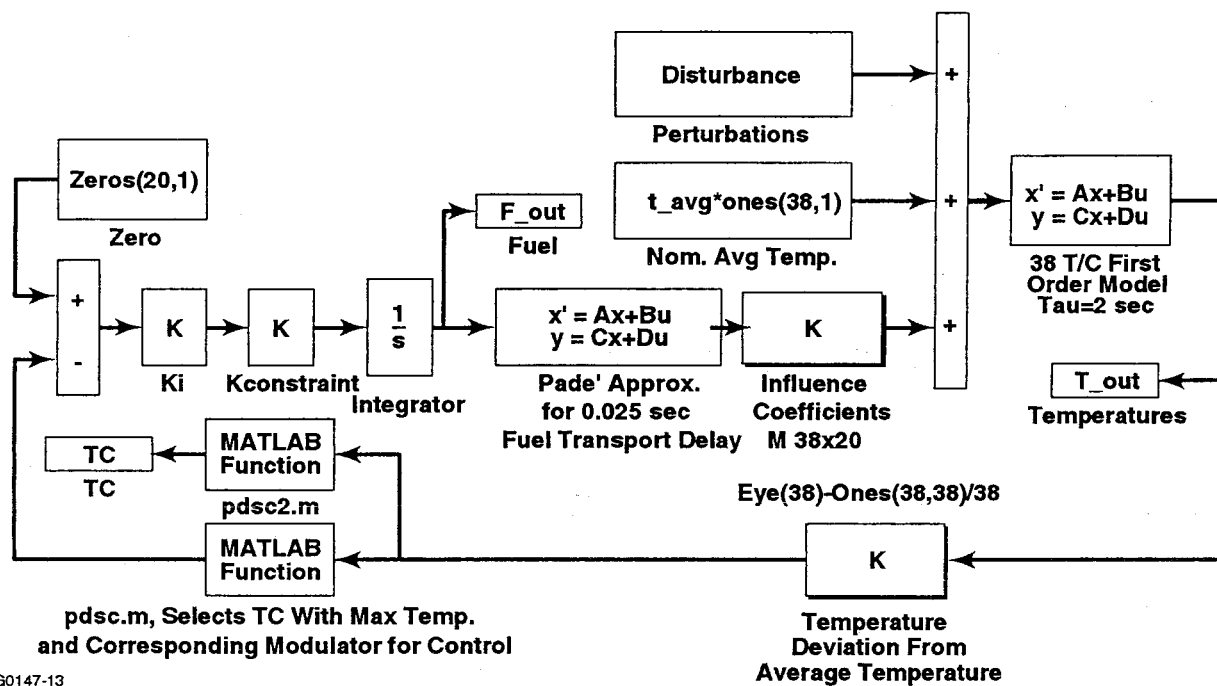


Figure 24. Simulink Block Diagram for Peak Detection Method.

Staging logic was also included. Staging consists of reducing the active number of fuel atomizers during conditions where very low fuel flow is necessary. It assures that each active atomizer has sufficient fuel flow so that a good fuel spray pattern and good combustor fuel/air ratio exists. The selection of pulse width modulation for the ACPFC fuel modulation concept is ideal for staging. This permits complete shutoff of the fuel flow to any atomizer. The other concepts considered for the ACPFC restricted the flow but could not completely shut off the flow.

The basic concept for staging is to turn every other atomizer off during starting and major unloading transients. The number of active atomizers is readily varied since each atomizer is under the control of the ACPFC. The logic can even change how many and which atomizers are shut down depending on the specific conditions. When the engine starting logic is active the staging logic can sequence the atomizers with respect to the location of the igniters. During unloading transients the staging logic would sense the requested speed of the power lever and actual speed of the engine. If actual speed is 3 percent higher then every other atomizer shall be turned off. The atomizers shall be opened again when the speed difference drops to less than 1 percent. An alternate approach would be to turn off an increasing number of the atomizers as the commanded fuel flow drops closer to the lean blowout schedule.

6. PATTERN FACTOR CONTROLLER

The hardware system interface is shown in Figure 25.

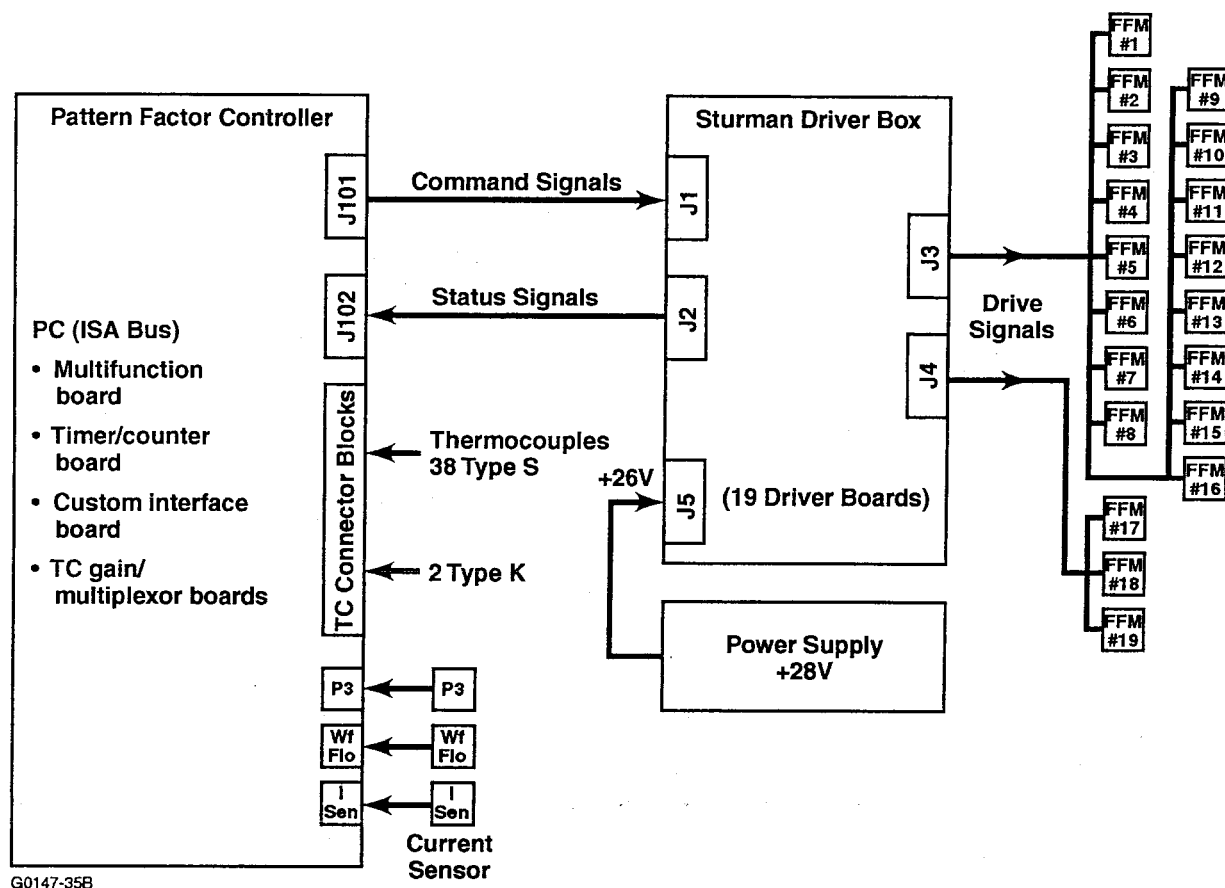


Figure 25. Pattern Factor Controller Interface Diagram.

The Pattern Factor Controller is a personal-computer (PC) based controller that incorporates ISA Bus I/O boards to provide the basic I/O functions required by the system. The system to be controlled consists of 19 pulse-width-modulated (PWM) fuel-flow modulator (FFM) valves. Each valve meters fuel flow to a fuel nozzle. A valve may be statically open for full flow, statically closed for no flow, or modulated to some partial flow. A modulated valve will be commanded open and shut during a frame time determined by the PWM repetition rate. There are 38 thin-film S type thermocouples mounted to a stator ring that are used to measure the temperatures. The temperature extremes determine the pattern factor. The purpose of this control is to provide research into various strategies to minimize the pattern factor by attempting to create a uniform temperature distribution. In Figure 26, the nozzles (each with a modulated valve) are indicated as circles.

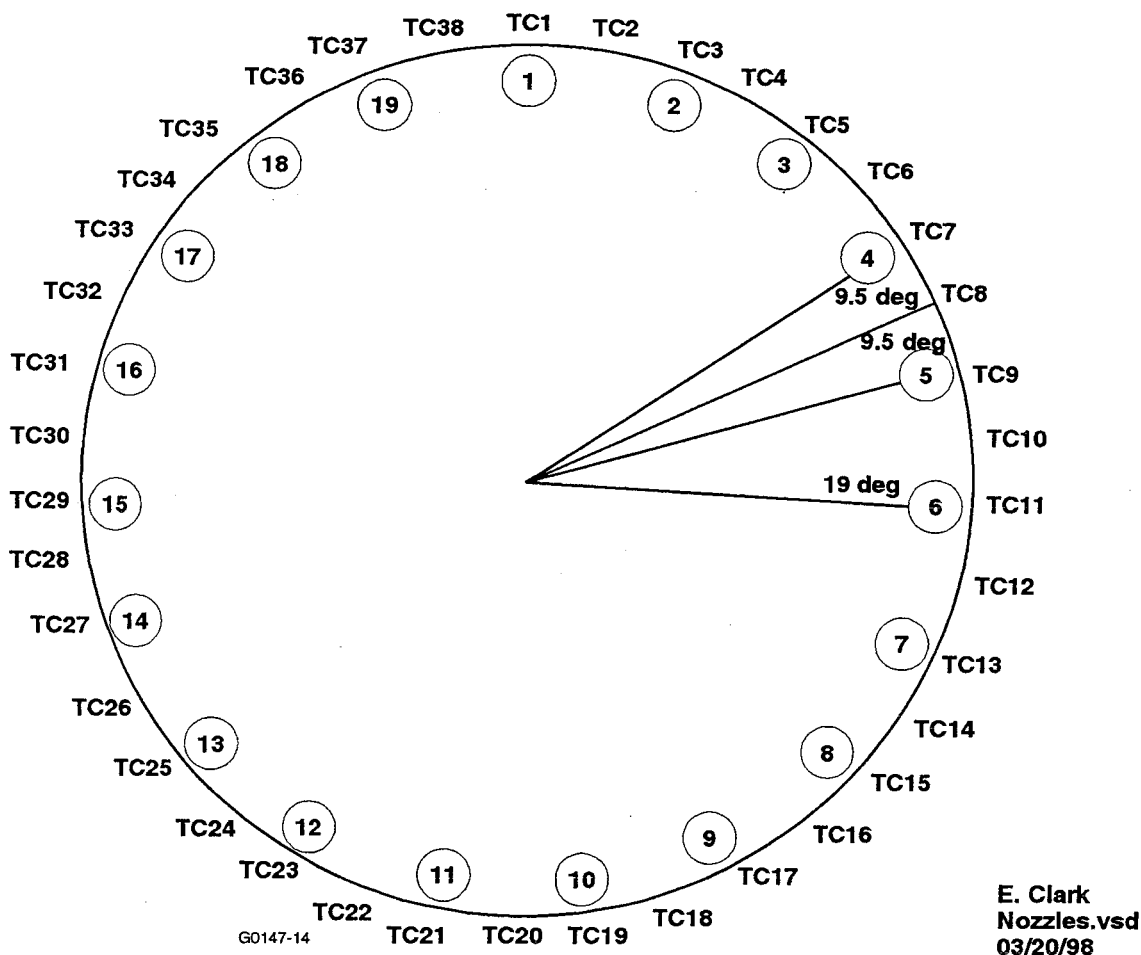
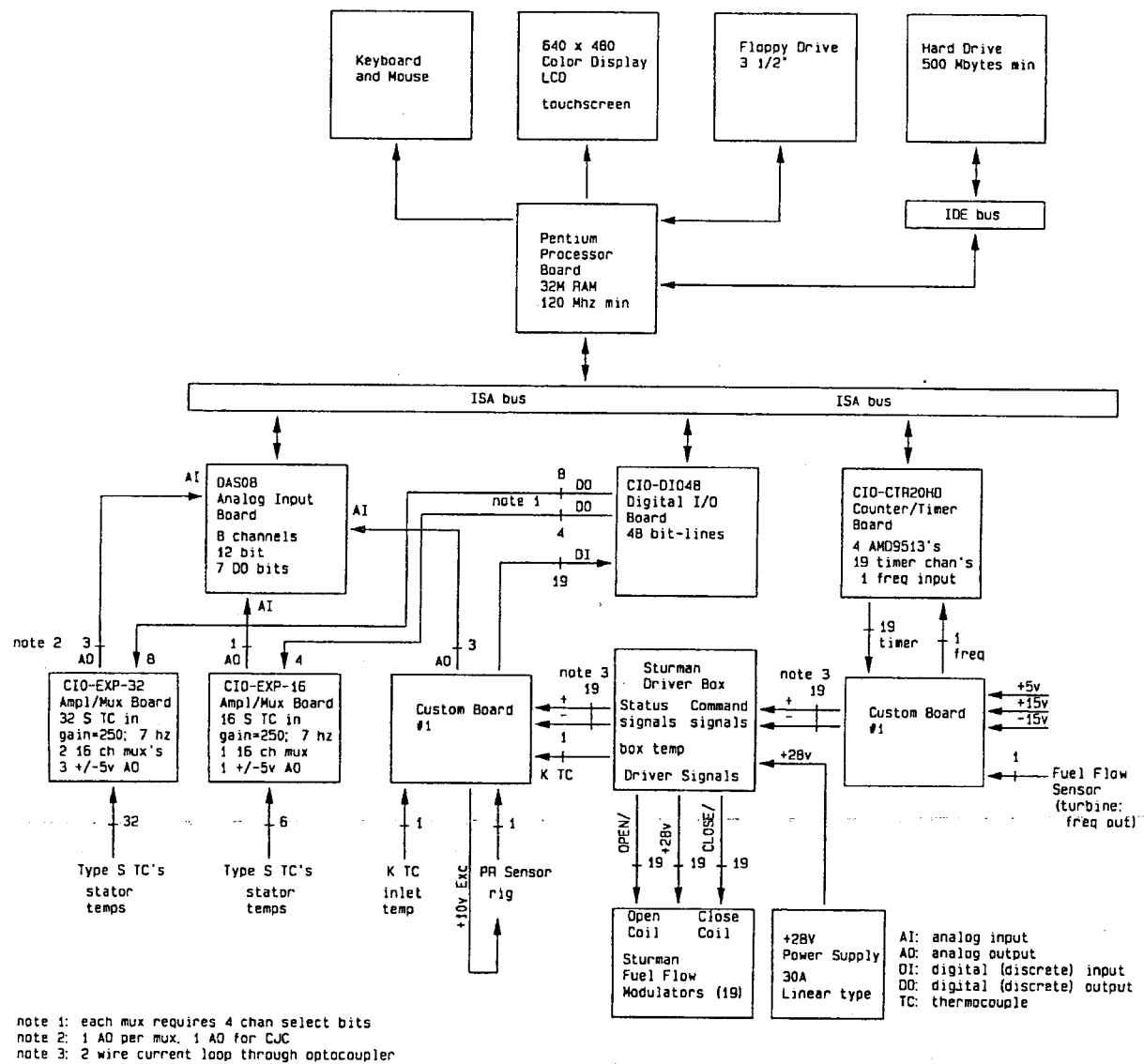


Figure 26. Thermocouple/Nozzle-Valve Orientation.

An FFM driver box (designed by Sturman Industries) receives PWM command signals from the controller and provides the drive currents to the fuel-flow modulator valves. The driver box also provides status signals back to the controller regarding FFM/driver operation. Figure 27 shows the system architecture.

The selected platform is a Hewlett Packard (HP) Vectra 5/90 PC that incorporates a Pentium processor running at 90 MHz. It incorporates four ISA slots, two of which are occupied by the add-in I/O boards selected for this program. There are 16 Mbytes of RAM available. The system timer peripheral is manipulated to provide a real-time clock to set up a fixed processing update rate.

A multifunction Analog-to-Digital (A/D) card includes 16 A/D channels with 16-bit resolution and also includes 32 discrete bit lines, and a timer peripheral. This board is I/O mapped to 0300H. (Consult the board manual for programming details.) Counter 0 of the 82C54 peripheral will be used to measure the fuel-flow sensor frequency signal.



GB404-12

Figure 27. Active Combustor Pattern Factor Controller (ACPFC) System Architecture.

The counter-timer board provides twenty 16-bit timers and an internal time-base clock. Nineteen channels are used in Mode J, hardware triggered one-shot, to provide the required PWM command outputs.

The 20th channel is set up in rate generator (mode D) to provide a reference clock that runs at 10 times the PWM frequency. A clock generator circuit on the custom board uses this clock to develop gate triggers for the 19 PWM timer outputs. This board is I/O mapped to 0310H.

(Consult the board manual and the AMD "MOS Microprocessors and Peripherals Manual" (1985) for programming details.)

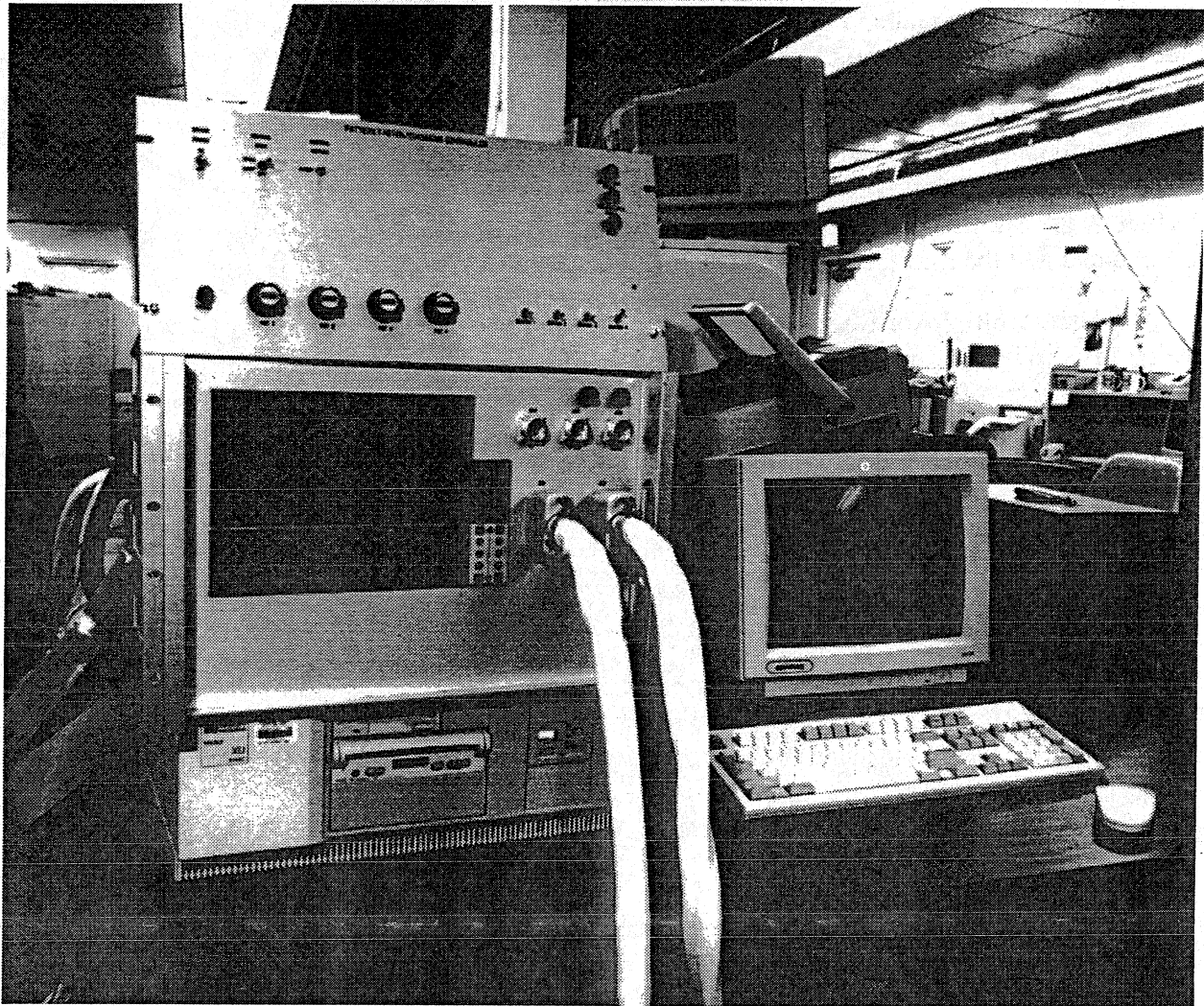
The I/O Box is an enclosure that incorporates one 32-channel thermocouple gain/multiplexor board, one 16-channel gain/multiplexor board, and the custom I/O board designed for this system. The 38 S and 2 K type thermocouple signals are conditioned in this box. The interface to the Sturman driver box is implemented on the custom board, as is the interface to the control panel and the interface to several other system sensors.

The Gain/Multiplexor Boards differ only in the number of channels supported. Each channel is a differential input that is multiplexed to an INA110 instrumentation amplifier. The low and high sides of the signal each have a 10K series resistor before the MUX. Optional solder pads on the boards have been configured such that a 1-uF filter capacitor is tied to the two 10K resistors, forming a 7-Hz hardware filter. Each thermocouple input has also been configured (via option solder pads) to tie in a biasing circuit so that an open thermocouple will cause a maximum downscale reading. The low side of each signal is also tied to signal common through a 100 K resistor. There are 3 multiplexors (3 banks) that each select 1 of 16 channels as commanded by 4 channel select bit lines under software (SW) control. Each bank output is wired to a separate analog input channel on the A/D board. There is also a cold-junction compensation (CJC) signal that is a linear function of volts versus temperature that reads the temperature of one of these MUX boards near the termination connectors. This signal (the other board CJC temperature is assumed to be the same) is routed to an A/D channel for measurement. One channel of each bank measures a ground reference signal and one channel of each bank measures a 20-mV nominal signal. The gain of the MUX boards has been switch selected to 301. The reference inputs are measured and used to compensate for any offset/gain differences between the banks.

The Custom I/O Board provides signal conditioning and level shifting required between the I/O boards and the rest of the system: the driver box interface, the control panel interface, and several other sensors. It also complements the timer board operation to add circuitry required to implement hardware (HW) triggered PWM command outputs. The PWM trigger signals are dispersed over time to even out the demand on the 28V supply used to power the FFMs.

The control panel provides an interface to the operator. Three software controlled indicators, four assignable pots, and seven switches are incorporated.

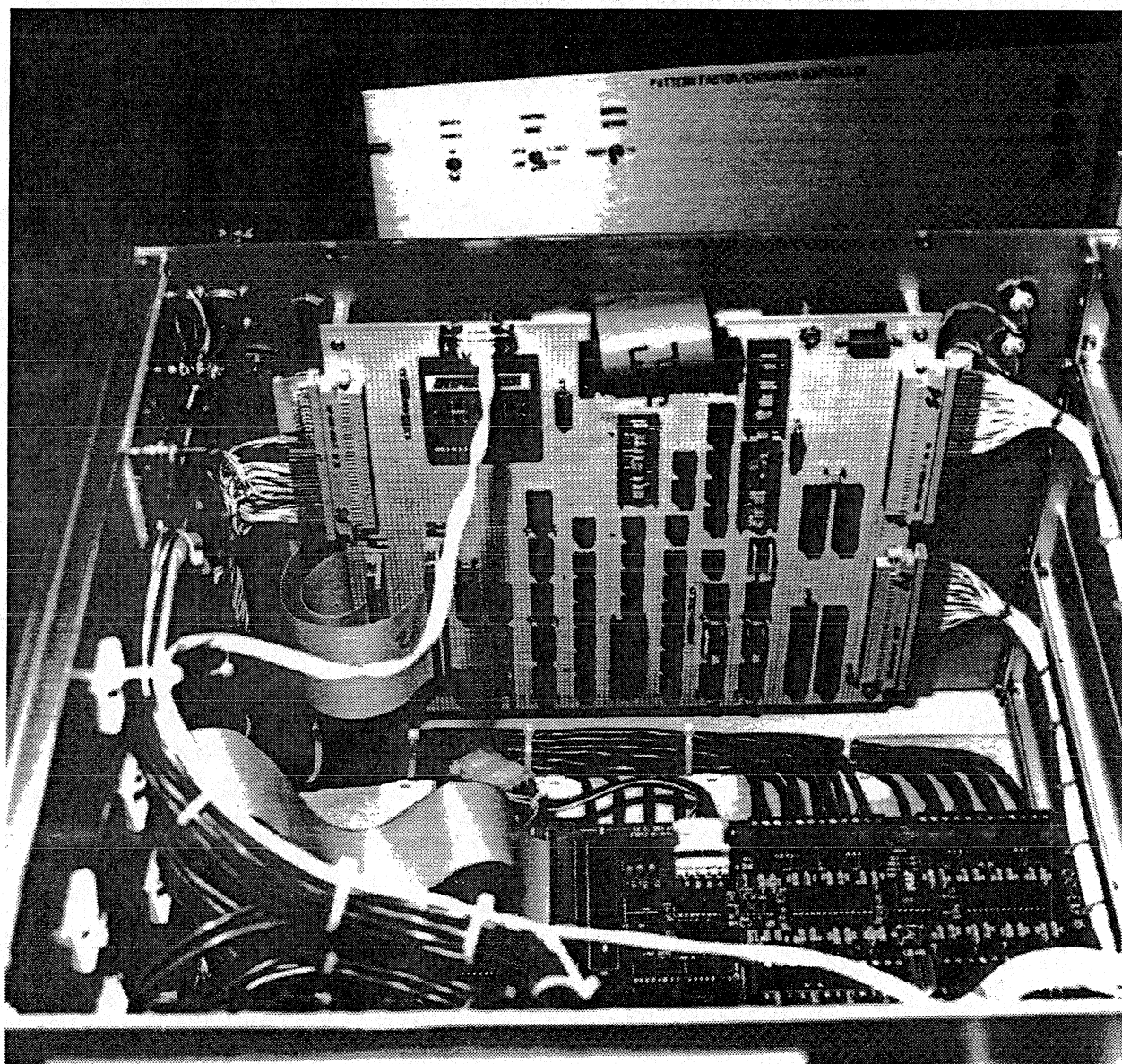
Photographs of the Rapid Prototype Controller are shown in Figures 28 and 29.



G8538-2

141084-1

Figure 28. Rapid Prototype Controller.



G8538-3

141084-4

Figure 29. Internal View of Rapid Prototype Controller.

The software to implement the control logic is run under the DOS operating system, with a processing frame time of 50 milliseconds. A PharLap tnt DOS extender package is utilized to increase available memory beyond the 640K DOS boundary. The system timer peripheral is set up for the desired frame time. A real-time interrupt handler is used to respond to this hardware signal to establish the real-time "foreground". A task dispatcher parcels out processing tasks in an "input-process-output" arrangement. When the foreground task completes, then a background task executes to provide operator interface support.

The flow chart in Figure 30 shows the PFC Mode Selection Logic.

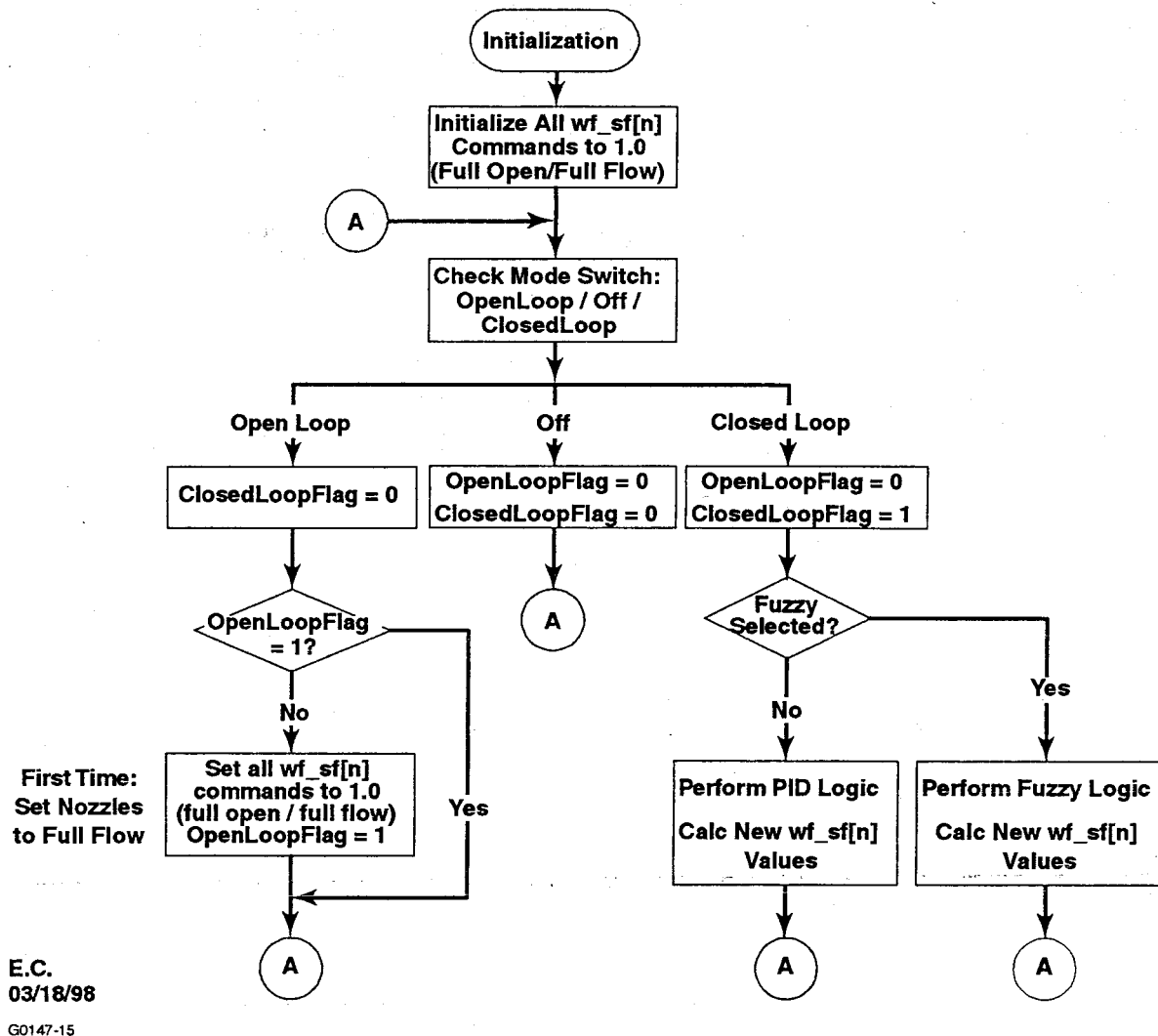


Figure 30. Pattern Factor Controller Mode Selection Logic.

There are three dedicated front panel switches that select the operating modes. The Open Loop/OFF/Closed Loop switch is to be utilized as follows:

- Open Loop: Manual mode; fuel-flow nozzles initialized to full flow. Moving the switch to this position is equivalent to the “reset” command. The monitor can be used to command settings other than full-flow; the switch action is a one-time reset to full open.
- Off: The Off position is interpreted as the “freeze” command, where fuel-flow commands are held at current settings.

- Closed Loop: This is the normal setting; system uses temperature readings and the selected control algorithm to control the fuel nozzles to optimize the pattern factor.

The Fuzzy/PID switch is interpreted as follows:

- Fuzzy: Perform fuzzy logic control algorithms.
- PID: Perform proportional-integral-derivative logic.

The system shall be capable of switching between fuzzy and PID operation during the same run.

The Odd/Even/All Thermocouple switch is a three-position switch used by both the PID and fuzzy control logic:

- Odd: Control on odd thermocouple readings.
- Even: Control on even thermocouple readings.
- All: Control on all thermocouple readings.

The system is capable of switching between these three modes of operation during a run.

For built-in testing, each fault test will use a persistence qualifier to help prevent nuisance indications. This is implemented using a count limit (default value = 10) for each sensor or measured quantity. An out-of-range or failed evaluation causes the associated fault counter to count up 2. An in-range or passed evaluation shall cause the associated fault counter to count down by 1 (if fault counter is greater than zero).

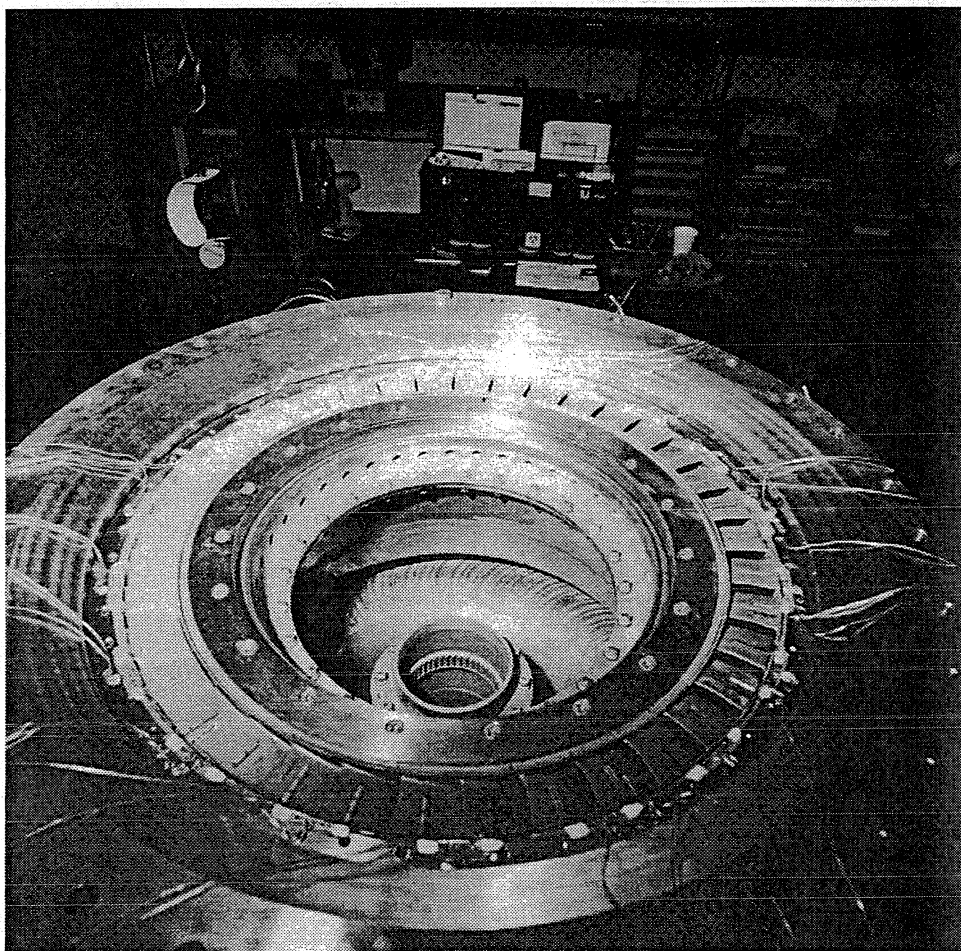
The Software Requirements Specification, from Document 21-9197(13), is provided in Appendix IV. A Software Problem Change Request is also provided in Appendix IV, Section 11.

7. COMBUSTOR RIG ASSEMBLY

The turbine-stator ring was sectioned into nineteen segments and then reassembled after processing of the thin-film sensors. The stator ring assembly was installed into the existing AS900 TVT Combustor rig. The rig was designed to allow the stator assembly to be positioned in relation to the injectors. The rig was modified to remove the bleed-air manifold and the temperature and pressure probes from the rake, and a cover plate installed in their place. The inner and outer cooling openings in each nozzle were blocked. The design of the rig modifications allows for thermal growth on the inner and outer flanges. The existing bleed-air exit fittings were used to remove the thermocouple leads.

There was no provision in the rig that would accommodate an emissions probe with the turbine nozzle installed. A rotating rake would not survive located directly behind the nozzle due to the high Mach number. A probe downstream in the tailpipe would be exposed to exhaust-duct cooling air. It was decided to design and fabricate a new emissions rake. A modified water-cooled emissions rake was designed to account for the turbine nozzle exit angle and was installed in the existing thermocouple rake drum assembly.

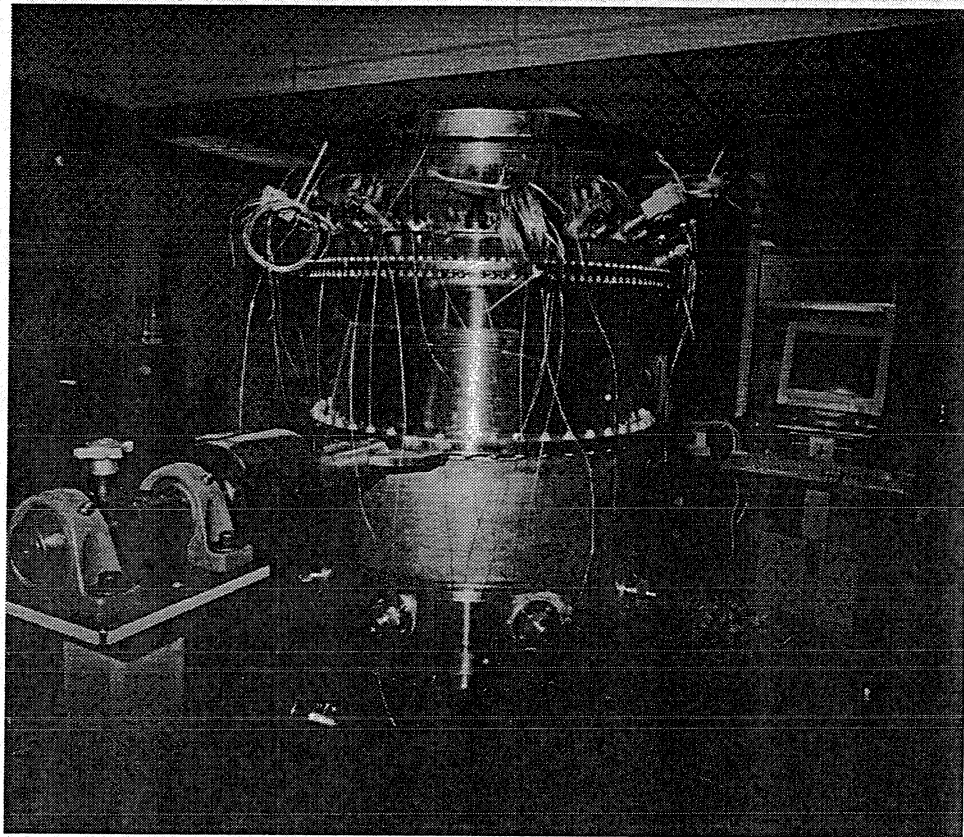
Figures 31 and 32 are photographs of the turbine nozzle ring assembly after installation in the combustor rig.



G8880-5

P142443-2

Figure 31. Combustor Rig Assembly After Installation of Instrumented Stator (Top View).



G8880-6

P142443-2

Figure 32. Combustor Rig Assembly After Installation of Instrumented Stator (Side View).

8. RAPID PROTOTYPE CONTROLLER BENCH TEST

A closed loop bench test of the Rapid Prototype Controller was conducted with the following objectives:

- (1) Confirm proper operation of the combined PC-controller, operator panel, Sturman driver box, and fuel-flow modulator (FFM) valves as a system.
- (2) Observe a sampling of several FFM driver current pulse shapes, widths, and magnitudes.
- (3) Measure +28v Power Supply loading at various pulse width modulation (pwm) frequencies and duty cycles with all valves being modulated.
- (4) Test the thermocouple measurement channels with a simulated temperature input from a calibrator.
- (5) Check out the controller response (hardware/software) to a simulated “hot zone”.

The test setup is shown in Figure 33.

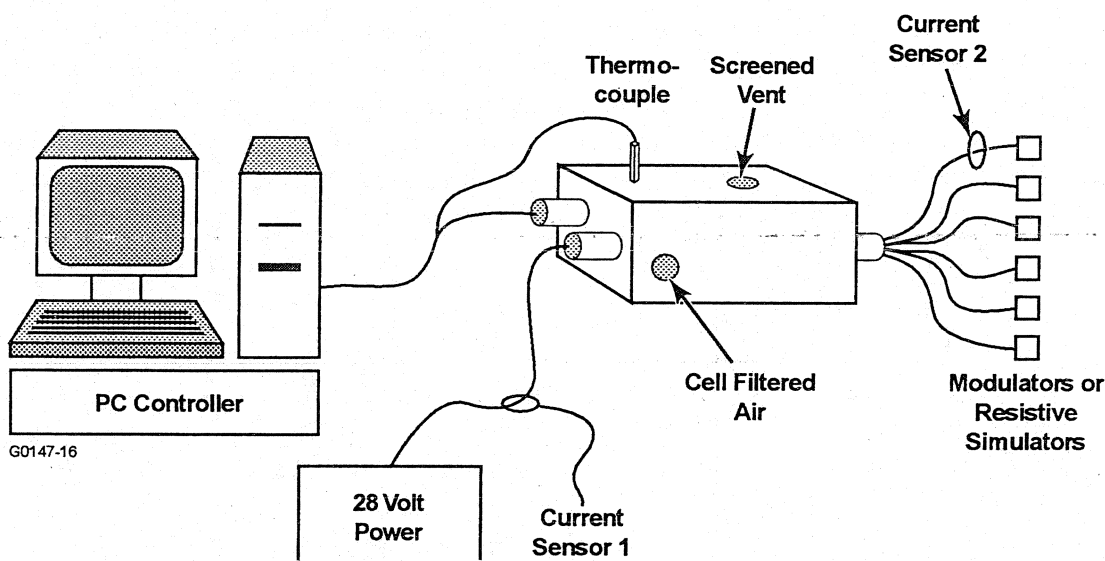


Figure 33. PC Controller Test Setup.

The bench test was successfully completed with all functions working properly and with favorable results in the area of thermocouple measurement channel accuracy, correlation, and low noise operation. The closed loop bench test also provided an opportunity to observe and gauge the correctness and effectiveness of the control logic and the code written to implement this logic. Improvements to the operator interface software (also known as the monitor software) were made to facilitate the testing process. Support was added for subscripted variables, which are used extensively in this controller. Several operator commands were enhanced. The strip

chart display-related command, for example, was enhanced to allow min/max scaling on the command line, which saved a recompile. A provision was also added to allow script files to be loaded (from a notebook PC) over the serial port. This allows new test-related script files to be loaded at any time while running, an improvement over the prior situation where a script file could be specified and loaded only at the time the control program was invoked.

In order to facilitate the “closed-loop” portion of the testing, a simple simulation was implemented that runs on the controller itself, in parallel with the control logic. The test strategy was to use a software switch to disconnect actual T4in measurements and to steer artificial (simulation computed) T4ol measurements to the control logic. These values (representing 38 thermocouple measurements) were initialized to a uniform value of 1500F. A single channel was then artificially set high (hot spot) or low (cold spot) and the simulation turned on via another software flag. The operator panel switches were then used to select the control method (fuzzy or PID) and the Odd / Even / All thermocouple group to control on. The system response was then monitored by observing the fuel-flow values of the fuel-flow modulator commands and the values of the T4ol variables being manipulated by the simulation.

One effect observed in the proportional-integral-derivative (PID) testing was a tendency for the FFM-valve commands to work increasingly toward the closed position. This is an undesirable effect in terms of having the modulation of the FFM valves appear “transparent” to a fuel control attempting to govern engine speed on a real engine. Logic was added to preserve a constant net-effective control area by maintaining a constant net-modulation duty cycle. A target average scale factor of 0.9 (90 percent duty cycle) was chosen to provide room for adjustment in both directions. An increment (or decrement) is computed to be added to each fuel-flow term to maintain the target control area. A software switch allows this mode of operation to be turned on and off to offer a comparison of system behavior. The fuzzy logic can also be operated with this mode turned On or Off.

The simulation logic implemented here uses the same gain matrix that is used by the PID control logic. Not surprisingly, in retrospect, the PID control behaved very well in these tests. The fuzzy logic performed less well against this simulation. The current simulation logic served its purpose in allowing several software bugs to be corrected and the overall logic to be deemed operational, while only a few minor areas of concern were exposed.

9. SIMULATOR BENCH TEST

The simulator bench test evaluates the system using the laboratory fuel supply and measures the ability of the system to control individual FFMs based on the commanded profiles. The controller incorporates a plant model that simulates a combustor based on data taken from a JTAGG combustion rig test. The controller predicts the control system response to a typical combustor temperature spread. The test also demonstrates, by measurement, the fuel flow to each nozzle to compensate for the simulated temperature errors.

The nineteen fuel-flow modulators were connected together by a manifold and supplied with fuel from the standard nozzle test stand. The discharge from the FFMs was fed through the engine fuel lines and spray nozzles. These were then connected by Tygon tubing to individual measuring beakers. Located nearby was the Sturman power supply box and power supply. The RPS was located outside the test cell area. This setup is shown in Figure 34.

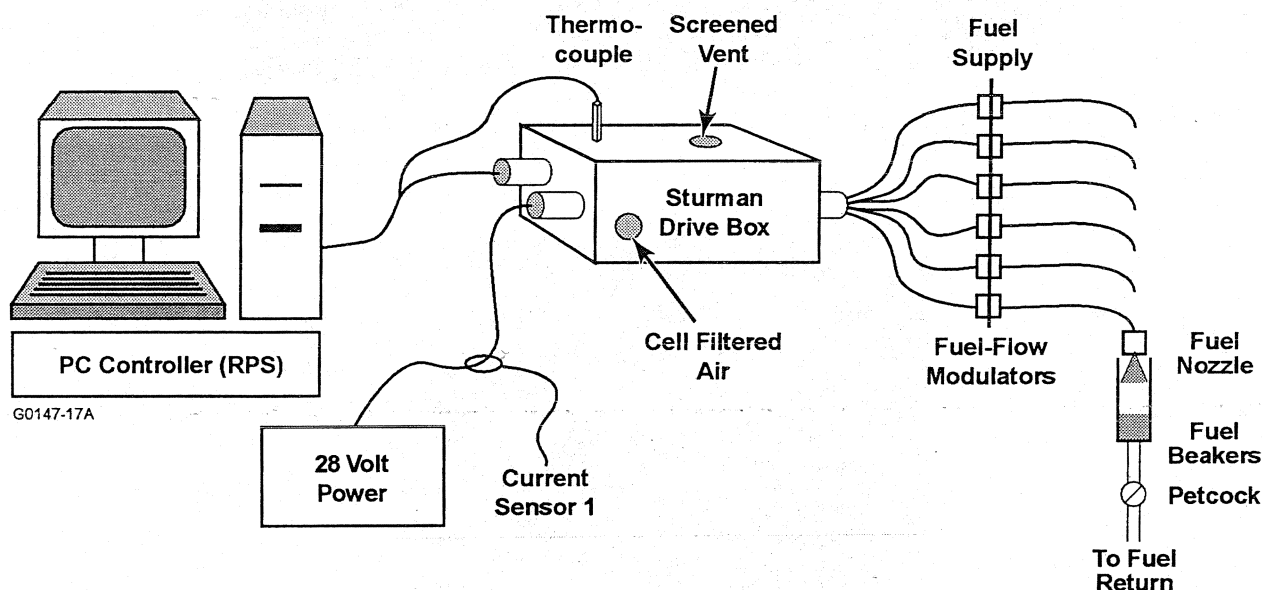


Figure 34. Simulator Bench Test Setup.

Several of the fuel-flow modulators with their connecting pipes, fuel nozzles, and Tygon tubing are shown in Figure 35, while Figures 36 and 37 show the PC-based controller and flow collection setup, respectively.

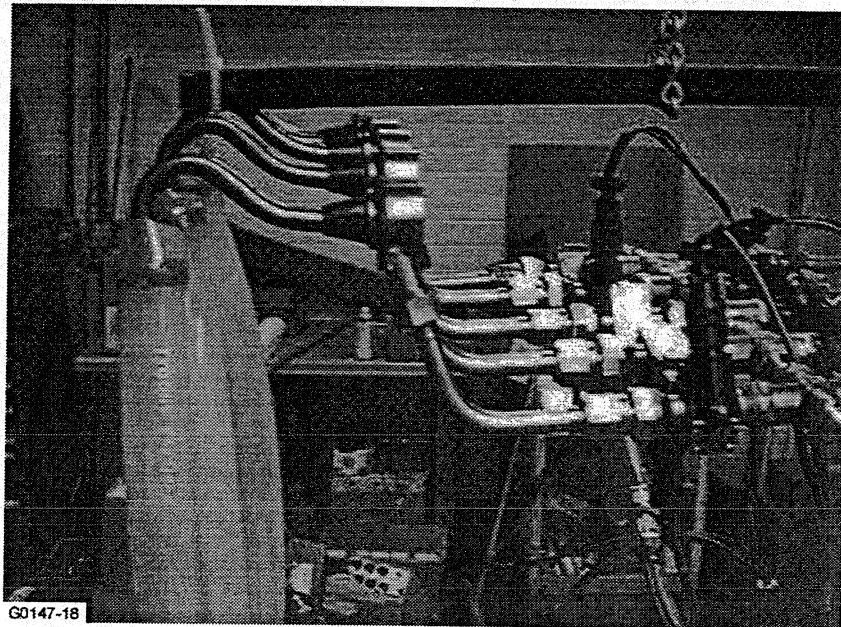


Figure 35. FFM's Connected To Fuel Nozzles.

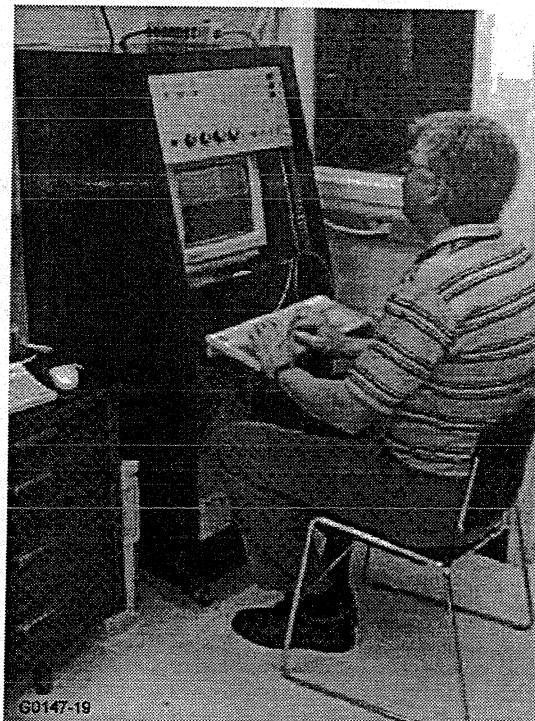


Figure 36. PC-Based Controller.

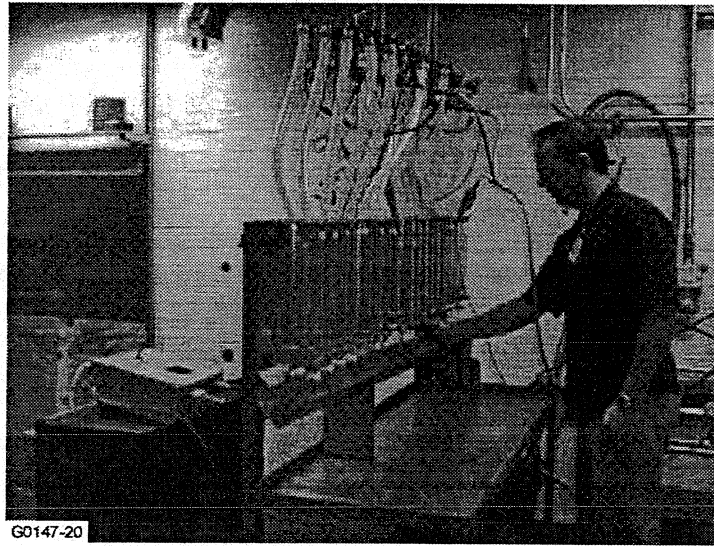


Figure 37. Flow Measurement Setup.

All fuel-flow modulators were operated uniformly at frequencies of 20, 30, and 40 Hz at three different supply pressures; 200, 400 and 600 psig. For each frequency and supply pressure, the duty cycle (percent ON time) was varied from 5 to 95 percent. The total fuel flow for all 19 modulators was measured at each condition. A plot of the resulting data is shown in Figure 38.

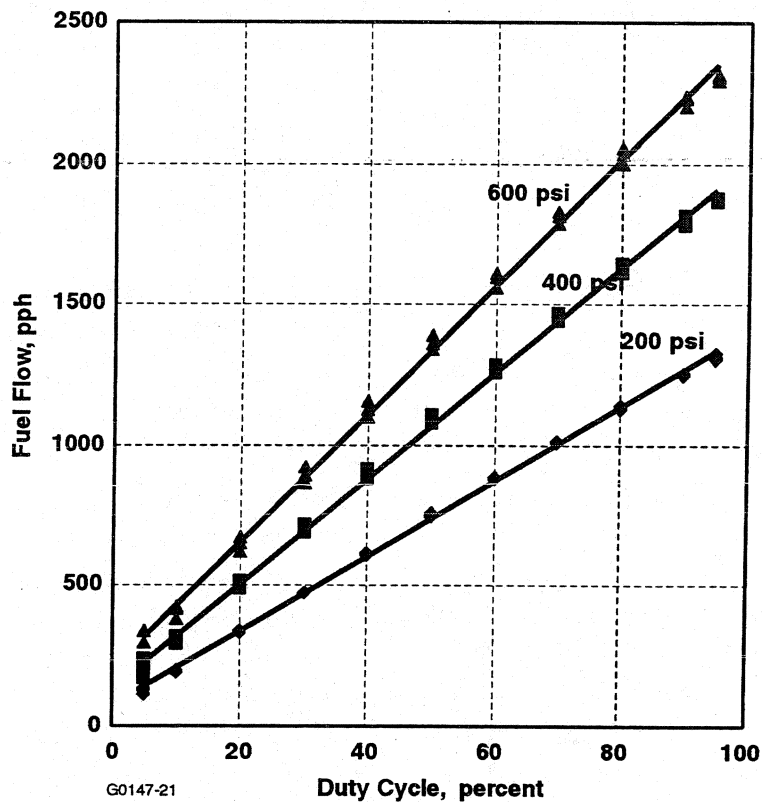


Figure 38. Calibration Data for Fuel-Flow Modulators.

As expected, the flow rate is very linear with duty cycle (percent full area ON time) and is proportional to the square root of the supply differential pressure. Flow was also found to be negligibly influenced by operating frequency, as noted by the fact that all data points (for 20, 30 and 40 Hz) are plotted together in Figure 38.

A baseline uniformity test was conducted to confirm that the system could compensate for non-uniform fuel nozzle flow characteristics. Initially, the RPS was set to 30 Hz and a constant duty cycle of 80 percent was commanded to all FFMs. Fuel was collected in the 19 beakers and measured. As shown in Figure 39, the average nozzle variation was approximately 3 percent, with the exception of nozzle number 2, which was almost 9 percent below average. These nozzles had been run several times in a development rig, and coking could have been present.

After measuring these flows, a series of “compensation factors” were introduced into the software as multipliers between the commanded and actual output signals. The system was then run again with constant commanded duty cycles and the actual fuel collected is shown by the compensated data curve. This shows that the system can dramatically reduce the variations in individual fuel flow due to atomizer variations or other effects. The compensation factors were left in the software for the remaining tests, so that the relationship between temperature errors, commanded flow and actual flow could be observed.

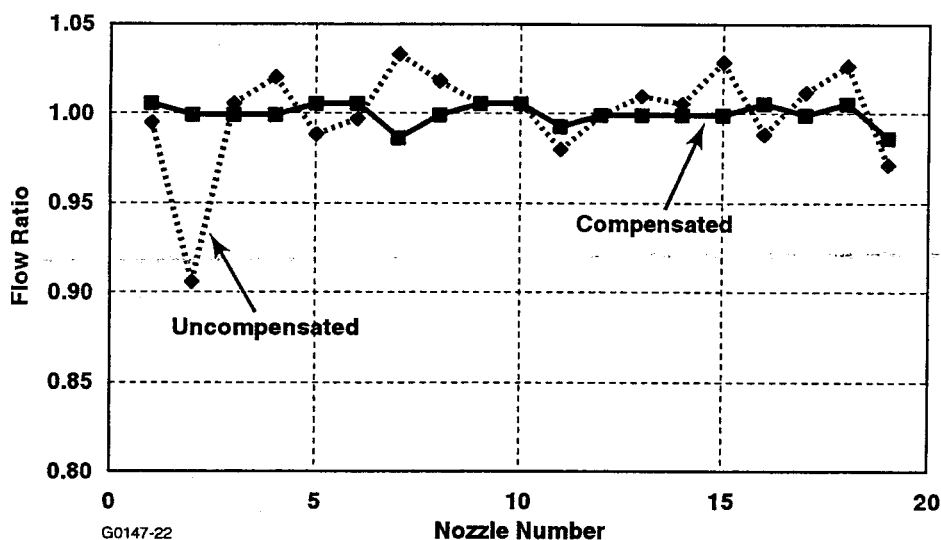


Figure 39. Nozzle Flow Distribution, Flow Uniformity Test Results.

In order to confirm the operability of the control software, a digital simulation of the combustor temperature exit profile, as a function of individual atomizer flow rates, was coded into the Rapid Prototype Controller. This simulation was based on data taken from a JTAGG I combustor during the preceding NASA Small Engines Technology program and used extensively during the analysis phase of the present program. The code was modified to allow the introduction of temperature distributions typical of operating combustors. This assumed initial temperatures, before control action is applied, which are shown in Figure 40. The pattern factor for this distribution is 0.136 and the standard deviation is 153.9F from the average of 1900F.

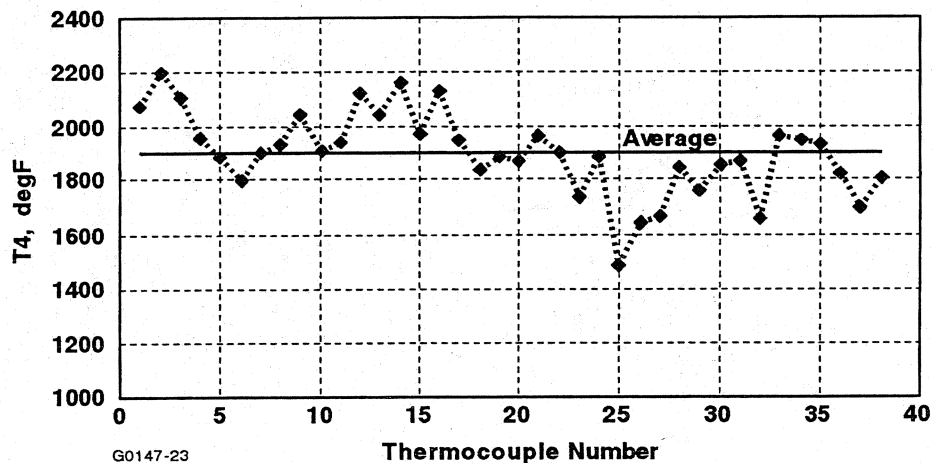


Figure 40. T4 Initial Temperatures.

As shown in Figure 41, the outputs from the combustor model have the starting temperature errors added. The resulting T4 temperatures are then acted upon by the control logic (either fuzzy or PID) and the individual modulator signals are adjusted. The combustor model then reacts to these signals and changes the simulated output temperatures.

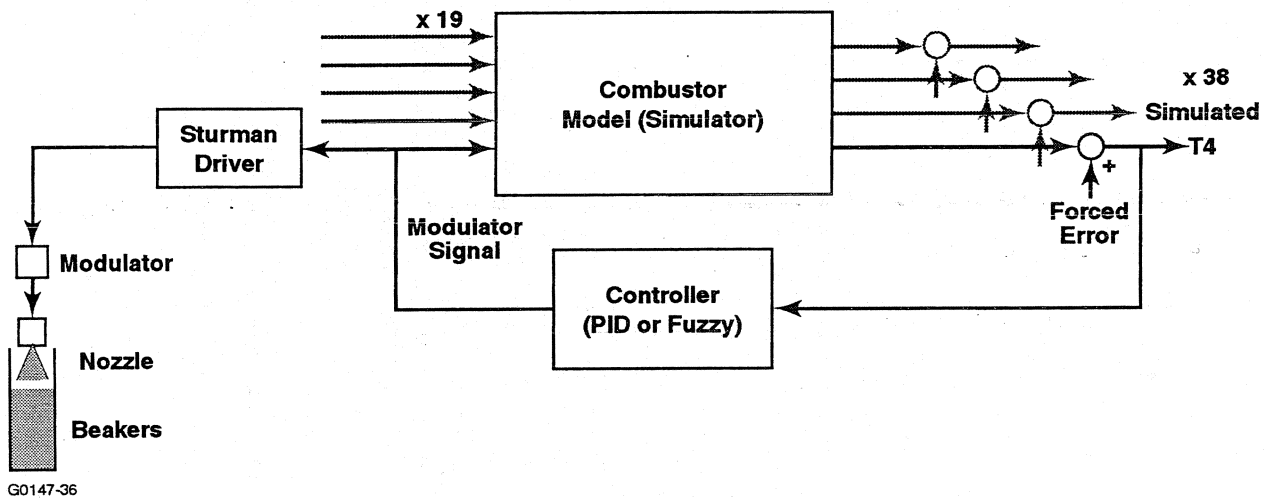


Figure 41. Simulation Schematic.

The controller output signals also drive the modulators through the Sturman driver circuits that permitted confirmation of the system operation through flow measurement. Using the temperature error values from the JTAGG combustor tests, the PID controller logic reduced the pattern factor from 0.231 to 0.057, or 75 percent. The standard deviation in the simulation final temperature distribution was 12.2F. The resulting temperature distribution under PID control and the fuel valve positions are shown in Figure 42.

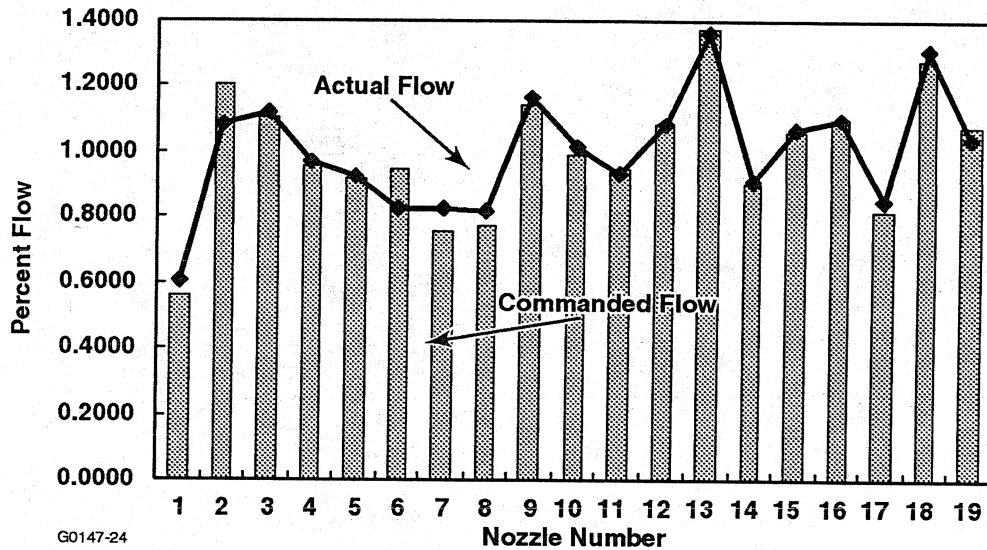


Figure 42. Commanded versus Actual Flow with PID.

The fuzzy logic controller was then applied to the same simulated temperature disturbance. The result is shown in Figure 43. Pattern factor for this control was 0.10, or a 57 percent reduction. The standard deviation in temperature errors was 11.8F.

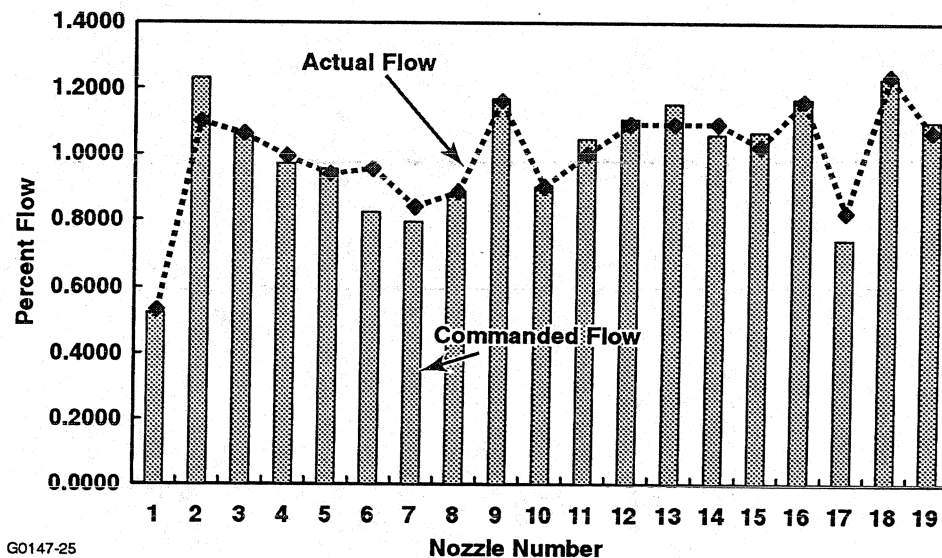


Figure 43. Commanded Versus Actual Flow with Fuzzy Logic.

It should be noted that neither controller was optimized for this plant simulation. When operated with the actual plant (combustor) the gains may be adjusted to obtain minimum pattern factors and emissions. Conversely, with an actual combustor the relationship between a given nozzle and turbine-stator segment may vary with operating conditions, such that further optimization may not be possible. However, it was demonstrated that the controller system does

act to significantly reduce the pattern factor and the physical fuel flows are reduced in the expected manner.

Successful completion of these bench simulation tests lead to the following conclusions:

- (1) The PC-based control responds appropriately to drive each of the FFMs correctly.
- (2) The FFMs deliver fuel in direct proportion to the ON duty cycle commanded within a band of approximately 5 percent.
- (3) The system responds in the appropriate direction and magnitude to simulated combustor temperature errors.
- (4) The two control logic schemes show the potential for significant reduction in the combustor exit pattern factor.
- (5) The PC control display provides excellent visualization of the commanded fuel flow and measured temperatures.

10. COMBUSTOR RIG TESTS

The objectives of the rig tests are to demonstrate a reduction in circumferential variation of vane temperatures (pattern factor), demonstrate the influence on overall combustion emissions, evaluate the benefits of staging, and demonstrate the stability of the control loop.

An AS907 prototype turbine-stator ring is located at the discharge of the annular combustor. Each of the 38 vanes is equipped with Type S thermocouples. The sensors are connected to the PC controller through the test cell wiring. This test setup is shown in Figure 44.

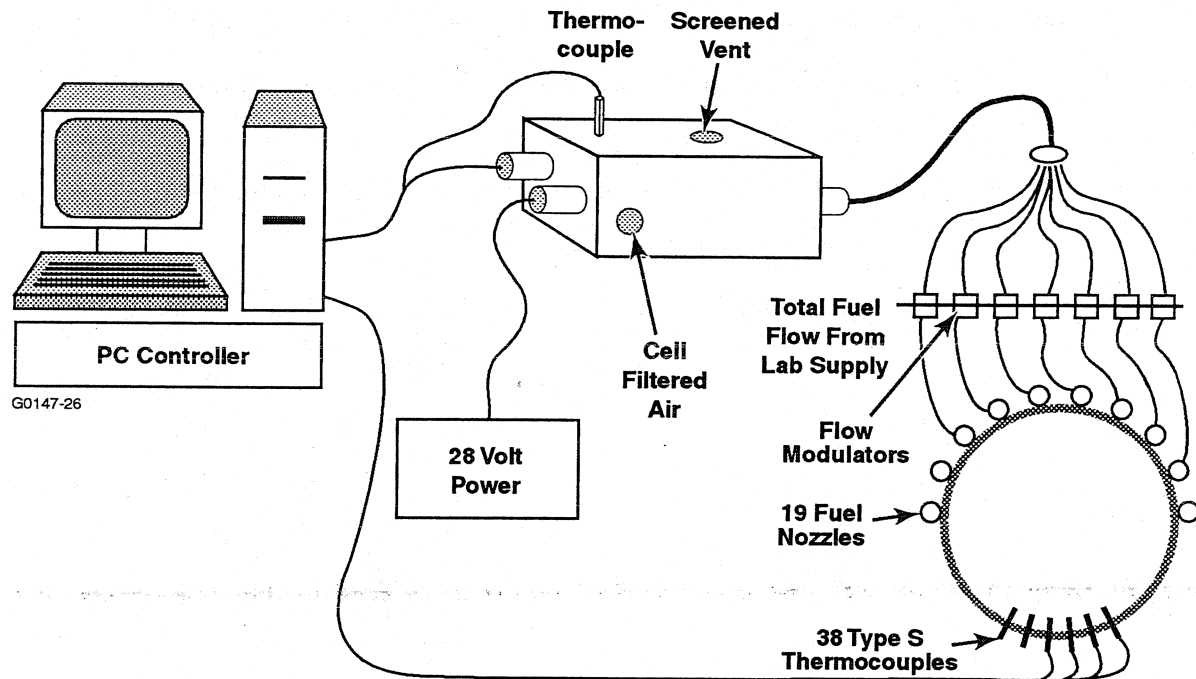


Figure 44. Combustor Rig Test Setup.

The PC control is located in the console room of the Honeywell test cell number C-100. The remaining equipment is located inside the cell near the combustor rig. The thermocouple signals are communicated from the in-cell "boom" to the console and then to the PC control. Rig inlet temperature (T3) and pressure (P3) are taken from the console data to the PC. Output signals to drive the Sturman box are connected directly. The test cell arrangement is shown in Figure 45.

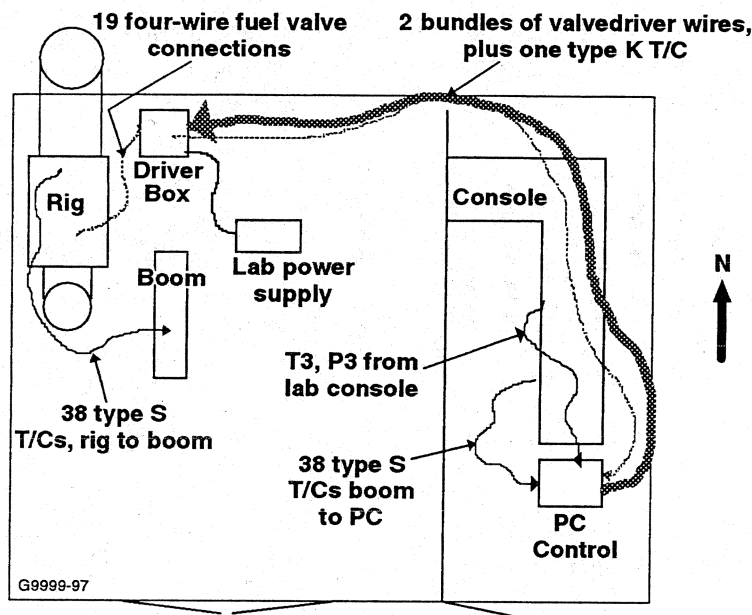


Figure 45. Engines & Systems Combustor Test Cell C-100 Top View.

Installation, instrumentation, and connection of the combustor rig to the electronic pattern factor controller was completed on May 25, 1999. It was noted that one external thermocouple lead had been irreparably damaged during the installation and showed as open circuit on the controller. Fault detection logic in the control substitutes the average of the two adjacent values for the faulty signal.

Airflow was initiated through the rig and the fuel system was pressurized with air to check for leaks. Several leaks were noted and the fittings were tightened. It was noted that several more thermocouples were reading "open" following this non-burning run. External connections were checked but the location of the open circuit was determined to be within the rig.

Combustion was then initiated and the rig was taken to an equivalent idle fuel/air/pressure condition. All of the fuel-flow modulators (FFMs) were energized at 20 Hz and set to 80 percent "on-time" and a baseline pattern factor was obtained. Figure 46 shows the modulator settings and distribution of the temperatures and pattern factor for this point.

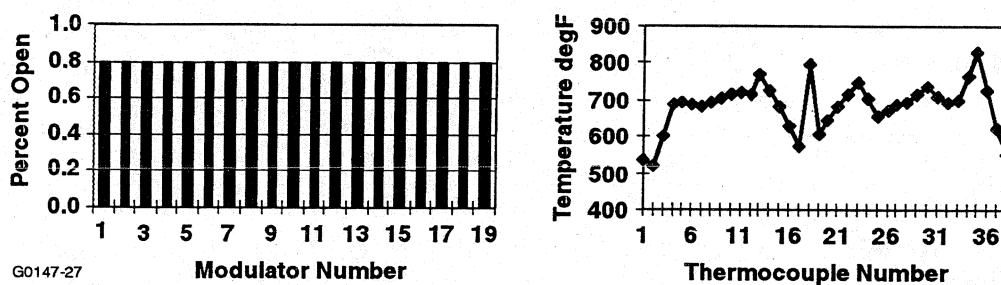


Figure 46. Baseline (no control): $T_{avg} = 684.6F$, $T_{hot} = 828.6$, Pattern Factor=0.42.

The ACPFC was set to Closed Loop operation in the Proportional/Integral/Derivative (PID) mode and energized. This resulted in a reduction in peak temperature from 828.6 to 762.7F and a reduction in pattern factor from 0.42 to 0.21 as shown in Figure 47.

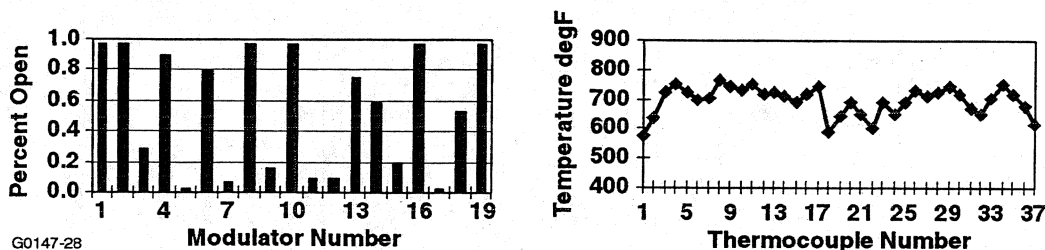


Figure 47. PID Control: $T_{avg}=692.2F$, $T_{hot} = 762.7F$, Pattern Factor =0.21.

The ACPFC was next set to closed loop operation in the Fuzzy Logic control mode. This resulted in a reduction peak temperature from the original baseline of 828.6 to 780F and a reduction in pattern factor from 0.42 to 0.23, as shown in Figure 48.

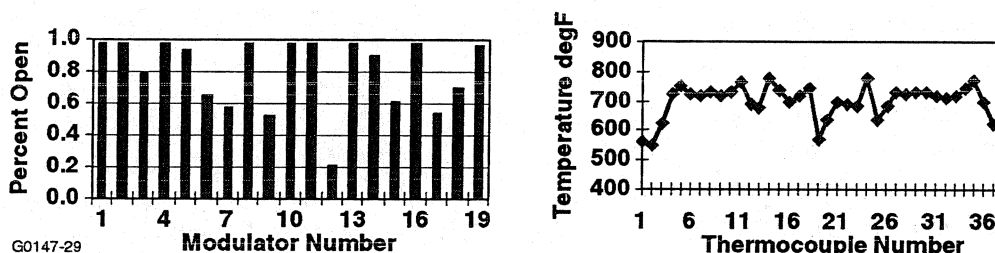


Figure 48. Fuzzy Control: $T_{avg}=697.6F$, $T_{hot} = 780F$, Pattern Factor =0.23.

Following this test it was noted that additional thermocouple signals were out of range. The control's fault accommodation logic is to substitute the average of the adjacent signals for the failed sensor. This system operates very well for a few, randomly distributed failures. However, when a number of adjacent sensors fail, it is possible that major hot spots are being missed and the control does not perform well.

Another run was made at an average blade temperature of approximately 1100F. In the open-loop mode, the high temperature blade was 1483F, and the pattern factor was 0.38. With the PID control operating, the maximum blade temperature observed was 1196F and the pattern factor was 0.28. The Fuzzy Logic control resulted in 1371F and a pattern factor of 0.34. This data is considered to be non-optimum since approximately half of the sensor signals were inoperative and being accommodated.

In order to assure that the fuel-flow modulators, which use PWM technology, do not have a detrimental effect on either emissions or acoustics, a series of uniform "pulsing" of the atomizers was conducted. In this test, the control was operated in the open-loop mode at several FFM frequencies and PWM duty cycles, or "on-times". The frequencies tested were 10, 20, and 30 Hz while the duty cycles were 90, 80, 60 and 40 percent.

Figure 49 shows the results of these tests, including a “no modulation” or baseline point (the square symbol, Test 1). As can be seen, Tests 2 and 3 (20 Hz at 90 and 80 percent duty cycle, respectively) produced a NO_x index higher than the baseline, while the remaining six conditions (Tests 4 through 9, which included 30 Hz and 10 Hz conditions) produced NO_x levels lower than the baseline. Inspection of other rig data, such as inlet temperature, fuel flow, and airflow, were held very closely for all data points. Consequently, no specific relationships could be determined from these runs; however, it was concluded that PWM fuel delivery by itself does not significantly affect NO_x production.

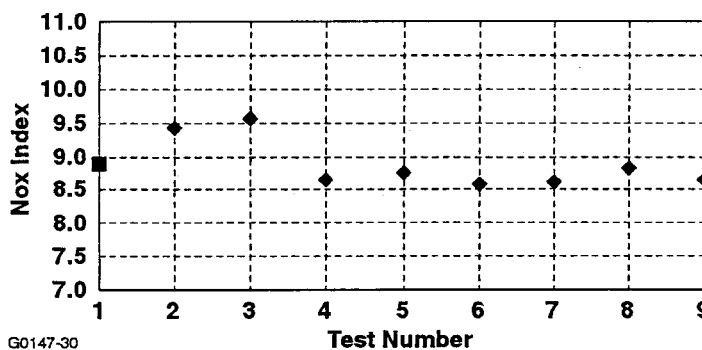


Figure 49. Uniform PWM at Various Frequencies and Duty Cycles.

Based on the bench test and burner rig testing conducted earlier in the program, there was an expectation of success with the thin-film, type-S thermocouples on the ACPFC stators. However, results indicated sensor losses from the outset of the pattern factor testing. At the conclusion of the testing, it was noted that only eleven of the thin-film temperature sensors were providing in-range signals. Visual examination disclosed that in several cases there was delamination of the metal platinum and platinum-rhodium thin-film legs, as well as cracking in the films. Splice locations also appeared to be compromised, with erosion and lifting of the WC16 ceramic cement, 3 mil to MGO conductors splices open, as well as damage to the 0.020-inch MGO. It was concluded that the configuration of the thin-film sensors required further development before being applied in a dynamic temperature based fuel control system. A decision was made to rebuild the rig using conventional platinum-rhodium thermocouples.

In addition to the problems with the temperature sensors, a water leak from the cooling water supply sprayed onto the fuel-flow modulator driver box, resulting in a short circuit and repeated tripping of the power supply circuit breaker.

Acoustic testing was conducted to ensure that the pulsing fuel delivery system would not cause an acoustical problem. Oscillations have been seen in the past on premix combustors. These oscillations cause vibrations that are severe enough to damage a number of engine components. Data was taken with steady flow (all modulators locked open) and then partial but uniform durations during the initial calibration phase. No oscillations were seen while viewing the frequency spectrum real time. This quick look provides the noise spectra of several operating conditions.

No change was seen in the noise spectra between the baseline (full open modulators) and pulsed modulation conditions. Plots of some of the different conditions recorded on May 27, 1999 are shown in Figures 50 through 52.

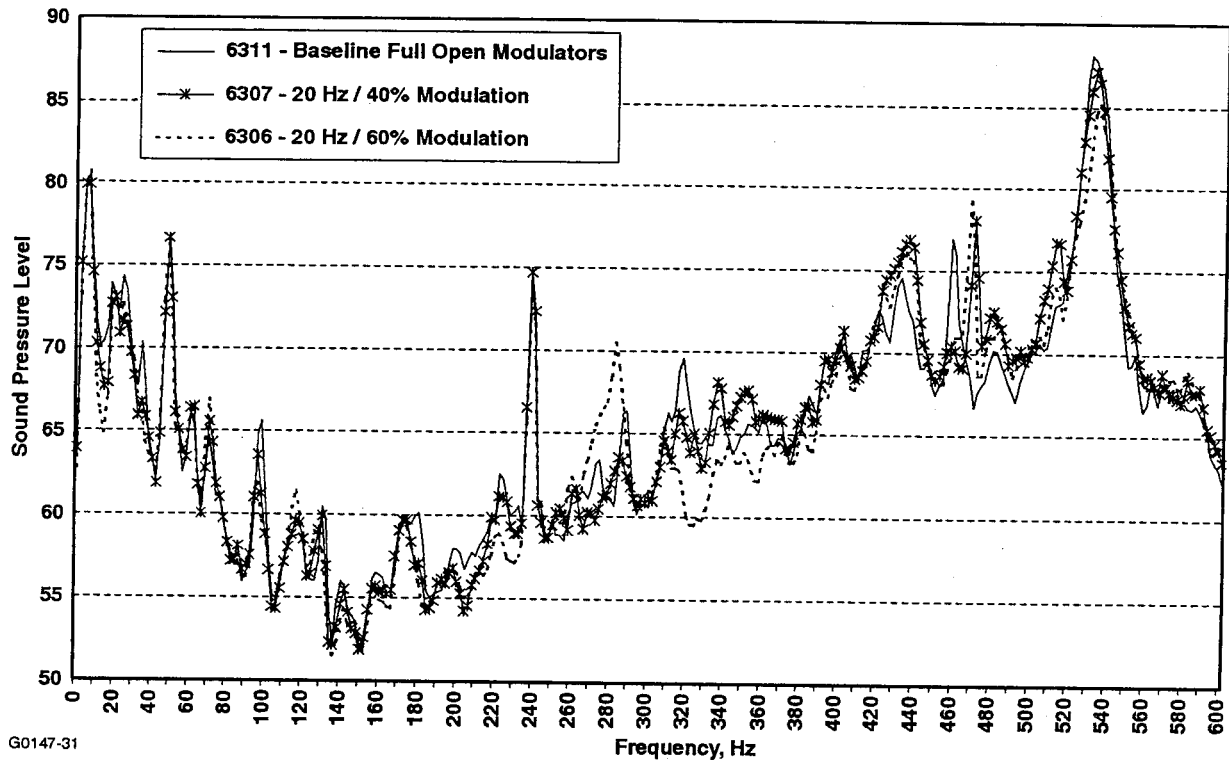


Figure 50. ACPFC Sound Pressure Levels (20 Hz Modulation Comparison).

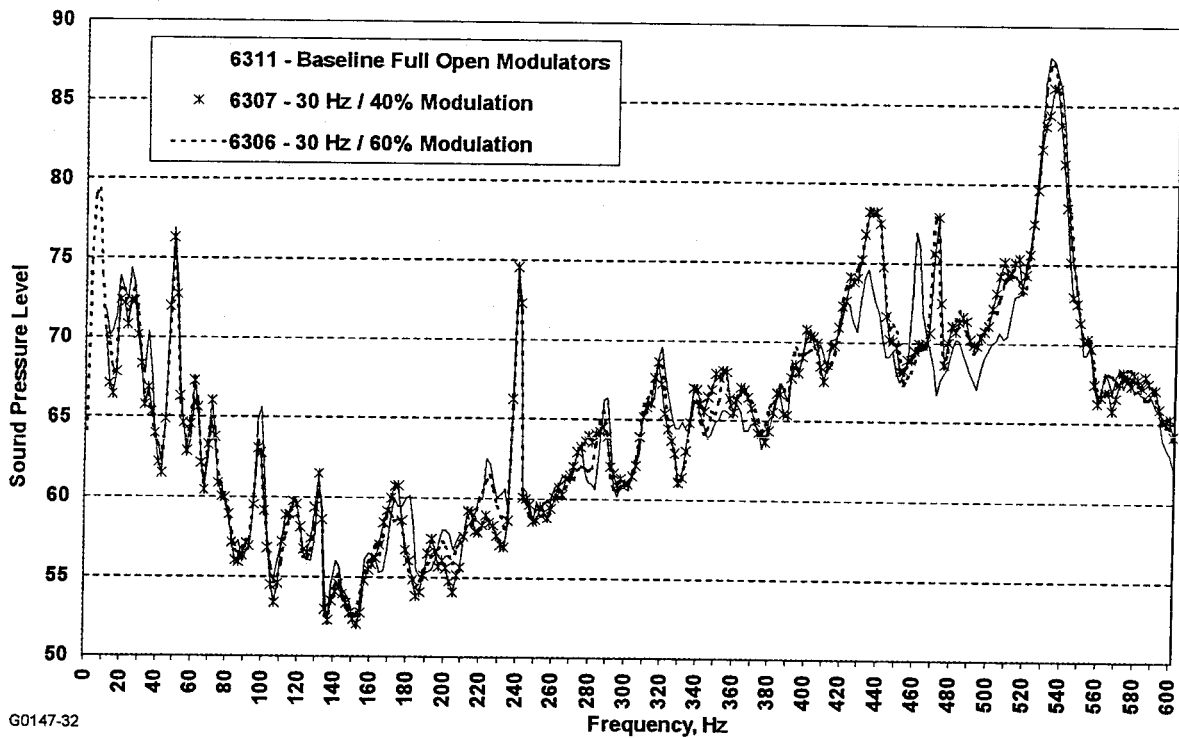


Figure 51. ACPFC Sound Pressure Levels (30 Hz Modulation Comparison).

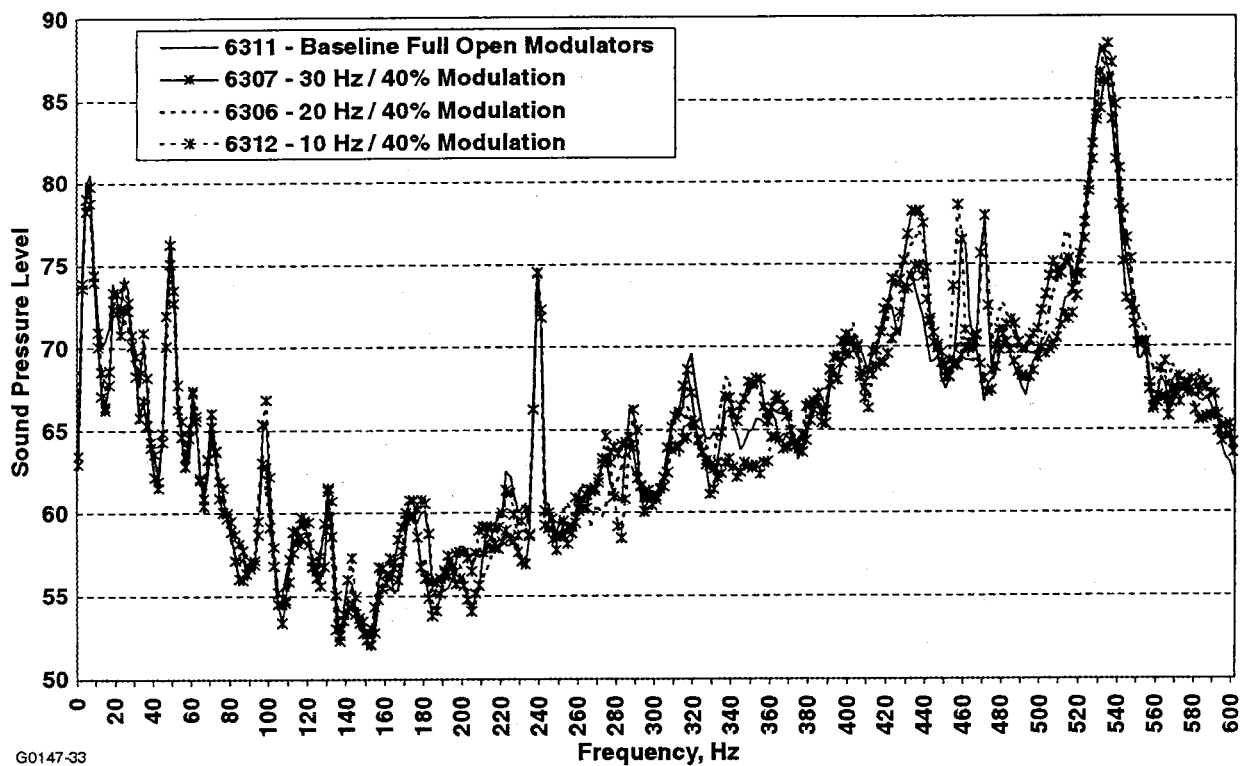


Figure 52. ACPFC Sound Pressure Levels (40 Percent Modulation Comparison).

It is known that premix combustors will resonate with the proper combination of equivalence ratio, air mass flow rate and hardware geometry. Although no resonances were measured for the conditions run during this test, it may still be possible to excite a resonance if any of the above parameters were changed.

No resonances were measured and it was concluded that pulse width modulation of the fuel delivery did not introduce any undesirable acoustic response.

Initiation of the **second test series** (using conventional thermocouples) revealed multiple failures in the modulator driver box supplied by Sturman. Each driver circuit has a board supplied by a 5 volt linear regulator. The boards have the drive transistors, a microcontroller, and the associated built-in test logic. Bench testing showed that many of the 5 volt regulators were not functional and consequently some of the microcontrollers had also failed. It is theorized that the system was subjected to an overvoltage event that occurred when water leaks from the rig were sprayed on the driver box and the lab power supply was subjected to multiple trips. The driver box was repaired and the linear regulator function replaced with a single 28 to 5 volt power supply to improve reliability. With this approach the individual built-in test circuits will not be masked by failure of the local power supply.

After repair of the driver box, testing of the Low Emissions Combustor resumed. Repairs that had been made to the driver circuit cards and fuel-flow modulators were successful and the control system worked as planned.

Two basic operating conditions were evaluated; idle (T3=344F, T4avg=1417F), and moderate power (T3=707F, T4avg=1890F). At each condition the system was operated "open loop" (no control) and then with the PID and Fuzzy control laws operating. Gains were adjusted in both control laws to minimize system "nervousness" as well as blade pattern factor.

The following table shows the preliminary data taken during the test:

| Condition | Control | T3 | P3 | Wf | T4avg | T4max | Pattern | %PF | NOX | %NOx | CO | UHC |
|-----------|---------|-------|-------|-----|-------|--------|---------|------|-------|------|-------|-------|
| | | deg F | psia | pph | deg F | deg F | Factor | Red. | ppm | Red. | ppm | ppm |
| Idle | none | 344 | 48.0 | 316 | 1417 | 1592 | 0.163 | - | 4.24 | - | 54.23 | 13.12 |
| Idle | fuzzy | 344 | 48.0 | 316 | 1417 | 1501 | 0.078 | 51.9 | 4.05 | 4.5 | 56.20 | 16.88 |
| Idle | PID | 337 | 48.0 | 316 | 1420 | 1513 | 0.086 | 47.0 | 3.93 | 7.3 | 58.01 | 23.35 |
| mod pwr | none | 708 | 145.0 | 808 | 1894 | 2015.2 | 0.102 | - | 14.38 | - | 1.97 | 0.13 |
| mod pwr | fuzzy | 707 | 145.0 | 807 | 1882 | 1952 | 0.059 | 42.5 | 14.19 | 1.3 | 2.13 | 0.21 |
| mod pwr | PID | 707 | 145.0 | 809 | 1897 | 1981 | 0.071 | 30.8 | 14.18 | 1.4 | 1.90 | 0.11 |

Following recording of the last data point, a bolt failed in the rig allowing the rake assembly and its seals to move rearward. This movement opened a large hole at the front of the rig to ambient, allowing rig pressure to escape. Minimal damage occurred; however, the rig would have to be partially disassembled to make repairs. It was decided to conclude the test at this point.

11. CONCLUSIONS

1. The control system clearly reduces pattern factor as measured by the single point thermocouples at the center of each turbine vane. Reductions in blade pattern factor of up to 52 percent were noted at idle and up to 43 percent at moderate power.
2. The PC control, electronic drivers and fuel-flow modulators operate as intended to directly control local vane temperature while providing the commanded total fuel flow to the combustor. The dynamics of the control system were well tolerated by the combustor and well within normal control system characteristics. Some additional thought should be given to programming fault accommodation for intermittent thermocouples. The present logic allows the controller to “chase” these momentary failures and ultimately slews the closest fuel actuator closed.
3. Reductions in NO_x were between 4 and 7 percent at idle and only 1.4 percent at moderate power with a corresponding increase in CO and UHC. This modest reduction in NO_x has been attributed to the burner configuration being a diffusion-flame system, and not a well-stirred system as analyzed by Jim May of NASA earlier in the program. In a diffusion flame, the mixture burns near stoichiometric at the interface of fuel and air. Moving the introduction of a constant-volume of fuel would, on average, produce the same emissions signature. Therefore, to see an emissions benefit, one would have to run the fuel controller with a better-mixed combustion system.

12. FURTHER DEVELOPMENT

1. With the present combustor, significant improvements in emissions cannot be demonstrated. Combustor inlet temperature could be lowered, to say 300 degF, and fuel flow raised to achieve the desired 1900 degF average blade temperature at the higher power condition. This would provide greater fuel flow and larger reductions in pattern factor may be demonstrated. Using fewer fuel modulators to control sector rather than vane temperatures could also be demonstrated. Different approaches to optimizing fuel staging could also be tested. The rig would need a modest amount of rework and, assuming the turbine nozzle is capable of additional use, this testing could be resumed in a short time.
2. The NASA AST program does have a combustor that has improved fuel-air mixing and is operated fuel-lean in the primary zone (referred to as the Fuel Preparation Chamber). Unfortunately this combustor is designed to fit in the AS907 engine/rig and not the AS900 TVT rig that is currently being used for the ACPFC. The AS907 program has no plans to install a turbine nozzle on the combustor rig, so to test the effectiveness of the controller on this well-mixed system, a modification to the rig would be required.
3. The ACPFC could be tested with a UEET combustor once it is available.

APPENDIX I
THIN-FILM SENSOR TEARDOWN REPORT
(17 pages)

APPENDIX I
NAS3-27752
THIN-FILM SENSOR TEARDOWN REPORT

1. SUMMARY

Nineteen AS900 stator segments were instrumented with thin-film type S thermocouples and run in the AS900 combustor rig as part of the active pattern factor control demonstration. A total of 25 stator segments were actually prepared and instrumented with thin-film thermocouples. Nineteen of these were then selected for assembly of the stator ring. The 38 sensors were connected to the control system which will pulse-width modulate the fuel flow to the combustor rig. Five of the 38 thin-film thermocouple sensors were replaced with conventional hardwire thermocouples, since the thin-film sensors were shorted to ground through the alumina dielectric. The processing history of each sensor at the onset of the test is documented in Table I-1 (reproduced from Progress Report No. 18). Failures were quickly detected during the test, leading to a posttest examination of the installation and investigation of the failure modes. The thin-film sensor installations were examined and improvements categorized into the following areas.:

- Splice and wire transition.
- Thin-film metal thermocouple elements, including delamination and bubbled metal films.
- Aluminum oxide thin-film dielectric.
- Overcoating.

As a result of the fabrication and testing experience gained in this project, recommendations are made for process improvements that will be implemented in thin-film sensor installations on future applications.

Table I-1. Stator Insulation Resistance and Processing History.

| Film Thermocouple Processing Status - 04/01/99 | | | | | | | | | | | | | | |
|--|---------------------------------|----------|-----------|----------|--------|---------------|-------------------|-----|------------|---------------|-----|-------------|--------------|----|
| Stator ID | Polish, RT278, Peen, Repolish | TGO | CVD Oxide | Platinum | Pt10Rh | Rground | Buildup weld pads | YSZ | Chromalloy | 3mil wire | MGO | Rgnd: final | Rloop: final | MN |
| | | | | | | | | | | processing NA | | | | |
| A1 | Y - processed 1998 @ Chromalloy | Y-Refrac | delam | Y | Y | >2Kohm short | Y | Y | | Y | Y | >20M | 53 | 1 |
| A2 | Y | Y | delam | Y | Y | >1Gohm | Y | Y | | Y | Y | >20M | 51 | 2 |
| B1 | Y | Y | N | Y | Y | >1Gohm | Y | Y | | Y | Y | >20M | 49 | 3 |
| B2 | Y | Y | N | Y | Y | >1Gohm | Y | Y | | Y | Y | >20M | 52 | 4 |
| C1 | Y | Y | delam | delam | Y | 100ohm short | Y | Y | | | | | | |
| C2 | Y | Y | delam | delam | Y | >14Kohm | Y | Y | | | | | | |
| D1 | Stator damaged by Chem Lab NG | | | NG | | | | | | | | | | |
| D2 | | | | NG | | | | | | | | | | |
| E1 | Y | Y | Y | Y | Y | >1Gohm | Y | Y | | Y | Y | >20M | 48 | 9 |
| E2 | Y | Y | Y | Y | Y | >1Gohm | Y | Y | | Y | Y | >20M | 59 | 10 |
| F1 | Y | Y | delam | NG | | | | | | | | | | |
| F2 | Y | Y | delam | NG | | | | | | | | | | |
| G1 | Y | Y | delam | Y | Y | 100ohms short | Y | Y | | Y | Y | 1K | 51 | 13 |
| G2 | Y | Y | delam | Y | Y | >1Gohm | Y | Y | | Y | Y | >20M | 50 | 14 |
| H1 | Y | Y | N | Y | Y | >12Mohm | Y | Y | | Y | Y | >20M | 50 | 15 |
| H2 | Y | Y | N | Y | Y | >30Mohm | Y | Y | | Y | Y | >20M | 52 | 16 |
| J1 | Y | Y | N | Y | Y | >20Mohm | Y | Y | | Y | Y | >20M | 51 | 17 |
| J2 | Y | Y | N | Y | Y | >20Mohm | Y | Y | | Y | Y | 1K | 56 | 18 |
| K1 | Y | Y | Y | Y | Y | >1Gohm | Y | Y | | Y | Y | >20M | 51 | 19 |
| K2 | Y | Y | Y | Y | Y | >1Gohm | Y | Y | | Y | Y | >20M | 50 | 20 |
| L1 | Y | Y | N | Y | Y | >300Kohm | Y | Y | | Y | Y | >20M | 32 | 21 |
| L2 | Y | Y | N | Y | Y | >20Mohm | Y | Y | | Y | Y | >20M | 27 | 22 |
| M1 | Y | Y | delam | Y | Y | >20Mohm | Y | Y | | Y | Y | >20M | 50 | 23 |
| M2 | Y | Y | delam | Y | Y | >20Mohm | Y | Y | | Y | Y | >20M | 49 | 24 |
| N1 | Y | Y | Y | Y | Y | >1Gohm | Y | Y | | Y | Y | >20M | 51 | 25 |
| N2 | Y | Y | Y | Y | Y | >800 Mohm | Y | Y | | Y | Y | >20M | 50 | 26 |
| O1 | Y | Y | delam | Y | Y | >200Kohm | Y | Y | | Y | Y | >20M | 65 | 27 |
| O2 | Y | Y | delam | Y | Y | >1Gohm | Y | Y | | Y | Y | >20M | 58 | 28 |
| P1 | Y | Y | delam | Y | Y | >1Gohm | Y | Y | | Y | Y | >20M | 50 | 29 |
| P2 | Y | Y | delam | Y | Y | >200Kohm | Y | Y | | Y | Y | >20M | 54 | 30 |
| Q1 | Y | Y | N | Y | delam | >25Mohm | Y | Y | | | | | | |
| Q2 | Y | Y | N | Y | delam | >1Gohm | Y | Y | | | | | | |
| R1 | Y | Y | Y | Y | Y | >1Gohm | Y | Y | | Y | Y | >20M | 47 | 33 |
| R2 | Y | Y | Y | Y | Y | >1Gohm | Y | Y | | Y | Y | >20M | 50 | 34 |
| S1 | Y | Y | delam | NG | | | | | | | | | | |
| S2 | Y | Y | delam | NG | | | | | | | | | | |
| T1 | Y | Y | delam | Y | NG | | | | | | | | | |
| T2 | Y | Y | delam | Y | NG | | | | | | | | | |
| U1 | Y - processed 1999 @ Chromalloy | YRefrac | N | Y | Y | >1Gohm | Y | Y | | Y | Y | >20M | 51 | 5 |
| U2 | Y | Y | N | Y | Y | >700Mohm | Y | Y | | Y | Y | >20M | 50 | 6 |
| V1 | Y | Y | N | Y | Y | >1Gohm | Y | Y | | Y | Y | >20M | 26 | 7 |
| V2 | Y | Y | N | Y | Y | >1Gohm | Y | Y | | Y | Y | >20M | 44 | 8 |
| W1 | Y | Y | N | Y | Y | >500Mohm | Y | Y | | Y | Y | 1K | 54 | 11 |
| W2 | Y | Y | N | Y | Y | >500Mohm | Y | Y | | Y | Y | >20M | 49 | 12 |
| X1 | Y | Y116 | N | Y | Y | >1Gohm | Y | Y | | Y | Y | >20M | 53 | 31 |
| X2 | Y | Y116 | N | Y | Y | >1Gohm | Y | Y | | Y | Y | >20M | 64 | 32 |
| Y1 | Y | Y | N | Y | Y | >1Gohm | Y | Y | | Y | Y | 1K | 49 | 35 |
| Y2 | Y | Y | N | Y | Y | >1Gohm | Y | Y | | Y | Y | 1K | 50 | 36 |
| Z1 | Y | Y | N | Y | Y | >1Gohm | Y | Y | | Y | Y | >20M | 50 | 37 |
| Z2 | Y | Y | N | Y | Y | >1Gohm | Y | Y | | Y | Y | >20M | 49 | 38 |
| NOTES | | | | | | | | | | | | | | |
| Summary | | | | | | | | | | | | | | |
| TGO - thermal grown oxide | | | | | | | | | | | | | | |
| CVD - chemical vapor deposition | | | | | | | | | | | | | | |
| Designation notes two separate airfoils on one stator eg: A1, A2 | | | | | | | | | | | | | | |
| 19 compl with wiring and ready for assembly | | | | | | | | | | | | | | |
| ASSEMBLY SEQUENCE: A,B,U,V,E,W,G,H,J,K,L,M,N,O,P,X,R,Y,Z | | | | | | | | | | | | | | |
| TGO Only [10] | | | | | | | | | | | | | | |
| TGO and good CVD [4] | | | | | | | | | | | | | | |
| Delam CVD [5] | | | | | | | | | | | | | | |

2. FABRICATION METHODS

Initial work on the program focused on process development using Hastelloy X flat bar stock to develop the methodology and processing techniques. To prove the sensor durability in a burner rig, several bars were subjected to temperature cycles from ambient to 1600F to simulate engine operational conditions. Durability and tracking of the bar sensors with respect to a reference thermocouple was acceptable and indicated a robust sensor fabrication process. The results of the bar tests were documented in the bimonthly status reports. In addition, the University of Rhode Island was funded to conduct base technology development and determine specific processing and material science issues. The evaluations included thermocouple combinations, thermocouple drift, dielectric thermal cycle evaluation, material chemistry, and overcoating technology. A master's thesis has been published by the University of Rhode Island (URI) documenting their efforts. Scanning Electron Microscopy (SEM) evaluations conducted at AlliedSignal Engines & Systems concluded that the thermally grown oxide (TGO) was 1.5 to 2.5 microns thick. X-ray diffraction (XRD) work at URI identified the alumina as primarily alpha phase. However, there was some concern that defects noted in the aluminum oxide micrographs could short circuit the sensor to ground. As a result, the work at Iowa State University (ISU) from the Small Engine Technology (SET) program was continued in the AST project to include chemical vapor deposition (CVD) as an enhancement on the thermally grown oxide surfaces. Sample stators were provided for this process development at ISU.

The general processing technique used can be outlined as follows:

1. Modification of hardware to allow for thin-film sensor transition to the flange.
2. Polish to 1 micron finish.
3. Application of 4 mils of RT270 NiCoCrAlY and peening at Chromalloy.
4. Repolish to 1 micron finish.
5. Oxidation in controlled environment to form alpha alumina dielectric.
6. Process a select group of stators using chemical vapor deposition (CVD) to enhance the aluminum oxide, supported by the work at Iowa State University in process development.
7. Use of resist, tape, and aluminum foil to define sensor geometry.
8. Sputter platinum, remasking, and sputter platinum 10% rhodium.
9. Remask and increase metal weld pad thickness; platinum and platinum 10% rhodium.
10. Heat treat at 700C.
11. Weld 3 mil extension wires to films.
12. Overcoat sputtered sensors with yttria stabilized zirconia.
13. Attach 0.020 diameter Magnesium Oxide (MgO) hardware.
14. Pot splices with aluminum oxide ceramic cement.

As noted previously, defects were noted in some of the thermally grown oxide (TGO) on the Hastelloy X bar samples used in the process development. It was then decided to complete the development of the chemical vapor deposition (CVD) technique to enhance the TGO dielectric quality at ISU and to use it on at least part of the rig stator set. Critical to the deposition of good CVD alumina is the control of the growth rate and uniformity. After the CVD processing, it was noted that some of the airfoils were "compromised" with highly stressed chemical vapor deposited alumina, as there were spots spalling off when the temperature was returned to ambient. A tumbler with a soft abrasive was used in a cleaning process to remove the CVD alumina and return to the thermal oxide layer. However, not all the CVD oxide was removed: adherence problems were noted and shorting to ground experienced on these reworked stators during deposition of the platinum and/or platinum-10% rhodium. Therefore, the processing was modified to include more extensive cleaning in an attempt to deal with spalling of the CVD alumina. The photofabrication process and deposition sequence was also changed to reduce resist contamination of the alumina, relieve residual film stresses, and improve the metal film adherence. A tape and aluminum foil physical mask proved to be the best solution to the photoresist contamination that was experienced.

Our thin-film process produced a 15,000 to 20,000Å sensor film across the airfoil and then a weld pad built to 30,000 to 35,000Å, required for the 3 mil wire transition. After deposition of the metal films and build up of the weldpads, the sensor was checked for insulation resistance. The parts were then cycled overnight to 700°C to condition the metal films, cleaned, and physically masked for the deposition of an yttria stabilized zirconia (YSZ) overcoating. After being ozoned, a 3-4 micron (µm) protective overcoat of YSZ was sputtered onto the airfoils. Table I-1 also details the final measurements and specifications of the processing on an individual stator basis. The final set of 19 stators sent out for test consisted of ten stators with TGO only, four with TGO and CVD alumina, and five with TGO and "delaminating" CVD.

The delamination of the CVD oxide from the TGO was attributed to an excessively high aluminum oxide growth rate in the CVD reactor at ISU, caused by lack of control of the aluminum propoxide precursor and heated flow distribution in the cold wall reactor. A softer columnar alumina is produced which created problems in the sensor photofabrication as the resist was absorbed into the oxide. Small amounts of resist impede the metal adherence. Thus one of the primary problems experienced during fabrication was the spalling of the CVD aluminum oxide applied at ISU.

After process modifications and rework of the CVD alumina, several of the stators required a 700°C bake, cleaning, and depositions to reapply or repair the platinum and platinum 10% rhodium films. After metal depositions, 0.020-inch diameter MgO insulated hardwire leads were installed onto the flange and a transition using 3 mil leads made from the film to the conductors in the MgO. Resistance welds were used to attach the 3 mil wire to the platinum and platinum rhodium weld pads. Once welded, WC16, a high-purity aluminum oxide ceramic cement was used to cover and protect the splice transitions. The YSZ overcoat was sputtered in three batches in the MRC903 only. As noted, the six backup stators were processed with TGO only. These proved to have good alumina and were included in the completed hardware set for the test. The six backups used were polished, coated with RT270, repolished, and then the TGO only was

processed at Refrac Systems. The thermocouples sputtered on these stators were good and the films survived the test intact as shown in the photos.

Two of the stators with TGO were sent to the University of California at Santa Barbara to Dr. David Clarke who is developing a new process to identify alpha phase aluminum oxide using a laser and interrogating the reflected spectra. The bulk of the evaluations using glancing angle xray diffraction [XRD] to identify phase type and percentage of composition. This was done on the both the TGO and CVD samples at the University of Rhode Island. Thus we were able to quantify phase percentages in which multiphase alumina is quite common. Energy dispersive xray [EDX] was also used to verify thin-film metal film composition constituents on sample sensors prior to the actual engine hardware.

3. TEST AND TEARDOWN

Results from the test showed delamination of the splice potting with failures in the wire transition (see Figures *I-4, I-5, I-8, I-9, I-12, and I-13), delamination and bubbles in the metal thermocouple elements (see Figures I-6 and I-7), and further delamination and failures in the CVD dielectric (see Figures I-2 and I-3).

The most extensive damage was noted at the splice location. It appears that airflow through the transition slot (flow over the film to 3 mil wire to MgO splices), and the thermal coefficient of expansion (TCE) mismatch in the metal to aluminum oxide to WC16 cement system caused the potting to lift off the surface and fail the thin-film to wire welds. The damage to the splices can be readily seen, due to the TCE induced splice stress and high velocity flow. The cement separation from the TGO caused the 3 mil wires to break; note that pieces of the cement are missing, and also lifting off the surface.

3.1 Splices and Wire Transition

- 3 of 38 splices good
- 6 of 38 splices exhibited stress cracks but were intact
- 29 of 38 splices were delaminated, splices broken, or the pieces of the cement missing

Only 9 of 38 splices were electrically continuous and intact.

3.2 Metal Thin-film Thermocouple Elements

Metal thin-film inspection only (includes grounded thermocouples)

- 11 of 38 had good films; no bubbling or spot delamination.
- 12 of 38 had spot delaminations of the films; film is electrically continuous.
- 6 of 38 had bubbled films.
- 9 of 38 were open - fracture or delamination.

29 of 38 thin-film sensors were electrically continuous.

3.3 Aluminum Oxide Thin-film Dielectric

- 21 of 38 were good: ungrounded.
- 8 of 38 grounded.
- 9 of 38 with CVD aluminum oxide delamination under the metal films.

21 of 38 thin-film sensors were electrically isolated from substrate.

3.4 Overcoating

- 17 of 38 had complete overcoat with no damage.
- 21 of 38 had spot delamination of the YSZ, along with the metal film and alumina delaminations noted above.

38 of 38 sensors overcoating survived test.

It was noted that the thin-film thermocouples on the six spare stator segments, which were processed as a second batch with TGO, fared better than the first set, processed as a mix of TGO and CVD aluminum oxide. Out of the 12 thermocouples on the second set of 6 stators, all 12 had loop continuity and 7 of 12 had good isolation from ground after testing. Since 3 of 12 were grounded before the test, 7 of the 9 films from the second processing batch were good through test. Stator U (Thermocouples No. 5 and No. 6) looked the best with little change other than some change in the YSZ overcoat appearance and the splice problem on No. 6 (see composite photo, Figure I-1). 29 of the 38 metal films were continuous with little or no visible change (see Figures I-10, I-11, I-14, and I-15].

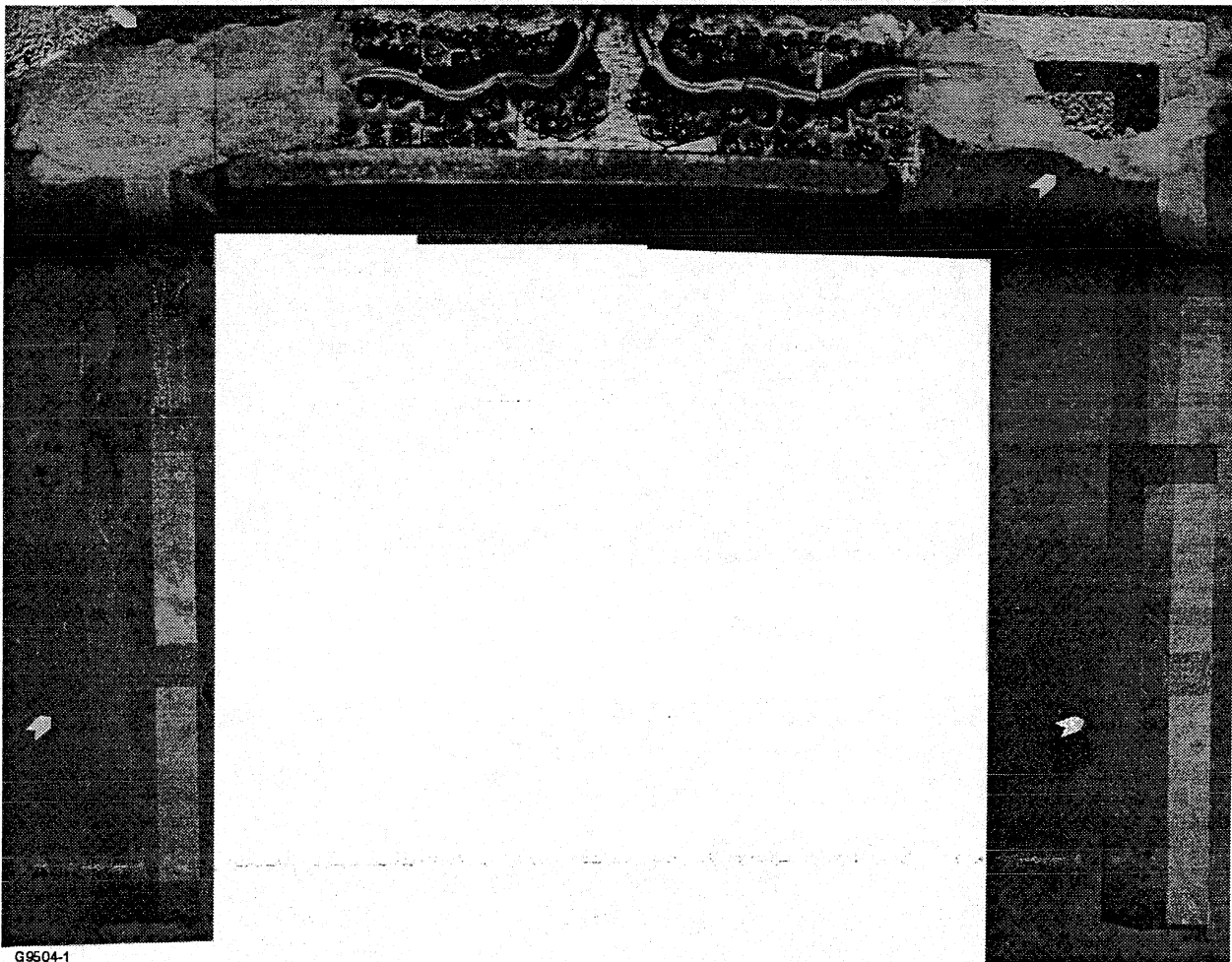


Figure I-1. Thermocouples No. 5 and No. 6, Composite Photo.

The metal film thermocouple elements are intact and overcoat is complete. Note the splice damage on Thermocouple No. 6, while the Thermocouple No. 5 splice is intact.

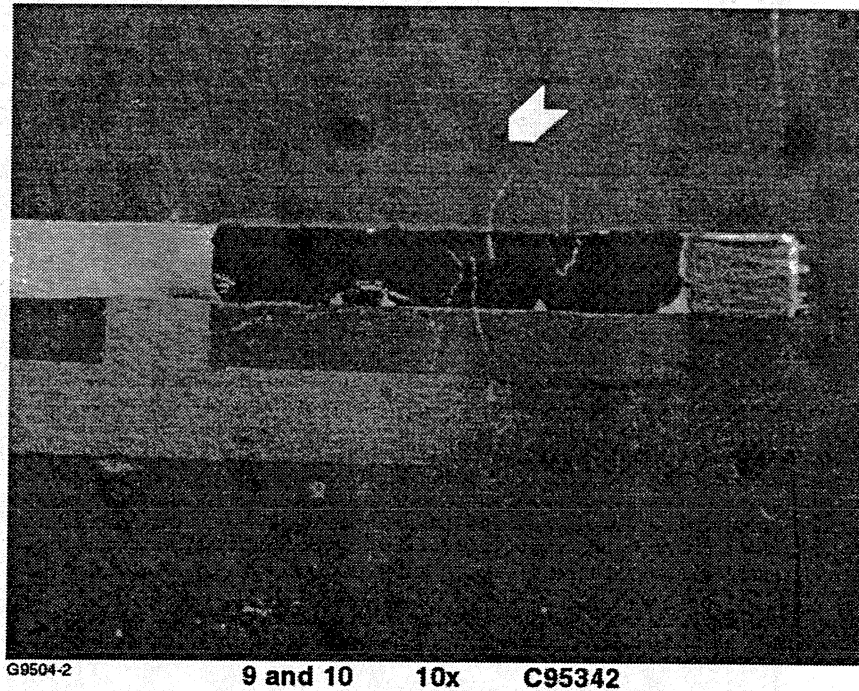


Figure I-2. Thermocouple No. 9.

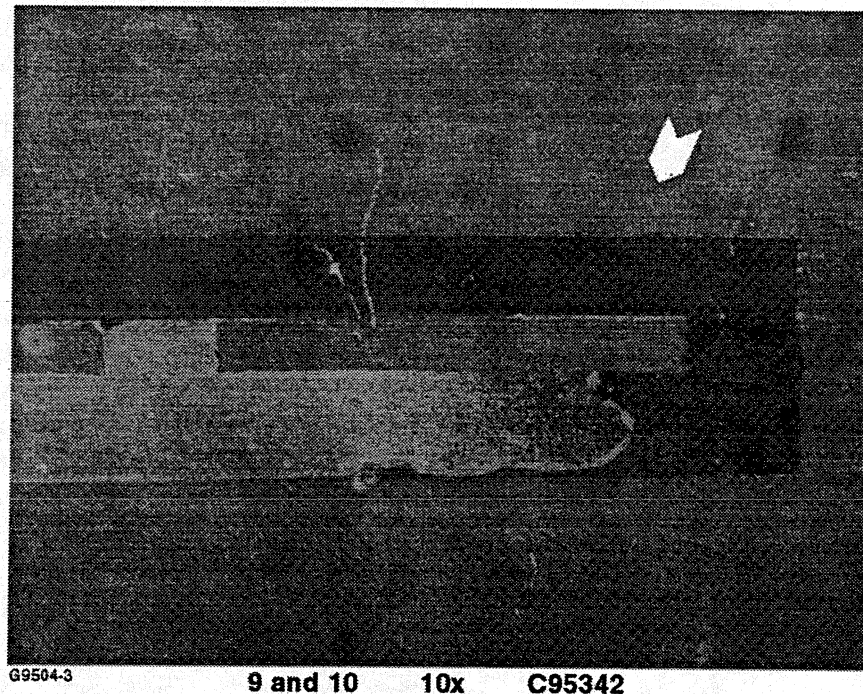


Figure I-3. Thermocouple No. 10.

Figures I-2 and I-3 – Thermocouples No. 9 and No. 10. Delamination of the CVD alumina off the thermally grown alumina failed the metal films.

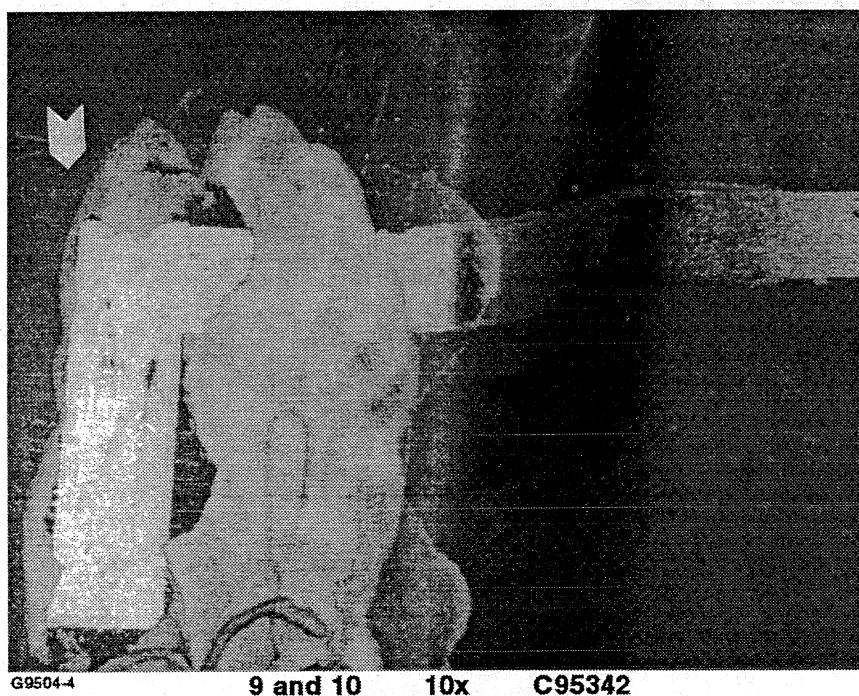


Figure I-4. Thermocouple No. 10.

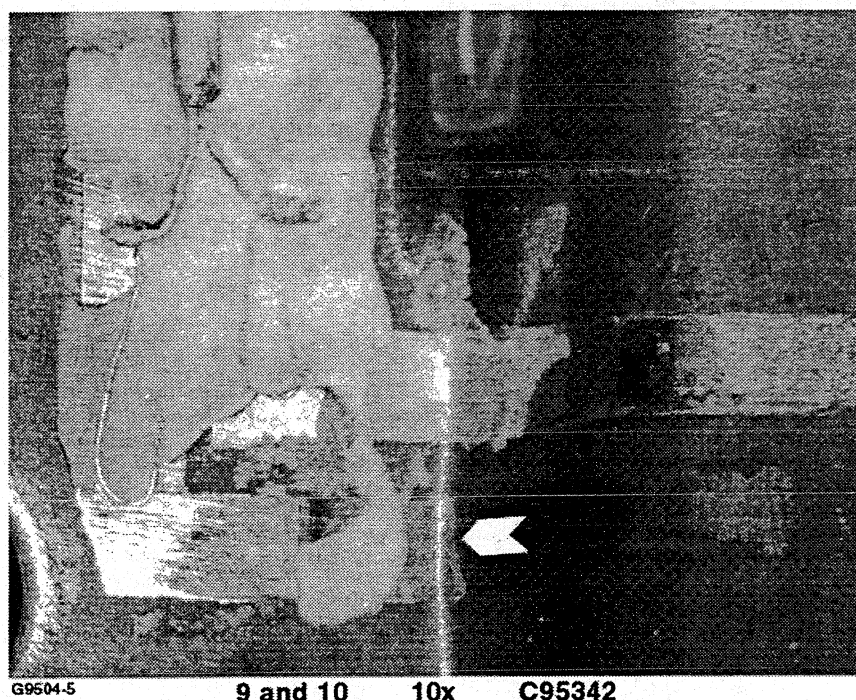
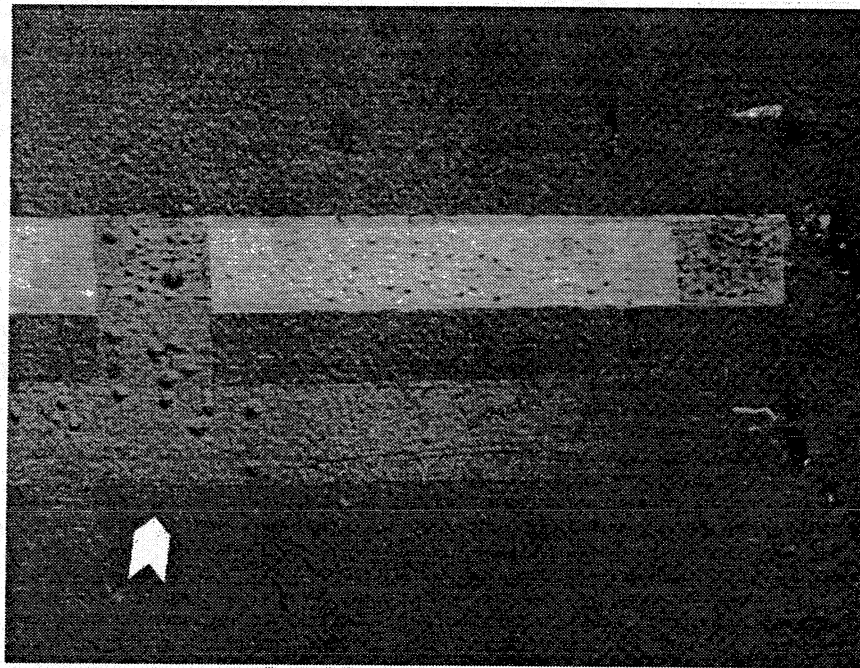


Figure I-5. Thermocouple No. 9.

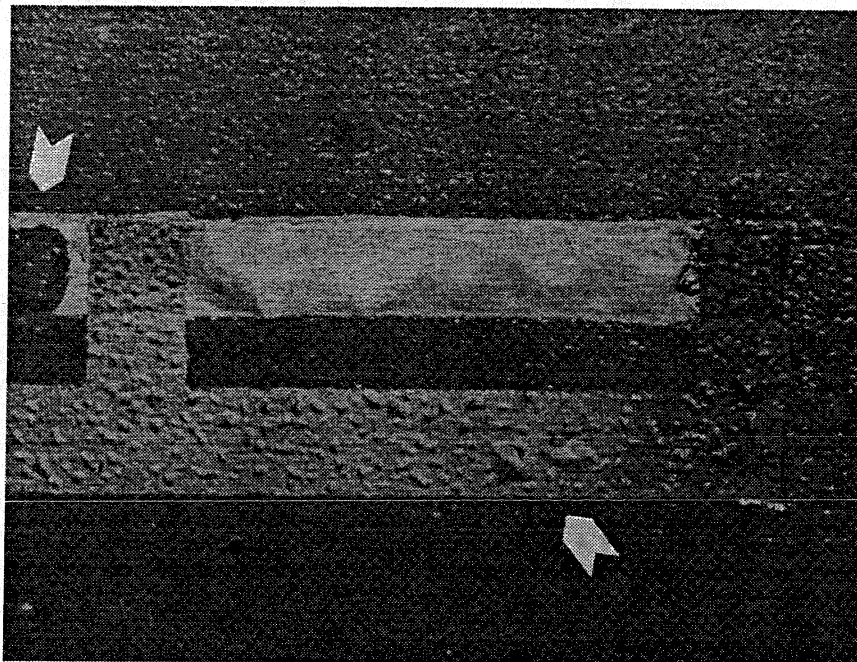
Figures I-4 and I-5 – Thermocouples No. 9 and No. 10. Splice potting delaminations and broken 3 mil wire to film transition.



G9504-6

3 and 4 10x C95342

Figure I-6. Thermocouple No. 3.



G9504-7

3 and 4 10x C95342

Figure I-7. Thermocouple No. 4.

Figures I-6 and I-7 – Thermocouples No. 3 and No. 4. Bubbles noted in films. In Figure I-7, note delamination of metal film off the thermally grown oxide.



G9504-8

3 and 4

10x

C95342

Figure I-8. Thermocouple No. 3.



G9504-9

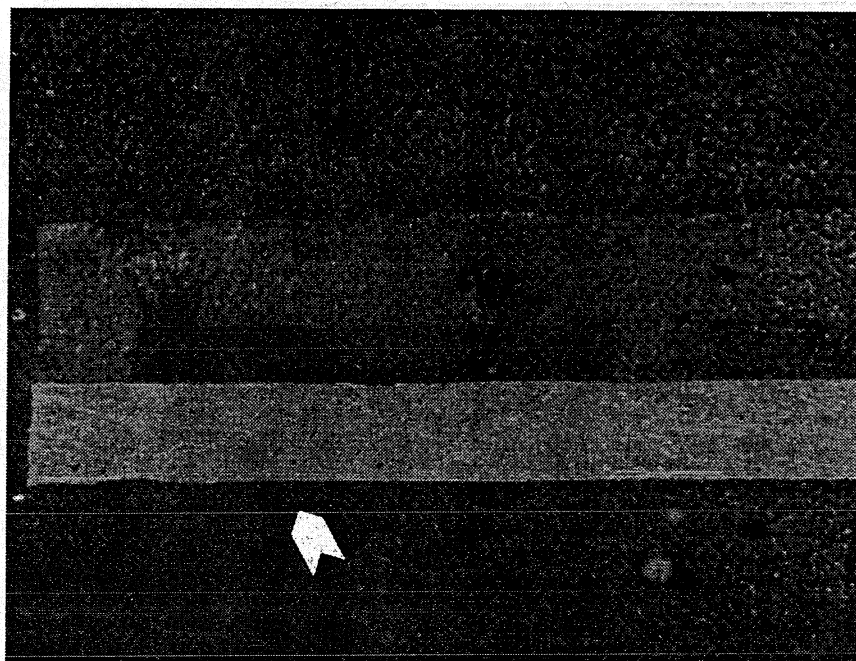
3 and 4

10x

C95342

Figure I-9. Thermocouple No. 4.

Figures I-8 and I-9 – Thermocouples No. 3 and No. 4. Splice potting delamination and broken 3 mil wire to film transitions.



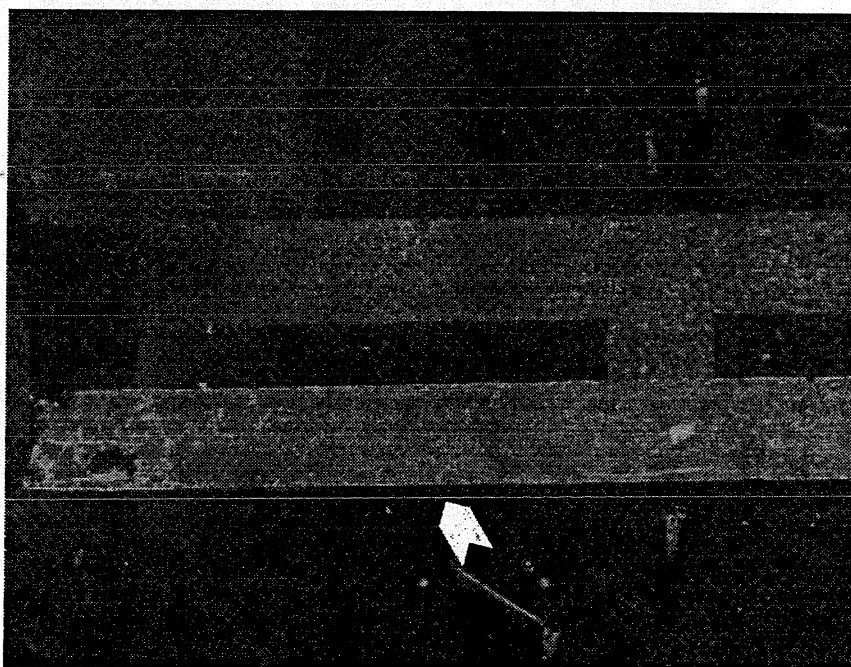
G9504-10

7 and 8

10x

C95342

Figure I-10. Thermocouple No. 7.



G9504-11

7 and 8

10x

C95342

Figure I-11. Thermocouple No. 8.

Figures I-10 and I-11 – Thermocouples No. 7 and No. 8. The metal film thermocouple elements are intact with small bubbles.



G9504-12

7 and 8

10x

C95342

Figure I-12. Thermocouple No. 7.



G9504-13

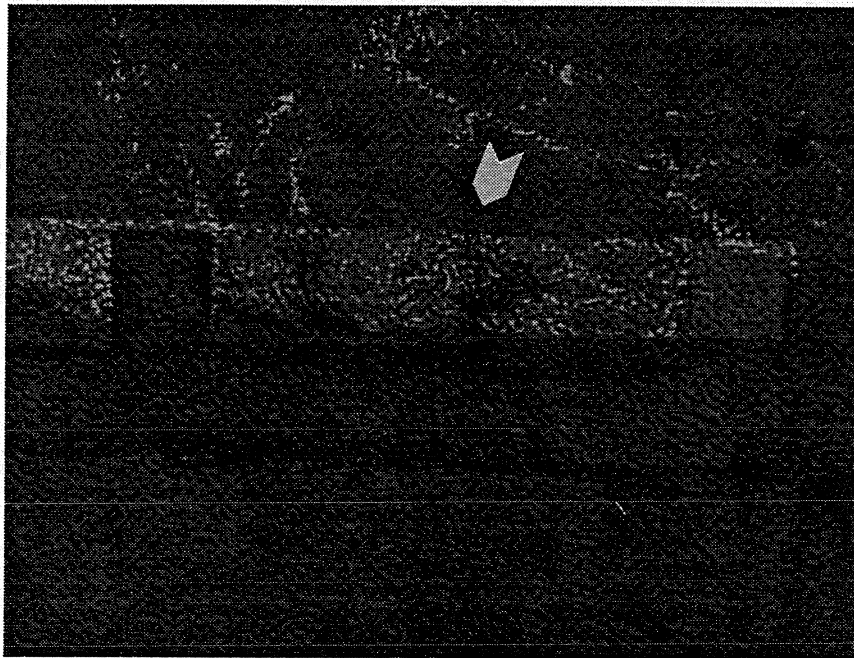
7 and 8

10x

C95342

Figure I-13. Thermocouple No. 8.

Figures I-12 and I-13 – Thermocouples No. 7 and No. 8. Splices delaminated with broken 3 mil wire to film transition.



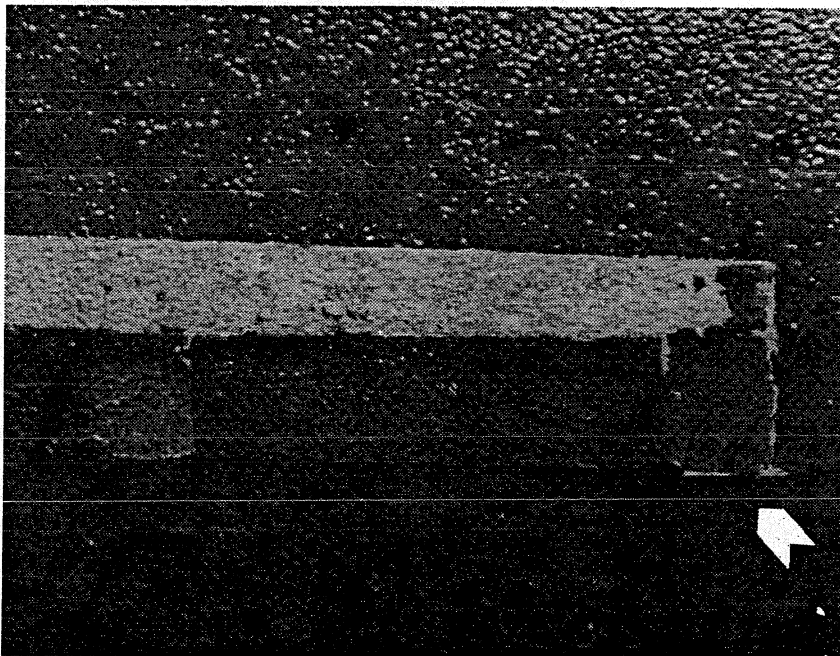
G9504-14

37 and 38

10x

C95342

Figure I-14. Thermocouple No. 37.



G9504-15

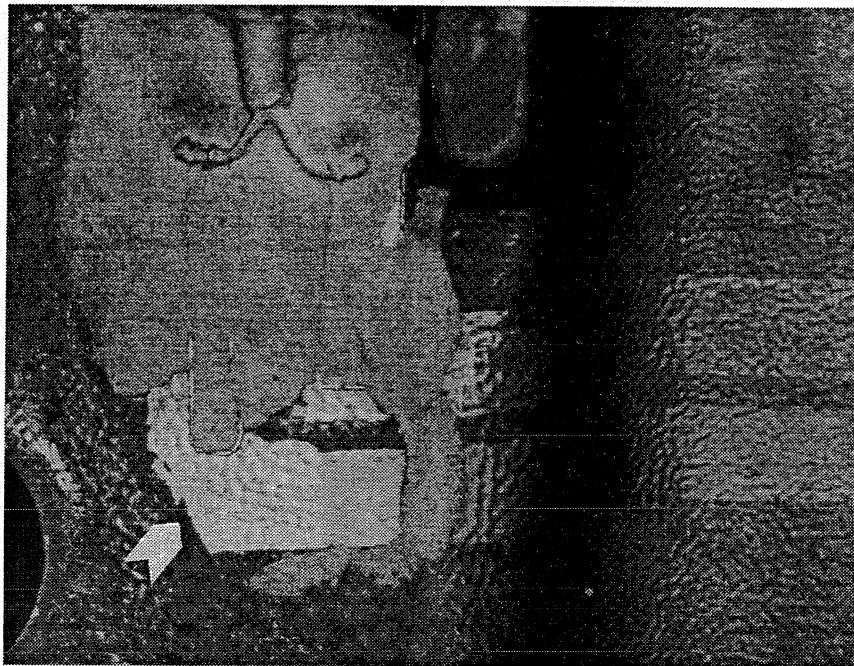
37 and 38

10x

C95342

Figure I-15. Thermocouple No. 38.

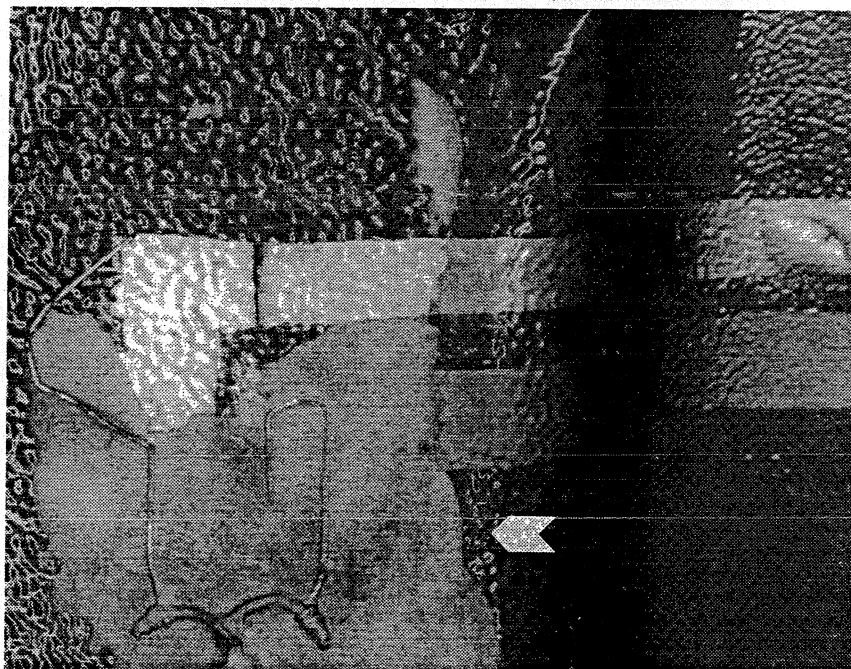
Figures I-14 and I-15 – Thermocouples No. 37 and No. 38. The metal film thermocouple elements are intact. Note the aluminum oxide finish underneath; also some overcoat missing from Thermocouple No. 38.



G9504-16

37 and 38 10x C95342

Figure I-16. Thermocouple No. 37.



G9504-17

37 and 38 10x C95342

Figure I-17. Thermocouple No. 38.

Figures I-16 and I-17 – Thermocouples No. 37 and No. 38.
Thermocouple No. 37 – 3 mil wire splices are intact; part of the potting has delaminated.
Thermocouple No. 38 – Partial delamination and weld break.

4. LESSONS LEARNED AND RECOMMENDED PROCESS CHANGES

Sensor fabrication and process improvements can be categorized into four specific areas. These are: dielectric processing, masking and metallization techniques, wire transition splicing and potting, and overcoating.

4.1 Dielectric Processing

The aluminum oxide dielectric provides us with the biggest opportunity for process improvement, where electrical insulation and adherence is the key to sensor quality and longevity. The thermocouples on the stators with only TGO appear to be intact with very adherent thin films, as well as being dielectrically isolated. Consistent replication of the thermal growth processing is critical. In contrast, the delamination of the CVD alumina was extensive and compromised good sensor basecoats. It appears that the CVD to TGO bond is weak, even weaker than the metal to CVD, as evidenced in the Figures I-6 and I-7. The XRD work at the University of Rhode Island of the CVD concluded that the alumina was primarily alpha phase, with some small gamma side peaks. The CVD aluminum oxide was good on structure, but poor on adherence and process film growth control. Note that the delamination of the CVD alumina occurred at the TGO to CVD interface, thus indicating that any further CVD work would require some type of interface surface preparation to increase adherence. Although the adherence to the thermal alumina appears to be the primary culprit, the growth rate of the CVD alumina also was not well defined and controlled, and resulted in a soft unstable structure.

Further CVD development will require improved process control and evaluation methods to improve the TGO to CVD film adherence. Because of the success with the second batch of backup stators as previously noted, an internal Green Belt team at AlliedSignal is currently focused on optimizing the thermally grown aluminum oxide processing. This is an opportunity to identify key process parameters and replicate results in the thermal oxide. A series of experiments has been set up to sort these critical parameters and lock in the best process methods. The balance of the backup stator set is currently being used for these experiments. The results should be available in November 1999.

4.2 Splicing

The film to hardwire transition and potting of this area proved to be the primary sensor failure mode. The thermal coefficient of expansion (TCE) mismatch between the parent metal, the aluminum oxide, the metal film, and the potting compound creates a structure that is susceptible to both high velocity and high temperature air gradients. The splice location on the stator segments was at the outside diameter of the airfoil and the access slot allowed flowpath air to course over the installation. A protective metal shim over the splice pad would increase the coverage of the cement. Note that the high velocity air flow over the installation works at the interface to the surface and combined with thermal stresses then lifts off the potting compound thus fracturing the wire to film bond (see Figures I-4, I-5, I-8, I-9, I-12, and I-13). Selection of a potting compound requires electrical stability through the expected operating range to minimize noise as well as that the TCE would match the hardware. Most nickel alloy substrates are 10 to 12 ppm/C and the aluminum oxide as well as the aluminum oxide cement is 4 to 6 ppm/C creating the interface stresses. Hitec Products suggested the use of a new NCC3 ceramic cement

which better matches a nickel alloy TCE yet contain little chrome oxide. Chrome oxide is quite common in other potting compounds, but breaks down dielectrically above 1800F. A second issue will be to use wedgewire bonding of the 3 mil wires to the films instead of resistance welding. This is a proven technique in the semiconductor industry and allows for a thinner weld pad profile and more repeatable welds.

4.3 Metal Films

Resist contamination of both the TGO and CVD aluminum oxide was experienced during the course of this project. Masking techniques need to be standardized and the use of physical methods is preferred over resist. Ultimately, a reusable electro-discharge machine (EDM) physical mask could be designed and fabricated that would eliminate the use of resist or tape, and thus contamination would not be an issue. Currently tape provides a very convenient masking technique, when supplemented with aluminum foil, as long as there is no heat buildup to cause outgassing of the adhesive onto the films. Physical masks in general provide a quicker means of creating the thermocouple pattern and remove any possibility of residual resist contamination in the CVD or TGO. Film stresses can be reduced by keeping all the metal film depositions to less than 15,000Å on both the airfoil and at the weld pads. In addition, the duration of heat treat could be increased to enable the removal of any trapped gases remaining from the sputtering process, which can be noted in the photos of film bubbling (see Figures I-6, I-7, I-10, and I-11).

Typically, a 30,000Å thick film is employed primarily to facilitate the attachment of the 3 mil wire to a weld pad. AlliedSignal Engines & Systems has been investigating wedge wirebonding techniques which are common in the semiconductor industry and used on precious metals. There are two advantages to the use of wedge bonding. First, it is very well controlled and repeatable, allowing weld to a film as thin as 1,000Å. 3 mil wire can easily be bonded ultrasonically to a 5,000Å to 10,000Å platinum or platinum rhodium film. This has been proven to result in good wire to film bond strength and will reduce film thickness, film stress, and process time, as well as precious metal cost.

4.4 Overcoating

Little damage was seen in the yttria stabilized zirconia (YSZ) overcoating. Some spot delamination can be attributed to the delamination of the metal or aluminum oxide underneath (see Figure I-15]. However, the long term durability of the YSZ overcoat is yet to be evaluated. It is planned that the sputtered YSZ would be coated with a thicker layer of YSZ at Chromalloy, similar to thermal barrier coatings common to turbine airfoils. This would allow for better long-term protection from environmental damage.

APPENDIX II

DEMONSTRATION OF A FUEL FLOW MODULATOR USING AN ADVANCED LATCHING MAGNETIC ACTUATOR

**AlliedSignal Ref. # PSC21-9246
Sturman Industries Report MPR.00001.01**

(39 pages)

Demonstration of a Fuel Flow Modulator Using an Advanced Latching Magnetic Actuator

FINAL REPORT

**AlliedSignal Ref # PSC21-9246
Sturman Industries Report MPR.00001.01**

November 12, 1998

Submitted to:

**AlliedSignal Aerospace
111 S. 34TH Street
Phoenix, AZ 85072-2180**

Submitted by:

**Sturman Industries
One Innovation Way
Woodland Park, CO 80863**

EXECUTIVE SUMMARY

This report is being submitted as per the requirements of Allied Signal Program 21-9246 and Sturman Industries proposal "Demonstration of a fuel flow modulator using an advanced latching magnetic actuator" dated November 5, 1996.

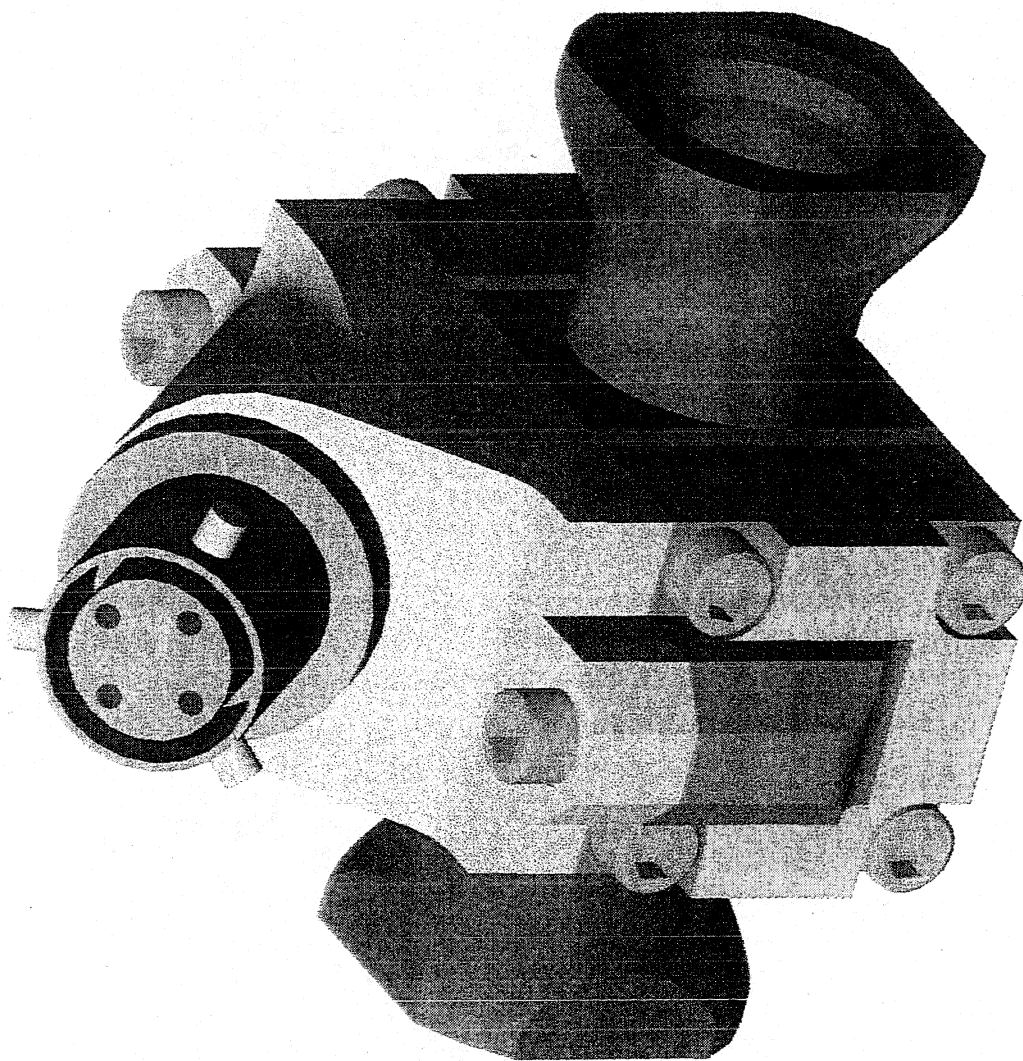
The program has been successfully completed and the hardware delivered to AlliedSignal for testing. This report summarizes project issues and provides detailed test data on the each fuel flow modulator.

The goal of the program was to supply one Fuel Flow Modulator (FFM) for the Pattern Factor Control Program that could meet the requirements of both the test bench portion of the program, 30 pounds per hour, and the full scale conditions at NASA, 100 pounds per hour. The challenge was to provide the dynamic range required for both requirements in one package. This goal has been fully achieved.

The design of the FFM allows it to meet and exceed the performance specifications as listed in the original RFP and yet it is an extremely simple design. Frequency response, flow range, overall pressure drop, linearity and gain, and hysteresis specifications have all been exceeded. And yet the design incorporates only one moving part weighing 4 grams. The total weight of the FFM is only 140 grams.

The FFM as delivered will work well for development and testing efforts. It is the opinion of Sturman Industries that after the initial evaluation, a second generation FFM be considered. There are several improvements to the current design that should be considered and with Quality Function Deployment considerations, and possibly a design FMEA conducted jointly between Sturman Industries and AlliedSignal, significant functional improvements could result.

Sturman Industries will continue to support AlliedSignal in the testing effort and looks forward to a successful program conclusion. The contact person at Sturman is Peter Petersen: (719) 686-6014



Fuel Flow Modulation Valve
Figure 1

TECHNICAL OVERVIEW

Sturman Industries has pioneered the use of digital latching valve technology for applications ranging from satellite thrusters, to diesel fuel injectors, to lawn sprinklers. The potential of the technology is such that it can positively impact the performance of any industry currently using conventional valve systems. One arena showing great promise of improvement is that of proportional valves. The digital valve, through its characteristic rapid response, can provide analog output with no hysteresis, at a fraction of the cost, complexity, and weight of an analog servovalve.

The main effort for this program was to apply Sturman Industries digital valve technology to the Fuel Flow Modulator concept. The valve is a simple two way spool valve that provides linear flow versus duty cycle when controlled with pulse width modulation.

An Introduction to Magnetic Latching Valves

The key to the development and operation of fully digital, magnetic-latching valves is residual magnetism. Residual magnetism is a small, permanent magnetic force that remains in a material after the primary magnetizing field is removed. For years, solenoid and valve manufacturers have been fighting residual magnetism because it degrades performance in a manner similar to that of mechanical friction or hysteresis. A wide range of materials and heat treating techniques have been used to minimize the effects with little success. New and exotic materials have also been developed to address the problem but have yielded only partial, and expensive, success.

Rather than working to eliminate it, engineers at Sturman Industries believe that residual magnetism, if properly understood, can enhance the performance of a valve. If enough residual magnetism can be retained, a stable state will exist and, thus, eliminate the need to use energy to hold the valve in the open or closed position. Conventional valves require energy to hold the valve open and since no work is being done, the energy is wasted and dissipated as heat. Subsequently, larger devices are required to prevent overheating which, in turn, equates to slower response. If a purely scientific look is taken as to the mechanical action sought, energy would only be consumed during each transient state i.e. only when work is being done.

While magnetic latching valves have been employed in a variety of fields already, it has been accomplished with the use of permanent magnets rather than the harnessing of the material's residual magnetism. Permanent magnets are costly, susceptible to demagnetization and cracking, sensitive to temperature changes, and have low magnetic efficiency. By contrast, residual magnetism can generate high latching forces, adds no additional cost, and can be applied through the use of materials with very good mechanical properties. Furthermore, the force only acts over a small distance, so residual magnetic latching does not inhibit armature motion.

Design Concepts

The current version of the FFM is the result of three earlier designs that were considered and evaluated based upon technical merit. The valve designs were evaluated based upon performance, reliability, maintainability, cost, and weight. The performance specification for the valve and the intent to use a single valve for two flow ranges requires that the valve is capable of rapid actuation as necessary to achieve high turn down ratio (maximum pulse width/minimum pulse width). Pursuant to this, a design employing two solenoids and no springs was considered ideal. The use of two coils allows the application of maximum force to the spool to achieve rapid actuation in both the opening and closing directions. As an alternative, a single coil and spring design that uses the coil to move the valve from one position to the other, and the spring to return it, was considered. However, because a large portion of the force generated by the solenoid is used only to compress the spring and not to accelerate the mass of the valve, this design was not considered optimum for the current test/development effort. It should be noted that once testing is completed and the actual performance specification for the valve has been identified, the use of a single coil design should be revisited as a possible cost savings alternative.

With the two coil configuration selected, three designs were considered. The first was a pressure balanced conical poppit valve that employed steel diaphragms. The valve would incorporate a semi-compliant seat to achieve positive sealing. The valve and diaphragm concepts are well understood by Sturman Industries and have been successfully applied to high reliability/high durability valves. Two diaphragms on the poppit valve would provide complete pressure balance and sealing however, the diaphragms typically require a significant level of development to achieve infinite life and are costly to manufacture. Furthermore, the use of diaphragms introduced additional leakage paths, additional weight and complexity, all of which contributed to the decision to pass over this design.

The second design was based upon the use of a flat lapped disc valving unit that is capable of high life and is simple to manufacture. For this valve, bellows were proposed to achieve the pressure balance. This valve had the benefits of the first option but would not require the development effort of the diaphragm. Unfortunately, the problems of weight, complexity, leakage paths, and cost affect this design as they did the first.

The final design was based upon development work completed at Sturman Industries to determine the effects of subjecting the ends of a pressure balanced spool to high pressure. If the pressure force can be limited, a simple spool valve has many advantages over the previously mentioned concepts with only one downside: leakage. Hydraulic pressure on the end of the spool causes a force imbalance when the spool is at the zero air gap position as the pressure affects the area of one end of the spool but not the other. To minimize the effects, the ends of the spool are profiled to limit contact area thereby limiting the hydraulic force component to an acceptable level. These spools were tested to determine any detrimental effects of minimizing the contact area that absorbs the impact of the spool and were successfully operated to two billion cycles.

FFM DESIGN DETAILS

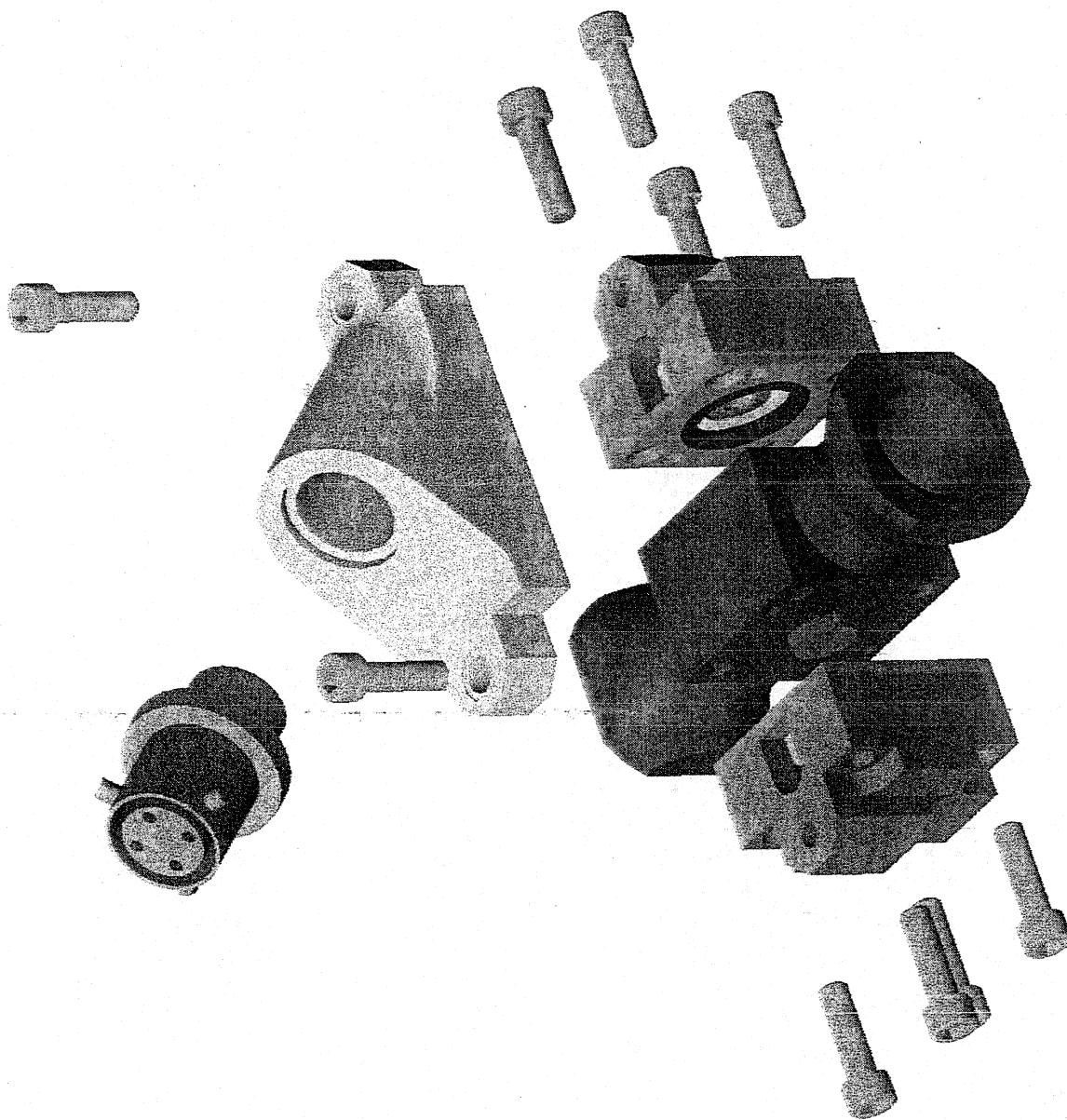
With the optimum FFM configuration selected, the design progressed rapidly. Initial design reviews showed that the proposed valve design was a good match to the application. The main features were as follows:

- Simple design, only five major components: the body, 2 end caps, the spool, and the connector base.
- The straight forward design results in a minimal envelope and an estimated weight of only 150 grams.
- Machining tolerances are compensated for with spacers, no field adjustments are possible.
- The FFM contains only one moving part and the low mass of the part, estimated to be 4 grams, results in unparalleled response times.
- The rapid response of the FFM results in a linear flow versus pulse width characteristic and provides high dynamic range.
- Valve to valve flow accuracy can be controlled during assembly by selecting the appropriate spacer.
- No special tooling is required to assemble the valve.
- High efficiency latching solenoid technology minimizes power requirements.
- Electronic driver can be configured for normally open or closed operation and fail-safe open conditions.
- By achieving the high turn down ratio, one FFM design can accommodate both program flow requirements.

Figure 2 is an exploded view of the FFM valve. There are five main components in the FFM: the valve body, the spool, two end caps with coils, and the connector base.

Magnetic Analysis

Magnetic analysis of the FFM's magnetic circuit was conducted with a two dimensional software package known by the trade name Maxwells. The two dimensional package can accurately estimate the performance of an axially symmetric magnetic system. The analysis of the circuit indicates that the actuators develop approximately 7.5 pounds of force. Residual magnetism is estimated to be 40 percent of the maximum, or 3 pounds.



FFM Exploded View
Figure 2

FUEL FLOW MODULATOR OPERATION

Operation of the FFM is quite simple. The spool, the only moving component, can be magnetically latched to one pole or the other. No intermediate position is used. Figures 3 and 4 show the FFM in the open and closed position. The spool in figure 3 is latched to the pole on the left while figure 4 is shown latched to the right. The total travel for the spool is .012 inches. As shown in figure 3, there is a 0.006 gap on each side of the central land on the valve body which permits flow from the inlet to the outlet. Figure 4 shows the spool latched to the pole on the right, the closed position. In this position, no flow is allowed from the inlet to the outlet port. To operate the FFM valve, the coils are alternately energized to shuttle the spool back and forth.

Electronic Driver

A digital valve uses current pulses to shift the spool from one position to another. Furthermore, the magnet wire used is of a larger diameter than typically used and hence the coils have fewer turns which results in low resistance and low inductance. This allows the coils to handle high current and generate extremely high magnetic forces, which translates to fast response. The solenoids are energized only for an instant, typically on the order of one millisecond. To accomplish switching of the voltage to the two coils, a special driver is required.

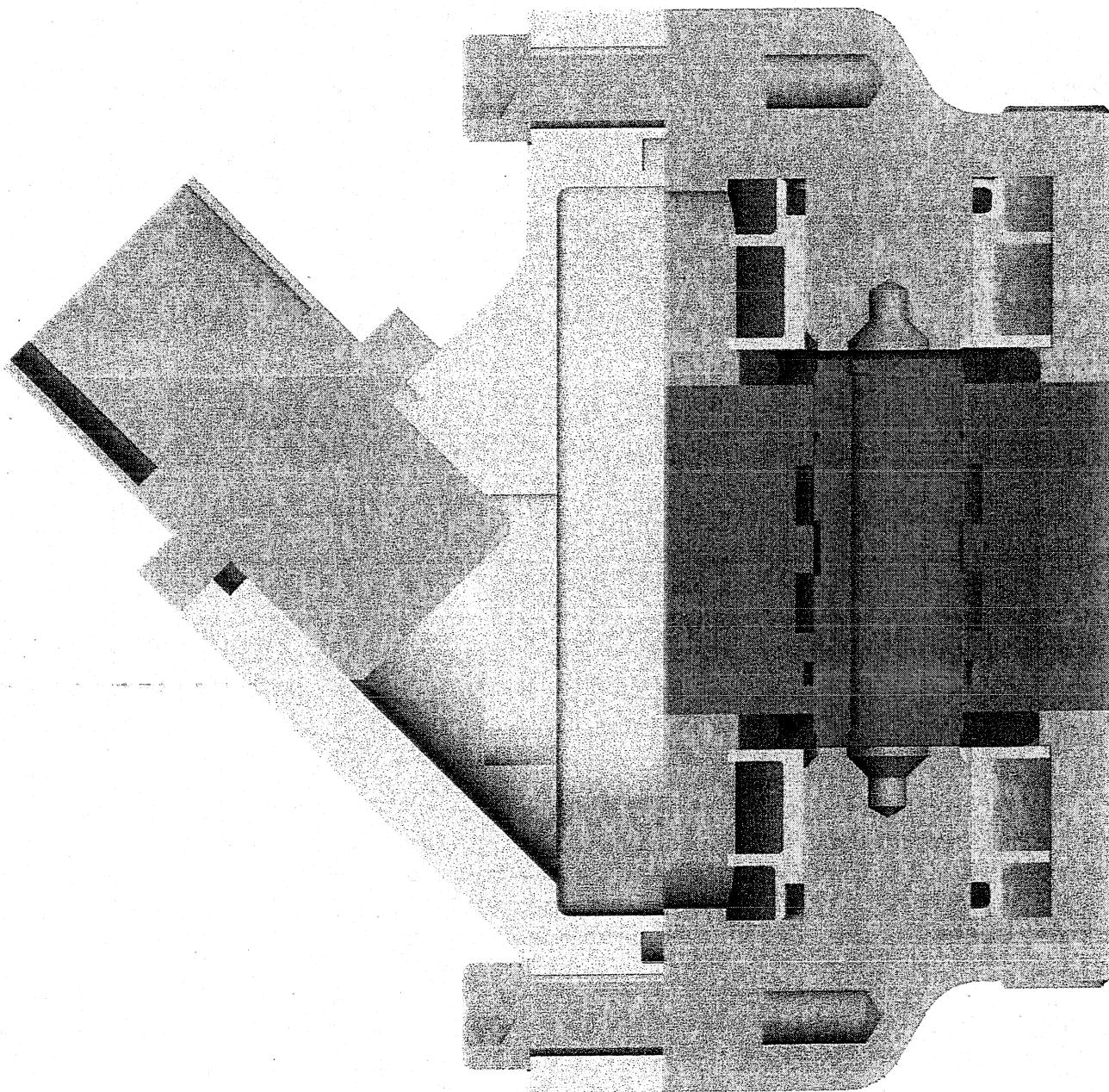
The driver is comprised of transistors in an H bridge configuration that allows current to pass through each coil in a forward and reverse direction. The driver can sense current and uses back EMF traces (from the non-energized coil) to detect the end of motion of the spool. The drivers supplied to AlliedSignal operate in this mode and as a result, provide consistent performance over a wide voltage range.

Basic Performance Measurements

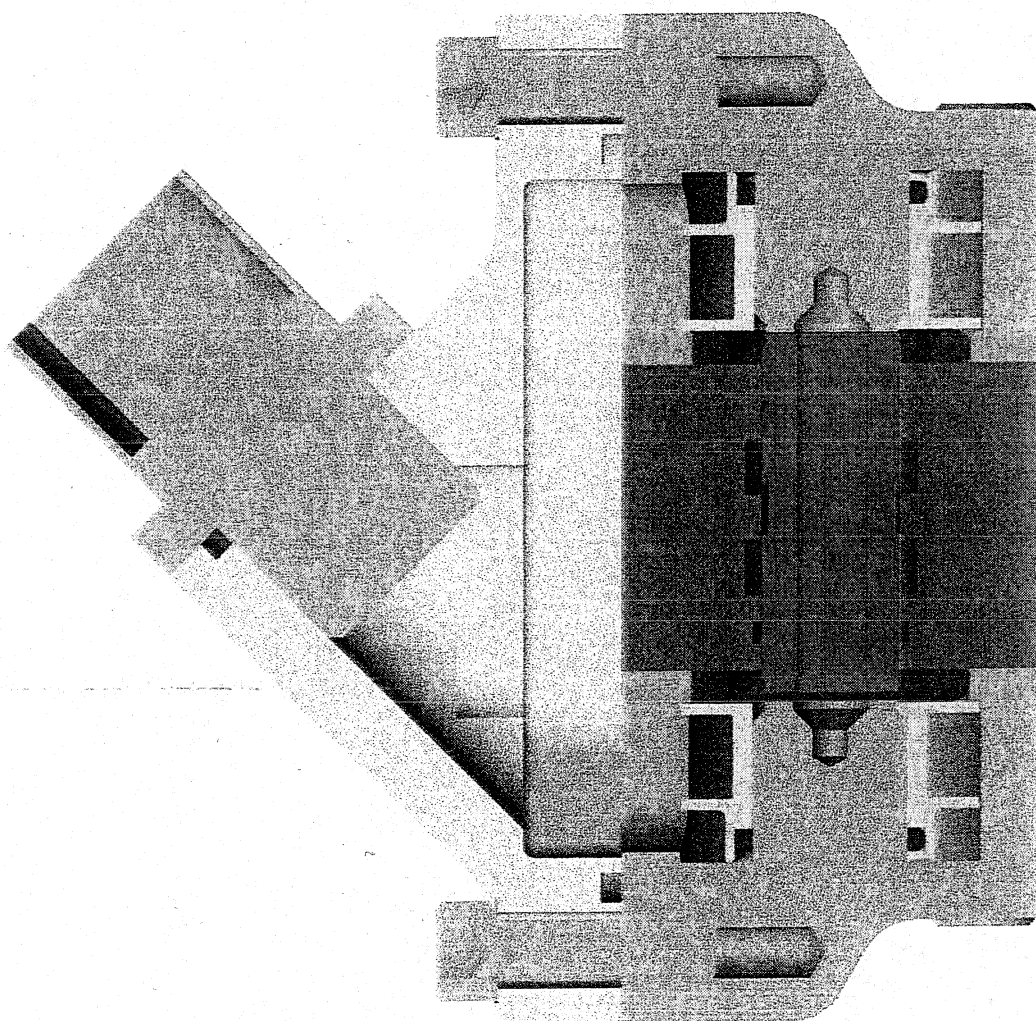
The performance of the FFM can be seen in the following oscilloscope traces, figures 5, 6, and 7. Figure 5 shows three traces. The logic or command signal is shown at the top: when the logic signal goes high, the valve is commanded to turn on. Below, the current trace to coil one is shown. The current to coil one increases until a cusp is detected by the driver circuit after which the coil is left on for approximately 100 microseconds to ensure a complete latch is achieved. When the logic goes low, coil two is turned on, again until the cusp is detected.

Figure 6 shows the same trace with cursors used to measure the maximum current. Delta voltage is measured to be 91.6 millivolts. The current probe was set to 10 millivolts per amp hence 9.1 amps were required to open the valve. Typically all FFM's will require 10 amps or less.

Figure 7 shows the voltage signature on each coil for the same event. Here the back EMF signal can be seen. This induced voltage signal is useful as a diagnostic tool.



FFM Cross Section Open
Figure 3



FFM Cross Section Closed
Figure 4

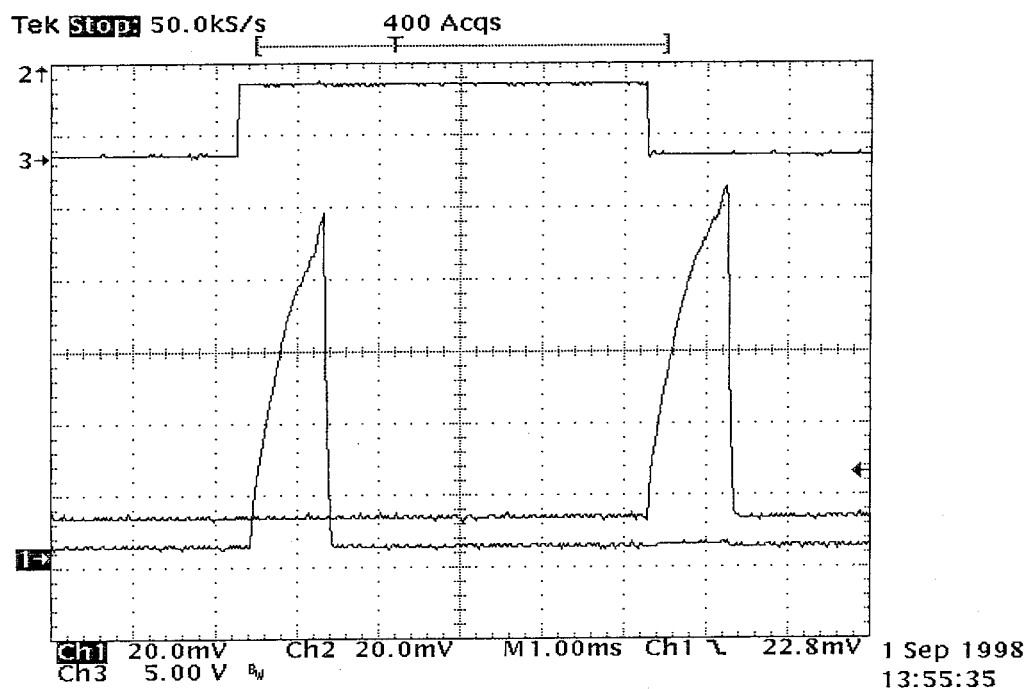


Figure 5: FFM Logic and Current Traces

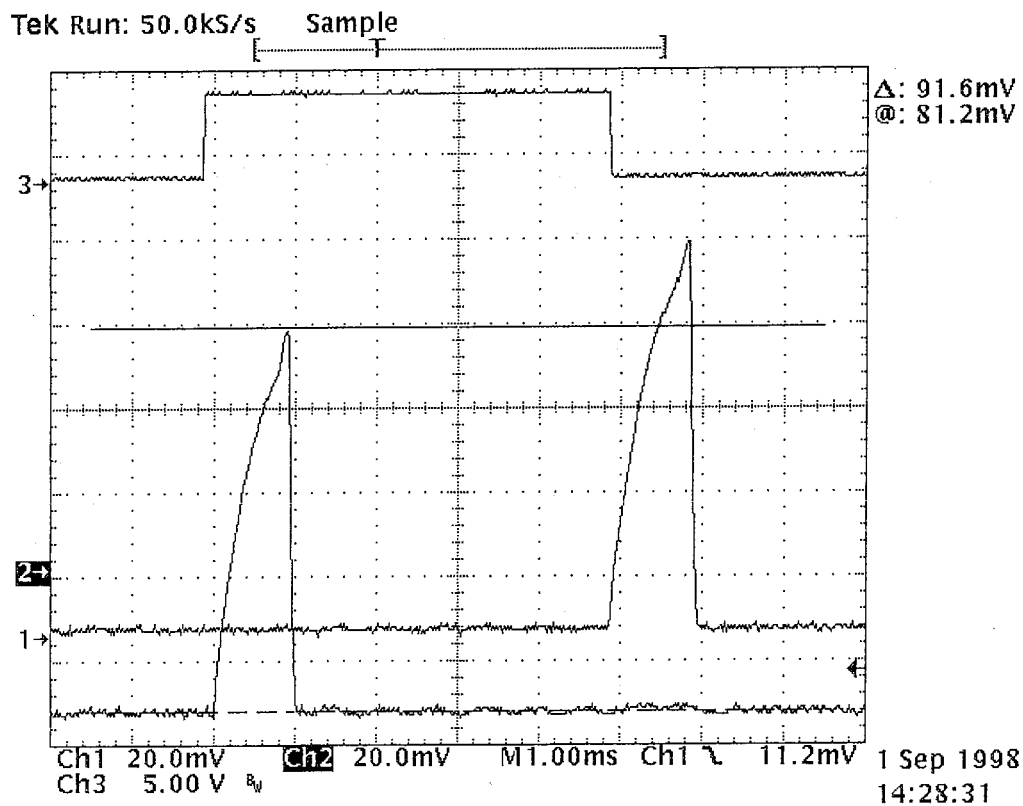


Figure 6: FFM Logic and Current Traces with Cursors

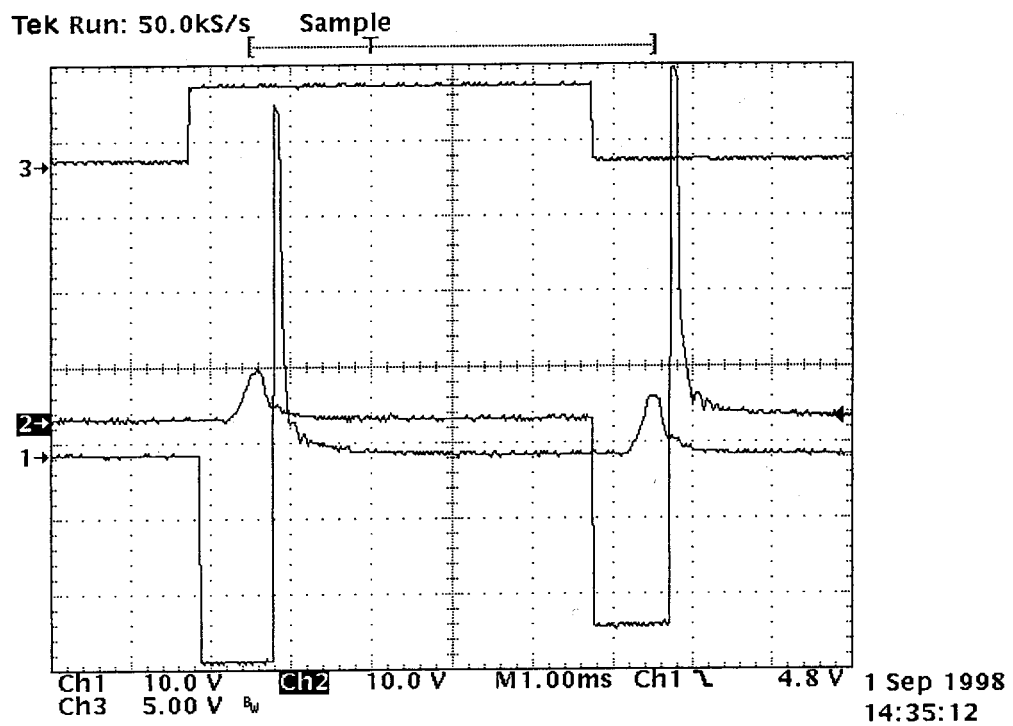


Figure 7: FFM Logic and Voltage Traces

TEST METHODS

Testing of the FFM's was conducted as required to confirm that each valve performed in accordance with the specification. A single test bench was fabricated which was used for all testing. Instrumentation included:

1. Pressure drop across the valve ($\pm 2\%$)
2. Fluid temperature (± 2 deg. F)
3. FFM inlet pressure ($\pm 2\%$)
4. Mass flow rate ($\pm 1\%$)
5. Four channel digital storage scope

The test bench was set up with diesel calibration fluid conforming to SAE specification J967. The calibration fluid is sold under the trade name Viscore.

TEST RESULTS

The following test sequence was completed for each valve.

1. SETUP - Attach the valve to the hydraulic test stand and run the valve at 20 Hz, 20 mSec pulse width, for approximately 5 minutes to allow the valve to stabilize.
2. RESPONSE - Record to disc two traces on the oscilloscope, showing the opening and closing events with response time shown on the cursors.
3. STABILITY - A cumulative trace should be recorded showing the stability of the valve for the opening event.
4. OVERALL PRESSURE DROP - First, adjust the upstream pressure to achieve a flow rate of 100 lb/hr. Next the valve will be latched open (100% duty cycle) and the supply pressure adjusted to the 100 lb/hr point. The pressure drop across the valve will be measured.
5. LINEARITY - The flow rate will be recorded for each valve at 5 pulse widths from 2 to 5 mSec energize time, while running at 10 Hz.
6. The valve will be removed from the test bench and the sequence repeated for the next valve.

Graphical results of the valve flow data are shown in the appendix.

The following test results apply to all the valves.

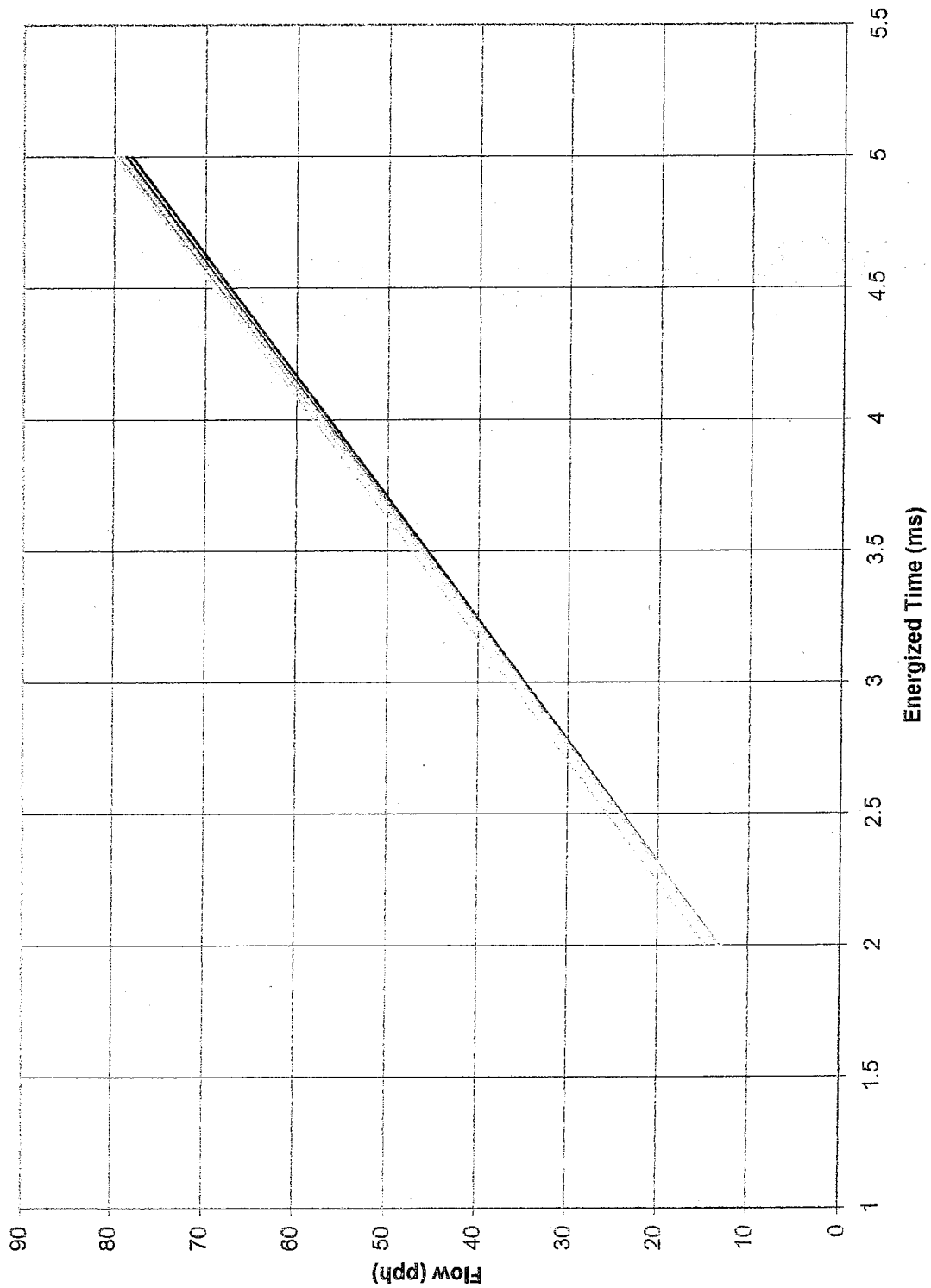
| | |
|--|----------------------------------|
| Valve Response Time: The time measured from the command signal to the completion of travel of the spool valve. | 0.9±.1 mSec |
| Frequency Response | N/A dependant upon system volume |
| Overall Pressure Drop: Worst case for conditions specified in RFP | L.T. 15 PSI |
| Valve Stability: The total range of time variation for the end of motion of the spool. | 100 µSec |
| Hysterisis | None measurable |

APPENDIX

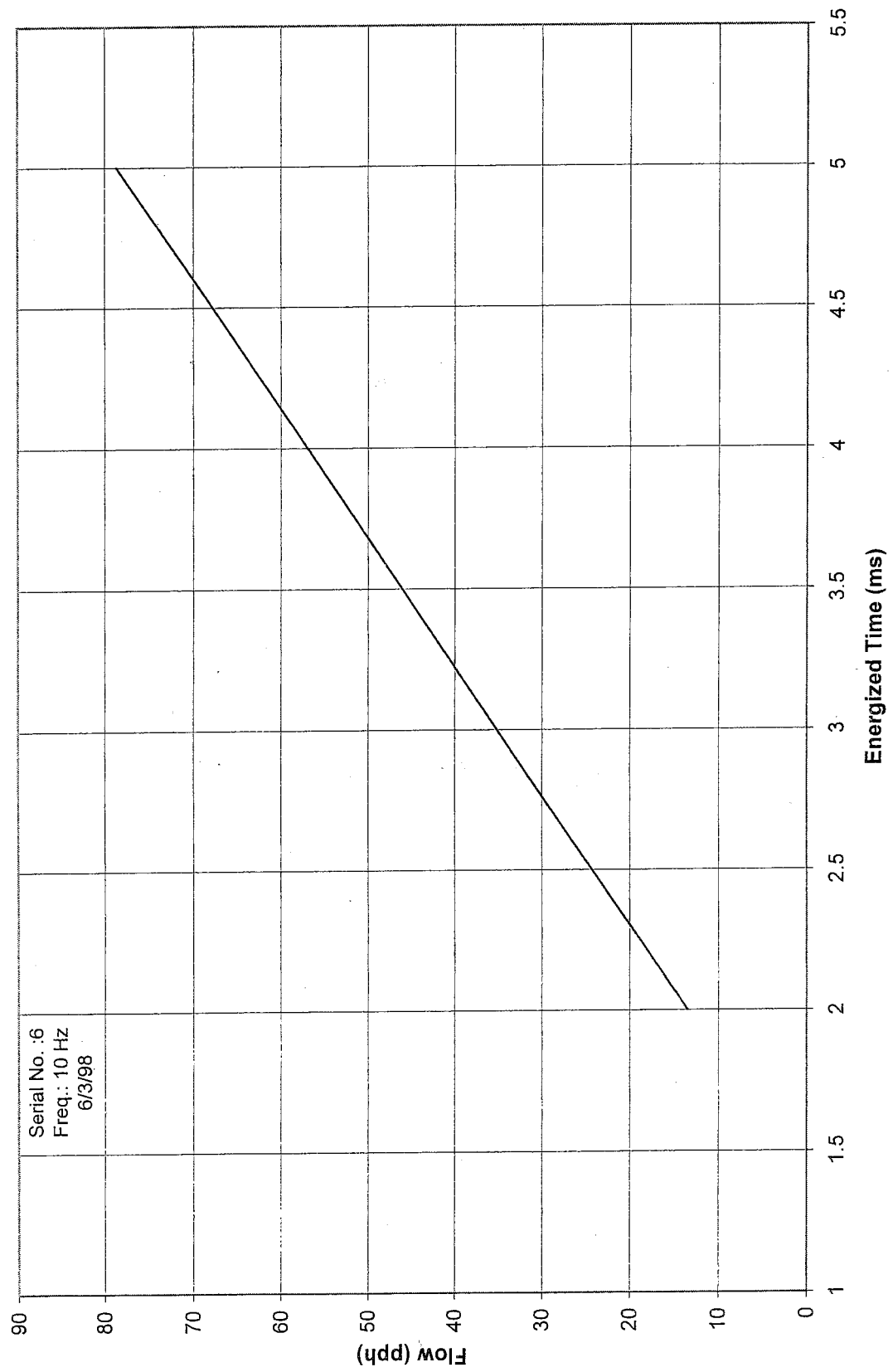
VALVE SPECIFICATION

| | |
|------------------------------------|---------------------------------------|
| AlliedSignal Part Number | R3559482 |
| Sturman Industries Part Number | 8300616 |
| FFM Weight | 140 g |
| Electrical Connector Specification | Mil-C26482 |
| Hydraulic Port Connection | MS33649 |
| Envelope | See Appendix, pg. A1 |
| | |
| Temperature | -40 to 250 deg. F |
| Operating Pressure | 750 PSIG |
| Proof Pressure | 1500 PSIG |
| Burst Pressure | 2000 PSIG |
| Pressure Drop @ 100% duty cycle | LT 15 psi within specified conditions |
| Steady State Flow Stability | LT 1% @ fixed voltage |
| Valve to Valve Variation | LT \pm 4% |
| | |
| Operating Voltage | 28 VDC Nom \pm 5 VDC |
| Frequency Response | N/A Dependant upon system |
| Response Time | 0.9 \pm .1 mSec |
| Max Current | 10 amps |
| Hysterisis | None measurable |
| | |

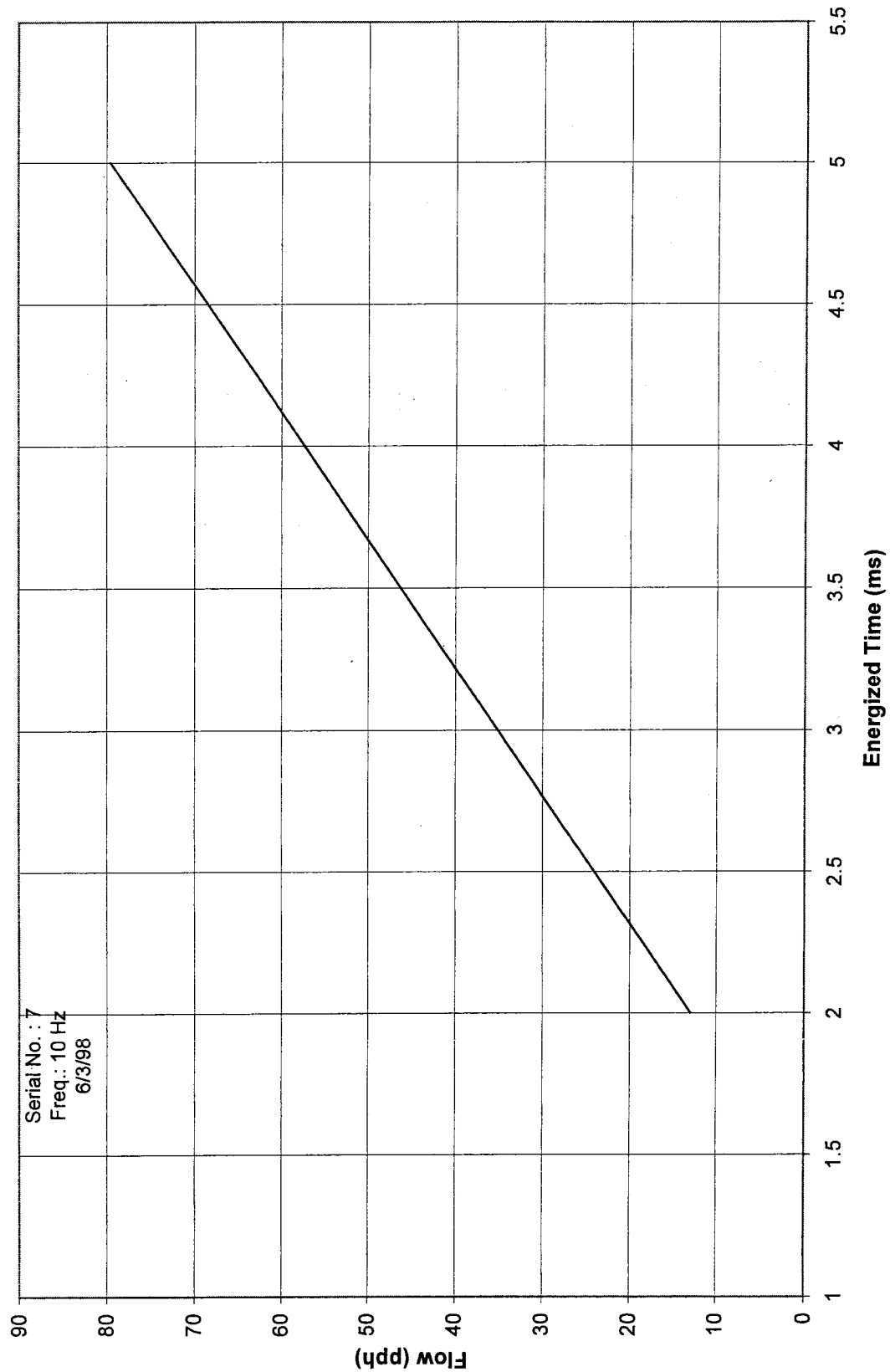
Allied Valve Comparison



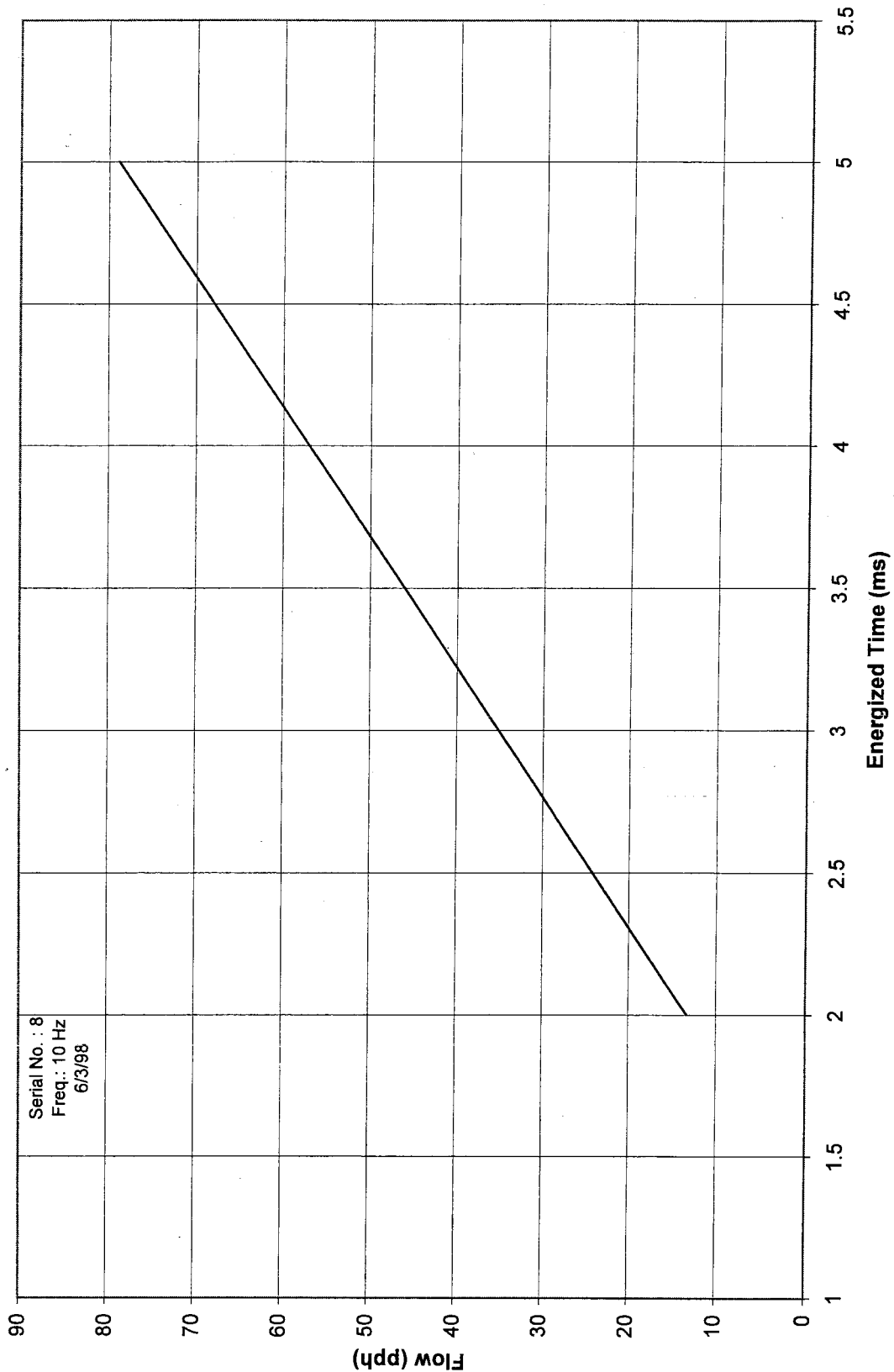
Allied Valve Comparison



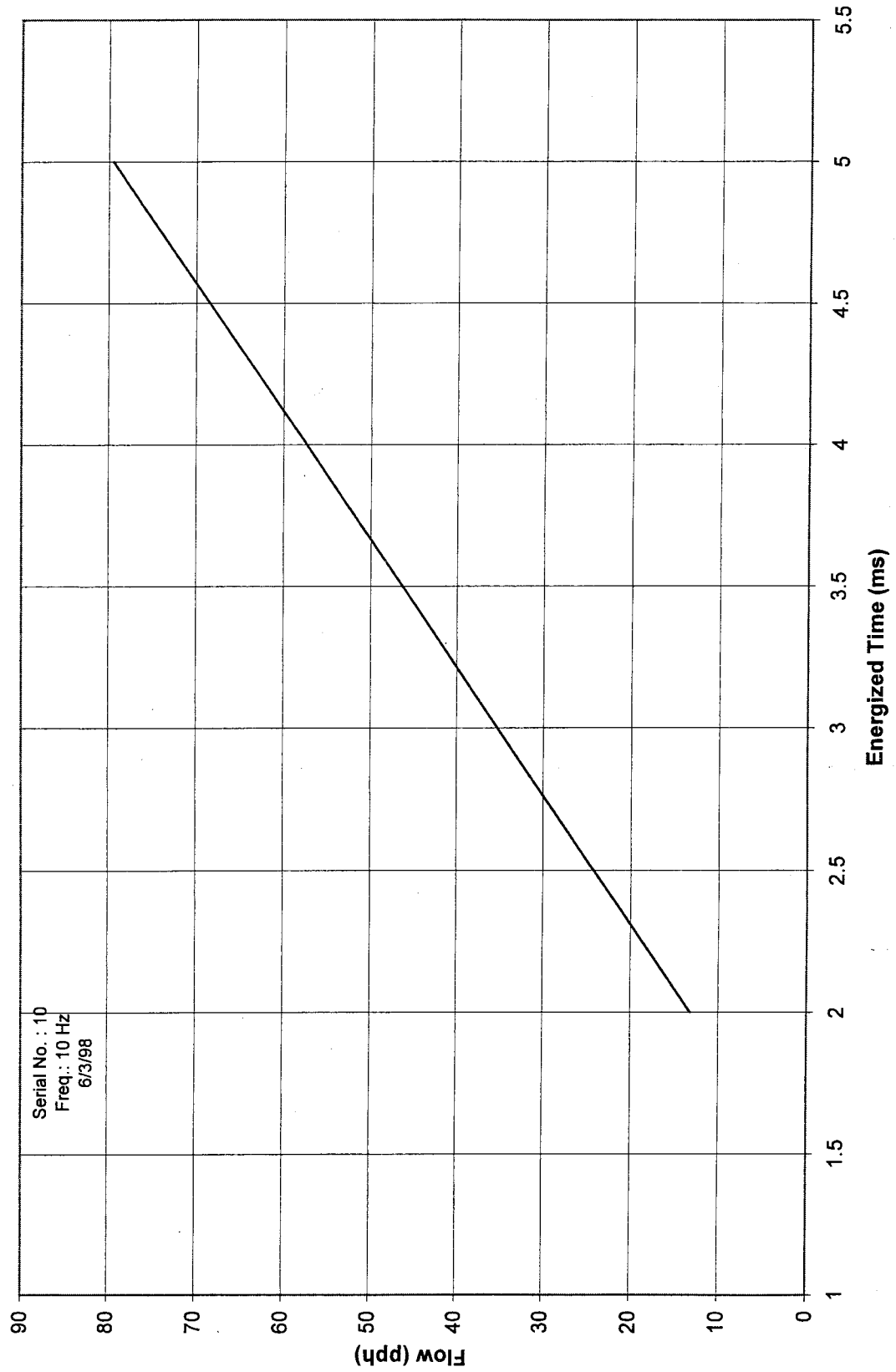
Allied Valve Comparison



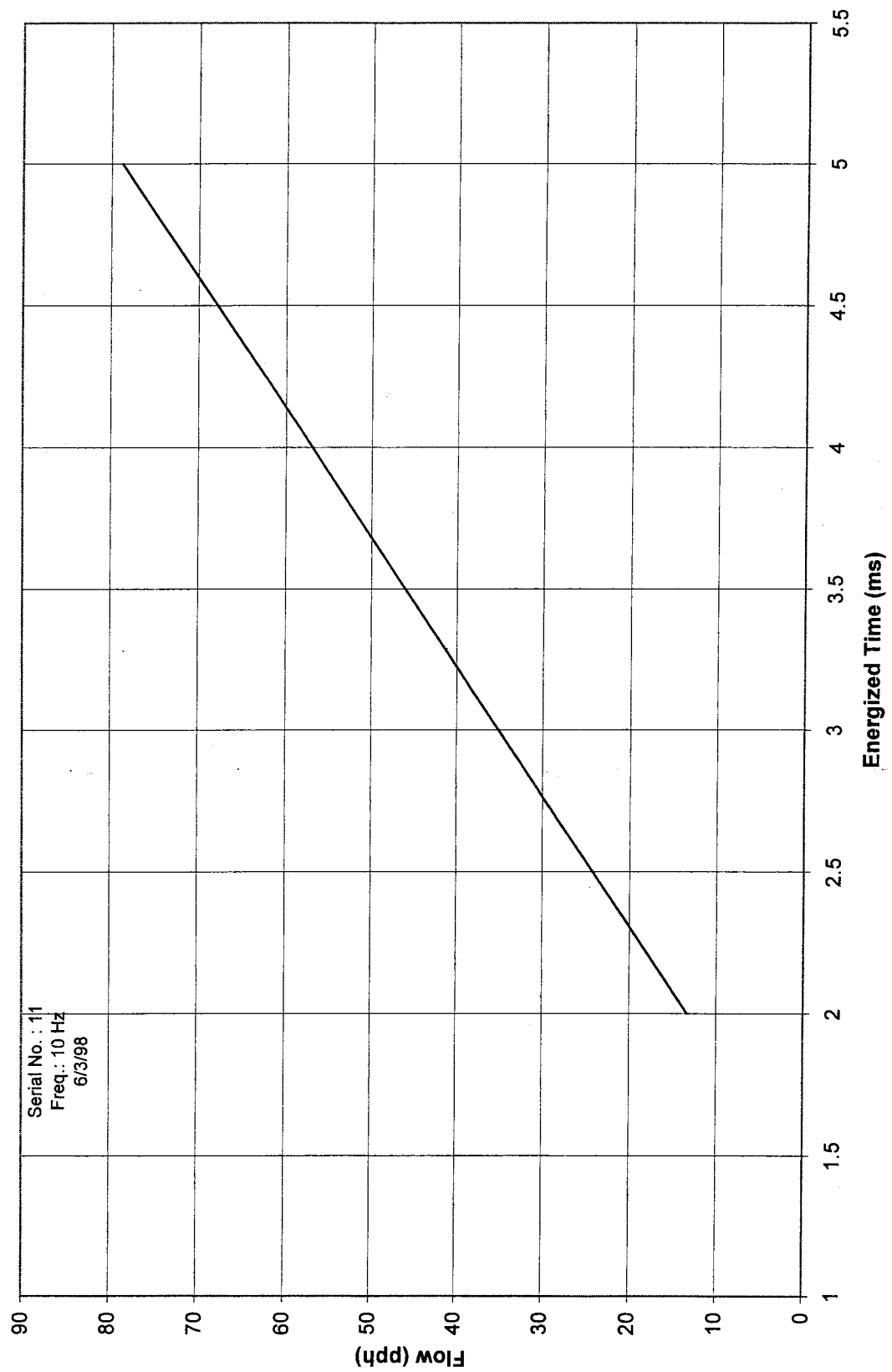
Allied Valve Comparison



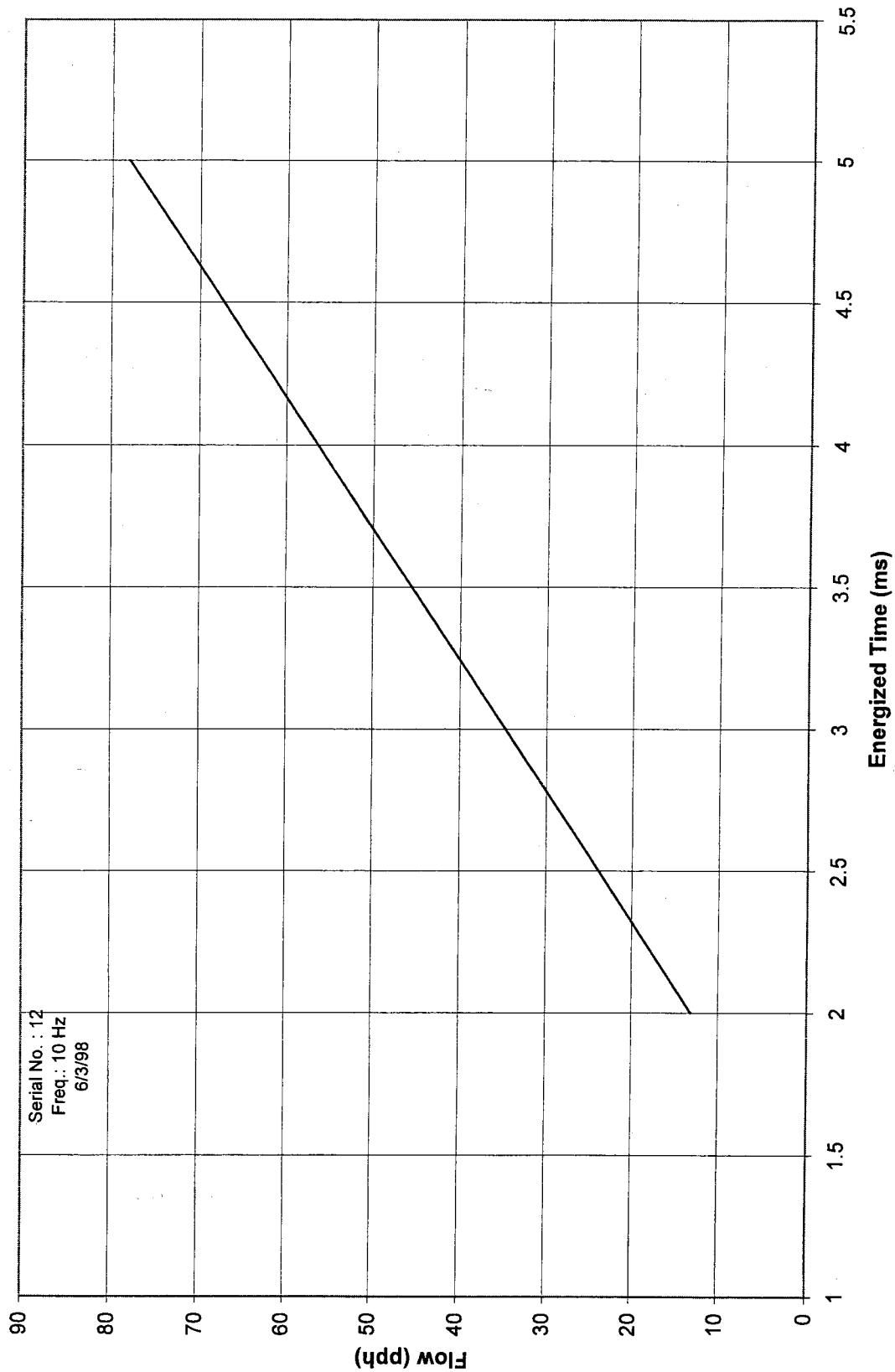
Allied Valve Comparison



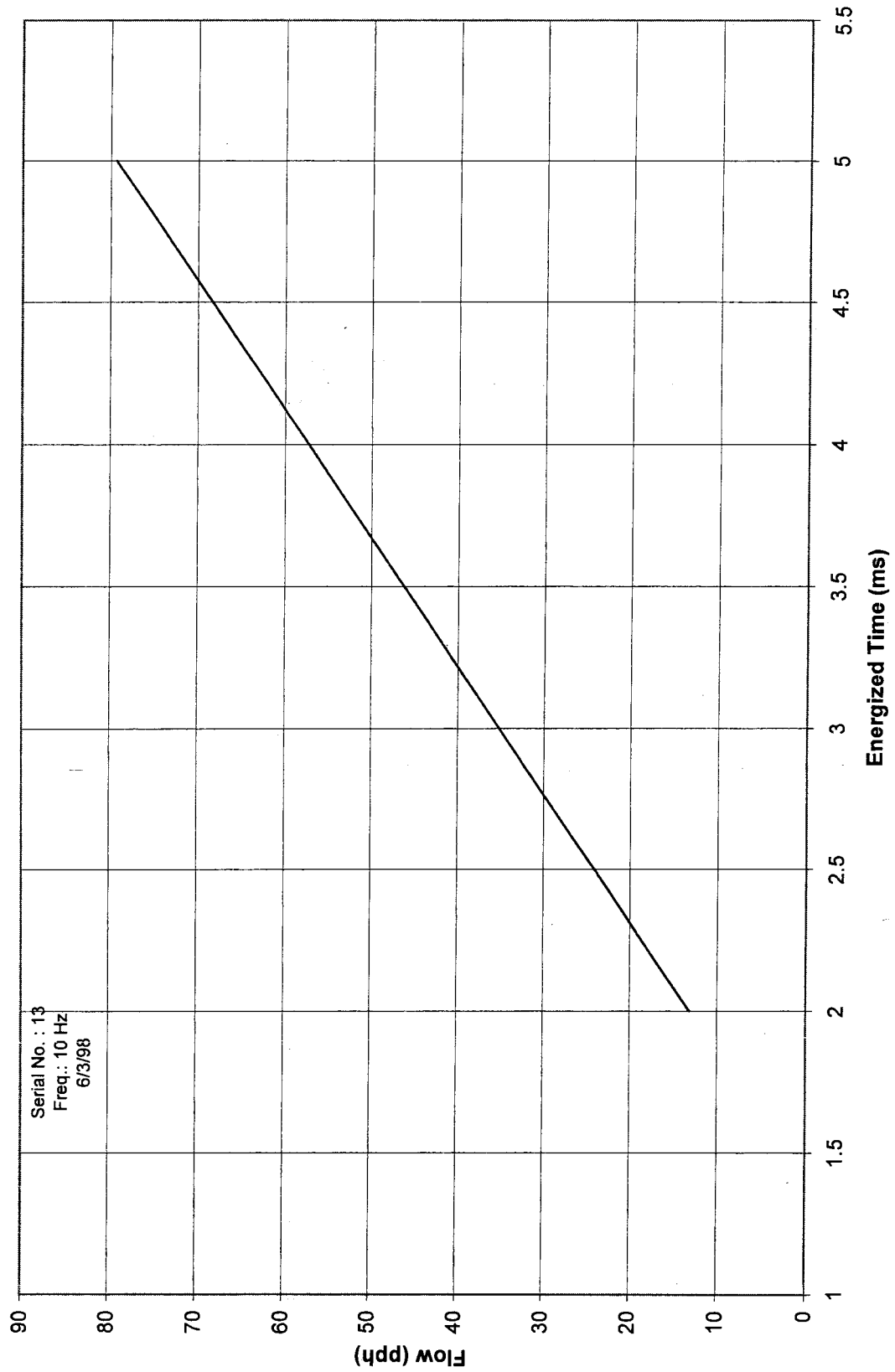
Allied Valve Comparison



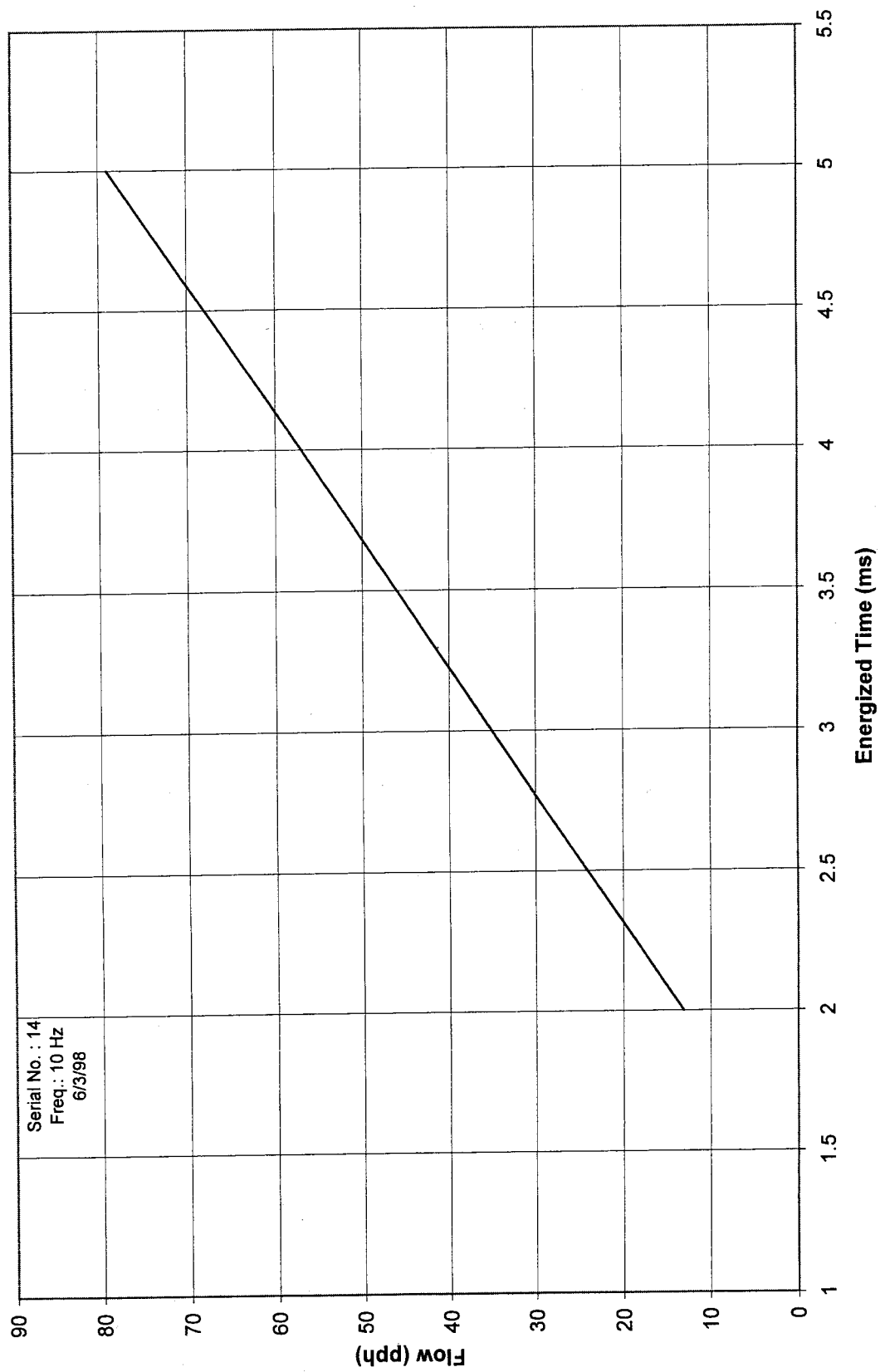
Allied Valve Comparison



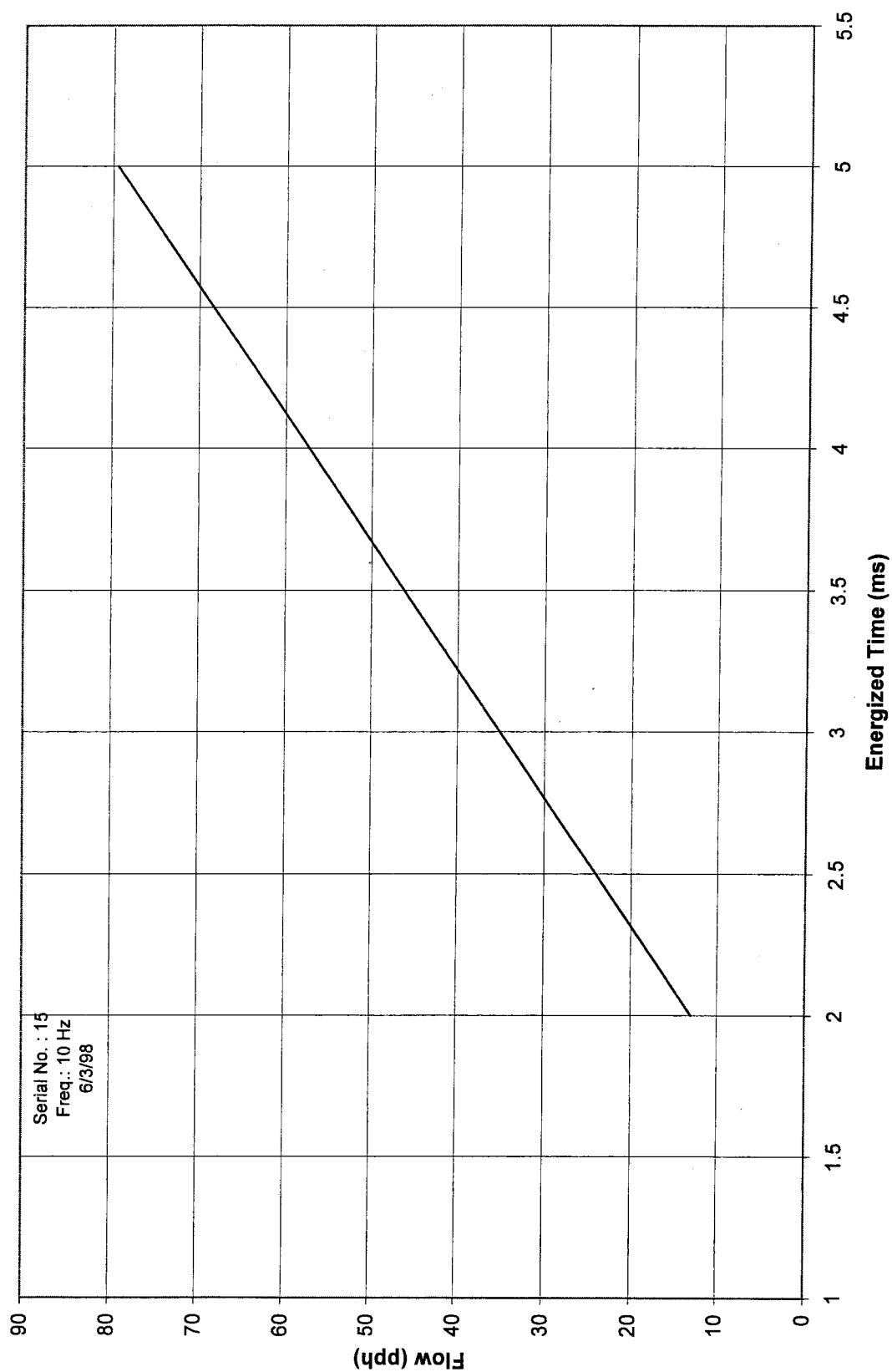
Allied Valve Comparison



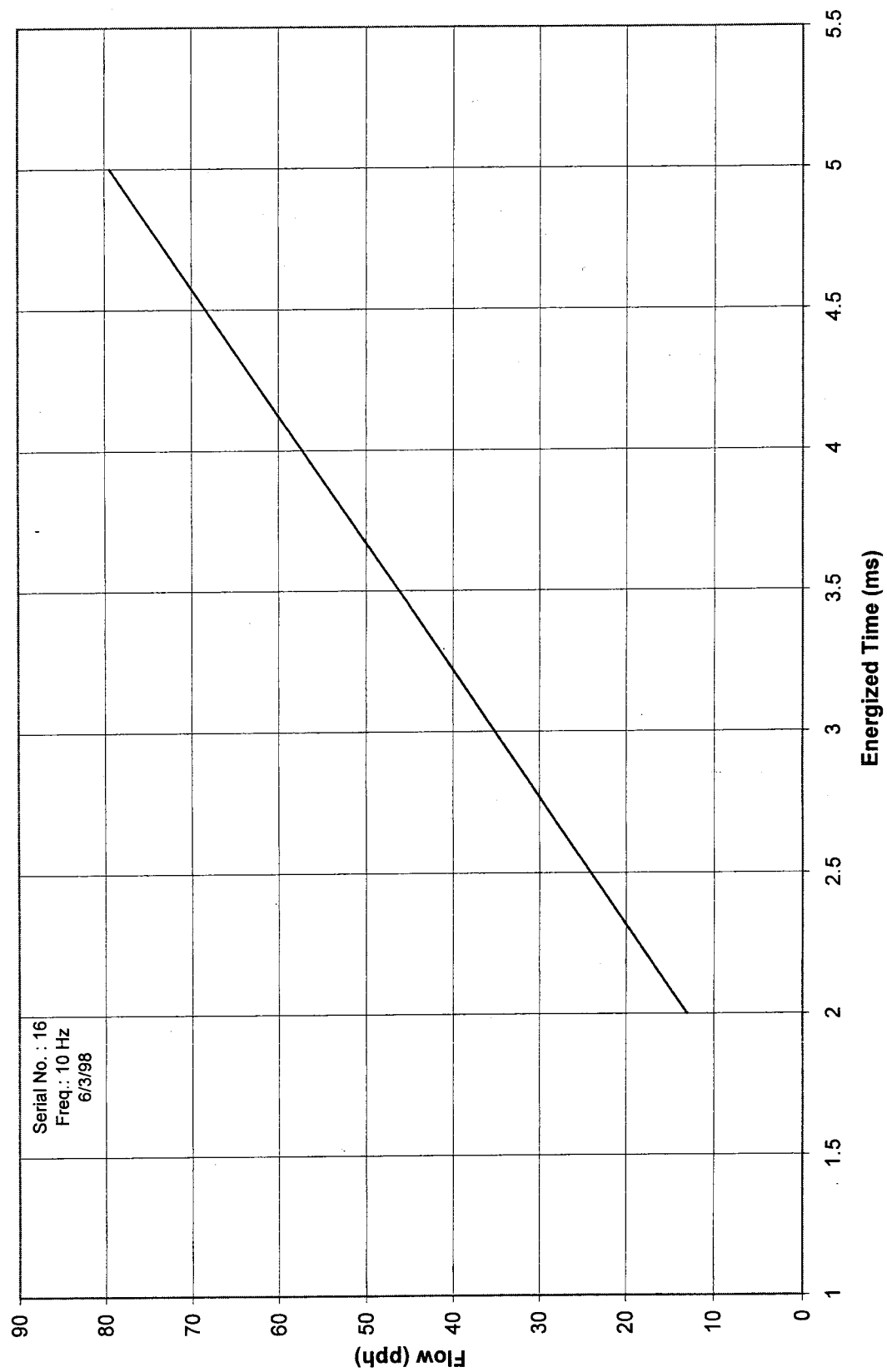
Allied Valve Comparison



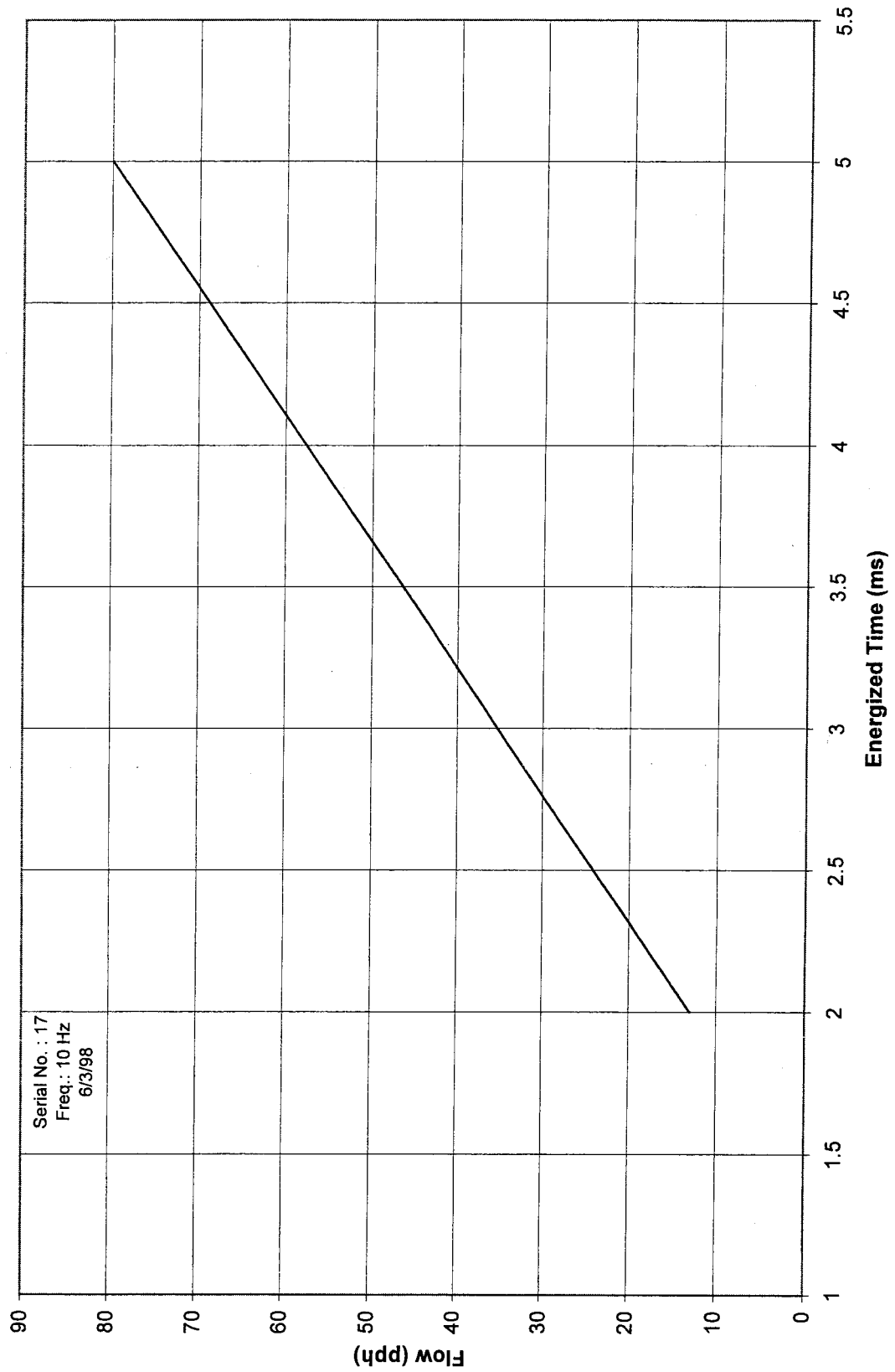
Allied Valve Comparison



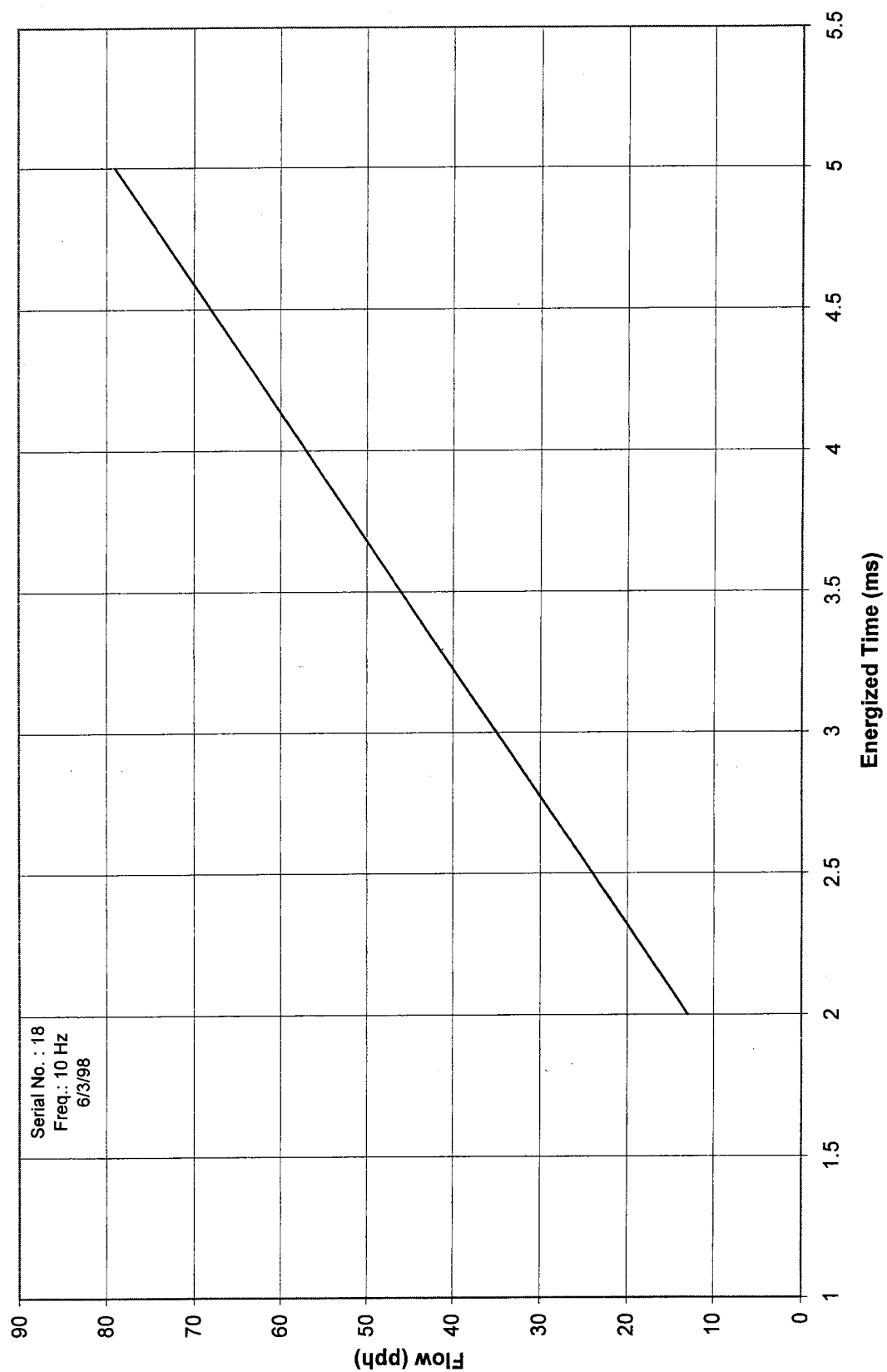
Allied Valve Comparison



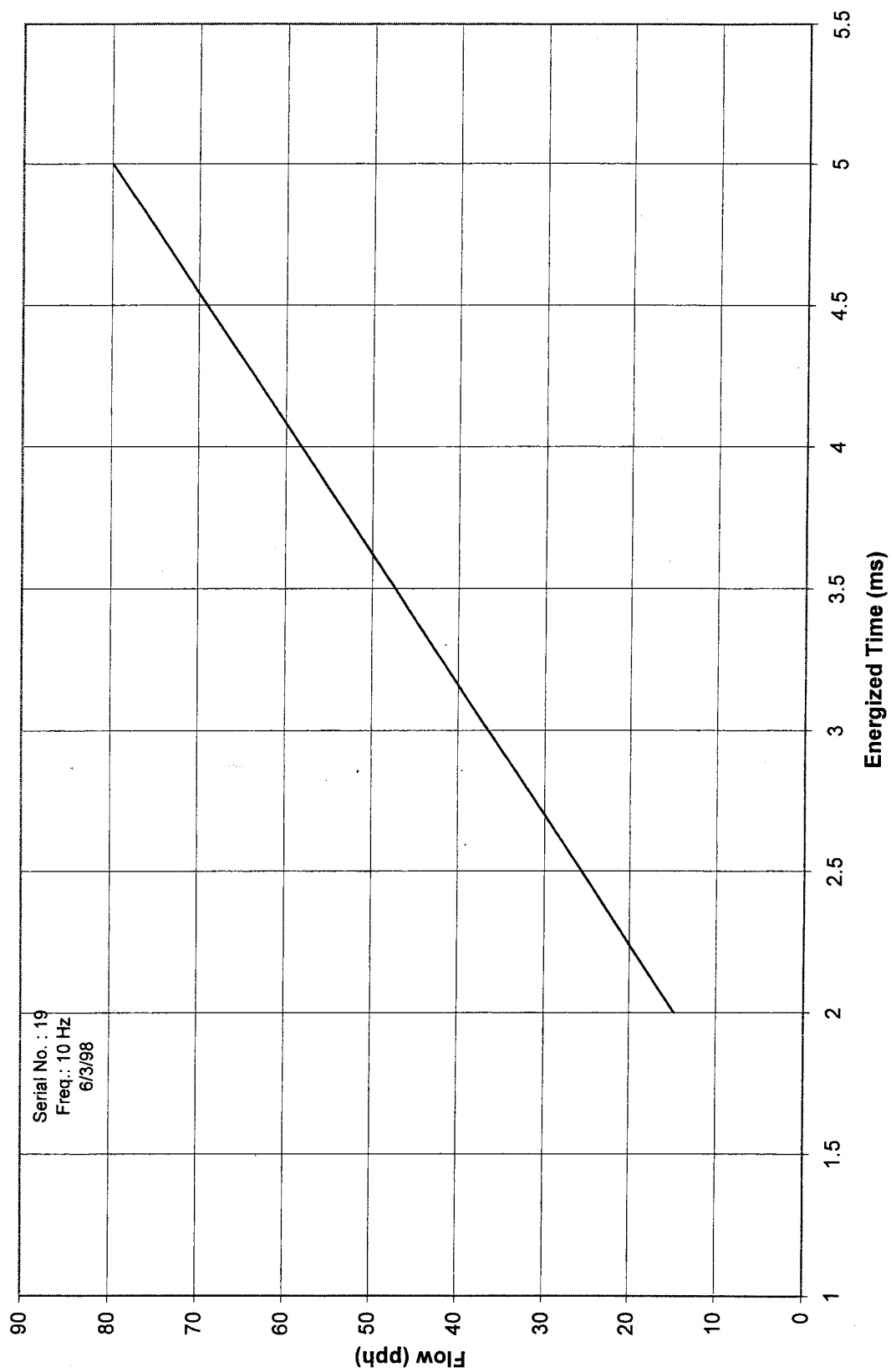
Allied Valve Comparison



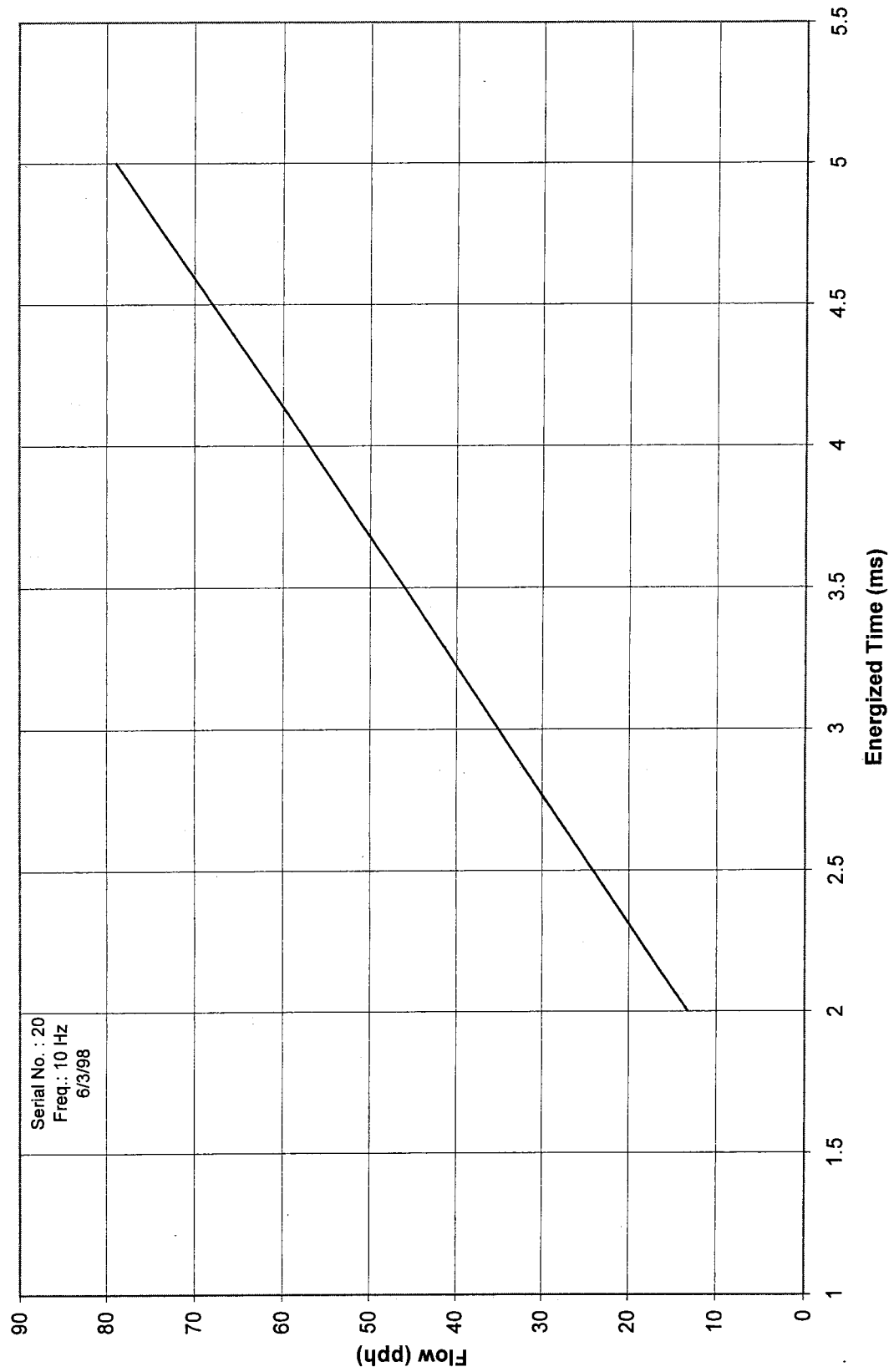
Allied Valve Comparison



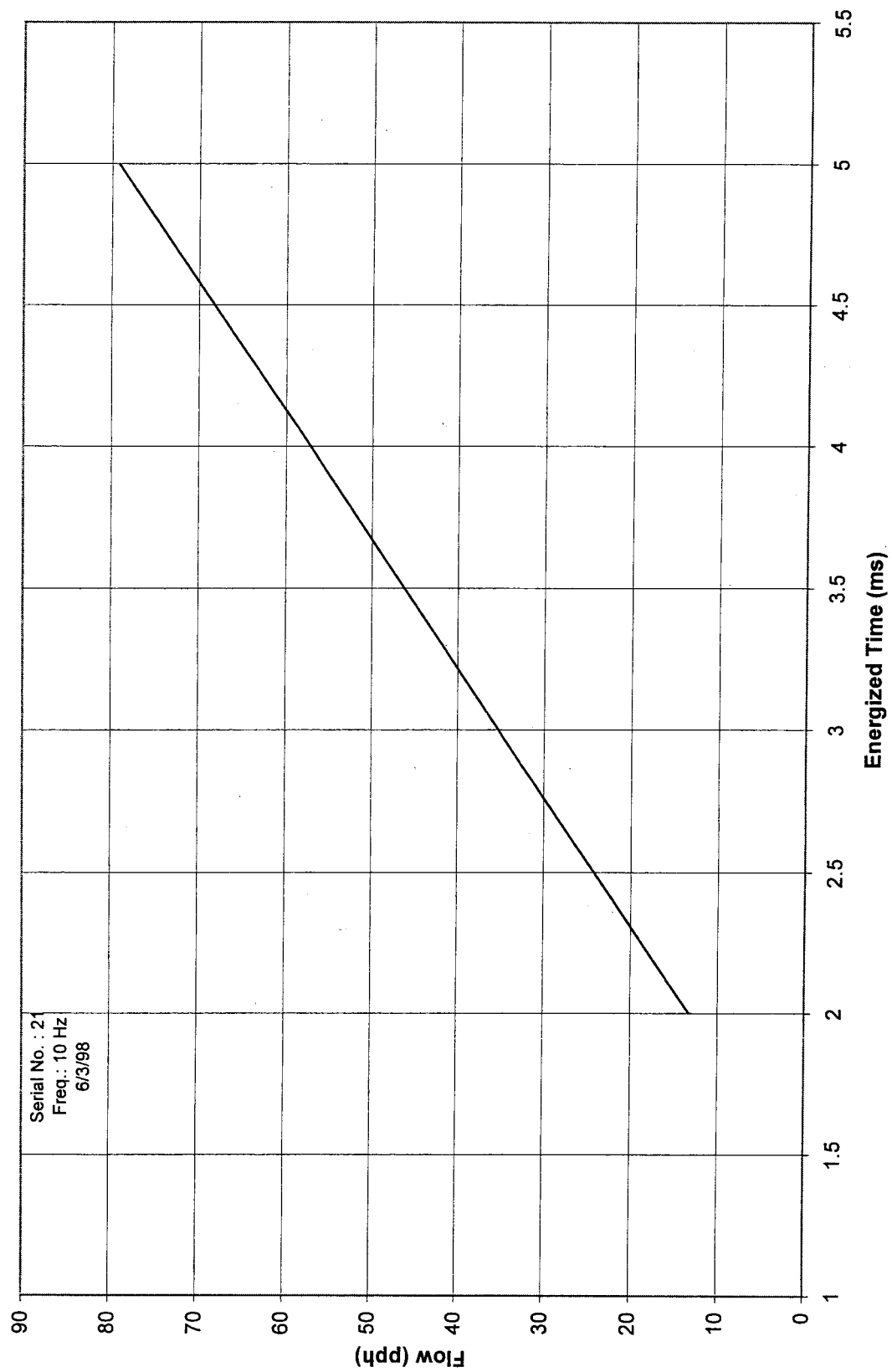
Allied Valve Comparison



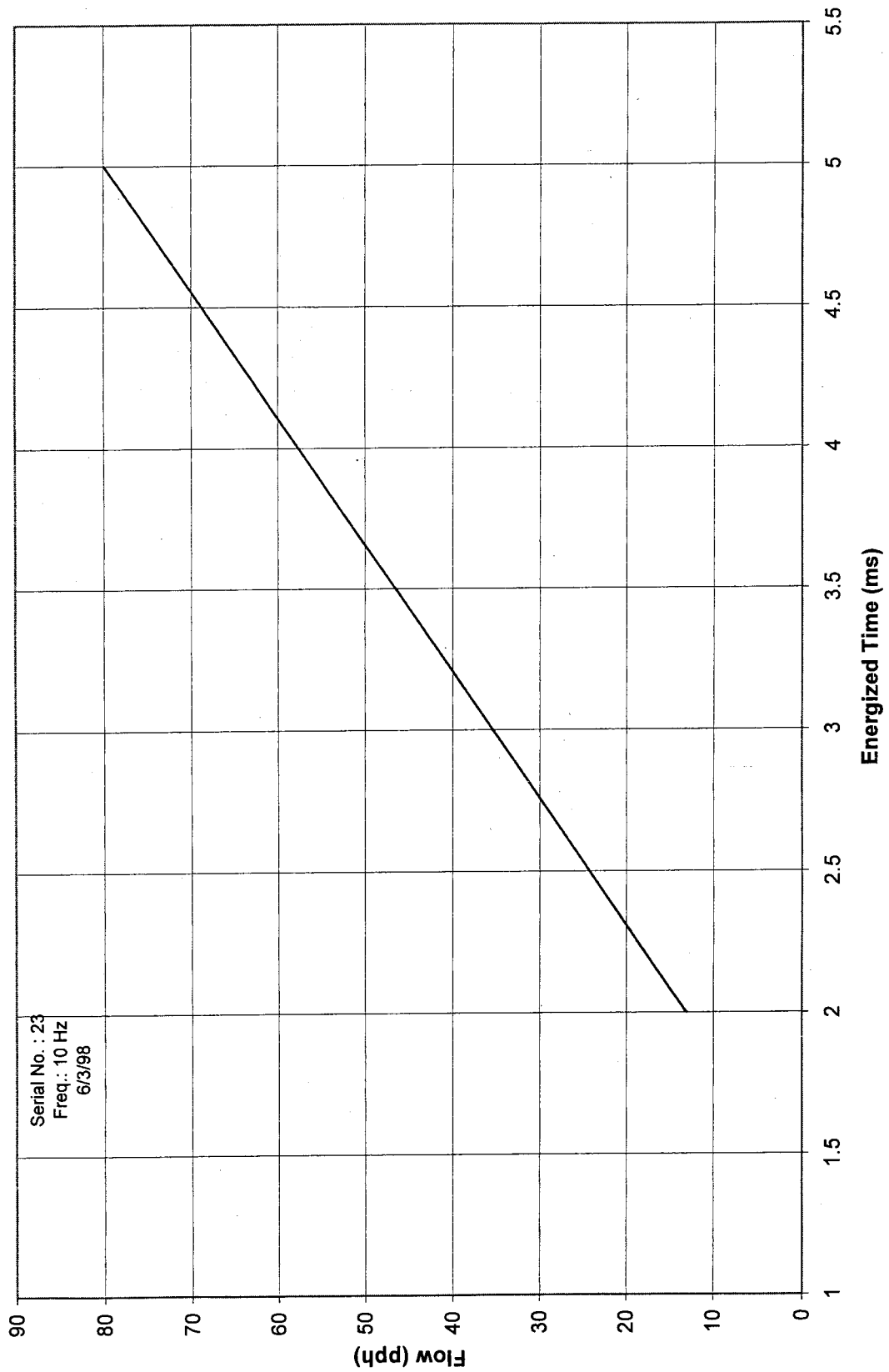
Allied Valve Comparison



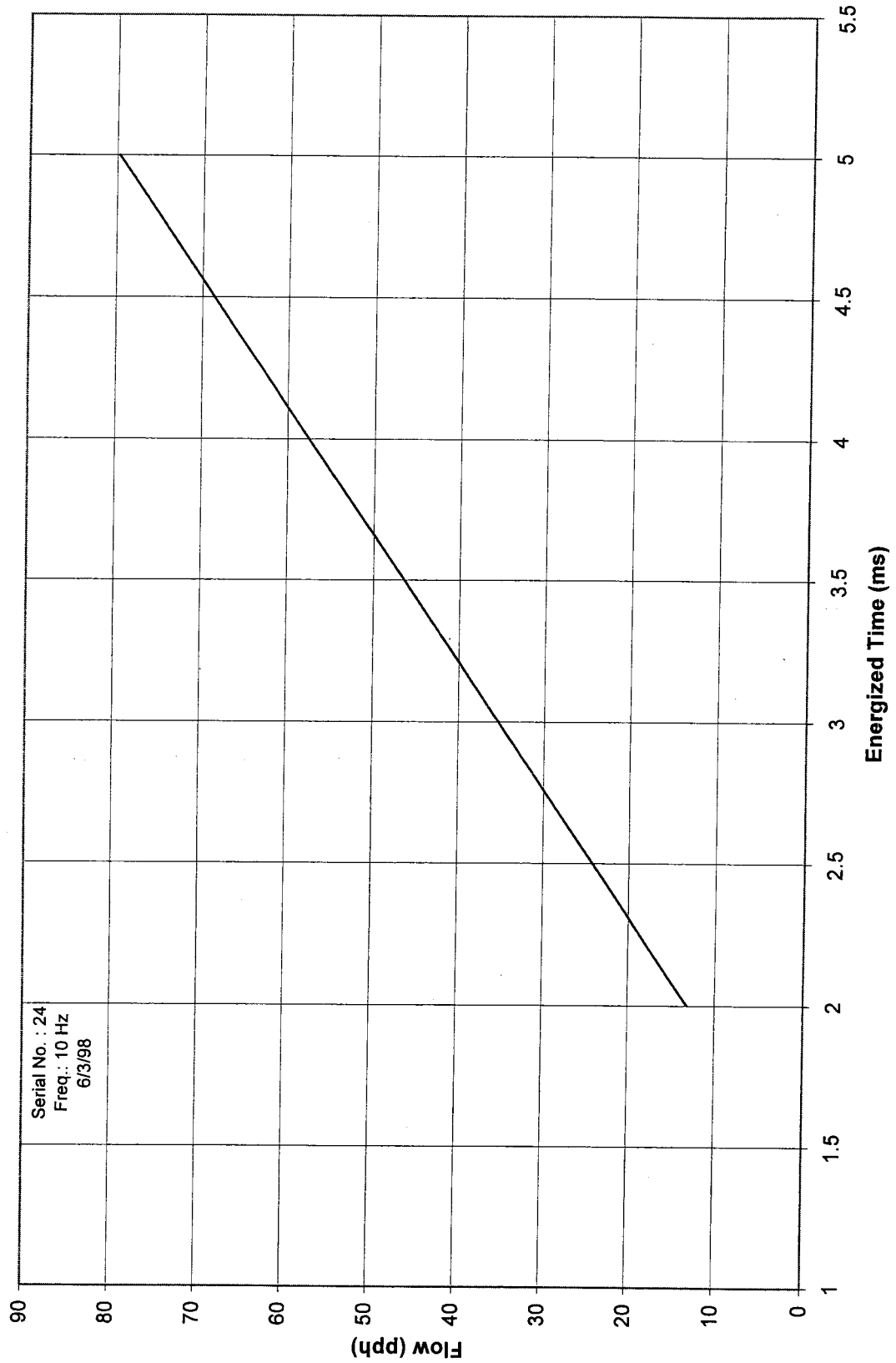
Allied Valve Comparison



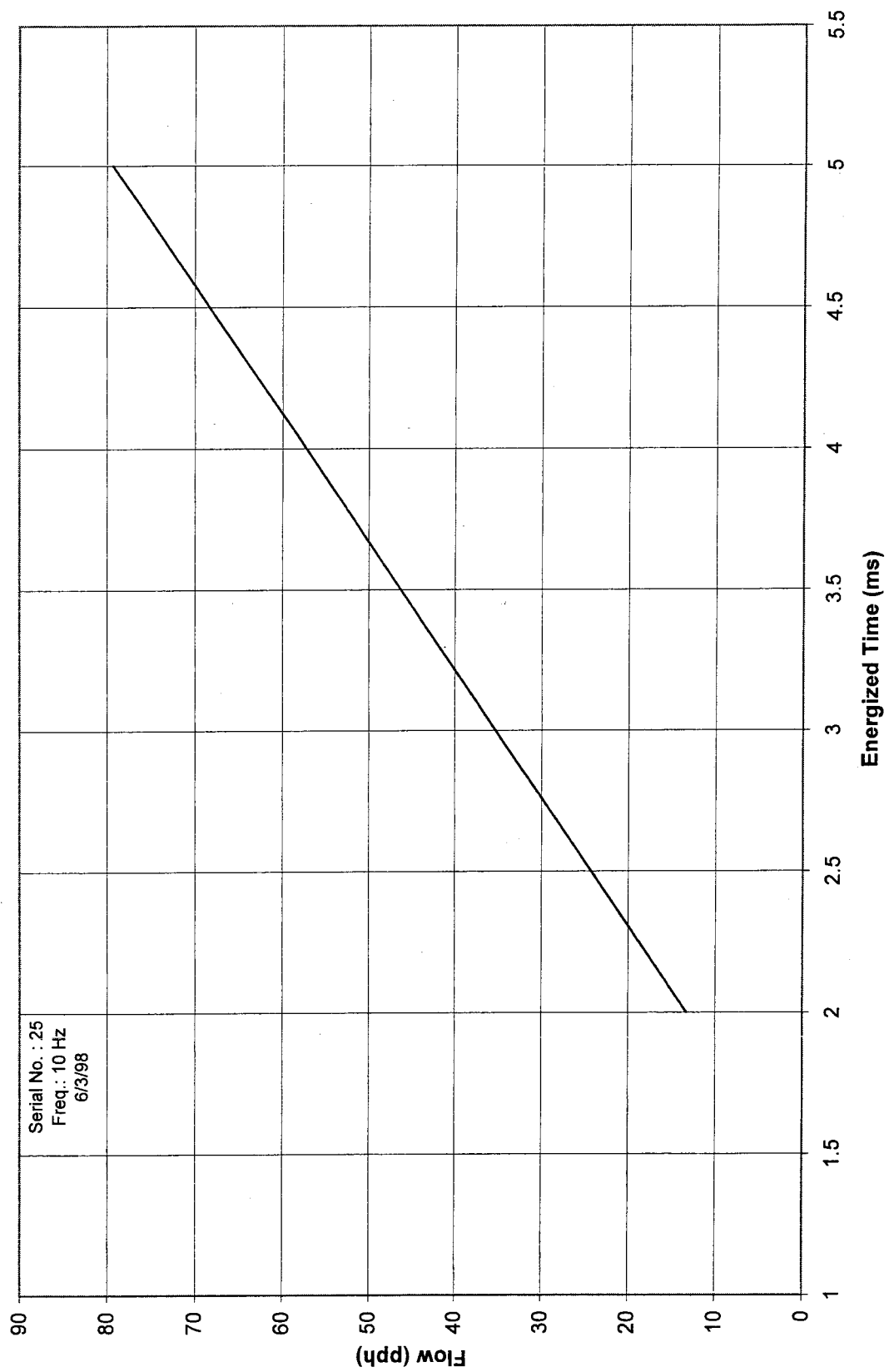
Allied Valve Comparison



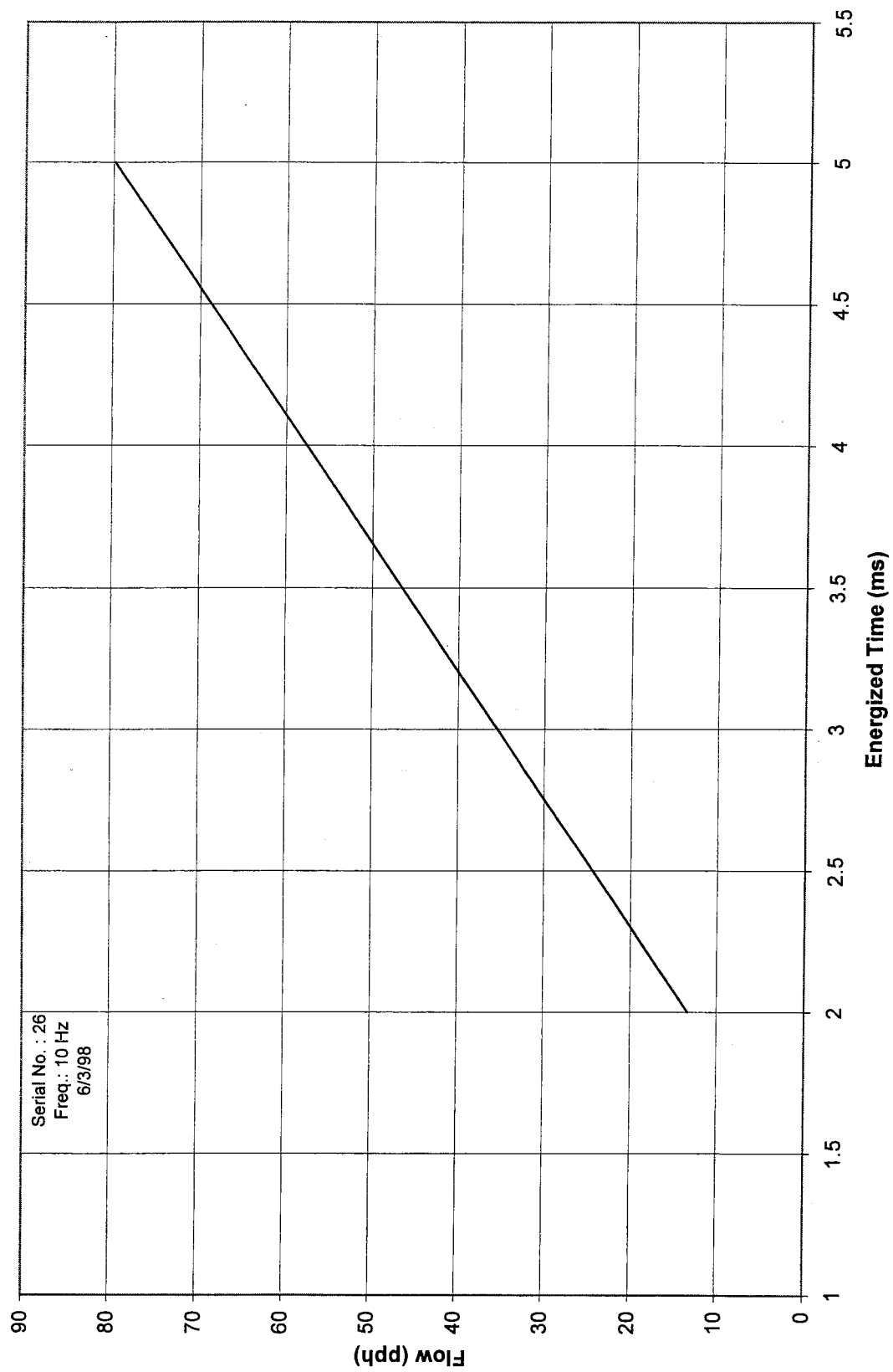
Allied Valve Comparison



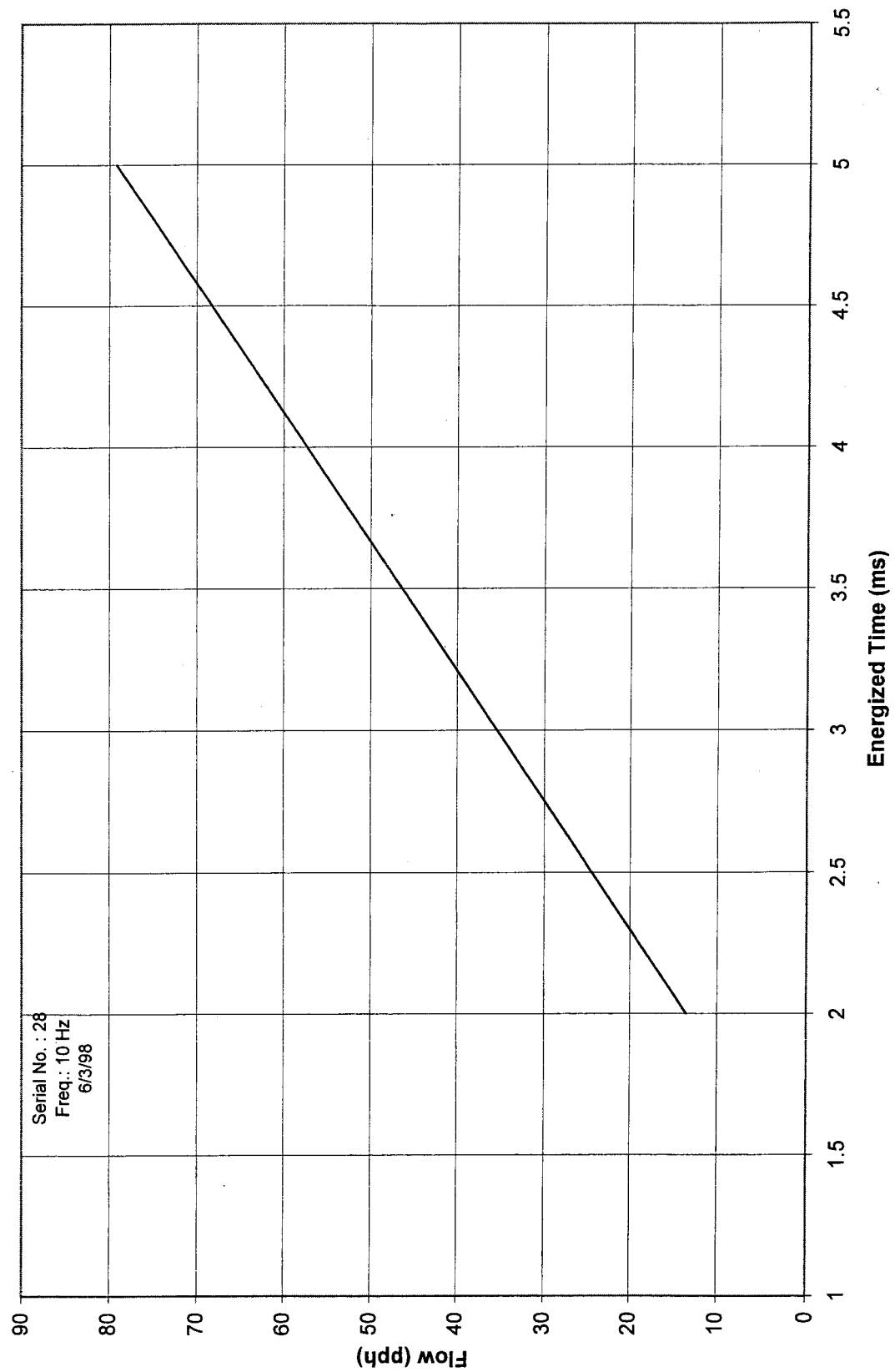
Allied Valve Comparison



Allied Valve Comparison



Allied Valve Comparison



APPENDIX III

**RELIABLE AND AFFORDABLE CONTROL SYSTEMS
ACTIVE COMBUSTOR PATTERN FACTOR CONTROL SYSTEM
MODES AND LOGIC DESIGN DOCUMENT**

Document No. 21-9690

(149 pages)

Prepared for:
NASA Lewis Research Center
Cleveland, Ohio

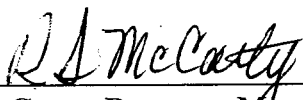
RELIABLE AND AFFORDABLE
CONTROL SYSTEMS
ACTIVE COMBUSTOR
PATTERN FACTOR CONTROL

SYSTEM MODES AND LOGIC DESIGN DOCUMENT

(NASA CONTRACT NO. NAS3-27752, TASK 1.2)

21-9690

June 10, 1997

Approved By: 
R. McCarty, Program Manager

Approved By: 
R. Stokes, Principal Investigator

REPORT NO.: 21-9690

This data is submitted with Limited Rights under Government Contract No. NAS3-27752. It may be reproduced and used by the Government with the express limitation that it will not, without permission of the Contractor, be used for purpose of manufacture nor disclosed outside the Government; except that the Government may disclose this data outside the Government for the following purposes, if any, provided that the Government makes such disclosure subject to prohibition against further use and disclosure.

ATTACHMENTS:

1. Interim Report, Combustor Pattern Factor Modeling And Control, Part II: Control Design; SMI, Inc., Tempe, AZ, February 5, 1997 (29 Pages)
2. PI Controller For Emissions Reduction Via Active Pattern Factor Control; J. Rushinsky, AlliedSignal Engines, Phoenix, AZ (35 Pages)
3. Fuzzy Logic Controller For Emissions Reduction Via Active Pattern Factor Control; T. Pfeifer, AlliedSignal Engines, Phoenix, AZ (77 Pages)

| Revision | By | Approved | Date | Pages and/or Paragraphs Affected |
|----------|-----|-------------------------|----------|----------------------------------|
| NC | GAL | R. McCarty R. Stokes | 06-10-97 | Initial Issue. |

AMENDMENT 1

ACTIVE COMBUSTOR PATTERN FACTOR CONTROL SYSTEM MODES AND LOGIC DESIGN DOCUMENT (NASA CONTRACT NO. NAS3-27752, TASK 1.2)

21-9690 AM 1

June 6, 2000

This amendment forms a part of Engines & Systems Document Number 21-9690, dated June 10, 1999, and is to be attached thereto. This amendment changes four figures in Attachment 3: Figure 12, page 15, and Figures 16-18, pages 26-28. The content is unchanged. The revisions are designed to make the charts more readable.

Affected Page(s)

Revision Summary

Pages 15-16

Page 15, Figure 12, dropped settling time for fuzzy logic controller, which obscured times for the PI Controller. Page 16 is unchanged and is provided as reverse to page 15.

Pages 25-28

Pages 26-28, Figures 16-18. Separated the actual and the sensed charting, which obscured each other in the initial document. Page 25 is unchanged and is provided as reverse to page 26.

Approved by: R. McGinley
R. McGinley
Principal Engineer

ACTIVE COMBUSTOR PATTERN FACTOR CONTROL (CONTRACT NO. NAS3-27752, TASK 1.2) SYSTEM MODES AND LOGIC DESIGN DOCUMENT

1.0 INTRODUCTION

This report, prepared by AlliedSignal Engines (AE), Phoenix, Arizona, for the National Aeronautics and Space Administration (NASA) Lewis Research Center, Cleveland, Ohio, comprises the System Modes and Logic Design document for the Active Pattern Factor Control Program, under Contract No. NAS3-27752, Task No. 1.2.

Active, closed-loop control of combustor emissions/pattern factor is a cooperative development effort being conducted by AlliedSignal Engines and the NASA Lewis Research Center to reduce emissions and turbine stator vane temperature variations, thereby enhancing engine performance and life, and reducing Direct Operating Costs (DOC). Total fuel flow supplied to the engine is established by the speed/power control, but the distribution to individual atomizers will be controlled by the Active Combustor Pattern Factor Control (ACPFC). The ACPFC system consists of three major components: multiple, thin-film temperature sensors located on the turbine stator vanes; fuel flow modulators for individual atomizers; and control logic and algorithms within the electronic control. A schematic of the system is shown in Figure 1.

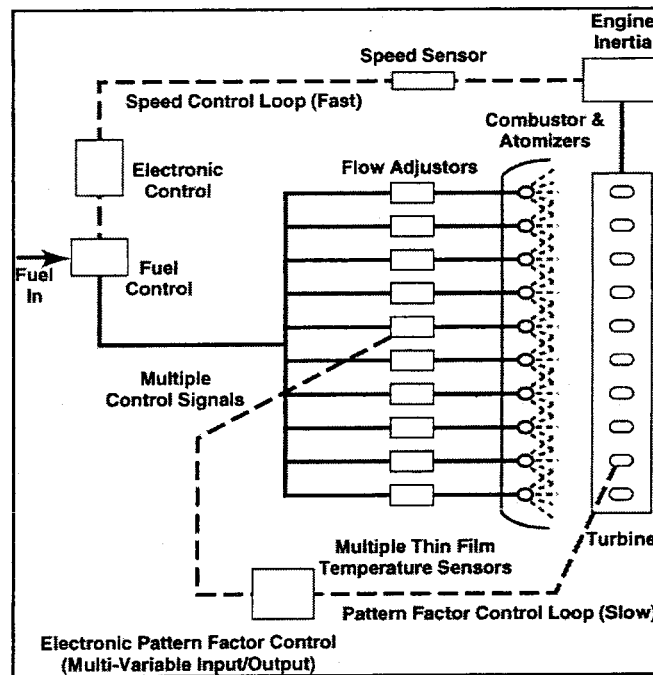


Figure 1: Basic Configuration for Active Combustor Pattern Factor Control

Various types of control logic were evaluated with respect to their performance on the Active Combustor Emissions/Pattern Factor Control System. This report documents the analysis performed to select the optimum control logic.

2.0 SUMMARY

Three reports are provided as attachments to this document, describing the development of and simulation results from several control algorithm designs for reducing engine emissions through Active Combustor Pattern Factor Control (ACPFC). From the outset of the ACPFC program (Reference NASA Contract No. NAS3-27752), our approach has been that AlliedSignal Engines and Scientific Monitoring, Inc., (Tempe, Arizona) would each independently develop a combustor plant model, and that each company would likewise develop candidate control strategies. This method offers a controls validation check using more than one model, and a variety of control options to consider. A version of the ACPFC model is described in AE Report 21-9645, titled "Reliable and Affordable Control Systems Active Combustor Pattern Factor Control -- Simulink Computer Simulation and Users Guide," which was submitted to NASA in mid-May, 1997. This model was used to evaluate the various control methods.

Included herein are details of the development and simulation results for the following control designs: (1) An optimization approach; (2) A spatial averaging Proportional plus Integral (PI) multi-input-multi-output (MIMO) control; (3) A harmonic control, using fast Fourier transforms (FFTs) to identify controllable spatial modes; (4) A peak detection/switching control; (5) An optimized, parallel Single-Input-Single-Output (SISO) PI control; and (6) Control algorithms based on "fuzzy" logic. Methods (1) through (4) and the results are described in Attachment 1 from Scientific Monitoring, Inc. Method (5) is detailed in Attachment 2. Method (6) is described in Attachment 3, including simulations over a range of failure modes.

The conclusion(s) from these studies were that Methods (4), (5), and (6) offer comparable benefits, but that other tradeoff factors, such as: ease of implementation, execution time, size of code, etc. need to be considered to make a final selection. These factors will be considered during the programming of the prototype control, scheduled to begin in November, 1997. The intent is to program more than one of the candidate control systems, so that comparison testing can be accomplished during the hardware rig testing.

ATTACHMENT 1

Interim Report, Combustor Pattern Factor Modeling And Control

Part II: Control Design

SMI, Inc., Tempe, AZ, February 5, 1997

(29 Pages)

Interim Report
Combustor Pattern Factor Modeling and Control

(Part II: Control Design)

Submitted to
AlliedSignal Engines
111 S. 34th Street
Phoenix, Arizona

As required by
Subcontractor Statement of Work
Dated on July 26, 1996

Reference P. O. no.: P0011026

Submitted by
Scientific Monitoring, Inc.
4801 S. Lakeshore Drive, Suite 103
Tempe, Arizona 85282-7156

February 5, 1997

Summary

This report contains SMI's effort in pattern factor control design on the Active Combustor Pattern Factor Control (ACPFC) program. The work on pattern factor modeling is summarized in a previous report which has been submitted to Allied-Signal Engines. In this report, system constraints and control design limitations are analyzed, and the following four control design approaches are investigated for a new temperature distribution:

- Optimization approach
- Spatial temperature averaging PI control
- Modal truncation and harmonic control
- Peak detection/switching control.

1.0. Problem Statement

The objective of pattern factor control is to minimize the pattern factor by adjusting the fuel flow rates in the modulated fuel nozzles while maintaining the total fuel flow rate the same. The definition of pattern factor used in this report is given below as

$$PF = \frac{T_{peak}}{T_{avg}} - 1 \quad (1)$$

where T_{peak} is the measured peak temperature at the combustor exit and T_{avg} is the averaged measured temperature.

A new combustor configuration is considered in which there are 20 modulated fuel nozzles (modulator) and 38 thermocouples. Both fuel modulators and thermocouples are distributed equally circumferentially, the first fuel modulator is placed at 0 degree mark and the first thermocouple is placed at 5 degree mark.

The nominal temperature profile around the circumference at the combustor exit is given in Figure 1. The averaged temperature of this nominal temperature profile is 2291.5 degree (F). The peak temperature is 2586.7 degree (F) which occurs at thermocouple #15 (angular position 137.6 degree), and the minimum temperature is 2004.4 at thermocouple #25 (angular position 232.4 degree).

The fuel flow rate through a modulator is controlled by its opening area which can also be considered as a control parameter. A fuel flow rate perturbation in a modulator can be considered as a variation of the modulator opening area. If each modulator

opening area is normalized to one for the nominal case, then the normalized opening area of a modulator corresponding to a fuel flow rate change ΔW can be written as

$$Marea = (1 + \frac{\Delta W}{W_{in}}) \quad (2)$$

where W_{in} is the nominal fuel flow rate through the modulator.

In the subsequent sections, the fuel flow rate perturbations are used as the control input, the corresponding variations in the normalized area can be computed according to Eq.(2).

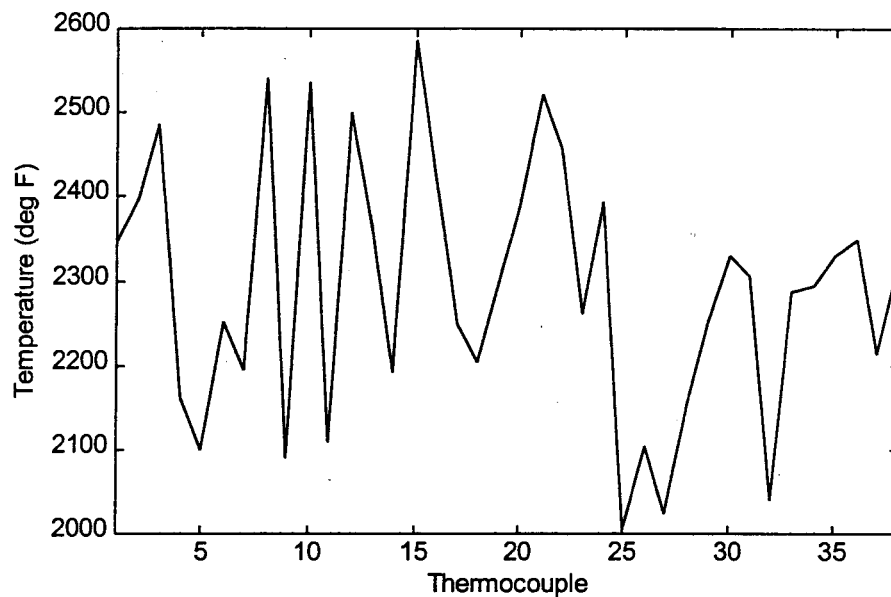


Figure 1. Nominal temperature profile.

2.0. Open-loop Pattern Factor Control Model

A linear combustor pattern factor control model developed in Simulink is shown in Figure 2. This is a perturbation model based on the given nominal operation condition. The control input vector is fuel flow rate variations from the nominal fuel flow rates through modulators and the output vector is the thermocouple readings. The nominal temperature profile is treated as two external constant inputs to the system, represented by the blocks: Perturbations and Nom. Avg. Temp.. The block Nom. Avg. Temp. represents the nominal averaged temperature and the block Perturbations represents the variations of the nominal temperatures from the nominal averaged temperature.

The central part of the open loop model is the influence coefficient matrix which describes (to the first order) the relationship between the fuel flow rate changes in the modulators and the corresponding temperature changes around the combustor circumference at the exit. The dynamics of fuel transportation and thermocouples are also considered in this model. The former is considered as a 0.025 second delay and the latter is considered as a first-order system with a time constant of 2.0 seconds. Furthermore, a Pade approximation is used to represent the 0.025 transportation delay.

In this open-loop model, there is no coupling among thermocouples. The influence coefficient matrix provides only static couplings between fuel modulators and thermocouples. The total fuel flow rate constraint also provides some coupling among fuel modulators.

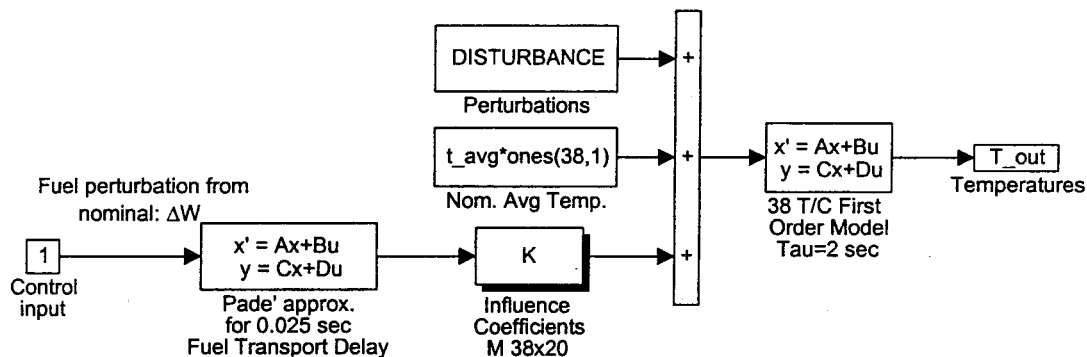


Figure 2. Open-loop block diagram of pattern factor control model.

Influence coefficient matrix

The influence coefficients for a single fuel modulator to all the downstream thermocouples have been generated from pattern factor test data in the Interim Report Part I-PF Modeling. The test data analyzed in Interim Report Part I is obtained through 36 thermocouples, while in the design configuration here they involve 38 thermocouples. Although an interpolation method can be used to generate the influence coefficients for 38 thermocouples from the influence coefficients for 36 thermocouples, the following normal Gaussian function is used to approximate the influence coefficients:

$$m_a = 34e^{\frac{-(\theta-10)^2}{2\sigma^2}} \quad (3)$$

where θ is the angular difference (degs) between thermocouple location and the modulator location, the number 10 in the exponent is for the circumferential shift of 10

degree in the experimental data, $\sigma=8$ is the standard deviation representing the spread of temperature profile for a single modulator.

As shown in Figure 3, this function fits the influence coefficients from test data very well. The circumferential variations in the influence coefficients from real data is probably due to flow variation and measurement noise.

All 20 modulators are assumed identical, the influence coefficient matrix M of dimension 38×20 is formed by applying the above influence coefficients obtained after functional fit to every modulator.

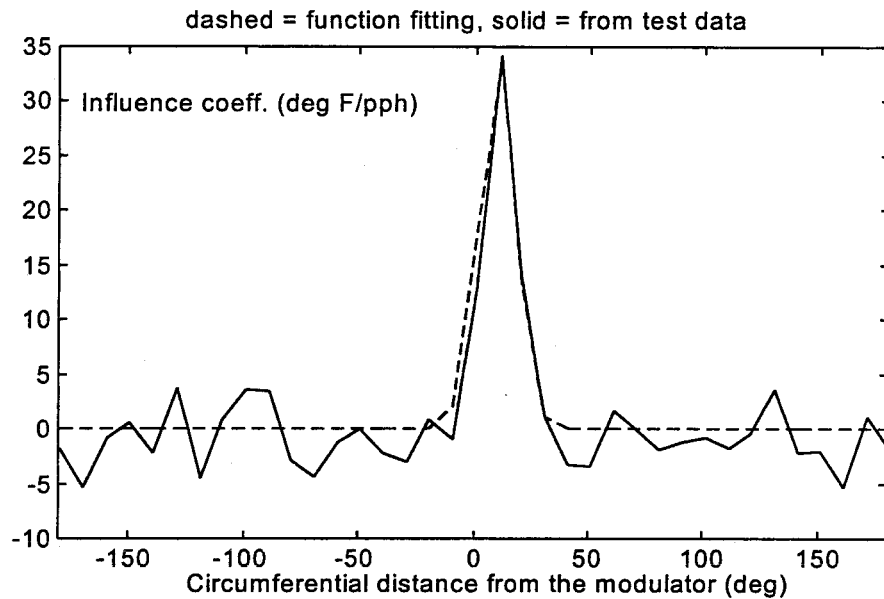


Figure 3. Functional fit of influence coefficients.

Dynamics of fuel transportation delay and thermocouples

For a single fuel modulator, the following Pade approximation is used to approximate the fuel transportation delay:

$$g_t(s) = \frac{1 - \frac{T}{2}s}{1 + \frac{T}{2}s} \quad (4)$$

where $T=0.025$ is the transportation delay time. The state space description of the block representing the fuel transportation delay is then given as

$$\begin{aligned} \dot{x}_d &= A_d x + B_d u \\ y_d &= C_d x + D_d u \end{aligned} \quad (5)$$

where $A_d = -80I_{20}$, $B_d = I_{20}$, $C_d = 160I_{20}$, and $D_d = -I_{20}$. The initial conditions of the state variables are set to zero.

The state space representation for the thermocouples is given as

$$\begin{aligned}\dot{x}_t &= A_t x + B_t u \\ y_t &= C_t x\end{aligned}\tag{6}$$

where $A_t = -0.5I_{38}$, $B_t = 0.5I_{38}$, and $C_t = I_{38}$. The initial conditions of the state variables are the thermocouple temperature readings at nominal condition.

3.0. Control Constraints and Design Limitations

3.1. Fuel flow rate conservation

A constraint on the pattern factor control is to maintain the total fuel flow rate the same. In terms of the perturbed fuel flow rates, this requires that

$$\sum_{i=1}^{20} \Delta W_{fi} = 0\tag{7}$$

where ΔW_{fi} is the perturbed fuel flow rate through the i th modulator. The total fuel flow rate conservation is implemented in the control designs by a fuel conservation matrix

$$K_{conservation} = \begin{bmatrix} 1 & -1/19 & \cdots & -1/19 \\ -1/19 & 1 & \cdots & -1/19 \\ \vdots & \vdots & \ddots & \vdots \\ -1/19 & -1/19 & \cdots & 1 \end{bmatrix}\tag{8}$$

This conservation matrix implies that a fuel flow rate increase in one modulator causes a uniform fuel flow rate decrease in all the other modulators.

3.2. Averaged temperature

From the pattern factor definition given in Eq.(1), it can be seen that one can control pattern factor by either reducing peak temperature or increasing the averaged temperature, or both. In closed-loop control, the temperature profile measured by the thermocouples is fed to a controller to generate the necessary fuel flow rate adjustments

to each modulator in order to control the pattern factor. When the closed-loop system reaches a steady state, we will show that the averaged temperature at the combustor exit is approximately constant as long as the total flow rate is maintained the same.

Referring to the open-loop system in Figure 2, the transfer function from the control input ΔW to the temperature reading T_{out} can be written as

$$G_o(s) = G_t(s)MG_d(s) \quad (9)$$

where $G_t(s)$ is the transfer function of thermocouple dynamics, M is the influence coefficient matrix, and $G_d(s)$ is the transfer function of fuel transportation delay. From Eqns.(5) and (6), the open-loop transfer function can be written as

$$G_o(s) = \frac{0.5}{s+0.5} \left(\frac{160}{s+80} - 1 \right) M \quad (10)$$

Suppose the perturbed fuel flow rates through the modulators reach constant at steady state, say ΔW_{fss} , then the steady state circumferential temperature deviations from nominal condition, ΔT_{ss} , become

$$\Delta T_{ss} = \lim_{s \rightarrow 0} s G_o(s) \left(\frac{1}{s} \Delta W_{ss} \right) = M \Delta W_{fss} \quad (11)$$

Since all the modulators are assumed identical, the sums of the columns of the matrix M are the same. Therefore, the averaged temperature deviation from the nominal condition is

$$C \Delta T_{ss} = C M \Delta W_{fss} = c_1 C \Delta W_{fss} = 0 \quad (12)$$

where $C = [1, 1, \dots, 1]_{1 \times 20}$ and c_1 is the sum of one column of the influence coefficient matrix M .

3.3 System controllability

Since there are no dynamic couplings among thermocouples, the influence coefficient matrix is constant, and the number of modulators is less than the number of thermocouples, the open-loop system is not completely controllable. Specifically, it is not possible to make an arbitrary circumferential temperature profile uniform at combustor exit. This can be easily verified by checking the controllability matrix of the open-loop system. As a matter of fact, the controllable subspace for the circumferential temperatures is the space spanned by the columns of influence coefficient matrix M .

A desired pattern factor control is to make the temperature profile uniform. This would require the perturbed fuel flow rates to generate a temperature distribution that is opposite to the temperature variations from the averaged temperature in the nominal case. Since the temperature variations in the nominal temperature profile do not fall into the controllable subspace, therefore, it is not possible to generate a perfect uniform temperature profile based on the model given in Figure 2.

Another way to look at the design constraint is to investigate the spatial modes of the temperature profile at steady state. For illustration purpose, the first two spatial modes are shown in Figure 4. As we know, 38 thermocouples can measure $(n/2-1)=18$ modes above the zero-th mode (with uniform temperature distribution). However, with 20 modulators, only 9 modes can be resolved. The higher modes are beyond the modulator resolution. The power spectral density of temperature variations from the averaged temperature in nominal case is shown in Figure 5. It can be seen that there is a substantial energy in the higher modes (10th ~ 18th modes).

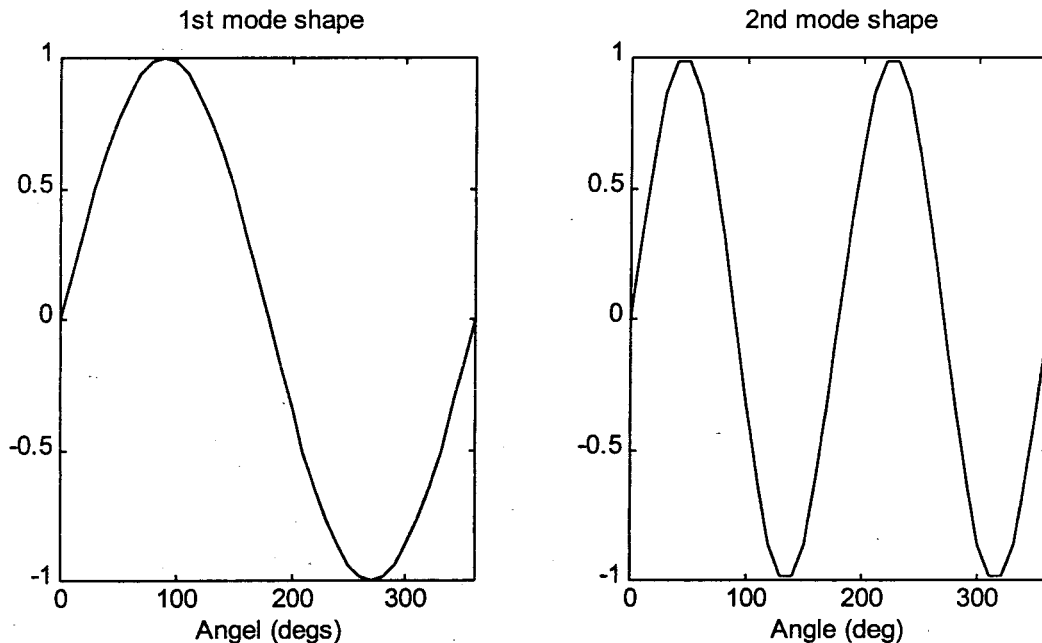


Figure 4. Plot of the first two spatial modes.

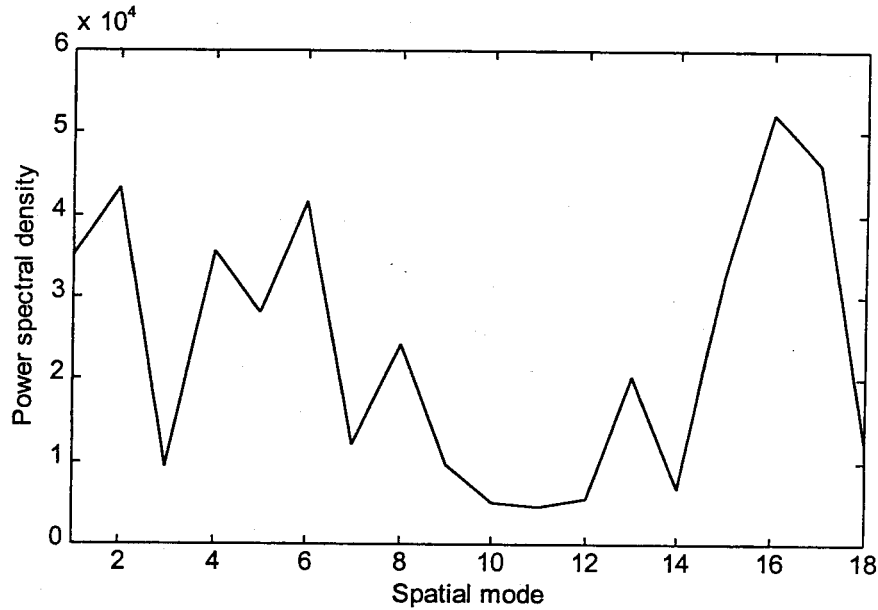


Figure 5. Power spectral density of the temperature variations of nominal temperature profile.

4.0. Control Design Approaches

4.1. Optimization approach

A static optimization approach is investigated which minimizes a *weighted quadratic sum* of the combustor exit temperature deviations between a desired temperature profile and the local temperatures measured at various circumferential locations. The optimization objective function is

$$J = (T - T_d)^T Q (T - T_d) \quad (13)$$

where T is the vector of measured temperature, T_d is the desired temperature profile, and $Q > 0$ is a positive weighting matrix. In the following, T_d is assumed a uniform temperature profile with its averaged temperature equal to the averaged measured temperature. The weighting matrix Q is a function of the measured temperatures and the desired temperatures as well. One can either reduce the peak temperature or reduce the maximum temperature deviation from the averaged temperature using the optimization approach.

The optimization of the objective function is subject to the constraint of maintaining the same total fuel flow rate during the pattern factor control process. The constraint equation can be expressed as

$$C * W_f^* = U_0 \quad (14)$$

where $C = [1, 1, \dots, 1]_{1 \times 20}$, W_f^* is the vector of optimal fuel flow rates through all the modulators, and U_0 is the nominal total fuel flow rate in the combustor.

The solution to the above constrained optimization problem is given by

$$\Delta W_f = -HM^T Q + HC^T (CHC^T)^{-1} CHM^T Q \quad (15)$$

where $H = (M^T Q M)^{-1}$ and ΔW_f is the vector of perturbed fuel flow rates from the nominal fuel flow rates.

The closed-loop control block diagram developed in Simulink is shown in Figure 6. The Matlab function block continuously updates the optimal fuel flow rate perturbations based on the measured temperature profile according to Eq.(15). If a constant weighting matrix is used, this Matlab function block can be replaced by a constant gain block. Two weighting matrices $Q1$ and $Q2$ are investigated in the following, with $Q1$ emphasizing the reduction of peak temperature and $Q2$ emphasizing the reduction of maximum temperature deviation. Both matrices are diagonal, the i th diagonal elements of the two matrices are

- 1) $Q1(i,i) = \max(0.1, \Delta T(i) / \Delta T_{\max})$;
- 2) $Q2(i,i) = \max(0.1, |\Delta T(i)| / \Delta T_{\max})$.

where $\Delta T(i)$ is the temperature difference between the measured temperature at the i th thermocouple and the averaged measured temperature, and ΔT_{\max} is the maximum temperature difference between the measured temperatures and the averaged measured temperature.

The time responses of thermocouple readings and perturbed fuel flow rates for both weightings are given in Figure 7, 8, 10, and 11, respectively. The temperature profiles at 10 seconds for both weightings are given in Figure 9 and 12, respectively. One may notice that there are small peaks of perturbed fuel flow rates in some fuel modulators, these may be caused by the updating of the weighting matrix during the control process.

The results of the optimization approach are summarized in Table 1 below. The RMS in the table indicates the root-mean-square of the temperature variations from the

averaged measured temperature. The peak temperature is reduced by about 103 deg (F) using *Q1* and 63 deg (F) using *Q2*. The minimum temperature is reduced by about 10 deg (F) using *Q1* and increased by about 57 deg (F) using *Q2*. The pattern factor (PF) is reduced from 0.1288 to 0.0837 using *Q1* and 0.1013 using *Q2*.

Table 1. Summary of the control results of optimization approach.

| | T_max (deg F) (change) | T_min (deg F) (change) | PF (change) | RMS (deg F) (change) |
|----------------|---------------------------|---------------------------|-----------------|-------------------------|
| Before control | 2586.7 | 2004.4 | 0.1288 | 151.7 |
| Q1 | 2483.4 (-103.3) | 1994.5 (-9.9) | 0.0837 (-35.0%) | 110.7 (-41.0) |
| Q2 | 2523.7 (-63.0) | 2061.8 (57.4) | 0.1013 (-21.4%) | 110.5 (-41.2) |

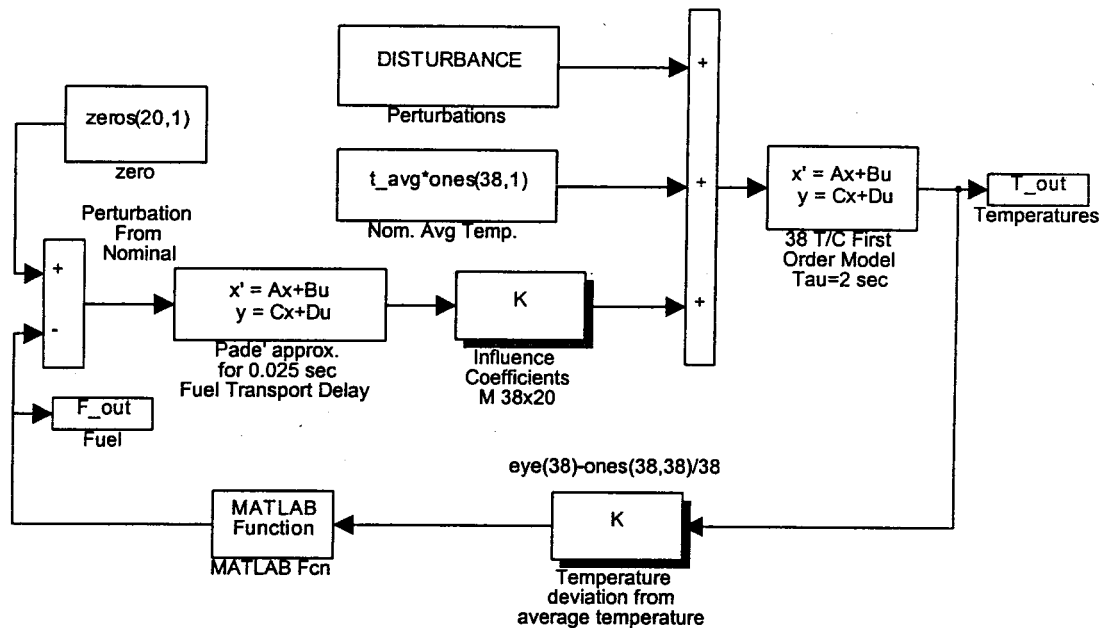


Figure 6. Simulink block diagram of the closed-loop system for optimization approach.

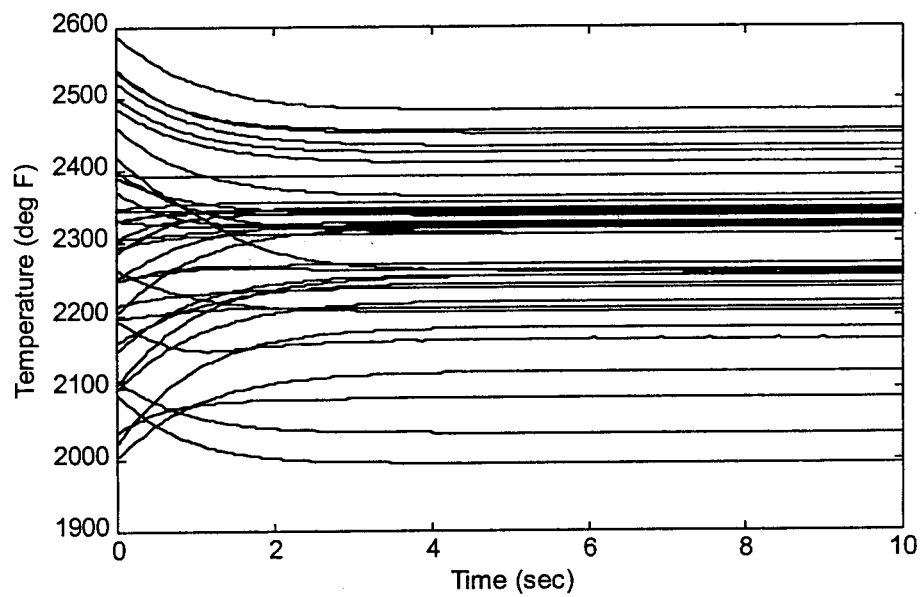


Figure 7. Optimization approach (Q1): time responses of 38 thermocouple readings.

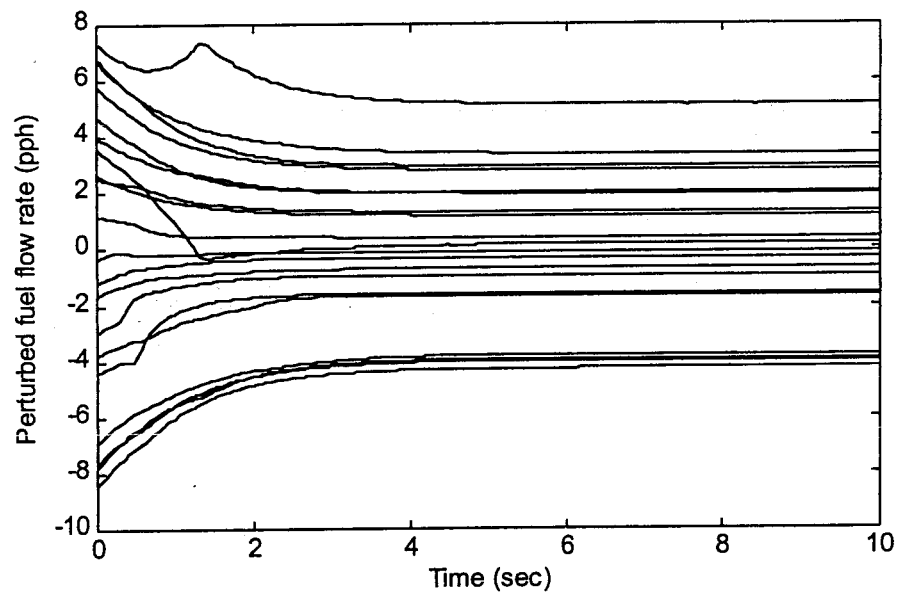


Figure 8. Optimization approach (Q1): time responses of the perturbed fuel flow rates.

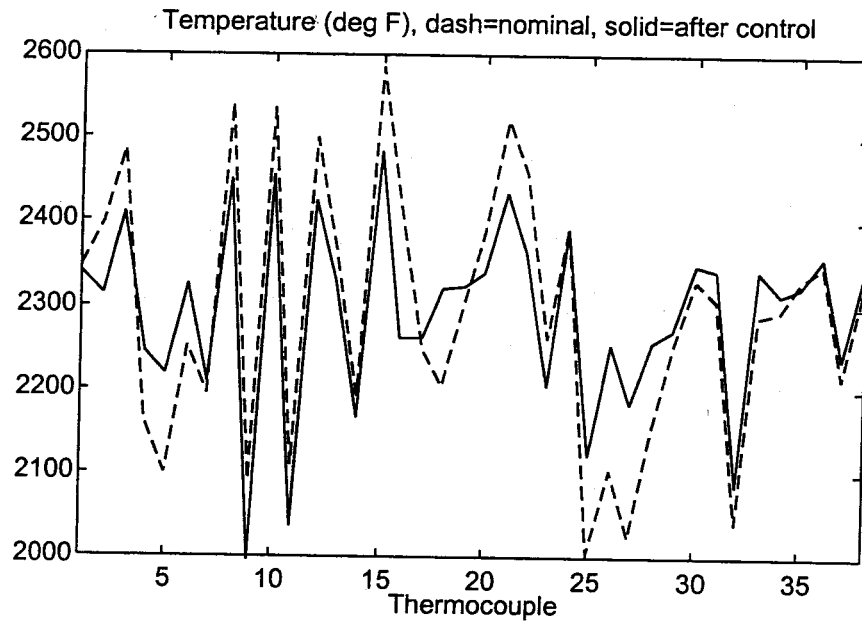


Figure 9. Optimization approach (Q1): temperature profile at 10 seconds.

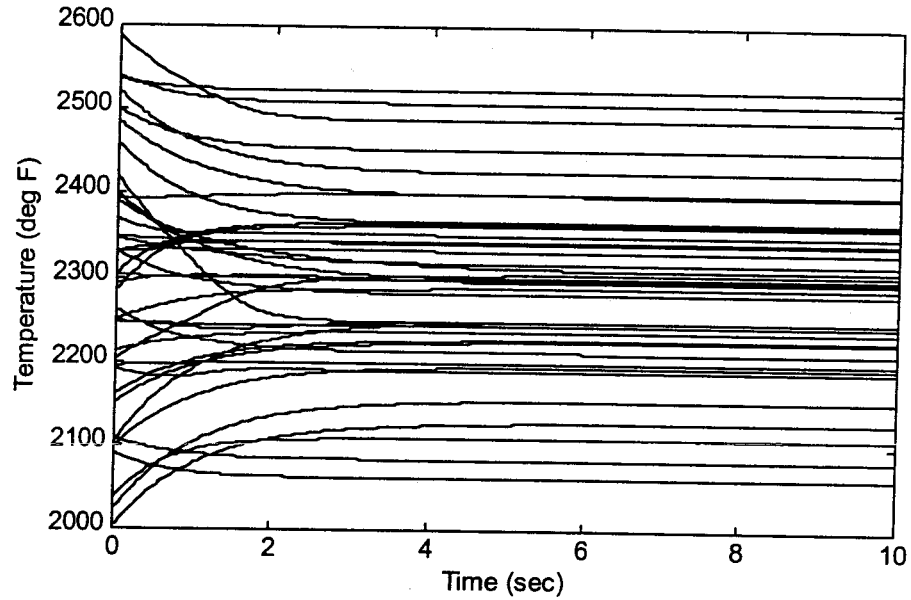


Figure 10. Optimization approach (Q2): time responses of 38 thermocouple readings.

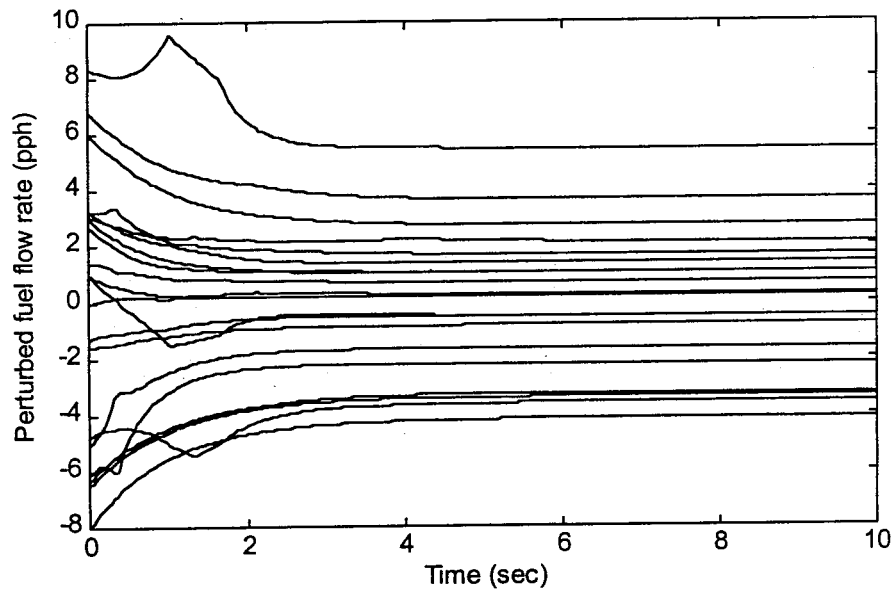


Figure 11. Optimization approach (Q2): time responses of the perturbed fuel flow rates.

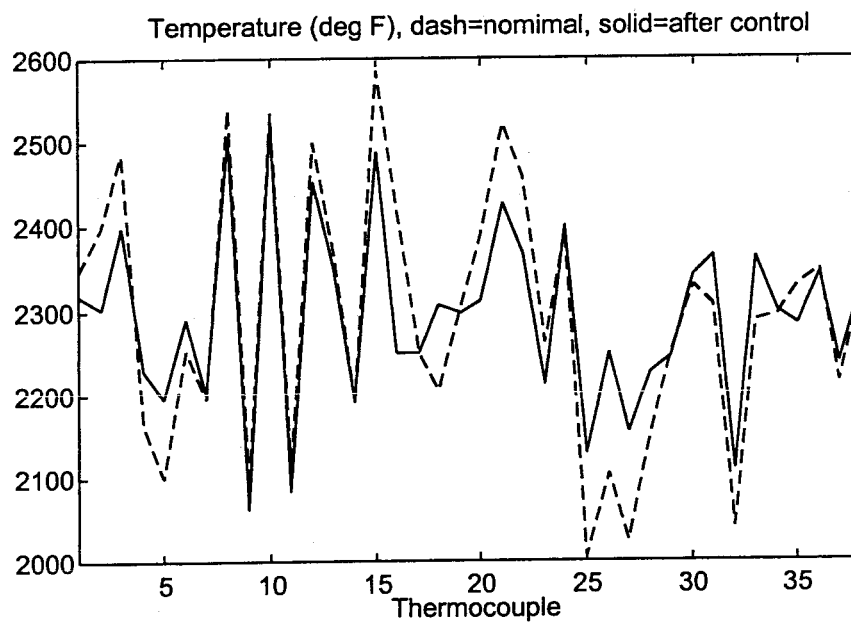


Figure 12. Optimization approach (Q2): temperature profile at 10 seconds.

4.2. Spatial averaging PI control

Since it is not possible to control 38 thermocouples with only 20 modulators, a spatial temperature averaging is used to obtain a square multi-input multi-output system. This is realized by a conversion matrix to convert 38 actual thermocouple reading to 20 pseudo thermocouple readings. A PI control is then used to average out the 20 pseudo temperatures.

Figure 13 shows the block diagram for spatial averaging PI control implementation in Simulink. The integral gain matrix is taken as $-0.033I_{20}$ and the proportional gain is taken as $-0.017I_{20}$. The fuel flow rate conservation matrix is the same as in Eq.(8). The matrix Sys3 which is used to convert 38 thermocouple readings to 20 pseudo thermocouple readings is generated based on the influence coefficient matrix by the following Matlab code:

```
for I=1:20
    Sys3(i,:)=M(:,i)/sum(M(:,i))
end;
% This loop just gets rid of the small values
for i=1:20,
    for j=1:38,
        if abs(Sys3(i,j)) < 1e-8
            Sys3(i,j)=0;
        end;
    end;
end;
```

Note that matrix Sys3 is just a weighting matrix for the spatial averaging and any other spatial averaging techniques could be used.

Figure 14 shows the pseudo temperature responses. It is seen that the 20 pseudo temperatures are indeed averaged out. However, as shown in Figure 15 and Figure 16, the 38 temperatures reach a steady state, but are not averaged out. As pointed out in previous section, there is not enough modulator spatial resolution to control the circumferential temperature profile formed by 38 thermocouple readings.

The peak temperature is reduced by about 57 deg F, the minimum temperature is increased by about 35 deg F, and the RMS of temperature variations from the averaged temperature is reduced to 99.6 deg F from 151.7 deg F. The pattern factor is 0.1039 at the steady state, a 19.3% reduction from the nominal case.

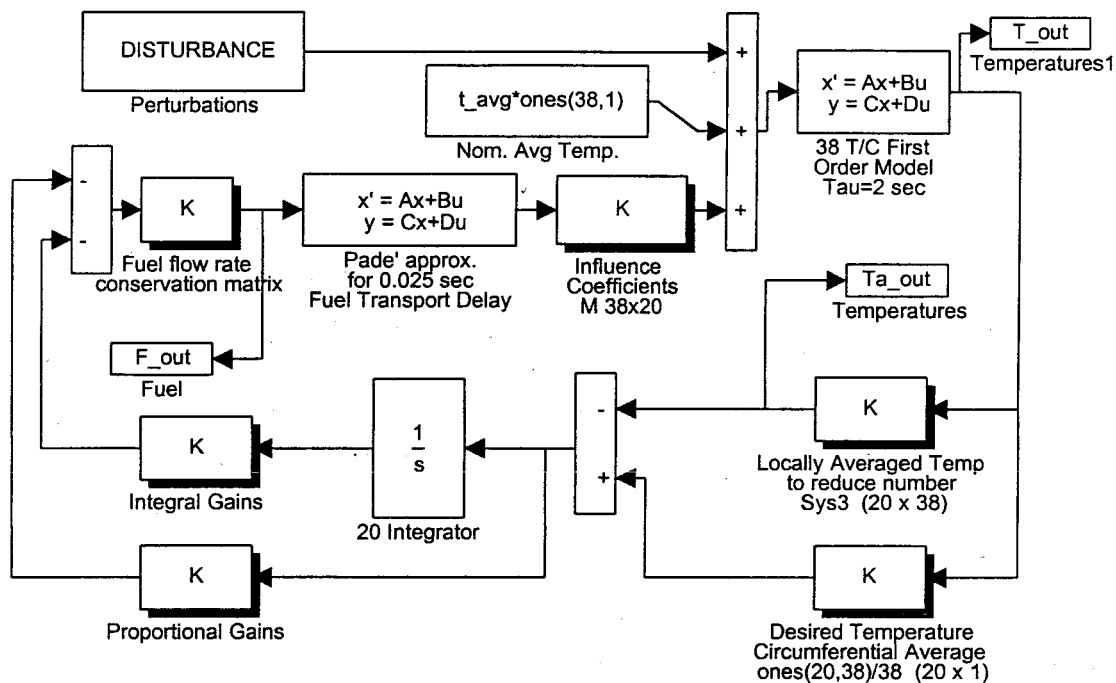


Figure 13. Simulink block diagram of the closed-loop system for spatial averaging control.

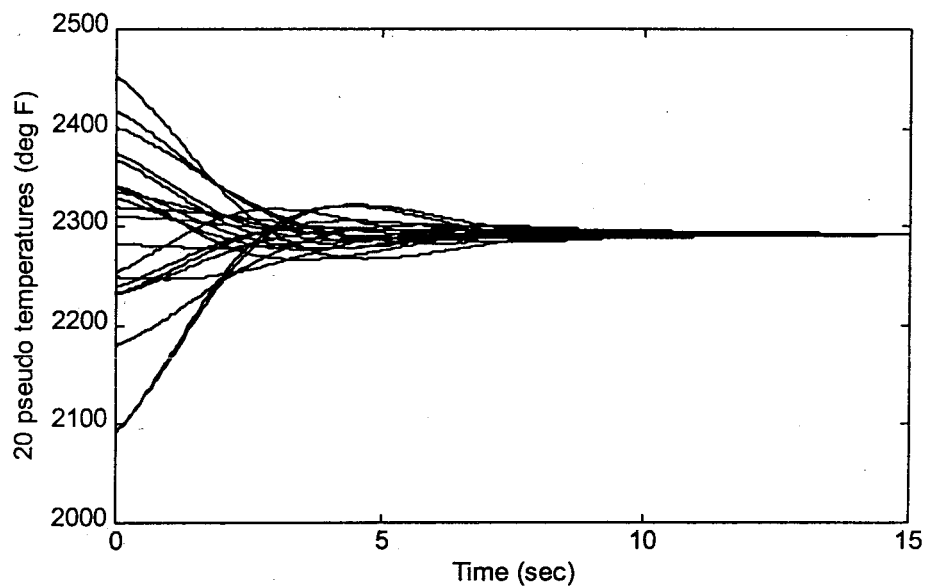


Figure 14. Spatial averaging control: time responses of 20 pseudo temperatures.

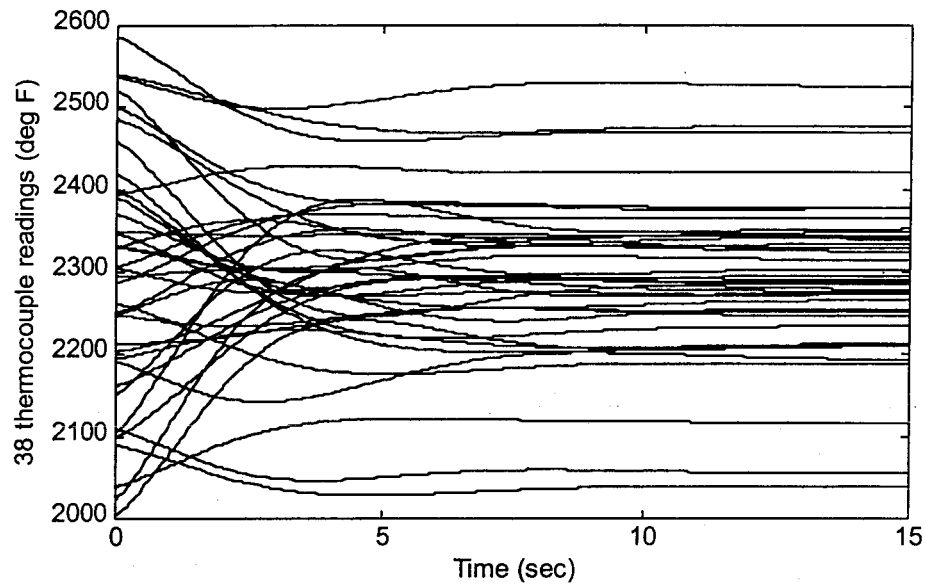


Figure 15. Spatial averaging control: time responses of 38 thermocouple readings.

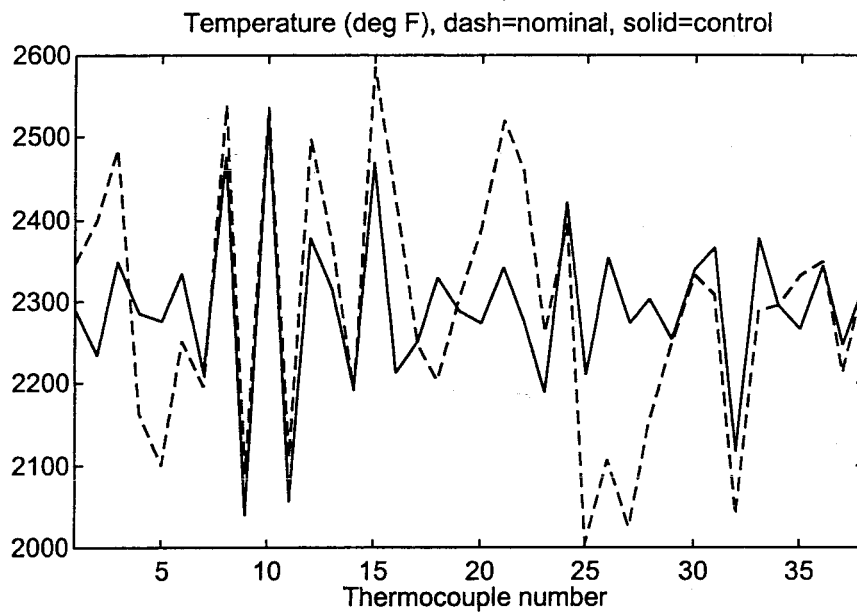


Figure 16. Spatial averaging control: temperature profile at 10 seconds.

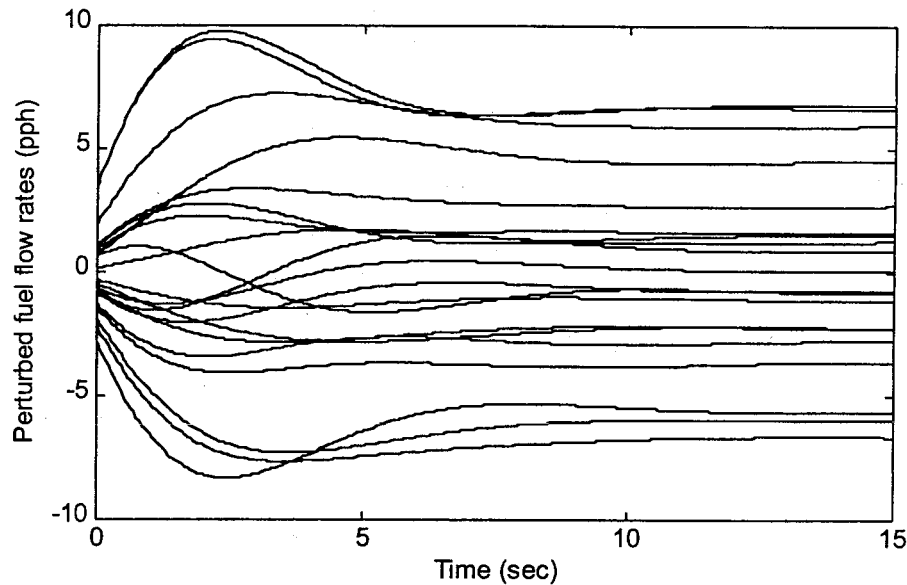


Figure 17. Spatial averaging control: time responses of perturbed fuel flow rates.

4.3. Harmonic control

The concept of harmonic control is based on the fact that 20 fuel modulators can only control the first 9 spatial modes in an arbitrary circumferential temperature profile. Figure 18 shows the harmonic control implementation in Simulink. A simple proportional controller is applied to cancel the first 9 spatial temperature deviation modes. The Matlab Function `smifft.m` is as follows:

```
function [y] = smifft(u);
u_fft = fft(u([1,2,3:38],1));
yfft = u_fft([1:10,20,30:38]); % Eliminate small period modes
yfft(1,1) = 0,                % NO DC COMPONENT
y = real(ifft(yfft));          % The imaginary parts are 1e-13 small.
```

This function routine calculates a discrete fast Fourier transformation (FFT) and truncates modes 10 and up, keeping the 9 lowest modes. The routine then calculates the corresponding inverse FFT and uses the negative of this function as the error in a proportional controller. Since the uncontrollable modes have been filtered out and we only try to control the modes that we have enough spatial resolution to control, this routine can be considered as a spatial filter.

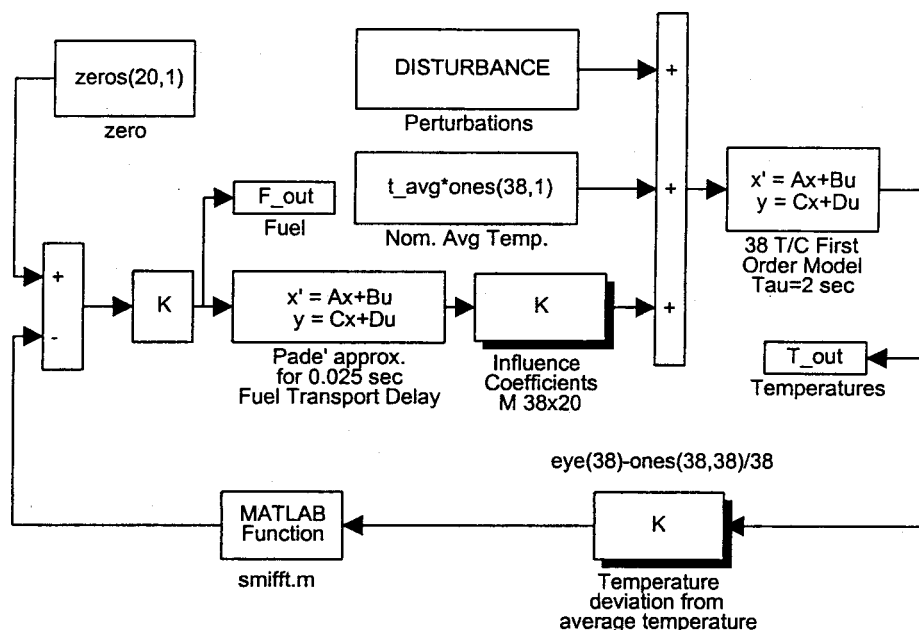


Figure 18. Simulink block diagram of the closed-loop system for harmonic control.

The time responses of thermocouple temperature readings and perturbed fuel flow rates are shown in Figure 19 and Figure 20. The temperature profile at 10 seconds is shown in Figure 21. The peak temperature is increased by about 32 degrees (F) and the minimum temperature is almost unchanged. The RMS of temperature variations from the averaged temperature is reduced by 24 degrees (F). Due to the peak temperature increase, the pattern factor is increased to 0.1427 from 0.1288 in nominal condition.

From Figure 22, it can be seen that harmonic control does significantly reduce the energy in the first 9 modes. The energy in higher modes changes very little. The main reason for the increase of peak temperature may be the spillover effect on the uncontrollable higher modes. A more sophisticated harmonic controller design may obtain better results, but still be limited to lower modes.

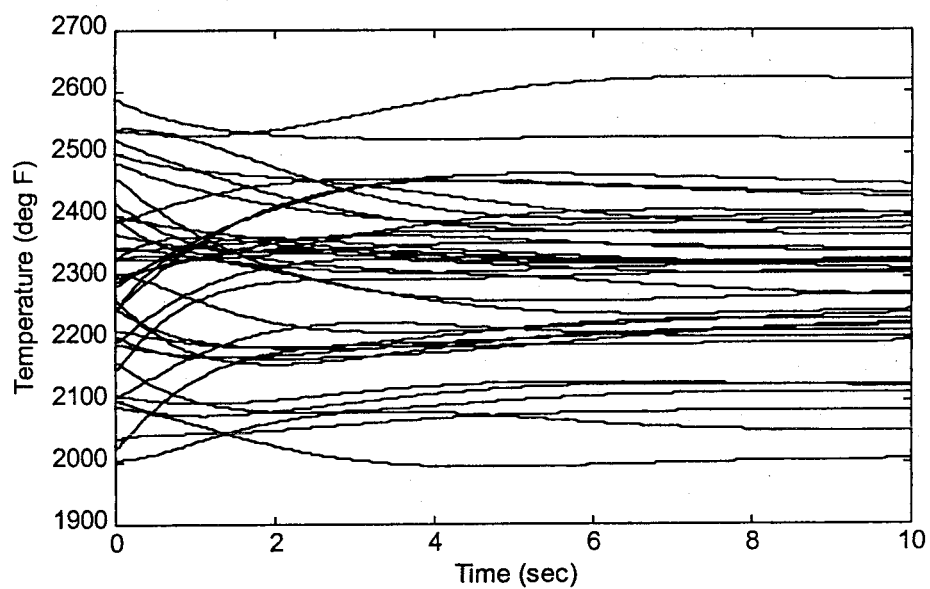


Figure 19. Harmonic control: time responses of 38 thermocouple readings.

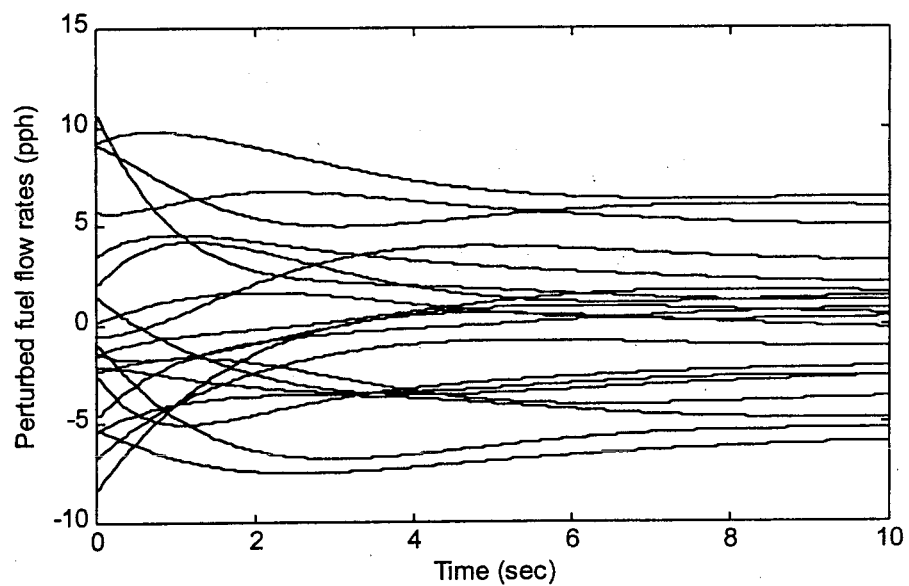


Figure 20. Harmonic control: time responses of perturbed fuel flow rates.

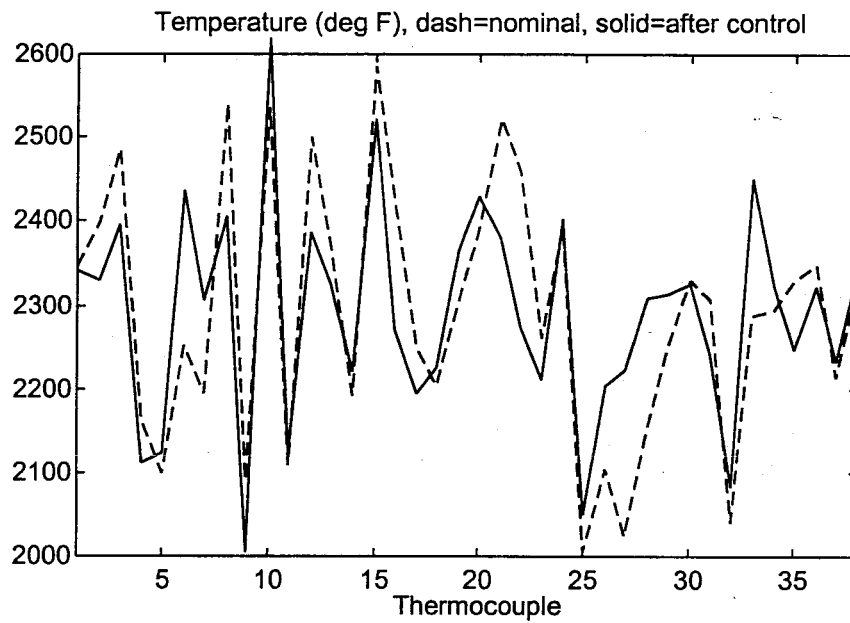


Figure 21. Harmonic control: temperature profile at 10 seconds.

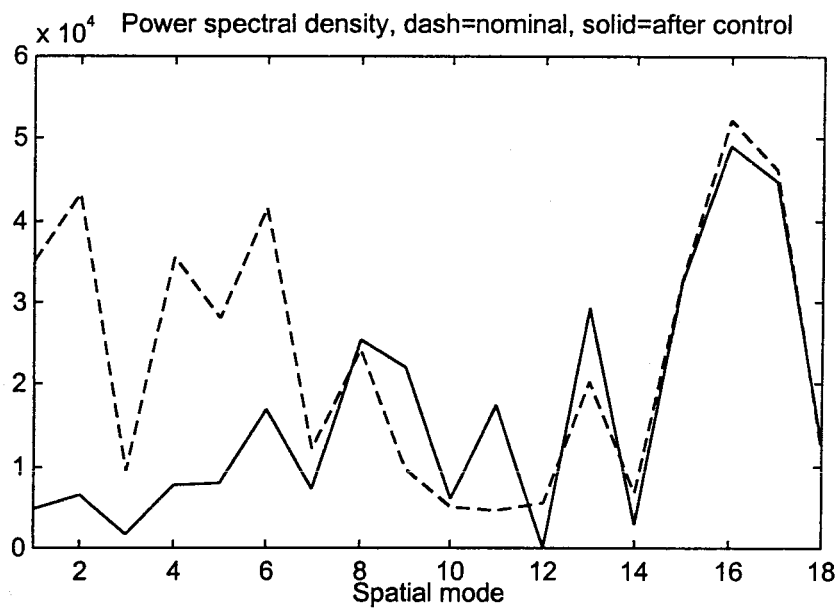


Figure 22. Harmonic control: power spectral density of temperature variations.

4.4. Peak detection/switching control

Figure 23 shows the implementation block diagram of the closed-loop system for peak detection/switching control. It includes a pure integral controller (K_i/s) with peak detecting and switching logic. The matrix $K_{\text{constraint}}$ is the fuel flow rate conservation matrix given in Eq.(8). Once a thermocouple is selected, the corresponding fuel modulator is determined for fuel flow modulation. The peak temperature deviation is used as a feedback through a constant gain to the integrator associated with that particular fuel modulator.

The routine `pdsc.m` selects the thermocouple with maximum temperature reading and computes the integer number associated with the corresponding fuel modulator for reducing the peak temperature. The Matlab code of `pdsc.m` is

```
function [feedback] = pdsc(u);
N=38; %t/c
M=20; %modulators
[T,n]=sort(u);
Tmax=T(N);
thermocouple =n(N);
%find t/c angle. #1 starts at 5 degs.
thermocouple_deg=5+360/(N)*(thermocouple-1);
mod=round((((thermocouple_deg-20)*M)/360+1));
if mod==0, mod=20, end;
feedback=zeros(20,1);
feedback(mod,1)=Tmax;    %20x1 vector with 1 nonzero scalar
```

The routine `pdsc2.m` selects only the thermocouple with the maximum temperature reading, its Matlab code contains only a part of the code of `pdsc.m`.

Figure 24 and Figure 25 show the time responses of thermocouple temperature readings and the perturbed fuel flow rates. Figure 26 shows the temperature profile at 10 seconds and Figure 27 shows the change of the thermocouple with maximum temperature reading with time. After 10 seconds, the peak temperature is reduced by about 195 degree (F) and the minimum temperature is also reduced by about 124 degree (F). The root-mean-square of the temperature variations from its averaged temperature is reduced to 135.4 from 151.7. The pattern factor is reduced to 0.0442 from 0.1288, a 65.7% reduction from nominal case.

This version of switched controller does not address low spots and thus cold spots are generated as part of average reduction mechanism. Modifications to this switched controller to include a lower limit are possible.

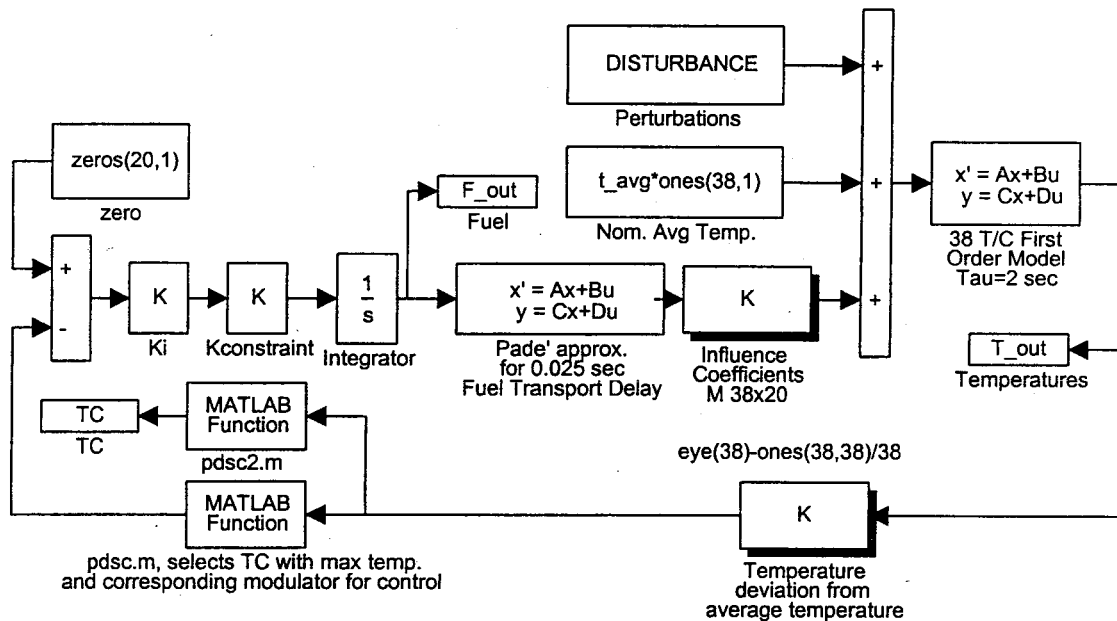


Figure 23. Simulink block diagram of the closed-loop system for peak detection/switching control.

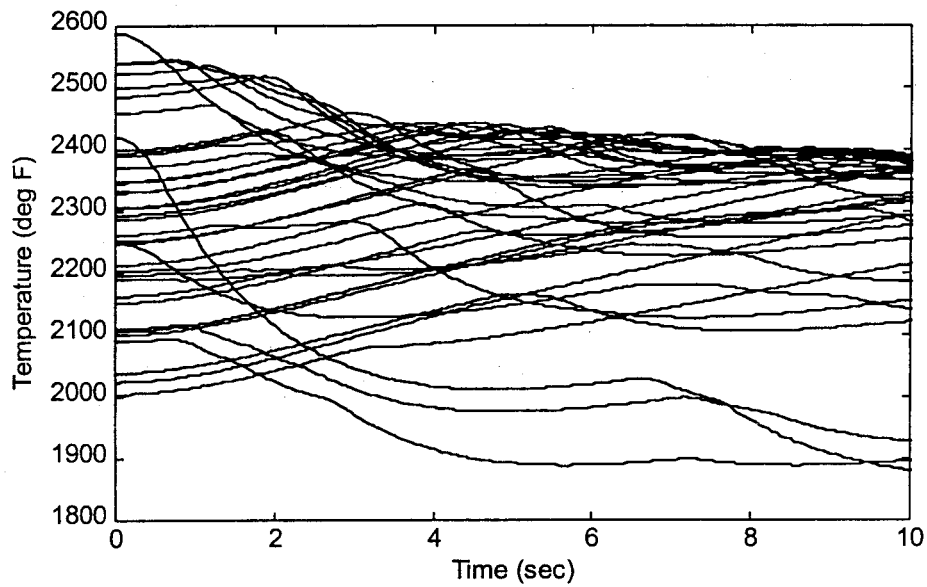


Figure 24. Peak detection/switching control: time responses of 38 thermocouple readings.

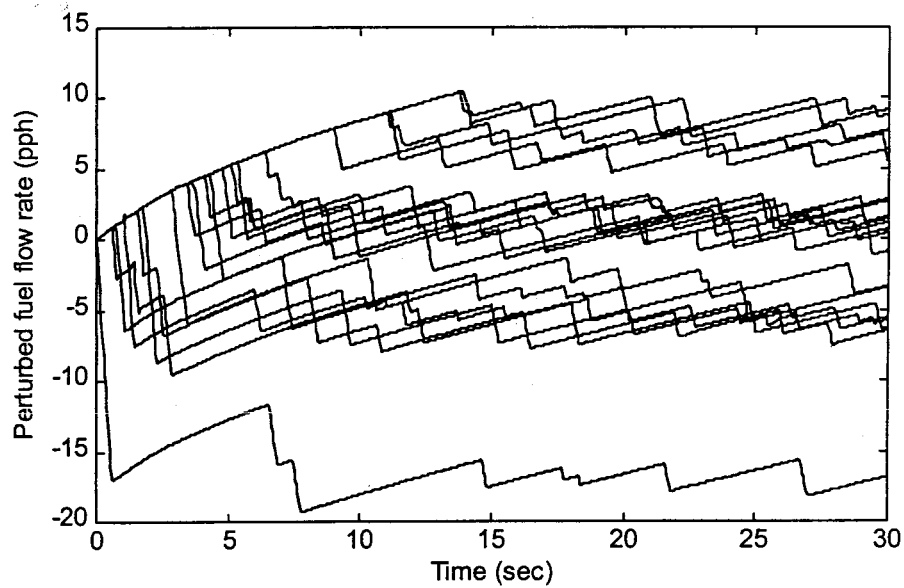


Figure 25. Peak detection/switching control: time responses of perturbed fuel flow rates.

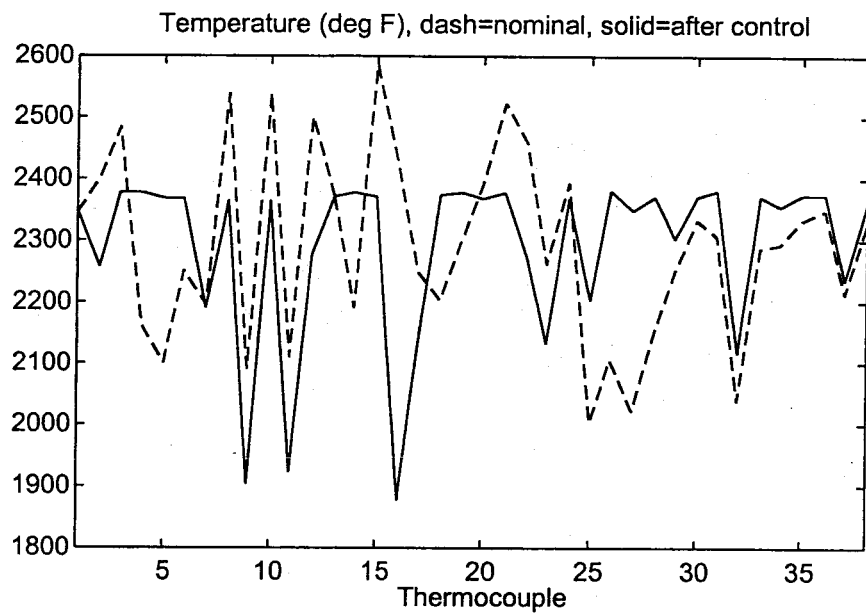


Figure 26. Peak detection/switching control: temperature profile at 10 seconds.

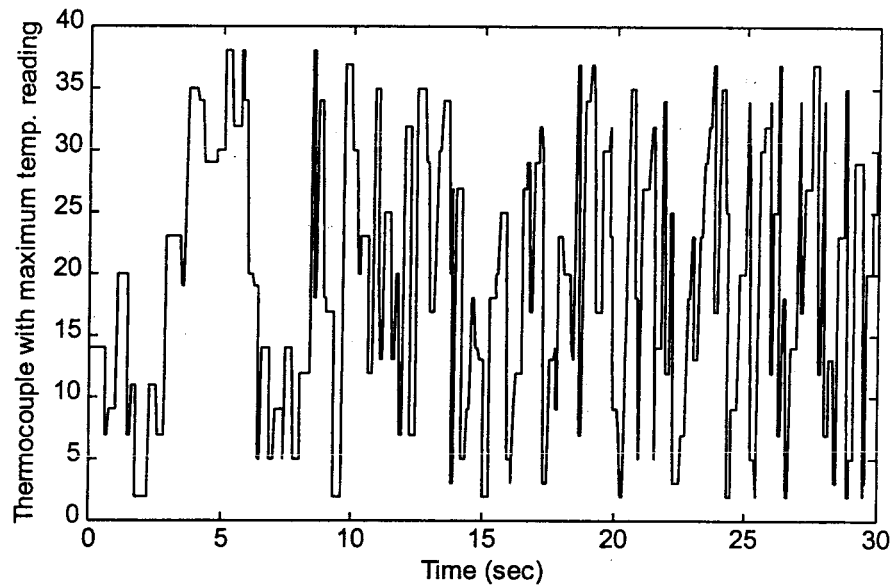


Figure 27. Peak detection/switching control: thermocouple with maximum temperature reading versus time.

4.5. Comparison and discussion

The results of the four control approaches discussed in above sections are summarized in Table 2 below. Following observations are made from the control design results:

- The pattern factor (or peak temperature) is reduced for all control approaches except the harmonic control. Maximum pattern factor reduction (66%) is achieved via the peak detection/switching control. The harmonic control needs to be further investigated to get better results.
- The root-mean-square of temperature variations from the average temperature is reduced for all the control approaches. The maximum reduction is achieved by the spatial averaging method.
- Changes in minimum temperature vary with the control approaches used. Enhancement of minimum temperature is achieved by optimization approach (with weighting $Q2$) and spatial averaging method. The minimum temperature is reduced in optimization control design (with weight $Q1$) and peak detection/switching control.

Table 2. Summary of results of the four control designs.

| | T_max (deg F) (change) | T_min (deg F) (change) | PF (change) | RMS (deg F) (change) |
|-------------------|---------------------------|---------------------------|-----------------|-------------------------|
| Before control | 2586.7 | 2004.4 | 0.1288 | 151.7 |
| Optimization(Q1) | 2483.4 (-103.3) | 1994.5 (-9.9) | 0.0837 (-35.0%) | 110.7 (-41.0) |
| Optimization(Q2) | 2523.7 (-63.0) | 2061.8 (57.4) | 0.1013 (-21.4%) | 110.5 (-41.2) |
| Spatial averaging | 2529.6 (-57.1) | 2038.9 (34.5) | 0.1039 (-19.3%) | 99.6 (-52.1) |
| Harmonic control | 2618.7 (32.0) | 2005.0 (0.6) | 0.1427 (10.8) | 127.1 (-24.6) |
| Switching control | 2392.0 (-194.7) | 1880.4 (-124.0) | 0.0442 (-65.7%) | 135.4 (-16.3) |

5.0. Conclusions and Recommendations

Conclusions

- With more thermocouples than fuel modulators, there is a fundamental limitation to the spatial control authority that we have with this problem.
- Even with the limited spatial resolution of the control inputs, it is still possible to significantly reduce the pattern factor, whether the interest is in the RMS temperature variations or the peak temperature.
- At least for a first order effect, the averaged thermocouple temperature is a function of total fuel flow rate. If the total fuel flow rate does not change, the circumferential average temperature should not change either, to the first order.
- It seems that the best way to reduce the peak temperature is to focus on it, like in the peak detection/switching control.

- The results raise an issue as to what is the critical control criteria? What performance index is important? Is it the peak temperature or some RMS deviation from the spatial average, or some other function that is important to minimize. For example, the switched controller causes some cold spots. Is it bad? Do we just want to reduce the peak temperature, or do we also want to prevent cold spots? Once these questions have been addressed, the control system design can be more easily finely tuned to the specific cost function.

Recommendations for further research

The following aspects need further research effort:

- More sophisticated harmonic control design which not only reduces the energy in the controllable modes but also reduce the peak temperature.
- Addressing the cold spots at the combustor exit so as to achieve more effective control of the pattern factor.
- Investigating the advantages and disadvantages of the control approaches at different operation conditions.
- Experimenting with different performance indices and weightings to achieve further reduction on peak temperature or RMS temperature variations.
- Studying the possibility of combining different control approaches/strategies to find a more effective way for pattern factor control.
- Collecting more data to create a better pattern factor control model.

ATTACHMENT 2

**PI Controller For Emissions Reduction
Via Active Pattern Factor Control
J. Rushinsky, AlliedSignal Engines, Phoenix, AZ**

(35 Pages)



PI Controller for Emissions Reduction via Active Pattern Factor Control

John Rushinsky



ACPFC System Mode and Logic Design Document

Overview

This report presents the design and performance results for several controllers evaluated on the Active Emissions Control project funded under NASA contract NAS3-27752. An optimized proportional + Integral (PI) controller is described in detail and simulations were performed along with various failure modes.

Model Definition

Refer to the ACPFC Simulink Simulation Users Guide for an explanation of the components contained in the simulation.

Design

Fig. #1 depicts the basic structure of the model utilized for design purposes. The block labeled APFC contains the controller that was designed to maintain some expected level of performance. The APFC block senses all the temperature readings and then adjusts the areas of each of the individual fuel flow modulators to maintain a desired temperature profile.

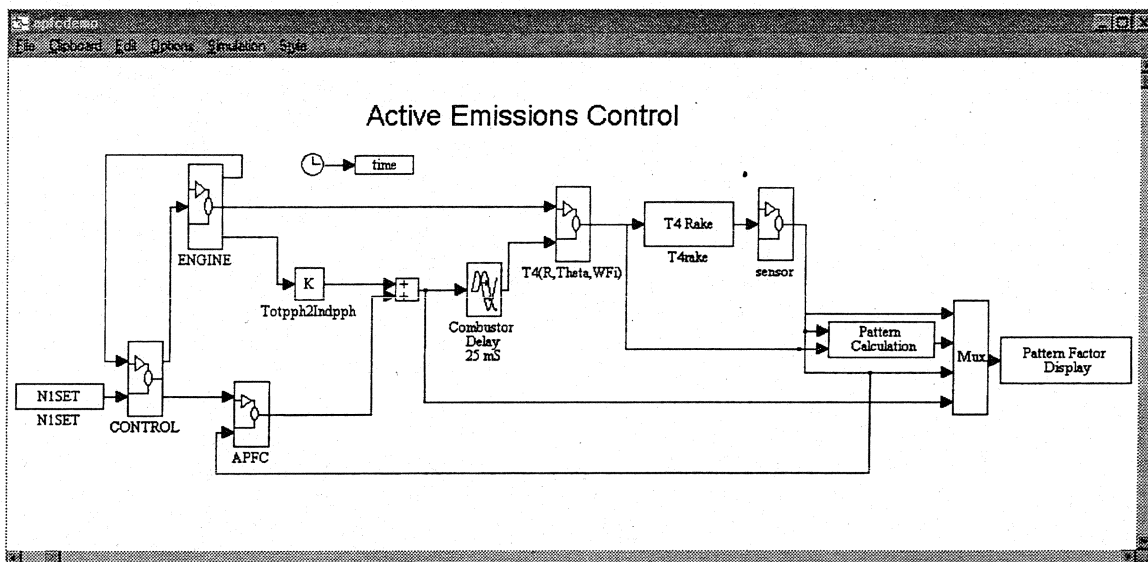


Fig. #1 Top Level Diagram of Active Pattern Factor Control Project

Open-Loop Optimization Study Performed

In order to assess the effect of number of temperature sensor, the location of the sensors, and initial angular placement of the sensors, an open-loop optimization study was performed.

In the computer simulation, it is possible to adjust the number of the thermocouples utilized, the initial degree location of the thermocouples, and the radial location of the thermocouples. For a particular initial temperature profile for the combustor, and assumed temperature sensitivity to fuel flow changes, an offline parametric study was performed in order to quantify the effect of sensor placement and quantity. This optimization was performed in the following manner.

A cost function was defined:

$$J = \left[\Delta T_{err} - \left[\frac{\partial T}{\partial W F} \right] \Delta W F \right]^T Q \left[\Delta T_{err} - \left[\frac{\partial T}{\partial W F} \right] \Delta W F \right]$$

ΔT_{err} represents the initial profile deviation from the mean combustor temperature. The number of sensors was varied from 19 to 38; therefore, this vector will also vary in length from 19 to 38.

$\delta T / \delta W F$ represents the change in temperature due to a change fuel flow

$\Delta W F$ represents the change in fuel flow in each nozzle. The number of fuel flow nozzles was set at 19.

Q represents the weighting matrix on the errors

The solution of this least squares problem is given by:

$$\Delta W F^* = \left[\left[\frac{\partial T}{\partial W F} \right]^T Q \left[\frac{\partial T}{\partial W F} \right] \right]^{-1} \left[\frac{\partial T}{\partial W F} \right]^T Q \Delta T_{err}$$

For this optimized fuel the resulting temperatures errors are

$$\Delta T_{err}^* = \Delta T_{err} - \left[\frac{\partial T}{\partial W F} \right] \Delta W F^*$$

As seen above, "optimal" fuel amounts to reduce the temperature deviations are a function of the weighting matrix Q . The designer is permitted to pick any Q matrix. Therefore, examine the resulting ΔT_{err} , for the particular Q used, find the element of ΔT_{err} that is a maximum, and then double the corresponding element of Q , and repeat the process. After iterating several times the max value of ΔT_{err} will no longer change. This Q matrix then yields the appropriate $\Delta W F$, resulting in the minimization of maximum temperature error. The **optim**

directory contains the file that will reproduce the open-loop plot. Fig #2 below shows a sample graph of the optimum temperature distribution.

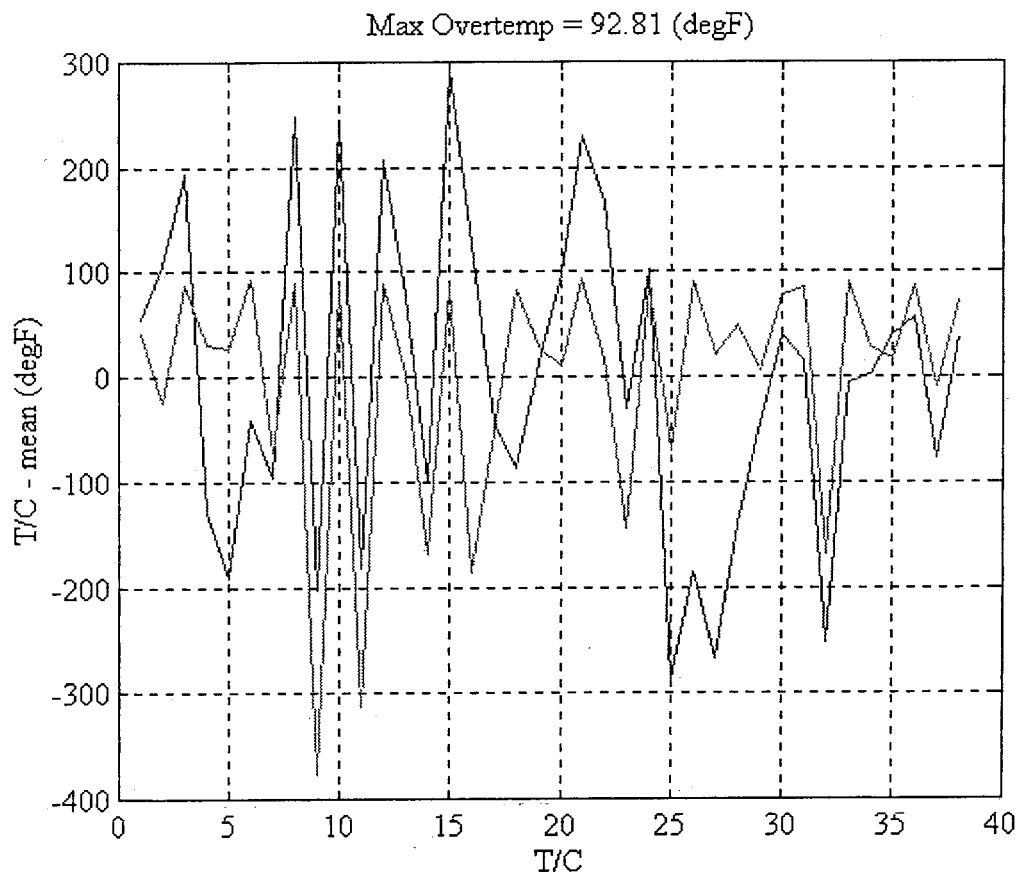


**Fig. #2: Optimum Temperature Distribution for the case: $\Theta = 5\text{deg}$,
Radius=4.0,#Sensors=38,#Nozzles=19**

After establishing the method for selecting an optimum fuel flow distribution to minimize the maximum temperature distribution, a parametric study was performed to calculate minimum temperature distributions for various radial locations, circumferential position, and number of temperature sensors used. Using the above method the resulting pattern factor is depicted in Fig #3.

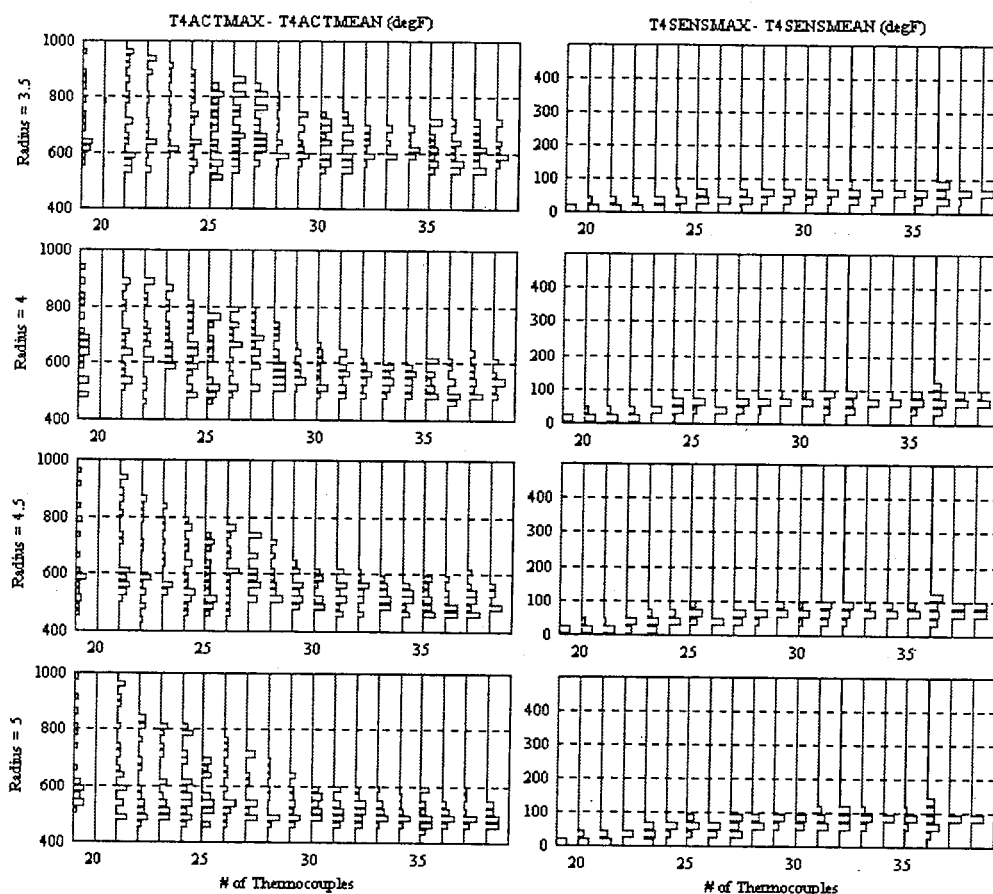


Fig. #3: Open-loop Sensitivity study for APFC project

The above six graphs should be interpreted as follows. Each pair of adjacent graphs is for the parametric study being performed at a particular radial location for the thermocouples {3.5,4.0,4.5, and 5.0}. The four graphs on the left contain the temperature difference of the MAX – MEAN for the overall combustor profile; whereas, the four graphs on the right contain the temperature difference of MAX – MEAN for the sensed values. The x-axis on all six graphs is the number of thermocouples evaluated. For each study at a particular number of thermocouples, a histogram plotted sideways is shown. The histogram itself results from varying the initial circumferential location of the sensors from 0 degrees to the location of thermocouple number two when thermocouple number one is located at zero degrees.

Some key observations may be made from Fig #3.

- The overall pattern factor is more greatly reduced when the number of sensors is large. View any graph on the left, in the increasing thermocouple direction and notice the reduction in the MAX – MEAN values.

- The overall pattern factor is more greatly reduced when the sensors are placed at a higher radial location. For example, view the graphs on the left for the number of thermocouples equal 38 cases. As the radial position increases from 3.5 to 5.0 the MAX-MEAN value reduces from about 650degF to 500degF.
- The temperature profile of the sensors is more greatly reduced for a fewer number of sensors; however, the overall pattern is actually made worse. This is to be expected since 19 fuel nozzles can more easily control a fewer number of sensors than a large number of sensors. View the graphs on the right, and radius location equal 5.0 for example. As the number of thermocouples decrease from 38 to 19 the sensed MAX – MEAN value decreases from about 100degF to 0degF. The equivalent plot on the left for the overall MAX-MEAN, shows the MAX-MEAN value getting worse it increases from about 500degF to 700degF as the thermocouples decrease from 38 to 19.

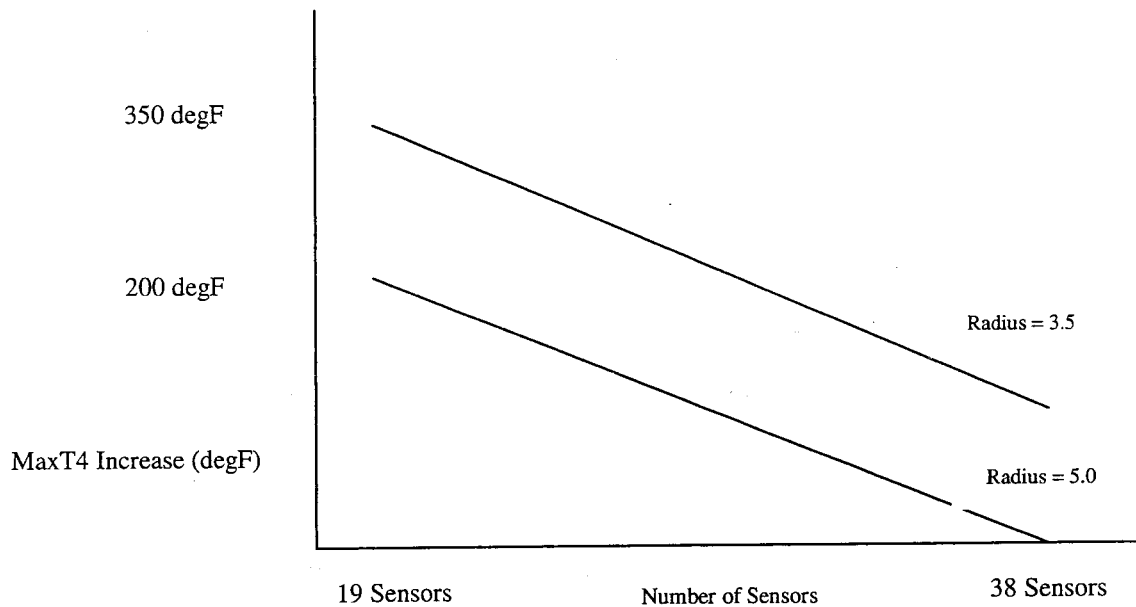


Fig #4: Summary plot of observations made from Fig #3

Fig #4 shows the general conclusions drawn from the parametric study presented in Fig #3. There is about a 200 degree decrease in the overall MAX-MEAN when the number of thermocouples is increased from 19 to 38. And there is an additional 150 degree decrease in the overall MAX – MEAN when the radial position of the thermocouples is increased from 3.5 to 5.0.

PI Controller Design

The capability of a PI controller was evaluated. The simple control law structure is depicted in Fig. #5. This simple controller consists of a lead-lag filter to compensate for sensor dynamics, error selection logic which only selects errors greater than 50 degF, an integral gain block which has the fuel constraint equation embedded in the gain, and a limited integrator. Using this controller the initial profile response is depicted in Fig #6. The controller is activated at 5 sec into the simulation.

The fuel constraint equation embedded the integral gain, is a 19x38 matrix which is constructed such that after multiplying by the constraint matrix, the sum of the errors into the integrator is zero. This insures that each increase fuel flow through one modulator, is compensated for by a decrease in fuel flow through all the other fuel modulators.

A 50-degree offset was used for the offset to determine when a thermocouple is reading a hot value. 50 degrees was selected as the offset based on the parametric study performed in Fig #3. From Fig #3, when the number of thermocouples is 38, it is seen that there is no way to do better than 50 to 100 degrees for the value of MAX-MEAN sensed. Based on that plot a value of 50 degrees was selected. This permits the controller to attack those areas that are warm, while ignoring temperatures that are already near the mean.

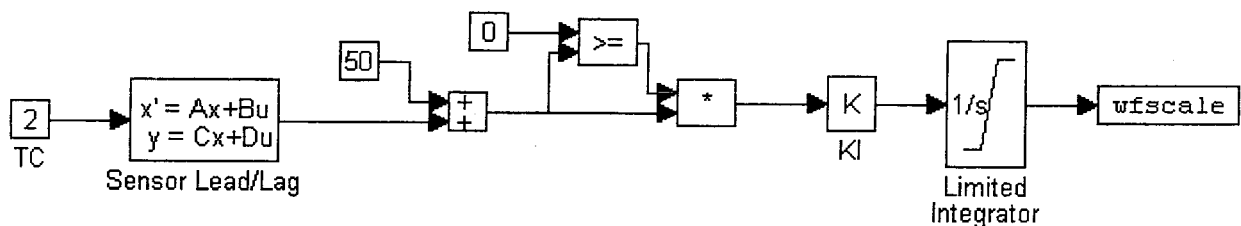


Fig #5: Simple Controller for APFC study

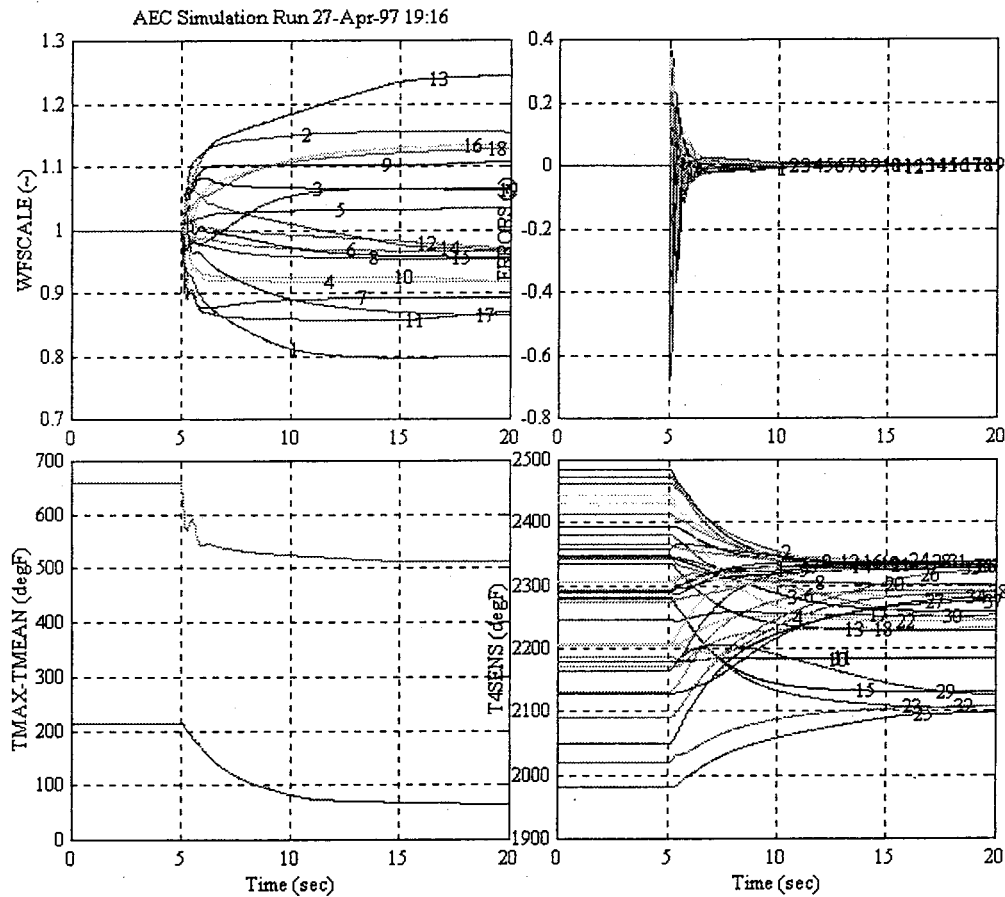


Fig #6: Sample Simulation Trace

Fig #6 shows in the bottom left plot the temperature difference between the maximum and the mean for the overall T4 profile (top line) and for sensed T4 profile (bottom line). The bottom right plot of Fig #6 shows the individual temperature readings, note the overall convergence of the temperature readings. The top left plot on Fig #6 shows the nozzle fuel flow scale factors required to improve the temperature profile, these scale factors are an indication of the fuel flow changes as a result of control action. The top right plot of Fig #6 shows the integrator errors being driven to zero. The reason the integrator errors can be driven to 0 but there is still some spread in the temperature readings, is due to the fact that there are 38 sensors and only 19 fuel actuators. The process of reducing the 38 temperature errors to 19 errors to send into the integrators, results in some information loss, this is unavoidable. It is not possible to exactly control 38 parameters with only 19 actuators.

| | Initial Condition | After Controller |
|---------------------------|-------------------|------------------|
| Max – Mean Overall (degF) | 658 | 517 |
| Max – Mean Sensed (degF) | 212 | 65 |
| Mean – Min Overall (degF) | 517 | 651 |
| Mean – Min Sensed (degF) | 290 | 185 |
| RMS Sens (degF) | 126 | 76 |

Table 1: Results for PI controller

Table 1 above summarizes the before and after effect for the controller. The bolded row shows the key purpose of the controller and the resulting reduction in temperature distribution. There is about a 147 degree improvement in the maximum sensed temperature (212-65). Additionally, the minimum temperature distribution is improved by 105 degrees. The reason for the improvement in the cold-spot, even with no direct design considerations, is that the fuel flow changes must be conserved. Since the fuel flow decreases to reduce the hot spot the excess fuel must go somewhere, thus resulting in increasing the temperature of the cold spots.

PI Controller tested on SMI model

The PI controller was tested on the SMI model. The SMI model consists of 20 Fuel actuators and 38 temperature sensors located at radial position 4.0 and an initial phase angle of 5 degrees. The only significant difference between the AlliedSignal model and the SMI model is the calculation of $dT4SENS/dWF$, and the three point average temperature sensing method. The difference between $dT4SENS/dWF$ between the two models is the result of using different test data matching algorithms. The AlliedSignal model was modified to the SMI temperature sensing method to permit a direct comparison of the PI controller with the SMI controller. Fig. 7 shows the controller operating on the AlliedSignal model. The only differences between Fig. #7, and Fig #6 is that Fig. #7 has 20 fuel modulators, and the `area_flag` calculation for the temperature sensors is not being used. This indicates that the temperatures are only being read at radius=4.0, whereas the results in Fig #6 are based on the three-point measurement method for the sensor readings. The effect of not using the three point method for calculating each thermocouple reading, is to alter the initial condition of each model. When the single point method is used the initial MAX -MEAN sensed reading is 295 degF (see Table1), while the three point method results in an initial MAX-MEAN sensed reading of 212 degF (see Table 2). The three point averaging method has a smoothing effect on the data.

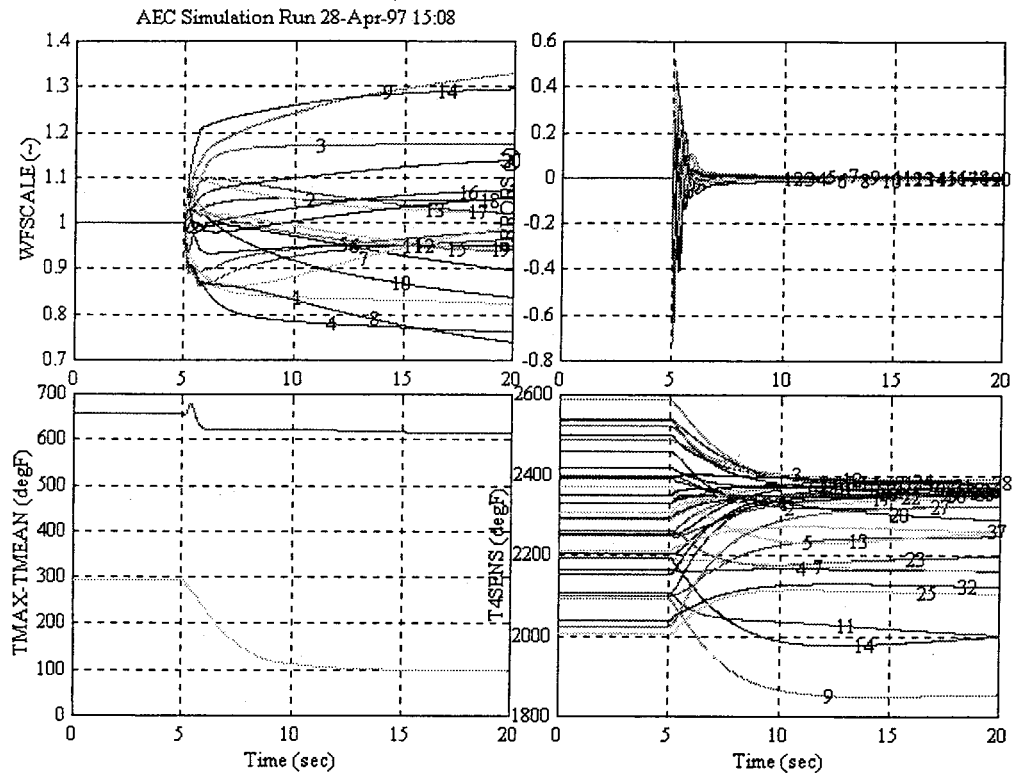


Fig #7: 38 T/C's, 20 Fuel Nozzles, AlliedSignal controller on AlliedSignal model, single point T/C measurement

The results of using the PI controller on the SMI model are shown in Fig #8. Table 2 compares the PI control operation on the two different models.

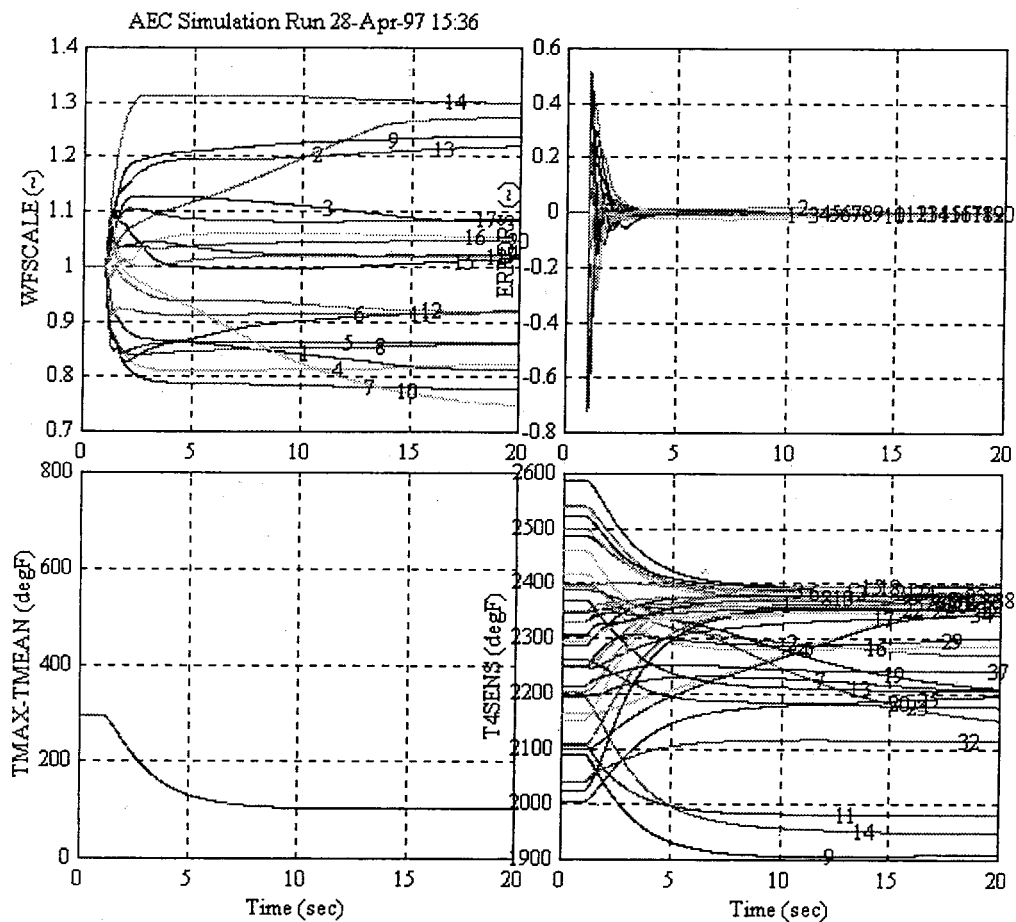


Fig #8: 38 T/C's, 20 Fuel Nozzles, AlliedSignal controller on SMI model, single point T/C measurement

| | Initial Condition | On AS Model Fig #7 | On SMI model Fig #8 | SMI results for Switching control |
|---------------------------|-------------------|-----------------------|------------------------|--------------------------------------|
| Max – Mean Overall (degF) | 658 | 613 | N/A on SMI | N/A on SMI |
| Max – Mean Sensed (degF) | 295 | 97 | 105 | 100 |
| Mean – Min Overall (degF) | 517 | 651 | N/A on SMI | N/A on SMI |
| Mean – Min Sensed (degF) | 287 | 437 | 380 | 411 |
| RMS Sens (degF) | 154 | 128 | 128 | 138 |

Table 2: Results for simple controller on SMI model

The AlliedSignal PI controller performs about 8 degrees (105-97) better on the plant model for which it was designed, and is still robust enough to control within 5 degrees (105-100) of the result obtained for SMI switching control. The standard deviation after control actuation is about 10 degrees better for the AlliedSignal controller than the SMI controller (128 vs 138). Overall, these controllers are equivalent in performance.

AlliedSignal controller modified to address cold spots

In response to discussions raised at the biannual review on 4/8/97, the PI controller was modified to allow for control of cold spot temperatures. The modified control block diagram is shown in Fig. # 9 below. The cold spot errors were not given equal weight to the hot spot errors. This is seen by the 75-degree offset for the cold spot determination versus the 50-degree offset for the hot spot determination. Furthermore, cold spot errors were only given 50% the credit of the hot spot errors. This was done to maintain the emphasis on hot-spot reduction while still attempting to effect the cold-spots. Fig. 10 shows the response for this control modification and is comparable to Fig #6.

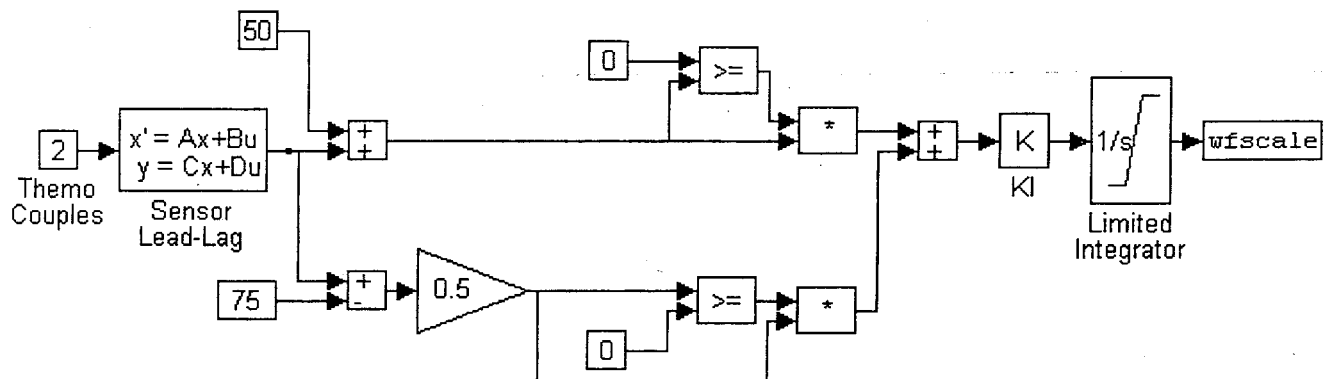


Fig #9: Modified PI Controller to include cold-spot control

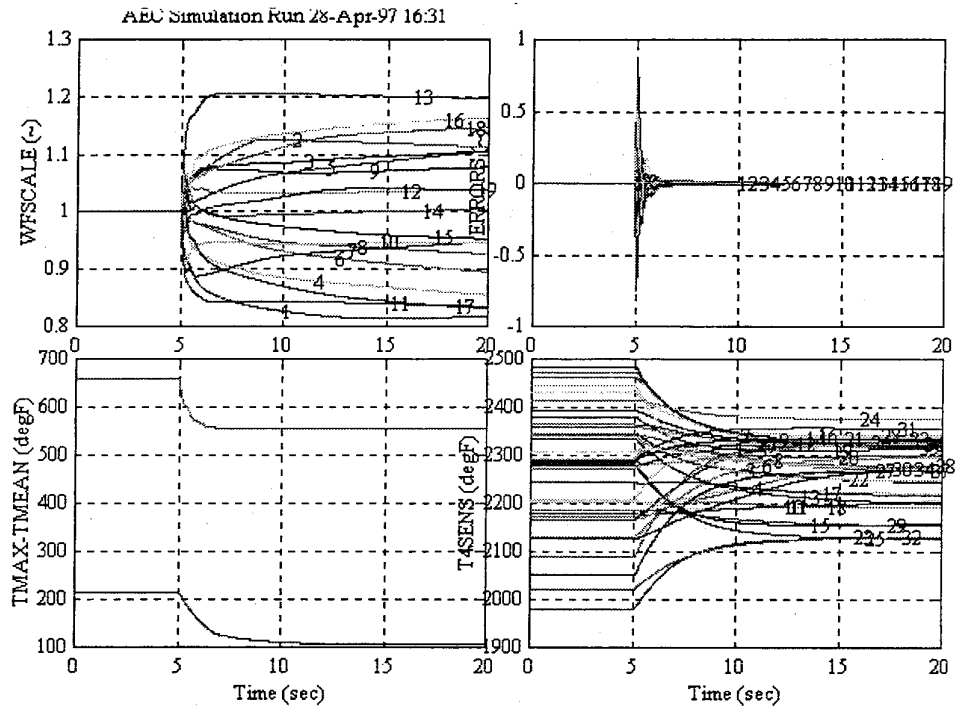


Fig #10: PI Controller result with cold-spot control added

| | Initial Condition | Hot-Spot PI Controller Fig # 6 | Hot/Cold PI Controller Fig #10 |
|---------------------------|-------------------|-----------------------------------|-----------------------------------|
| Max – Mean Overall (degF) | 658 | 517 | 555 |
| Max – Mean Sensed (degF) | 212 | 65 | 106 |
| Mean – Min Overall (degF) | 517 | 651 | 617 |
| Mean – Min Sensed (degF) | 290 | 185 | 143 |
| RMS Sens (degF) | 126 | 76 | 70 |

Table 3: Comparison of hot/cold focused PI controller with nominal PI controller

The summary information in Table 3 shows that the addition of the cold spot logic does decrease the difference between the mean temperature and the minimum temperature, now 143 deg instead of 185 degree without the cold-spot logic. A 42 degree improvement. However, the improvement comes at the expense of making the hot spot worse by 41 degrees. The hot spot increased from 65 degF with no cold-spot logic to 106 with the cold spot logic. Additionally the overall combustor profile was likewise affected. There was a marginal 6-degrees (76 to 70) of improvement in the standard deviation after the inclusion of the cold-spot logic.

The most significant reason for the penalty incurred on the hot-spot values, when including the cold-spot logic, can be seen by reviewing Fig #2. It is easy enough to see in Fig #2 that there are large changes in adjacent temperature readings around the combustor. The fuel flow required to raise a cold-spot temperature will also raise a hot spot temperature, this is a consequence of the physics of the model. So, although cold spots may be addressed in a manner similar to hot-spots it should be noted that the benefit of cold-spot control may come at the expense of hot-spot control, especially for adjacent hot and cold zones.

Failure modes investigated

In order to assess the response of the controller to various failures, a failure study was performed. The controller used is the one first presented which addresses primarily hot-spot control with cold-spot control being a secondary benefit. The nature of the failures consisted of combinations of: temperature reading failed high (high = 2600degF), temperature reading failed low (low = 2000 degF), fuel nozzle failed open (scale factor = 2), fuel nozzle failed closed (scale factor = 0). Table 4 below lists the specific failures investigated. The controller was activated 5 seconds into the simulation, and the failure(s) occurred at 15 seconds into the simulation. Appendix 1 contains the time traces for each of the failure tests performed.

These results are somewhat different than those presented at the biannual review. The key difference is that a lead-lag filter was introduced on the temperature sensors to permit a higher responding system to be designed. The lead-lag filter is designed to compensate for the temperature sensor dynamics. The presence of the lead-lag filters causes the errors to vary slightly during the transient and thus a differently equilibrium point is obtained for the steady-state behavior of the system. Recall, that 38 sensors are being reduced to 19 fuel actuators commands and as a result, some information loss occurs.

| Test Point | Failure Description | Simulation Figure Results |
|------------|---|---------------------------|
| -1 | Initial Condition | Fig #6 |
| 0 | Baseline | Fig #6 |
| 1 | FN 4 failed open | Appendix #1: Fig #1 |
| 2 | FN 4 failed closed | Appendix #1: Fig #2 |
| 3 | TC 10 low | Appendix #1: Fig #3 |
| 4 | TC 5 low | Appendix #1: Fig #4 |
| 5 | FN 4 failed open, TC 10 low | Appendix #1: Fig #5 |
| 6 | FN 4 failed closed, TC 10 low | Appendix #1: Fig #6 |
| 7 | FN 4 failed open, TC 10 high | Appendix #1: Fig #7 |
| 8 | FN 4 failed closed, TC 10 high | Appendix #1: Fig #8 |
| 9 | TC 10 and 5 low | Appendix #1: Fig #9 |
| 10 | TC 10 and 5 high | Appendix #1: Fig #10 |
| 11 | TC 10 low and TC 5 high | Appendix #1: Fig #11 |
| 12 | FN 4 failed open, TC 10 low, TC 5 low | Appendix #1: Fig #12 |
| 13 | FN 4 failed closed, TC 10 low, TC 5 low | Appendix #1: Fig #13 |
| 14 | FN 4 failed open, TC 10 high, TC 5 high | Appendix #1: Fig #14 |
| 15 | FN 4 failed closed, TC 10 high, TC 5 high | Appendix #1: Fig #15 |
| 16 | FN 4 failed open, TC 10 high, TC 5 low | Appendix #1: Fig #16 |
| 17 | FN 4 failed closed, TC 10 high, TC 5 low | Appendix #1: Fig #17 |
| 18 | FN 12 failed open, TC 3 high, TC 17 low | Appendix #1: Fig #18 |
| 19 | FN 12 failed closed, TC 3 high, TC 17 low | Appendix #1: Fig #19 |

Table 4: Failure Mode Test Matrix Description

| Test Point | Max - Mean (Sensed) (degF) | Max - Mean (Overall) (degF) | Mean - Min (Sensed) (degF) | Min - Mean (Overall) (degF) | Stndrd Dev (Sensed) (degF) |
|--------------|----------------------------------|-----------------------------------|----------------------------------|-----------------------------------|----------------------------------|
| Initial Cond | 212 | 658 | 290 | -517 | 126 |
| Baseline | 65 | 517 | 185 | -651 | 76 |
| 1 | 115 | 575 | 416 | -750 | 133 |
| 2 | 152 | 691 | 602 | -843 | 161 |
| 3 | 71 | 518 | 266 | -651 | 86 |
| 4 | 70 | 511 | 260 | -659 | 87 |
| 5 | 113 | 576 | 426 | -748 | 130 |
| 6 | 158 | 693 | 596 | -838 | 165 |
| 7 | 291 | 626 | 983 | -1420 | 219 |
| 8 | 271 | 726 | 1633 | -2022 | 350 |
| 9 | 77 | 515 | 255 | -660 | 96 |
| 10 | 260 | 763 | 876 | -1406 | 280 |
| 11 | 297 | 705 | 1042 | -1467 | 284 |
| 12 | 123 | 575 | 389 | -756 | 133 |
| 13 | 170 | 695 | 705 | -954 | 187 |
| 14 | 263 | 774 | 1056 | -1307 | 293 |
| 15 | 260 | 752 | 1448 | -1832 | 329 |
| 16 | 304 | 625 | 958 | -1426 | 223 |
| 17 | 293 | 752 | 1632 | -2026 | 359 |
| 18 | 299 | 727 | 1165 | -1494 | 270 |
| 19 | 305 | 648 | 1027 | -1367 | 266 |

Table 5: Failure Mode Results

Table 5 shows the pattern values at the completion of each test run. Some points of interest are:

- About ½ the testruns maintain the sensed Max-Mean value below the initial condition. These are testruns 1,2,3,4,5,6,9,12,13
- About ½ the testruns maintain the overall Max-Mean value below the initial condition. These are testruns 1,3,4,5,7,9,12,16,19
- Only three of the failure modes maintain the standard deviation below the initial condition. These are testruns 3,4,9

These observations are somewhat expected, since in general the well-behaved failure modes include those in which a thermocouple is failed low. Since the PI controller does not directly attack cold-spots these failures are in general ignored by the controller. In fact, none of the failures in which a thermocouple is failed high do a very good job on the sensed value. This is a result of the controller continuing to attack the “perceived” hot spot to no avail. Note, that no special failure protection has been introduced in the controller, this is the natural response of the controller with the sensor values provided and actuators available. In general, the controller is fairly well behaved in the presence of the failures investigated.

Appendix #1

Simulation Traces for Failure Modes Investigated

maxT4 - aveT4 for PI Control, failure at 10 sec: FN 4 failed open

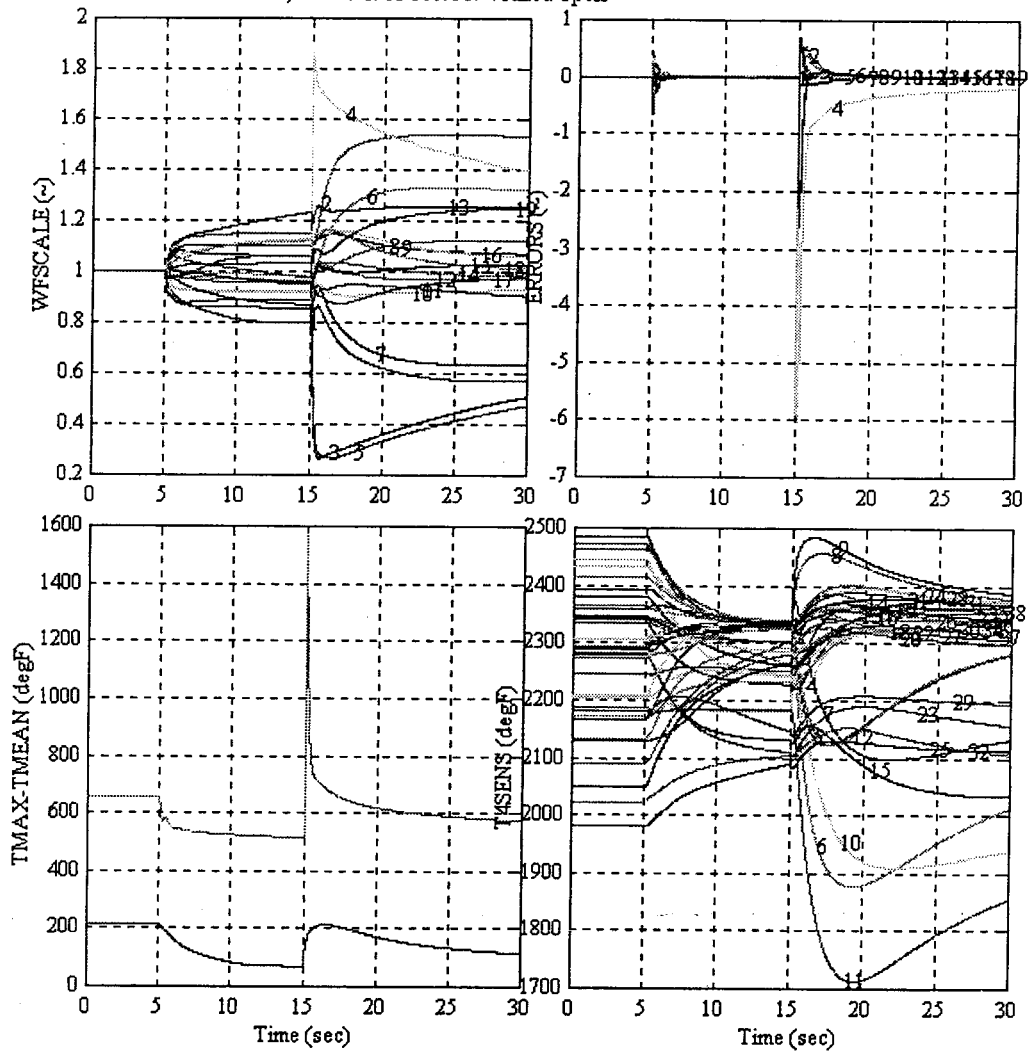


Fig. #1: Fuel Nozzle #4 Failed Open

maxT4- aveT4 for PI Control, failure at 10 sec: FN 4 failed closed

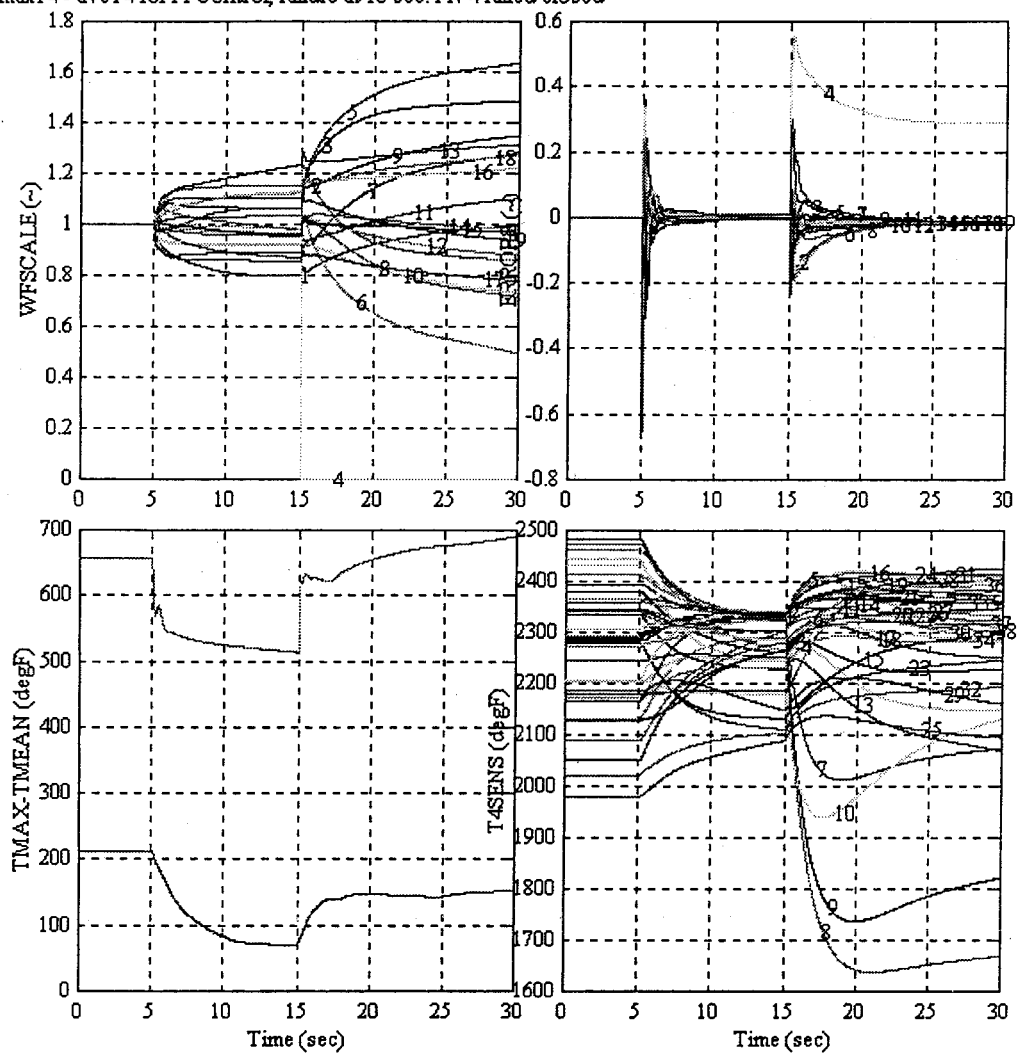


Fig. #2: Fuel Nozzle #4 Failed Closed

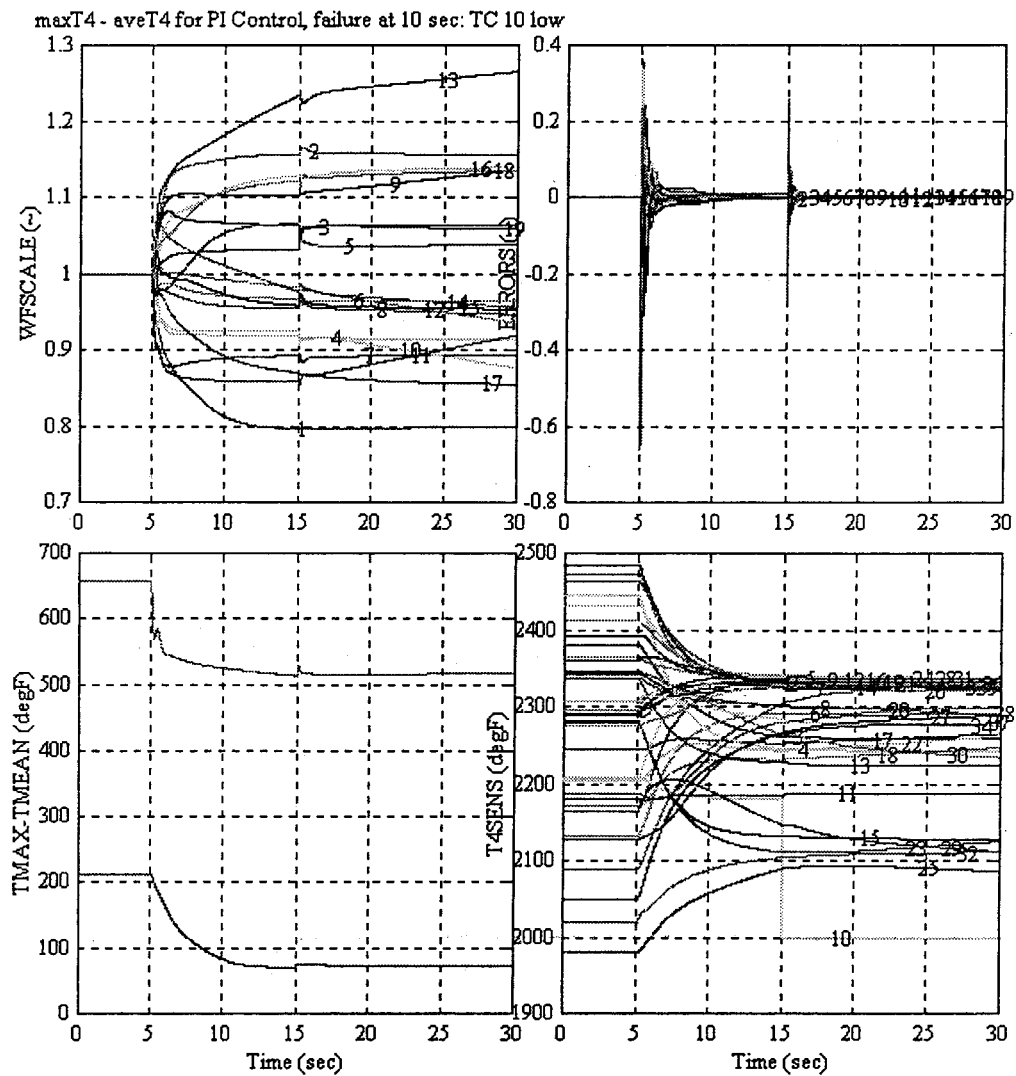


Fig. #3: Thermocouple #10 Failed Low

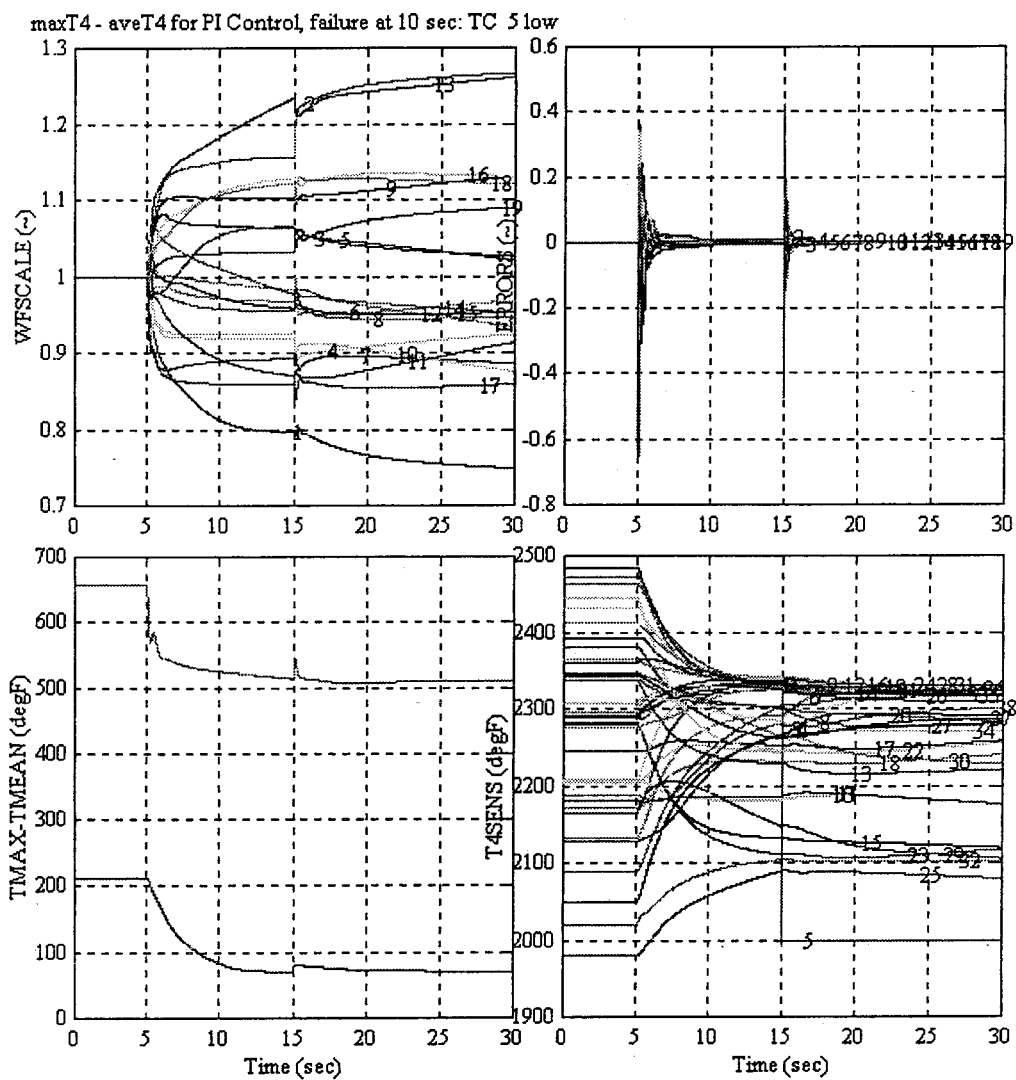


Fig. #4: Thermocouple #5 Failed Low

ixT4 - aveT4 for PI Control, failure at 10 sec: FN 4 failed open, TC 10 low

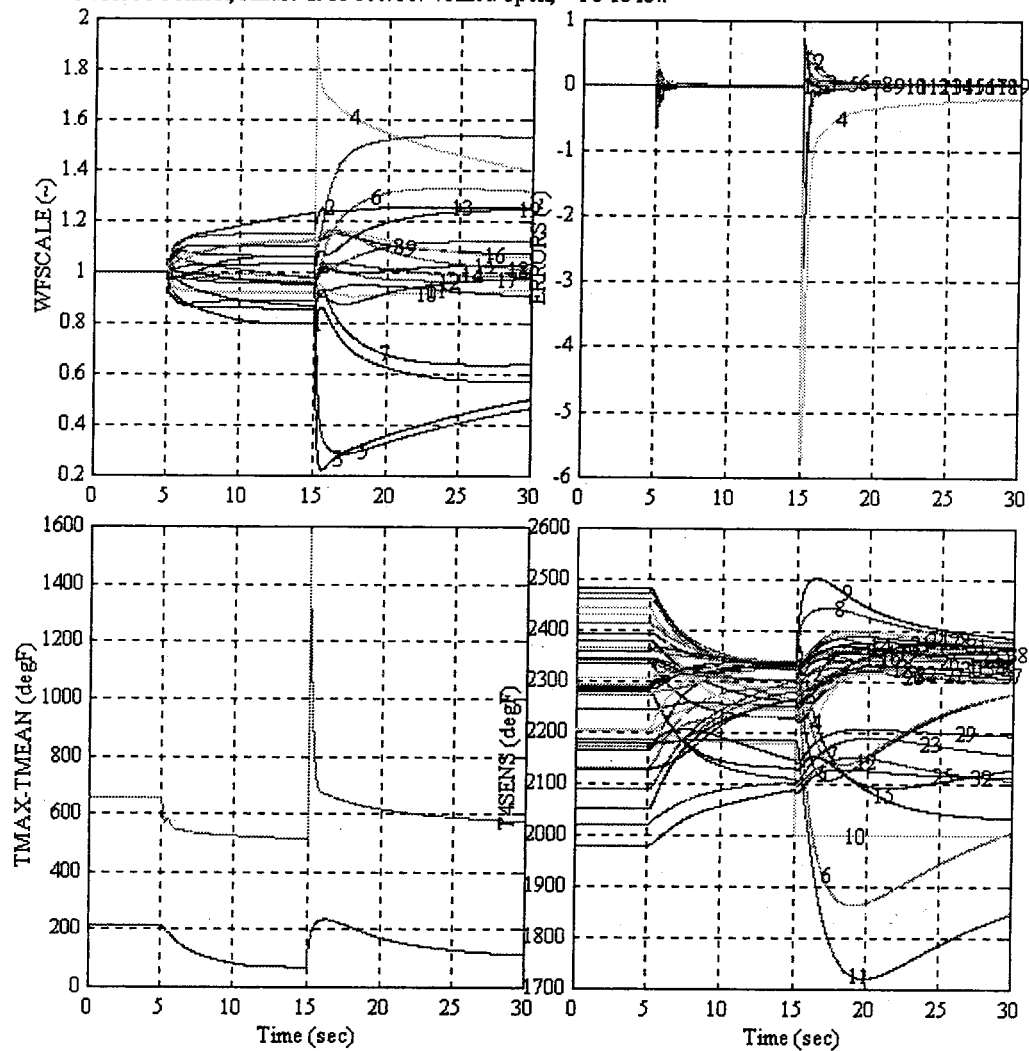


Fig. #5: Fuel Nozzle #4 Failed Open, Thermocouple #10 Failed Low

$\alpha T4$ - aveT4 for PI Control, failure at 10 sec: FN 4 failed closed, TC 10 low

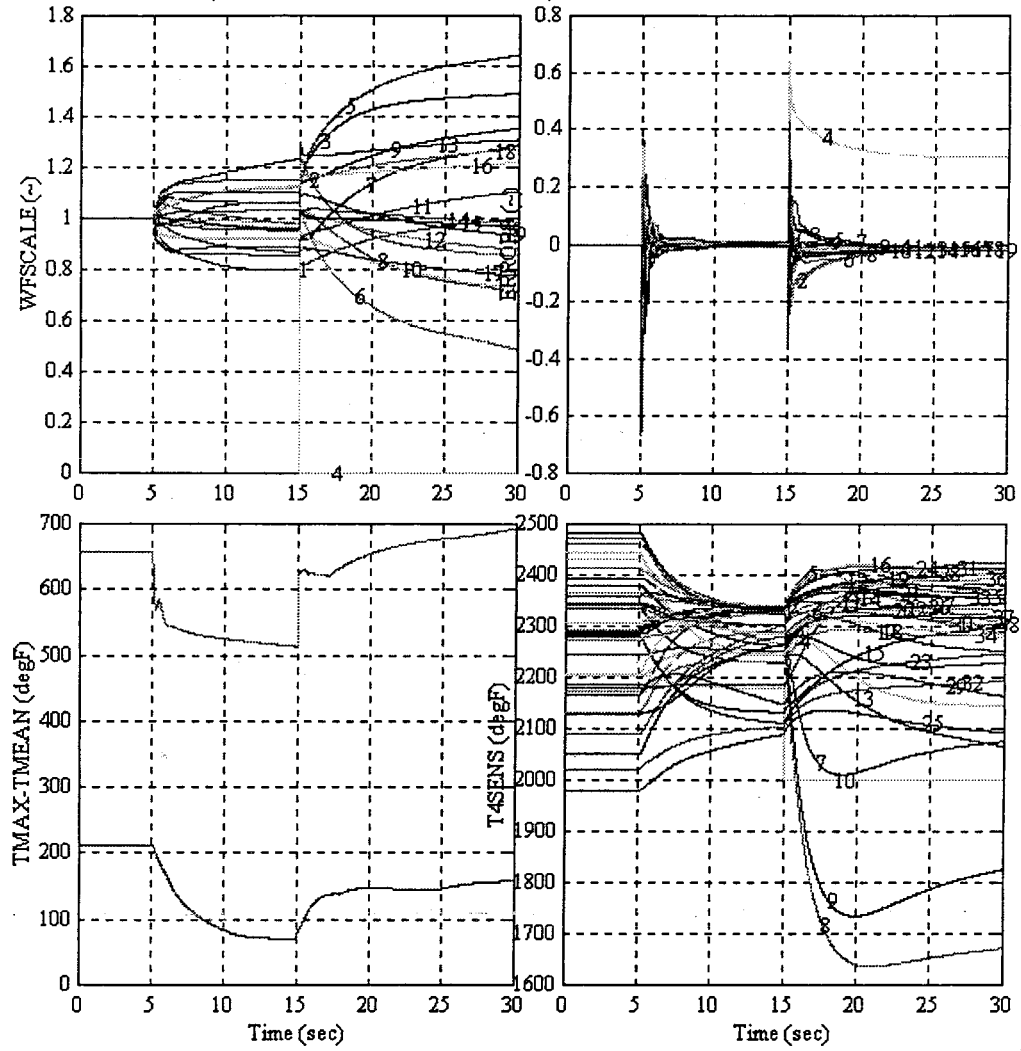


Fig. #6: Fuel Nozzle #4 Failed Closed, Thermocouple #10 Failed Low

xT4 - aveT4 for PI Control, failure at 10 sec: FN 4 failed open, TC 10 high

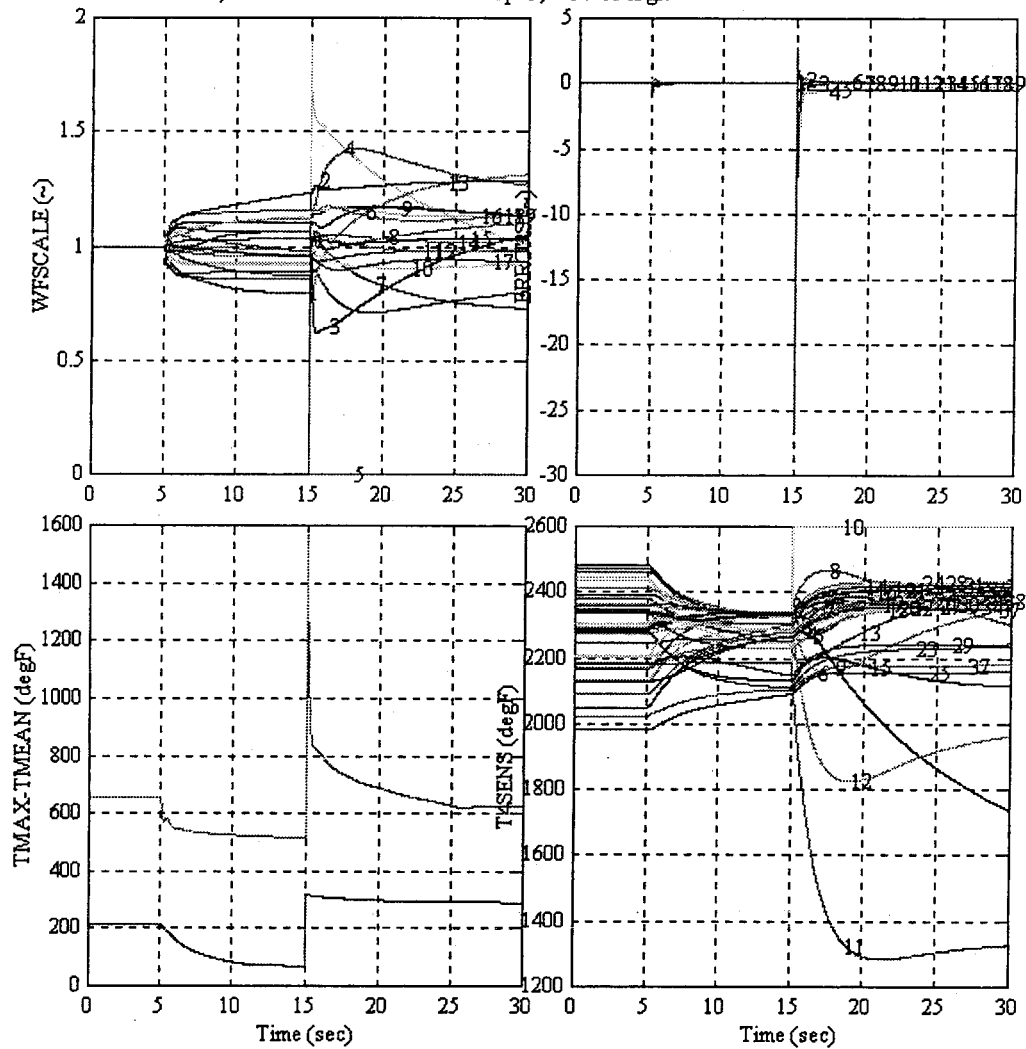


Fig. #7: Fuel Nozzle #4 Failed Open, Thermocouple #10 Failed High

xT4 - aveT4 for PI Control, failure at 10 sec: FN 4 failed closed, TC 10 high

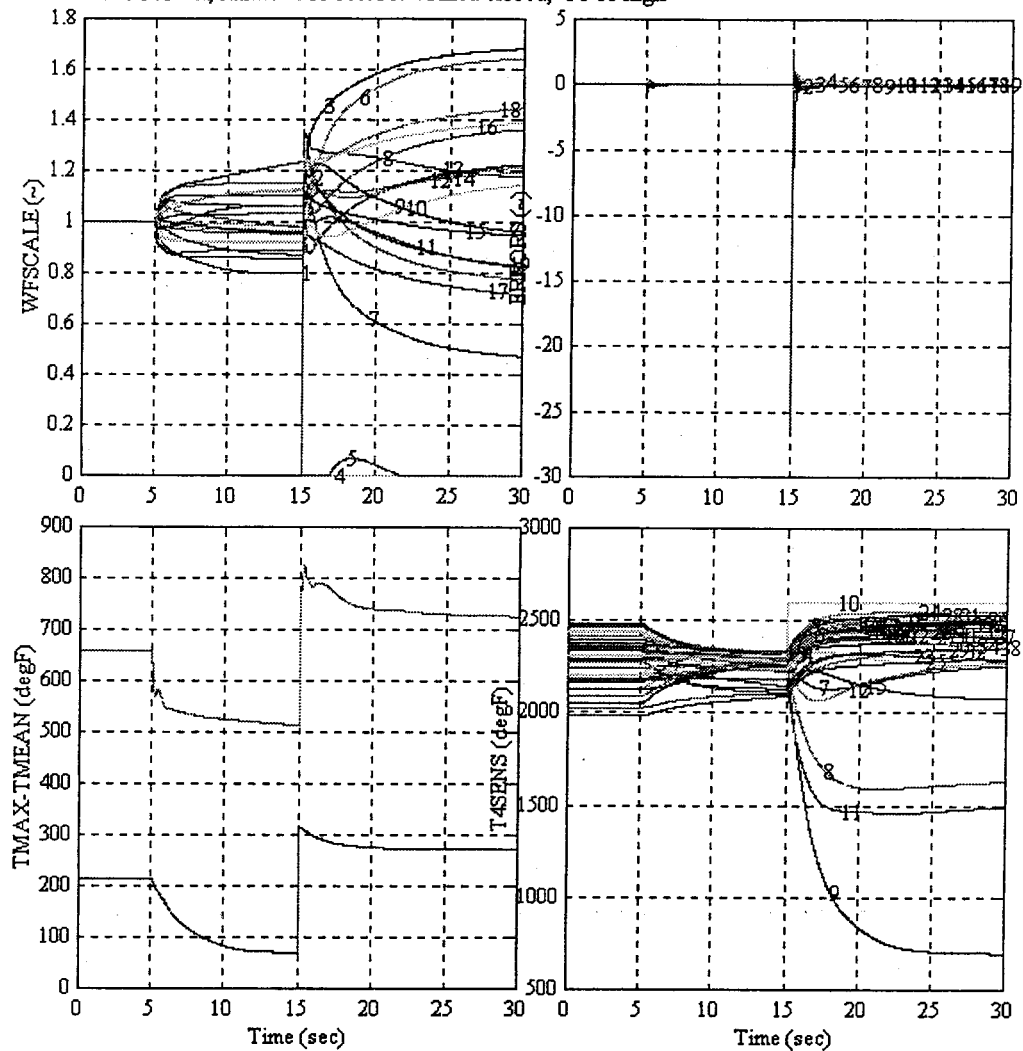


Fig. #8: Fuel Nozzle #4 Failed Closed, Thermocouple #10 Failed High

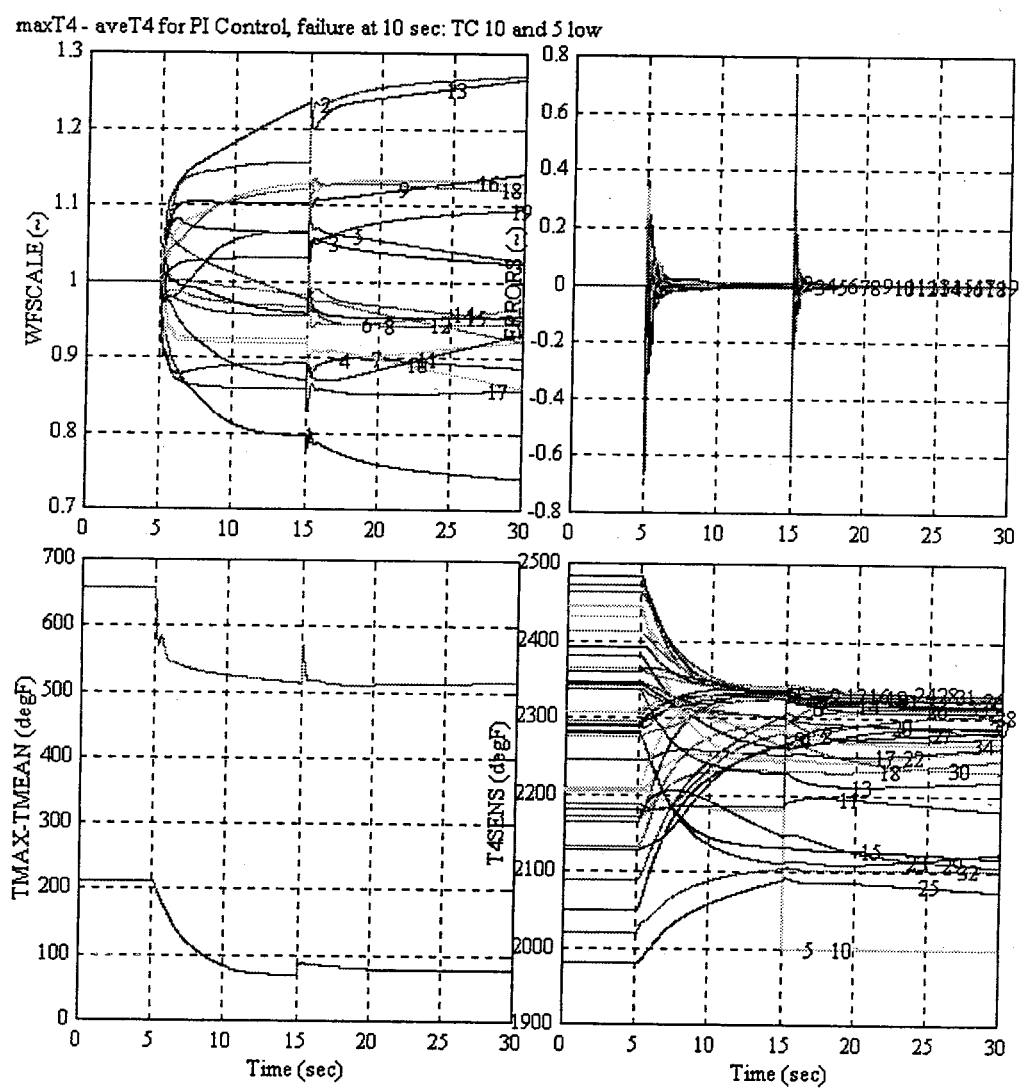


Fig. #9: Thermocouple #5 Failed Low, Thermocouple #10 Failed Low

maxT4 - aveT4 for PI Control, failure at 10 sec: TC 10 and 5 high

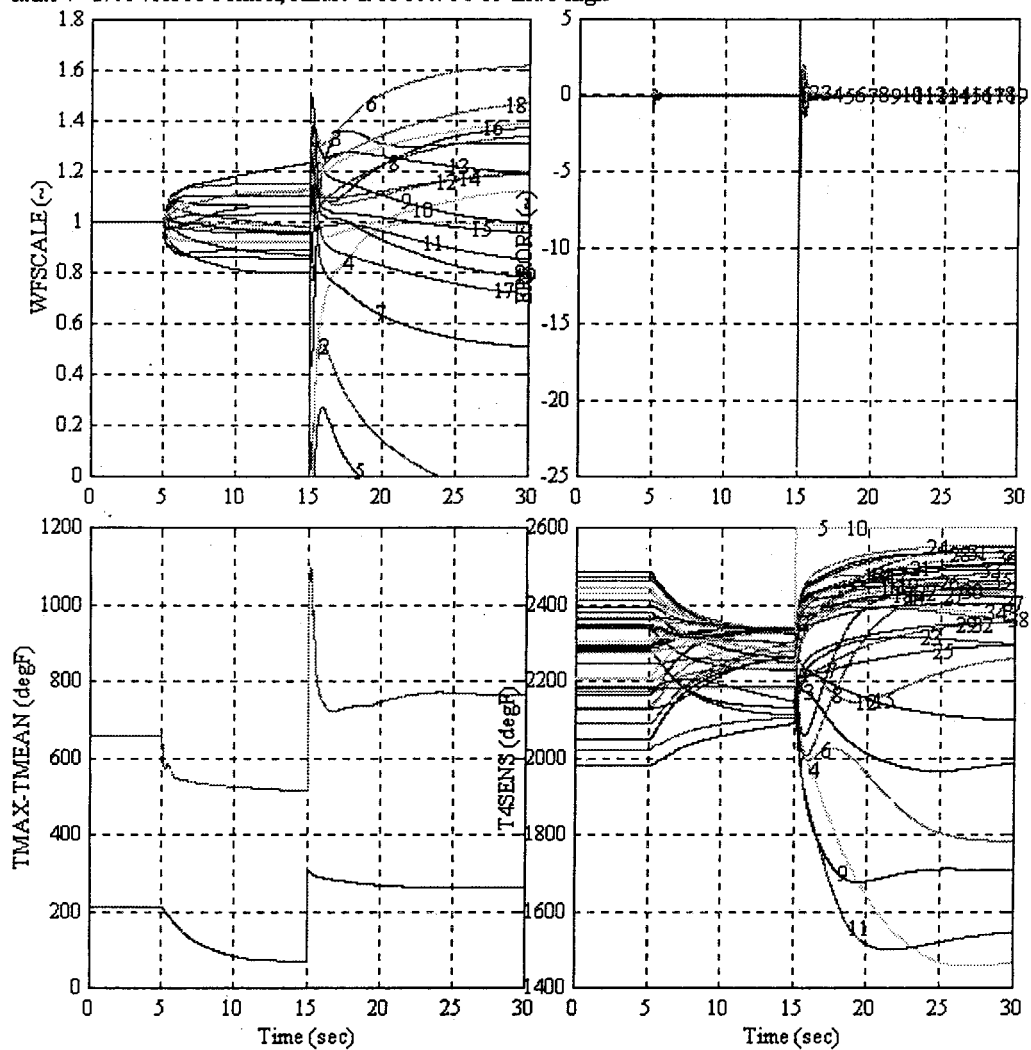


Fig #10: Thermocouple #5 Failed High, Thermocouple #10 Failed High

maxT4 - aveT4 for PI Control, failure at 10 sec: TC 10 low and TC 5 high

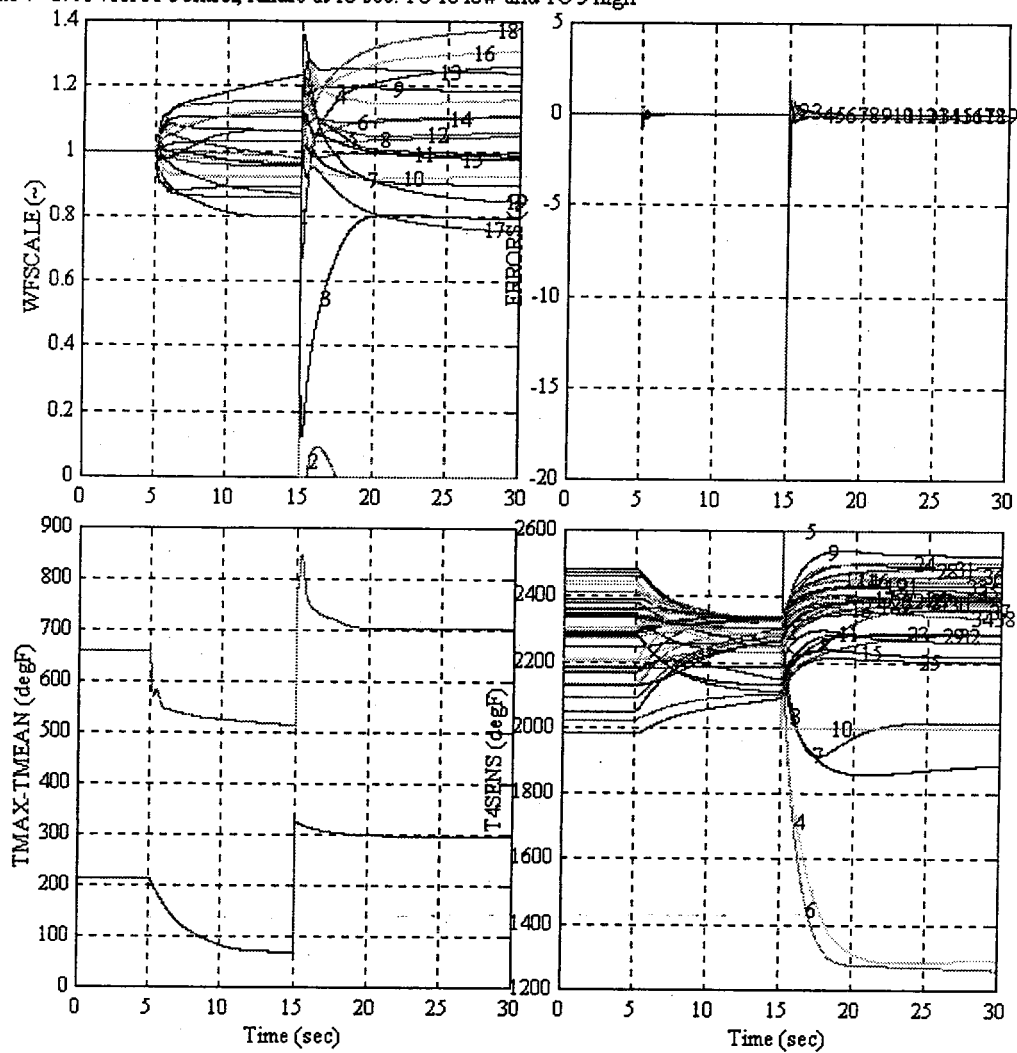


Fig. #11: Thermocouple #5 Failed High, Thermocouple #10 Failed Low

aveT4 for PI Control, failure at 10 sec: FN 4 failed open, TC 10 low, TC 5 low

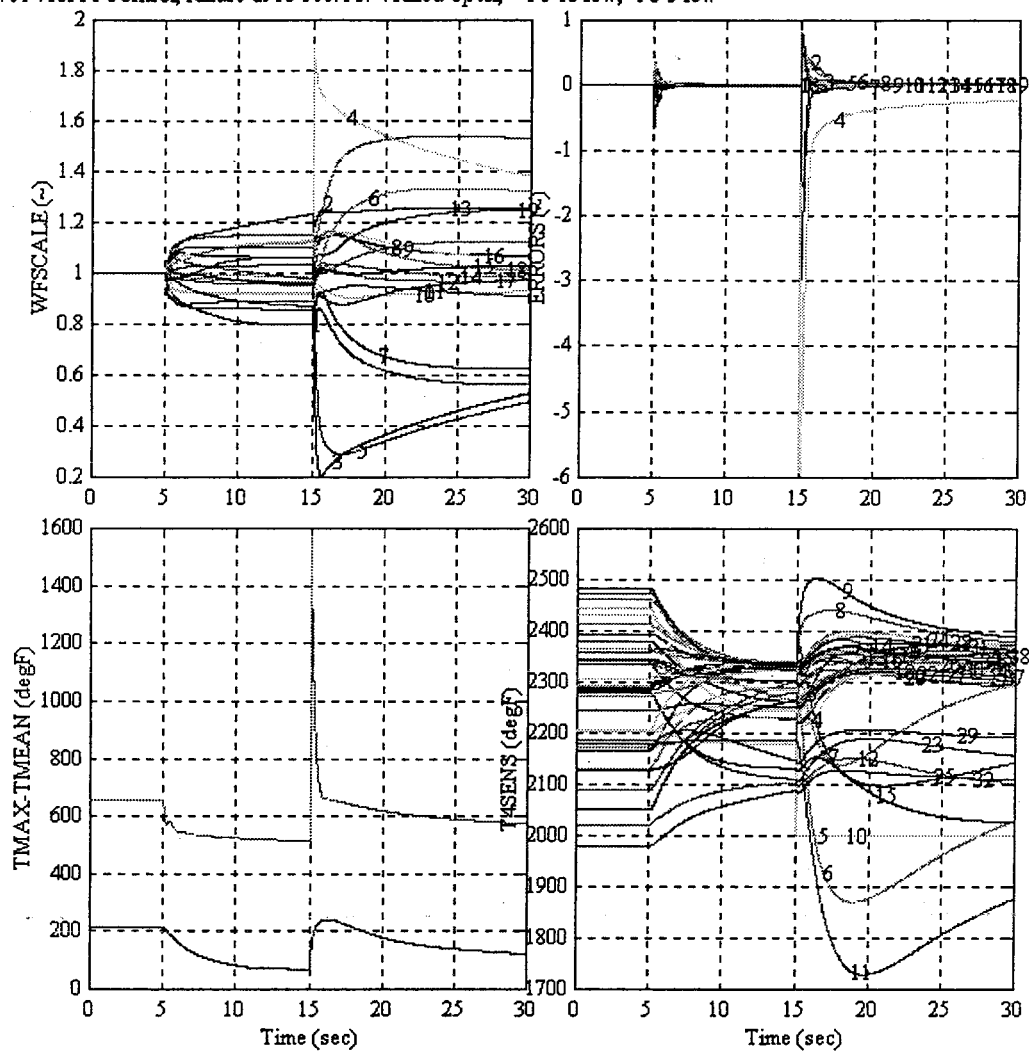


Fig. #12: Fuel Nozzle #4 Failed Open, Thermocouple #5 Failed Low, Thermocouple #10 Failed Low

aveT4 for PI Control, failure at 10 sec: FN 4 failed closed, TC 10 low, TC 5 low

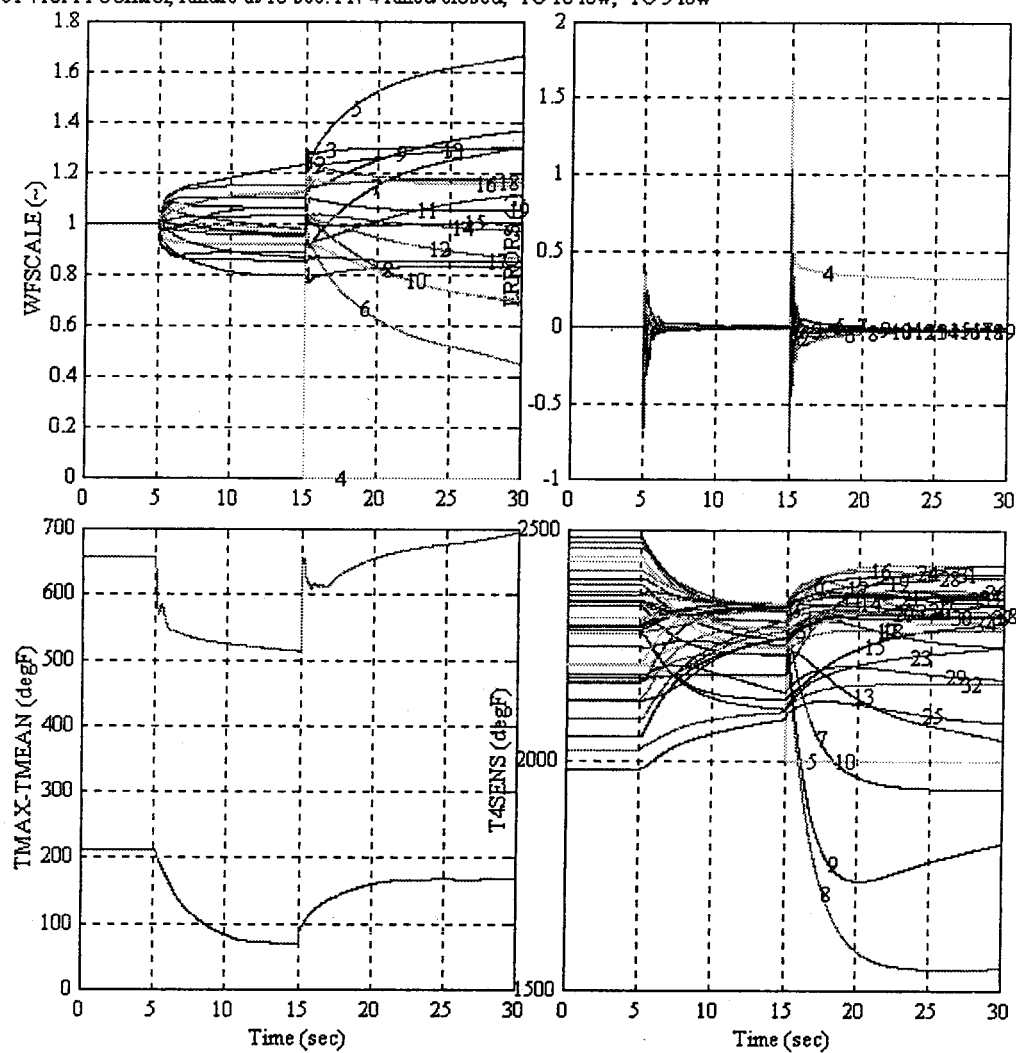


Fig. #13: Fuel Nozzle #4 Failed Closed, Thermocouple #5 Failed Low, Thermocouple #10 Failed Low

aveT4 for PI Control, failure at 10 sec: FN 4 failed open, TC 10 high, TC 5 high

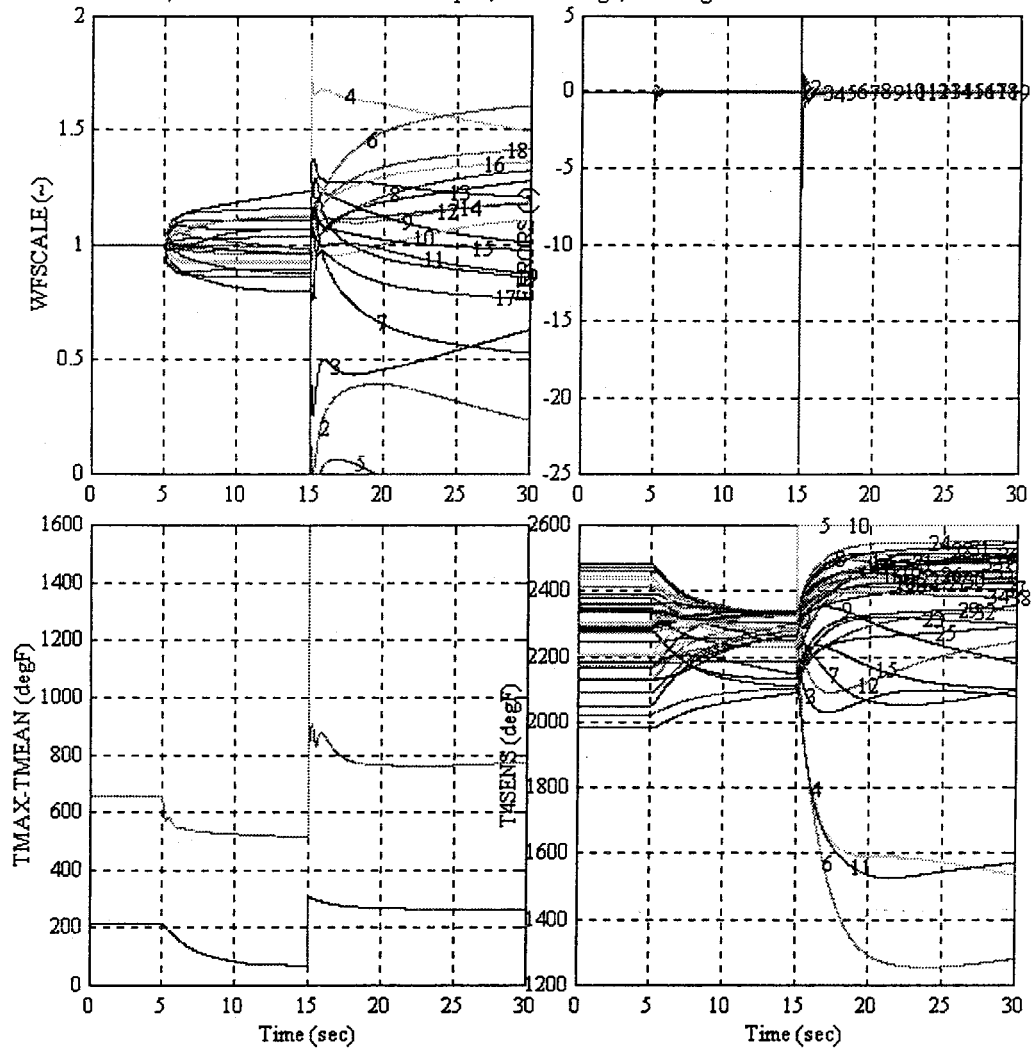


Fig. #14: Fuel Nozzle #4 Failed Open, Thermocouple #5 Failed High, Thermocouple #10 Failed High

aveT4 for PI Control, failure at 10 sec: FN 4 failed closed, TC 10 high, TC 5 high

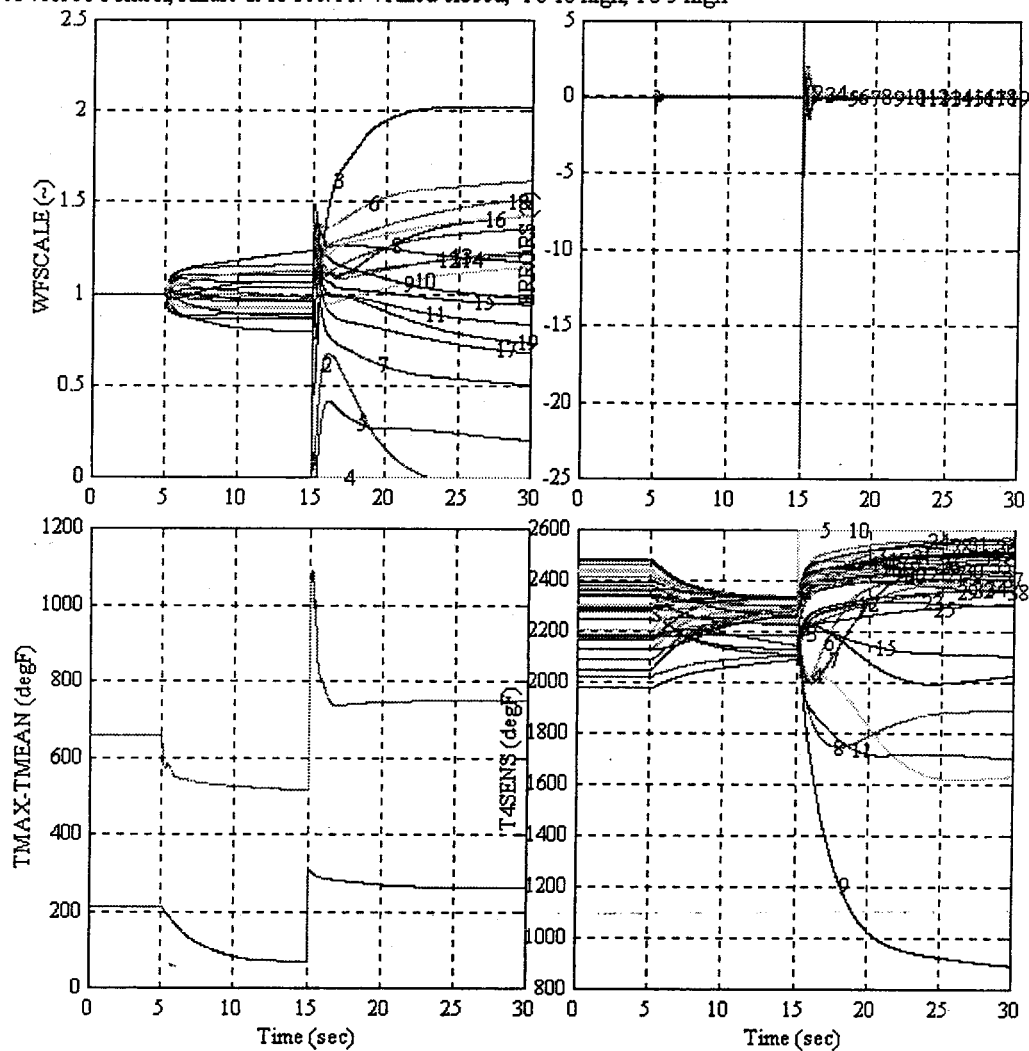


Fig. #15: Fuel Nozzle #4 Failed Closed, Thermocouple #5 Failed High, Thermocouple #10 Failed High

aveT4 for PI Control, failure at 10 sec: FN 4 failed open, TC 10 high, TC 5 low

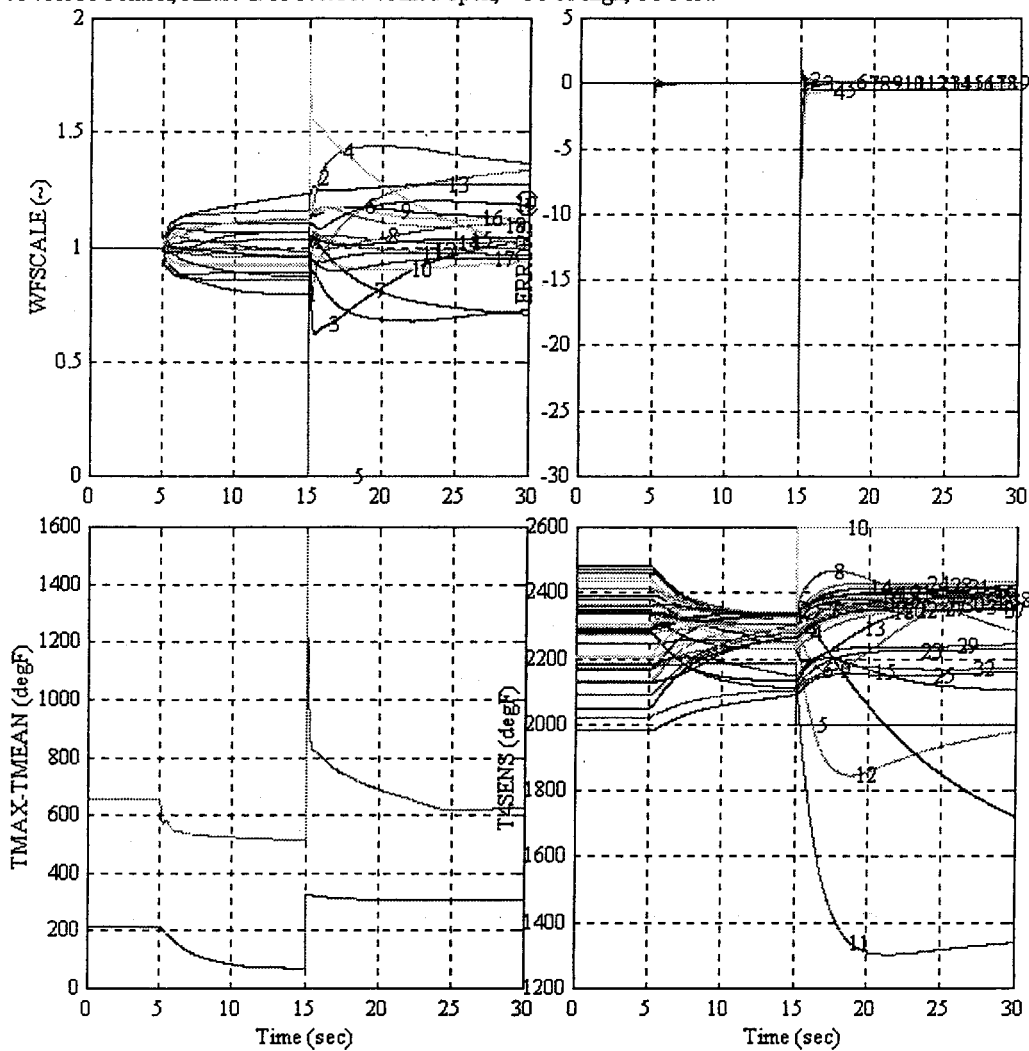


Fig. #16: Fuel Nozzle #4 Failed Open, Thermocouple #5 Failed Low, Thermocouple #10 Failed High

aveT4 for PI Control, failure at 10 sec: FN 4 failed closed, TC 10 high, TC 5 low

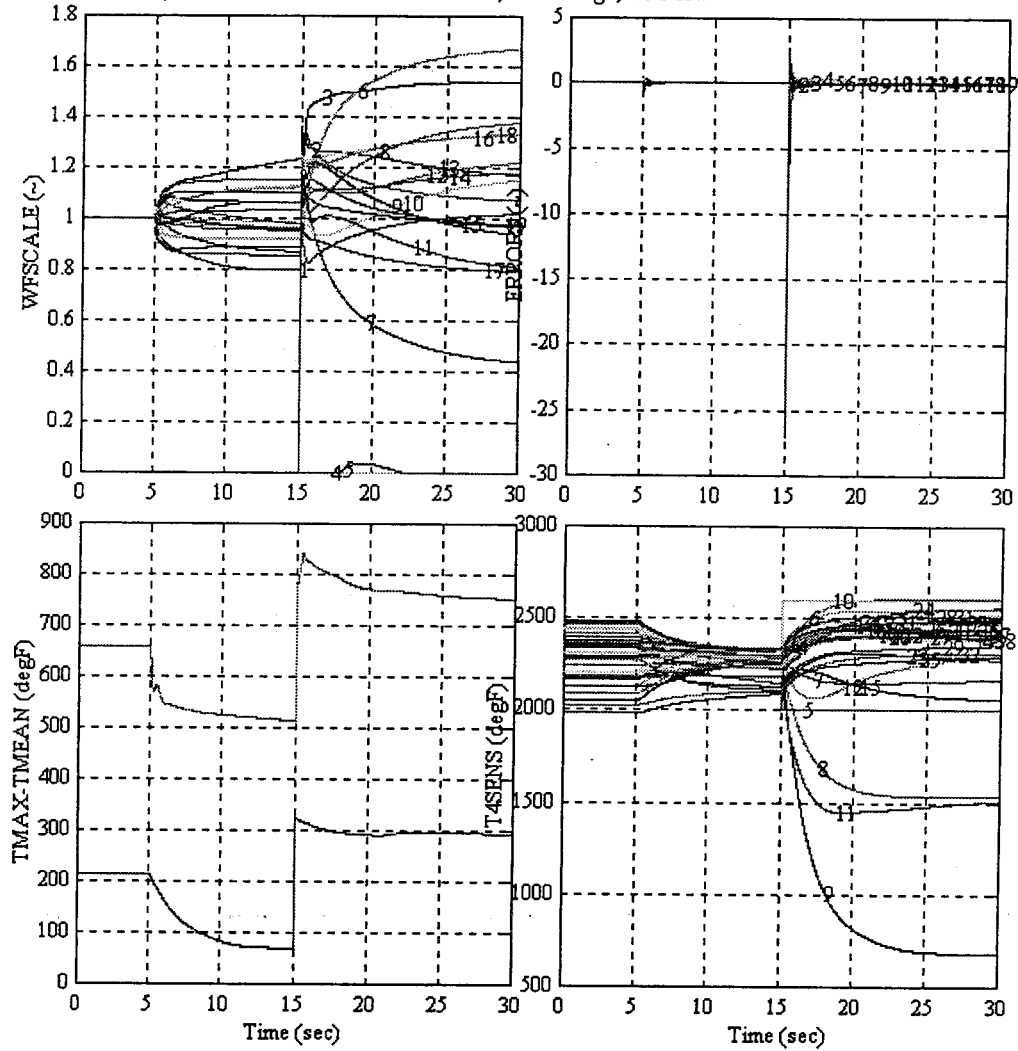


Fig. #17: Fuel Nozzle #4 Failed Closed, Thermocouple #5 Failed Low, Thermocouple #10 Failed High

aveT4 for PI Control, failure at 10 sec: FN 12 failed open, TC 3 high, TC 17 low

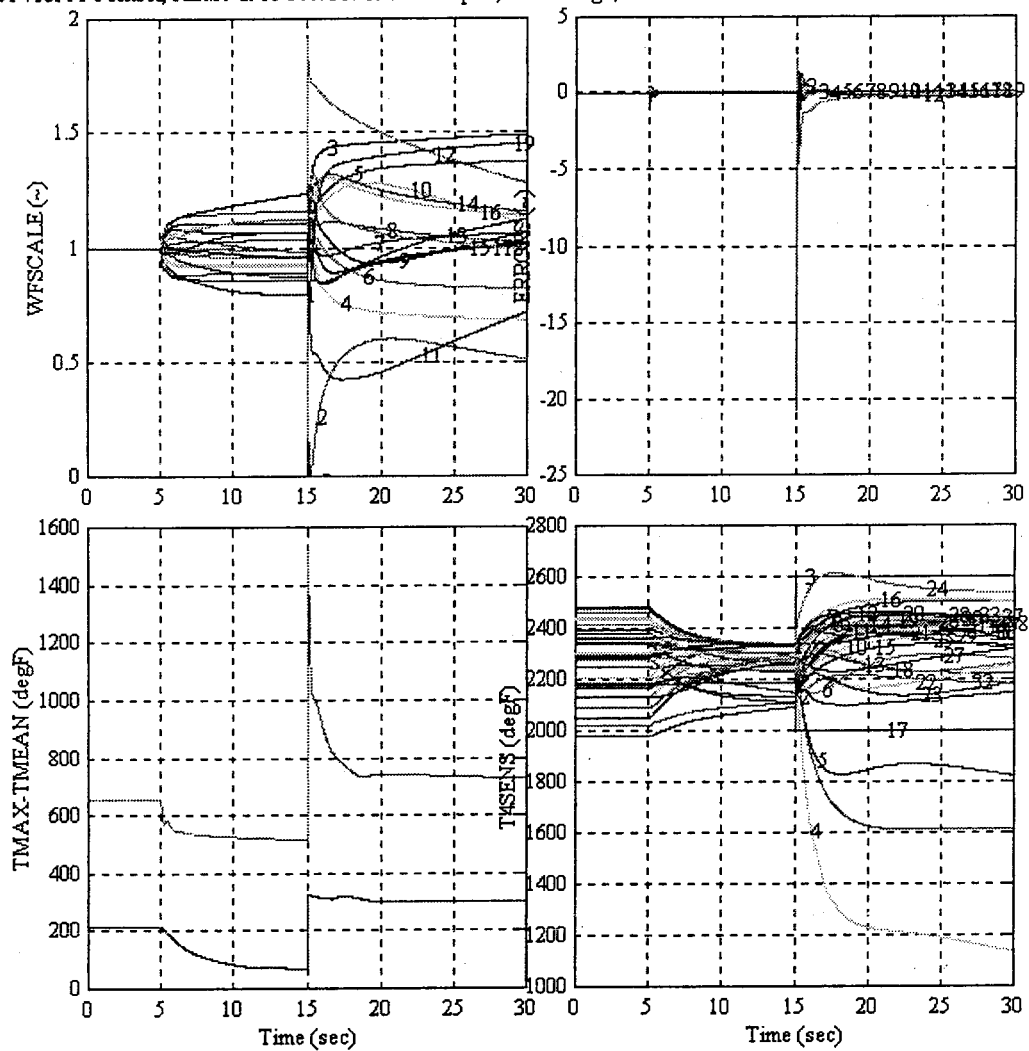


Fig. #18: Fuel Nozzle #12 Failed Open, Thermocouple #3 Failed High, Thermocouple #17 Failed Low

aveT4 for PI Control, failure at 10 sec: FN 12 failed closed, TC 3 high, TC 17 low

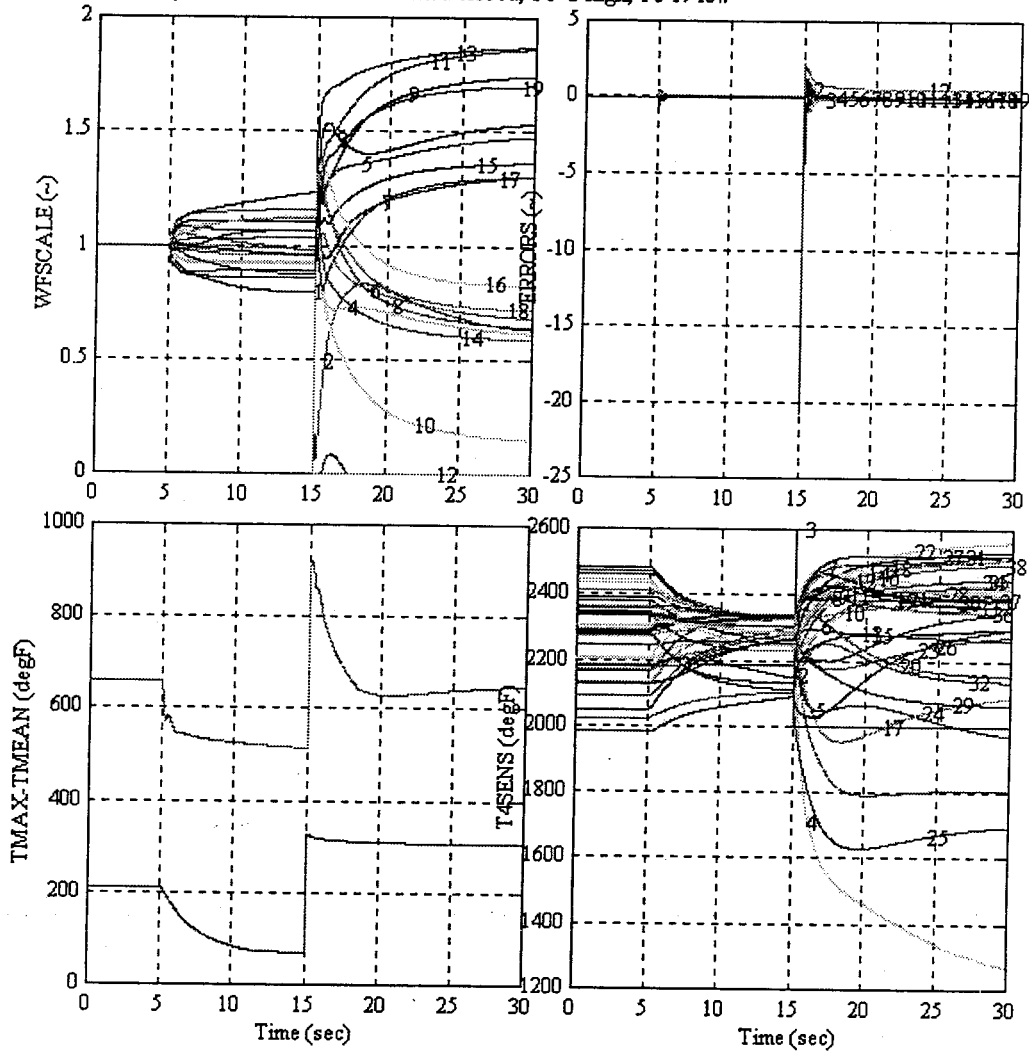


Fig. #19: Fuel Nozzle #12 Failed Closed, Thermocouple #3 Failed High, Thermocouple #17 Failed Low

ATTACHMENT 3

**Fuzzy Logic Controller For Emissions Reduction
Via Active Pattern Factor Control
T. Pfeifer, AlliedSignal Engines, Phoenix, AZ**

(77 Pages)



Fuzzy Controller for Emissions Reduction via Active Pattern Factor Control

Teresa Pfeifer



Introduction:

The fuzzy logic investigation described in this section was conducted in two phases. In phase one, the structure of the controller was developed, which addressed an ideal model of the combustor fuel nozzle and thermocouple system. To determine the ability of the controller to decrease hot spots both thermocouple failure modes and baseline runs were simulated and analyzed. A simple proportional plus integral (PI) controller was used as a benchmark for the fuzzy logic controller performance.

Phase Two addressed a more specific combustor system. Modifications were made to the simple phase one model in order to allow an asymmetric arrangement of thermocouples and fuel nozzles. Ability to reduce both cold and hot spots across a combustor was evaluated. Two fuzzy rule sets were evaluated, in addition to simulations on a larger array of failure modes for both thermocouples and fuel nozzles. A model that integrated the Allied Signal fuzzy logic control logic and the SMI combustor model was also created, executed, and compared against previous results.

What is a Fuzzy-Rule-Based System?

A Fuzzy-rule-based system is the process of mapping from a given input space to an output space defined by a set of fuzzy rules, and membership functions. In the APFC system two inputs and one output are defined. Input one is the change in temperature (T_4), as sensed by the thermocouples in the dispersion area of a fuel nozzle, with respect to the average temperature (T_4) of the combustor. Input one is called the error (e) of the system. Input two is the derivative of input one, (\dot{e} or $derror$) The output is the change in scale factor (sf , or $areaout$), or congruently, the change in fuel nozzle flow, dwf or du . [3],[4]

The first step of the mapping process is to 'fuzzify' the inputs. This means that each input, in parallel, is evaluated over all the membership functions. For example, if the input error was -150 degrees then the corresponding fuzzified input would be 'error is hot' and the graphical definition would be 1. (See membership function for input variable, error.) [1],[4]

The second step of the mapping process is to evaluate the inputs according to the rules. An example rule is: 'If error is hot and $derror$ is normal then sf is close.' The interpretation of this rule says if the change in sensed temperature with respect to the average temperature is high and the rate of change in sensed temperature is small then close the fuel nozzle. [3] With that example one can see how the fuzzified input, 'error is hot,' along with the input, 'derror is normal,' is evaluated by a rule. The result of the rule evaluation is the output. In this case if 'error is hot' and 'derror is normal' then the output, sf , will be 'close.'

The outputs from each rule are represented by an individual fuzzy set. Defuzzification, the final step, is the combination of each set that represents the output of a rule into a single fuzzy set. Defuzzification provides a single crisp number that represents each of the previous inputs, membership functions, and rules. The APFC fuzzy logic inference system used the centroid calculation. It returns the area under the curve. In this case the curve is the sum of the graphical representations from each rule. The area under the curve represents the controlled value, areaout or scale factor (sf). [1]

Phase One:

Fuzzy logic can be a powerful, efficient tool when dealing with nonlinearities. In this case, as a Pattern Factor Controller (T4 combustor temperature distribution), the relationship between the thermocouple measurements and individual fuel nozzle area was non-linear. The effectiveness of a fuzzy logic controller was devised by comparing the capability of a Fuzzy Inference System (FIS) in decreasing peak T4 temperatures to that of a traditional Proportional Integral (PI) controller. The fuzzy logic controller was shown to be capable of recovering from five defined thermocouple failure modes.

The FIS was modeled as a traditional PI controller that can be described as:

$$\begin{aligned} u &= K_p \cdot e + K_i \cdot \int e dt \\ &= \int \left(K_p \dot{e} + K_i \cdot e \right) dt \\ \text{or} \\ du &= \left(K_p \dot{e} + K_i e \right) dt \end{aligned}$$

where: e = the input, or error, to the control logic,
 K_p, K_i = constants,
 dt = incremental change in time (for Simulink model $dt = 0.2$ sec.),
 du = the output from the fuzzy logic control,
 u = the output from the PI control logic, also the integrated value of du .

The proportional term (K_p) provides control action equal to some multiple of the error, whereas the integral term (K_i) forces the steady-state error to zero. [2].

The input, or error, used in the fuzzy logic control was the same as the current PI control:
 $\text{error} = \text{average T4} - T4(i)$.

where: error = the input to the control logic, e ,
 $T4(i)$ = the individual T4 thermocouple temperature value,
 average T4 = the average of all T4 thermocouples values at a given time.

The output from the fuzzy logic control was the change in fuel nozzle area, or \dot{u} , (referred to as *areaout* in Simulink model). To obtain *area(i)*, the individual fuel nozzle area, an integrator is added to the FIS output. The variable *area(i)* corresponds to u in the above equations.

Fuzzy Inference System

The first step in the study was to develop the Fuzzy Inference System (FIS) for the ideal case, ie. no noise or failure modes. To enable comparison to a traditional PI controller the fuzzy logic controller was 'set' to match the existing PI controller in the Simulink model.

The FIS was designed with two input membership functions, each with five levels. Inputs were the error, average T_4 - $T_4(i)$ and its first derivative. The output membership function, *areaout*, was also five levels. Nineteen rules were written to define the output. The FIS membership functions, rules and error space are shown in Figures 1, 2, 3 and 4. The rules are listed below.

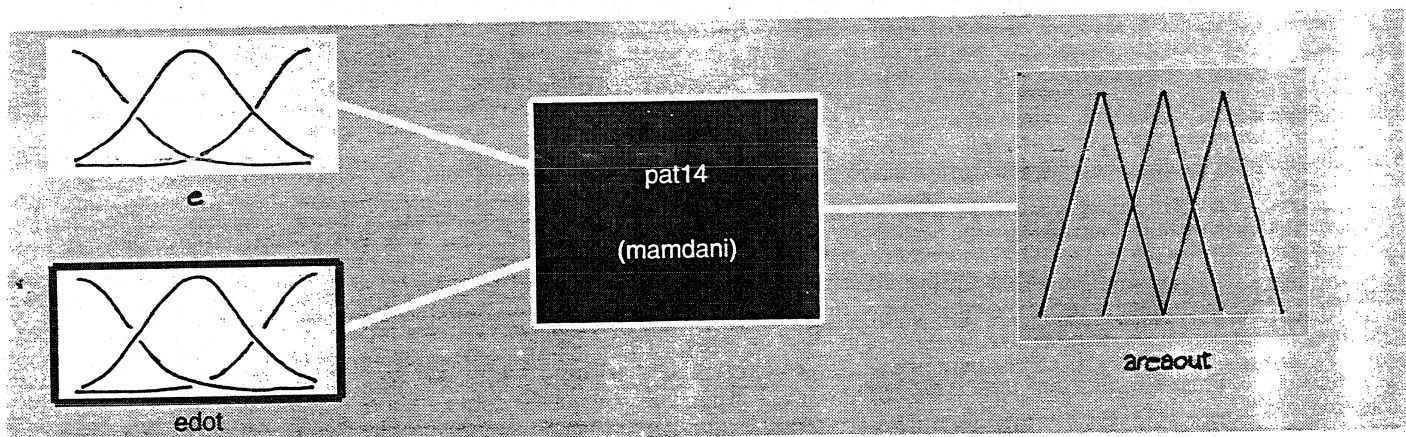


Figure 1. Fuzzy Logic Inference System (FIS), ideal case. This block diagram shows that two inputs e and \dot{e} generate one output, *areaout* when analyzed by the FIS *pat14* (*mamdani*). The FIS structure contains two 5 level input membership functions, one 5 level output membership function and 19 rules.

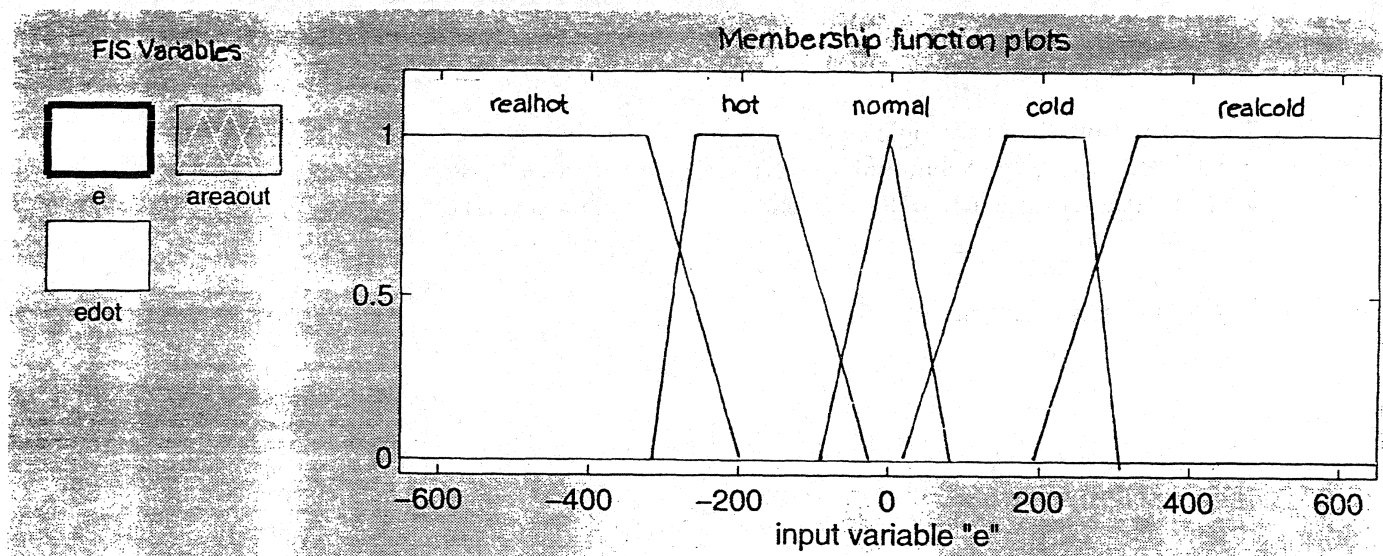


Figure 2. Input e Membership Function. e, or average $T4 - T4(i)$, is defined at five levels:

realhot $-650 < e < -200$
hot $-300 < e < -10$
normal $-75 < e < 75$
cold $10 < e < 300$
realcold $200 < e < 650$.

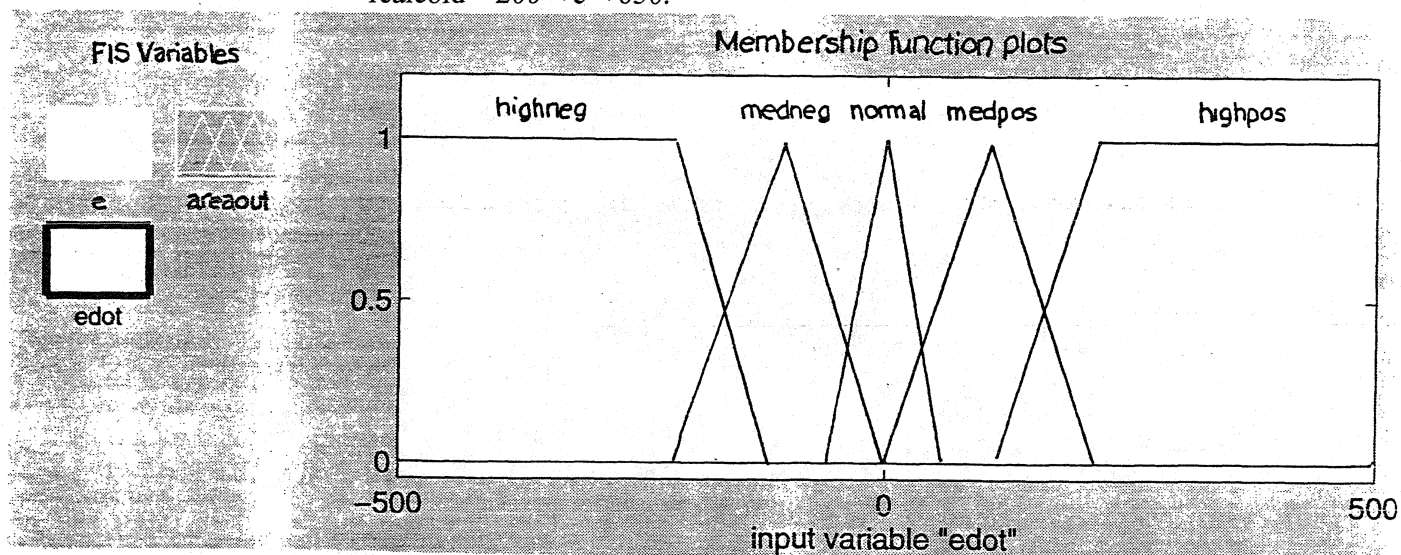


Figure 3. Input edot Membership Function. edot, or the 1st derivative of average $T4 - T4(i)$ is defined at five levels:

highneg $-500 < edot < -117$
medneg $-215 < edot < 0$
normal $-60 < edot < 60$
medpos $0 < edot < 215$
highpos $117 < edot < 500$.

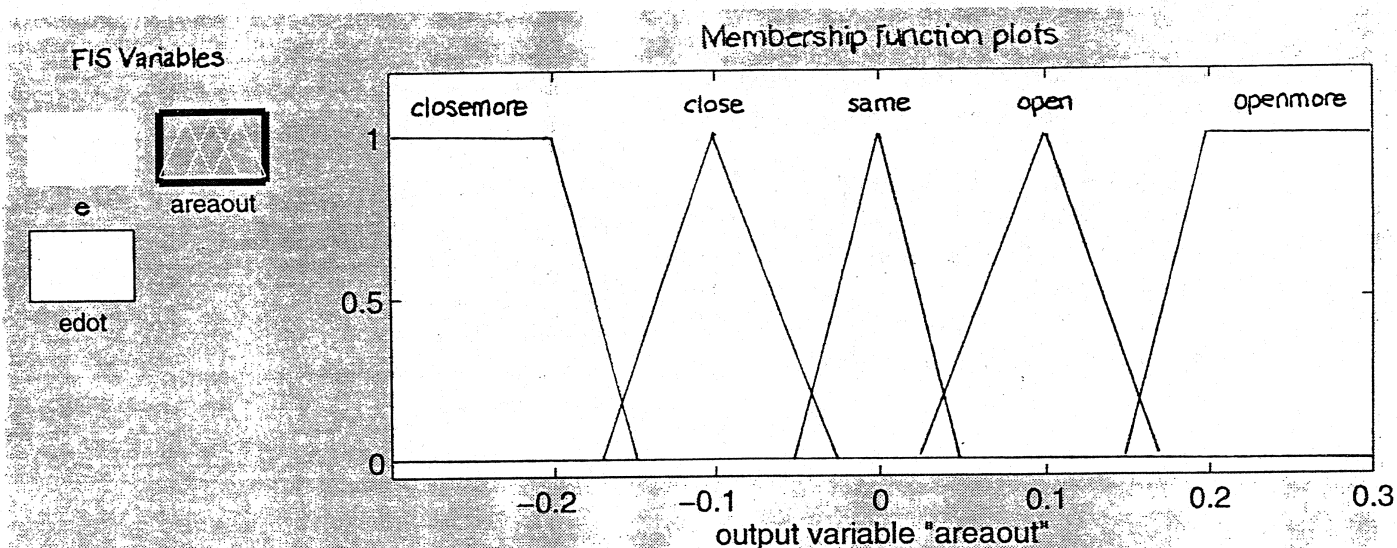


Figure 4. Output areaout Membership Function. areaout, or the change in individual fuel nozzle area, is defined at five levels:

| | |
|-----------|----------------------------------|
| closemore | $-0.3 < \text{areaout} < -0.15$ |
| close | $-0.17 < \text{areaout} < -0.03$ |
| same | $-0.05 < \text{areaout} < 0.05$ |
| open | $0.03 < \text{areaout} < 0.17$ |
| openmore | $0.15 < \text{areaout} < 0.3$ |

The fuzzy logic rules are listed below:

1. If e is realhot and edot is highneg then areaout is closemore.
2. If e is realhot and edot is normal then areaout is closemore.
3. If e is realhot and edot is medpos then areaout is close.
4. If e is realhot and edot is highpos then areaout is same.
5. If e is hot and edot is medneg then areaout is close.
6. If e is hot and edot is normal then areaout is close.
7. If e is hot and edot is medpos then areaout is same.
8. If e is cold and edot is medneg then areaout is same.
9. If e is cold and edot is normal then areaout is open.
10. If e is cold and edot is medpos then areaout is open.
11. If e is realcold and edot is highneg then areaout is same.
12. If e is realcold and edot is medneg then areaout is open.
13. If e is realcold and edot is normal then areaout is openmore.
14. If e is realcold and edot is highpos then areaout is openmore.
15. If e is normal and edot is highneg then areaout is closemore.
16. If e is normal and edot is medneg then areaout is close.
17. If e is normal and edot is normal then areaout is same.
18. If e is normal and edot is medpos then areaout is open.
19. If e is normal and edot is highpos then areaout is openmore.

Here is an example interpretation of rule number one. If e is in the level of realhot and edot is in the level of highneg then areaout is in the level of closemore. Another way of saying this is if average $T4 - T4(i)$ is between -200 and 650 degrees and it is getting much hotter (edot is highneg) then close the fuel nozzle as much as you can.

The fuzzy logic levels of the membership functions and rules were adjusted to match the PI controller with $K_P = 4$ and $K_I = 2$, steady state performance [2]. For a given input set (e, edot) or ($T4(i) - \text{average } T4, d[T4(i) - \text{average } T4]$), the corresponding output, areaout , can be set by adjusting the slope of the surface plot. See Figure 5. The actual peak temperature difference from average was 75 degrees lower than the PI controller and 50 degrees higher at the thermocouples for a system of 20 thermocouples and 20 fuel nozzles.

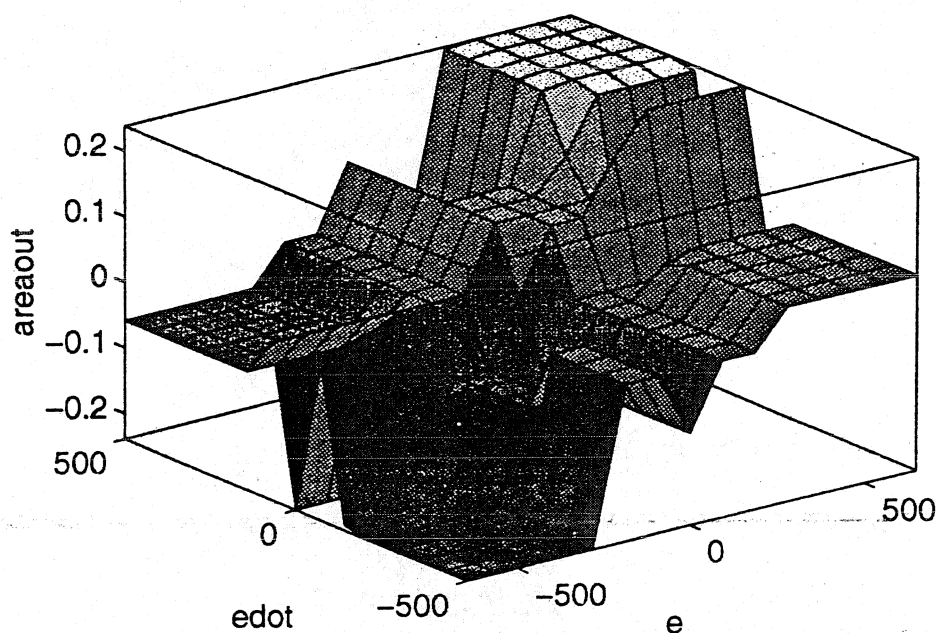


Figure 5. Fuzzy Logic (FIS) Error Space. This surface plot shows the surface defined by the membership functions and rules. It represents the anticipated inputs of e and edot for the ideal case. Its slope was adjusted to match the gains of the traditional PI controller. Here: $e = \text{average } T4 - T4(i)$, and $\text{edot} = \text{the 1st derivative of average } T4 - T4(i)$.

Active Pattern Factor Model Modification

After the FIS strategy was developed the next step was to modify the $T4$ combustor temperature distribution model to include the FIS. The model was changed to include the fuzzy logic controller. An Allied Signal / Engines MATLAB function, which allows an array to be passed to the MATLAB/Simulink Fuzzy Logic Toolbox EVAL_FIS CMEX function, (see Figure 6), was put into the Simulink model, and depicted in Figures 7 and 8, in submodule 'patdemo/Controller'. As can be seen in the submodule diagram the error and its derivative was fed into a Mux block which was then fed into the `multinput_evalfis` MATLAB function.

```

% Teresa Pfeifer
% Multiple inputs evaluated with evalfis in Matlab Fuzzy Logic Toolbox
% /users/e064443/nasa/active_fuzzy/multinput_evalfis.m
%

function [output_vector] = multinput_evalfis(N,input);

global fismat; % if change fis then must type at command line
               %      fismat = readfis(fisname);

% this is for square matrix, ie. all inputs have N elements
% input1 is a scalar , input2 is a vector of N elements, input3 is a vector of
%      N elements, ...
% when at matlab prompt and indicating the fisname must use quotes around the name
%      of the fis, ie. fisname = 'pat1' not fisname = pat1

% massage inputs into matrix format needed for evalfis
%      evalfis([input1(i); input2(i); input3(i)],fismat)

input1 = input(1:N);           % Average T4 - Max T4(i)
input2 = input((N+1):(2*N));    % d(Average T4 - Max T4(i))
input3 = input((2*N+1):(3*N));  % the following three inputs are
input4 = input((3*N+1):(4*N));  %      available for development purposes
input5 = input((4*N+1):(5*N));

array = [];

for i = 1:N

    % five inputs - delete input in not using it
    % eval(['array = [array; ' num2str(input1(i)) ' ' num2str(input2(i)) ' ' num2str(input3
    %      num2str(input4(i)) ' ' num2str(input5(i)) '];']);

    % two inputs only
    eval(['array = [array; ' num2str(input1(i)) ' ' num2str(input2(i)) ' ' '];']);

end % i

output_vector = evalfis([array],fismat); % in this case output_vector is
                                         %      dareaout

clear array;

```

Figure 6. Multinput_evalfis Allied Signal / Engines Matlab Function.

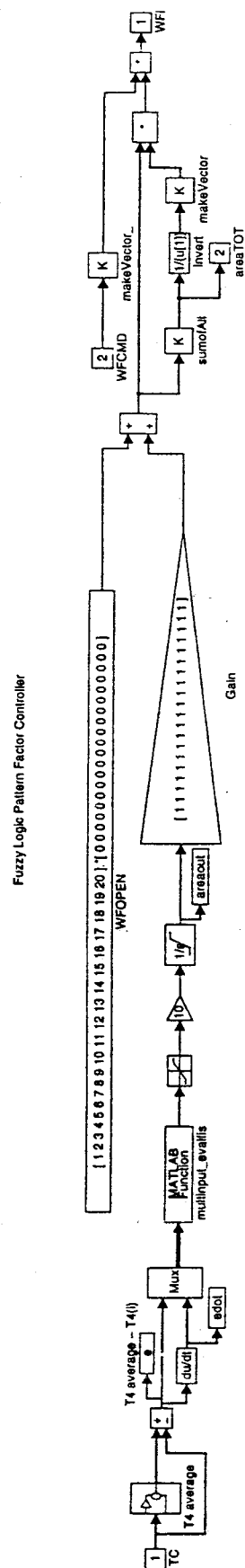


Figure 8. Fuzzy Logic Pattern Factor Controller Matlab/Simulink Diagram.

The MATLAB function 'multinput_evalfis' evaluated the fuzzy logic algorithm. Its output is an array of change in fuel nozzle area, areaout. The output is passed through a saturation block with an upper limit of 5 and a lower limit of 0. The output is then passed through a gain of 10 before the integrator stage. The integrator had a lower bound of .5, upper bound of 2 and an initial condition of 1. This is now the new fuel nozzle area, area(i).

These values are used to calculate the actual fuel at each nozzle. A change in area at one fuel nozzle effects the amount of commanded fuel ratio at all the other fuel nozzles. This is due to there being a constant total fuel flow for a given N1 speed. Individual fuel flow at each nozzle is related to the total fuel by the following:

$$W_f(i) = W_{f,total} \cdot \frac{area(i)}{\sum_{i=1}^N area(i)}$$

where: area(i) = the individual nozzle area,
 N = the number of fuel nozzles,
 Wf(i) = the individual fuel nozzle flow,
 Wf,total = constant total fuel flow for a given N1 speed.

Evaluation of the Fuzzy Logic Controller

Evaluation of the Fuzzy Logic Controller consisted of observing the magnitude of T4 temperature fluctuations and comparing them to a traditional PI controller. The overall max T4 value minus the average T4 value for both the measured thermocouple readings and the actual temperatures (as calculated in the model) were used as metrics. Actual temperature was considered to be of higher priority than measured temperature in this case. It is important to note that in operation the measured temperature is the only information that will be available. Settling time was also observed.

Table 1 summarizes those metrics for both the Fuzzy Logic Controller and the Traditional PI controller when the number of thermocouples and fuel nozzles was varied from 15 to 40. Note: more than 20 thermocouples are not realistic for this application. Values greater than 20 are used to obtain an understanding of the control logic.

Figure 9 and Figure 10 present a comparison of the controllers as the number of thermocouples were varied, with no failure modes.

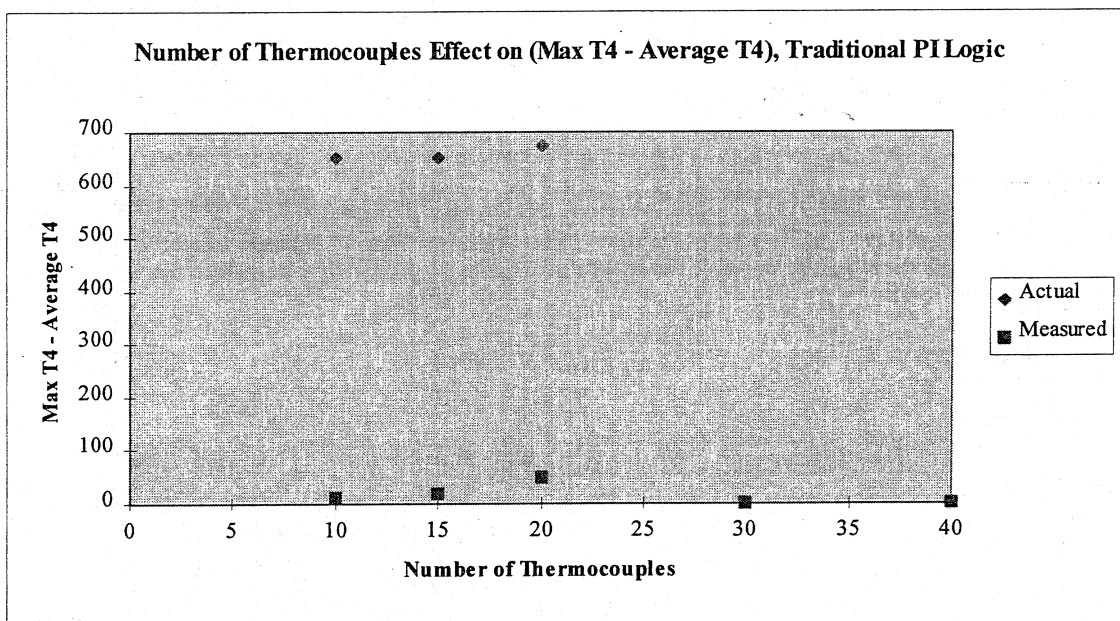


Figure 9. Note: As the number of thermocouples increased past 20 the temperature difference (Max T4 - Average T4) no longer settled out within a reasonable period of time, ie. two minutes. The points at 30 and 40 are at zero to symbolize that the system did not settle to any value.

| item no. | No. of | | Controller Type | Settle Time | | Maximum T4 - Average T4 | | Failure Mode | FIS | Gain |
|--|---------------|---------|-----------------|-------------|----------|-------------------------|-----------|--------------|-------|------|
| | Thermocouples | Nozzles | | Actual | Measured | Actual | Measured | | | |
| 1 | 10 | 10 | fuzzy | 5 | 10 | 625 | 100 | 0 | pat14 | 10 |
| 2 | 10 | 10 | fuzzy | 5 | 5 | 600 | 250 | 0 | pat14 | 100 |
| 3 | 15 | 15 | fuzzy | 20 | 10 | 675 | 50 | 0 | pat14 | 5 |
| 4 | 15 | 15 | fuzzy | 10 | 10 | 650 | 150 | 0 | pat14 | 10 |
| 5 | 20 | 20 | fuzzy | 5 | 5 | 600 | 100 | 0 | pat14 | 10 |
| 6 | 30 | 30 | fuzzy | 5 | 5 | 525 | 200 | 0 | pat14 | 10 |
| 7 | 40 | 40 | fuzzy | 5 | 10 | 475 | 300 | 0 | pat14 | 10 |
| 8 | 50 | 50 | fuzzy | 5 | 10 | 500 | 375 | 0 | pat14 | 10 |
| 9 | 60 | 60 | fuzzy | 5 | 5 | 475 | 375 | 0 | pat14 | 10 |
| 10 | 10 | 10 | PI | 5 | 10 | 650 | 10 | 0 | - | - |
| 11 | 15 | 15 | PI | 10 | 10 | 650 | 20 | 0 | - | - |
| 12 | 20 | 20 | PI | 20 | 5 | 675 | 50 | 0 | - | - |
| 13 | 30 | 30 | PI | - | - | unsettled | unsettled | 0 | - | - |
| 14 | 40 | 40 | PI | - | - | unsettled | unsettled | 0 | - | - |
| Failure modes: 0 = ideal case, 1 = one sensor fixed low (2000 deg), 2 = one sensor fixed high (2600 deg), 3 = both sensors low, 4 = both sensors high, 5 = one sensor low, one sensor high | | | | | | | | | | |
| 15 | 15 | 15 | fuzzy | 5 | 10 | 650 | 150 | 1 | pat14 | 10 |
| 16 | 15 | 15 | fuzzy | 5 | 10 | 625 | 150 | 3 | pat14 | 10 |
| 17 | 15 | 15 | fuzzy | 5 | 5 | 725 | 350 | 5 | pat14 | 10 |
| 18 | 20 | 20 | fuzzy | 5 | 5 | 610 | 150 | 1 | pat14 | 10 |
| 19 | 20 | 20 | fuzzy | 5 | 5 | 700 | 325 | 2 | pat14 | 10 |
| 20 | 20 | 20 | fuzzy | 5 | 5 | 650 | 325 | 3 | pat14 | 10 |
| 21 | 20 | 20 | fuzzy | 5 | 5 | 775 | 300 | 4 | pat14 | 10 |
| 22 | 20 | 20 | fuzzy | 5 | 5 | 675 | 350 | 5 | pat14 | 10 |
| 23 | 20 | 20 | PI | 60 | 10 | 875 | 200 | 1 | - | - |
| 24 | 20 | 20 | PI | 25 | 5 | 900 | 325 | 2 | - | - |
| 25 | 20 | 20 | PI | 60 | 25 | 950 | 175 | 3 | - | - |
| 26 | 20 | 20 | PI | 25 | 5 | 875 | 275 | 4 | - | - |
| 27 | 20 | 20 | PI | 25 | 5 | 1050 | 350 | 5 | - | - |

Note 1: Thermocouples used for failure modes were number ten and five

Note 2: Phase is zero for all cases

Table 1. Summary of Results. Items 1 - 14 are the results for a number of thermocouple sensors series, Items 15 - 27 are the results for a failure mode series.

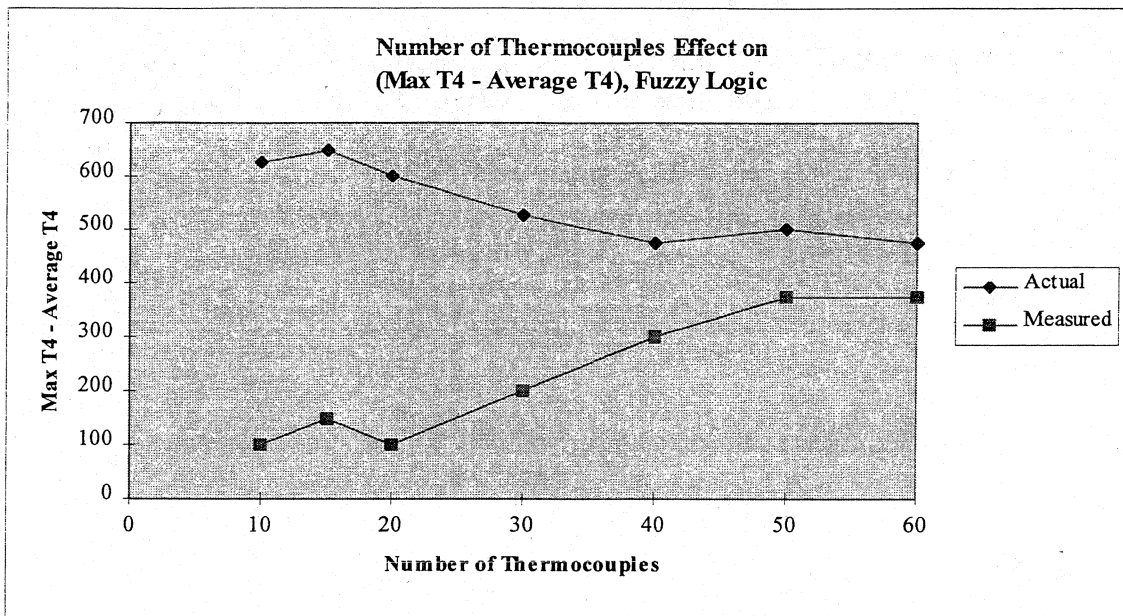


Figure 10. Note: As the number of thermocouples increased the measured and actual temperatures approach the same value. Considering that the measured data is a subset of the actual data it makes sense that the final values and measured data sets begin to look the same. As the number of thermocouples increase the measured data set becomes a larger subset of the actual data set.

What do these plots tell us about the controllers? If you relate the number of thermocouples to actual combustor area then this can be looked at from the view point of combustor area. As the number of thermocouples increases the controlled area of the combustor increases. Thus the controller is required to work harder with more thermocouples. The PI controller couldn't handle more than 20 thermocouples within a reasonable period of time (ie. two minutes). The fuzzy logic controller continued to settle out within five seconds and began to approach a limiting temperature difference of approximately 425 degrees. At this stage of the study the fuzzy logic controller seems more robust to thermocouple quantity variation. Thus better control of more area within the combustor. The question remains as to whether or not an optimized PI controller would perform in a more robust fashion.

Failure Modes

The second step of the evaluation investigated thermocouple failure modes. With failure modes the performance difference between the two was controllers shown. The actual temperature difference was higher by 200 to 300 degrees for the PI controller when compared to the fuzzy logic controller. The PI controller did not settle out after two minutes for two of the failure modes which fixed a thermocouple sensor low. The fuzzy logic controller performed consistently across all failure modes with regards to both pattern factor reduction and settling time.

Failure modes were defined as: 1) one thermocouple was fixed to read 300 degrees lower than the settled average T4; 2) one thermocouple was fixed to read 300 degrees high; 3) both thermocouple sensors fixed low; 4) both thermocouples fixed high; and 5) one thermocouple fixed high and one thermocouple fixed low.

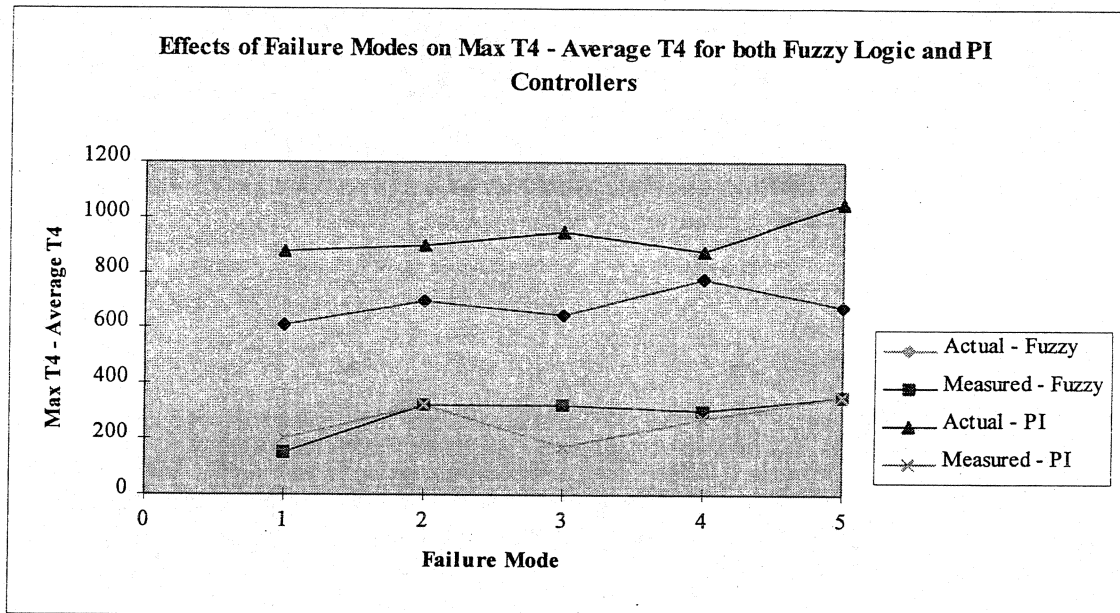


Figure 11. Note: The measured temperature difference was the same for both the PI and fuzzy logic controllers across all five failure modes. The actual temperature difference highlights the performance difference between the controllers. The fuzzy logic controller had a consistently lower temperature difference than the PI controller.

For the Fuzzy Controller the actual T4 temperature remained in the range of 650 degrees for all failure modes. (Using the baseline case of 20 thermocouples and 20 fuel nozzles, gain equal to ten for the test). When 15 thermocouples were tested the actual temperature increased to 725 for failure mode 3 only. In all cases the settling time was by 5 seconds. This was in contrast to the PI controller which displayed a range of $675 < \text{actual temperature} < 1050$ deg when failure modes were tested. The typical settling time for the PI controller was 25 seconds. See results in Table 1, Figure 11, and Figure 12.

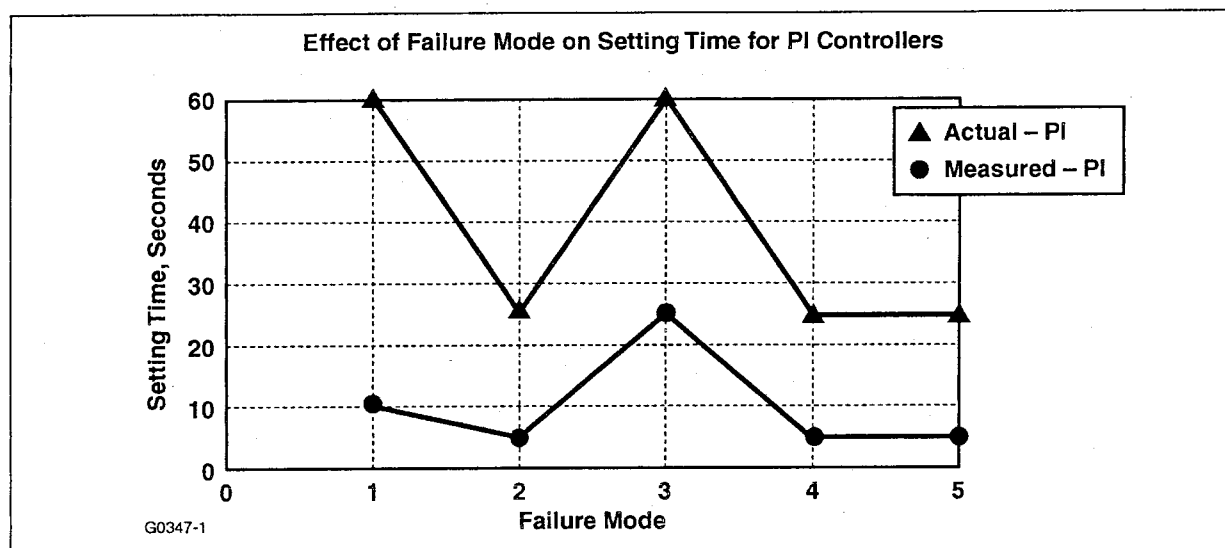


Figure 12. Note: The settling time for the PI controller was high for failure mode cases that fixed on or both thermocouples low, drastically so for the actual temperature difference. The fuzzy logic controller settled out in five seconds for all failure modes.

Phase One Conclusions:

The results show that the fuzzy logic controller can be set to match the steady state performance of the traditional PI controller by membership range selection [2]. For the ideal case of no failure modes both control schemes gave comparable results, although the fuzzy controller settled out quicker by 5 to 15 seconds. Failure modes revealed the differences in the performance of the controllers. Using the categories of settling time, shorter is better; actual temperature, lower is better; and robustness to number of thermocouples the fuzzy logic controller was revealed to be superior. Investigation into the effectiveness of a Fuzzy Logic Controller was continued in with Phase Two.

Phase Two:

The Active Pattern Factor Fuzzy Logic Controller was designed to reduce hot and cold spots within a combustor. Modifications were made to allow an asymmetric arrangement of thermocouples and fuel nozzles. The controller was evaluated on both Allied Signal models and SMI models. Failure modes for both thermocouples and fuel modulators were tested on a model that represented the actual test rig. The controller was transportable from model to model with comparable results.

The asymmetric fuzzy logic control system was evaluated in both the Allied Signal Model and the SMI Model. The original symmetric fuzzy logic controller, with 20 thermocouples and 20 fuel nozzles, resulted in an actual temperature difference of 600 degrees and sensed difference of 100 degrees. The asymmetric fuzzy controller (baseline) with 38 thermocouples and 19 fuel nozzles, resulted in an actual temperature difference of +590 and -600 degrees (hot and cold spots, respectively) and a sensed difference of +125 and -225 degrees.

The difference in performance is due to an unlike arrangement of thermocouples. The system with 38 thermocouples and 19 fuel nozzles is controlling a greater area within the combustor; you could say that it was working harder. It also used the nonlinear relationship of fuel dispersion to thermocouple in the error term. When the SMI model, an arrangement of 38 thermocouples and 20 fuel nozzles, was combined with the asymmetric fuzzy controller a sensed temperature difference of +/- 125 degrees resulted. Those results are comparable to the AE model with the fuzzy controller.

Modification of Symmetric model to Asymmetric:

Asymmetric arrangements are unequal numbers of thermocouples and fuel nozzles. The original fuzzy logic pattern factor controller allowed an asymmetric fuel nozzle and thermocouple arrangement. In order to make the model accept non equal numbers of components the relationship of fuel distribution to sensed thermocouple values was needed. The change of fuel flow with respect to the change sensed at the thermocouples was defined as a relationship of angular distribution from a fuel atomizer to

thermocouples. This relationship was established by test data. Note that this relationship could be modeled in many ways. The following was selected based upon its use elsewhere in the Allied Signal engine model.

The influence of fuel flow as sensed by a thermocouple was modeled as a cosine function. This influence was called the weight of the fuel nozzle on the thermocouple measurement and is described as:

$$\text{weight} = \begin{cases} \cos\left(d\Theta \cdot 3 \cdot \frac{\pi}{180}\right) & \text{for } d\Theta < |30^\circ| \\ 0 & \text{elsewhere} \end{cases}$$

where: $d\Theta$ is the angular distance of a thermocouple to a given fuel atomizer

The input, or error, used in the symmetric model was:

$$\text{error} = \text{average T4} - \text{T4(i)}$$

where: error = the input to the control logic, e,
 T4(i) = the individual T4 thermocouple temperature value,
 average T4 = the average of all T4 thermocouple values at a given time.

The modified asymmetric system uses the an effective thermocouple value in place of T4(i) . The effective thermocouple value reflected the weighted sum of all the thermocouple measurements that are influenced by a fuel atomizer:

$$\text{error} = \text{average T4} - \frac{\sum_{j=1}^N \text{T4}(i)_{<30^\circ} \cdot \text{weight}}{\sum \text{weight}}$$

where: error = the input to the control logic, e,
 average T4 = the average of all T4 thermocouple values at a given time,
 $\text{T4}(i)$ = the individual T4 thermocouple temperature values (for $d\Theta < 30^\circ$).

The asymmetric model was placed into both Allied Signal and SMI models. For the SMI model slight adjustments to the saturation limit and gain after the fuzzy logic block were made to allow a more stable approach to the final temperature difference. SMI provided an influence coefficient matrix which affected the error into the controller. AS also had an influence coefficient matrix. The matrices were comparable but the SMI matrix was more narrow than the AS matrix. The Fuzzy logic controller could be used with either influence coefficient matrix. Noise on the derivative of the error term, reduced by the AS influence coefficient matrix, was the only difference noticed. The SMI model did not allow for an actual temperature difference to be calculated.

Failure Modes:

Failure Modes were defined for both thermocouples and fuel flow modulators. They are listed below:

Thermocouples:

- 1) Temperature reading fixed High,
- 2) Temperature reading fixed Low,
- 3) Combinations of 1 & 2.

Fuel Flow Modulator (FFM):

- 4) Modulator area fixed open (primary failure mode),
- 5) Modulator area fixed closed (rare event),

The thermocouple failure modes were simulated by fixing a thermocouple temperature high or low, 2600 deg. or 2000 deg. respectively. The fuel nozzles were tested in the same manner by fixing one open or closed. Combinations of fuel nozzle and thermocouples failure modes were also performed. The following is a table of the failure modes considered. The simulation results using various fuzzy controllers are described subsequent to discussions on development of various fuzzy inference systems.

No. Failure Mode Definitions

| | | |
|----|-------------------------|-------------------------|
| 0 | Baseline | |
| 1 | FN 4 open | |
| 2 | FN 4 closed | |
| 3 | TC 10 low | |
| 4 | TC 5 low | |
| 5 | FN 4 open | TC 10 low |
| 6 | FN 4 closed | TC 10 low |
| 7 | FN 4 open | TC 10 high |
| 8 | FN 4 closed | TC 10 high |
| 9 | TC 10 and 5 low | |
| 10 | TC 10 and 5 high | |
| 11 | TC 10 low and TC 5 high | |
| 12 | FN 4 open | TC 10 and 5 low |
| 13 | FN 4 closed | TC 10 and 5 low |
| 14 | FN 4 open | TC 10 and 5 high |
| 15 | FN 4 closed | TC 10 and 5 high |
| 16 | FN 4 open | TC 10 high and TC 5 low |
| 17 | FN 4 closed | TC 10 and TC 5 low |
| 18 | FN 12 open | TC 3 high TC 17 low |
| 19 | FN 12 closed | TC 3 high TC 17 low |

A Short Discussion on the APFC Fuzzy Rules

A set of fuzzy rules describes the Active Pattern Factor Controller for a fuzzy-rule-based system. The fuzzy rule set maps the input vectors, (error,derror), into a fuzzy output set that defines the incremental control actions of the system. In the case of two inputs and one output a three dimensional space is defined by the membership function levels and the fuzzy rule set. The three dimensional space is called the error space. The set of fuzzy rules can be notated with a control matrix. [2]

A control matrix is a good way to organize a two-input and one-output fuzzy system. The first input defines the columns of the matrix, while the second input defines the rows. Column and row headings, or terms, correspond to the levels in the membership functions. Matrix data are the fuzzy output set elements.

An example of a seven level control matrix with two inputs and one output can be seen below. The seven levels are zero, negative low, negative medium, negative high, positive low, positive medium, and positive high. The same seven levels can also be used to define the output for a given combination error and derror, as summarized in the matrix below. Fuzzy logic rules that define the seven-level system are below the control matrix. The error space is steplike with gradations between steps defined by the rules and a slope defined by the membership function level definitions. Note that as the number of levels increase the number of rules and correspondingly the amount of time to execute the model increases.

| | | error | | | | | | | | | |
|--------|----|-------|----|----|----|----|----|----|----|----------|----------|
| | | NH | NM | NL | ZE | PL | PM | PH | | | |
| derror | NH | ph | ph | ph | ph | pm | pl | ze | ze | 7 levels | |
| | NM | ph | pm | pm | pm | pl | ze | nl | nl | | zero |
| | NL | ph | pm | pm | pl | ze | nl | nm | nm | | neg low |
| | ZE | ph | pm | pl | ze | nl | nm | nh | nh | | neg med |
| | PL | pm | pl | ze | nl | nm | nm | nh | nh | | neg high |
| | PM | pl | ze | nl | nm | nm | nm | nh | nh | | pos high |
| | PH | ze | nl | nm | nh | nh | nh | nh | nh | | pos med |
| | | | | | | | | | | | pos low |

Fuzzy Logic Rules - Seven Level System

1. If error is neghigh and derror is neghigh then areaout is poshigh.
2. If error is negmed and derror is neghigh then areaout is poshigh.
3. If error is neglow and derror is neghigh then areaout is poshigh.
4. If error is zero and derror is neghigh then areaout is poshigh.
5. If error is poslow and derror is neghigh then areaout is posmed.
6. If error is posmed and derror is neghigh then areaout is poslow.
7. If error is poshigh and derror is neghigh then areaout is zero.
8. If error is neghigh and derror is negmed then areaout is poshigh.
9. If error is negmed and derror is negmed then areaout is posmed.
10. If error is neglow and derror is negmed then areaout is posmed.

- | | |
|-------------------------|--|
| 11. If error is zero | and derror is negmed then areaout is posmed. |
| 12. If error is poslow | and derror is negmed then areaout is poslow. |
| 13. If error is posmed | and derror is negmed then areaout is zero. |
| 14. If error is poshigh | and derror is negmed then areaout is neglow. |
| 15. If error is neghigh | and derror is neglow then areaout is poshigh. |
| 16. If error is negmed | and derror is neglow then areaout is posmed. |
| 17. If error is neglow | and derror is neglow then areaout is posmed. |
| 18. If error is zero | and derror is neglow then areaout is poslow. |
| 19. If error is poslow | and derror is neglow then areaout is zero. |
| 20. If error is posmed | and derror is neglow then areaout is neglow. |
| 21. If error is poshigh | and derror is neglow then areaout is negmed. |
| 22. If error is neghigh | and derror is zero then areaout is poshigh. |
| 23. If error is negmed | and derror is zero then areaout is posmed. |
| 24. If error is neglow | and derror is zero then areaout is poslow. |
| 25. If error is zero | and derror is zero then areaout is zero. |
| 26. If error is poslow | and derror is zero then areaout is neglow. |
| 27. If error is posmed | and derror is zero then areaout is negmed. |
| 28. If error is poshigh | and derror is zero then areaout is neghigh. |
| 29. If error is neghigh | and derror is poslow then areaout is posmed. |
| 30. If error is negmed | and derror is poslow then areaout is poslow. |
| 31. If error is neglow | and derror is poslow then areaout is zero. |
| 32. If error is zero | and derror is poslow then areaout is neglow. |
| 33. If error is poslow | and derror is poslow then areaout is negmed. |
| 34. If error is posmed | and derror is poslow then areaout is negmed. |
| 35. If error is poshigh | and derror is poslow then areaout is neghigh. |
| 36. If error is neghigh | and derror is posmed then areaout is poslow. |
| 37. If error is negmed | and derror is posmed then areaout is zero. |
| 38. If error is neglow | and derror is posmed then areaout is neglow. |
| 39. If error is zero | and derror is posmed then areaout is negmed. |
| 40. If error is poslow | and derror is posmed then areaout is negmed. |
| 41. If error is posmed | and derror is posmed then areaout is negmed. |
| 42. If error is poshigh | and derror is posmed then areaout is neghigh. |
| 43. If error is neghigh | and derror is poshigh then areaout is zero. |
| 44. If error is negmed | and derror is poshigh then areaout is neglow. |
| 45. If error is neglow | and derror is poshigh then areaout is negmed. |
| 46. If error is zero | and derror is poshigh then areaout is neghigh. |
| 47. If error is poslow | and derror is poshigh then areaout is neghigh. |
| 48. If error is posmed | and derror is poshigh then areaout is neghigh. |
| 49. If error is poshigh | and derror is poshigh then areaout is neghigh. |

One way to decrease the amount of time to run is to decrease the number of levels in the membership functions. An example of a five level control matrix, along with the defining rules, is shown below. To the left and atop of the control matrix are abbreviations of the terms used in the APFC system. To the right of the control matrix are the actual terms used in the two input, (error, derror), and one output fuzzy system. For clarity in describing the output, the same nomenclature to represent the output, which was used during the phase 1 study, can be applied, ie; open, close, open more, close more, or same. For comparison the terms used in the seven level matrix are also shown. An FIS was written, pat21.fis, and run with the combustor model, and the results are described in a subsequent section of this report.

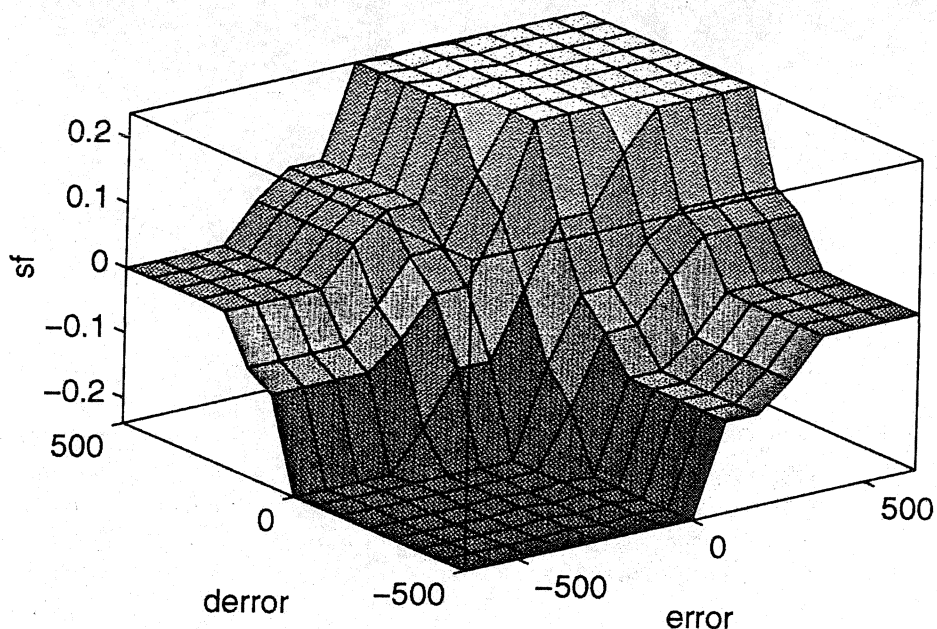


Figure 13. Five-level error space, pat21

Another way to decrease the amount of time to run is to decrease the number of rules that define the error space. This can be seen by modifying the seven level control matrix. Terms are removed until there are five levels for one or both of the inputs and the output. This corresponds to removing rules. Although there are only five levels defined the seven level error space is still represented. It should be noted that this method is possible with the Mathworks fuzzy logic toolbox used for this analysis, but might not be possible if another software package were used. An interpolation routine that takes neighboring elements to predict the output value is used in the Mathworks Fuzzy Logic Toolbox whenever an input is not defined by a rule and level.

Two examples of combined, or hybrid, seven level matrices with five terms for inputs and outputs are shown below. The error space as plotted with Mathworks Matlab Fuzzy Logic Toolbox is also shown. Note that the Mathworks plot does not show the interpolation. FIS names for these systems are pat20.fis and pat22.fis.

| | | error | | | | | | | |
|--------|----|-------|----|----|----|----|----|----|--|
| | | rh | h | n | c | rc | | | |
| derror | | NH | NM | NL | ZE | PL | PM | PH | |
| hn | NH | cm | | | c | | | s | |
| mn | NM | | | c | c | s | | o | |
| | NL | | | | | | | | |
| n | ZE | cm | | c | s | o | | om | |
| | PL | | | | | | | | |
| mp | PM | c | | s | o | o | | | |
| hp | PH | s | | | o | | | om | |

| 5 levels | error | derror |
|----------|-----------|----------|
| NM | Real Hot | High Neg |
| NL | Hot | Med Neg |
| ZE | Normal | Normal |
| PL | Cold | Med Pos |
| PM | Real Cold | High Pos |

pat22.fis

Fuzzy Logic Rules - Hybrid System One

1. If error is realhot and derror is highneg then sf is closemore.
2. If error is realhot and derror is normal then sf is closemore.
3. If error is realhot and derror is medpos then areaout is close.
4. If error is realhot and derror is highpos then areaout is same.
5. If error is hot and derror is medneg then areaout is close.
6. If error is hot and derror is normal then areaout is close.
7. If error is hot and derror is medpos then areaout is same.
8. If error is cold and derror is medneg then areaout is same.
9. If error is cold and derror is normal then areaout is open.
10. If error is cold and derror is medpos then areaout is open.
11. If error is realcold and derror is highneg then areaout is same.
12. If error is realcold and derror is medneg then areaout is open.
13. If error is realcold and derror is normal then areaout is openmore.
14. If error is realcold and derror is highpos then areaout is openmore.
15. If error is normal and derror is highneg then areaout is same.
16. If error is normal and derror is medneg then areaout is close.
17. If error is normal and derror is normal then areaout is open.
18. If error is normal and derror is medpos then areaout is close.
19. If error is normal and derror is highpos then areaout is open.

The corresponding error space:

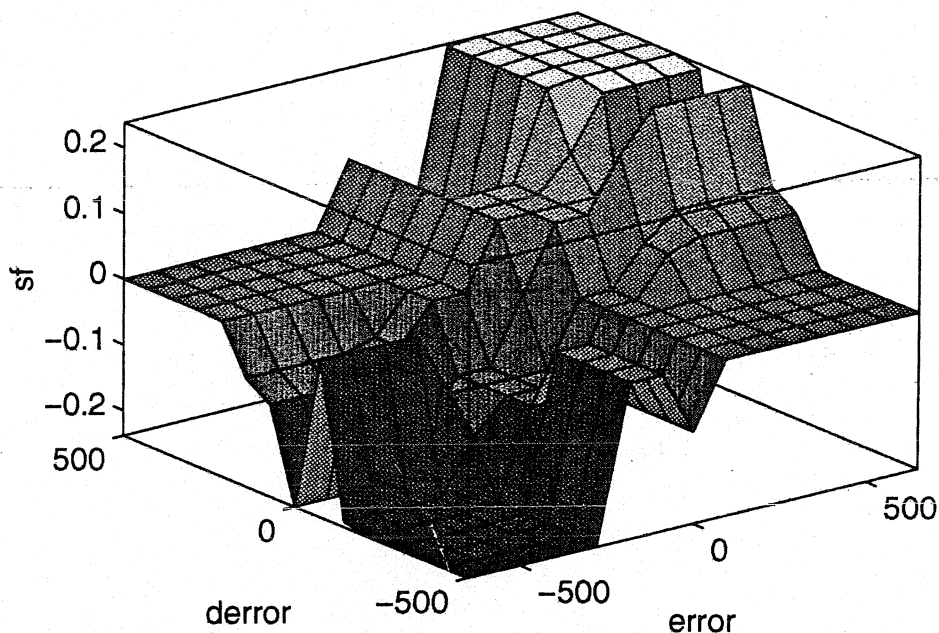


Figure 14. Hybrid-one 7-level error space, pat20

pat20.fis

| | | erro r | | | | | | | | | |
|--------|----|-----------|----|----|----|----|----|----|----------|-----------|----------|
| | | rh | h | n | c | | | rc | | | |
| derror | | NH | NM | NL | ZE | PL | PM | PH | 5 levels | error | derror |
| hn | NH | cm | | | cm | | | s | | | |
| mn | NM | | | c | c | s | | o | NM | Real Hot | High Neg |
| | NL | | | | | | | | NL | Hot | Med Neg |
| n | ZE | cm | | c | s | o | | om | ZE | Normal | Normal |
| | PL | | | | | | | | PL | Cold | Med Pos |
| mp | PM | c | | s | o | o | | | PM | Real Cold | High Pos |
| hp | PH | s | | | om | | | om | | | |
| | | | | | | | | | | | |

Fuzzy Logic Rules - Hybrid System Two

1. If error is realhot and derror is highneg then areaout is closemore.
2. If error is realhot and derror is normal then areaout is closemore.
3. If error is realhot and derror is medpos then areaout is close.
4. If error is realhot and derror is highpos then areaout is same.
5. If error is hot and derror is medneg then areaout is close.
6. If error is hot and derror is normal then areaout is close.
7. If error is hot and derror is medpos then areaout is same.
8. If error is cold and derror is medneg then areaout is same.
9. If error is cold and derror is normal then areaout is open.
10. If error is cold and derror is medpos then areaout is open.
11. If error is realcold and derror is highneg then areaout is same.
12. If error is realcold and derror is medneg then areaout is open.
13. If error is realcold and derror is normal then areaout is openmore.
14. If error is realcold and derror is highpos then areaout is openmore.
15. If error is normal and derror is highneg then areaout is closemore.
16. If error is normal and derror is medneg then areaout is close.
17. If error is normal and derror is normal then areaout is same.
18. If error is normal and derror is medpos then areaout is open.
19. If error is normal and derror is highpos then areaout is openmore.

The corresponding error space:

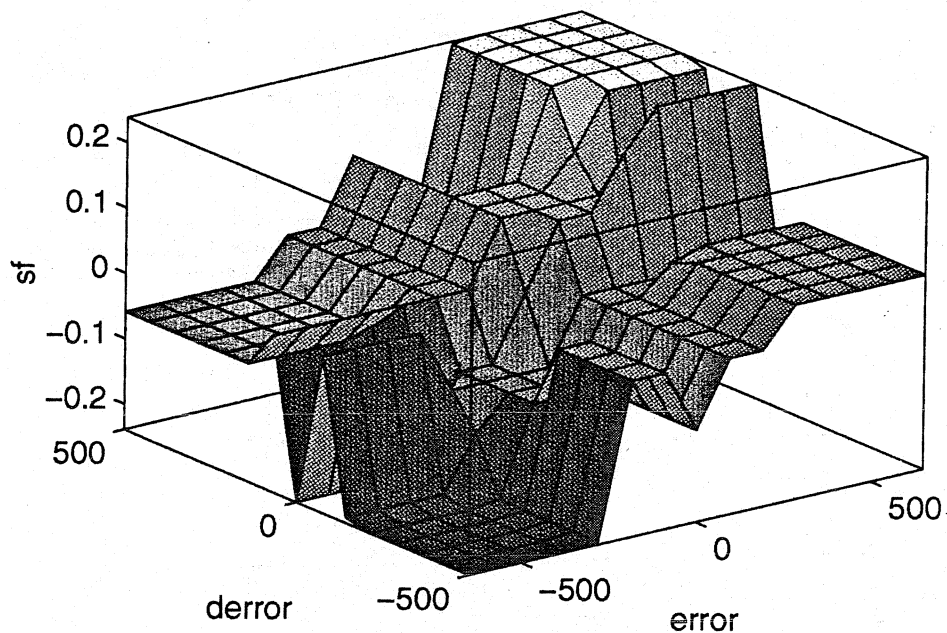


Figure 15. Hybrid-two seven-level error space, pat 22

Results

Figure 16 shows a comparison of the results of the five-level system and the hybrid seven-level system for Maximum and Minimum (hotspot versus coldspot) control. Notice that the results are comparable. Figure 17 displays the comparison of the pat20 fuzzy controller versus the PI controller. Notice that, with few failure mode exceptions, the results are comparable for control of the maximum combustor temperature. Although the control of “coldspots” was not a design requirement for either control, the fuzzy method seemed to keep the “coldspots” at a narrower range than the PI control. This can be more easily visualized through re-grouping of the failure modes as listed below and displayed in figure 18.

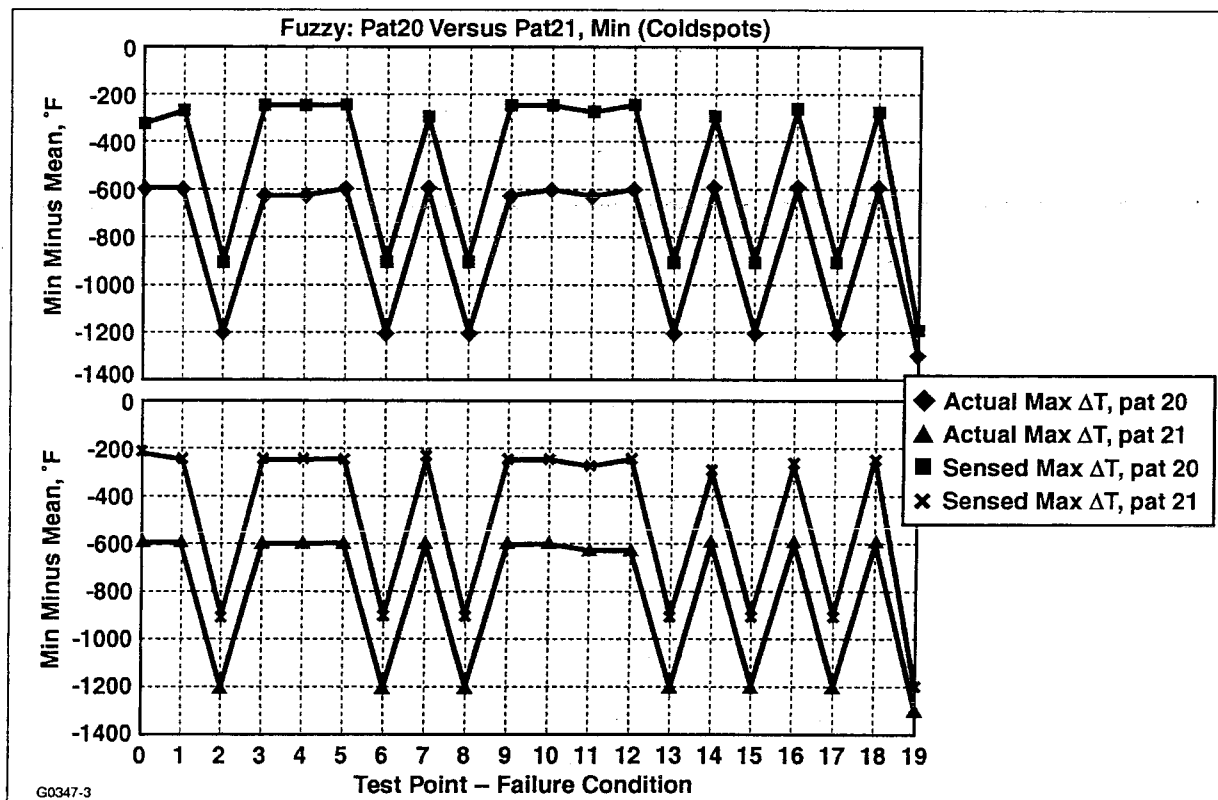
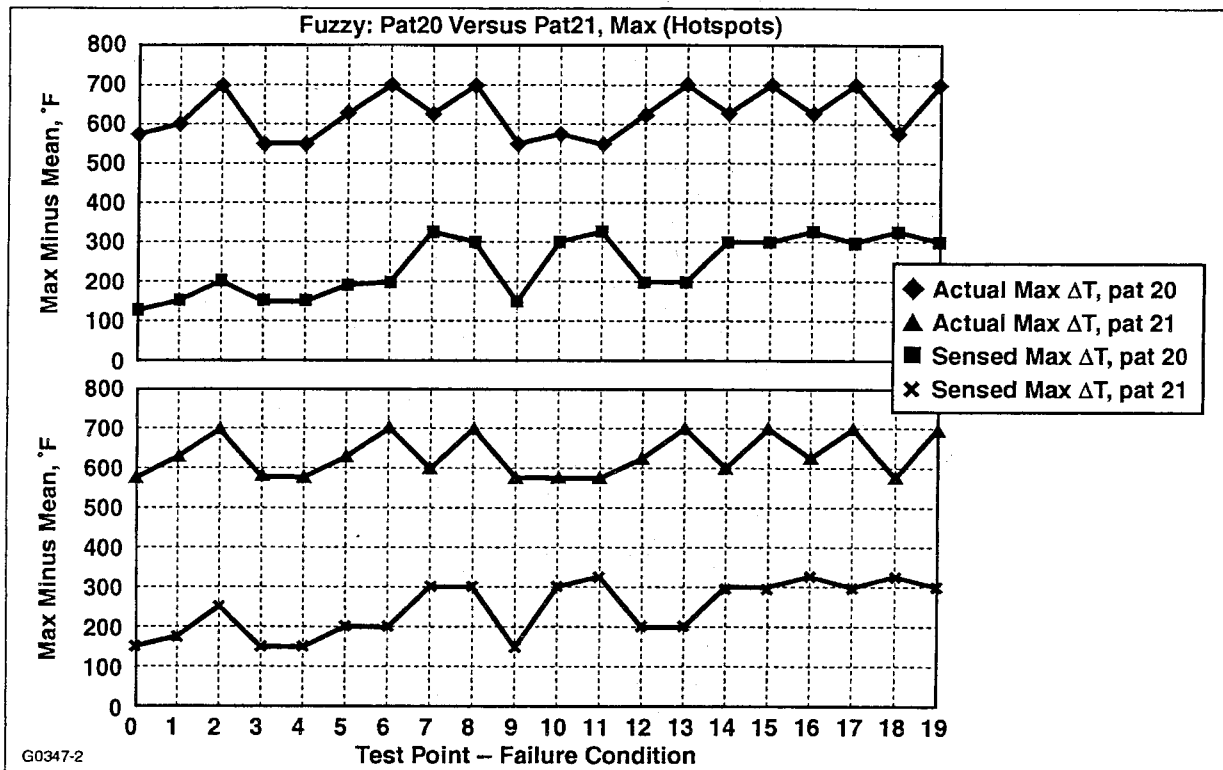


Figure 16. Test run comparisons for five-level (pat 21 – 25 rules), versus hybrid seven-level (pat 20 – 19 rules) fuzzy control.

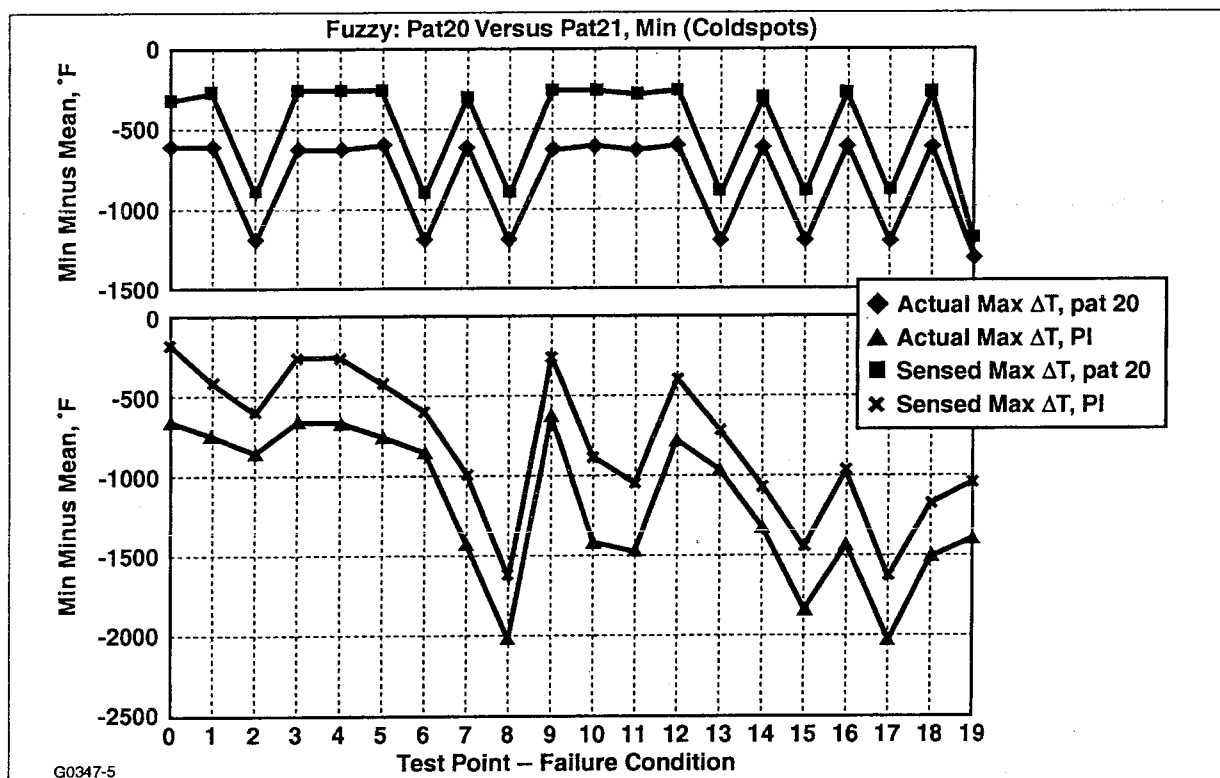
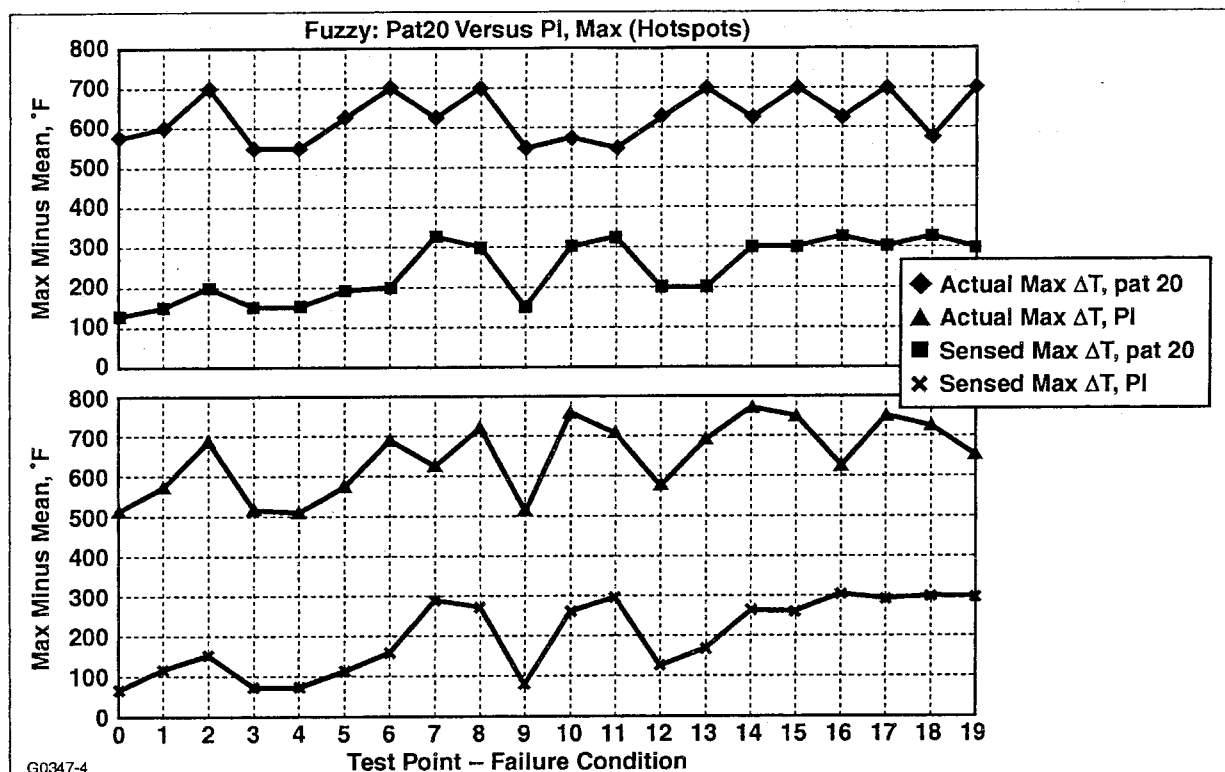


Figure 17. Test run comparisons for hybrid even-level (pat 21 – 19 rules) fuzzy control versus PI control.

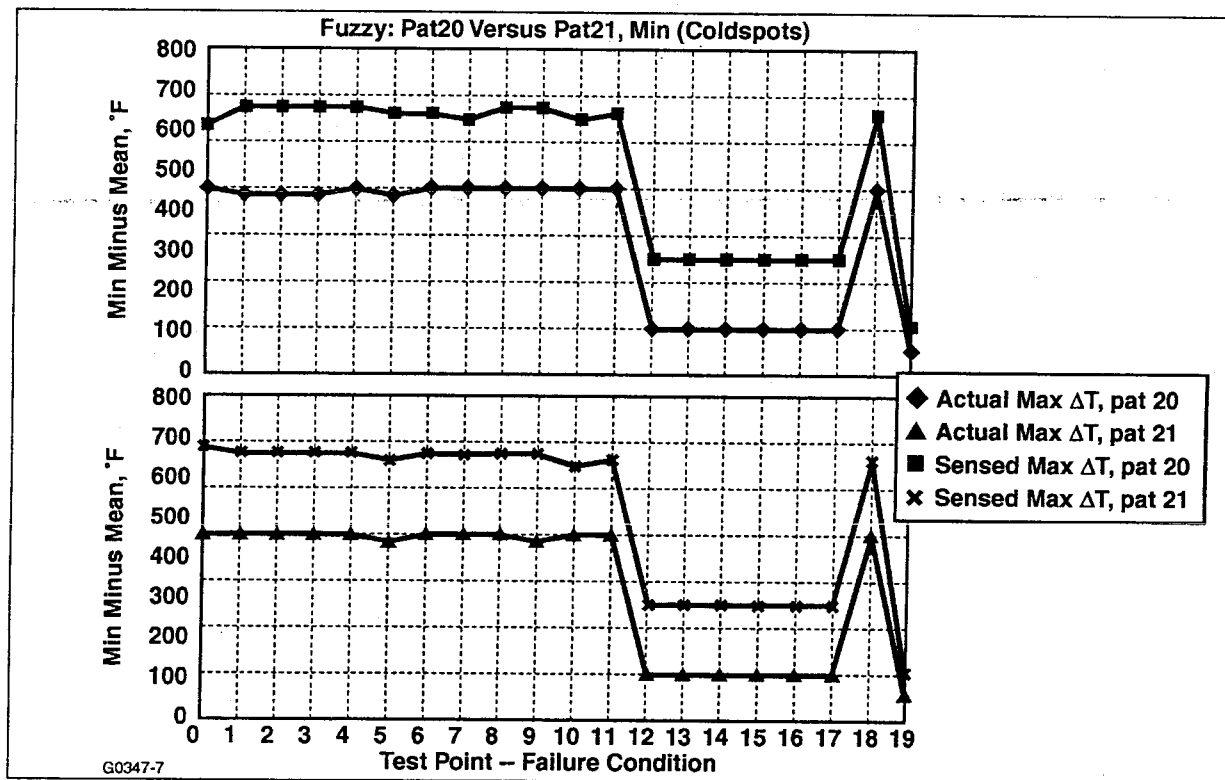
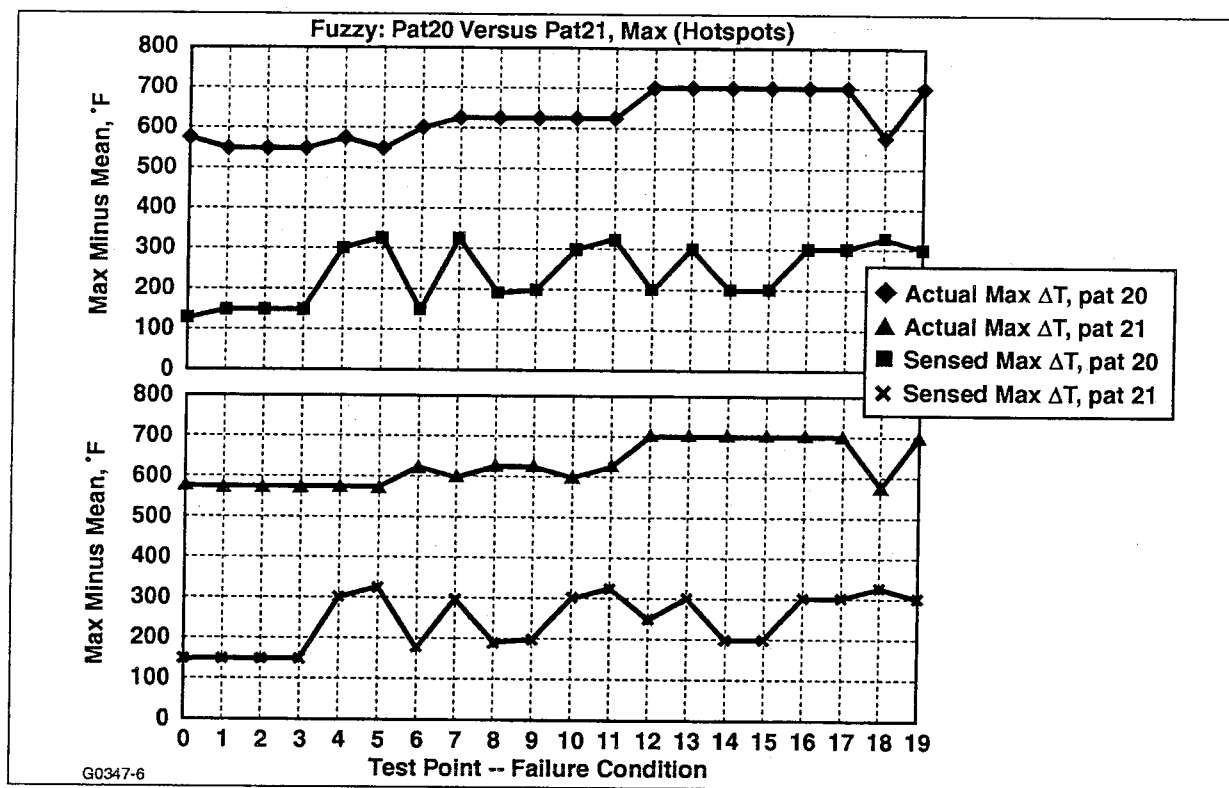


Figure 18. Test run comparisons for hybrid seven-level (pat 21 – 19 rules) fuzzy control versus PI control. Same test runs as Figure 17, except failure modes are regrouped.

No. Failure Mode Definitions

| | | |
|----|---------------------|---------------------|
| 1 | Baseline | |
| 2 | TC 10 low | |
| 3 | TC 5 low | |
| 4 | TC 10 & 5 low | |
| 5 | TC 10 & 5 high | |
| 6 | TC 10 low TC 5 high | |
| 7 | FN 4 open | |
| 8 | FN 4 open | TC 10 high |
| 9 | FN 4 open | TC 10 low |
| 10 | FN 4 open | TC 10 & 5 low |
| 11 | FN 4 open | TC 10 & 5 high |
| 12 | FN 4 closed | |
| 13 | FN 4 closed | TC 10 high |
| 14 | FN 4 closed | TC 10 low |
| 15 | FN 4 closed | TC 10 & 5 low |
| 16 | FN 4 closed | TC 10 & 5 high |
| 17 | FN 4 closed | TC 10 high TC 5 low |
| 18 | FN 12 open | TC 3 high TC 17 low |
| 19 | FN 12 closed | TC 3 high TC 17 low |

Results from the simulations show that the actual temperature difference was +600 and -600 degrees except for cases where the modulator was fixed closed. In those cases the actual temperature difference increased to +700 and -1200 degrees. The sensed temperature difference for hot spots remained within the range of +125 to 300 for all failure modes. Cold spots were -225 degrees for all failure modes except those with a modulator fixed closed in which case the value was -925 degrees.

The main points from this discussion are in the following text. Fuzzy systems are defined by fuzzy sets. The elements within those sets are defined by membership functions and rules. There is not always a unique system that will provide a single crisp number that represents each of the previous inputs, membership functions, and rules from the defuzzification step. For the case of the Active Pattern Factor Controller a seven-level system defined with 19 rules will give essentially the same crisp number as a five level system defined with 25 rules. A careful selection of membership function levels, or terms, can allow the fuzzy system to execute faster without impacting the results. These savings are during the development phase. For implementation into controller software a lookup table can be generated instead of executing each of the rules for each step through the control logic.

Associated Figures.

The following figures are included as an appendix to this report:

Figures A1 - A3 Membership functions for two inputs and one output.

Figures A4 - A23 Complete runs for pat20.fis, baseline and failure modes [4].

Figures A24 – A43 Complete runs for pat21.fis, baseline and failure modes [4].

Conclusion:

In this application the fuzzy logic controller can be designed to exhibit response similar to a conventional PI controller. Phase One showed that a fuzzy logic controller can be set to match the steady state performance of a traditional PI controller by membership level and range selection [2]. Output from the fuzzy logic FIS was the analogue of the proportional constant, K_p . Pass the output through an integrator and you have a PI controller. The output fuzzy set can be 'fine tuned' to match any PI controller by adjusting the membership levels. Once the combustor model was modified to include the nonlinear relationship of fuel dispersion to thermocouples the fuzzy logic controller still performed as well as a PI controller.

In phase two a more complex combustor system was controlled with fuzzy logic. The more complex system used more thermocouples than the symmetric case. Although the asymmetric model was controlling more area [3] the performance of the fuzzy logic controller was virtually unchanged. This displayed the ability of a fuzzy logic controller to adapt to configuration changes.

The effectiveness of the fuzzy logic controller on both hot and cold spots was quantified. It was robust to failure modes for both except for failure cases corresponding to a fuel nozzle fixed closed. In those cases the cold spots were double the normally controlled value of -600 degrees. Considering that the case of a fuel nozzle fixed closed would be a rare event it is safe to claim that the controller has the capability to accommodate failure modes.

When the Allied Signal Fuzzy Logic Controller was integrated with the SMI combustor logic the performance did not change. Thus the fuzzy logic controller was not only robust to combustor complexity, thermocouple - fuel nozzle arrangement, and failure modes but also to plant variations.

In order to implement this fuzzy logic controller, a lookup table which reflect the fuzzy logic FIS would need to be generated. The lookup table would take the error and derivative of the error, as described above, and output the corresponding areaout command. The same lookup table would be used for all fuel flow modulators. A scheme to code this concept into the rapid prototyping electronic control would need to handle all nineteen thermocouple inputs at once or with a sequencing routine. Ease of coding, and lines of code required, and CPU execution time, etc. should be factors in selecting the proper fuzzy control algorithm.

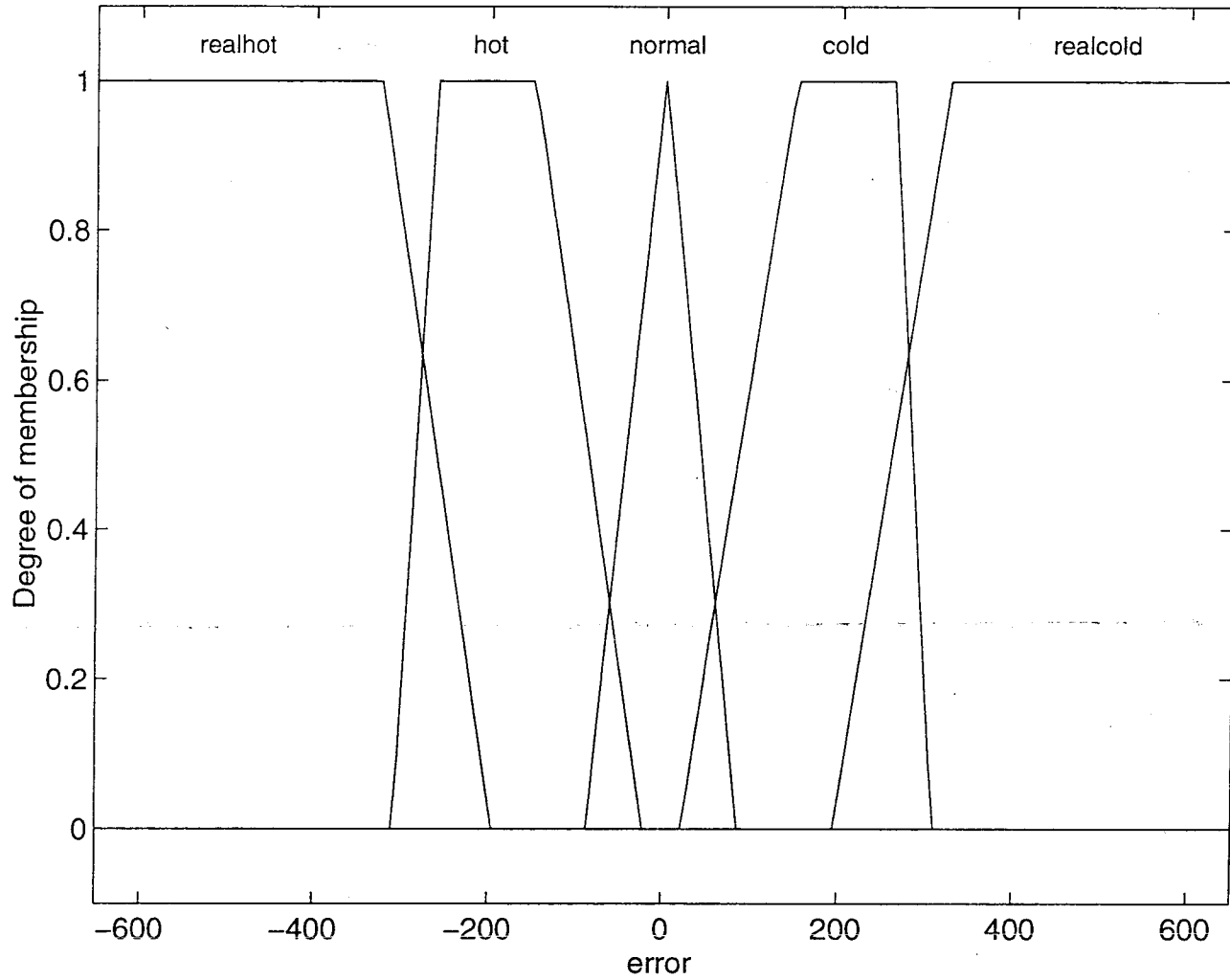
References:

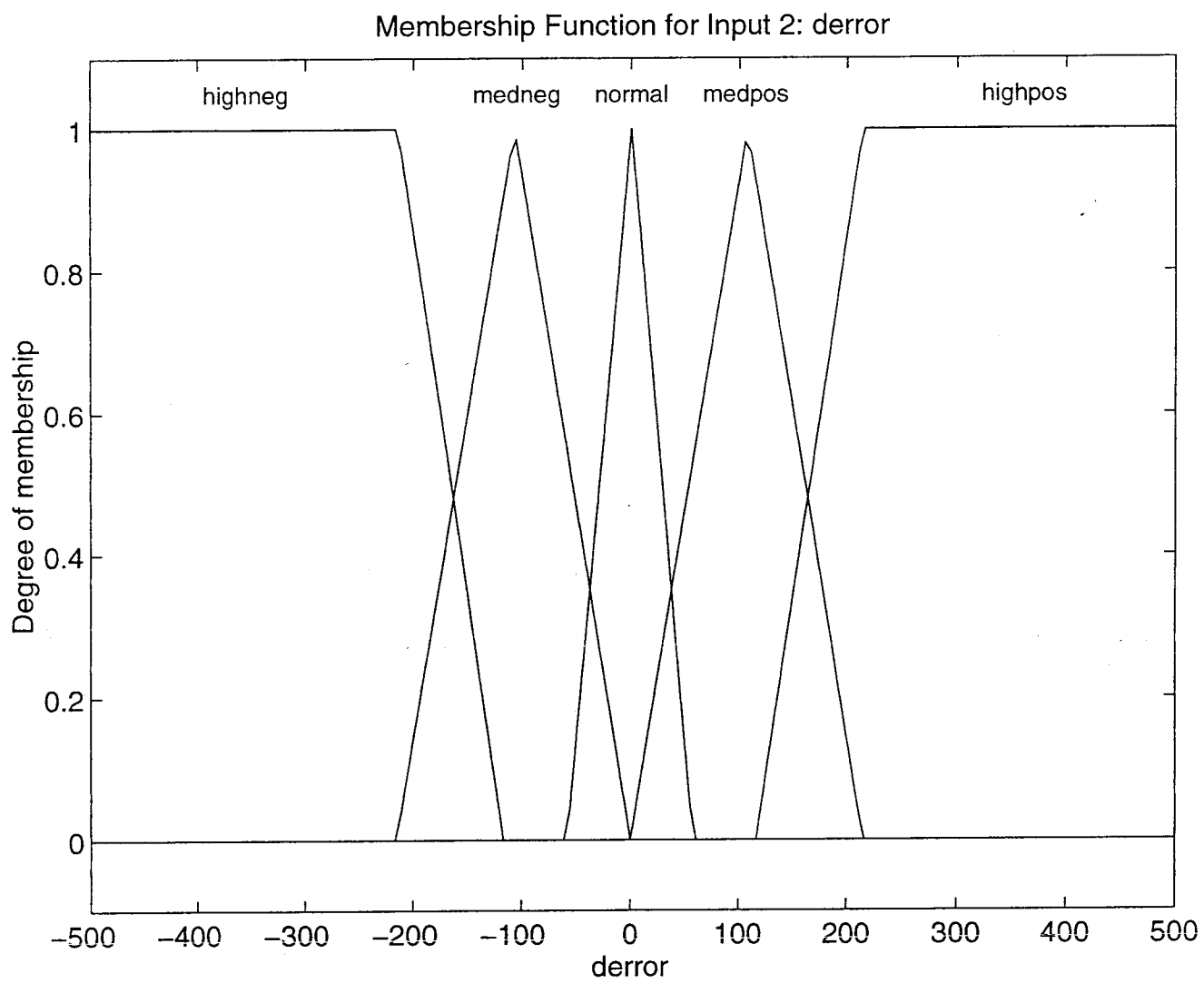
- [1] Gulley, Jang. 1/95. *Fuzzy Logic ToolBox User's Guide*, The Mathworks, Inc., pp. 2 - 50.
- [2] Bonissone, Chiang. 1995. Fuzzy Logic Hierarchical Controller for a Recuperative Turbohaft Engine. *Industrial Applications of Fuzzy Logic and Intelligent Systems*, IEEE Press, pp. 131-156.
- [3] Stokes, Krech. 1996. *Reliable and Affordable Control Systems, Active Combustor Pattern Factor Control*, NASA AST Technical Progress Report No. 4, Appendix I. AE Report 21-9197(4).
- [4] Stokes, Krech. 4/97. *Active Combustor Emissions/Pattern Factor Control Bi-annual Status Review*, pp 108-126. AE Report No. 21-9617.

APPENDIX I
ASSOCIATED FIGURES
(43 Pages)

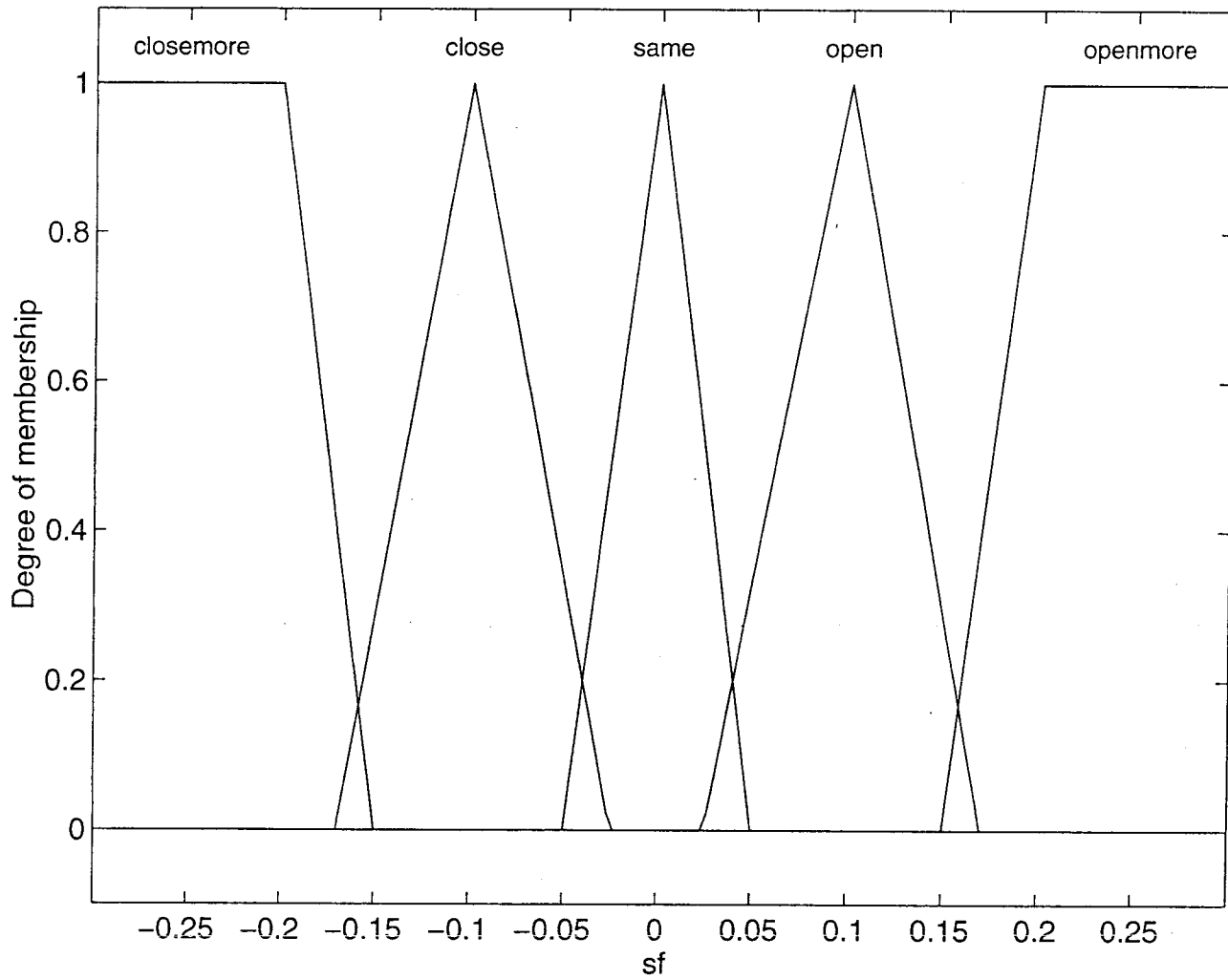
| <u>Fig. No.</u> | <u>Title</u> | <u>Page</u> |
|------------------------|---|--------------------|
| A1 - A3 | Membership functions for two inputs and one output | 34-36 |
| A4 - A23 | Complete runs for pat20.fis, baseline and failure modes [4] | 37-56 |
| A24 - A43 | Complete runs for pat21.fis, baseline and failure modes [4] | 57-76 |

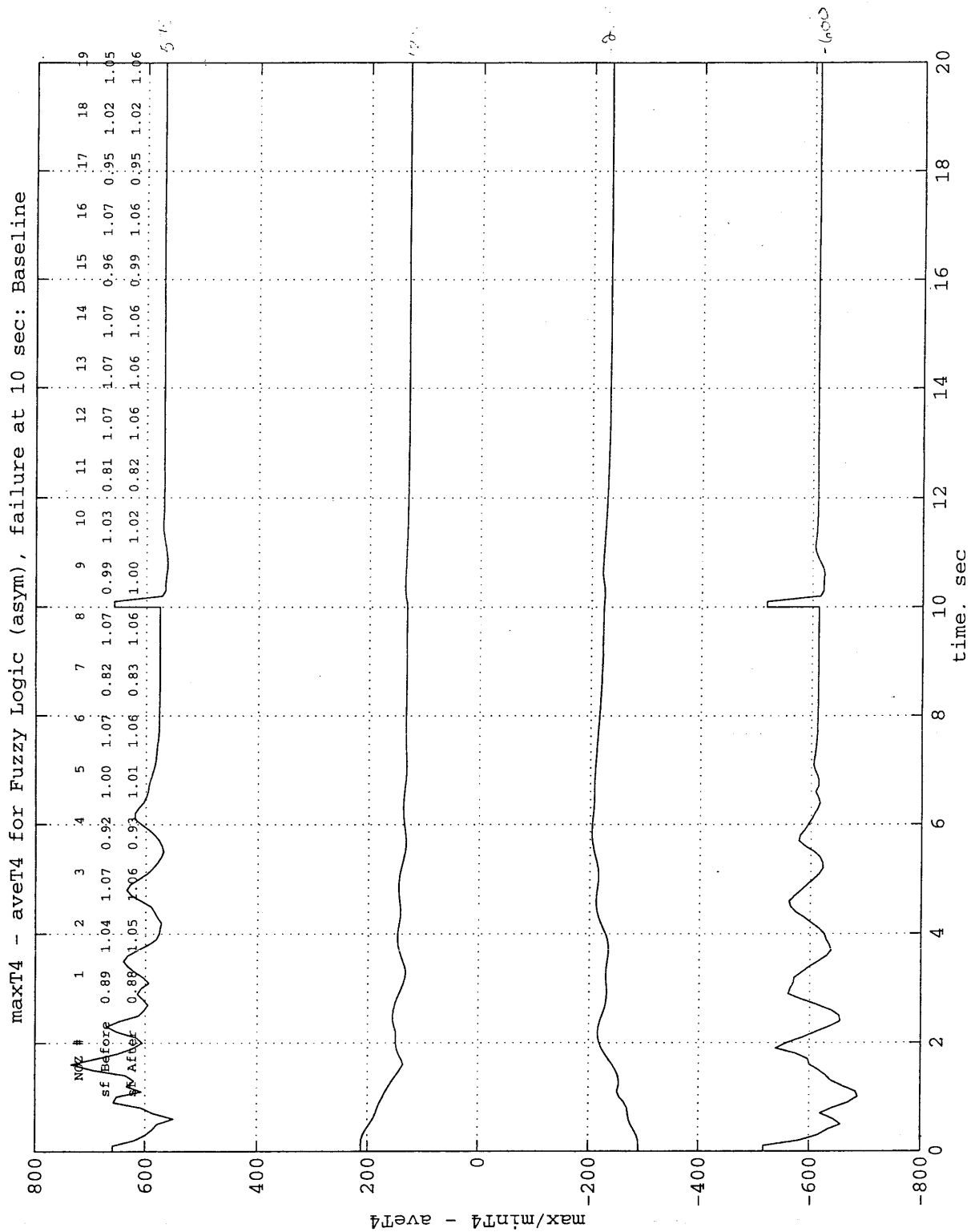
Membership Function for Input 1: error



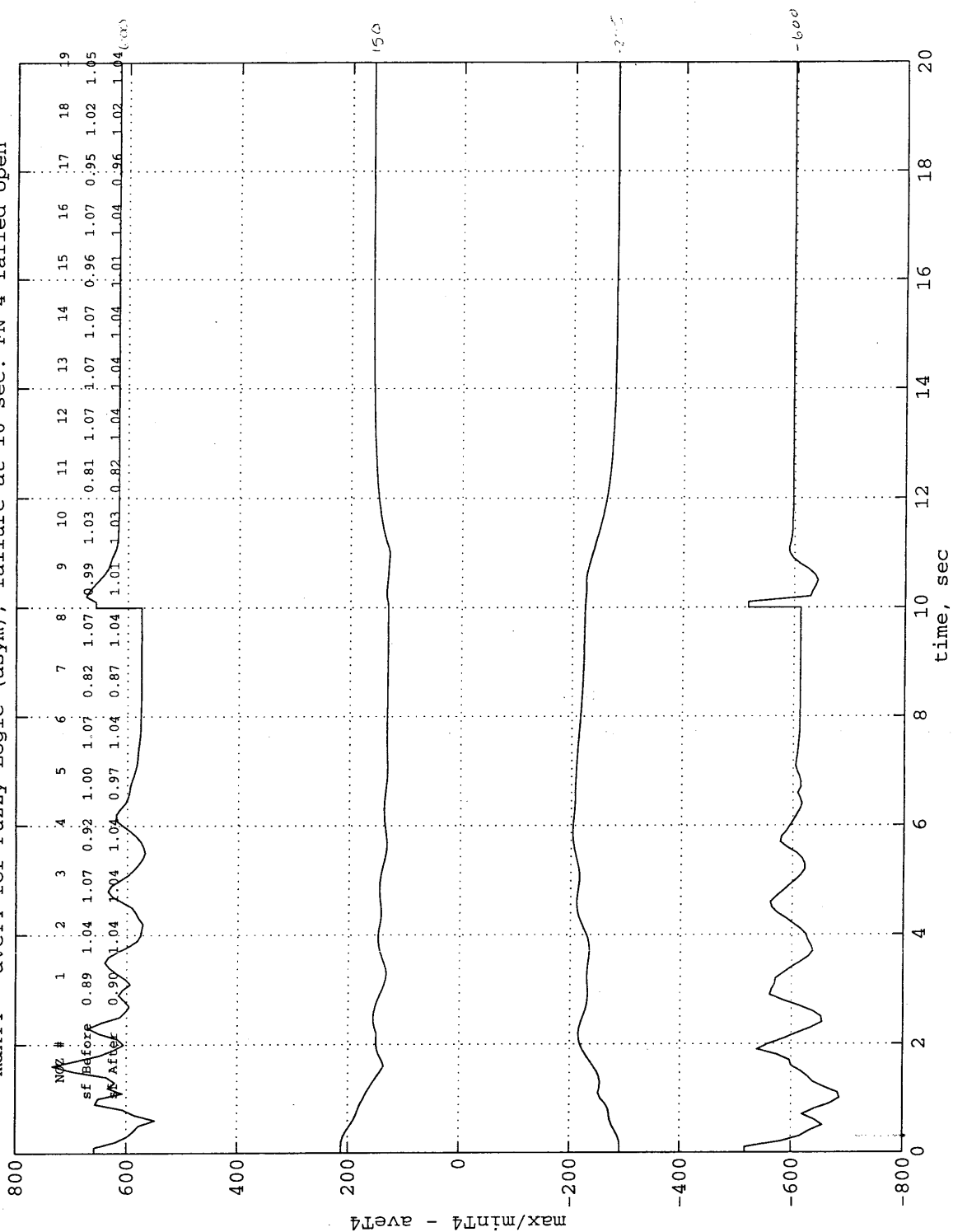


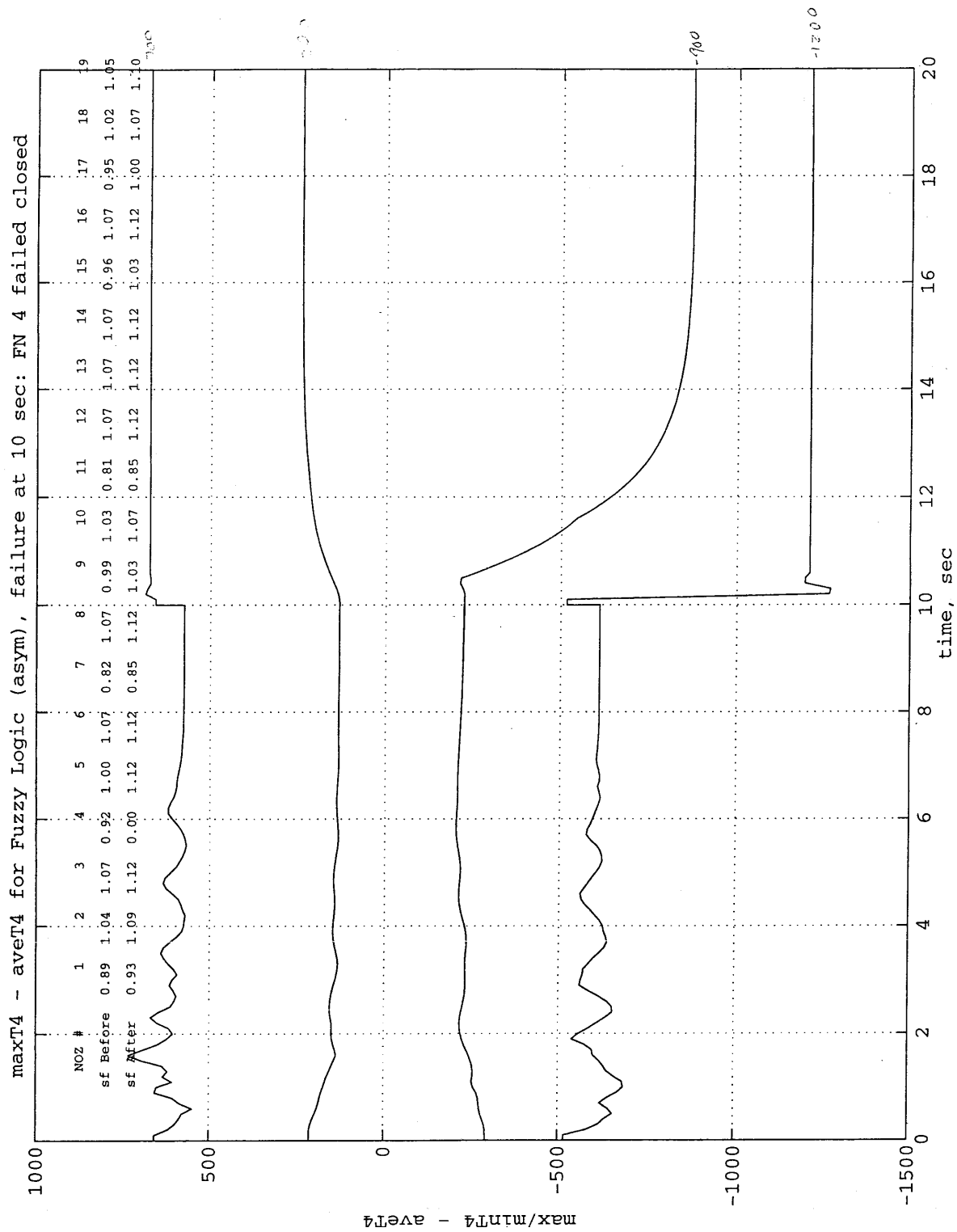
Membership Function for Output: sf

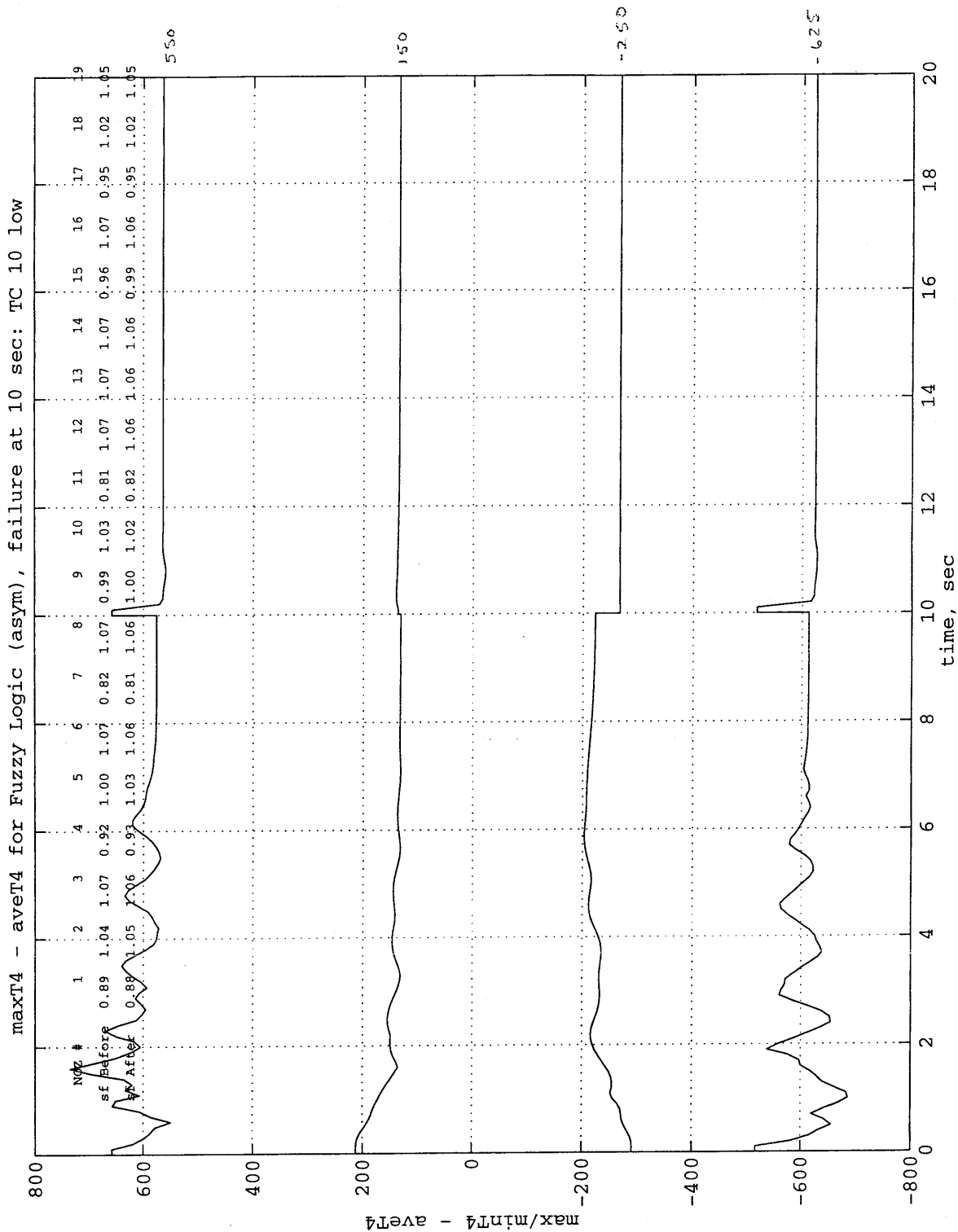


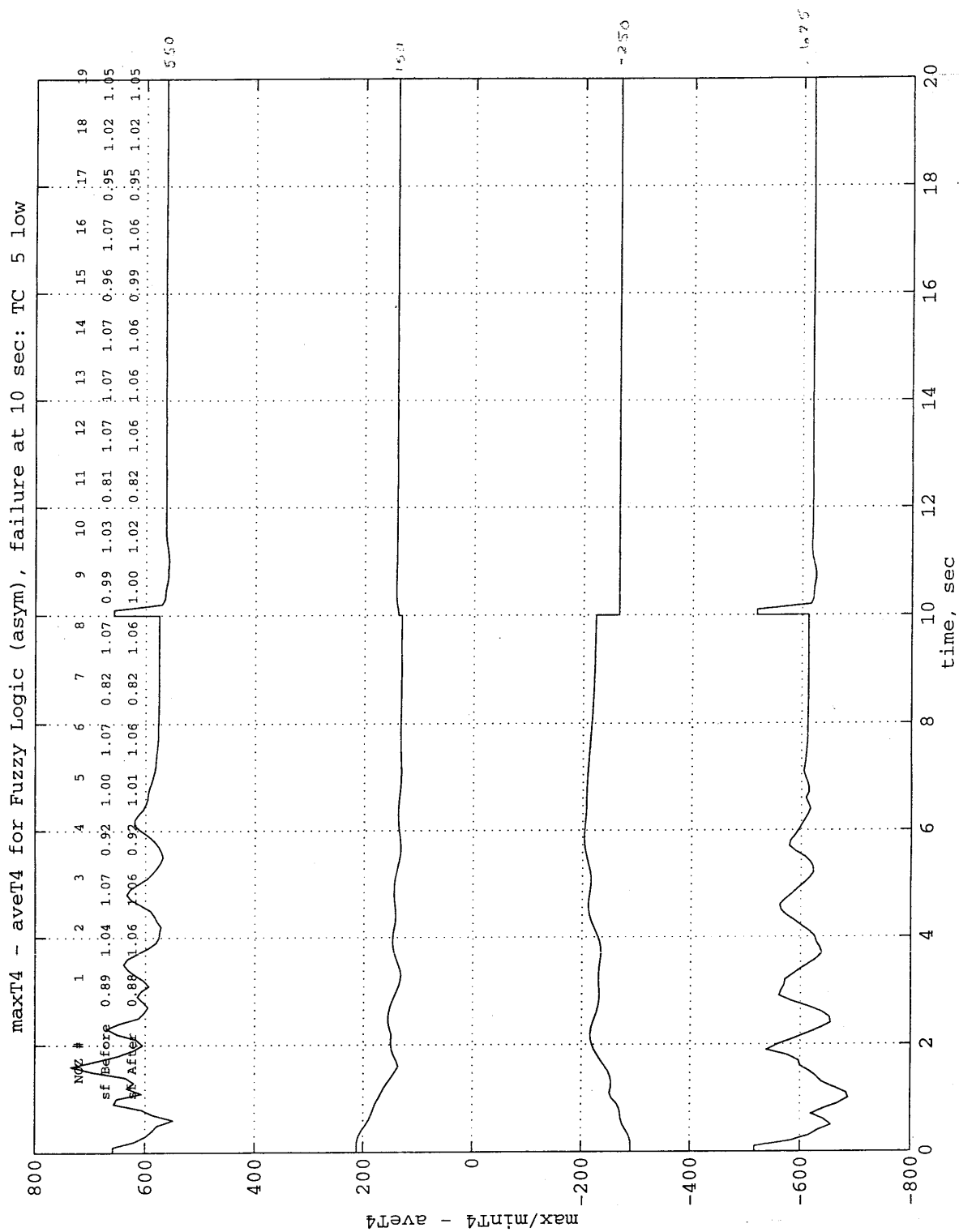


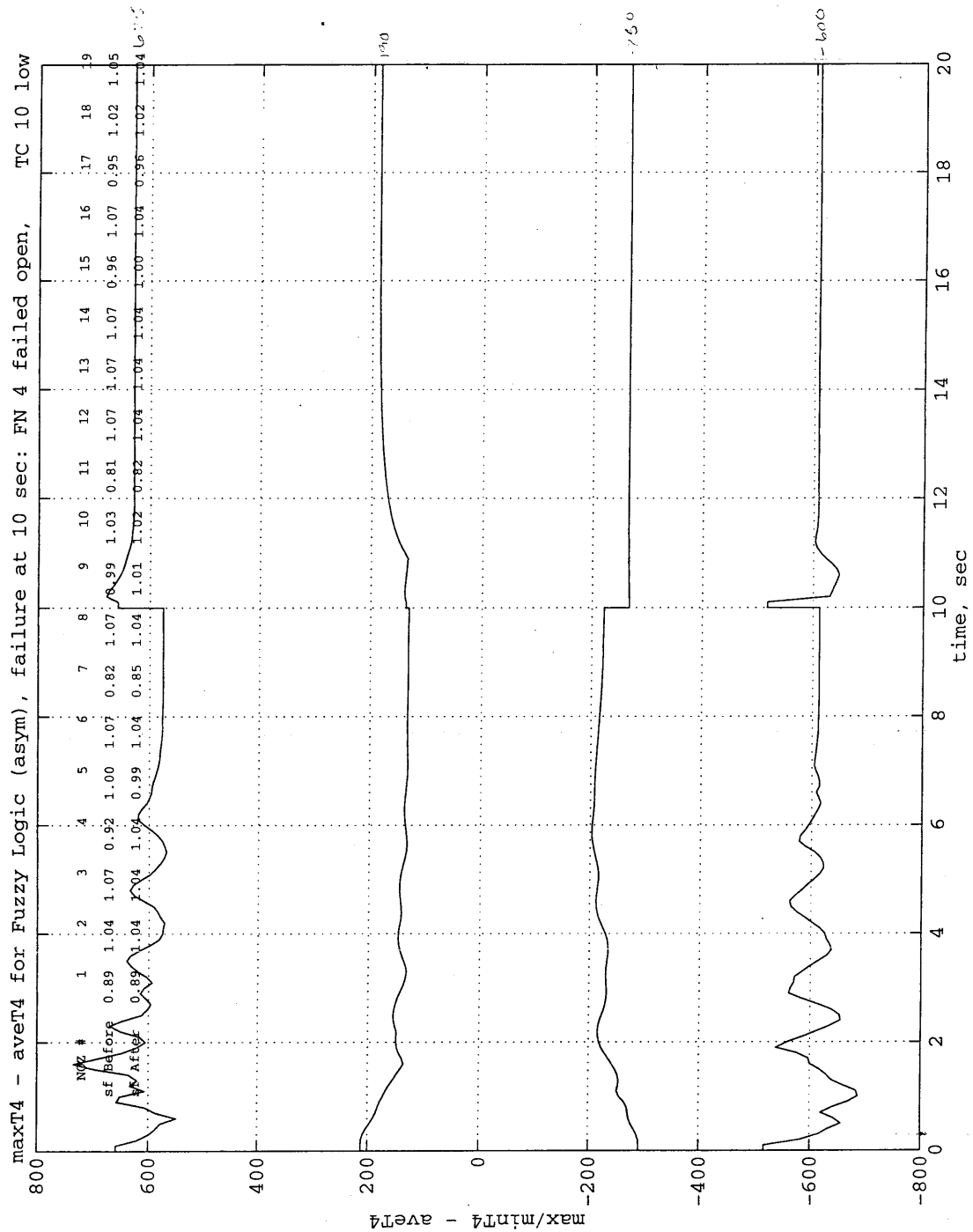
maxT4 - aveT4 for Fuzzy Logic (asym), failure at 10 sec: FN 4 failed open



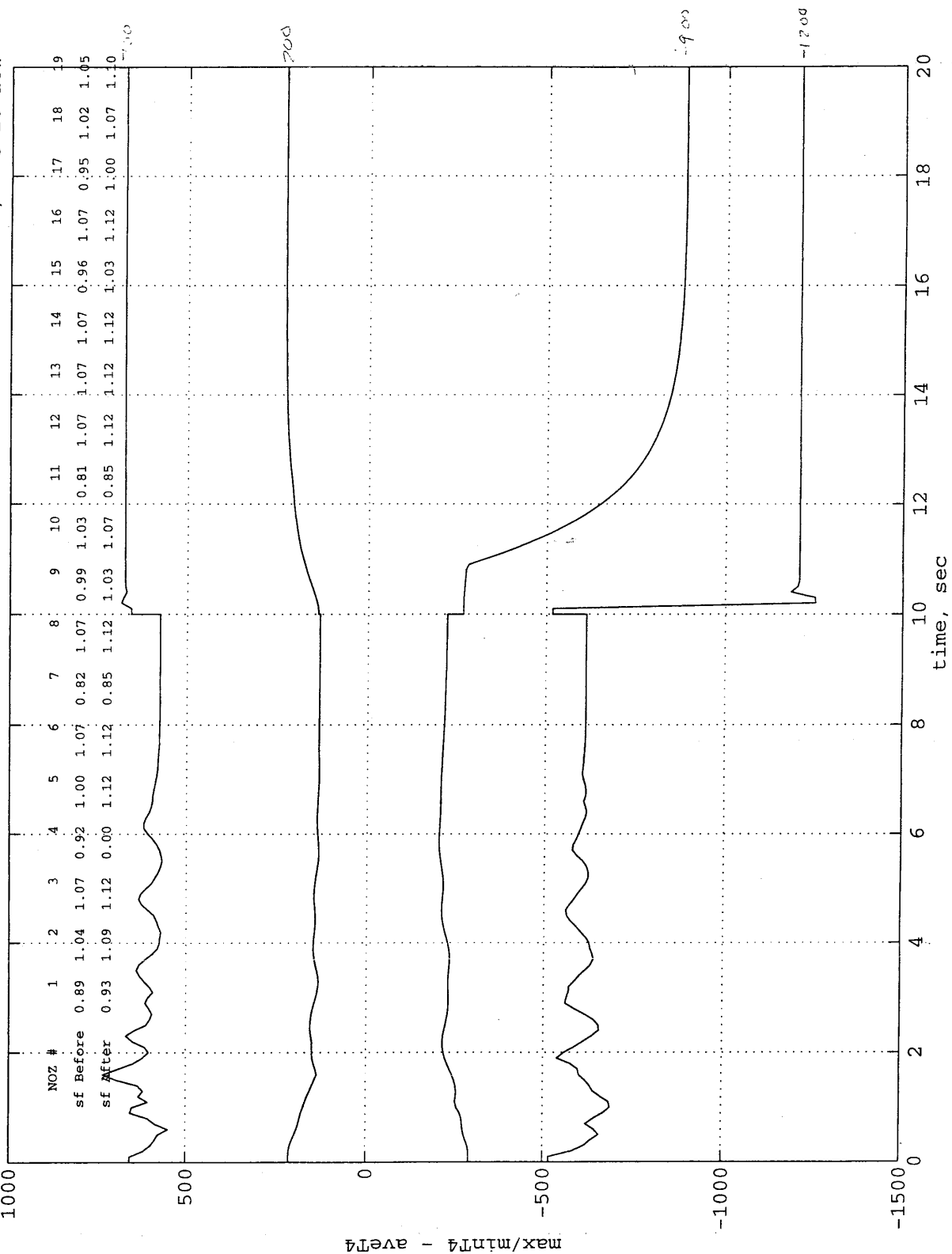


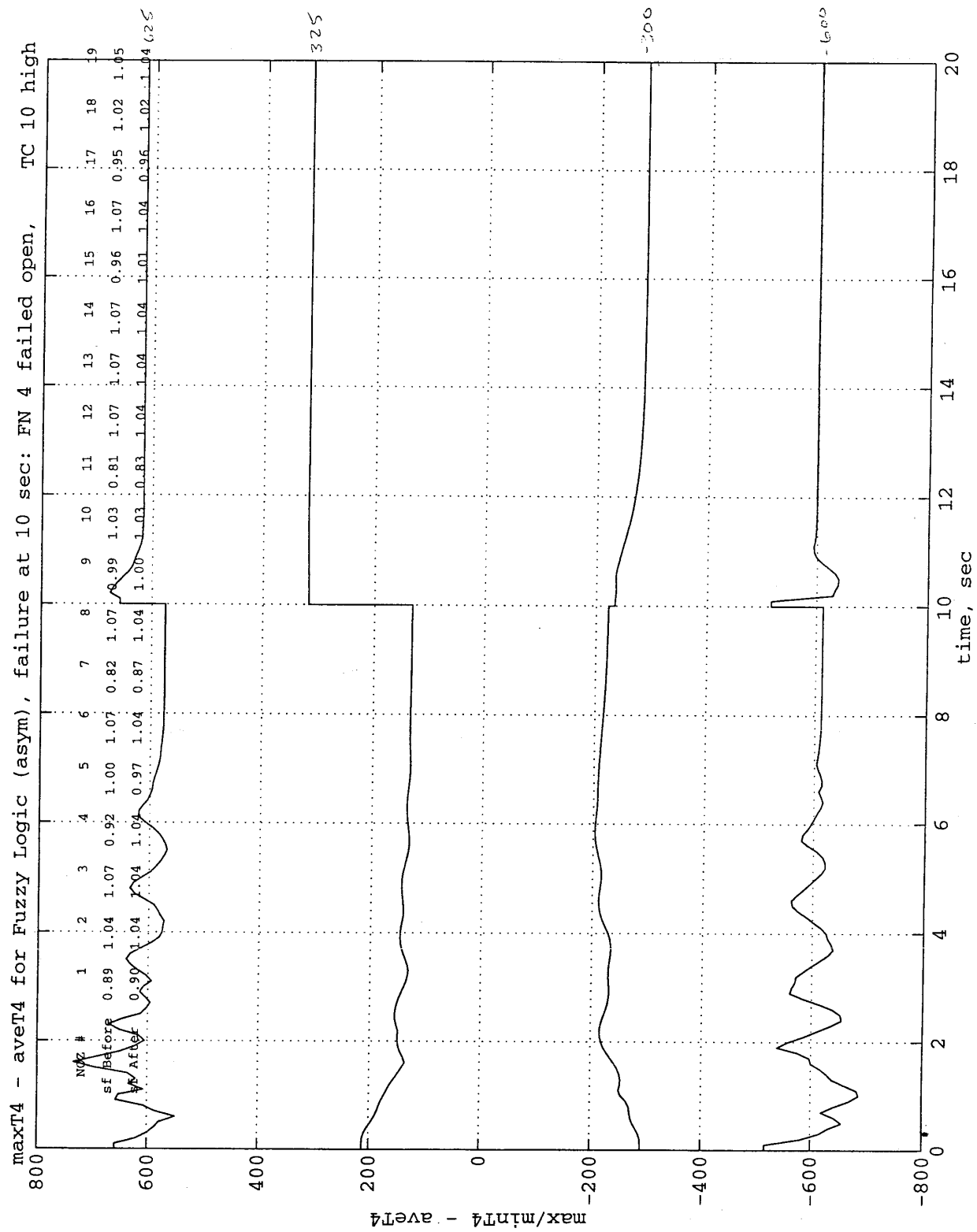




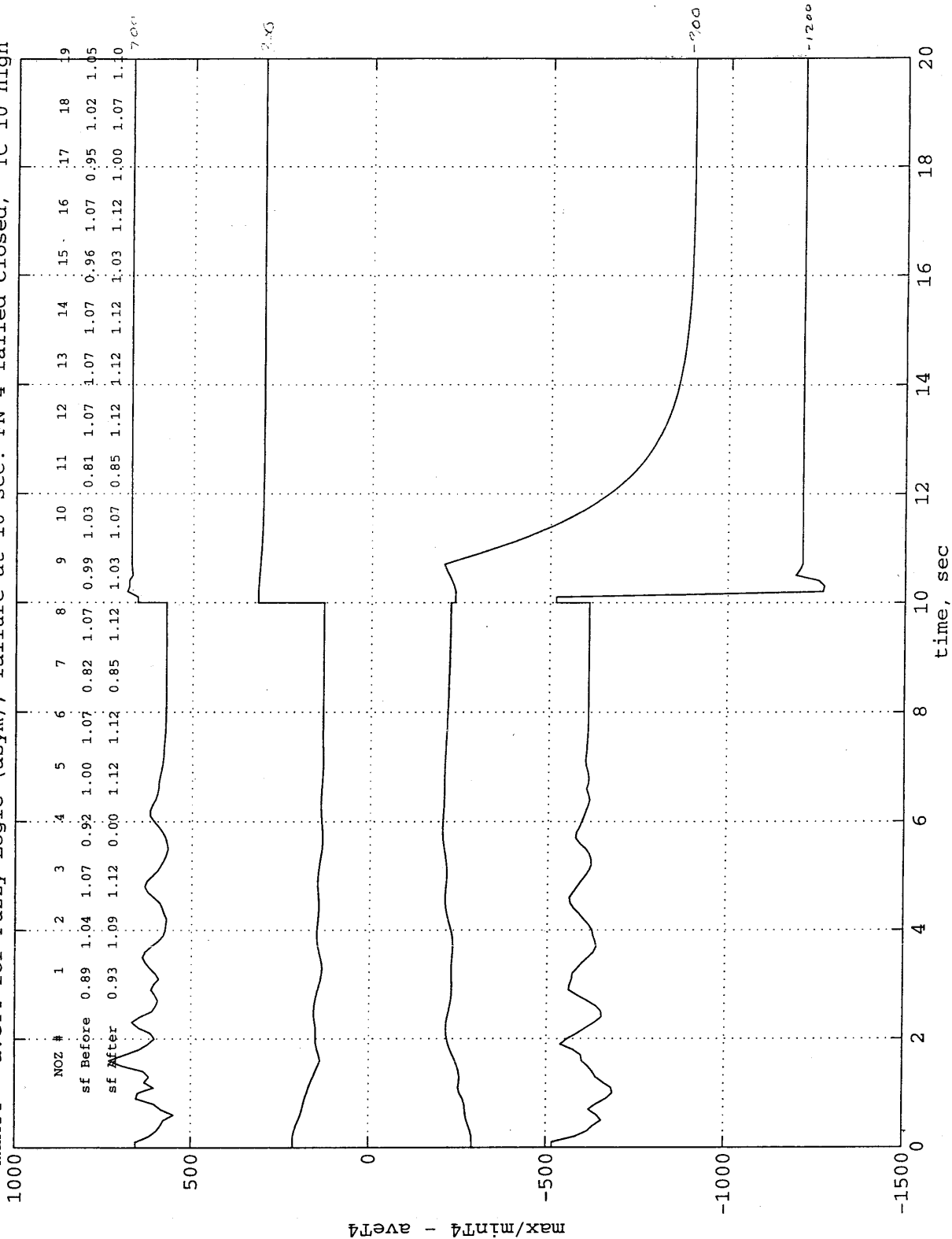


maxT4 - aveT4 for Fuzzy Logic (asym), failure at 10 sec: FN 4 failed closed, TC 10 low

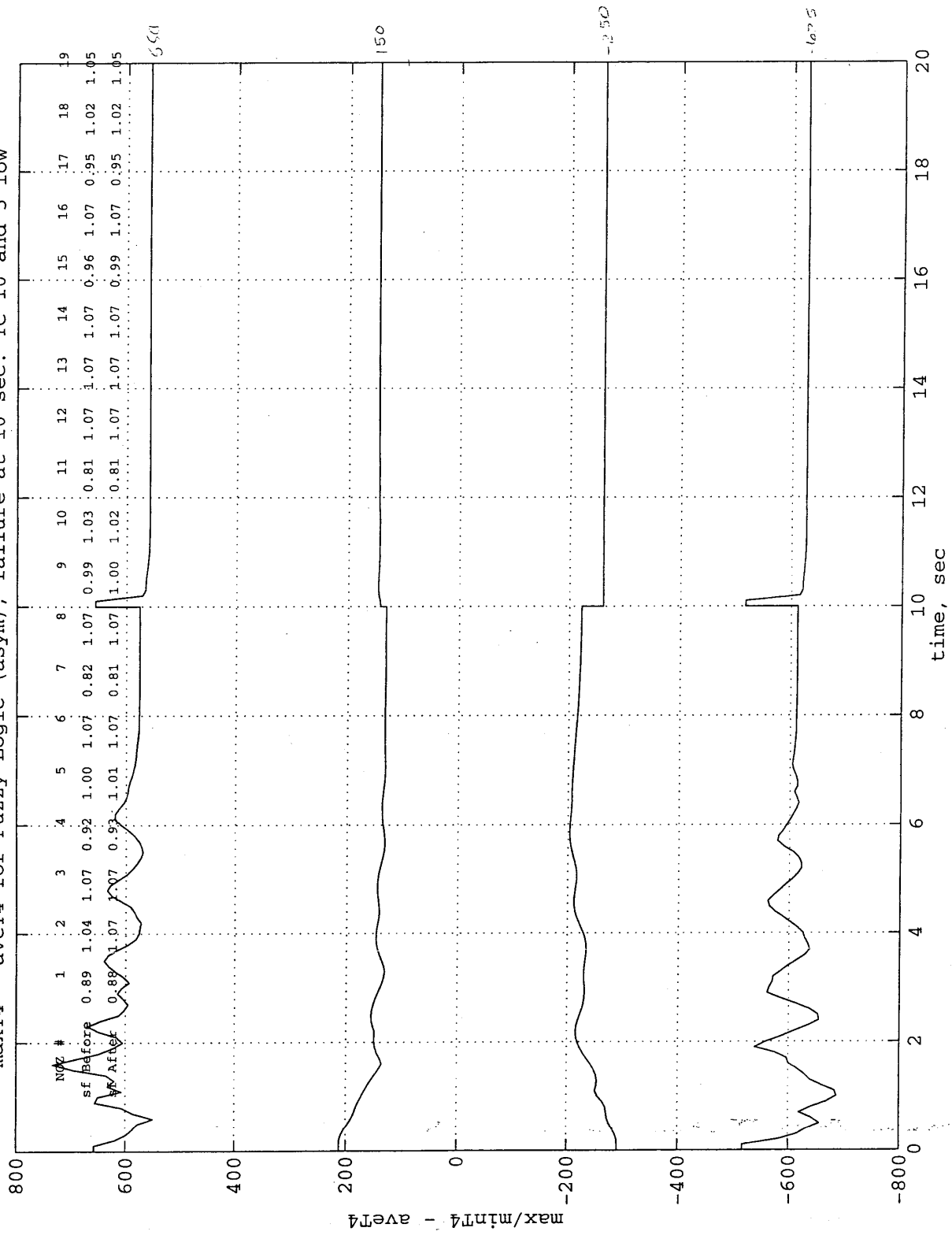


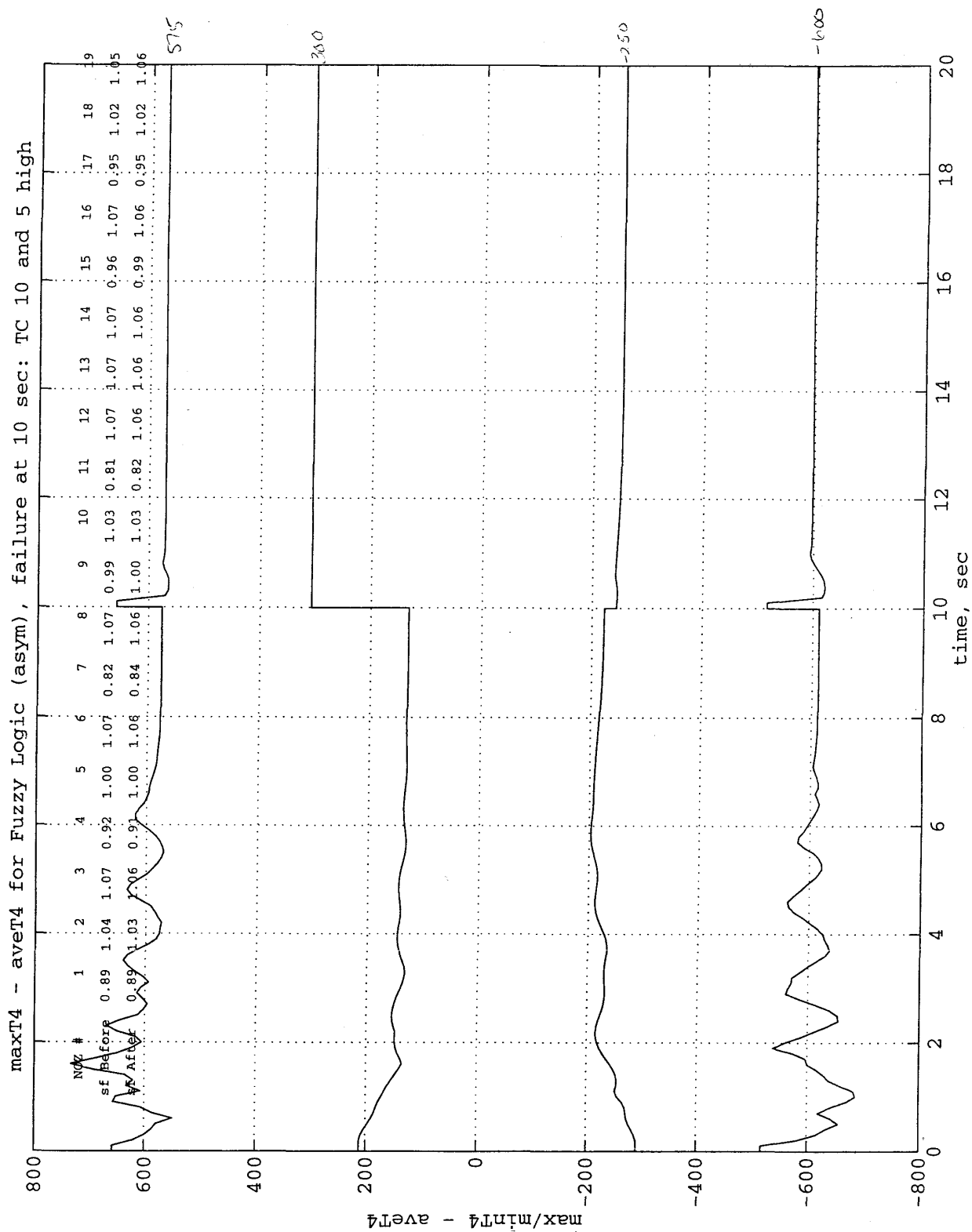


maxT4 - aveT4 for Fuzzy Logic (asym), failure at 10 sec: FN 4 failed closed, TC 10 high

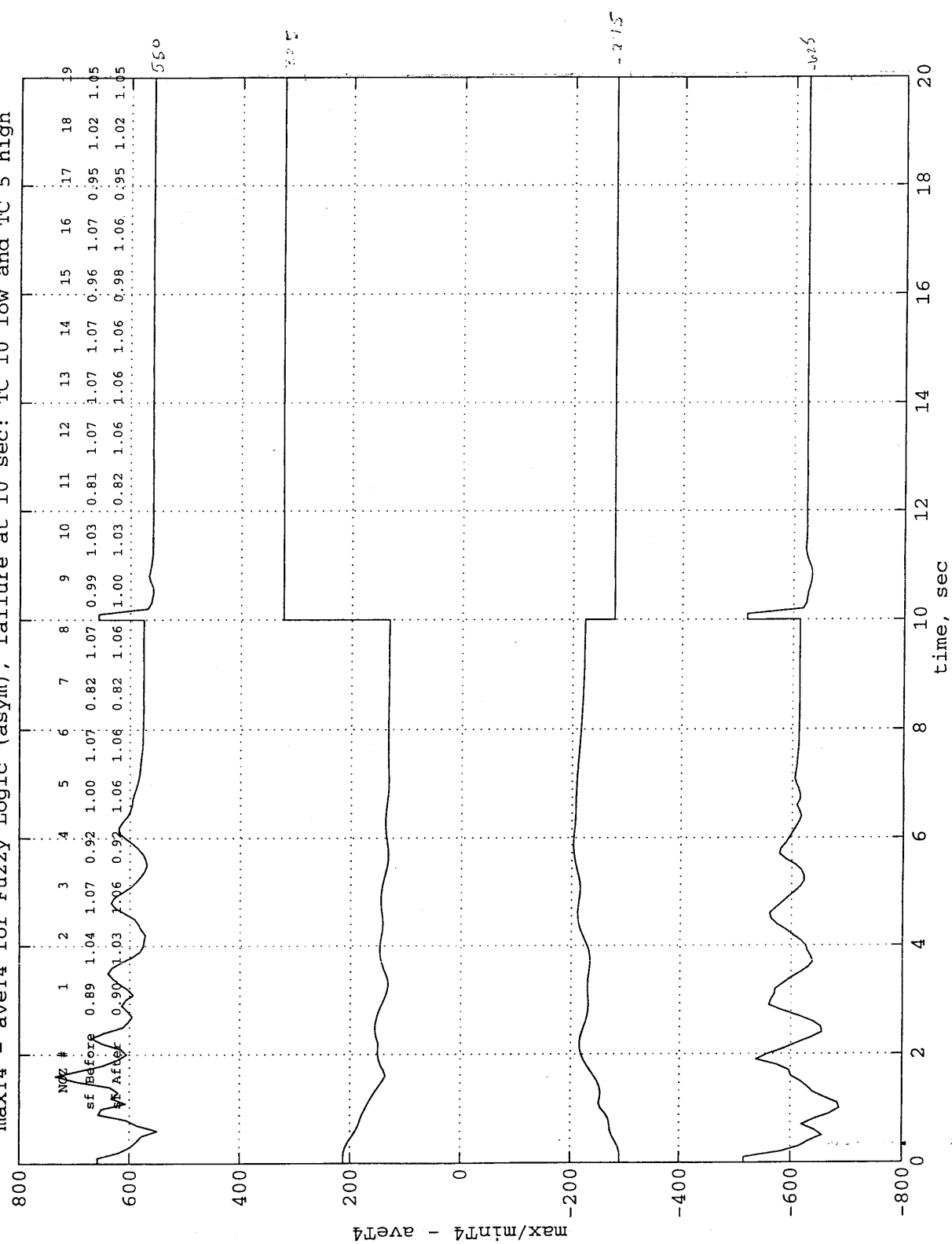


maxT4 - aveT4 for Fuzzy Logic (asym), failure at 10 sec: TC 10 and 5 low

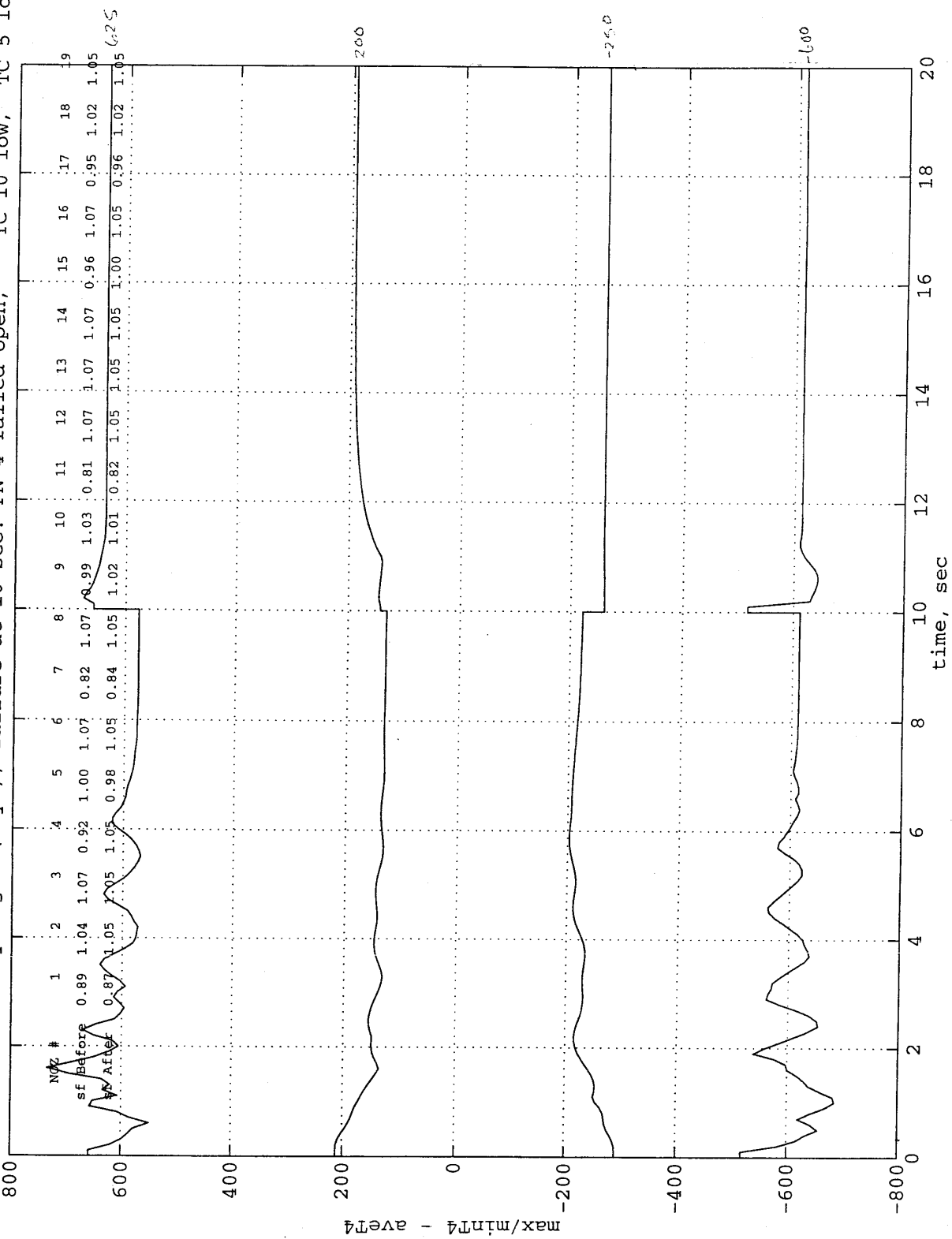




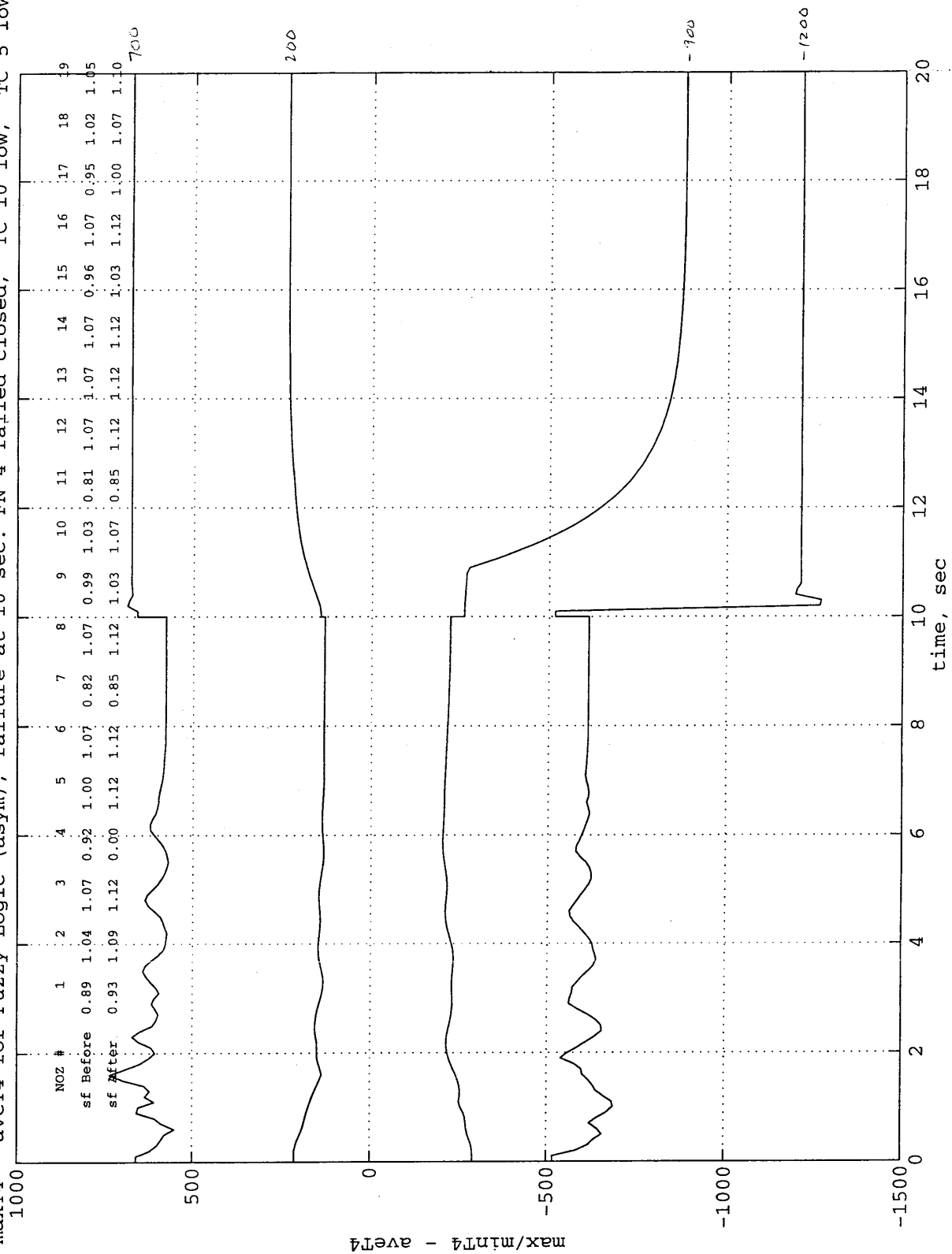
maxT4 - aveT4 for Fuzzy Logic (asym), failure at 10 sec: TC 10 low and TC 5 high



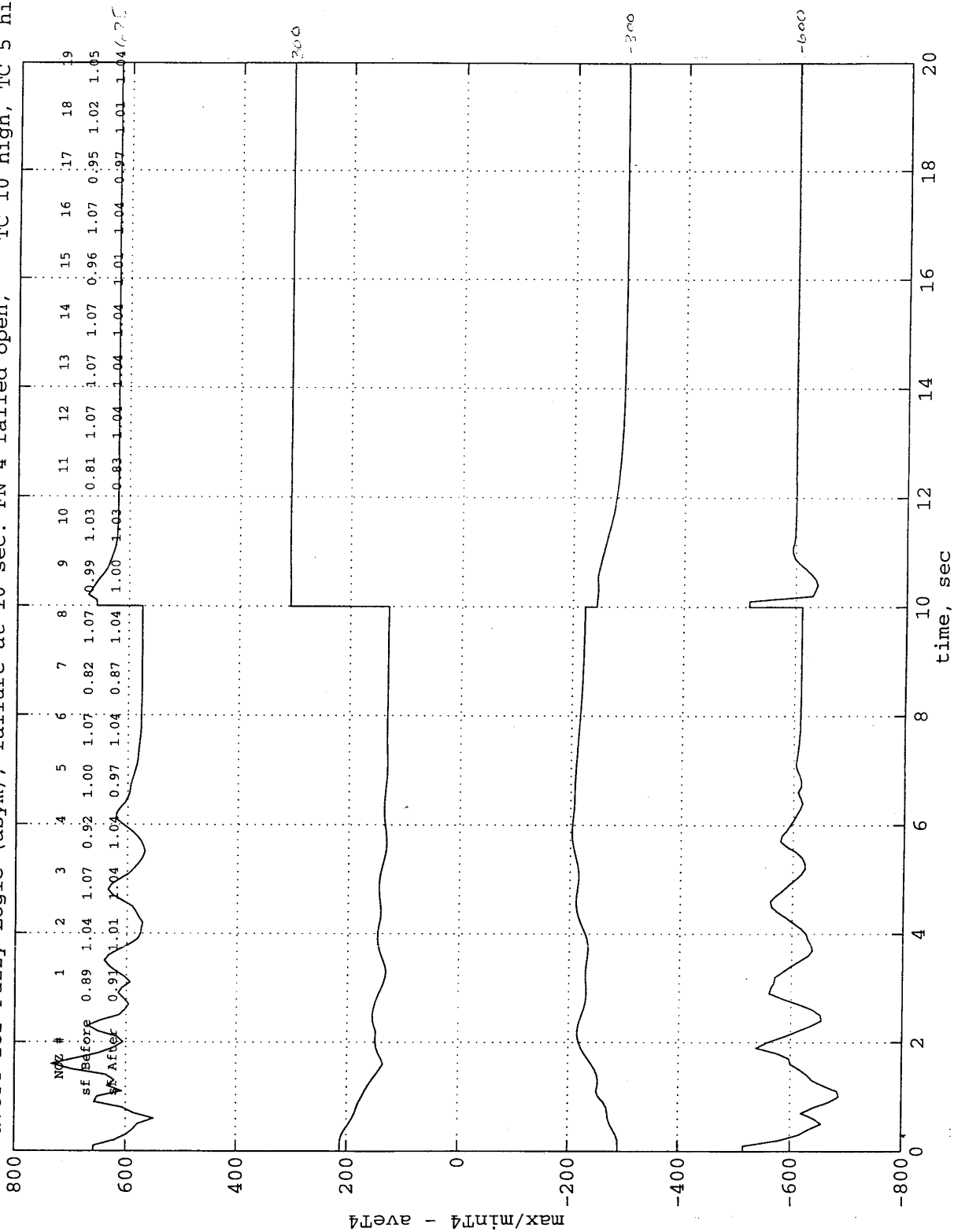
maxT4 - aveT4 for Fuzzy Logic (asym), failure at 10 sec: FN 4 failed open, TC 10 low, TC 5 low



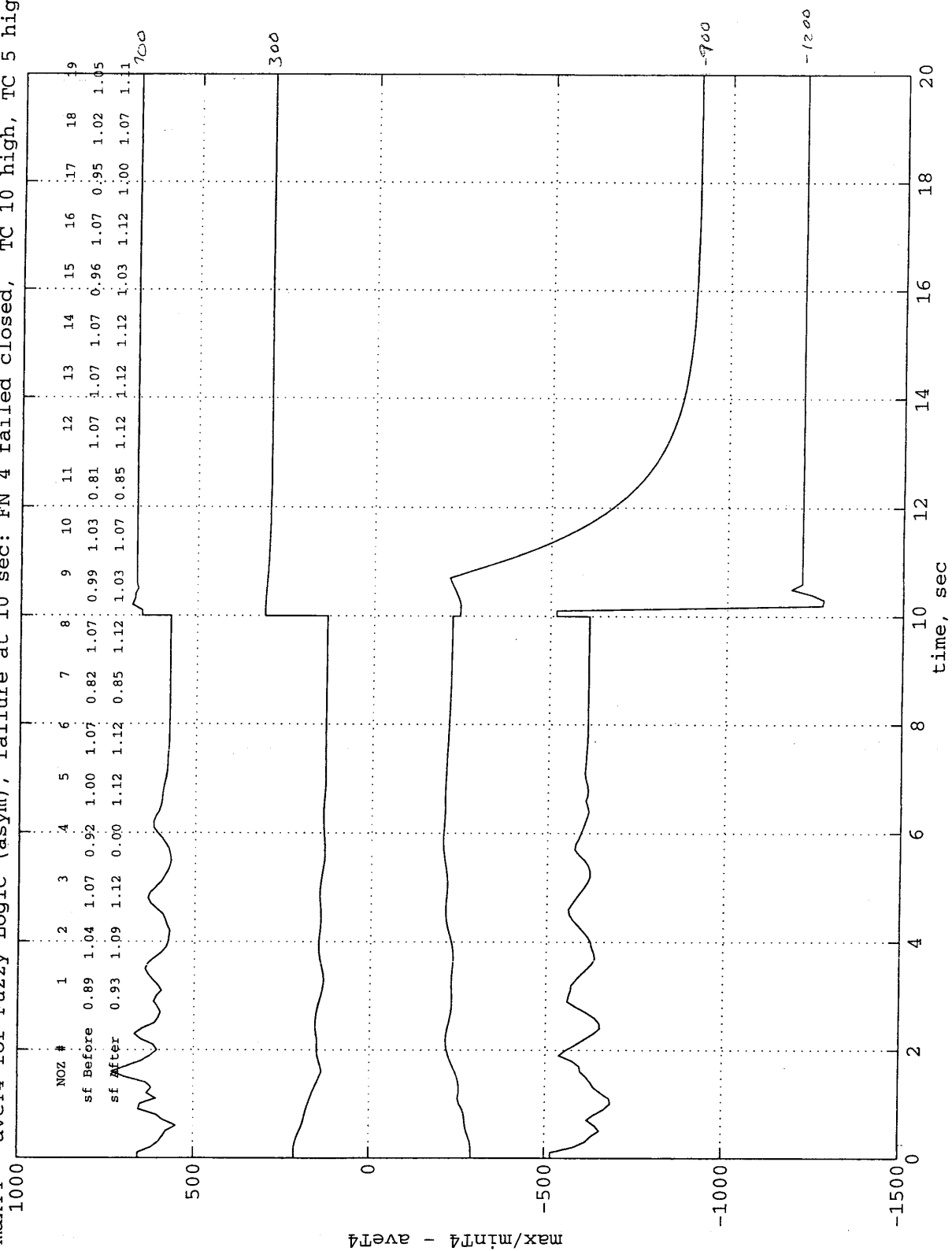
maxT4 - aveT4 for Fuzzy Logic (asym), failure at 10 sec: FN 4 failed closed, TC 10 low, TC 5 low



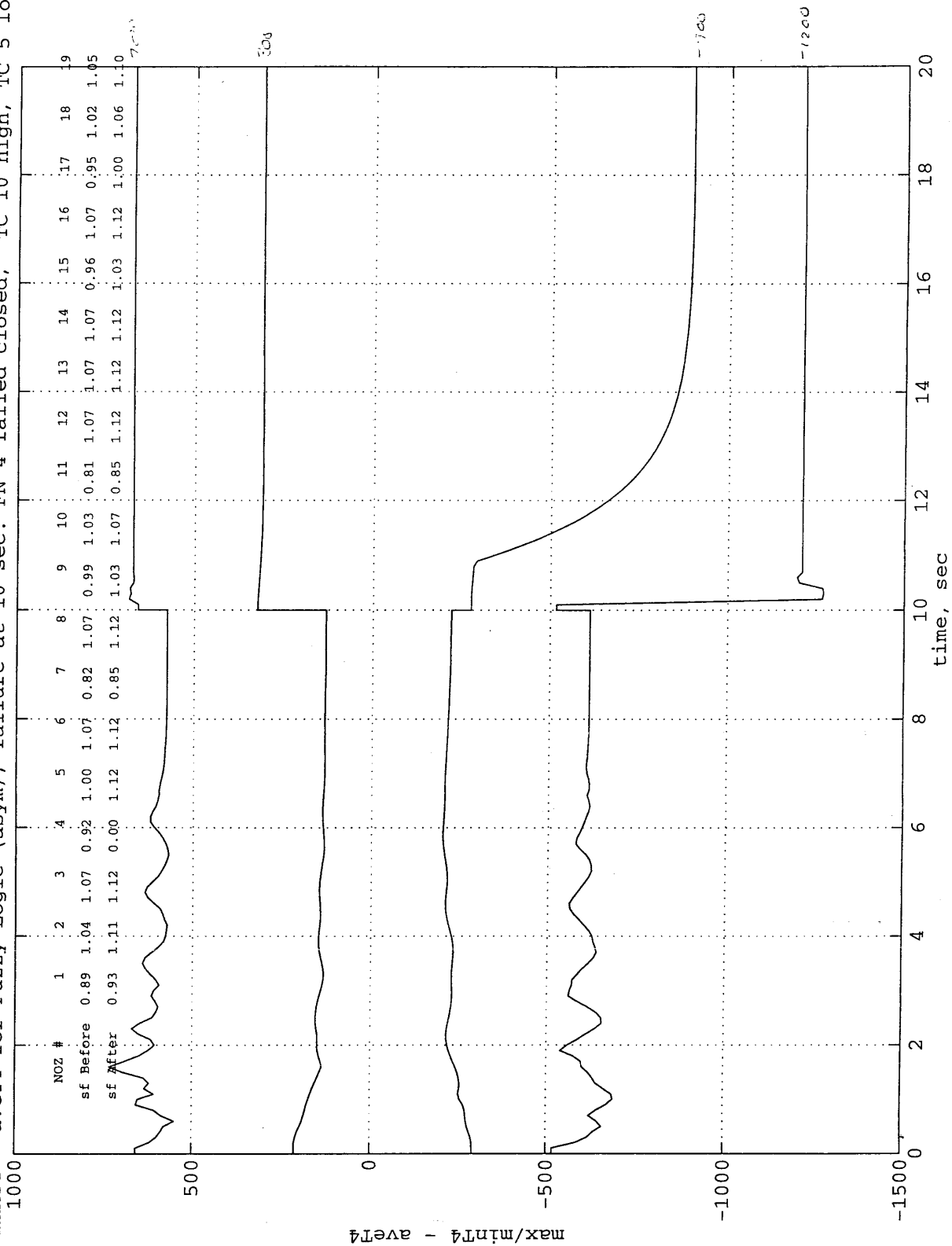
maxT4 - aveT4 for Fuzzy Logic (asym), failure at 10 sec: FN 4 failed open, TC 10 high, TC 5 high



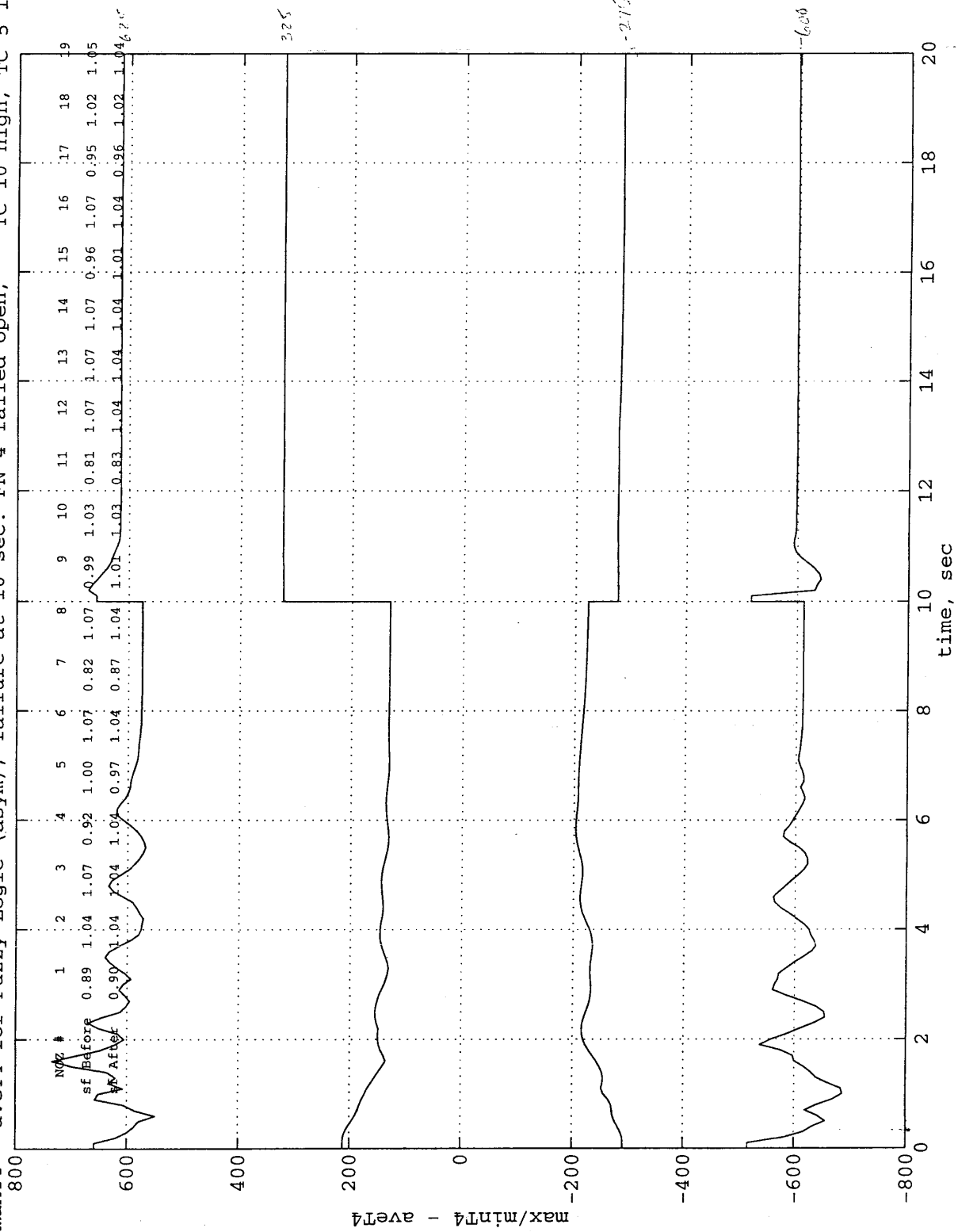
maxT4 - aveT4 for Fuzzy Logic (asym), failure at 10 sec: FN 4 failed closed, TC 10 high, TC 5 high



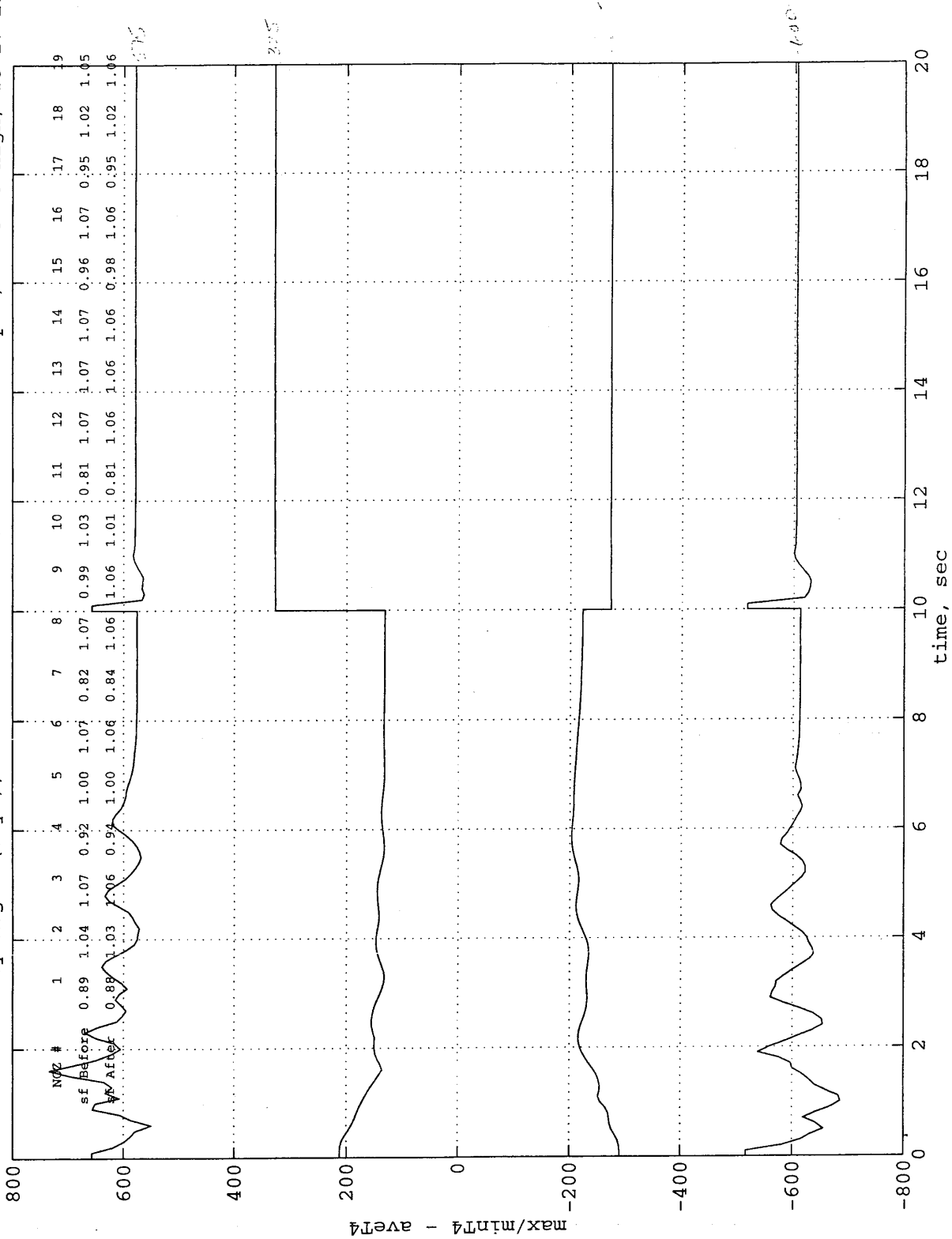
maxT4 - aveT4 for Fuzzy Logic (asym), failure at 10 sec: FN 4 failed closed, TC 10 high, TC 5 low



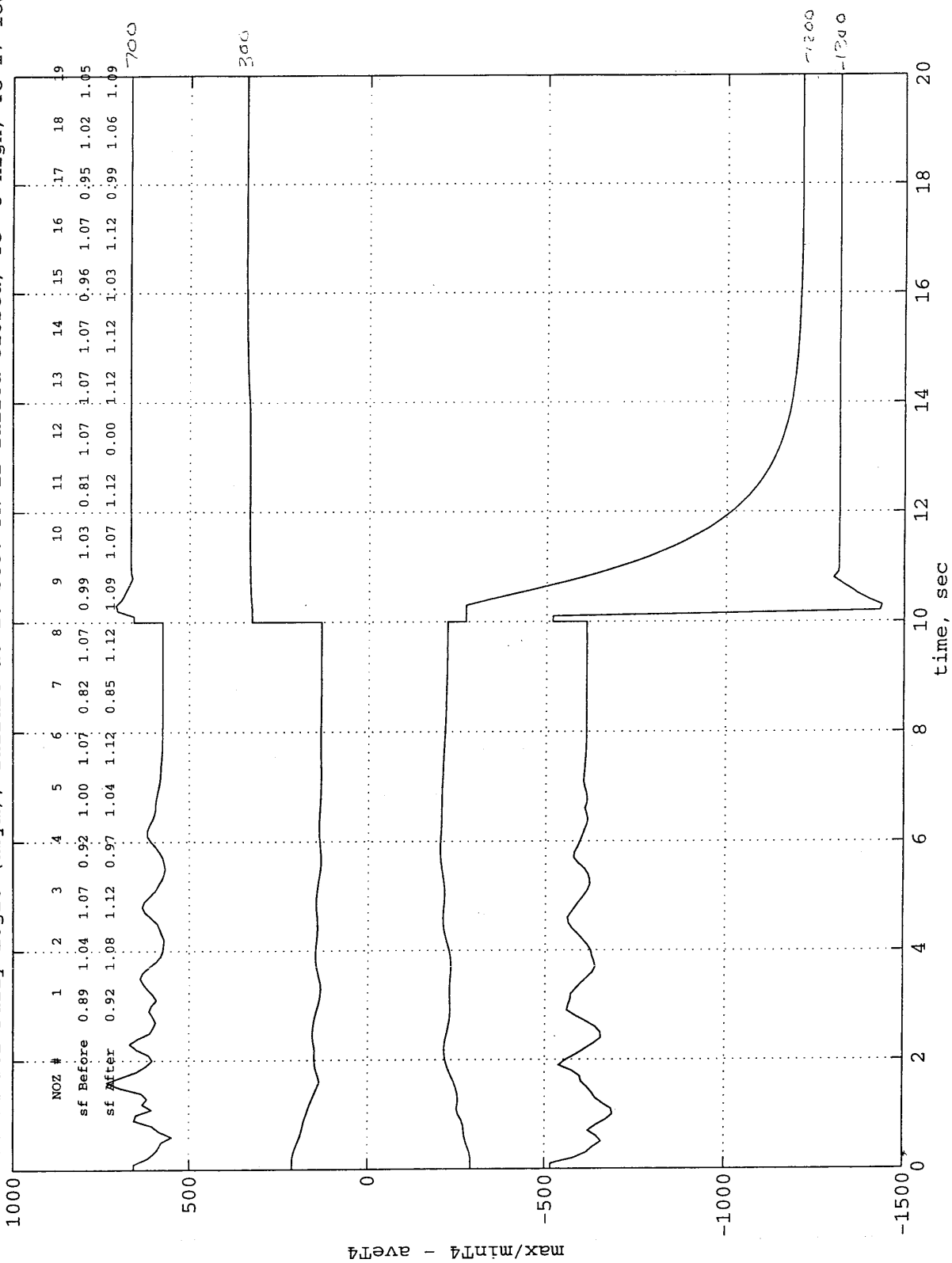
maxT4 - aveT4 for Fuzzy Logic (asym), failure at 10 sec: FN 4 failed open, TC 10 high, TC 5 low



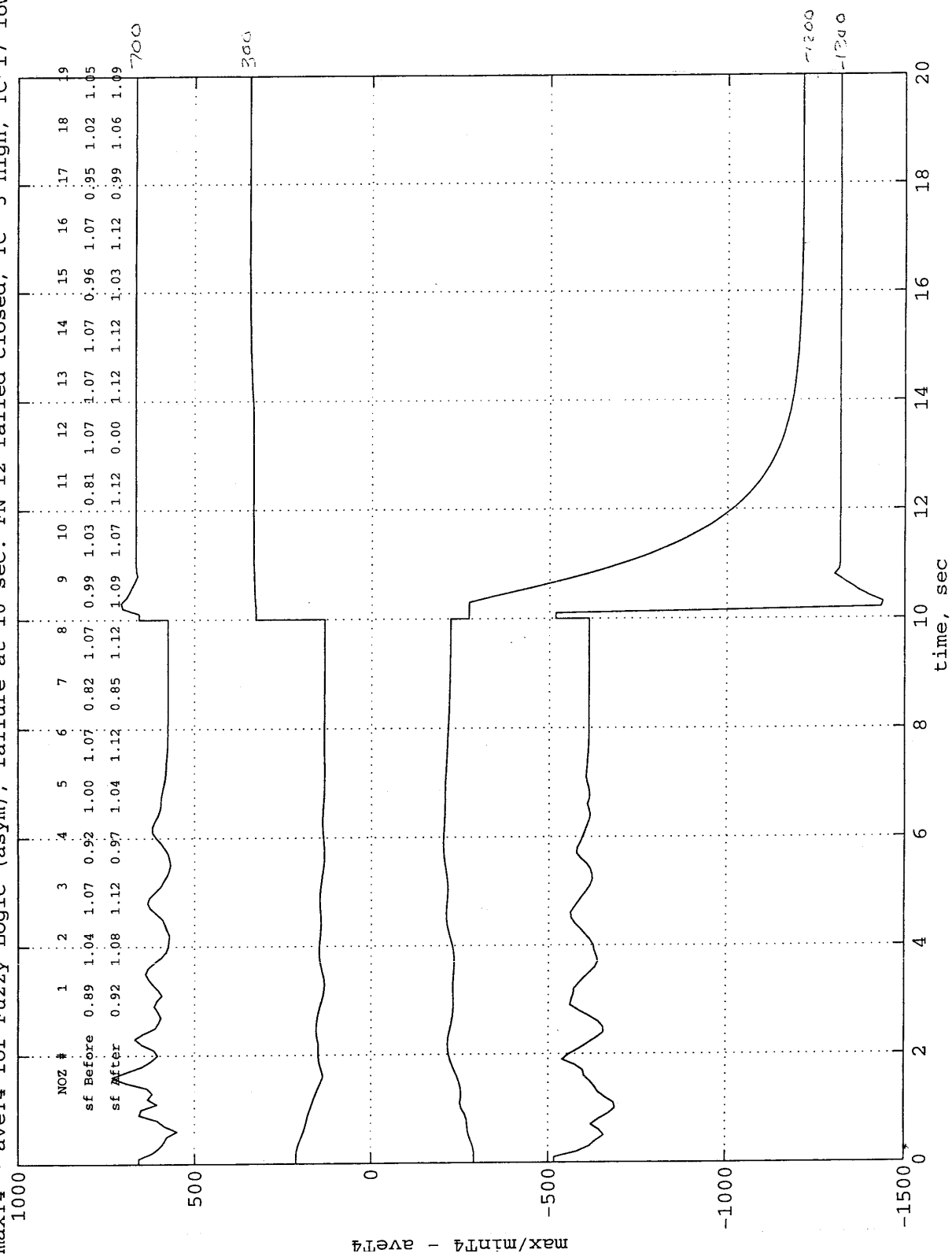
maxT4 - aveT4 for Fuzzy Logic (asym), failure at 10 sec: FN 12 failed open, TC 3 high, TC 17 low



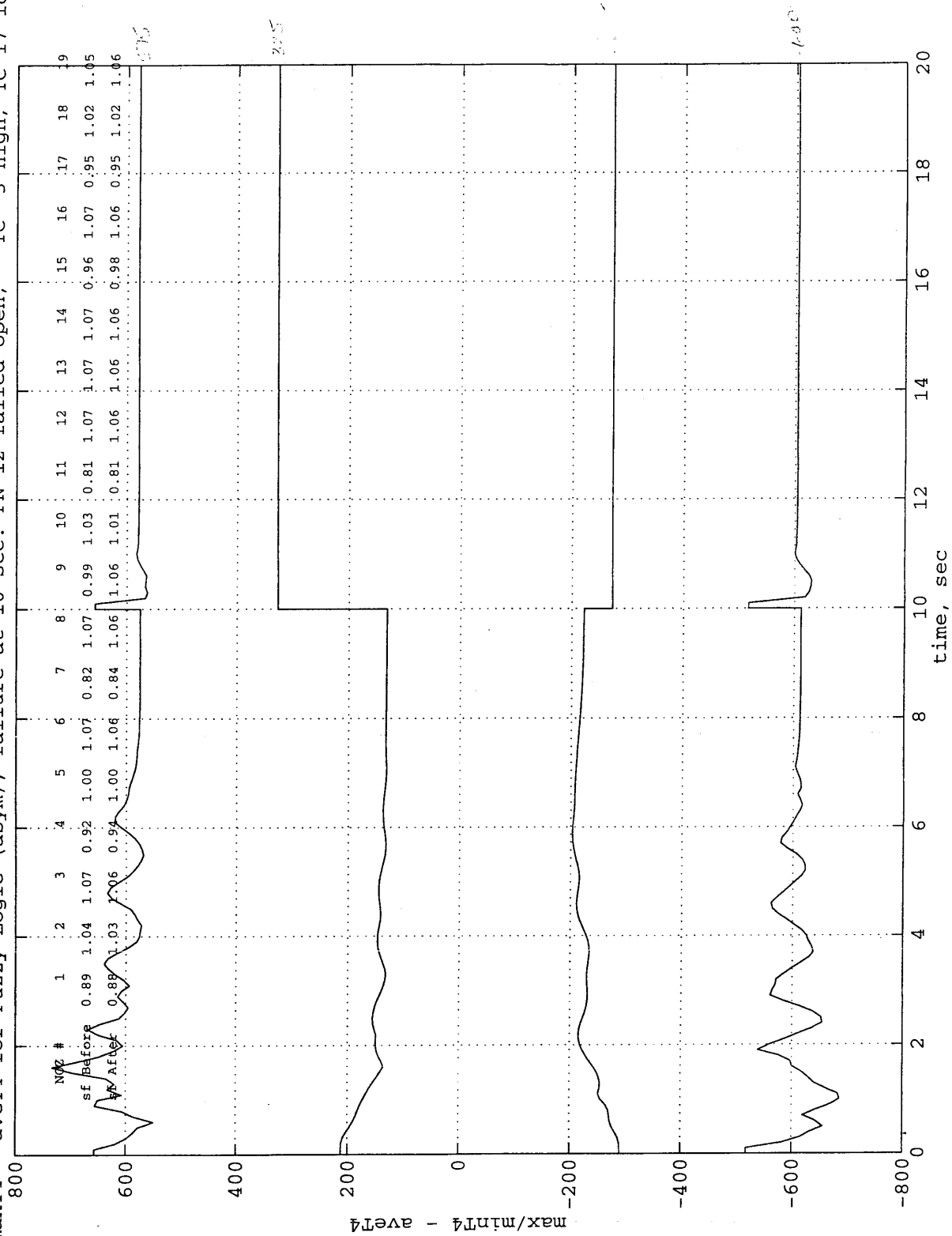
maxT4 - aveT4 for Fuzzy Logic (asym), failure at 10 sec: FN 12 failed closed, TC 3 high, TC 17 low



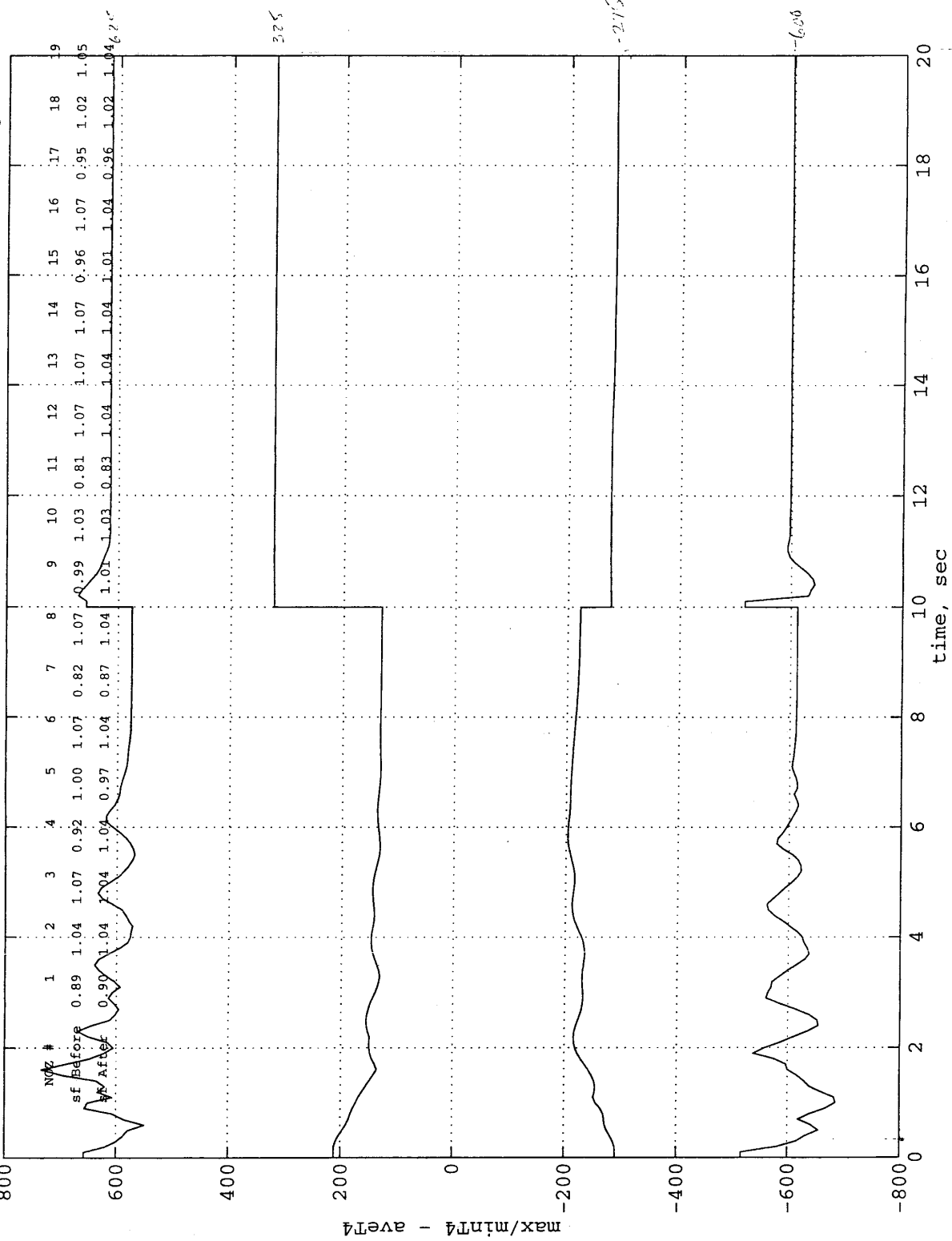
maxT4 - aveT4 for Fuzzy Logic (asym), failure at 10 sec: FN 12 failed closed, TC 3 high, TC 17 low



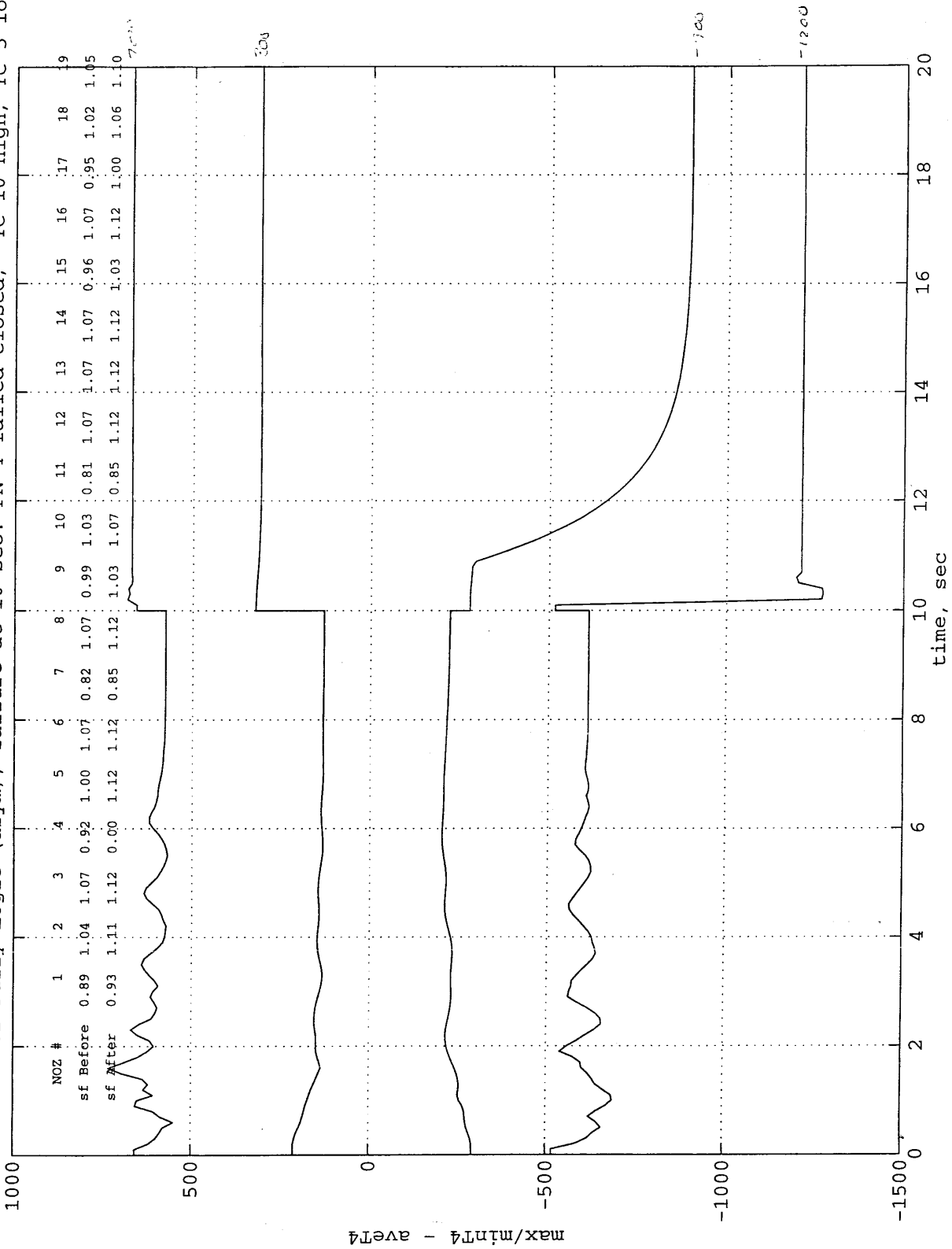
maxT4 - aveT4 for Fuzzy Logic (asym), failure at 10 sec: FN 12 failed open, TC 3 high, TC 17 low



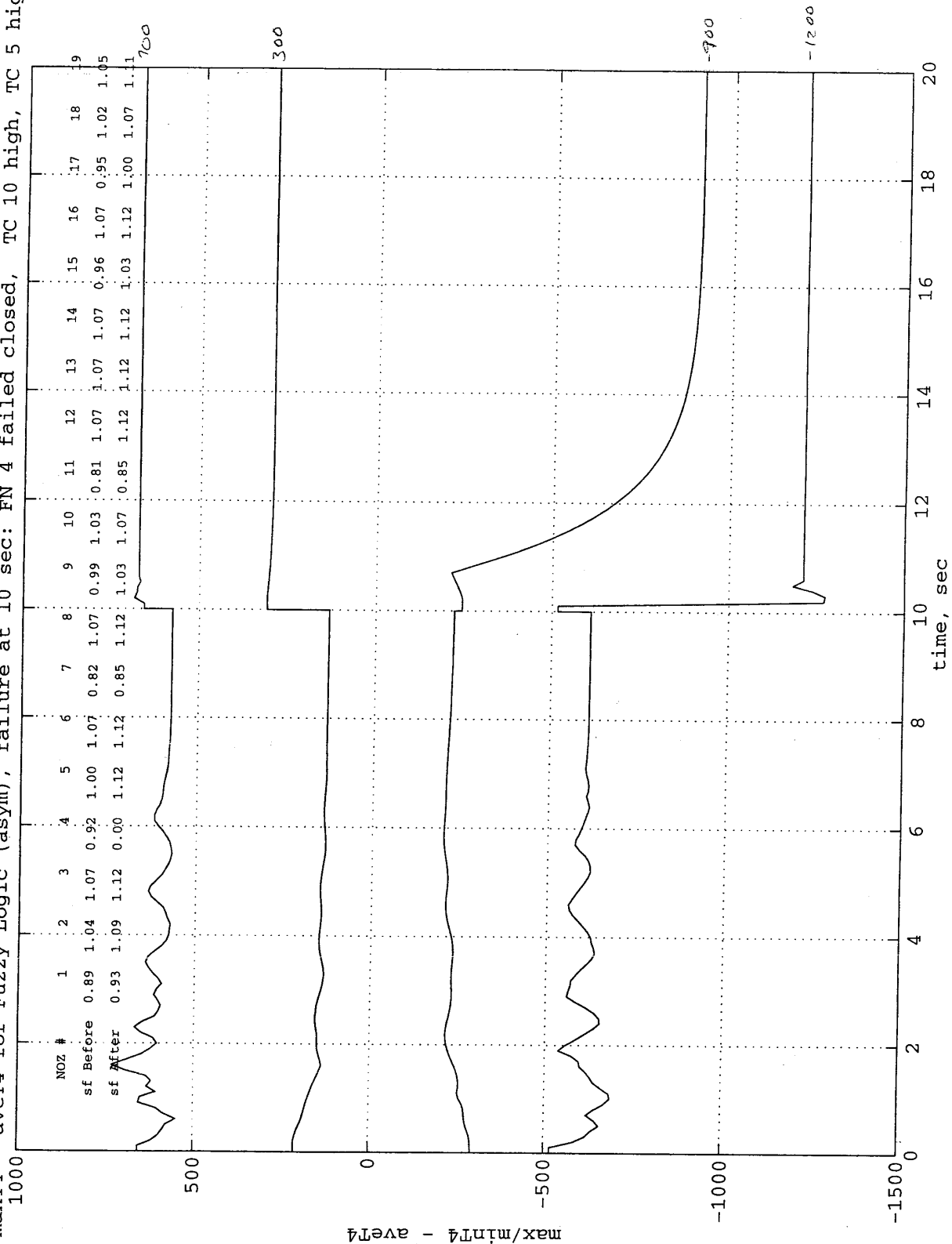
maxT4 - aveT4 for Fuzzy Logic (asym), failure at 10 sec: FN 4 failed open, TC 10 high, TC 5 low



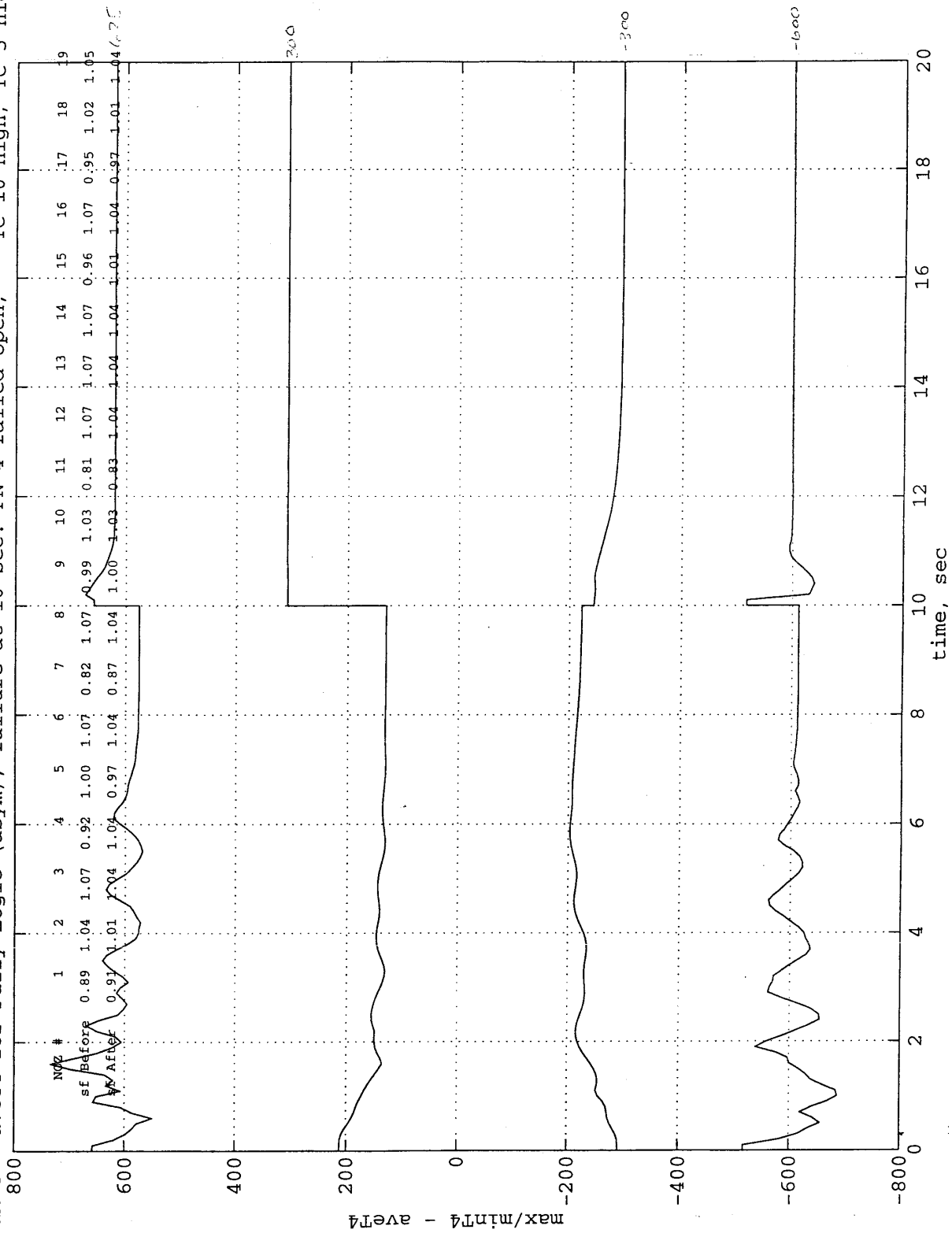
maxT4 - aveT4 for Fuzzy Logic (asym), failure at 10 sec: FN 4 failed closed, TC 10 high, TC 5 low



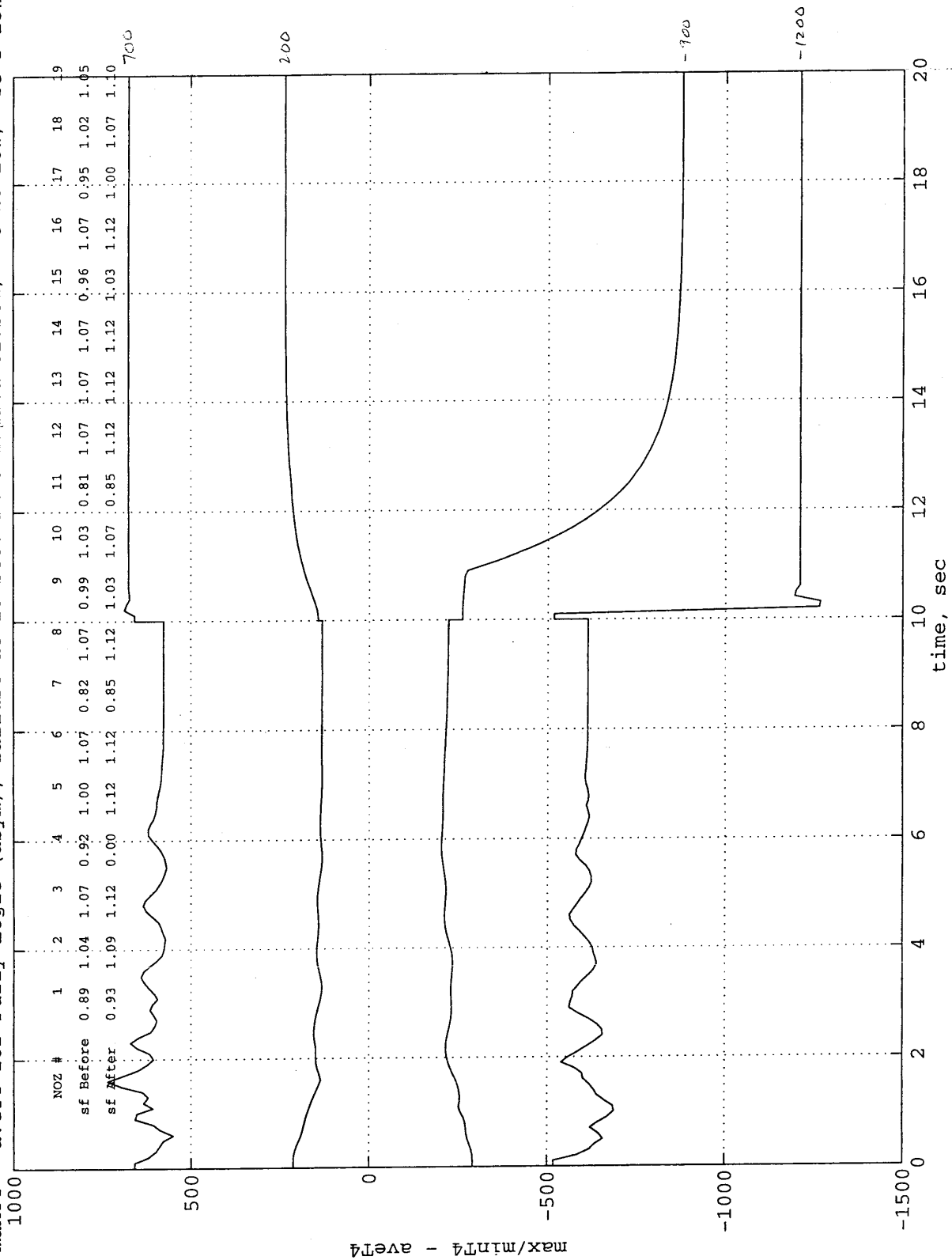
maxT4 - aveT4 for Fuzzy Logic (asym), failure at 10 sec: FN 4 failed closed, TC 10 high, TC 5 high



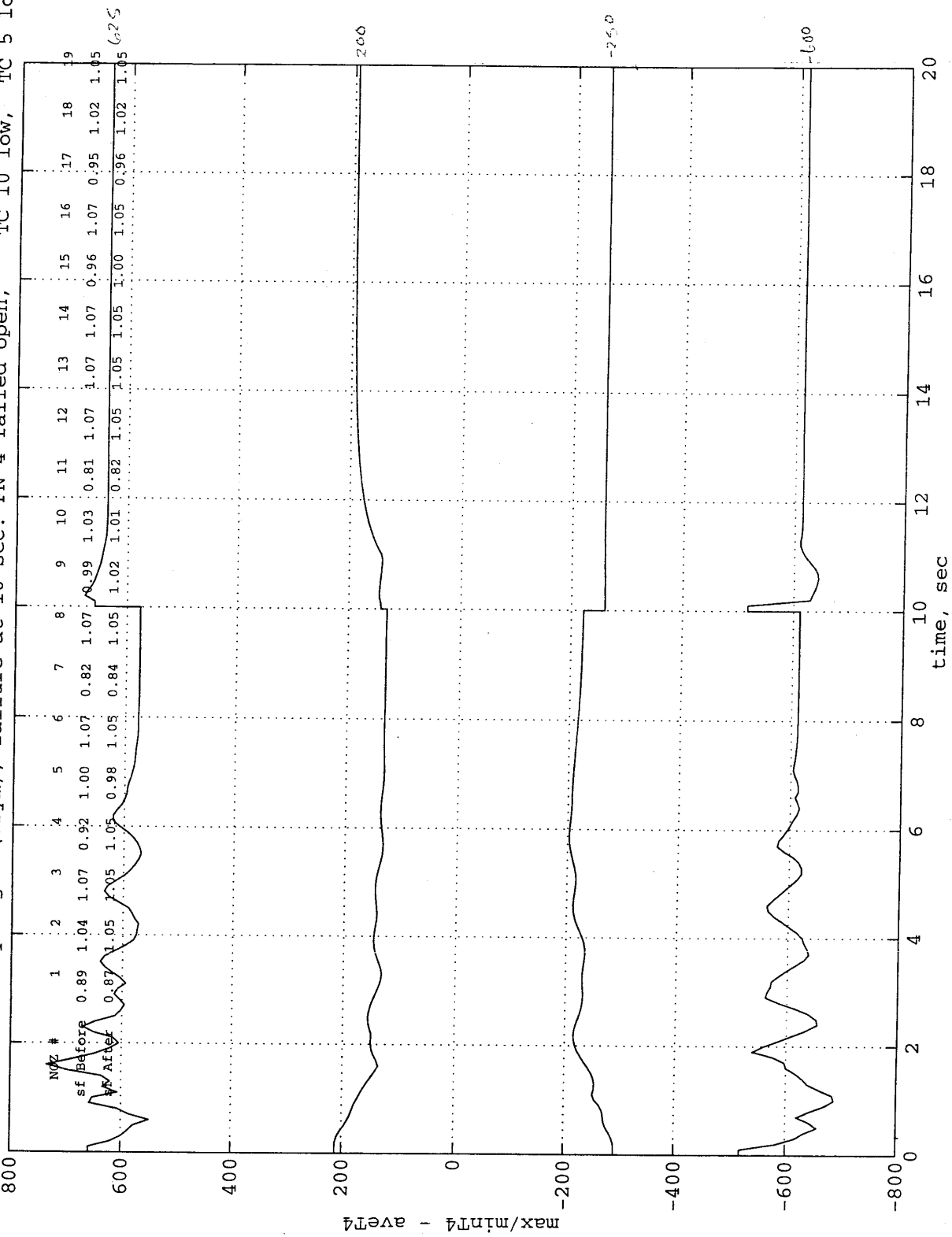
maxT4 - aveT4 for Fuzzy Logic (asym), failure at 10 sec: FN 4 failed open, TC 10 high, TC 5 high

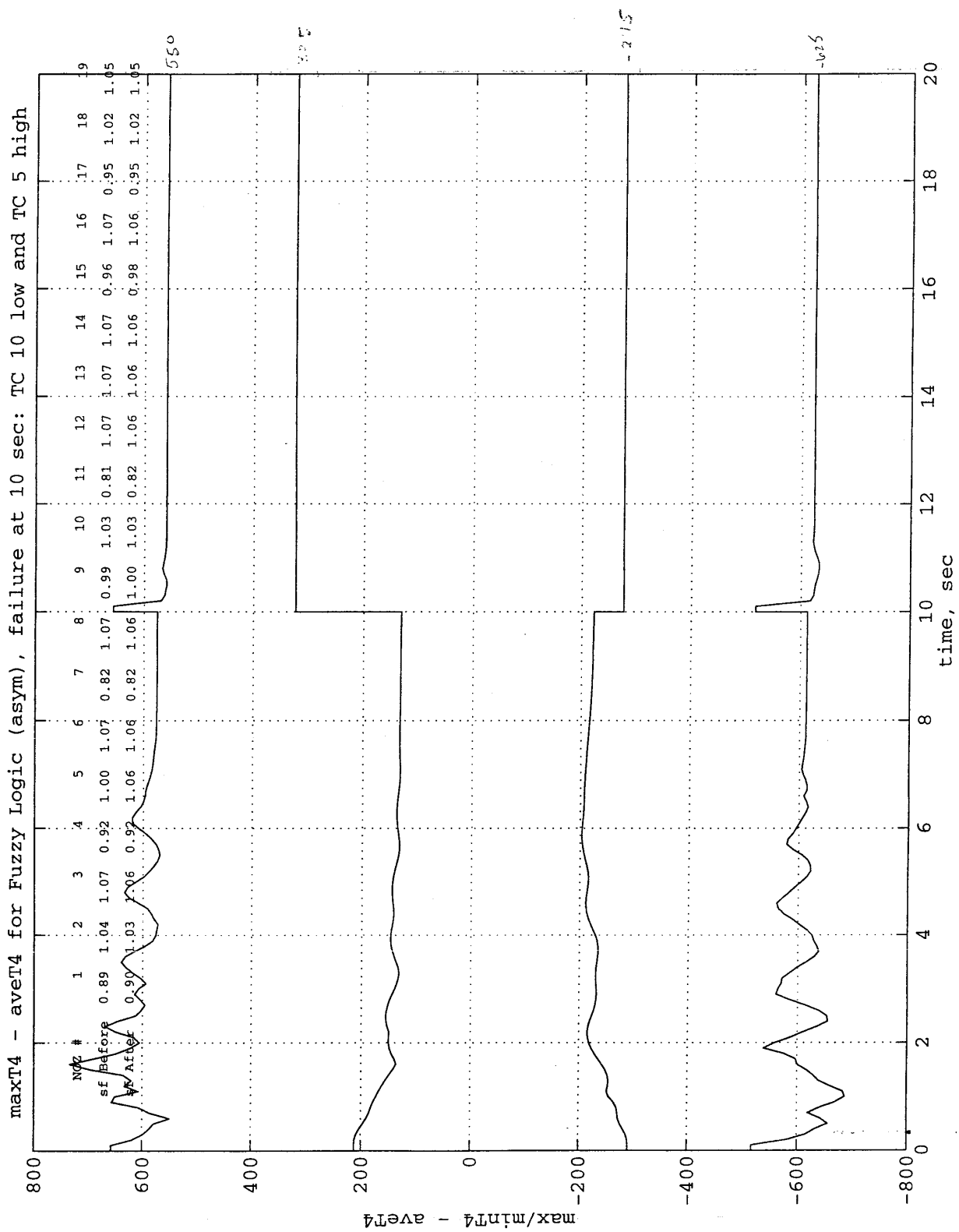


maxT4 - aveT4 for Fuzzy Logic (asym), failure at 10 sec: FN 4 failed closed, TC 10 low, TC 5 low

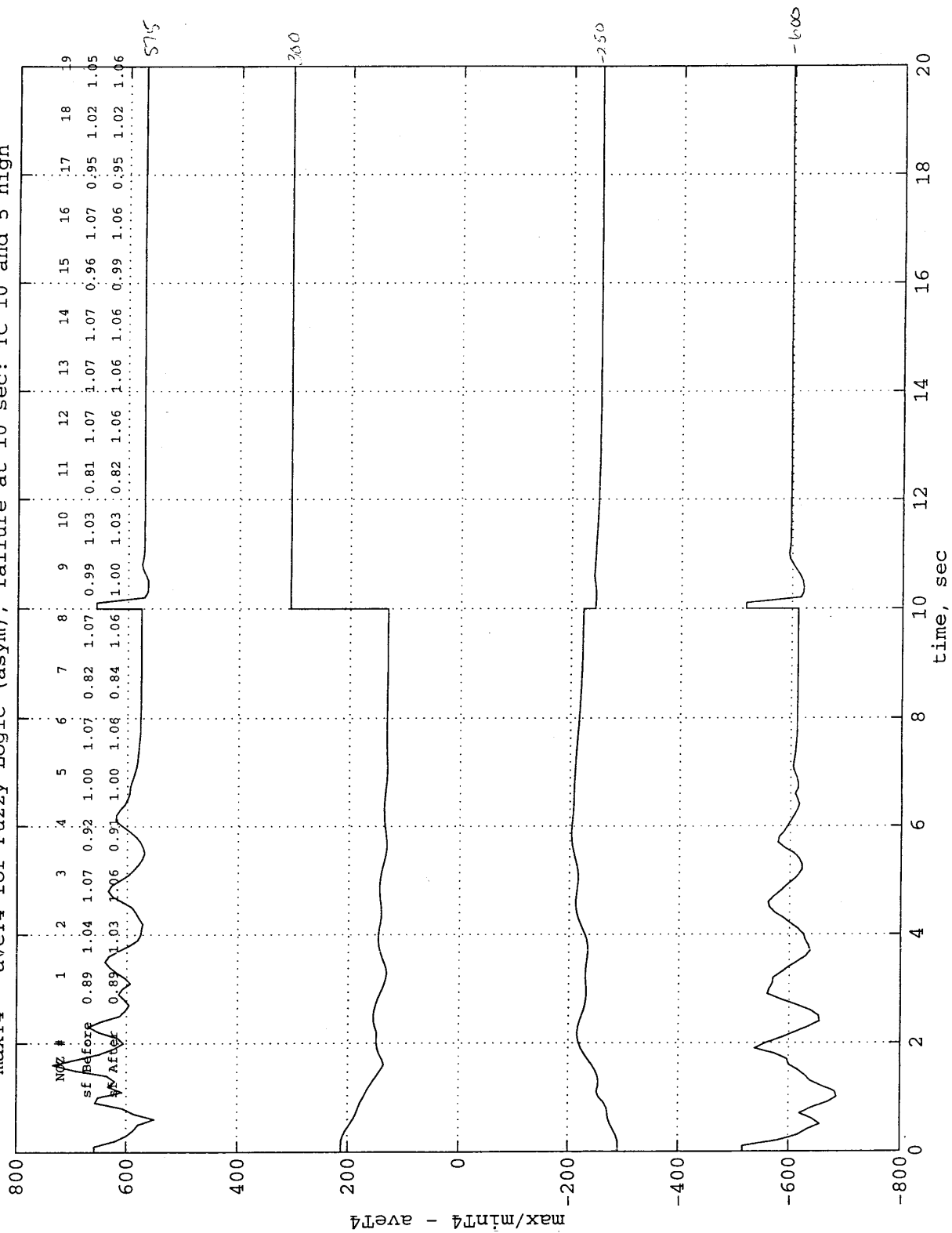


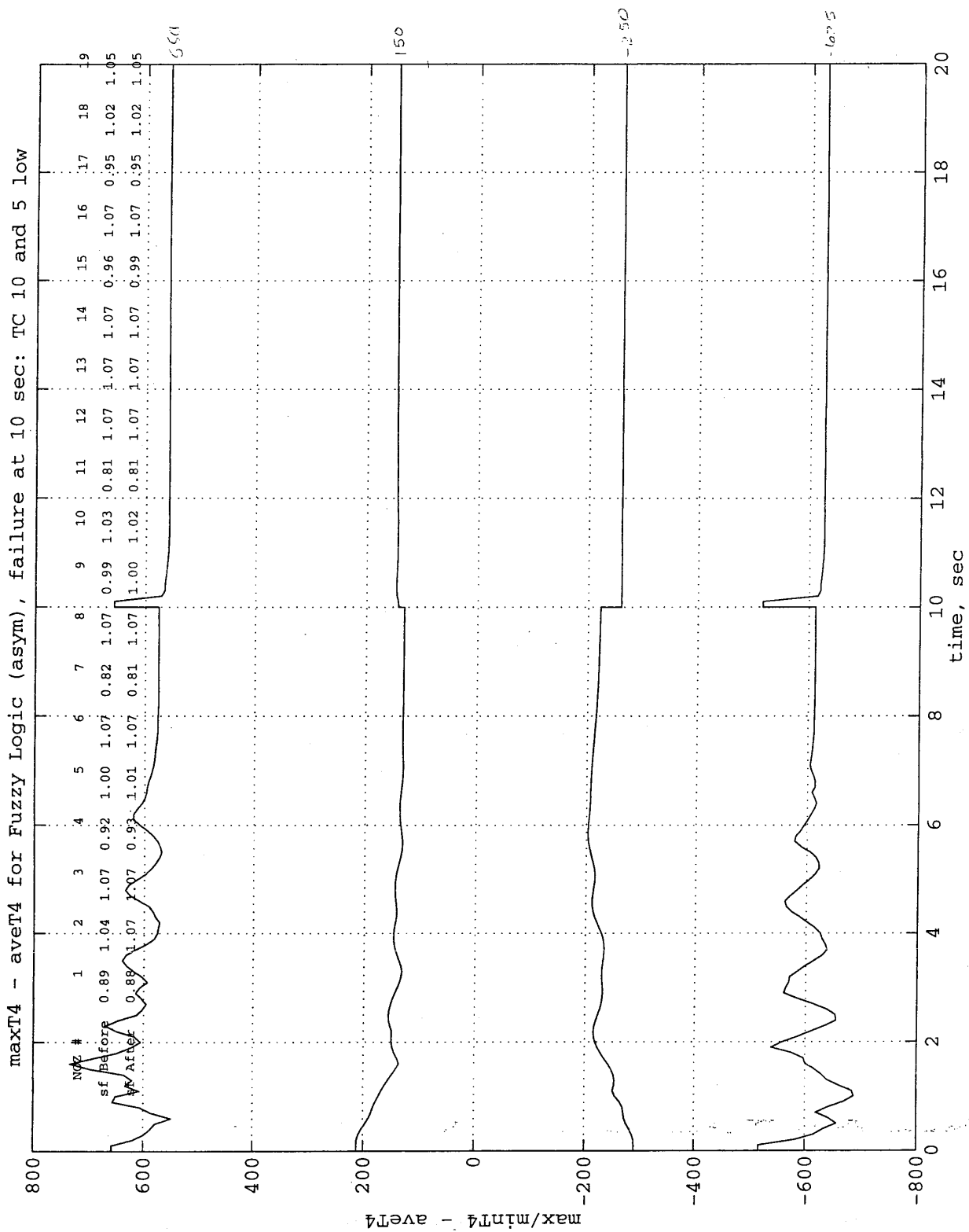
maxT4 - aveT4 for Fuzzy Logic (asym), failure at 10 sec: FN 4 failed open, TC 10 low, TC 5 low

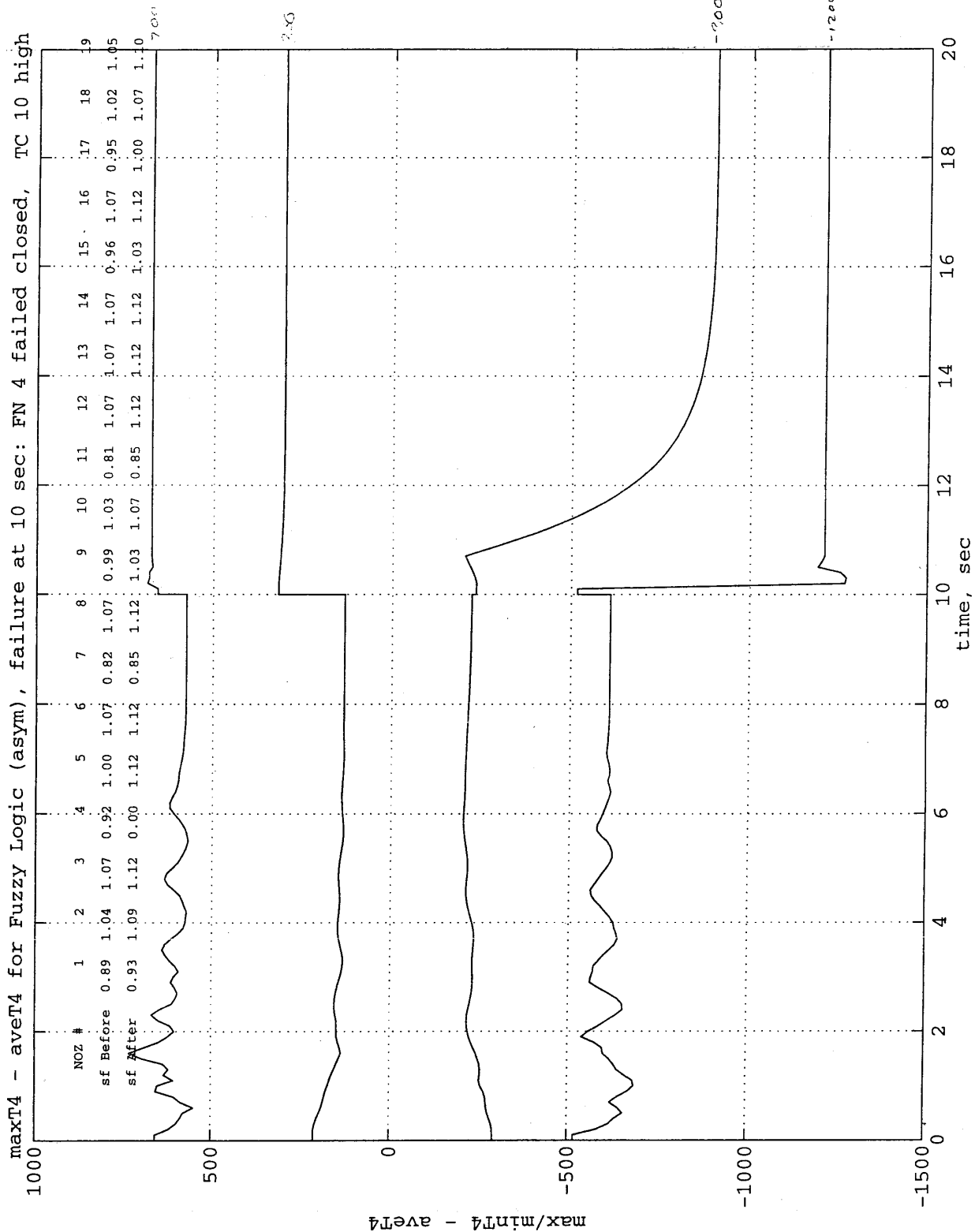


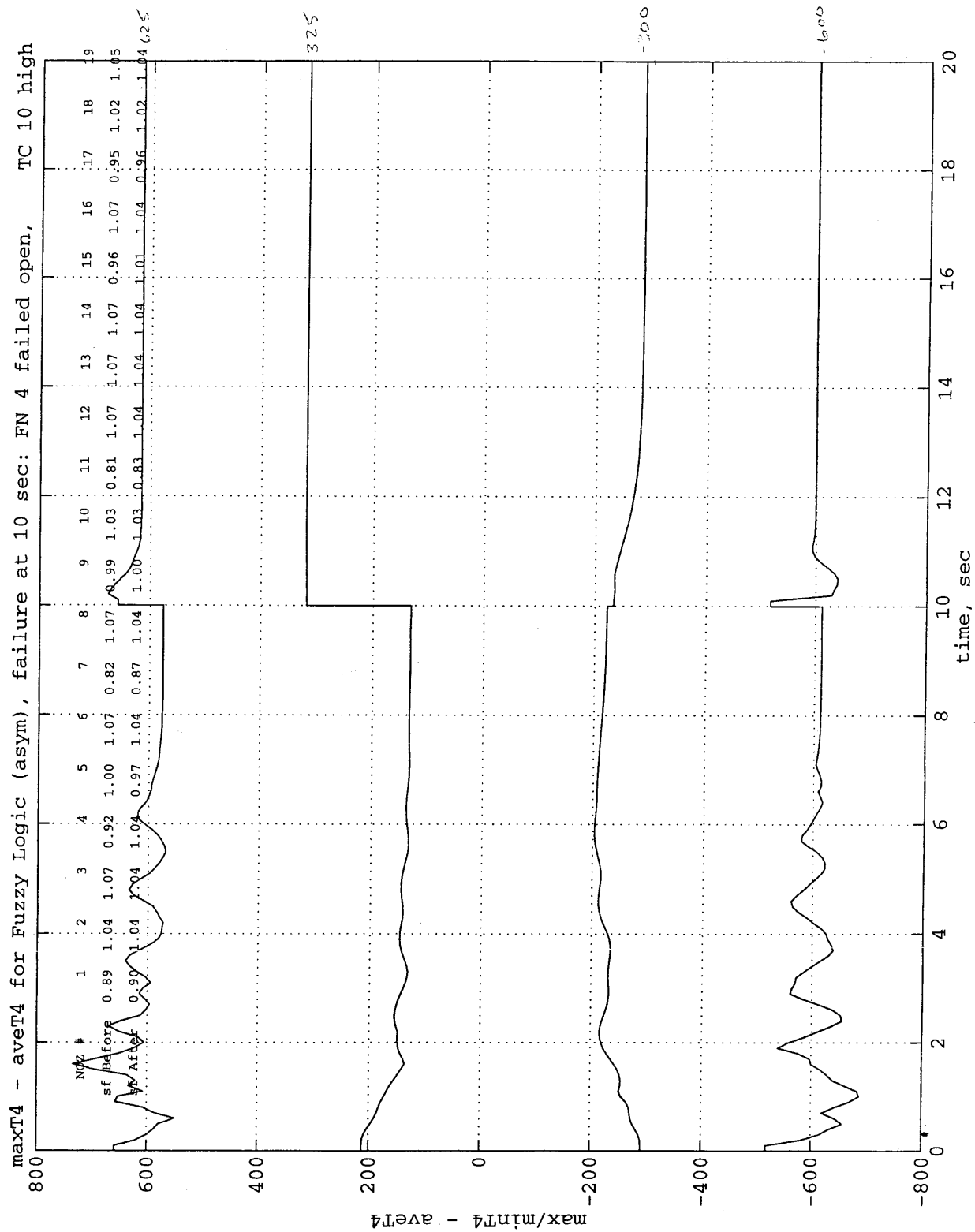


maxT4 - aveT4 for Fuzzy Logic (asym), failure at 10 sec: TC 10 and 5 high

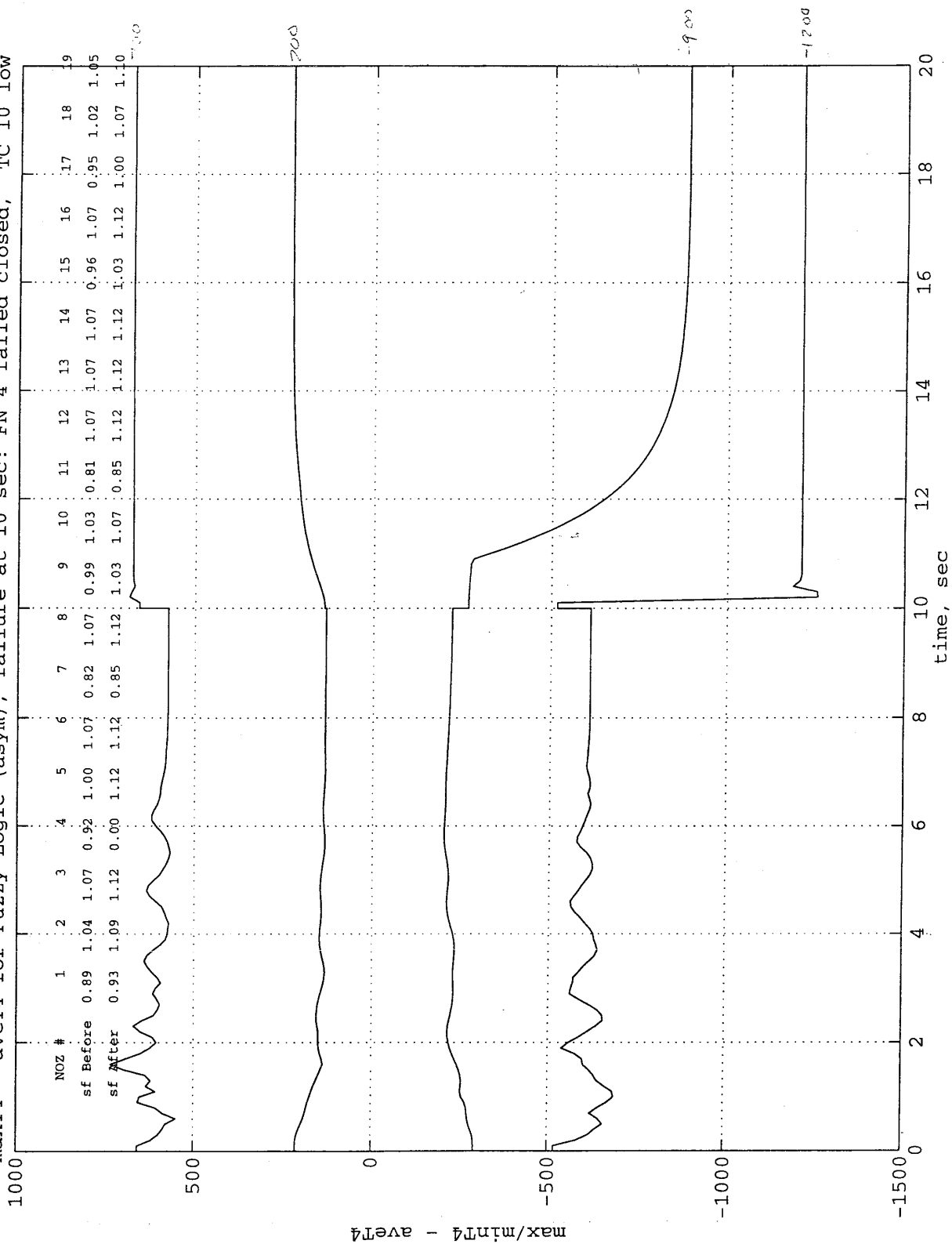


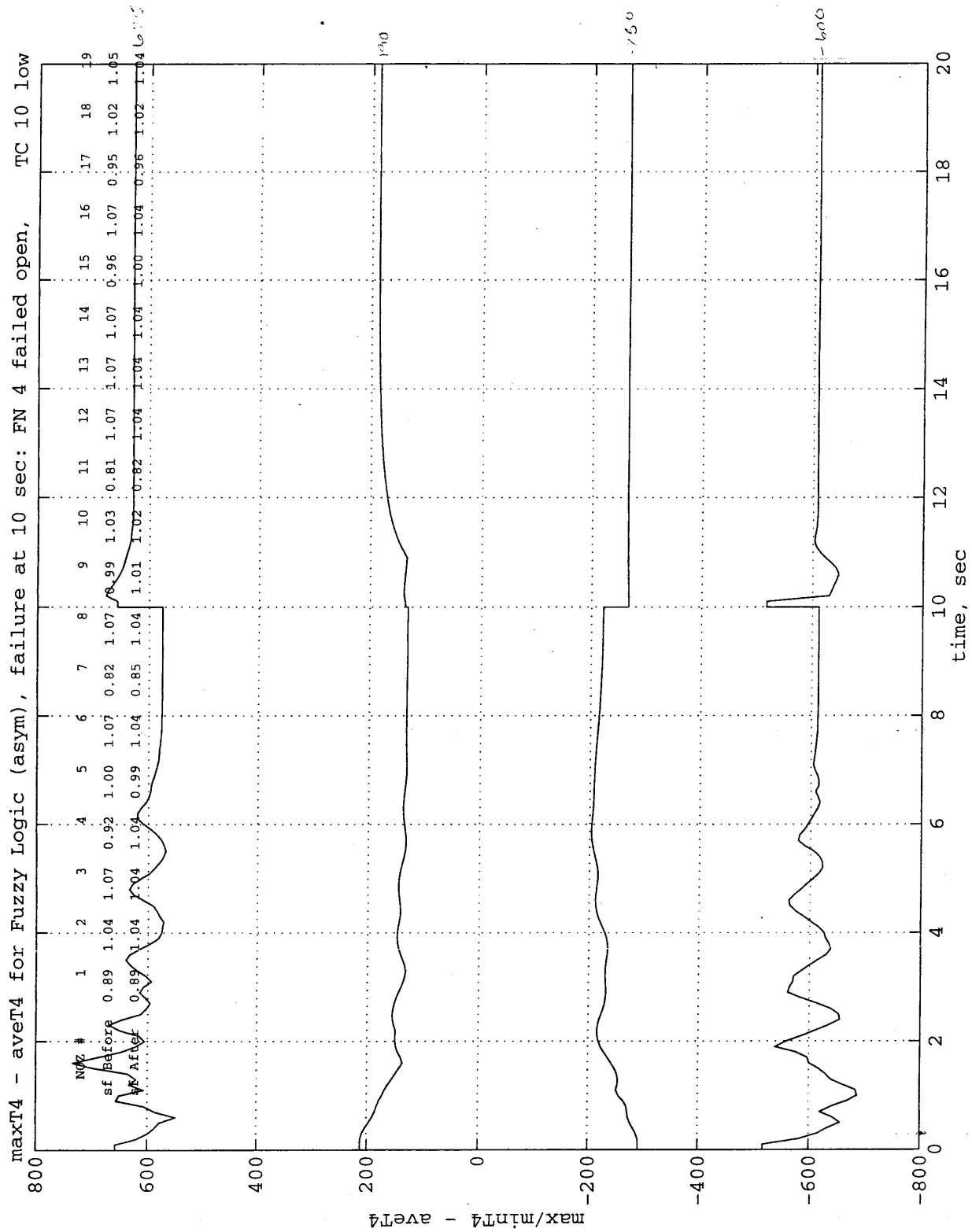




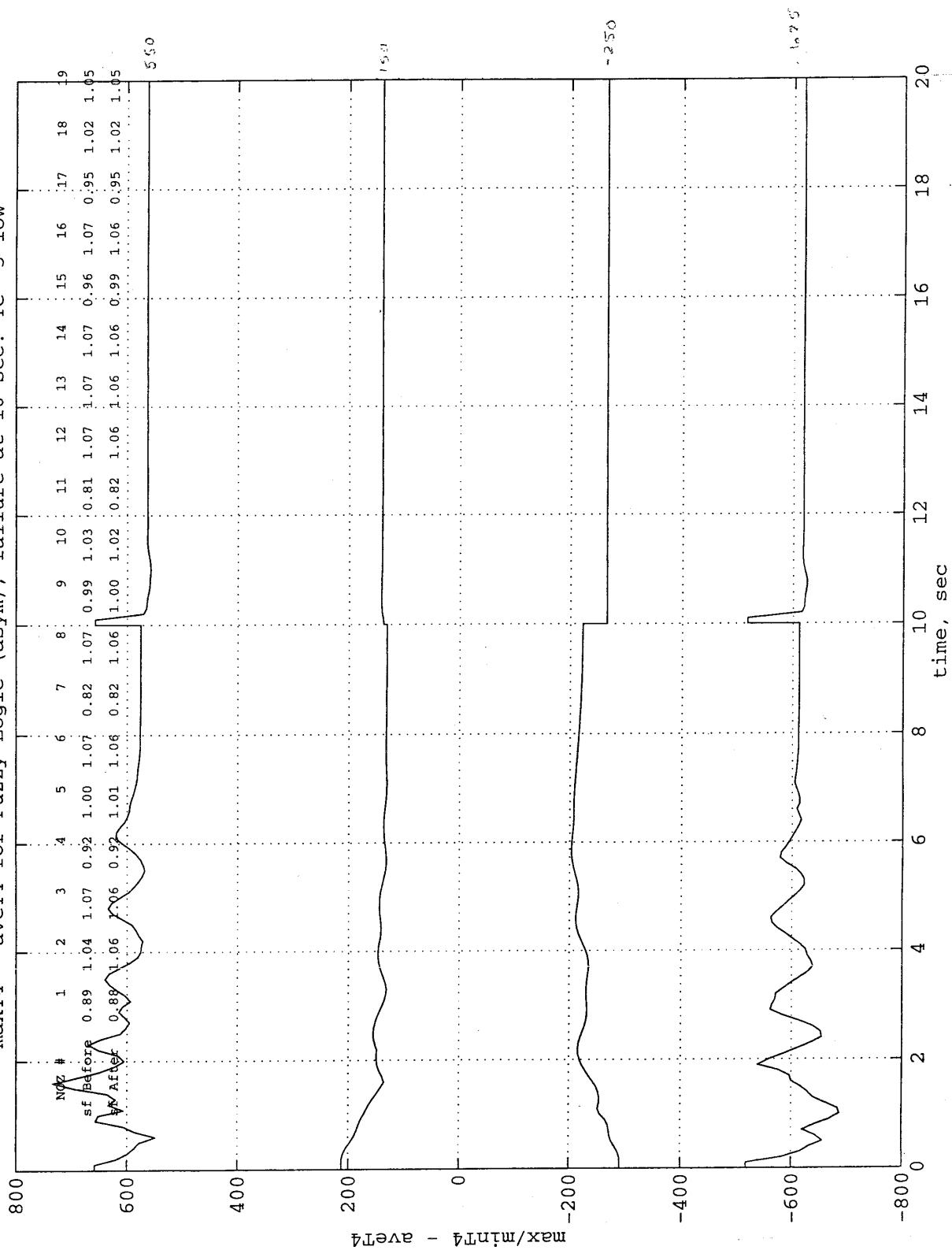


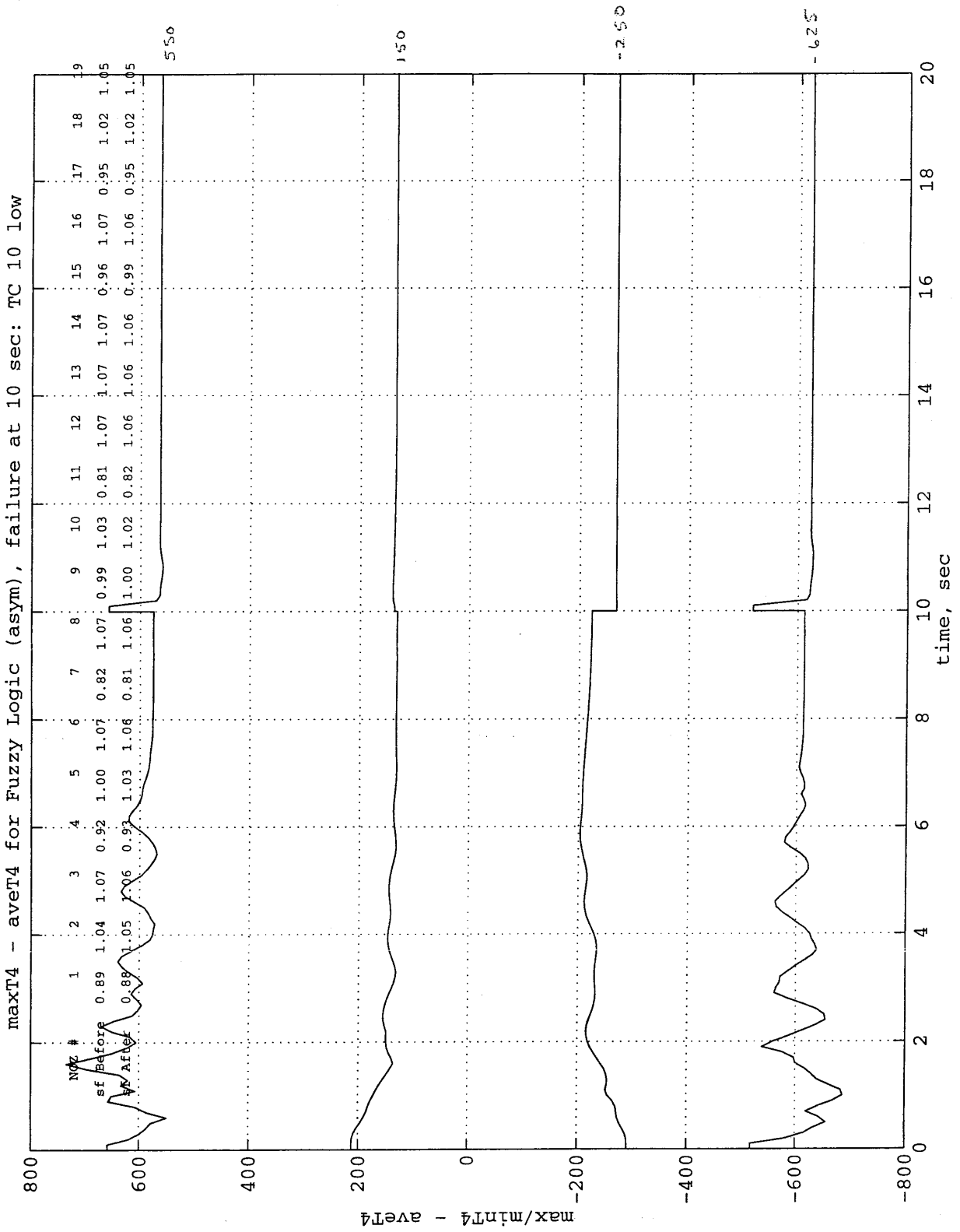
maxT4 - aveT4 for Fuzzy Logic (asym), failure at 10 sec: FN 4 failed closed, TC 10 low



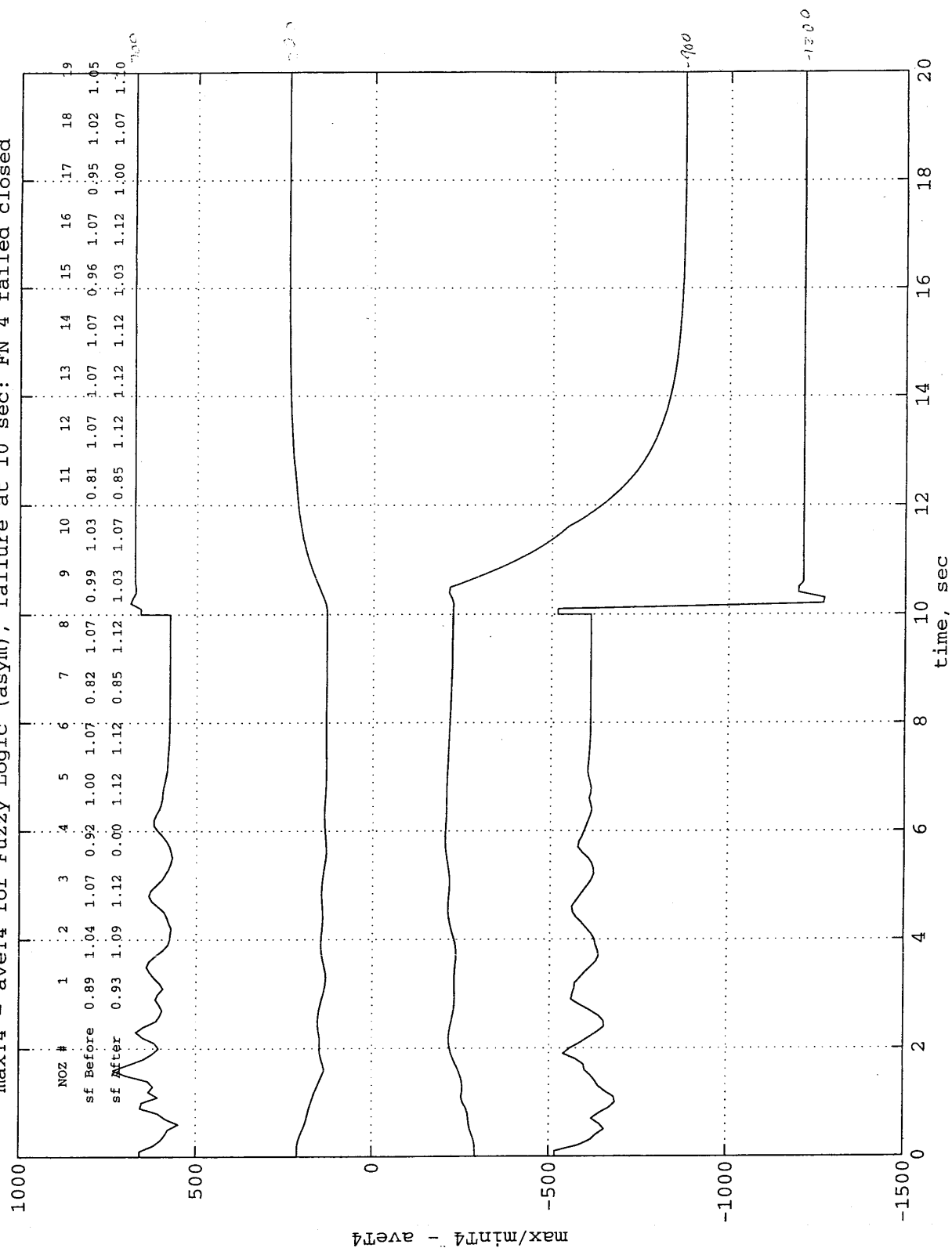


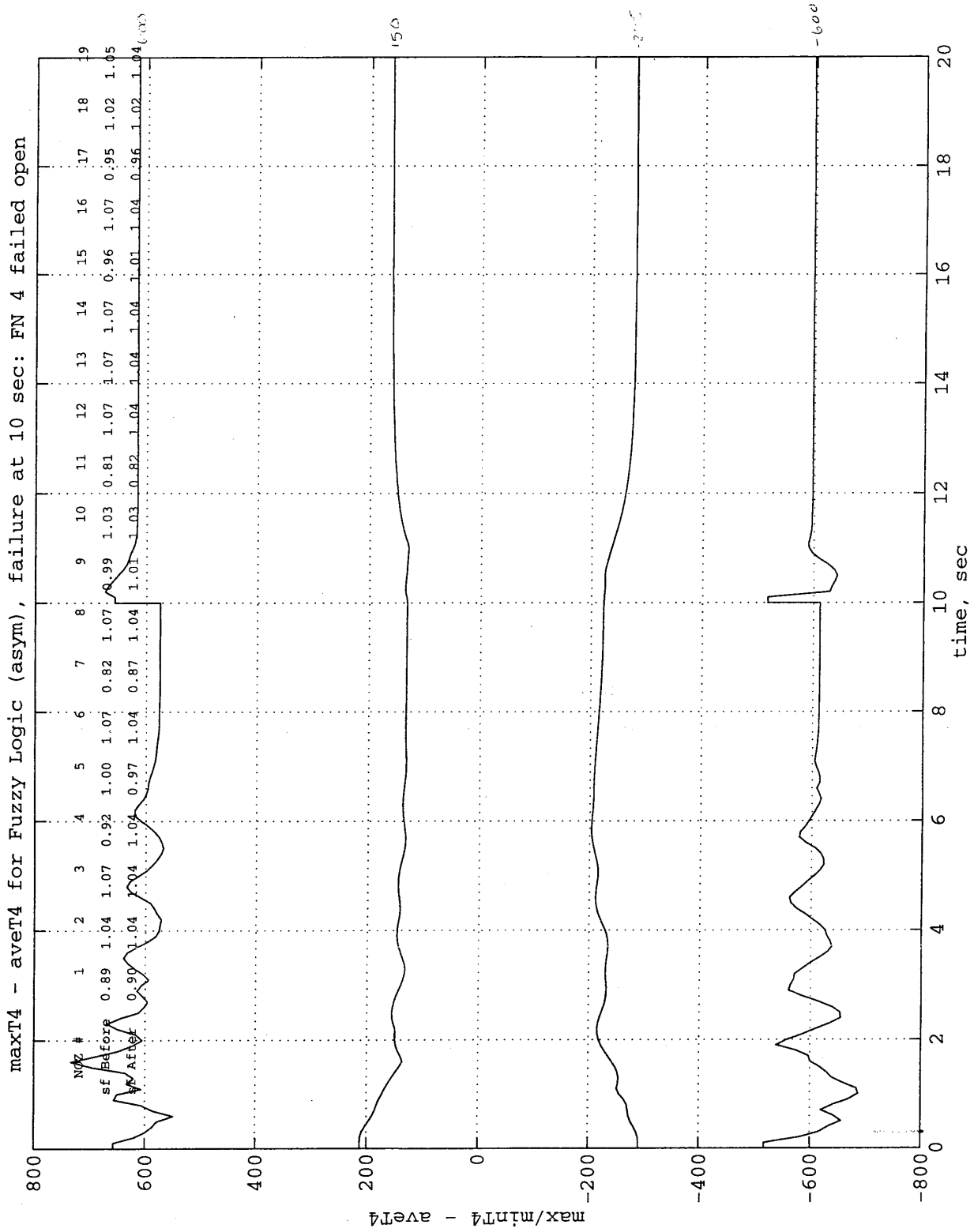
maxT4 - aveT4 for Fuzzy Logic (asym), failure at 10 sec: TC 5 low

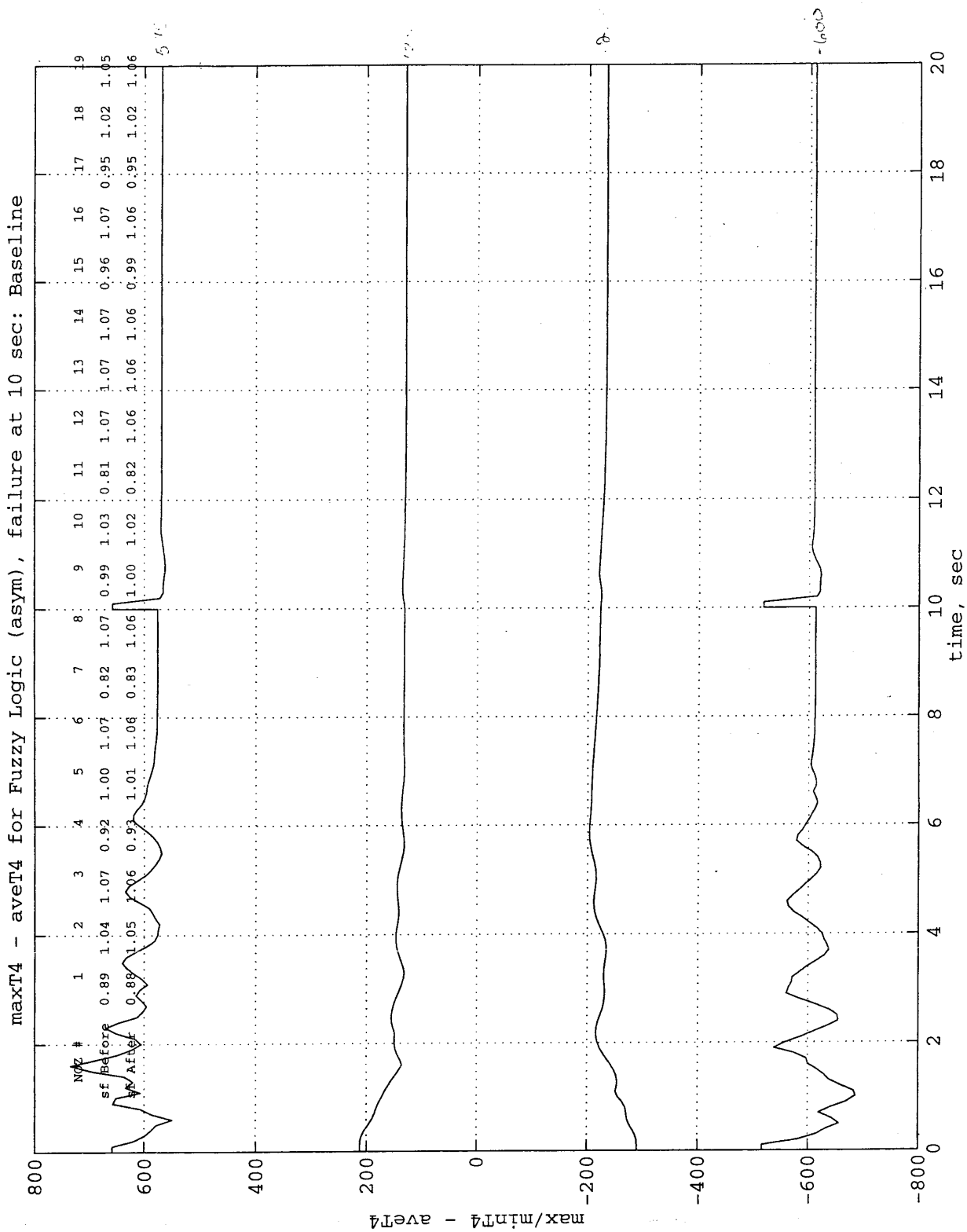


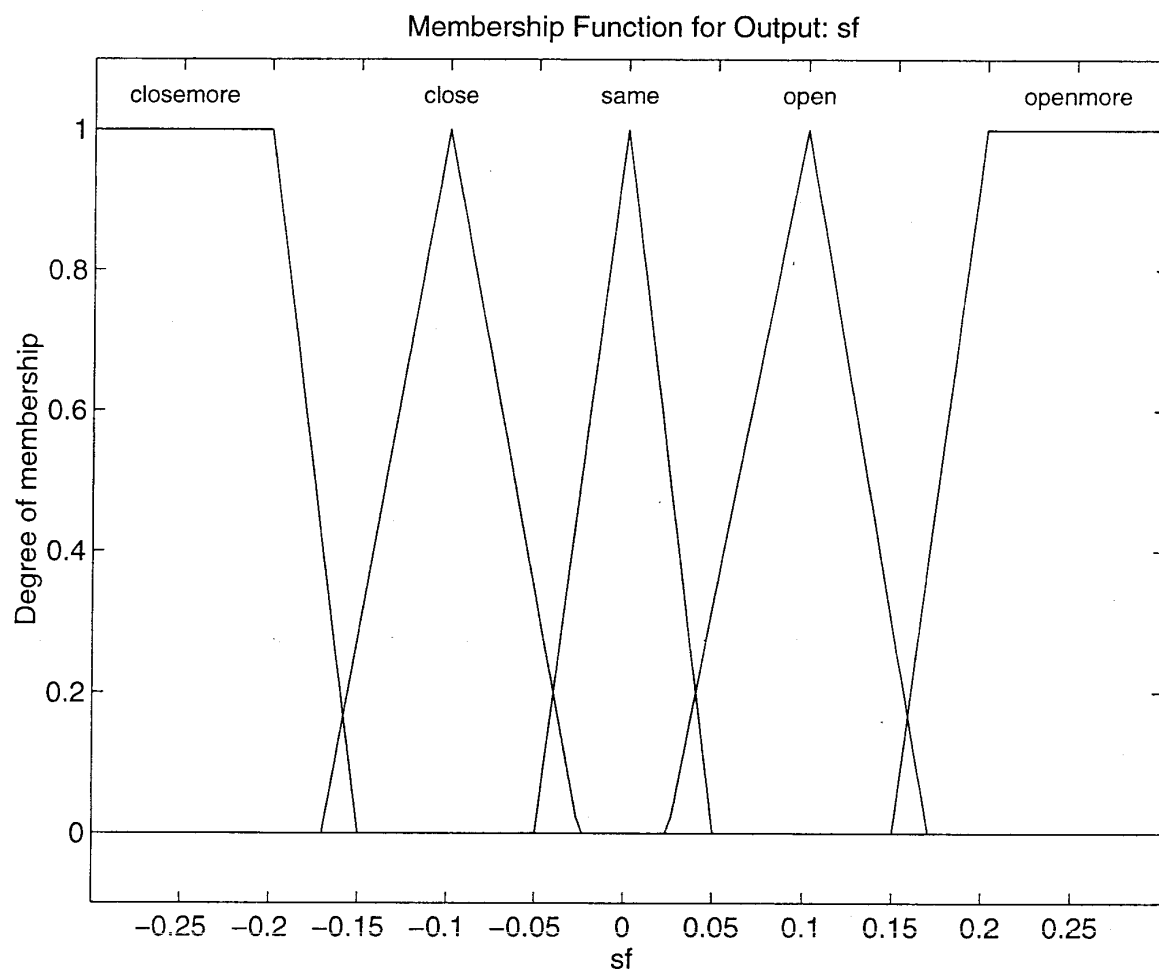


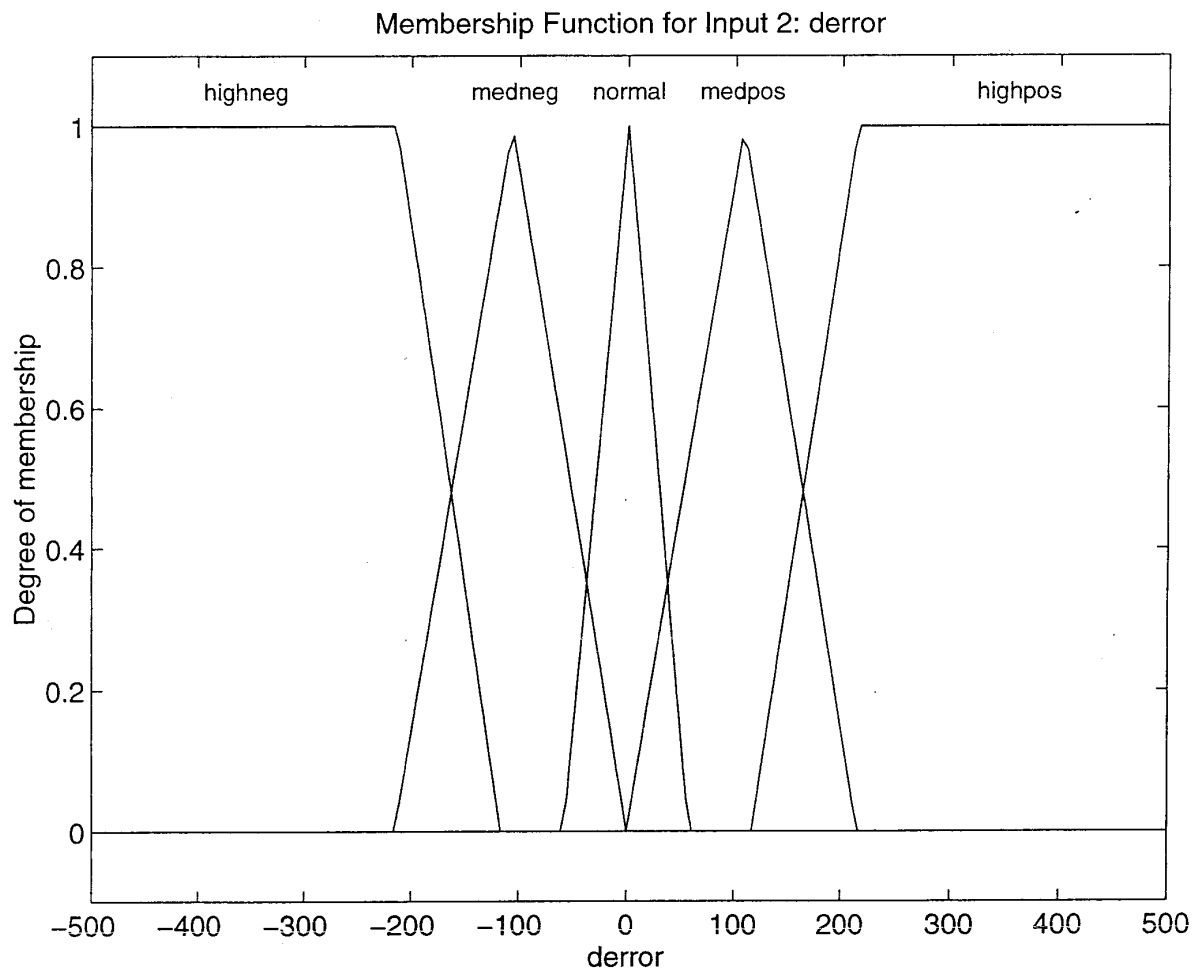
maxT4 - aveT4 for Fuzzy Logic (asym), failure at 10 sec: FN 4 failed closed

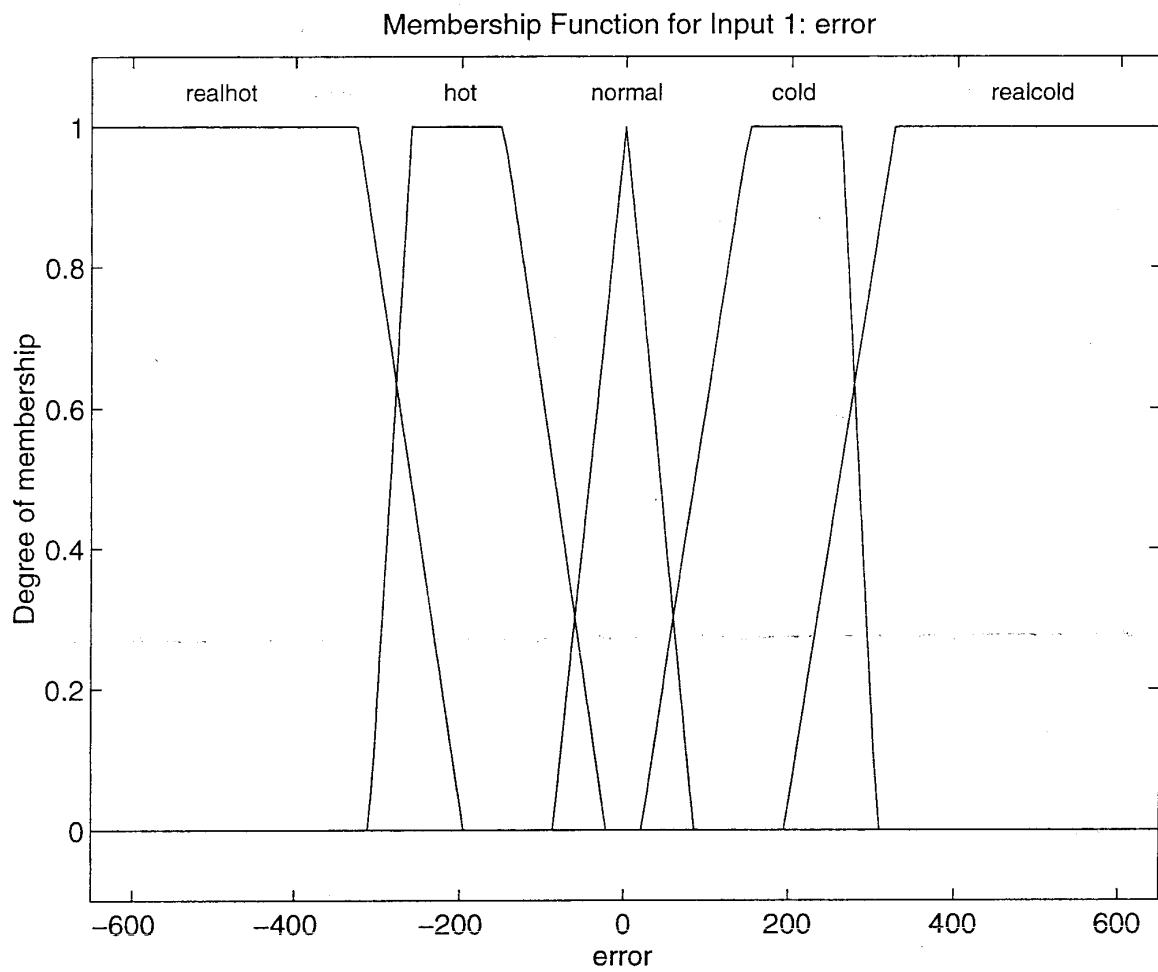












APPENDIX I
ASSOCIATED FIGURES
(43 Pages)

| <u>Fig. No.</u> | <u>Title</u> | <u>Page</u> |
|------------------------|---|--------------------|
| A1 - A3 | Membership functions for two inputs and one output | 34-36 |
| A4 - A23 | Complete runs for pat20.fis, baseline and failure modes [4] | 37-56 |
| A24 - A43 | Complete runs for pat21.fis, baseline and failure modes [4] | 57-76 |

References:

- [1] Gulley, Jang. 1/95. *Fuzzy Logic ToolBox User's Guide*, The Mathworks, Inc., pp. 2 - 50.
- [2] Bonissone, Chiang. 1995. Fuzzy Logic Hierarchical Controller for a Recuperative Turboshift Engine. *Industrial Applications of Fuzzy Logic and Intelligent Systems*, IEEE Press, pp. 131-156.
- [3] Stokes, Krech. 1996. *Reliable and Affordable Control Systems, Active Combustor Pattern Factor Control*, NASA AST Technical Progress Report No. 4, Appendix I. AE Report 21-9197(4).
- [4] Stokes, Krech. 4/97. *Active Combustor Emissions/Pattern Factor Control Bi-annual Status Review*, pp 108-126. AE Report No. 21-9617.

Conclusion:

In this application the fuzzy logic controller can be designed to exhibit response similar to a conventional PI controller. Phase One showed that a fuzzy logic controller can be set to match the steady state performance of a traditional PI controller by membership level and range selection [2]. Output from the fuzzy logic FIS was the analogue of the proportional constant, K_p . Pass the output through an integrator and you have a PI controller. The output fuzzy set can be 'fine tuned' to match any PI controller by adjusting the membership levels. Once the combustor model was modified to include the nonlinear relationship of fuel dispersion to thermocouples the fuzzy logic controller still performed as well as a PI controller.

In phase two a more complex combustor system was controlled with fuzzy logic. The more complex system used more thermocouples than the symmetric case. Although the asymmetric model was controlling more area [3] the performance of the fuzzy logic controller was virtually unchanged. This displayed the ability of a fuzzy logic controller to adapt to configuration changes.

The effectiveness of the fuzzy logic controller on both hot and cold spots was quantified. It was robust to failure modes for both except for failure cases corresponding to a fuel nozzle fixed closed. In those cases the cold spots were double the normally controlled value of -600 degrees. Considering that the case of a fuel nozzle fixed closed would be a rare event it is safe to claim that the controller has the capability to accommodate failure modes.

When the Allied Signal Fuzzy Logic Controller was integrated with the SMI combustor logic the performance did not change. Thus the fuzzy logic controller was not only robust to combustor complexity, thermocouple - fuel nozzle arrangement, and failure modes but also to plant variations.

In order to implement this fuzzy logic controller, a lookup table which reflect the fuzzy logic FIS would need to be generated. The lookup table would take the error and derivative of the error, as described above, and output the corresponding areaout command. The same lookup table would be used for all fuel flow modulators. A scheme to code this concept into the rapid prototyping electronic control would need to handle all nineteen thermocouple inputs at once or with a sequencing routine. Ease of coding, and lines of code required, and CPU execution time, etc. should be factors in selecting the proper fuzzy control algorithm.

Associated Figures.

The following figures are included as an appendix to this report:

Figures A1 - A3 Membership functions for two inputs and one output.

Figures A4 - A23 Complete runs for pat20.fis, baseline and failure modes [4].

Figures A24 – A43 Complete runs for pat21.fis, baseline and failure modes [4].

No. Failure Mode Definitions

| | | |
|----|---------------------|---------------------|
| 1 | Baseline | |
| 2 | TC 10 low | |
| 3 | TC 5 low | |
| 4 | TC 10 & 5 low | |
| 5 | TC 10 & 5 high | |
| 6 | TC 10 low TC 5 high | |
| 7 | FN 4 open | |
| 8 | FN 4 open | TC 10 high |
| 9 | FN 4 open | TC 10 low |
| 10 | FN 4 open | TC 10 & 5 low |
| 11 | FN 4 open | TC 10 & 5 high |
| 12 | FN 4 closed | |
| 13 | FN 4 closed | TC 10 high |
| 14 | FN 4 closed | TC 10 low |
| 15 | FN 4 closed | TC 10 & 5 low |
| 16 | FN 4 closed | TC 10 & 5 high |
| 17 | FN 4 closed | TC 10 high TC 5 low |
| 18 | FN 12 open | TC 3 high TC 17 low |
| 19 | FN 12 closed | TC 3 high TC 17 low |

Results from the simulations show that the actual temperature difference was +600 and -600 degrees except for cases where the modulator was fixed closed. In those cases the actual temperature difference increased to +700 and -1200 degrees. The sensed temperature difference for hot spots remained within the range of +125 to 300 for all failure modes. Cold spots were -225 degrees for all failure modes except those with a modulator fixed closed in which case the value was -925 degrees.

The main points from this discussion are in the following text. Fuzzy systems are defined by fuzzy sets. The elements within those sets are defined by membership functions and rules. There is not always a unique system that will provide a single crisp number that represents each of the previous inputs, membership functions, and rules from the defuzzification step. For the case of the Active Pattern Factor Controller a seven-level system defined with 19 rules will give essentially the same crisp number as a five level system defined with 25 rules. A careful selection of membership function levels, or terms, can allow the fuzzy system to execute faster without impacting the results. These savings are during the development phase. For implementation into controller software a lookup table can be generated instead of executing each of the rules for each step through the control logic.

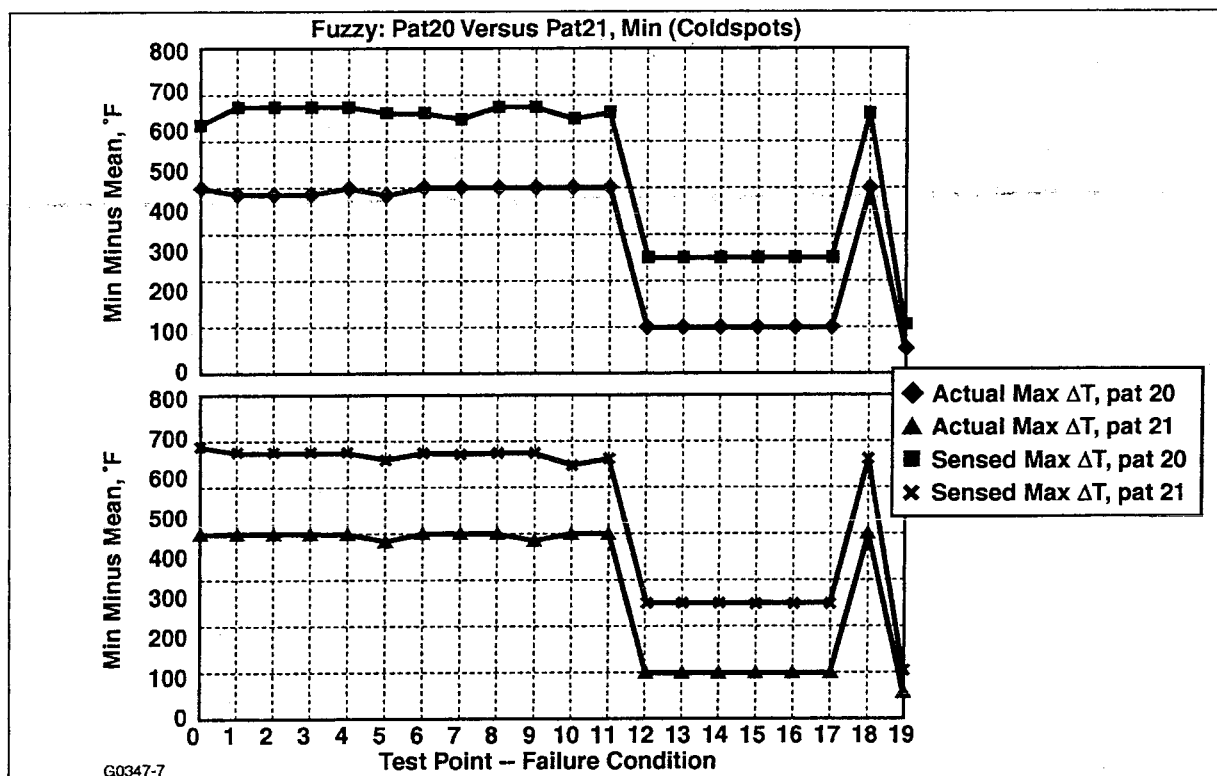
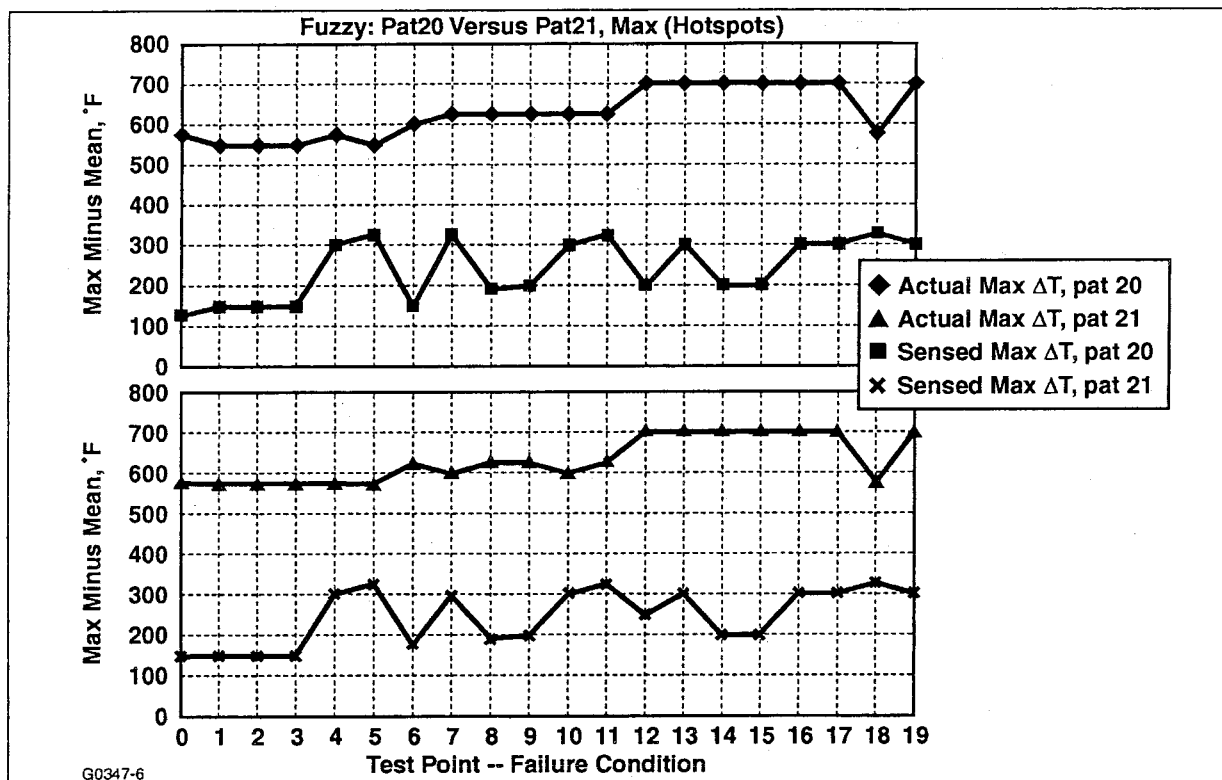


Figure 18. Test run comparisons for hybrid seven-level (pat 21 – 19 rules) fuzzy control versus PI control. Same test runs as Figure 17, except failure modes are regrouped.

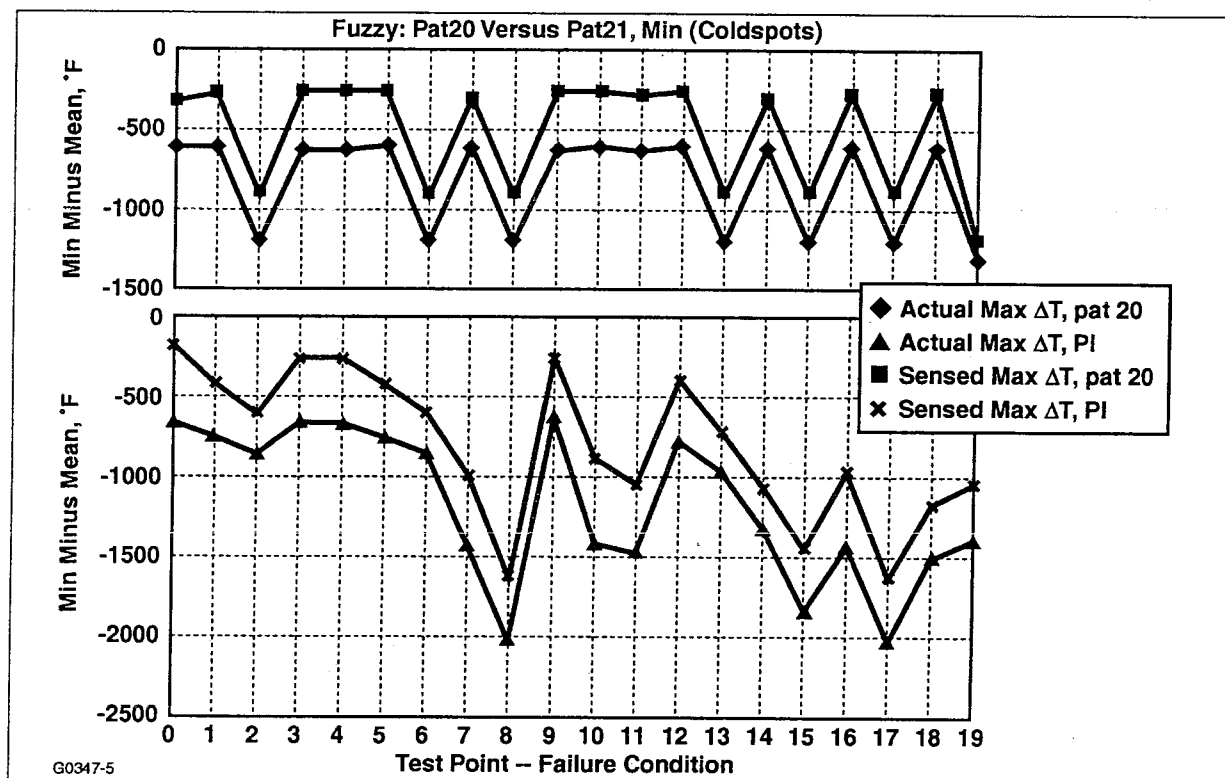
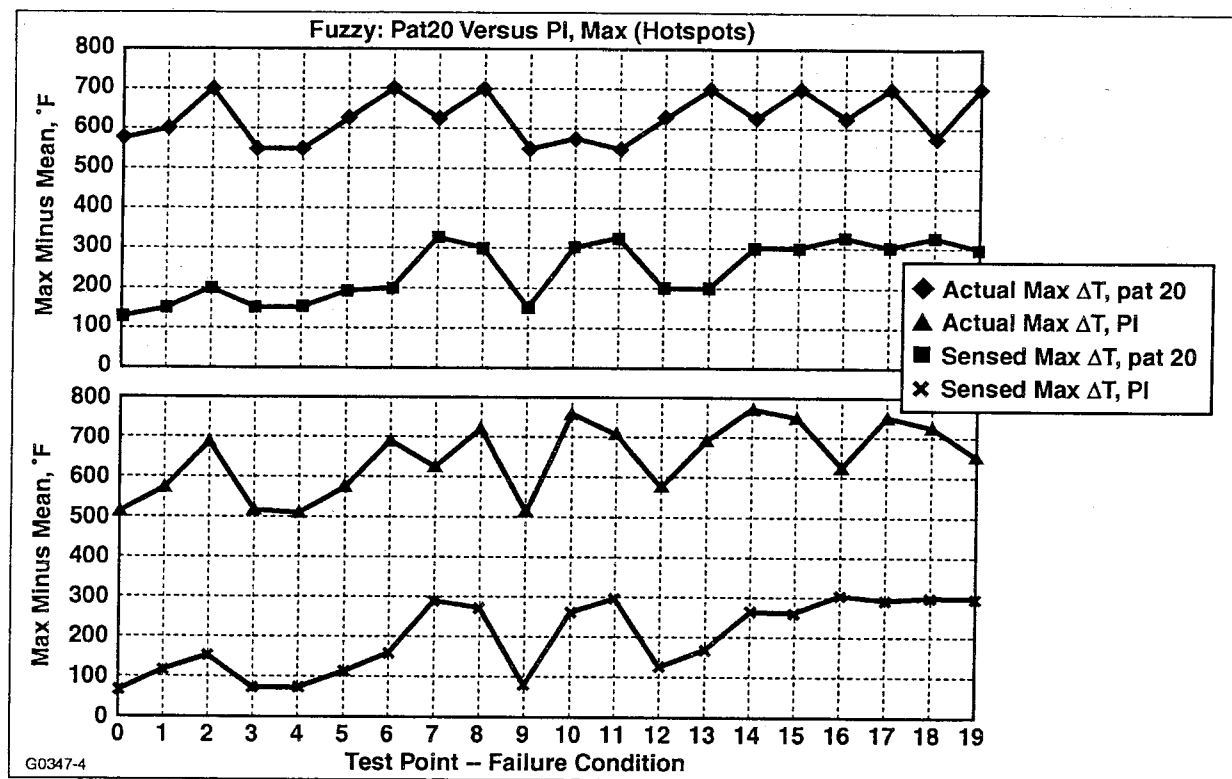
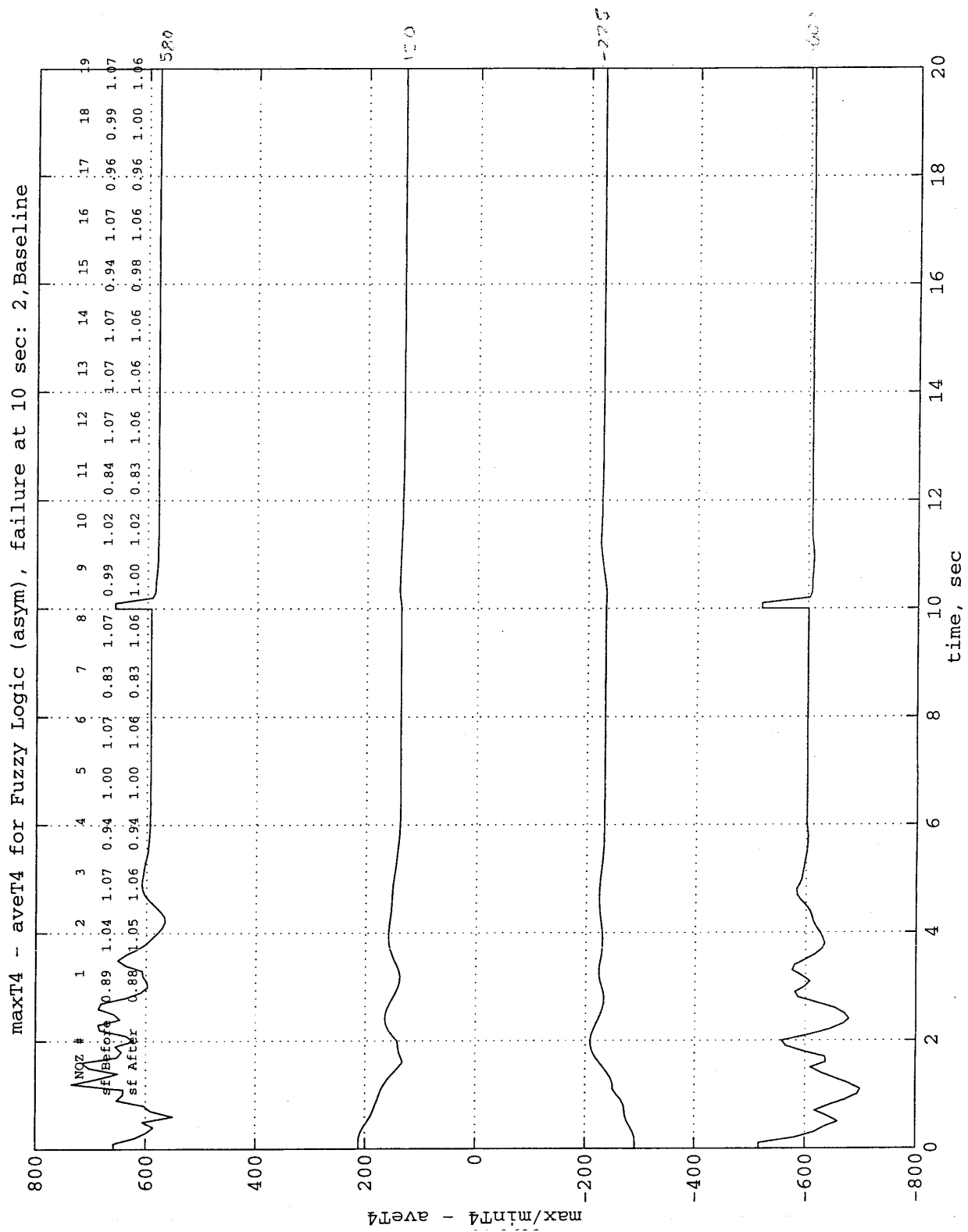
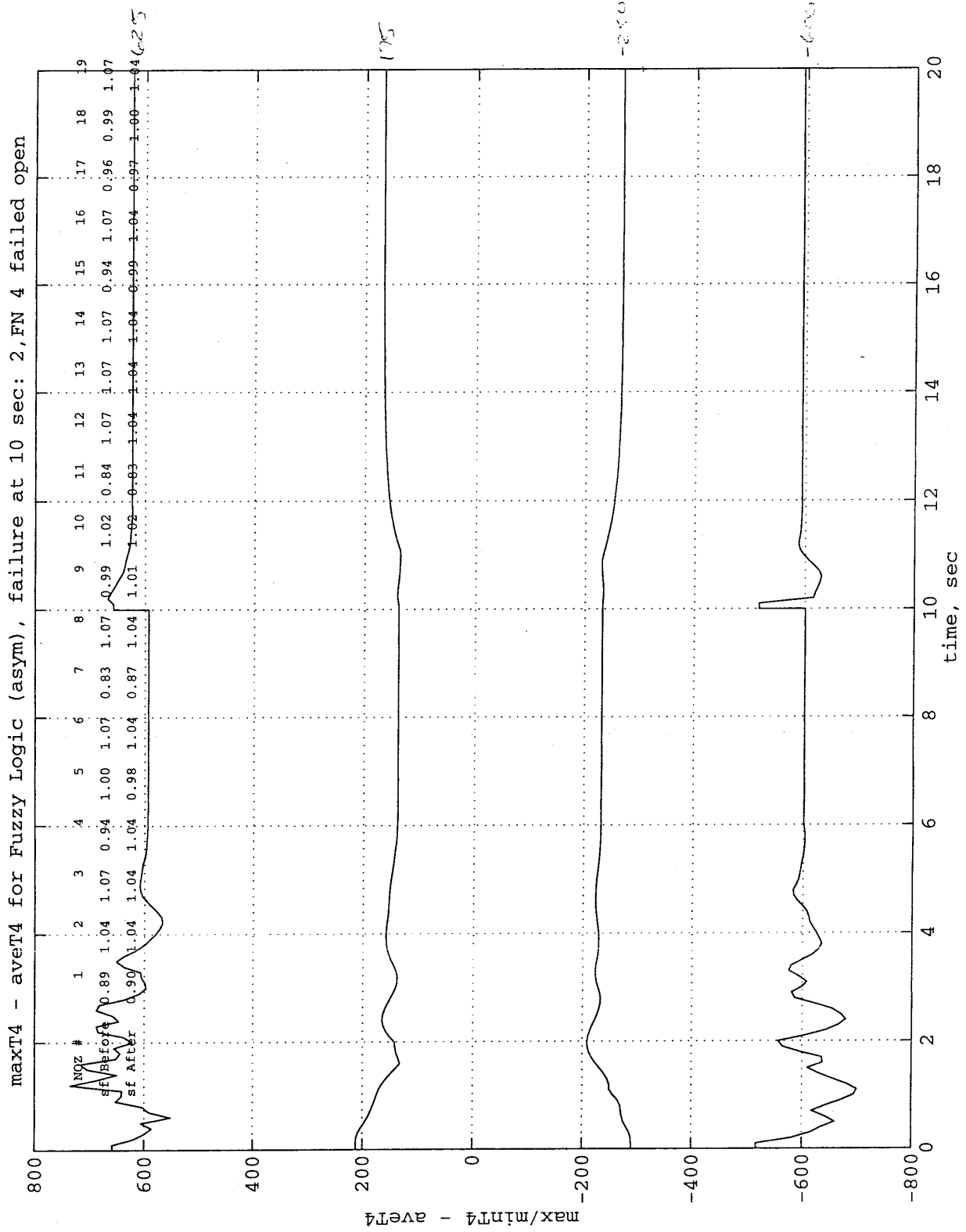
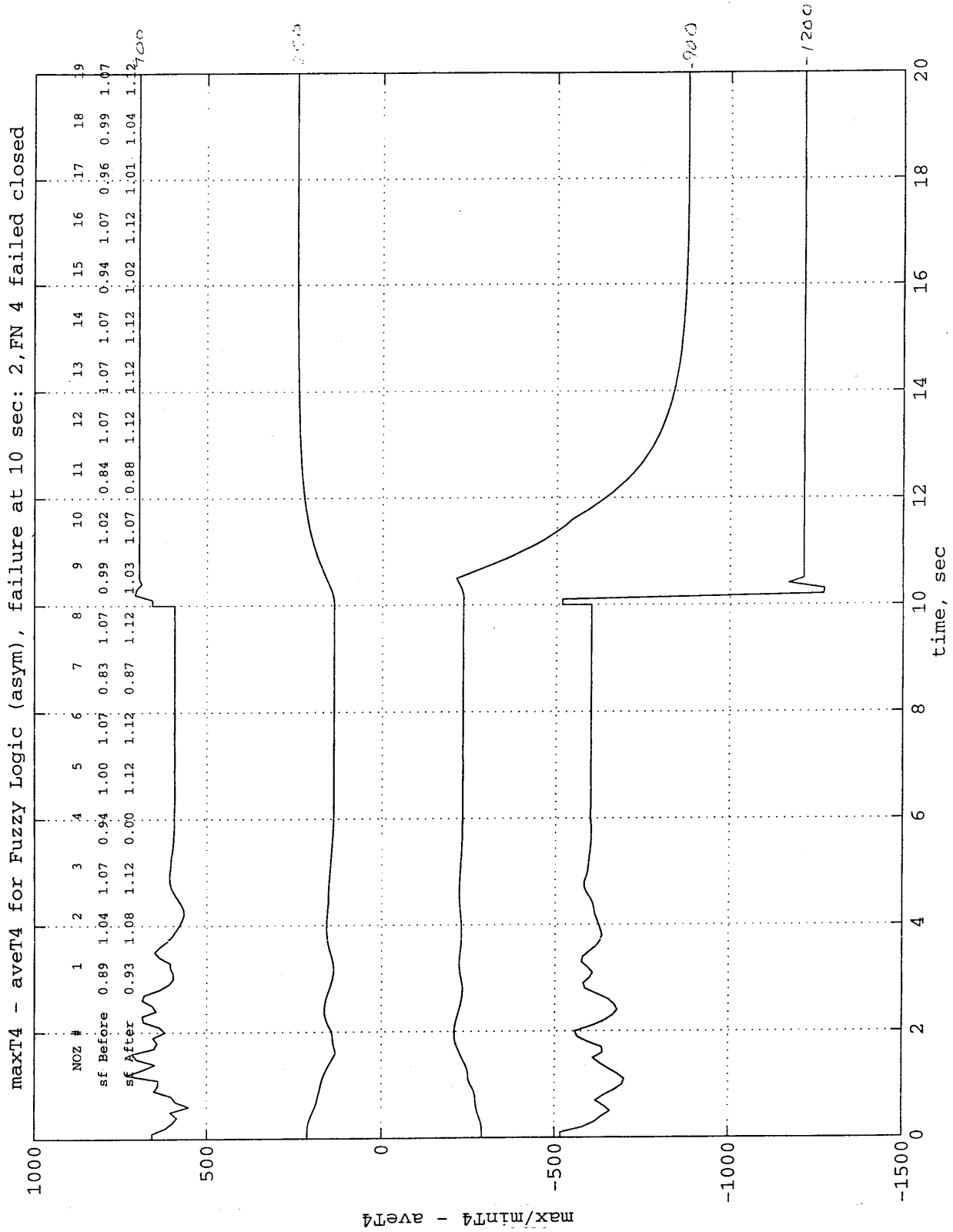
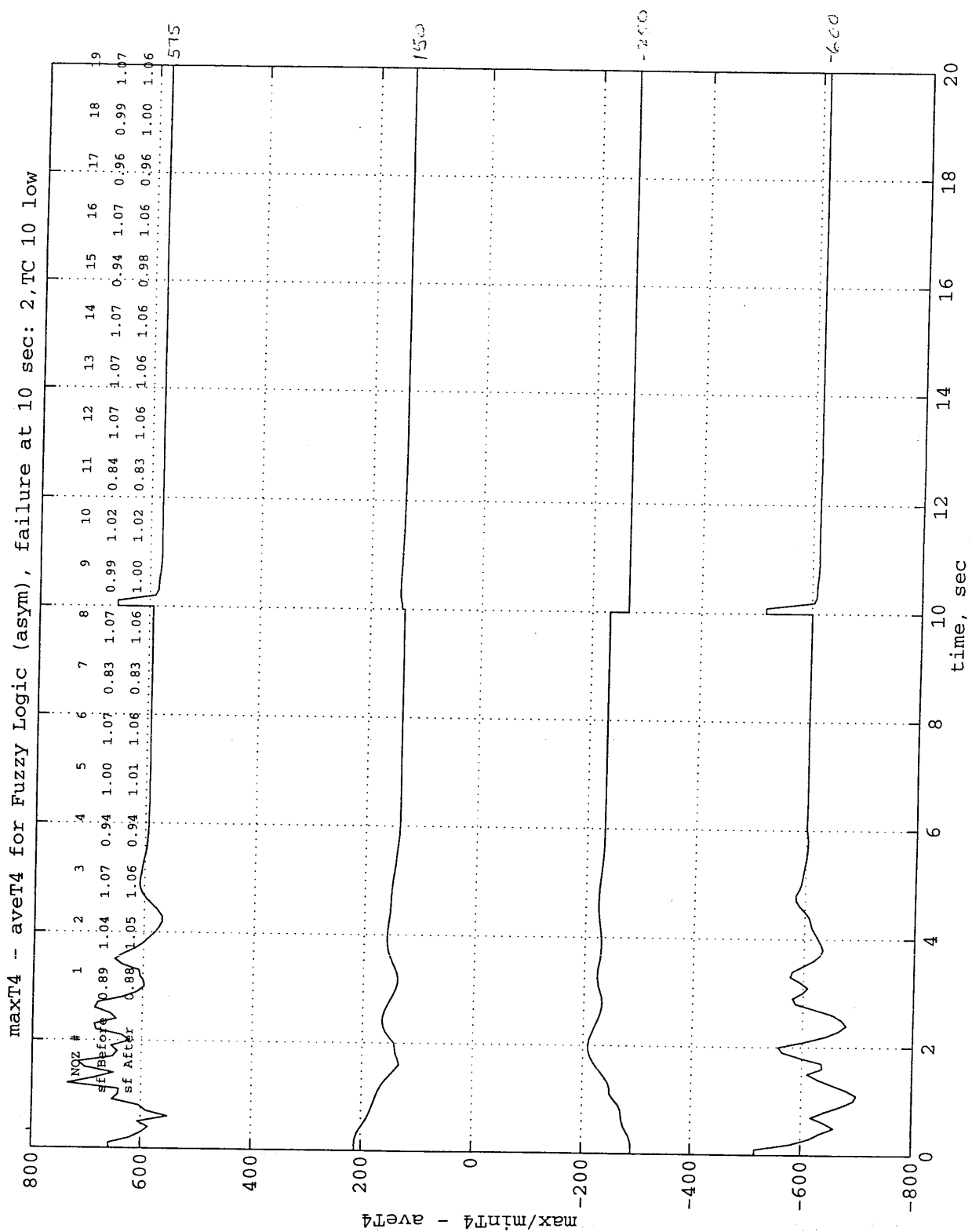


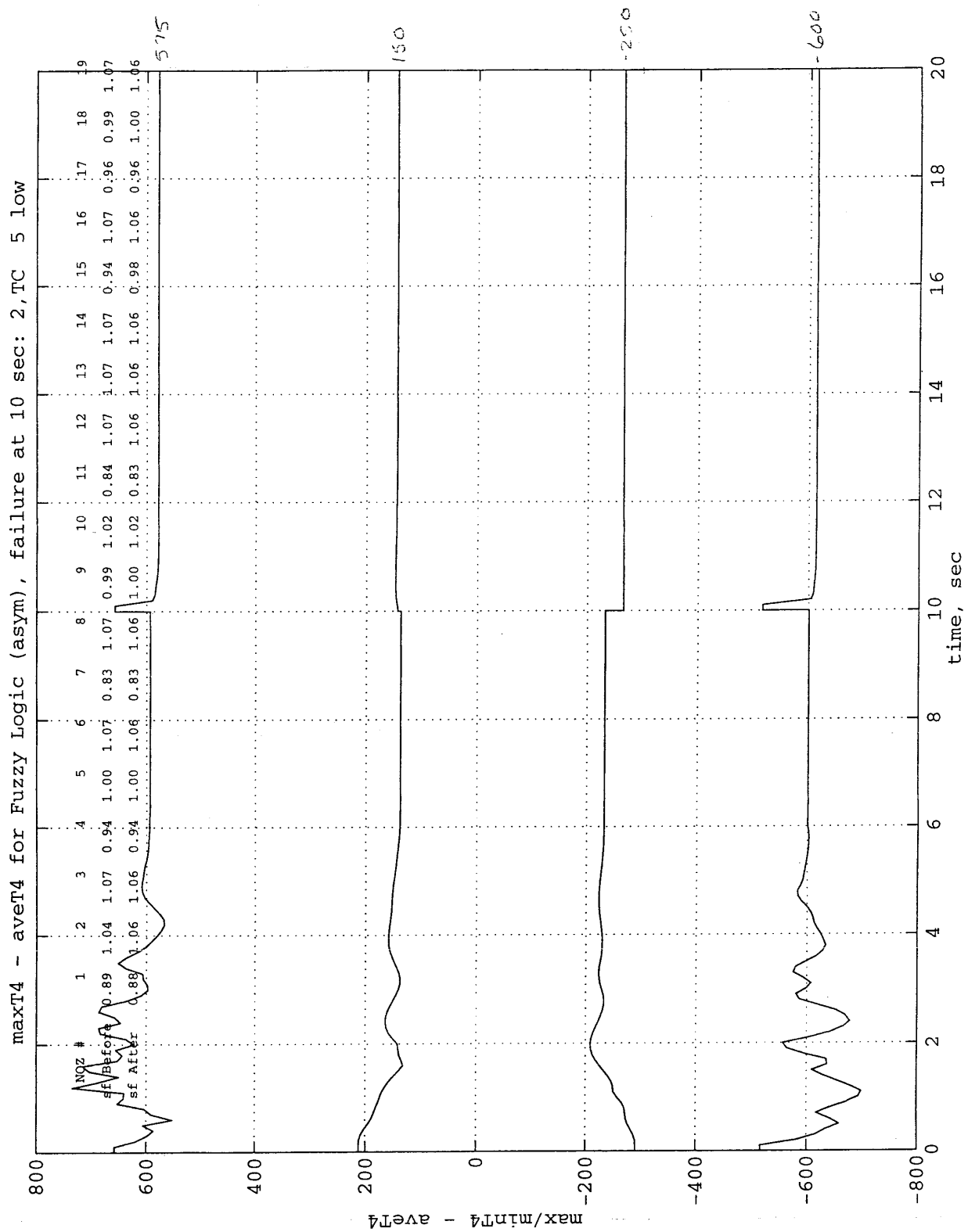
Figure 17. Test run comparisons for hybrid even-level (pat 21 – 19 rules) fuzzy control versus PI control.

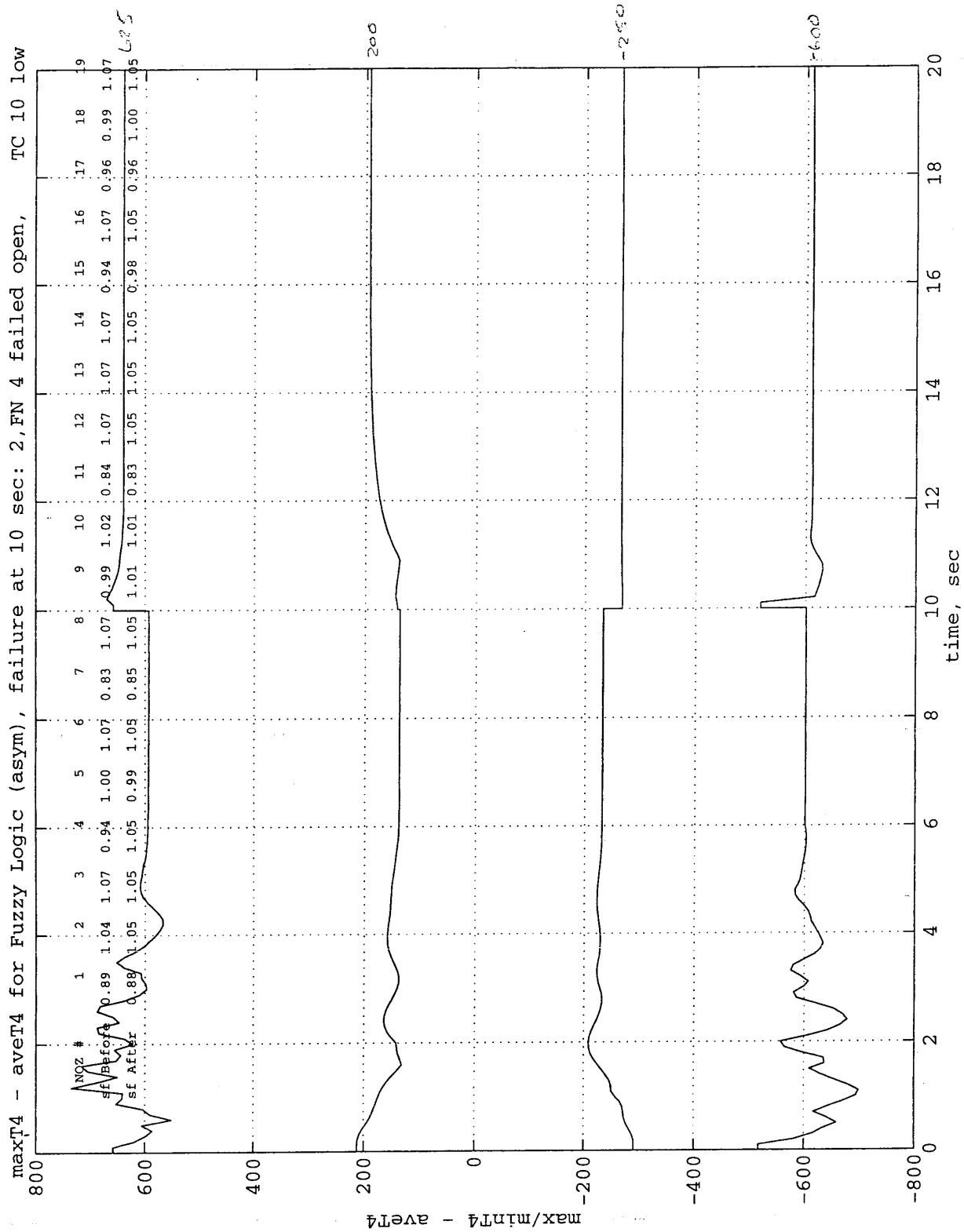


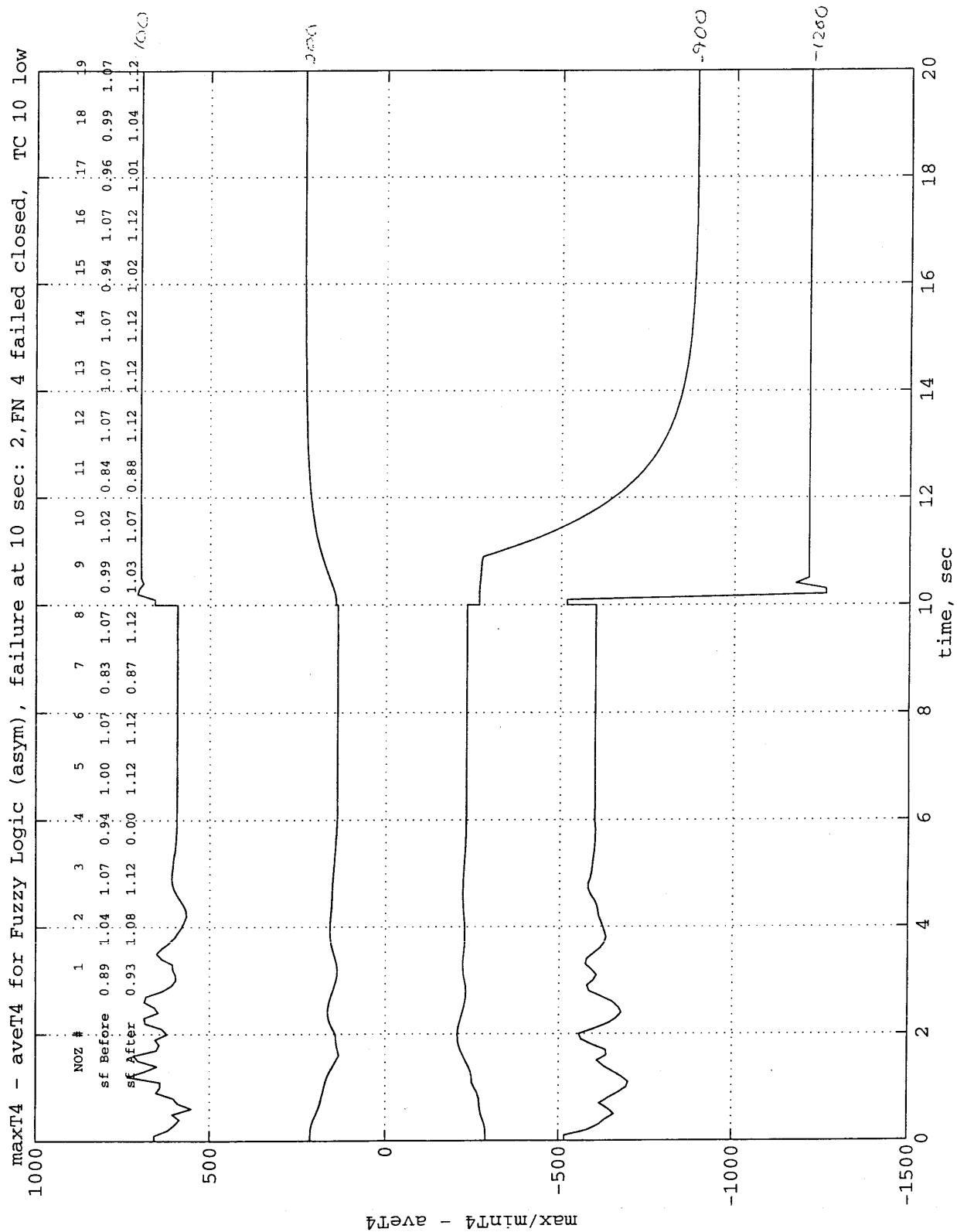


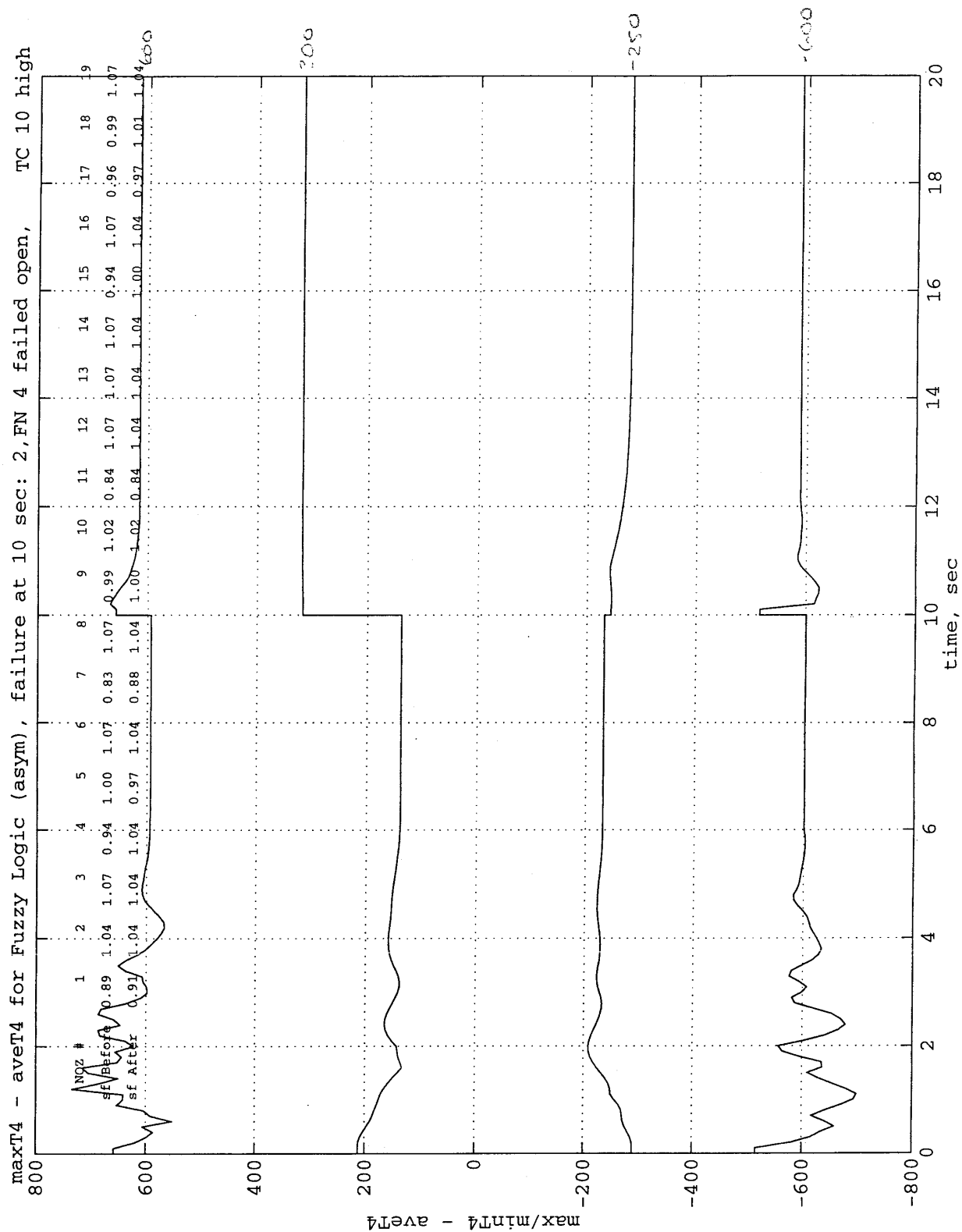




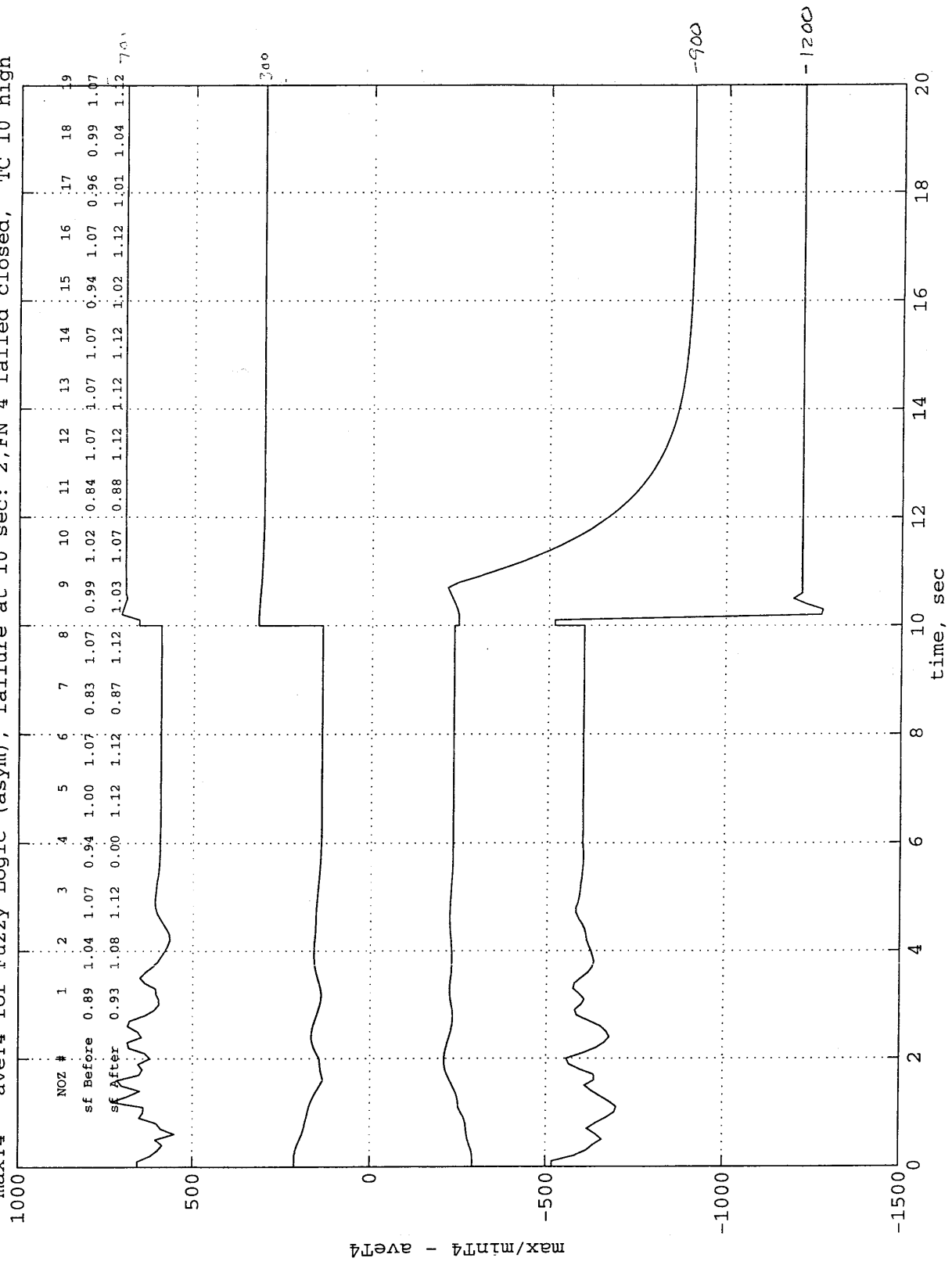




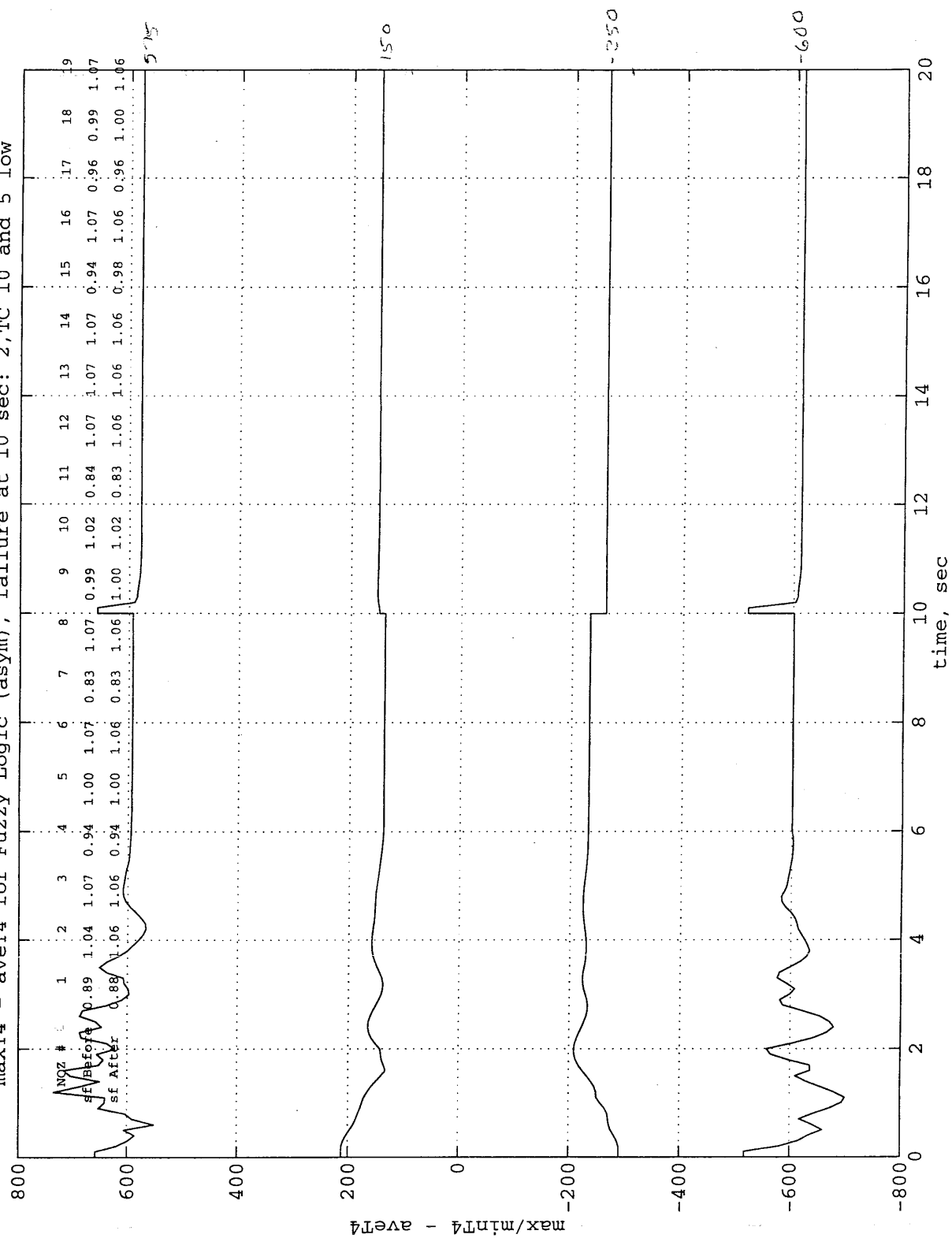




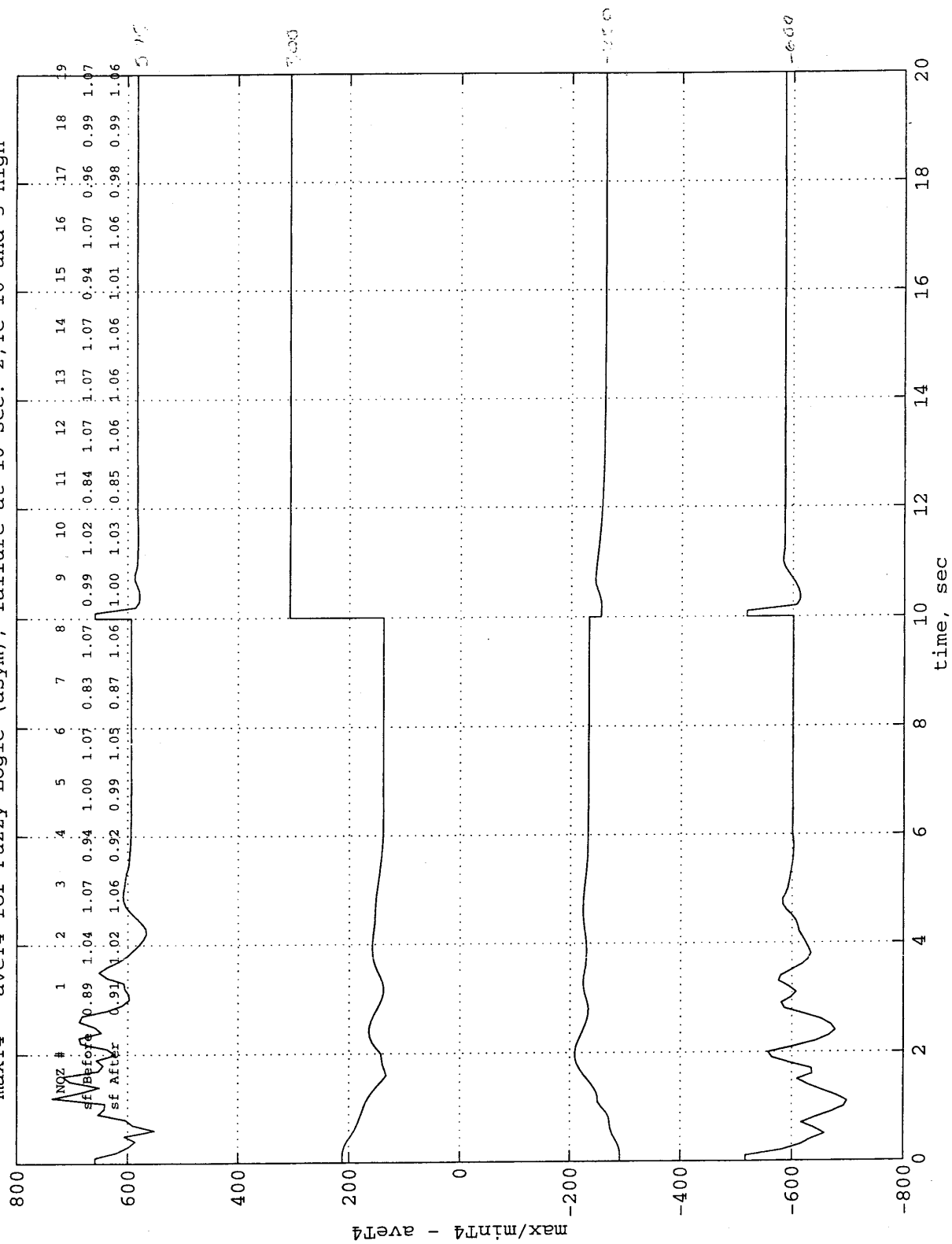
maxT4 - aveT4 for Fuzzy Logic (asym), failure at 10 sec: 2, FN 4 failed closed, TC 10 high

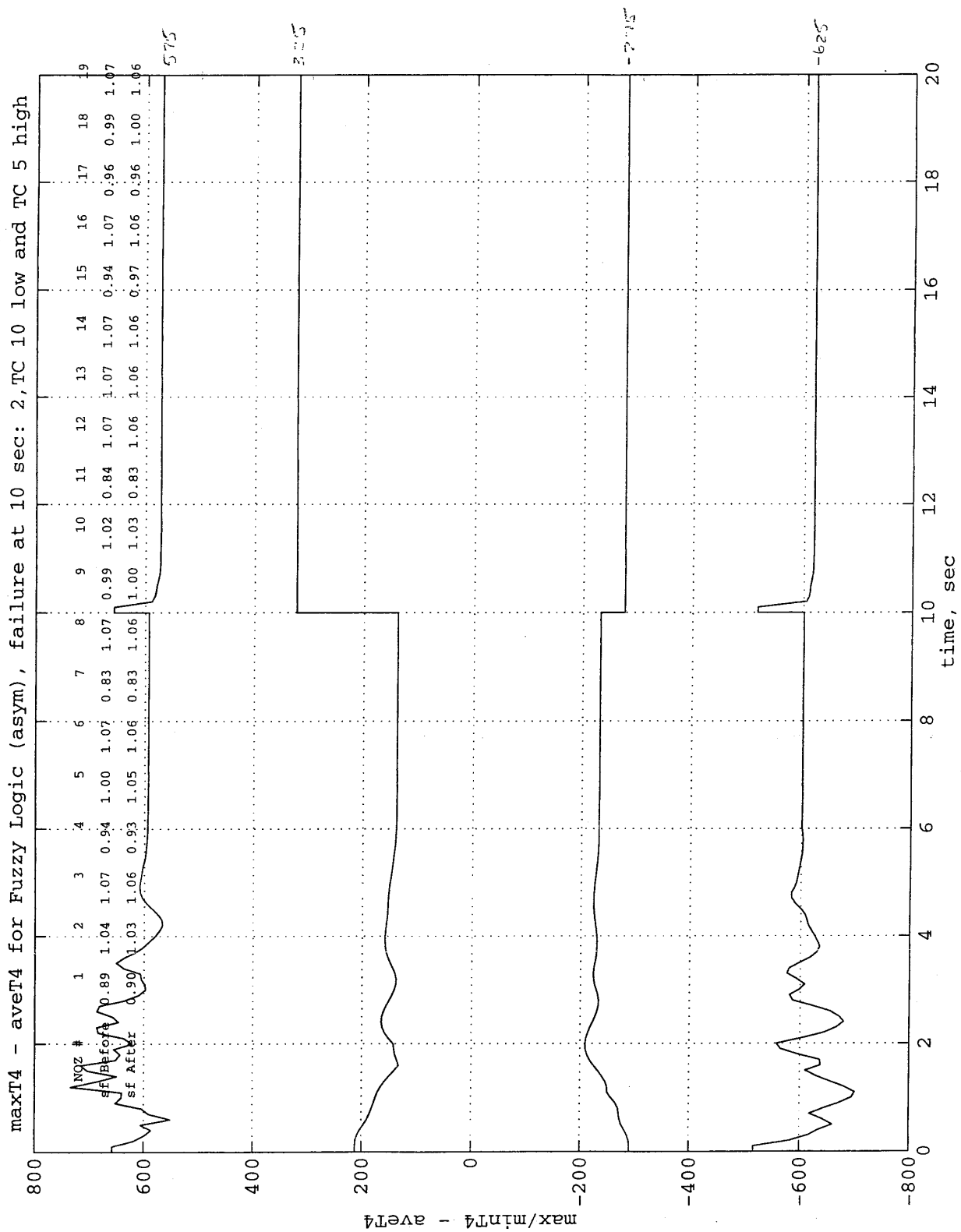


maxT4 - aveT4 for Fuzzy Logic (asym), failure at 10 sec: 2, TC 10 and 5 low

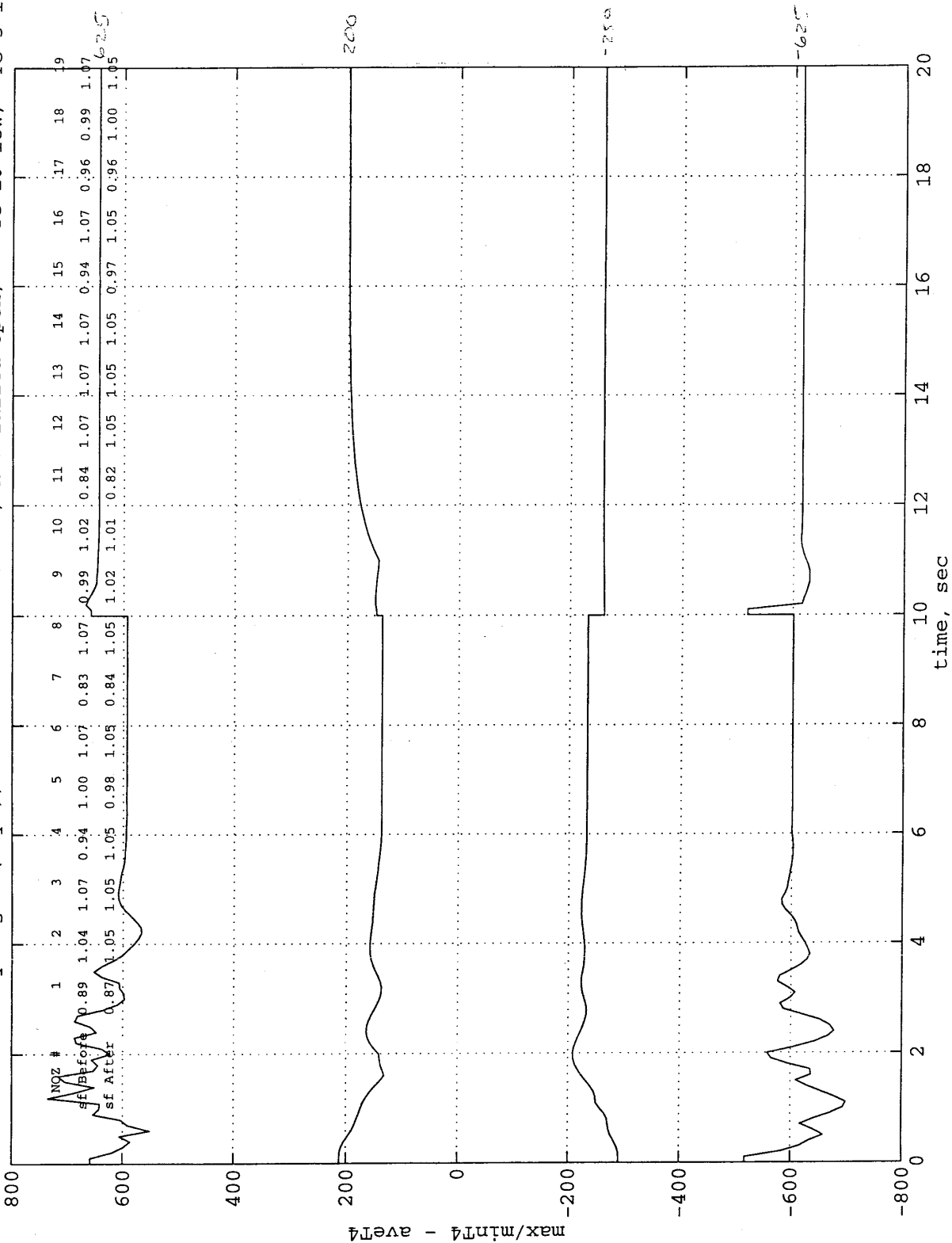


maxT4 - aveT4 for Fuzzy Logic (asym), failure at 10 sec: 2, TC 10 and 5 high

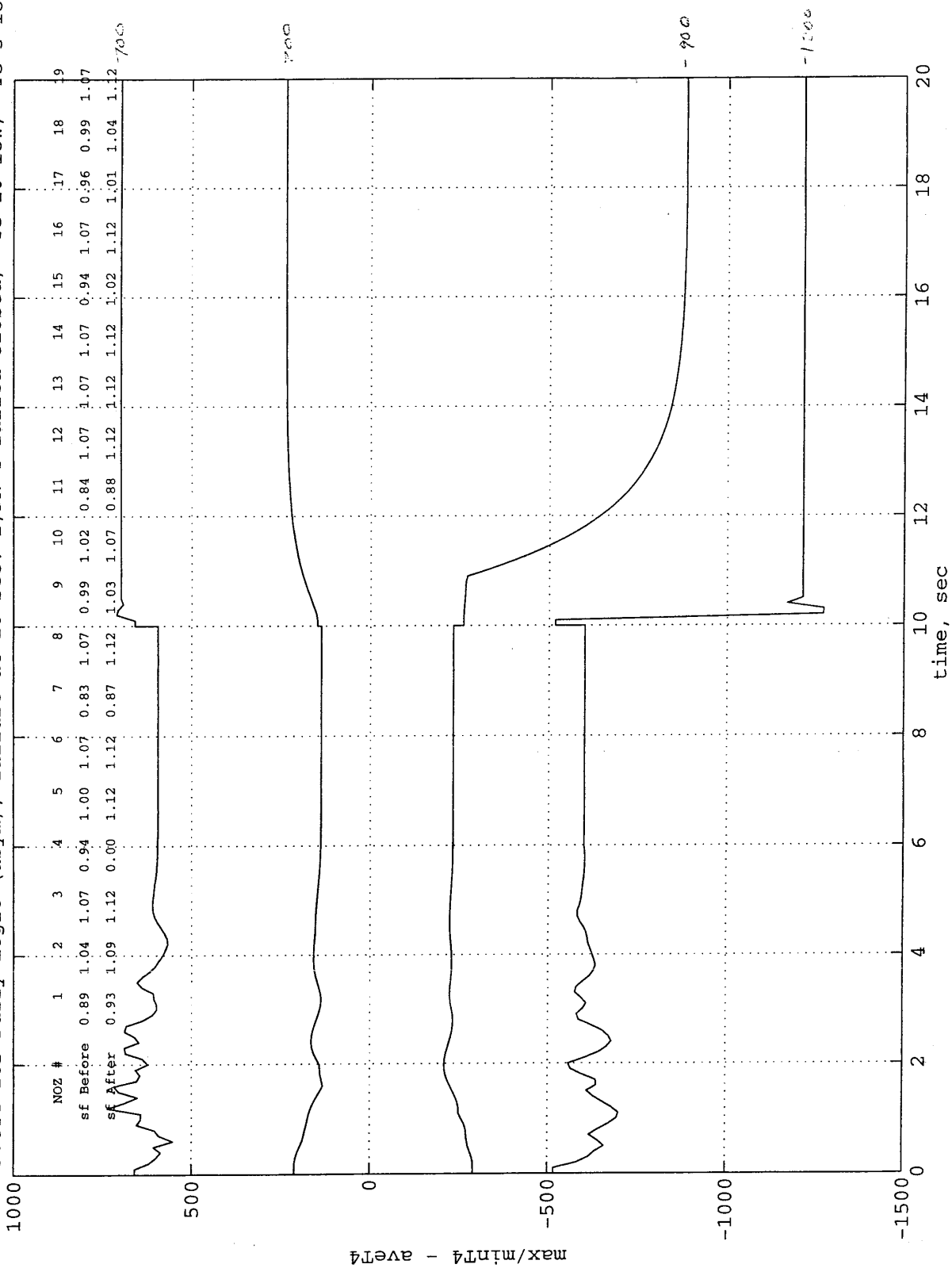




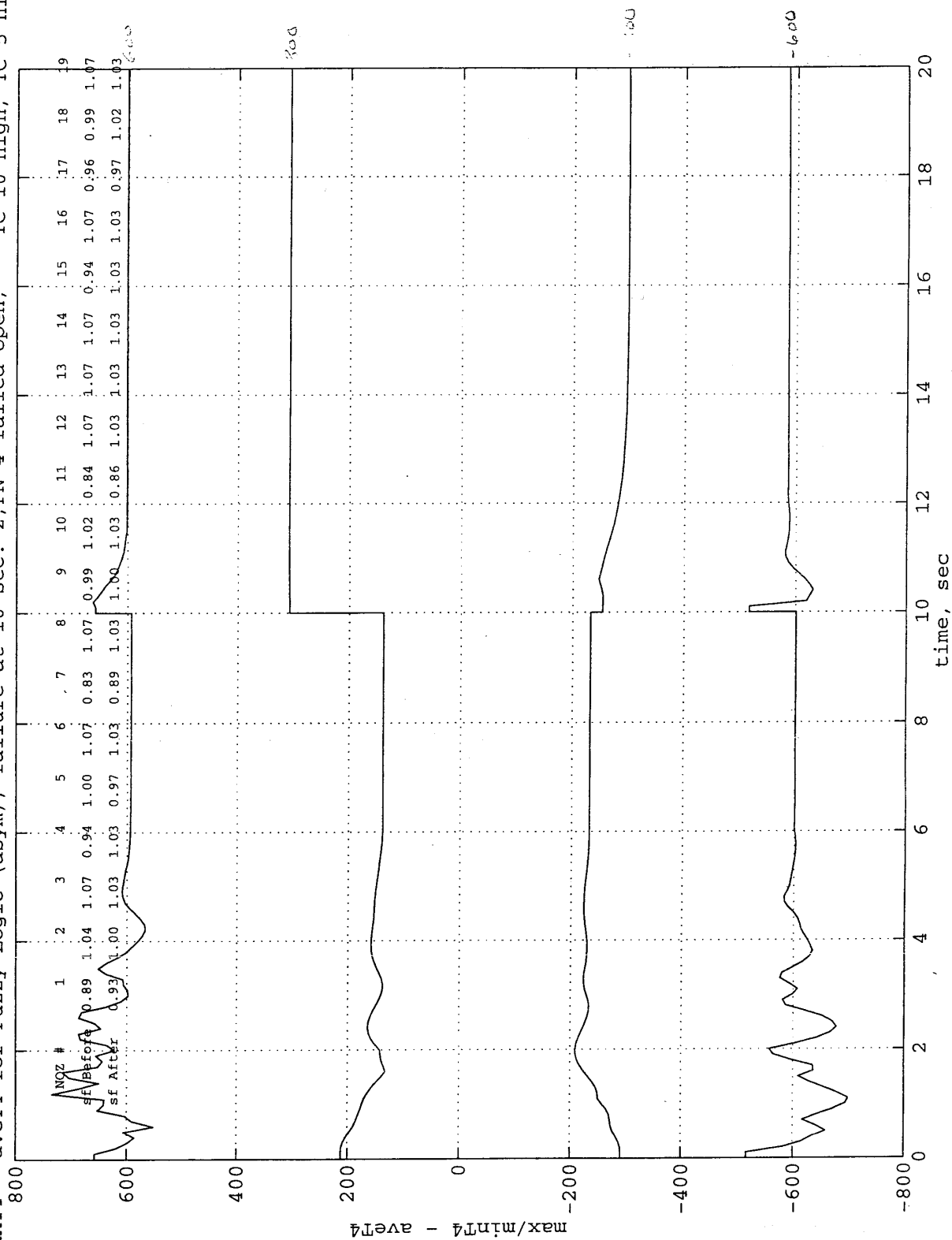
maxT4 - aveT4 for Fuzzy Logic (asym), failure at 10 sec: 2, FN 4 failed open, TC 10 low, TC 5 low



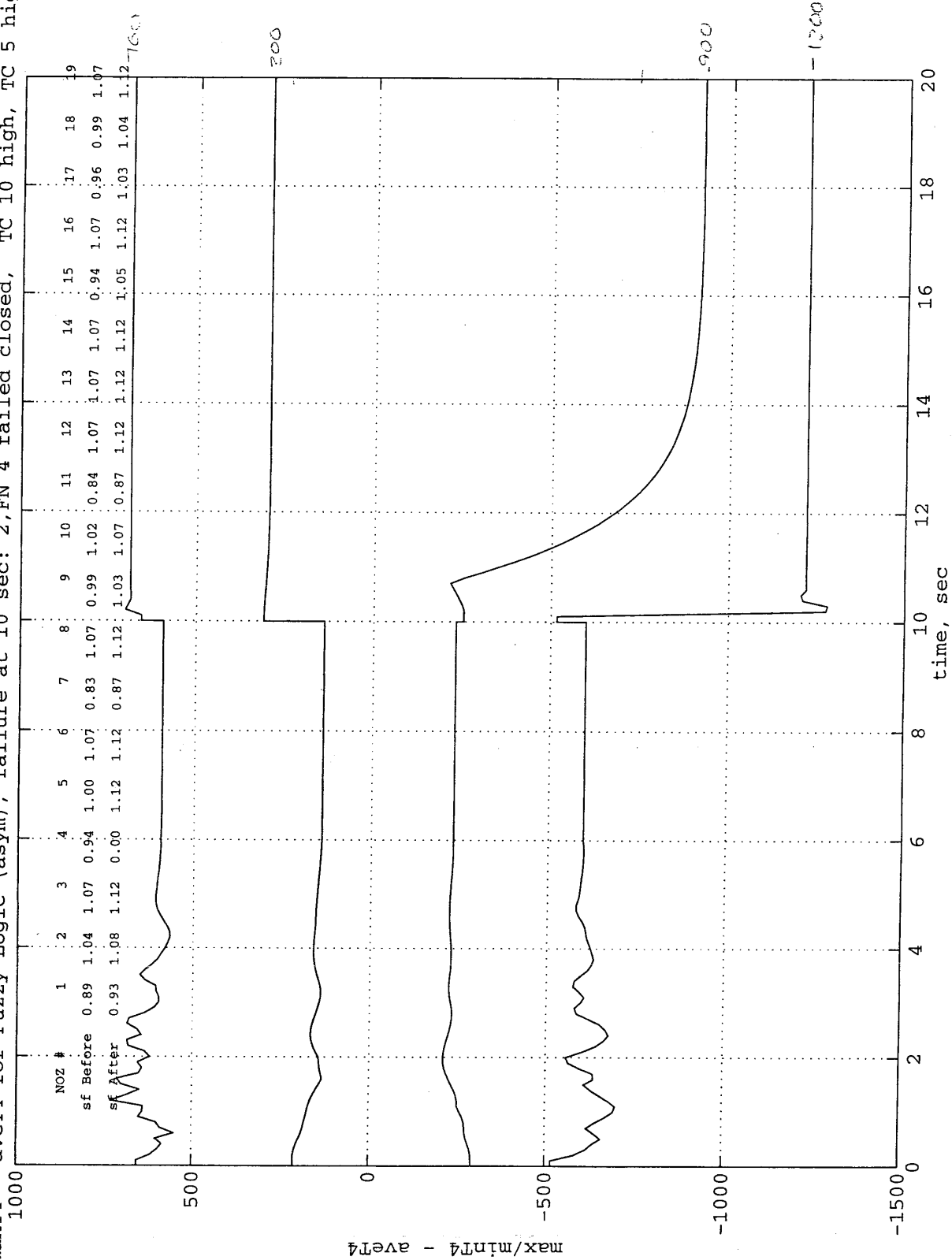
maxT4 - aveT4 for Fuzzy Logic (asym), failure at 10 sec: 2 FN 4 failed closed, TC 10 low, TC 5 low



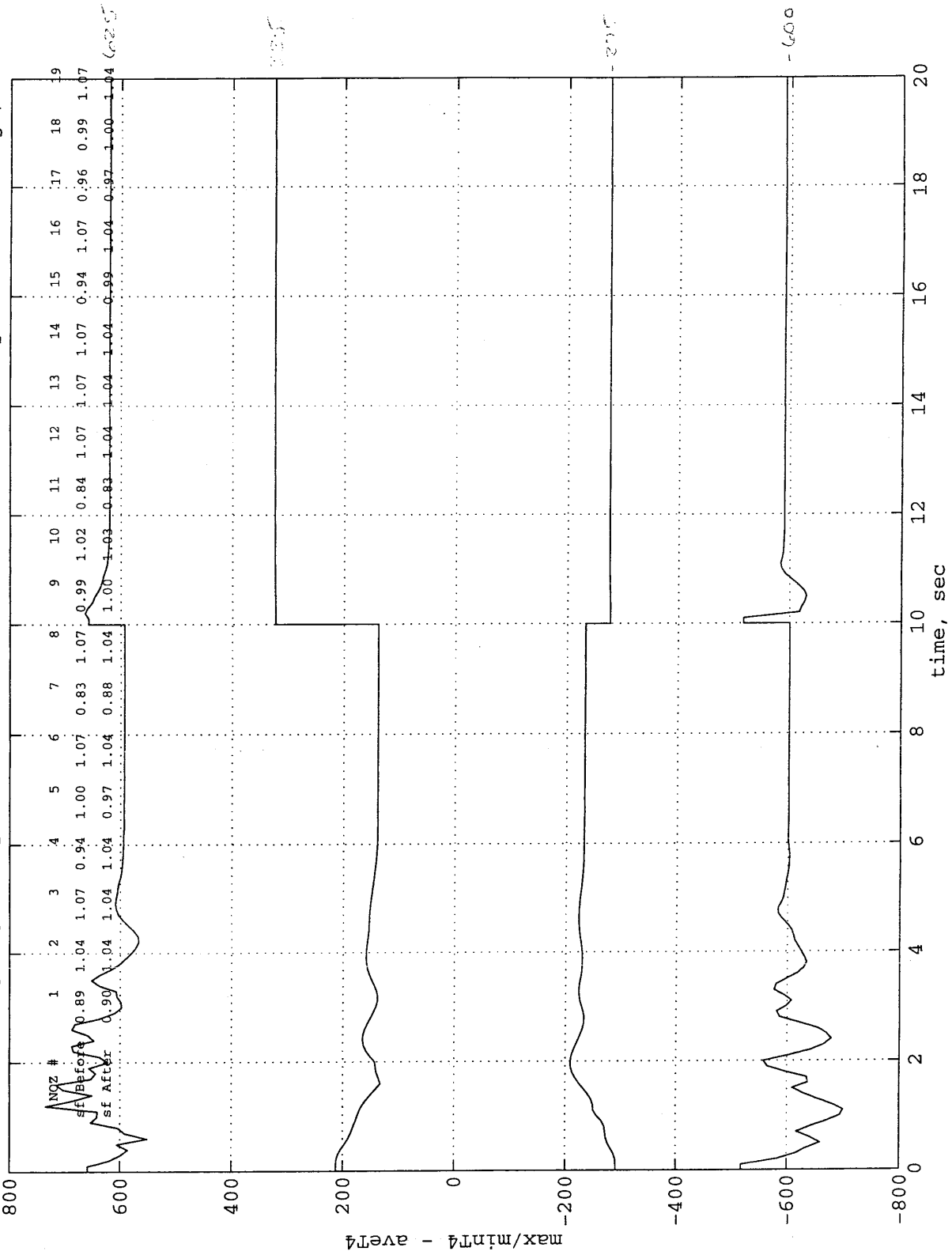
maxT4 - aveT4 for Fuzzy Logic (asym), failure at 10 sec: 2, FN 4 failed open, TC 10 high, TC 5 high



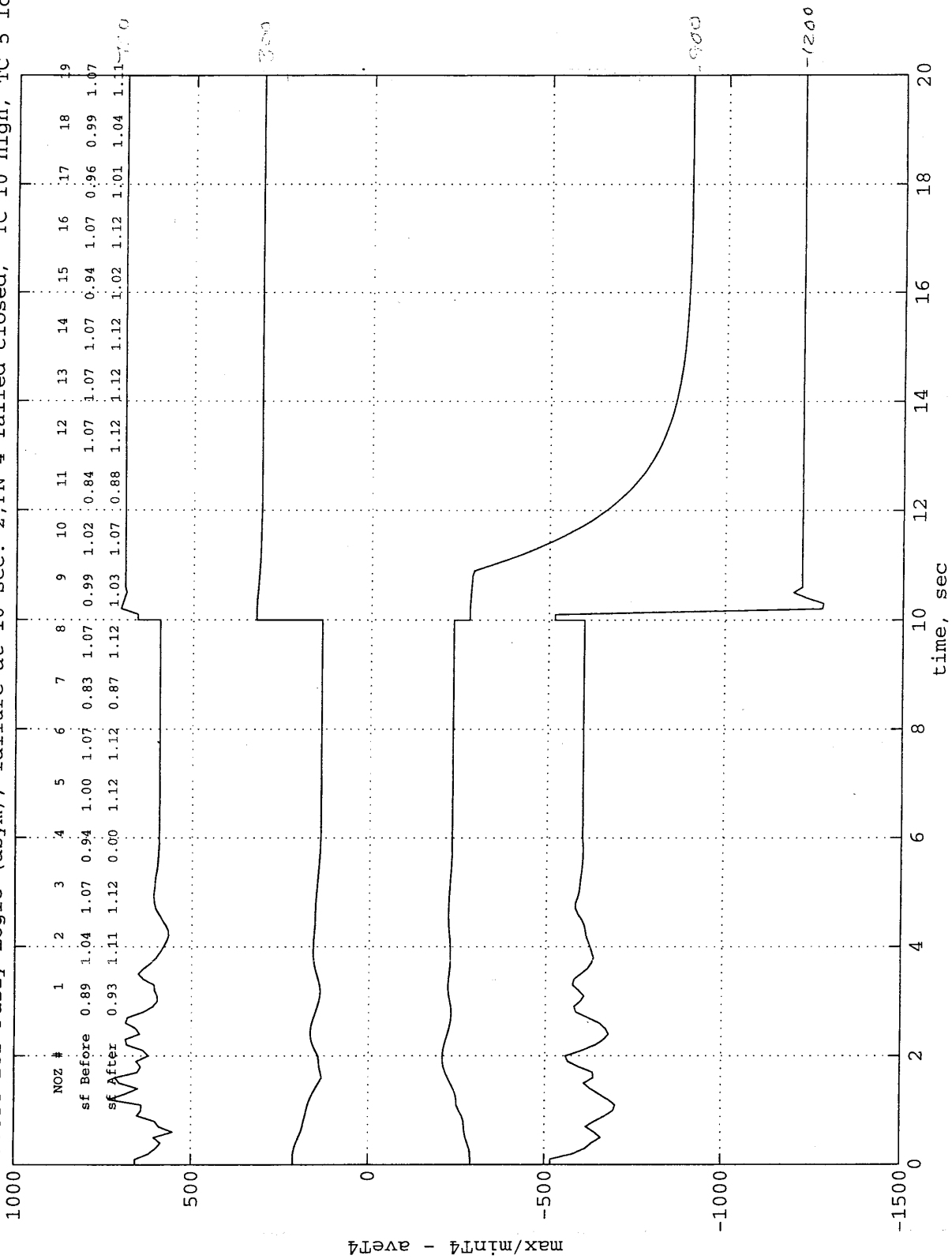
maxT4 - aveT4 for Fuzzy Logic (asym), failure at 10 sec: 2, FN 4 failed closed, TC 10 high, TC 5 high



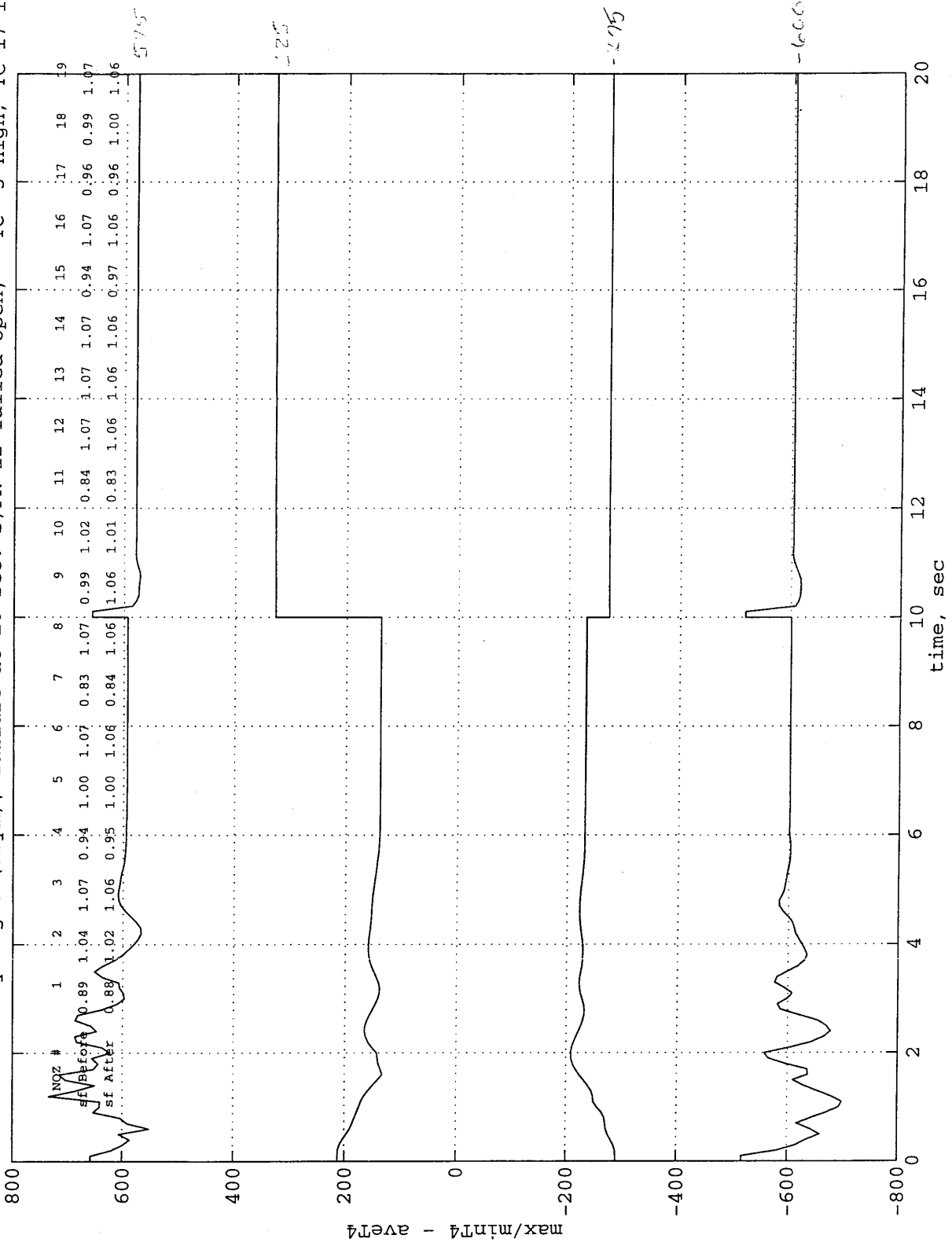
maxT4 - aveT4 for Fuzzy Logic (asym), failure at 10 sec: 2,FN 4 failed open, TC 10 high, TC 5 low



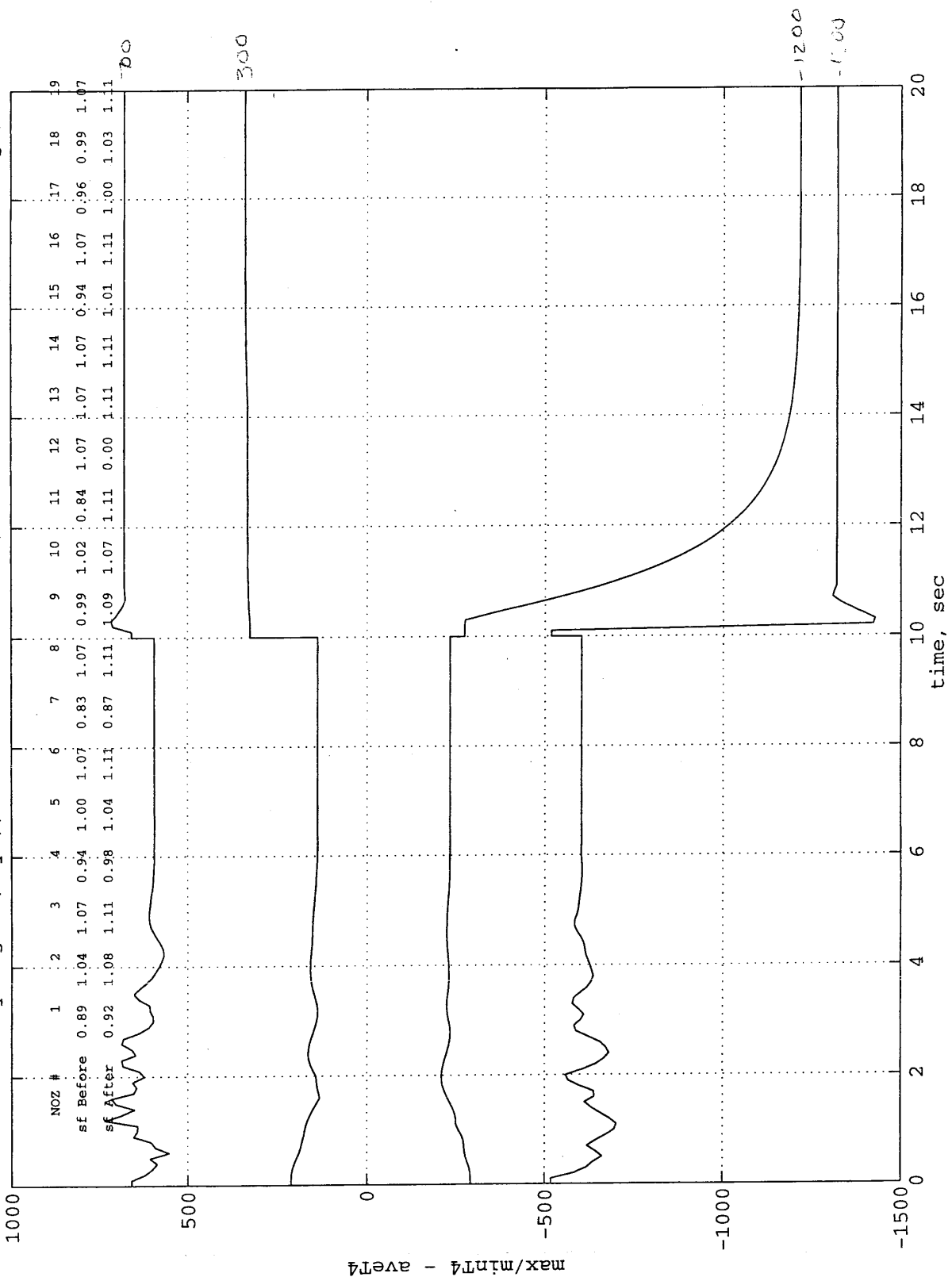
maxT4 - aveT4 for Fuzzy Logic (asym), failure at 10 sec: 2, FN 4 failed closed, TC 10 high, TC 5 low



maxT4 - aveT4 for Fuzzy Logic (asym), failure at 10 sec: 2, FN 12 failed open, TC 3 high, TC 17 low



maxT4 - aveT4 for Fuzzy Logic (asym), failure at 10 sec: 2, FN 12 failed closed, TC 3 high, TC 17 low



APPENDIX IV

SOFTWARE REQUIREMENTS SPECIFICATION FOR THE PATTERN FACTOR CONTROLLER

(32 pages)

1. INTRODUCTION: SYSTEM DESCRIPTION

The Pattern Factor Controller is a personal-computer (PC) based controller that incorporates ISA Bus I/O boards to provide the basic I/O functions required by the system. The system to be controlled consists of 19 pulse-width-modulated (PWM) fuel-flow modulator (FFM) valves. Each valve meters fuel flow to a fuel nozzle. A valve may be static open for full flow, static closed for no flow, or modulated to some partial flow. A modulated valve will be commanded open and shut during a frame time determined by the PWM repetition rate. There are 38 thin-film S type thermocouples mounted to a stator wheel that are used to measure the temperatures. The temperature extremes determine the pattern factor. The purpose of this control is to provide research into various strategies to minimize the pattern factor by attempting to create a uniform temperature distribution. In Figure IV-1, the nozzles (each with a modulated valve) are indicated as circles.

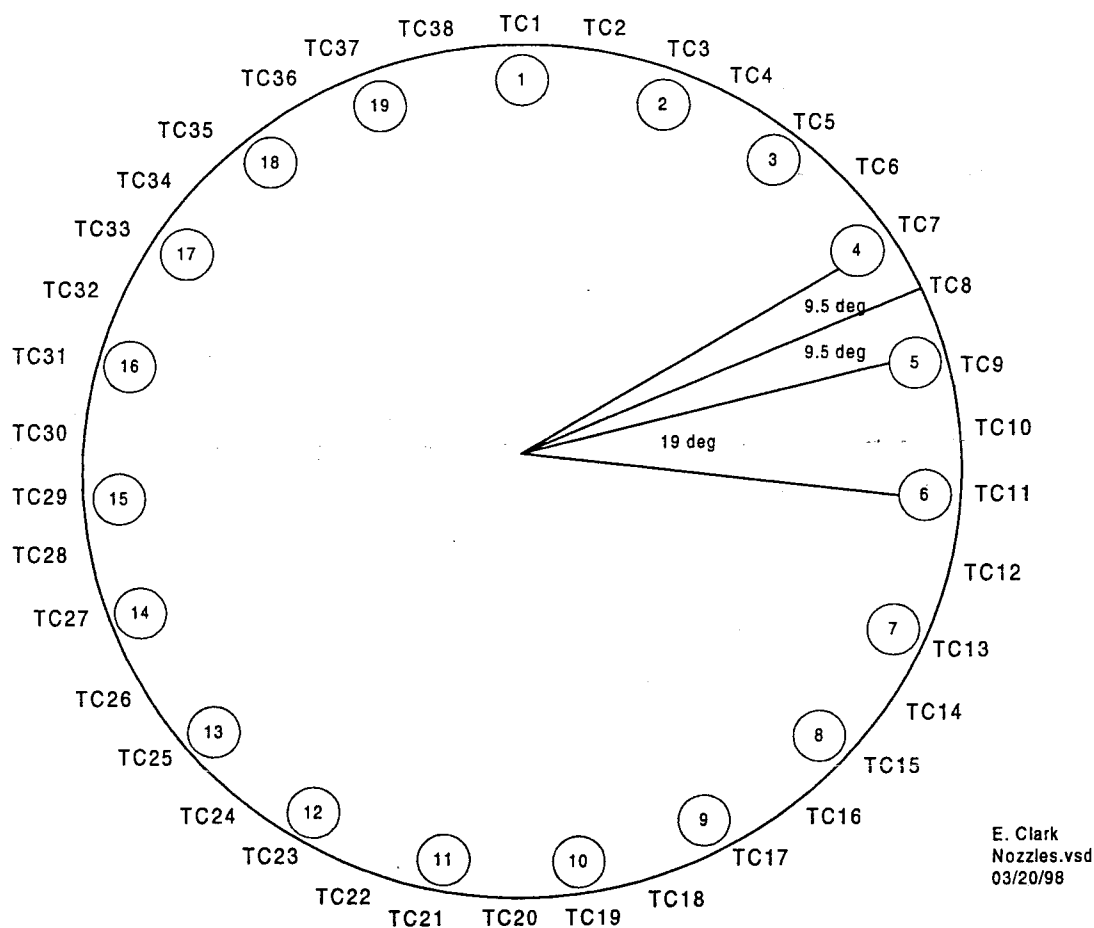
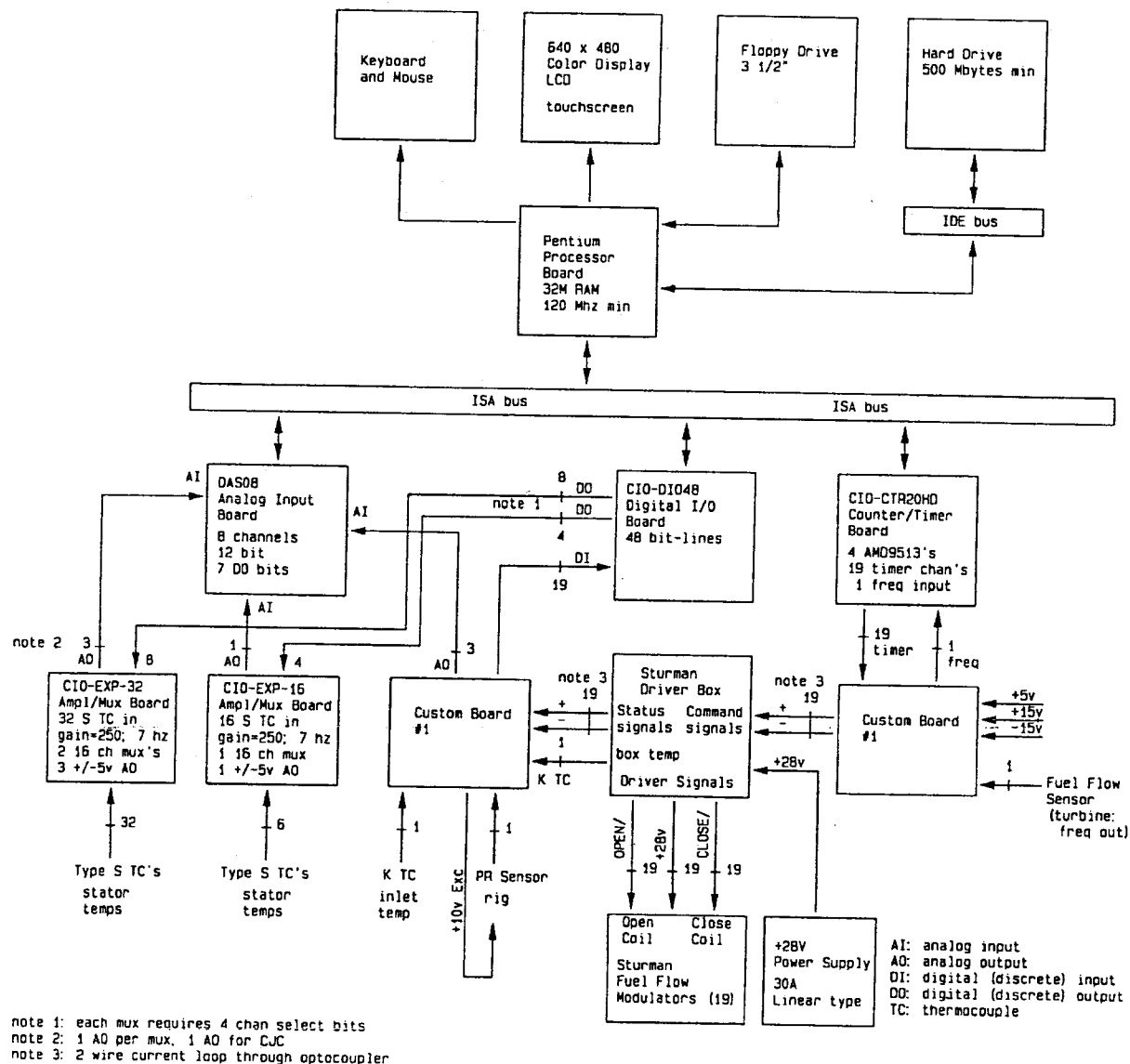


Figure IV-1. Thermocouple/Nozzle-Valve Orientation.

An FFM driver box (designed by Sturman Industries) receives PWM command signals from the controller and provides the drive currents to the fuel flow modulator valves. The driver box also provides status signals back to the controller regarding FFM/driver operation. Figure IV-2 shows the system architecture.



G8404-12

Figure IV-2. Active Combustor Pattern Factor Controller (ACPFC) System Architecture.

1.1 PC Platform

The target platform is a Hewlett Packard (HP) Vectra 5/90 PC that incorporates a Pentium processor running at 90 MHz. It incorporates four ISA slots, two of which are occupied by the add-in I/O boards selected for this program. There are 16 Mbytes of RAM available. The system timer peripheral is manipulated to provide a real-time clock to set up a fixed processing update rate.

1.1.1 CIO-DAS1602/16 Multifunction Board

This board is a multifunction Analog-to-Digital (A/D) card that includes 16 A/D channels with 16-bit resolution. It also includes 32 discrete bit lines, and a timer peripheral. This board is I/O mapped to 0300H. Consult the board manual for programming details. Counter 0 of the 82C54 peripheral will be used to measure the fuel-flow sensor frequency signal.

1.1.2 CIO-CTR20HD Counter-Timer Board

This board provides twenty 16-bit timers and an internal time-base clock. Nineteen channels are used in Mode J, hardware triggered one-shot, to provide the required PWM command outputs.

The 20th channel is set up in rate generator (mode D) to provide a reference clock that runs at 10 times the PWM frequency. A clock generator circuit on the custom board uses this clock to develop gate triggers for the 19 PWM timer outputs. This board is I/O mapped to 0310H. Consult the board manual and the AMD "MOS Microprocessors and Peripherals Manual" (1985) for programming details.

1.2 I/O Box

The I/O Box is an enclosure that incorporates one 32-channel thermocouple gain/multiplexor board, one 16-channel gain/multiplexor board, and the custom I/O board designed for this system. The 38 S and 2 K type thermocouple signals are conditioned in this box. The interface to the Sturman driver box is implemented on the custom board, as is the interface to the control panel and the interface to several other system sensors.

1.2.1 CIO-MUX32, CIO-MUX16 Gain/Multiplexor Boards

These boards differ only in the number of channels supported. Each channel is a differential input that is multiplexed to an INA110 instrumentation amplifier. The low and high side of the signal each have a 10K series resistor before the MUX. Optional solder pads on the boards have been configured such that a 1-uF filter capacitor is tied to the two 10K resistors, forming a 7-Hz hardware filter. Each thermocouple input has also been configured (via option solder pads) to tie in a biasing circuit so that an open thermocouple will cause a maximum downscale reading. The low side of each signal is also tied to signal common through a 100 K resistor. There are 3 multiplexors (3 banks) that each select 1 of 16 channels as commanded by 4 channel select bit lines under software (SW) control. Each bank output is wired to a separate analog input channel on the A/D board. There is also a cold-junction compensation (CJC) signal

that is a linear function of volts versus temperature that reads the temperature of one of these MUX boards near the termination connectors. This signal (the other board CJC temperature is assumed to be the same) is routed to an A/D channel for measurement. One channel of each bank measures a ground reference signal and one channel of each bank measures a 20-mV nominal signal. The gain of the MUX boards has been switch selected to 301. The reference inputs are measured and used to compensate for any offset/gain differences between the banks.

1.2.2 Custom I/O Board

This board provides signal conditioning and level shifting required between the I/O boards and the rest of the system: the driver box interface, the control panel interface, and several other sensors. It also complements the timer board operation to add circuitry required to implement hardware (HW) triggered PWM command outputs. The PWM trigger signals are dispersed over time to even out the demand on the 28V supply used to power the FFM's.

PFCKT1.DWG - PFCKT7.DWG are the schematics for this board.

1.2.3 Control Panel

The control panel provides an interface to the operator. There are 3 SW controlled indicators, 4 assignable pots, and 7 switches incorporated. The requirements associated with these functions are described in detail in paragraphs 3.14 and 3.3.2 of this document.

2. REAL-TIME AND OTHER PROCESSING REQUIREMENTS

The required processing frame time is 50 msec. The PharLap tnt DOS extender package is to be utilized to increase available memory beyond the 640K DOS boundary. This program is to run under the DOS operating system. The system timer peripheral is to be set up for the desired frame time. A real-time interrupt handler is to be used to respond to this HW signal to establish the real-time "foreground". A task dispatcher is to be created to parcel out processing tasks in an "input-process-output" arrangement. When the foreground task completes then a background task executes to provide operator interface support. Requirements for the operator interface are detailed in Sections 8 and 9 of this document.

3. INPUT/OUTPUT SIGNAL PROCESSING REQUIREMENTS

3.1 Analog Input Measurements

Table IV-1 shows the analog input (AI) channel assignments into the analog-to-digital (A/D) board. This board has been configured for bipolar measurements in the range of -10V to +10V. Table IV-2 shows the sensor assignments to the gain/multiplexor board inputs. A fullscale negative reading will yield an A/D count of 0. A fullscale positive reading will yield an A/D count of 65535. The following equation is used to scale a reading in volts:

$$\text{volts} = ((\text{AD_count} - 32768) / 32768) * 10.0.$$

Note that an open thermocouple will lead to a full downscale (-10V) signal out of the amplifier when connected to that thermocouple.

Table IV-1 - Analog Input Channel Assignments

| AI Channel | Signal Name | Voltage Range | Comment |
|------------|--------------|---------------|---|
| 0 | MUX32B1_OUT | -10 to 6V | MUX32 board bank 1 output |
| 1 | MUX32B2_OUT | -10 to 6V | MUX32 board bank 2 output |
| 2 | MUX16B1_OUT | -10 to 6V | MUX16 board bank 1 output |
| 3 | MUX32CJC_OUT | 0 to 2V | MUX32 board CJC output |
| 4 | P3 | 0 to 10V | - |
| 5 | I_SENSE | - | - |
| 6 | POT1 | 0 to 10V | - |
| 7 | POT2 | 0 to 10V | - |
| 8 | POT3 | 0 to 10V | - |
| 9 | POT4 | 0 to 10V | - |
| 10 | Spare | - | - |
| 11 | Spare | - | - |
| 12 | Spare | - | - |
| 13 | Spare | - | - |
| 14 | Spare | - | - |
| 15 | Gndref | 0V nom | Use to measure offset correction factor |

Table IV-2 - MUX Board Channel Assignments

| Channel | Bank 1 (MUX32 B1) | Bank 2 (MUX32 B2) | Bank 3 (MUX16 B1) |
|---------|-------------------|-------------------|-------------------|
| 0 | TC1 | TC14 | TC27 |
| 1 | TC2 | TC15 | TC28 |
| 2 | TC3 | TC16 | TC29 |
| 3 | TC4 | TC17 | TC30 |
| 4 | TC5 | TC18 | TC31 |
| 5 | TC6 | TC19 | TC32 |
| 6 | TC7 | TC20 | TC33 |
| 7 | TC8 | TC21 | TC34 |
| 8 | TC9 | TC22 | TC35 |
| 9 | TC10 | TC23 | TC36 |
| 10 | TC11 | TC24 | TC37 |
| 11 | TC12 | TC25 | TC38 |
| 12 | TC13 | TC26 | spare |
| 13 | T3 (K) | Tdriver (K) | spare |
| 14 | gndref_0 | gndref_1 | gndref_2 |
| 15 | 20mvref_0 | 20mvref_1 | 20mvref_2 |

3.1.1 Temperature Measurements

3.1.1.1 Mux Bank Offset/Gain Compensation

The thermocouple signal assignments are intended to group adjacent thermocouples to the same bank to the extent possible. The gndref signals simply jumper the high, low inputs of the

input channel together. The 20mvref signal was measured at 19.52 mV using an external voltmeter. Apply a low pass filter with a 1-second time constant to these reference measurements before performing the following calculations for each of the 3 banks

Bank gain = (20mvref reading (volts)- gndref reading (volts)) / 0.01952

Bank offset = gndref reading (volts)

Bank factor = 1000.0 / Bank gain; (used by temperature calculation)

Do a one-time calibration after the system has been operating for 40 seconds. On 100 successive frames, make measurements and calculate final values based on an average of these 100 readings. The default values for the three bank gains are to be set to 301 in the initialization process. The default values for the bank offsets are to be set to 0. The BITE logic monitors the reference signal readings. A failure of any of these signals shall cause the default gain and offset values to be used. Execution of the calibration routine causes these gains and offset values to be trimmed to reflect the average measured values.

Use the FGseconds variable and a latching cal_done flag to mechanize the operation of this:

IF ((cal_done FALSE) AND (FGseconds > 40)) THEN calibrate_muxes();

The monitor can be used to clear the cal_done flag to request an updated calibration at any time in the run.

3.1.1.2 Cold Junction Temperature Measurement / Compensation

The gain / MUX boards each provide an on-board temperature sensor intended to measure the ambient temperature of the signal connector terminals that the thermocouples are wired to. This is a linear electronic sensing element with the following transfer function:

0 mv at 32 degF (0 deg C)

13.333 mv / degF; (24 mv / degC)

Convert the raw A/D count to degrees F using the equation:

$$T_{cj} = ((T_{cj}.count - 32768) / 32768) * 750) + 32$$

Apply a low pass filter with a one second time constant to this reading.

Once this has been done, then the equivalent “cold junction” voltages (mV) need to be determined for both an S thermocouple and a K thermocouple. These mV offsets will be added as correction factors to the S and K thermocouple sensor measurements. Table IV-3 lists the CJC S mV and K mV versus degrees F relationships to be implemented.

Table IV-3. S and K mV Corrections Versus CJ Temperature, F

| CJ Temperature, F | CJ mV correction, Type S | CJ mV correction, Type K |
|-------------------|-----------------------------|-----------------------------|
| 32 | 0.000 | 0.000 |
| 50 | 0.055 | 0.397 |
| 60 | 0.087 | 0.619 |
| 70 | 0.119 | 0.843 |
| 80 | 0.153 | 1.068 |
| 90 | 0.186 | 1.294 |
| 100 | 0.221 | 1.520 |
| 110 | 0.256 | 1.748 |
| 120 | 0.292 | 1.977 |
| 130 | 0.328 | 2.206 |
| 140 | 0.365 | 2.436 |
| 150 | 0.402 | 2.666 |

3.1.1.3 S Thermocouple (TC1 - TC38) Temperature Measurements

The raw voltage for the amplified thermocouple is scaled from the raw count read from the A/D conversion for this signal.

$$TC[I].volts = ((TC[I].count - 32768) / 32768) * 10.0$$

This needs to be corrected for offset and gain, for the particular MUX bank used, and converted to mV prior to a lookup process that references a degrees F versus S mV standard table. A cold junction adjustment is also made based on the Tcj, the temperature of the connector blocks on the MUX boards.

TC1 - TC13:

```
mv = (TC[I].volts - b1_offset) * b1_factor; /* correct for offset, gain */
mv = mv + S_CJC_mv_adj;                    /* adjust for cold junction effects */
```

TC14 - TC27:

```
mv = (TC[I].volts - b2_offset) * b2_factor; /* correct for offset, gain */
mv = mv + S_CJC_mv_adj;                    /* adjust for cold junction effects */
```

TC28 - TC38:

```
mv = (TC[I].volts - b3_offset) * b3_factor; /* correct for offset, gain */
mv = mv + S_CJC_mv_adj;                    /* adjust for cold junction effects */
```

Then use Table IV-4, Temperature, F) versus S mV, to determine the temperature from the measured mV value. Table IV-4 is dimensioned for a range of readings from 32F to 3200F.

Table IV-4: Temperature, F versus S mV

| S mV | Temperature, F | S mV | Temperature, F |
|--------|----------------|--------|----------------|
| -0.218 | -50.0 | 8.749 | 1700.0 |
| 0.000 | 32.0 | 9.382 | 1800.0 |
| 0.119 | 70.0 | 10.025 | 1900.0 |
| 0.221 | 100.0 | 10.678 | 2000.0 |
| 0.597 | 200.0 | 11.335 | 2100.0 |
| 1.478 | 400.0 | 12.004 | 2200.0 |
| 2.466 | 600.0 | 12.675 | 2300.0 |
| 3.516 | 800.0 | 13.348 | 2400.0 |
| 4.610 | 1000.0 | 14.022 | 2500.0 |
| 5.741 | 1200.0 | 14.696 | 2600.0 |
| 6.322 | 1300.0 | 16.035 | 2800.0 |
| 6.913 | 1400.0 | 17.353 | 3000.0 |
| 7.514 | 1500.0 | 18.609 | 3200.0 |
| 8.127 | 1600.0 | - | - |

3.1.1.4 K Thermocouple (T3, Tdriver) Measurements

The raw voltage for the amplified thermocouple is scaled from the raw count read from the A/D conversion for these signals:

$$T3.volts = ((T3.count - 32768) / 32768) * 10.0$$

$$Tdriver.volts = ((Tdriver.count - 32768) / 32768) * 10.0$$

This needs to be corrected for offset and gain and converted to mV prior to a lookup process that references a degrees F versus mV standard table. A cold junction adjustment is also made based on the Tcj, the temperature of the connector blocks on the MUX boards.

```

mv = (T3.volts - b1_offset) * b1_factor;      /* correct for offset, gain */
mv = mv + K_CJC_mv_adj;                      /* adjust for cold junction effects */
T3 (degF) = lookup(Table IV-5, mv)
mv = (Tdriver.volts - b2_offset) * b2_factor; /* correct for offset, gain */
mv = mv + K_CJC_mv_adj;                      /* adjust for cold junction effects */
Tdriver (degF) = lookup(Table IV-5, mv)

```

The expected range of T3 is 32F to 500F. The expected range of Tdriver is 32 to 250F. Table IV-5 is dimensioned for a range of readings from 32F to 600F.

T3 and Tdriver readings are used for data collection purposes only. The system does not control on these readings.

The Tdriver (driver box internal temperature) does have an alarm threshold of 140F. A reading above this threshold shall cause the front panel "Driver/FFM Fault" lamp to be lighted. This indication signifies that the driver box is overheating, due to a power overload or an interruption of lab cooling air to the box.

Table IV-5: Temperature, F versus K mV

| K mV | Temperature, F | K mV | Temperature, F |
|-------|----------------|--------|----------------|
| 0.000 | 32.0 | 2.896 | 160.0 |
| 0.397 | 50.0 | 3.358 | 180.0 |
| 0.619 | 60.0 | 3.819 | 200.0 |
| 0.843 | 70.0 | 4.279 | 220.0 |
| 1.068 | 80.0 | 4.964 | 250.0 |
| 1.294 | 90.0 | 6.092 | 300.0 |
| 1.520 | 100.0 | 7.205 | 350.0 |
| 1.748 | 110.0 | 8.314 | 400.0 |
| 1.977 | 120.0 | 9.430 | 450.0 |
| 2.206 | 130.0 | 10.560 | 500.0 |
| 2.436 | 140.0 | 11.702 | 550.0 |
| 2.666 | 150.0 | 12.854 | 600.0 |

The T3 sensor measures the temperature of the compressed air supplied to the combustor. The lab provides the capability of pre-heating this air to simulate compressor discharge conditions.

3.1.2 P3 Measurement

The P3 sensor reading is received by the Pattern Factor Controller (PFC) as a 4 - 20 mA signal. The terminating resistor is 243.1 ohms and the sensing amplifier has a gain measured at 2.004. A 1.948 to 9.739V signal is developed. The pressure sensor has a span of 0 to 100 psi.

$P3_{null_voltage} = 1.948v.$

$P3_{scale_factor} = 100 \text{ psi} / (9.739v - 1.948v) = 12.835 \text{ psi} / \text{volt}$

$P3_{reading} = (P3_{volts} - P3_{null_voltage}) * P3_{scale_factor};$ /* bite logic: section 4.4 */

The P3 sensor measures the pressure of the compressed air supplied to the combustor inlet.

3.1.3 Current Sensor Measurement

A 0 to 50A hall-effect current sensor (F.W. Bell Model CLN-50) has been selected. This is a fast response sensor that will allow a drive coil current of a selected fuel flow modulator valve to be observed. The sensor provides 1mA/Amp response into a 100 ohm burden resistor, to provide a 0.1V/Amp signal that can be observed on an oscilloscope. The controller will provide $\pm 15V$ power to the sensor but will not process the current sensor signal. An oscilloscope will allow the driver current pulse width and amplitude to be observed and characterized. Another sensor can be used to monitor the overall current delivered by the 28V power supply.

3.1.4 Control Panel (SW Assignable) Potentiometer Measurements

These are four 0 to 10V signals. Apply a 100 msec lag filter to these input measurements.

These signals are to be software assignable to any integer, float, or double variable that has a symbol table entry, using the "pot" operator interface command (see Section 7 of this Appendix IV. This allows the pot to vary the value of the variable over a range specified by the min/max elements of the symbol table entry.

3.2 Analog Outputs

There are two unipolar (by jumper selection), 0 to 10V output, 12-bit DAC outputs. These are to be software assignable so that two variables may be mapped to these outputs to allow strip chart traces to be generated. These outputs are wired to the I/O box rear panel and marked DAC0 and DAC1.

3.3 Digital Input / Output Lines

The DAS1602/15 multifunction board supports 32 bits of discrete (digital) I/O. The custom board implements a 1 of 4 multiplexor arrangement to concentrate 32 input bit lines into a single 8-bit port (port A), part of an onboard 82C55 peripheral IC. The 82C55 has a total of three 8-bit ports. Port B is programmed to be an output port. Port C is set up to be an input port, but these lines are currently unused. The DAS1602 board has an additional 4-bit output port and 4 bit input port, that are referred to as P0out and P0in respectively.

3.3.1 Digital Output Lines

The four output bits of P0out are the 1 of 16 gain/MUX channel select lines. Straight hex coding provides a 4-bit output code of from 0 to F (0 to 15) that selects the same channel on each of the three multiplexor banks (MUX32 board has 2 banks). Table IV-6 shows the other, Port B, digital output assignments.

Table IV-6: Port B Output Bit Assignments

| Port B: | Signal Name | Comment |
|---------|---------------------|---|
| bit 0 | Discrete MUX 0 | One of two bits (0 to 3 value) used to manipulate the 1 of 4 (32:8) discrete input multiplexor |
| bit 1 | Discrete MUX 1 | |
| bit 2 | FFM Fault Drive | Lamp: high (on) = fuel flow modulator fault |
| bit 3 | TC Fault Drive | Lamp: high (on) = thermocouple fault |
| bit 4 | Alert Drive | Lamp: high (on) = BITE or SW programmed alert |
| bit 5 | spare | - |
| bit 6 | spare | - |
| bit 7 | Foreground test bit | Set high on entry to foreground interrupt, clear on exit from foreground intr routine. This allows measurement of FG usage. |

3.3.2 Digital Input Lines

Table IV-7 lists the digital input lines multiplexed through Port A.

Table IV-7: Multiplexed Port A Bit Assignments

| Port A: | MUX Select: 0 Signal Name | MUX Select: 1 Signal Name | MUX Select: 2 Signal Name | MUX Select: 3 Signal Name |
|---------|------------------------------|------------------------------|------------------------------|------------------------------|
| bit 0 | FFM Status 1 | FFM Status 9 | FFM Status 17 | Open Loop |
| bit 1 | FFM Status 2 | FFM Status 10 | FFM Status 18 | Closed Loop |
| bit 2 | FFM Status 3 | FFM Status 11 | FFM Status 19 | Fuzzy Mode |
| bit 3 | FFM Status 4 | FFM Status 12 | spare | Assignable Switch 1 |
| bit 4 | FFM Status 5 | FFM Status 13 | spare | Assignable Switch 2 |
| bit 5 | FFM Status 6 | FFM Status 14 | spare | Assignable Switch 3 |
| bit 6 | FFM Status 7 | FFM Status 15 | spare | All Thermocouples |
| bit 7 | FFM Status 8 | FFM Status 16 | spare | Odd Thermocouples |

The flow chart in Figure IV-3 shows the PFC Mode Selection Logic.

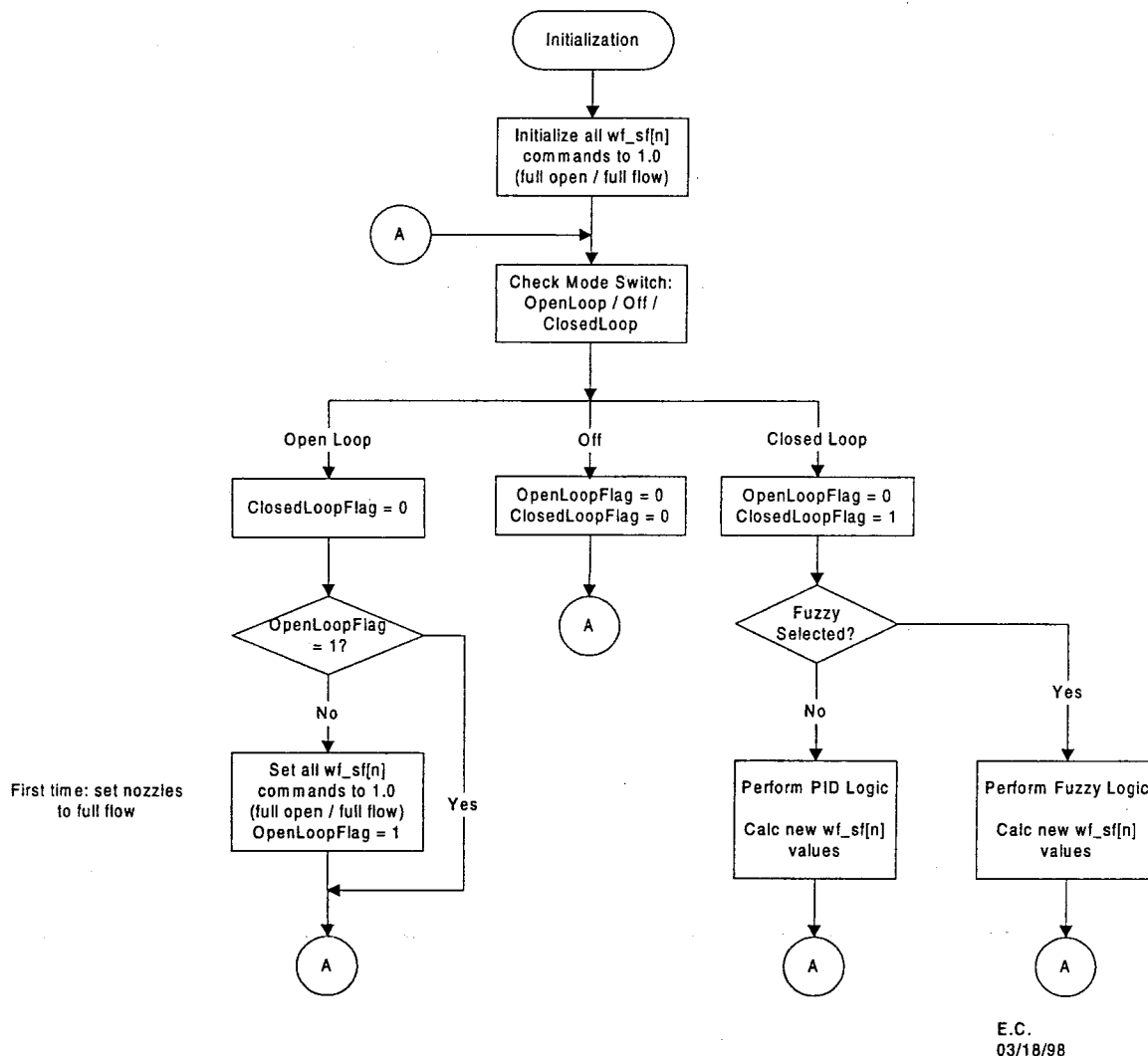


Figure IV-3. Pattern Factor Controller Mode Selection Logic.

There are three dedicated front panel switches that select the operating modes. The Open Loop/OFF/Closed Loop switch is to be utilized as follows:

- Open Loop - manual mode; fuel flow nozzles initialized to full flow. Moving switch to this position is equivalent to the 'reset' command. The monitor can be used to command settings other than full-flow; the switch action is a one-time reset to full open.
- Off - the Off position is interpreted as the 'freeze' command, where fuel flow commands are held at current settings.
- Closed Loop - this is the normal setting; system uses temperature readings and the selected control algorithm to control the fuel nozzles to optimize the pattern factor.

The Fuzzy/PID switch is interpreted as follows:

- Fuzzy - perform fuzzy logic control algorithms
- PID - perform proportional-integral-derivative logic

The system shall be capable of switching between fuzzy and PID operation during the same run.

The Odd/Even/All Thermocouple switch is a three position switch used by both the PID and fuzzy control logic:

- Odd - control on odd thermocouple readings
- Even - control on even thermocouple readings
- All - control on all thermocouple readings.

The system shall be capable of switching between these three modes of operation during a run.

There are three software assignable switch discrete inputs. These are to be assignable to any boolean variable that has a symbol table entry, using the “swi” operator interface command (see Section 7 of this Appendix IV). The variable will take on a value of zero when the switch is down, and a value of one when the switch is up (activated).

The four input lines of P0in and the 8 input lines of Port C are unused and represent spare discrete input lines, available if needed.

3.3.3 Timer (PWM) Outputs

The CIO-CTR20HD board provides twenty 16-bit programmable timers. Timer 20 is to be set up in rate generator mode to produce a square wave at 10 times the desired PWM frequency. A clock generator circuit on the custom board divides this down by 10 and provides time-staggered triggering pulses. The default PWM frequency is to be programmable through the operator interface, with a default of 20 Hz and an allowable range of 5 Hz through 50 Hz.

Timers 1 through 19 are to be set up in HW triggered one-shot mode with the one-shot duration count normalized to the PWM frequency in effect in order to produce the desired PWM duty cycle. The PWM command output shall be capable of being commanded to a static on, static off, or PWM signal adjustable from 0.1 to 99.9 percent minimum range with a minimum of 1 part in 1000 resolution. A command of 0.0 shall produce a static low output from the PWM circuit. A command of 1.0 shall produce a static high output from the PWM circuit.

3.3.4 Timer Input / Fuel Flow Sensor

The spare 82C54 timer channel on the DAS1602 board is to be set up as a frequency counter used to measure the fuel-flow sensor signal. This signal provides a frequency that is proportional to fuel flow.

The sensor measurement span is 0 to 1500 pph. The output frequency is 0 to TBD Hz.

Use 82C54 mode 0 (interrupt on terminal count) to accumulate the frequency count. The gate input is held high (On) via a pull-up resistor. The process is started by loading a count of 0FFFFh into the 16-bit counter in a LSB, MSB sequence of two byte writes. Establish a slow

task dispatcher to execute every 500 msec. Call the frequency measurement routine at this rate, establishing a 500 msec measurement gate. Read the count from the down-counting timer, invert it to get the count, multiply by 2 to determine the frequency. After this, load 0FFFFh back into the counter for the next measurement cycle.

4. BUILT-IN TEST EQUIPMENT (BITE) REQUIREMENTS

Each fault test will use a persistence qualifier to help prevent nuisance indications. This is to be implemented using a count limit (default value = 10) for each sensor or measured quantity. An out-of-range or failed evaluation shall cause the associated fault counter to count up 2. An in-range or passed evaluation shall cause the associated fault counter to count down by 1 (if fault counter is greater than zero).

4.1 Thermocouple Fault Detection

The thermocouple input circuits on the gain/MUX boards are biased such that an open thermocouple produces a maximum downscale reading. A fault of any of the S or K thermocouples shall cause the control panel TC Fault indicator to be turned on.

Substitute the previous reading for a thermocouple until the fault persists long enough to be considered a "hard fault". At this point, mark the thermocouple as failed and thereafter substitute the overall T4_avg for this thermocouple's reading.

4.1.1 S Thermocouple Fault Detection

Range checks shall be performed, against the following programmable limits:

low limit: -10 degF (detects open or miswired thermocouple)

high limit: 3000 degF; /* T4_avg + 500 as limit is under consideration */

4.1.2 K Thermocouple Fault Detection

Range checks shall be performed, against the following programmable limits:

low limit: -10 degF (detects open or miswired thermocouple)

high limit: 300 degF for Tdriver

550 degF for T3

4.2 Driver/FFM Fault Detection

The status signals provide by the Sturman driver box shall be examined. A logic high is assumed to indicate a failure. A fault of any of the drivers shall cause the control panel FFM Driver fault indicator to light up.

4.3 Gain/MUX Board Faults

The gain/multiplexor boards are tested using ground reference and 20 mV (actually 19.52 mV) reference signals. Each of the three-gain/MUX banks receives one each of these reference signals. The nominal gain of each of three banks of the gain/MUX boards is 301.

Range checks shall be performed on these reference signals against the following programmable limits:

mv20 (19.52 actual in; nominal is 5.8755v out) reference:

high limit: 6.0 volts

low limit: 5.75 volts

ground reference (after amplification):

high limit: 100 mV

low limit: -100 mV

A fault of any of the reference signals shall cause the control panel Alert indicator to light up.

4.4 Other System / Sensor Faults

The P3 sensor has a 4 to 20 mA interface, developing a 1.948 to 9.739V signal for normal operation. A voltage below a low limit of 1.8V indicates a fault of the P3 sensor.

A fault of P3 shall cause the control panel Alert indicator to be turned on.

5. PATTERN FACTOR CONTROL LOGIC

5.1.1 Modes of Operation

The following methods and modes of operation shall be supported in both PI (traditional) and fuzzy logic control:

- All - All thermocouples utilized in calculating error terms
- Even - Only the even numbered thermocouples utilized in calculating error terms
- Odd - Only the odd numbered thermocouples utilized in calculating error terms
- Reset - Reset the wf.sf (fuel flow commands) back to full open values of 1.0
- Freeze - Hold wf.sf (fuel valve scale factor) commands at current settings

See paragraph 3.3.2 for a description of control panel switches that select these modes of operation.

5.1.2 T4 Measurement Averaging

In order to provide best noise cancellation, provide a three (or five, if processing time is available) point average of each T4 thermocouple. This applies to both PID and fuzzy processing. Provide a software switch (label name: T4avgEn) to allow averaging to be turned On or Off.

T4avgEn: 1 = average readings, 0 = no averaging; use one reading only.

Default to T4avgEn = 1, averaging on.

5.2 Proportional-Integral-Derivative (“Traditional”) Logic

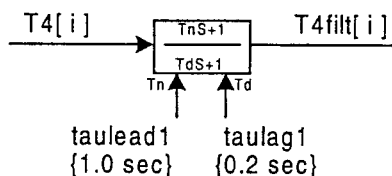
This paragraph summarizes the logic presented in Attachment 2 of AE Document No. 21-9690, System Modes and Logic Design Document, June 10, 1997.

The pseudo-code definition received as definition of the pattern factor proportional-integral-derivative control logic is listed in Section 10 of the current document.

5.2.1.1 T4 Dynamic Compensation

Provide a lead-lag compensation on each T4 measurement. Both the lead and lag time constants shall be adjustable using the monitor. The initial value of the lead term shall be 1.0 sec. The initial value of the lag term shall be 0.2 sec. Use the Tustin transform method.

Precalculate the three coefficients to simplify the processing. Recalculate these coefficients periodically to accommodate operator manipulation of the time constants.



Provide a software switch (label name: T4compEn) to allow dynamic compensation to be turned On or Off.

T4compEn: 1 = provide dynamic compensation, 0 = no compensation; use unfiltered readings.

Default to T4compEn = 0; compensation Off.

5.2.1.2 Calculate Averages

Calculate the min, max, and average of the odd and even thermocouples. Maintain an index or pointer to the min and max thermocouples in each group. Next determine the min and max thermocouples from the min and max thermocouples of these two groups.

Any thermocouples that are ‘faulted’ shall be assigned the average of its two nearest non-faulted neighbors (one to each side).

```
T4odd[i] = T4filt[i * 2 + 1];      /* ie T4[1, 3, 5 ... 37].reading; (i: 0 to 18) */
T4even[i] = T4filt[i * 2];        /* ie T4[0, 2, 4 ... 38].reading (i: 0 to 18) */
```

```
T4odd_avg = ( Σ T4_odd readings ) / 19;
T4even_avg = ( Σ T4_even readings ) / 19;
T4_avg = 0.5 * (T4odd_avg + T4even_avg);
```

5.2.2 Calculate Pattern Factors

```
Pattern_Factor_Odd = T4odd_max - T4odd_avg;
```

$\text{Pattern_Factor_Even} = \text{T4even_max} - \text{T4even_avg};$
 $\text{Pattern_Factor} = \text{T4_max} - \text{T4_avg};$

5.2.3 Generate Control Errors

Calculate 19 odd error terms: $\text{T4odd_err}[i] = \text{T4odd_avg} - \text{T4odd}[i];$ /* i: 0 - 18 */
 Calculate 19 even error terms: $\text{T4even_err}[i] = \text{T4even_avg} - \text{T4even}[i];$
 Calculate 38 error terms (All option): $\text{T4err}[j] = \text{T4_avg} - \text{T4}[j];$ /* (j: 0 to 37) */

Compare these individual error terms to a 'HOT_Error' threshold of 50 degr (adjustable) and a 'COLD_Error' threshold of 1000 degr (adjustable); note that HOT dominates.

Compare individual error terms against these thresholds. Clear errors between thresholds to zero, retain those that exceed thresholds. Figures IV-4 and IV-5 shows this processing for the odd error terms and all error terms.

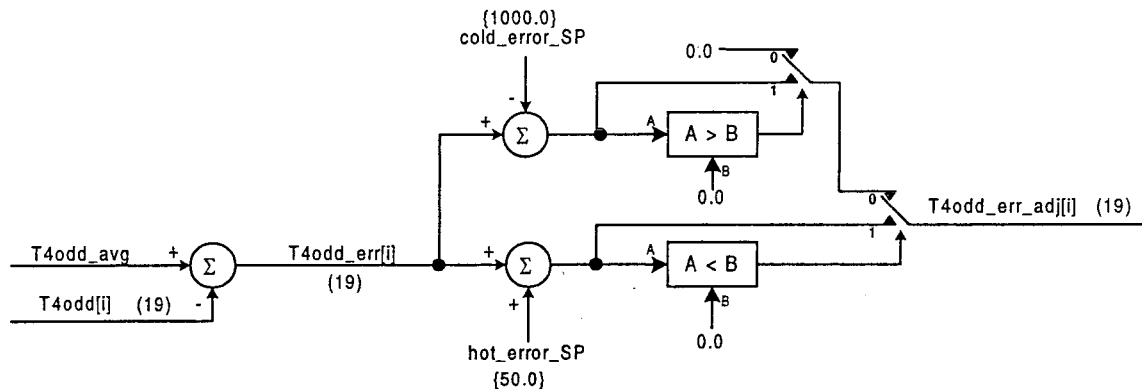


Figure IV-4. T4Odd Error Term Processing.

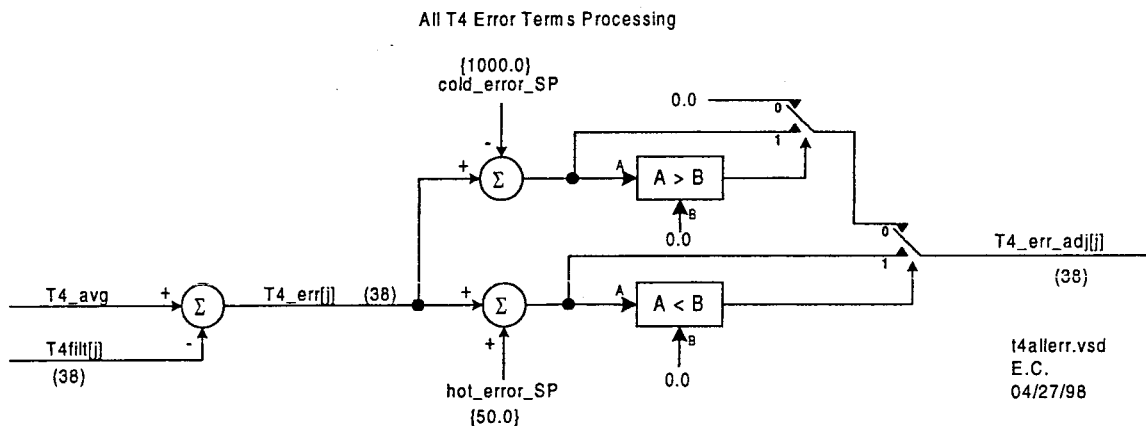


Figure IV-5. All T4 Error Terms Processing.

5.2.4 Output Control Logic

In Figure IV-6, wf_sf[i] represents the 19 control outputs to the 19 FFMs, scaled 0 to 1.0.

Initialize all to 1.0 to start with. This represents the full on or full flow state of the fuel flow modulator valves.

Initialize wf_sf_max to 1.0 also. Limit wf_sf[i] outputs to a maximum of 1.0.

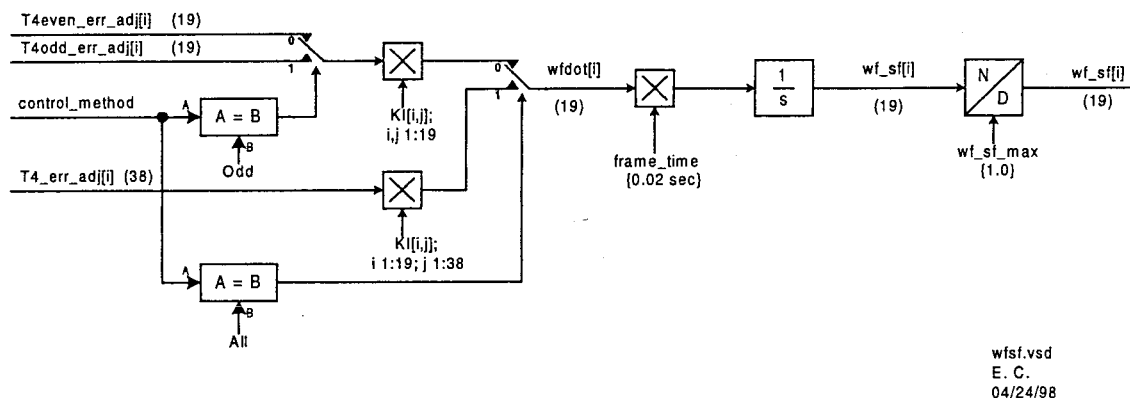


Figure IV-6. PI Control: wfdot and wf_sf Calculations.

5.2.4.1 Reset Logic

Reset all wf_sf[i] parameters back to 1.0.

Reset wf_sf_max parameter to 1.0.

5.2.4.2 All Thermocouples Mode

Calculate 19 wfdot[i] error terms, using all 38 thermocouple error terms:

$wfdot[i] = wfdot[i] + KI[i, j] * T4_err[j]$; /* for i = 0:18; for j = 0:18 */
/* KI is a 19 x 38 matrix of gains */

5.2.4.3 ODD Thermocouples Mode

Calculate 19 wfdot[i] error terms using 19 error terms:

$wfdot[i] = wfdot[i] + KI[i, 2 * j + 1] * T4odd_err[j]$; /* for i = 0:18, for j = 0:18 */

5.2.4.4 EVEN Thermocouples Mode

Calculate 19 wfdot[i] error terms using 19 error terms:

$wfdot[i] = wfdot[i] + KI[i, 2 * j] * T4even_err[j]$; /* for i = 0:18, for j = 0:18 */

5.2.4.5 Scale Factor Normalization and Output Calculation (All modes)

Compute new wf_sf[i] control parameters and readjust max command as required. Feed errors into slow trim integrators:

$wf_sf[i] = wf_sf[i] + FRAME_TIME * wfdot[i]$;

```

if (wf_sf[i] > wf_sf_max )           /* initialize wf_sf_max to 1.0 */
    wf_sf_max = wf_sf[i];           /* wf_sf_max should always be >= 1.0 */

Normalize wf_sf commands:
wf_sf[i] = wf_sf[i] / wf_sf_max;

```

5.3 Fuzzy Logic

This paragraph summarizes the logic presented in Attachment 3 of AE Document No. 21-9690, System Modes and Logic Design Document, June 10, 1997.

5.3.1 Calculate Average Temperature

$T4_avg = (\sum T4[i]) / 38$; $i = 1$ to 38 for the 38 S thermocouples. Any thermocouples that are “faulted” shall be assigned the average value of the non-faulted thermocouples.

5.3.2 Calculate Error Terms

As with the PI logic odd, even, or all thermocouples can be utilized as the sensor inputs for control of the modulating valves.

The error terms to be used are selected by the Odd/ Even/All switch on the control panel. The error terms utilize a cosine weighted average of adjacent thermocouples, described as follows:

```

weight = cos( $\Theta$  * 3);    /*  $\Theta$  is angular displacement of thermocouples from nozzle */
                          /* thermocouples have 9.5 deg separation from each other */

```

using the following angles and weights:

| Angle Θ | Weight |
|----------------|--------|
| 0 deg | 1.0 |
| 9.5 deg | 0.87 |
| 19 deg | 0.54 |

5.3.2.1 Calculate “Odd” Error Terms

Calculate 19 odd error terms:

```
T4odd_err[i] = T4odd_avg - T4odd_wa[i];
```

```
T4odd_wa[i] = ( 0.54 * ( T4odd[i-1] + T4odd[i+1] ) + T4odd[i] ) / 2.08;
```

5.3.2.2 Calculate “Even” Error Terms

Calculate 19 even error terms:

```
T4even_err[i] = T4even_avg - T4even_wa[i];
```

```
T4even_wa[i] = ( 0.54 * ( T4even[i-1] + T4even[i+1] ) + T4even[i] ) / 2.08;
```

5.3.2.3 Calculate ‘All’ Error Terms

Calculate 19 error terms:

$T4adj_err[i] = T4_avg - T4wa[i];$ /* $T4wa[i]$ is weighted average about $T4[i]$ */

$T4wa[i] = (0.54 * (T4[i-2] + T4[i+2]) + 0.87 * (T4[i-1] + T4[i+1]) + T4[i]) / 3.82;$

Not using all 38. Use i of 0, 2, 4, ... 38 (assume even thermocouples are aligned with fuel nozzles).

5.3.2.4 Calculate Rate Error Terms

Calculate 19 odd rate terms: $T4odd_edot[i] = (T4odd_lv[i] - T4odd[i]) * frame_rate;$

Calculate 19 even rate terms: $T4even_edot[i] = (T4even_lv[i] - T4even[i]) * frame_rate;$

Calculate 19 all rate terms: $T4adj_edot[i] = (T4adj_lv[i] - T4adj[i]) * frame_rate;$

/* lv is last value or previous value */

/* temp incr yields neg error term. */

5.3.3 Fuzzification / Input Membership Functions

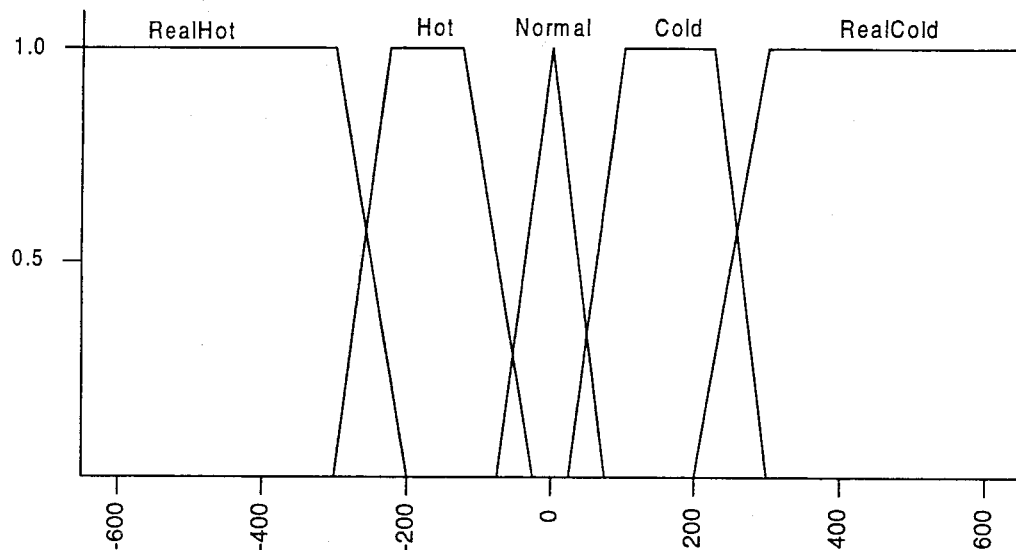
Trapezoidal shaped membership function graphs shall be employed.

5.3.3.1 T4 Error Input Membership Function

The $T4err$ input membership function is defined at five levels or classes (the function graph is shown in Figure IV-7):

- RealHot: $-650 < T4err < -200$
- Hot: $-300 < T4err < -10$
- Normal: $-75 < T4err < 75$
- Cold: $10 < T4err < 300$
- RealCold: $200 < T4err < 650$

Measurement units of $T4err$ is degrees F.



T4EM.VSD
E.C.
03/18/98

Figure IV-7. T4 Error Membership Function Graph.

For a given T4err term (x-axis input), 5 y-axis degree-of-membership values will be determined that will range in value from 0.0 to 1.0. An array of 38 is required for each class, to store the degree-of-membership value for each of the 38 T4err terms.

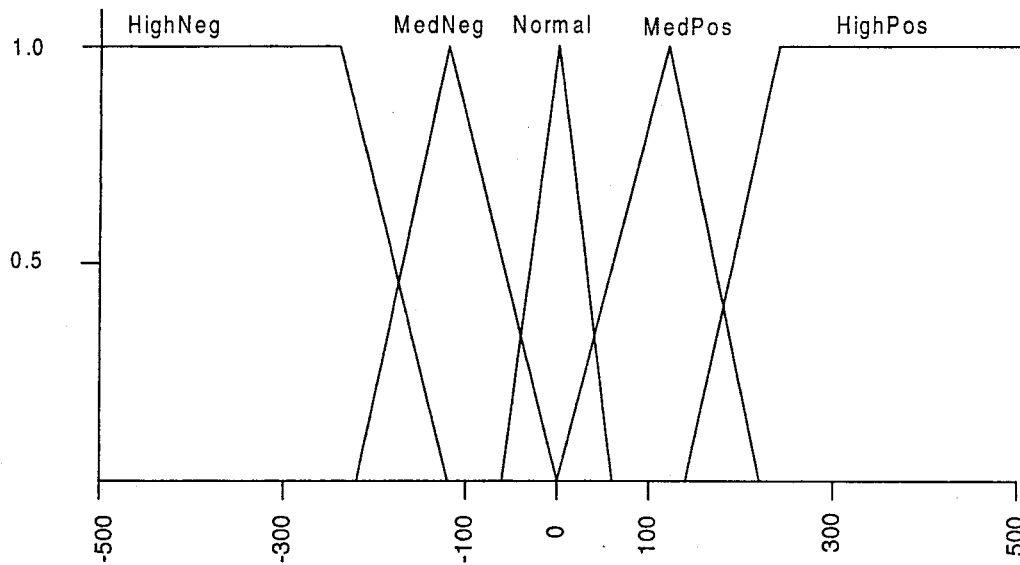
5.3.3.1 T4 edot Input Membership Function

The T4 edot input membership function is defined at five levels or classes (the function graph is shown in Figure IV-8):

- highneg: $-500 < T4edot < -117$
- medneg: $-215 < T4edot < 0$
- normal: $-60 < T4edot < 60$
- medpos: $0 < T4edot < 215$
- highpos: $117 < T4edot < 500$

Measurement units of edot is degrees F/sec.

For a given T4edot term (x-axis input), 5 y-axis degree-of-membership values will be determined that will range in value from 0.0 to 1.0. An array of 38 is required for each class, to store the degree-of-membership value for each of the 38 T4edot terms.



T4EDOT.VSD
E.C.
03/18/98

Figure IV-8. T4 edot Membership Function Graph.

5.3.4 Inference/Rules

A matrix of rules for T4 Error, T4 edot, and Wf delta is shown in Table IV-8.

Table IV-8. T4 Error, T4 edot, and Wf delta Rules.

| Rule | T4 Error | T4 edot | Wf delta |
|------|-----------|----------|-----------|
| 1 | real hot | high neg | closemore |
| 2 | real hot | normal | closemore |
| 3 | real hot | med pos | close |
| 4 | real hot | high pos | same |
| 5 | hot | med neg | close |
| 6 | hot | normal | close |
| 7 | hot | med pos | same |
| 8 | cold | med neg | same |
| 9 | cold | normal | open |
| 10 | cold | med pos | open |
| 11 | real cold | high neg | same |
| 12 | real cold | med neg | open |
| 13 | real cold | normal | openmore |
| 14 | real cold | high pos | openmore |
| 15 | normal | high neg | closemore |
| 16 | normal | med neg | close |
| 17 | normal | normal | same |
| 18 | normal | med pos | open |
| 19 | normal | high pos | openmore |

For example, interpret rule 1 as:

“if T4err is REALHOT and T4edot is HIGHNEG then wf_delta is CLOSEMORE”

The inference rules can be drawn as a matrix table (Table IV-9) with the columns shown as T4err membership terms and the rows shown as T4edot membership terms:

Table IV-9. Inference Rules:
T4err (= T4avg - T4[n])

| wf delta: | RealHot | Hot | Normal | Cold | RealCold |
|-----------|-------------|-------------|--------------|------------|-------------|
| HighNeg | CloseMore 1 | (CloseMore) | CloseMore 15 | (Close) | Same 11 |
| MedNeg | (CloseMore) | Close 5 | Close 16 | Same 8 | Open 12 |
| Normal | CloseMore 2 | Close 6 | Same 17 | Open 9 | OpenMore 13 |
| MedPos | Close 3 | Same 7 | Open 18 | Open 10 | (OpenMore) |
| HighPos | Same 4 | (Open) | OpenMore 19 | (OpenMore) | OpenMore 14 |

The rule number is shown along with the output membership function activated. Entries in parentheses were not specified by the 19 rules listed in AE Document No. 21-9690 (Appendix 3). This is how they would appear if the rule set were extended to the full 25 possible. Note the symmetry in the table.

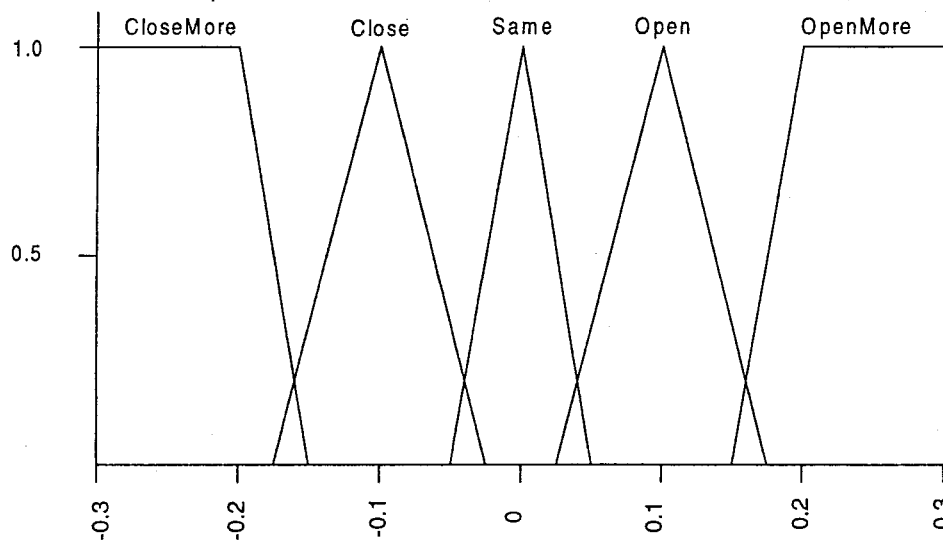
T4edot = (d/dt) T4err is on the left, as the row categorization.

5.3.5 Output Membership Functions

The wf_delta (change to FFM nozzle command) output membership function is defined at five levels (the function graph is shown in Figure IV-9):

- closemore: $-0.3 < wf_delta < -0.15$
- close: $-0.17 < wf_delta < -0.03$
- same: $-0.05 < wf_delta < 0.05$
- open: $0.03 < wf_delta < 0.17$
- openmore: $0.15 < wf_delta < 0.3$

For each T4 thermocouple, the T4edot membership entries (5) are compared to the T4err membership entries (5) in a “low-wins” comparison for each cell in the matrix (see Table IV-9) to determine 5 output membership terms ranging in value from 0 to 1.



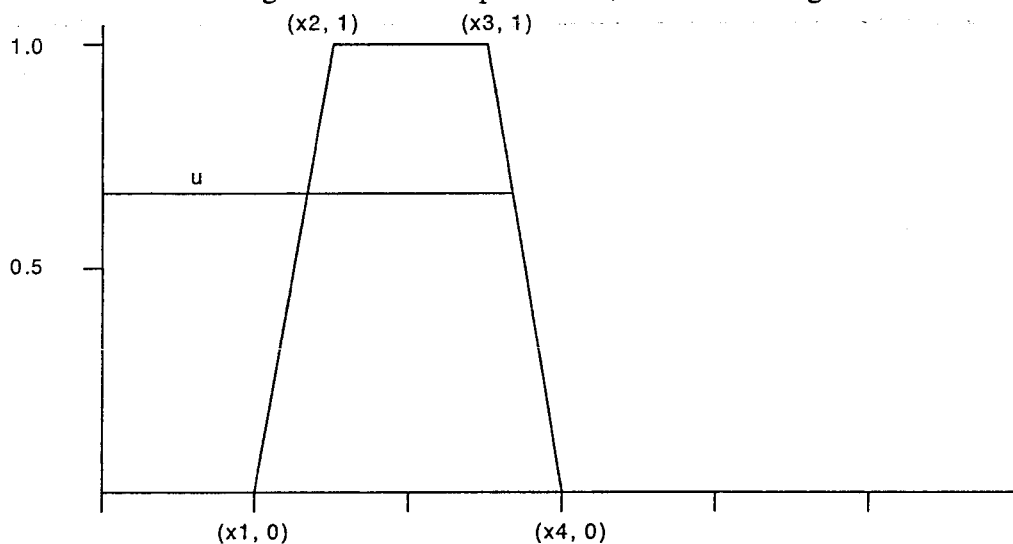
WFDelta.VSD
E.C.
03/19/98

Figure IV-9. Wf delta Membership Function Graph.

5.3.5 De-Fuzzification of Output Control Terms

The contributions of these output membership terms are then 'de-fuzzified', using the centroid method, to produce a single 'crisp' output for the wf_delta term.

Consider the four x intercepts required to characterize a trapezoidal membership function: x_1 , x_2 , x_3 , x_4 (Figure IV-10). The y intercepts would be 0 for x_1 and x_4 and 1 for x_2 and x_3 . For the case of a triangular membership function, x_2 and x_3 are given the same values.



DEFUZZ.VSD
E.C.
04/11/98

Figure IV-10. De-Fuzzification Processing, Output Membership Graph.

In Figure IV-10, u is the degree-of-membership of the output membership function activated by a rules “hit”. The area under the intersection of u in the output membership graph (Figure IV-10) is:

$$\text{Area} = (x_4 - x_1) * u + (x_1 - x_2 + x_3 - x_4) * u^2 / 2;$$

The moment of this area is given by:

$$\begin{aligned} \text{Moment} = & 0.5 * (x_4^2 - x_1^2) * u - (x_1 * (x_2 - x_1) + x_4 * (x_4 - x_3)) * u^2 \\ & + ((x_4 - x_3)^2 - (x_2 - x_1)^2) * u^3 / 3; \end{aligned}$$

(While the above equations appear computationally intensive, $x_1 - x_4$ values are effectively static until the operator changes them. Therefore, the terms of the equations can be boiled down to coefficients that need be computed only during initialization and at a TBD rate in the background thereafter, to support changes by the operator to the output membership graphs via manipulation of x values.)

The area and moment are calculated for each output membership function activated by a rules hit. The final crisp output value is calculated as the sum of the moments divided by the sum of the areas:

$$\text{Centroid} = \sum(\text{Moment}) / \sum(\text{Area});$$

Measurement units of wf_delta are a dimensionless fraction. wf_delta is the increment (or decrement if negative) added to the current nozzle command $wf_scale[i]$.

$$wf_scale[i] = wf_scale[i] + wf_delta[i];$$

Limit wf_scale to between 0.0 (full closed) and 1.0 (full-open).

6. OPEN-LOOP TEST ACCOMMODATION

In order to accommodate software testing and debug, as well as hardware/software integration testing, it will be necessary to “break the loop” and allow the operator to substitute fixed “open-loop” values for strategic inputs and outputs, such as the T4 temperature sensor readings and the T4edot error terms. Provide the data structures, logic, and symbol table entries required to support the mode of operation.

7. DATA LOGGING

The following is a list of signals most likely to be selected for data logging. The operator interface shall provide a flexible means of selecting which parameters are to be recorded, as well as the command interface to begin and end the recording process. The existing logic limits the number of stored variables to 16. Any variable with an entry in the symbol table is a candidate for data logging. The requirement related to this is to make a symbol table entry for each significant variable, including, but not limited to, the variables listed below.

The data logging SW being carried over from the gdm package stores each parameter as a “double” type, which uses 8 bytes of storage. See the “dav” and “hds” command descriptions in Section 8 for more details regarding operator control of the data logging process.

- P3
- T3
- Tdriver
- Wf.sf1 - Wf.sf19 (19 FFM commands (0.0 to 1.0 range))
- Status1 - bit packed (16 bit) status word
- Status2 - bit packed (16 bit) status word
- min temp reading
- high temp reading
- T4_avg
- T4even_avg
- T4odd_avg
- pattern_factor

8. OPERATOR INTERFACE

8.1 Command Interface Description

The following commands/syntax are to be supported by the command interpreter:

Syntax denotes syntax of command entry.

<CR> denotes carriage return or enter key.

varname is label corresponding to software variable of interest.

- var - display variable value in text field. Allow operator to enter new value for var.
Syntax: var varname<CR>
- shv - continuous text field display variable.
Syntax: shv varname<CR> (ESC key exits command)
- dav - continuous text field display variable in a reserved field.
Syntax: dav varname n (n is field number (0 through 15))
- stc - (strip chart) display variable as one of four strip chart traces.
Syntax: stc varname n (n is trace number (0, 1, 2 or 3))
- pot - maps a control panel assignable pot over a user specified (non-boolean) variable
Syntax: pot varname n (n is potentiometer number (0, 1, 2, or 3))
- swi - maps a control panel assignable switch over a user supplied (boolean) variable
Syntax: swi varname n (n is assignable switch number (0, 1, 2, or 3))
- hds - (hard disk storage) toggles a record mode flag on/off.
The variables to be stored are those defined or set up by the 'dav' command.
With the existing logic, this limits the number of stored variables to 16.

8.2 Display Fields/Screens

Further work remains to be completed in this area.

9.0 Logic Implementation

AE Document No. 22-4418, "Engineering Report - Logic Symbol Definitions" shall be used as a guide for implementing the logic operations called out.

9.1 Low Pass Filters

Low Pass (lag) Filter:
$$Y(n) = e^{(-\text{FRAME-TIME} / T_d)} (Y(n-1) - X(n)) + X(n)$$
$$Y(n-1) = Y(n)$$

(this is the discrete rectangular implementation)

Where possible, the filter output should be initialized to the nominal, expected value. This minimizes the startup transient.

mv20ref[I].filt - initialize to value of 5.8755v (the expected value)

Tcj.filt - initialize to value of 75 degF (the expected value)

9.2 Lead-Lag Filters

Use the rectangular (or Tustin transform) method described in AE Document No. 22-4418.

10. PSEUDO-CODE FOR PID CONTROL LOGIC

```
/* PFCLOGIC.TXT */
// John Rushinsky
// 01/05/97

// Pattern Factor Control Law

// Read in all 38 T/C call them TC(i) i = 1:38

// Mode Select for Control
// 0 = All T/C's used
// 1 = Odd T/C's used
// 2 = Even T/C's used

// Set every scan update to clear values

TC_ave = 0.0;
TCodd_ave = 0.0;
TCodd_max = 0.0;
TCodd_min = 10000;
TCeven_ave = 0.0;
TCeven_max = 0.0;
TCeven_min = 10000.0;

for i = 1:19,

    // Odd T/C's

    TCodd(i) = TC(2 * i - 1);
    TCodd_ave = TCodd_ave + TCodd(i);
    if TCodd(i) > TCodd_max,
        TCodd_max = TCodd(i);
        oddmax_index = 2 * i - 1;
    elseif TCodd(i) < TCodd_min;
        TCodd_min = TCodd(i);
        oddmin_index = 2 * i - 1;
    end

    // Even T/C's

    TCeven(i) = TC(2 * i);
    TCeven_ave = TCeven_ave + TCeven(i);
    if TCeven(i) > TCeven_max,
        TCeven_max = TCeven(i);
        evenmax_index = 2 * i;
    elseif TCeven(i) < TCeven_min;
        TCeven_min = TCeven(i);
        evenmin_index = 2 * i;
    end

end
```

```

//OverAll

if TCeven_max > TCodd_max,
    TC_max = TCeven_max;
    max_index = evenmax_index;
else,
    TC_max = TCodd_max;
    max_index = oddmax_index;
end

if TCeven_min < TCodd_min,
    TC_min = TCeven_min;
    min_index = evenmin_index;
else,
    TC_min = TCodd_min;
    min_index = oddmin_index;
end

// compute Averages

TCodd_ave = TCodd_max / 19;
TCeven_ave = TCeven_max / 19;
TC_ave = 0.5 * (TCodd_ave + TCeven_ave);

// Compute Pattern Factors

Pattern_Factor_Odd = TCodd_max - TCodd_ave;
Pattern_Factor_Even = TCeven_max - TCeven_ave;
Pattern_Factor = TC_max - TC_ave;

// generate Control Errors

Hot_Error = 50;           // TC's 50deg above mean are considered HOT (Adjustable
                           from console)
Cold_Error = 1000;        // TC's 1000deg below mean are considered COLD (Adjustable
                           from console)
for i = 1:19,
    // Odd Errors

    error_odd(i) = TCodd_ave - TCodd(i);
    if (error_odd(i) + Hot_Error) < 0 ,
        error_odd(i) = error_odd(i) + Hot_Error;
    elseif (error_odd(i) - Cold_Error) > 0.0,
        error_odd(i) = error_odd(i) - Cold_Error;
    else,
        error_odd(i) = 0.0;           // Clear Errors between the Thresholds
    end

    // Even Errors

```

```

error_even(i) = TCeven_ave - TCeven(i);
if (error_even(i) + Hot_Error) < 0 ,
    error_even(i) = error_even(i) + Hot_Error;
elseif (error_even(i) - Cold_Error) > 0.0,
    error_even(i) = error_even(i) - Cold_Error;
else,
    error_even(i) = 0.0;      // Clear Errors between the Thresholds
end

// All errors

error(2 * i - 1) = TC_ave - TC(2 * i - 1);
if (error(2 * i - 1) + Hot_Error) < 0 ,
    error(2 * i - 1) = error_even(2 * i - 1) + Hot_Error;
elseif (error(2 * i - 1) - Cold_Error) > 0.0,
    error(2 * i - 1) = error_even(2 * i - 1) - Cold_Error;
else,
    error(2 * i - 1) = 0.0;      // Clear Errors between the Thresholds
end
error(2 * i) = TC_ave - TC(2 * i);
if (error(2 * i) + Hot_Error) < 0 ,
    error(2 * i) = error_even(2 * i) + Hot_Error;
elseif (error(2 * i) - Cold_Error) > 0.0,
    error(2 * i) = error_even(2 * i) - Cold_Error;
else,
    error(2 * i) = 0.0; // Clear Errors between the Thresholds
end

end

// Feed errors into slow trim integrators
// Initialize all wf_sf(i) = 1.0 FULL OPEN

wf_sf_max = 1.0;

if control = 'RESET',      // Set all wf_sf = 1.0
    for i = 1:19,
        wf_sf(i) = 1.0;
    end

elseif control = 'FREEZE'

elseif control = 'ALL SENSORS'
    // KI = 19x38 Matrix of Gains
    for i = 1:19,
        wfdot(i) = 0;
        for j = 1:38,
            wfdot(i) = wfdot(i) + KI(i, j) * error(j);
        end
        wf_sf(i) = wf_sf(i) + UPDATE_RATE * wfdot(i);
        if wf_sf(i) > wf_sf_max,
            wf_sf_max = wf_sf(i);
        end
    end
end

```



```

// Normalize wf_sf commands

for i = 1:19,
    wf_sf(i) = wf_sf(i)/wf_sf_max;
end
elseif control = 'ODD'
    for i = 1:19,
        wfdot(i) = 0;
        for j = 1:19,
            wfdot(i) = wfdot(i) + KI(i, 2 * j - 1) * error_odd(j);
        end
        wf_sf(i) = wf_sf(i) + UPDATE_RATE * wfdot(i);
        if wf_sf(i) > wf_sf_max,
            wf_sf_max = wf_sf(i);
        end
    end
end
// Normalize wf_sf commands
for i = 1:19,
    wf_sf(i) = wf_sf(i)/wf_sf_max;
end
elseif control = 'EVEN'
    for i = 1:19,
        wfdot(i) = 0;
        for j = 1:19,
            wfdot(i) = wfdot(i) + KI(i, 2 * j) * error_even(j);
        end
        wf_sf(i) = wf_sf(i) + UPDATE_RATE * wfdot(i);
        if wf_sf(i) > wf_sf_max,
            wf_sf_max = wf_sf(i);
        end
    end
end
// Normalize wf_sf commands
for i = 1:19,
    wf_sf(i) = wf_sf(i) / wf_sf_max;
end
end

```

11. SOFTWARE PROBLEM CHANGE REQUEST

Honeywell Engines & Systems

Software Problem Change Request

SPCR Title: Document SW Changes Made During 1st Pattern Factor Rig Tests

SPCR Log Number: 01

Date: 06/02/99

Page 1 of 2

System: Pattern Factor Controller

Documentation affected: PFCSRSp1.doc, PFCSRSp2.doc

Software modules affected: pfcvars.c, publics.h, pfcbite.c, pfcio.c, pfcmain.c, picntrl.c, fuzcntrl.c, auxtasks.c

Requested by: E. Clark

Department: 93-43

Extension: 231-3732

Reason for request:

Document SW corrections or enhancements made during the first Pattern Factor rig tests. Modified modules need to be changed from version 1.0 to version 1.1. Add a display statement to display overall program version during program initialization. Send out (and store as a quality record) notice of the release of version 1.1. Archive the source files as of the end of the rig testing, and archive the source files that have now been annotated with version 1.1 modification header information.

Update PFCSRSp1.doc and PFCSRSp2.doc as required to bring requirements specification into alignment with current state of the design.

Description of change:

| Module | Subroutine | Change Description / Comment |
|------------|---|--|
| pfcmain.c | performFG main | move check_thermocouples() call ahead of map_openloop_input_vars() call to correct T4val[0] calculation problem add printf statement to display current overall version of program |
| pfcbite.c | check_thermocouples get_adjacent_average | WAS: T4reading[i] = T4lv[i]; (in out-of-range logic) NOW: T4reading[i] = get_adjacent_average[i]; WAS: good_one_found = ! T4[i].fail; (obs storage structure) NOW: good_one_found = ! T4fail[i]; (2 places) |
| picntrl.c | perform_PI_logic | ADD: if (wf_sf[i] < ffmxit_sf) wf_sf[i] = ffmxit_sf; (adds min bound check to already present max bound check) |
| fuzcntrl.c | perform_fuzzy_logic | ADD: if (wf_sf[i] < ffmxit_sf) wf_sf[i] = ffmxit_sf; (adds min bound check to already present max bound check) |

| Module | Subroutine | Change Description / Comment |
|------------|--|---|
| pfcio.c | read_analogs | ADD: P3.volts = - P3.volts; (invert to sort out HW polarity problem) |
| auxtasks.c | update_last_values write_remote_data send_word | remove write_remote_data, send_word routines and calls. This is unused code not fully implemented as part of attempt to use parallel port for data transmission. |
| backgnd.c | update_scattergram | ADD: if (T4fail[i]) _setcolor(_LIGHTRED); (this visually flags failed TC's by changing their color in scattergram to red) |
| pfcvars.c | N/A – var definitions | ADD: T4hil, T4lol, T4tol, T4tolK; these used to provide adjustable TC BITE limits as a function of average temp rather than previous hard limits of -50 and 3000 degF. WAS: P3scale_factor = 12.853; NOW: P3scale_factor = 38.51; (use 300 instead of 100 psi sensor) |
| publics.h | N/A – ext variable declarations | accommodate the variable additions made to pfcvars.c |

Approvals:

Primary Systems Engineer: E. Clark

Program: NA

Other: NA

| REPORT DOCUMENTATION PAGE | | | Form Approved OMB No. 0704-0188 | |
|---|--|---|---|--|
| Public reporting burden for this collection of information is estimated to average 1 hour per response, including the time for reviewing instructions, searching existing data sources, gathering and maintaining the data needed, and completing and reviewing the collection of information. Send comments regarding this burden estimate or any other aspect of this collection of information, including suggestions for reducing this burden, to Washington Headquarters Services, Directorate for Information Operations and Reports, 1215 Jefferson Davis Highway, Suite 1204, Arlington, VA 22202-4302, and to the Office of Management and Budget, Paperwork Reduction Project (0704-0188), Washington, DC 20503. | | | | |
| 1. AGENCY USE ONLY (Leave blank) | | 2. REPORT DATE July 2004 | 3. REPORT TYPE AND DATES COVERED Final Contractor Report—March 1996–Dec. 1999 | |
| 4. TITLE AND SUBTITLE Reliable and Affordable Control Systems Active Combustor Pattern Factor Control | | | 5. FUNDING NUMBERS WBS–22–714–20–04 NAS3–27752, AOI Task 1.2 | |
| 6. AUTHOR(S) Bob McCarty, Chris Tomondi, and Ray McGinley | | | | |
| 7. PERFORMING ORGANIZATION NAME(S) AND ADDRESS(ES) Honeywell Engines and Systems 111 S. 34th Street P.O. Box 52180 Phoenix, Arizona 85072–2180 | | | 8. PERFORMING ORGANIZATION REPORT NUMBER E–14572 | |
| 9. SPONSORING/MONITORING AGENCY NAME(S) AND ADDRESS(ES) National Aeronautics and Space Administration Washington, DC 20546–0001 | | | 10. SPONSORING/MONITORING AGENCY REPORT NUMBER NASA CR—2004-213097 21–11165 | |
| 11. SUPPLEMENTARY NOTES This research was originally published internally as AST034 in June 2000. Project Manager, Joseph R. Saus (retired). Responsible person, John Rohde, Aeropropulsion Projects Office, NASA Glenn Research Center, organization code 2600, 216–433–3949. | | | | |
| 12a. DISTRIBUTION/AVAILABILITY STATEMENT Unclassified - Unlimited Subject Category: 07 Available electronically at http://gltrs.grc.nasa.gov This publication is available from the NASA Center for AeroSpace Information, 301–621–0390. | | | 12b. DISTRIBUTION CODE | |
| 13. ABSTRACT (Maximum 200 words) Active, closed-loop control of combustor pattern factor is a cooperative effort between Honeywell (formerly AlliedSignal) Engines and Systems and the NASA Glenn Research Center to reduce emissions and turbine-stator vane temperature variations, thereby enhancing engine performance and life, and reducing direct operating costs. Total fuel flow supplied to the engine is established by the speed/power control, but the distribution to individual atomizers will be controlled by the Active Combustor Pattern Factor Control (ACPFC). This system consist of three major components: multiple, thin-film sensors located on the turbine-stator vanes; fuel-flow modulators for individual atomizers; and control logic and algorithms within the electronic control. | | | | |
| 14. SUBJECT TERMS Combustor; Pattern factor control; Emissions; Thin-film sensors; Engine life; Turbine-stator vanes; Fuel-flow modulators; Electronic control | | | 15. NUMBER OF PAGES 335 | |
| | | | 16. PRICE CODE | |
| 17. SECURITY CLASSIFICATION OF REPORT Unclassified | 18. SECURITY CLASSIFICATION OF THIS PAGE Unclassified | 19. SECURITY CLASSIFICATION OF ABSTRACT Unclassified | 20. LIMITATION OF ABSTRACT | |

